NAM

Laboratory Component Testing: Modelling Post-Test Predictions and Analysis Cross Validation

ARUP, Eucentre and TU Delft

Date February 2016

Editors Jan van Elk & Dirk Doornhof

General Introduction

The effort to model the seismic response of buildings in the Groningen area, commenced with the benchmarking and cross-validation study (Ref. 1). ARUP, Eucentre and TU Delft participated in this study, each using a different modelling software. The benchmarking and cross-validation study showed further validation of the modelling was required using large scale masonry components.

This report describes the modelling of large scale component tests, including in-plane and out-of-plane shaking of slender and wider walls of calcium silicate and clay brick masonry and cavity walls. Much attention was given to the modelling of the crack patterns.

Each participant in the study prepared a "blind" prediction before the experiment. These were also useful in preparing the experiments. The "blind" prediction results were compared with the actual experimental results and post-test refined predict ion prepared. This procedure of blind prediction, experiment followed by a refined prediction allowed improvement of the modelling of masonry components.

References

1. URM Modelling and Analysis Cross Validation – Arup, Eucentre, TU Delft, Reference 229746_032.0_REP127_Rev.0.03 April 2015.

NAM

Title	**Laboratory Component Testing: Modelling Post-Test Predictions and Analysis Cross Validation**		**Date**	February 2016
			Initiator	NAM
Autor(s)	**Staff of ARUP, Eucentre and TU Delft**	**Editors**	Jan van Elk and Dirk Doornhof	
Organisation	ARUP, Eucentre and TU Delft	**Organisation**	NAM	
Place in the Study and Data Acquisition Plan	Study Theme: Modelling Seismic response URM Buildings Comment: The effort to model the seismic response of buildings in the Groningen area, commenced with the benchmarking and cross-validation study (Ref. 1). ARUP, Eucentre and TU Delft participated in this study, each using a different modelling software. The benchmarking and cross-validation study showed further validation of the modelling was required using large scale masonry components. This report describes the modelling of large scale component tests, including in-plane and out-of-plane shaking of slender and wider walls of calcium silicate and clay brick masonry and cavity walls. Much attention was given to the modelling of the crack patterns. Each participant in the study prepared a "blind" prediction before the experiment. These were also useful in preparing the experiments. The "blind" prediction results were compared with the actual experimental results and post-test refined predict ion prepared. This procedure of blind prediction, experiment followed by a refined prediction allowed improvement of the modelling of masonry components.			
Directliy linked research	(1) Experiments on URM walls (2) Development of Fragility Curves (URM buildings) (3) Risk Assessment			
Used data				
Associated organisation	NAM			
Assurance	Across ARUP, Eucentre and TU Delft			

Client: Nederlandse Aardolie Maatschappij

Arup Project Title: Groningen Earthquakes - Structural Upgrading

Laboratory Component Testing: Modelling Post-Test Predictions and Analysis Cross Validation

229746_031.0_REP1006

Issue | 16 February 2016

Job number 229746

Arup bv
Naritaweg 118
1043 CA Amsterdam
PO box 57145
1040 BA Amsterdam
The Netherlands

ARUP

Contents

1 Introduction

There are a number of modelling and analysis approaches presently used for assessment of the seismic performance of unreinforced masonry (URM) structures. The approaches employ different idealisations for modelling the behaviour of masonry, potentially leading to differences in the resulting assessment of the expected seismic performance.

A previous benchmarking and cross-validation exercise [1] was performed by Arup, the European Centre for Training and Research in Earthquake Engineering (EUCENTRE) and the Technical University of Delft (TU-Delft) in 2014. The three Consultants used different analysis software: LS-DYNA, TREMURI and DIANA (see Appendix B). This previous work highlighted the need for further validation of the analysis methods with large scale component tests, which are the subject of this report. The test campaign was performed at EUCENTRE and TU-Delft between May and December 2015, is outlined briefly in Section 2, and reported fully in [2], [3] and [4].

To demonstrate the robustness of the different approaches, each Consultant generated a "blind prediction" of the expected laboratory result, based on the planned test protocol. The physical test was then performed and the blind prediction was compared to the test. In practice, the actual loading applied in many of the tests differed from the planned protocol significantly (for example, in respect of the applied overburden). Comparisons between the blind predictions and the actual test results are therefore of limited value for those tests. Because the blind predictions may distract from the main purpose of this report, they are documented in a separate annex [13].

A "post-test refined prediction" was then analysed, taking into account the most up-to-date input information concerning material properties and the loading and boundary conditions applied during the tests. The results are described in Sections 3.3 and 4.3. The post-test refined predictions provide a measure of the robustness and accuracy of the current simulation methods and software for URM. Further work remains to absorb the wealth of information revealed by the tests and use it to improve the simulation methods and material models.

Figure 1 - Collaboration partners of Arup

2 Test Programme

The experimental campaign is divided between the laboratories of EUCENTRE (EUC) and TU-Delft (TUD) and is designed to investigate the most recurrent types of wall structures encountered in terraced houses of the Groningen area.

Table 1: Summary of the full integrated tasting campaign

Category	Type	Lab	ID	Geometry [m]	Description
In-plane	Quasi-Static	EUC	COMP-1	2.75 x 1.1	Double-fixed - 0.5 MPa
		EUC	COMP-2	2.75 x 1.1	Double-fixed - 0.7 MPa
		EUC	COMP-3	2.75 x 4	Cantilever - 0.3 MPa
		TUD	COMP-0a	2.75 x 1.1	Double-fixed - 0.7 MPa
		TUD	COMP-1	2.75 x 1.1	Cantilever - 0.5 MPa
		TUD	COMP-2	2.75 x 1.1	Cantilever - 0.7 MPa
		TUD	COMP-3	2.75 x 1.1	Double-fixed - 0.3 MPa
		TUD	COMP-4	2.75 x 4	Double-fixed - 0.5 MPa
		TUD	COMP-5	2.75 x 4	Double-fixed - 0.3 MPa
		TUD	COMP-6	2.75 x 4	Cantilever - 0.5 MPa
Out-of-plane	Quasi-Static	TUD	COMP-0b (*)	2.75 x 1.45	One-way Bending - 0.2 MPa
		TUD	COMP-7	2.75 x 1.45	One-way Bending - 0.2 MPa
		TUD	COMP-10	2.75 x 4	Two-ways Bending
		TUD	COMP-11	2.75 x 4	Two-ways Bending
		TUD	COMP-12	2.75 x 4	Two-ways Bending
	Dynamic	EUC	COMP-4	2.75 x 1.45	Single leaf CS - 0.3, 0.1 MPa
		EUC	COMP-5	2.75 x 1.45	Cavity system 2ties/m^2 - 0.1 MPa
		EUC	COMP-6	2.75 x 1.45	Cavity system 2ties/m^2 - 0.3 MPa
		EUC	COMP-7	2.75 x 1.45	Cavity system 4ties/m^2 - 0.1 MPa

(*) TUD-COMP-0b test was stopped due to instability of the test system. It was repeated as TUD-COMP-7 with all the same boundary conditions. Therefore, analysis of TUD-COMP-0b is not reported

The series of tests was planned to investigate both in-plane and out-of-plane response, in order to capture most of the failure mechanisms expected during the seismic response of these walls. The test set-ups and results are described in detail in [2], [3] and [4].

3 In-Plane Component Tests

3.1 Blind Predictions for In-Plane Component Tests

Blind prediction results are reported in a separate annex [13] to this report.

3.2 Changes to Analysis Models for Post-Test Refined Predictions of In-Plane Component Tests

After receipt of the laboratory test results, the analysis models were updated. This section describes the changes made.

3.2.1 Arup changes to LS-DYNA models for in-plane post-test predictions

A consistent set of assumptions, inputs and modelling methods has been used across all the post-test LS-DYNA analyses. In general terms the differences compared to the blind prediction models are:

- Most of the blind prediction LS-DYNA models were run before the material properties were measured by EUC and TUD and used material properties from NAM's Basis for Design (Appendix A). The post-test models all used the material properties of masonry measured by EUC and TUD.
- The material characteristics modelled in the post-test analyses include better non-linear representation of masonry as it approaches compression failure, enabling collapse of certain specimens to be better predicted.
- The overburden loads and applied displacements were changed to reflect those actually applied during the tests.
- After completing the displacement protocol that was applied in the laboratory, further larger cycles were applied to the LS-DYNA models to find the drift at which LS-DYNA predicted collapse.

All the post-test analyses were run using the October 2015 version of LS-DYNA's masonry material model.

3.2.1.1 Material properties

The calcium silicate and clay properties measured by EUC [2] differed somewhat from those measured by TUD [5]. LS-DYNA models of tests performed by EUC used the material properties measured by EUC, while the models of tests performed by TUD used material properties measured by TUD. In all other respects, the same consistent set of material properties was used for all the post-test analyses reported here. The key differences in the material properties are summarised in Table 2 and Table 3 below.

Table 2: Calcium silicate material properties used in LS-DYNA blind predictions and post-test refined predictions

	NAM Basis for Design (used in blind prediction models unless noted otherwise)	**Measured properties (used in post-test models)**	
		EUC	TUD
Young's Modulus	3500 MPa	4182 MPa	5091 MPa
Compressive strength	6.0 MPa	6.2 MPa	6.2 MPa (*)
Compressive behaviour	Elastic-perfectly-plastic	Stress-strain curve with softening	
Poisson's ratio	---	0.14 (+)	0.14
Bed joint tensile strength (f_w)	150 kPa	238 kPa	270 kPa
Bed joint shear strength (f_{v0})	300 kPa	210 kPa	140 kPa
Bed joint friction coefficient (μ)	0.75	0.42	0.43

(*) The TUD measured compressive strength of masonry was 5.9 MPa but no stress-strain curve was provided. Therefore, the compression properties measured by EUC were used for tests from both test centres.

(+) Properties not reported by EUC – data from TUD used.

Table 3: Clay material properties used in LS-DYNA blind predictions and post-test refined predictions

	NAM Basis for Design (used in blind prediction models unless noted otherwise)	**Measured properties (used in post-test models)**	
		EUC	TUD
Young's Modulus	6000 MPa	6033 MPa	6921 MPa
Compressive strength	8.0 MPa	11.3 MPa	11.3 MPa (*)
Compressive behaviour	Elastic-perfectly-plastic	Stress-strain curve with softening	
Bed joint tensile strength (f_w)	150 kPa	158 kPa	170 kPa (**)
Bed joint shear strength (f_{v0})	300 kPa	150 kPa (+)	150 kPa
Bed joint friction coefficient (μ)	0.75	0.87 (+)	0.87

(*) The TUD measured compressive strength of masonry was 14.7 MPa but no stress-strain curve was provided. Therefore, the compression properties measured by EUC were used for tests from both test centres.

(**) Measured tensile strength was 270 kPa but LS-DYNA's masonry material model does not permit f_w exceeding f_{v0}/μ

(+) Properties not reported by EUC – data from TUD used.

3.2.1.2 Compression behaviour, toe crushing and collapse

The application of a more realistic compressive stress-strain curve with post-peak softening influences the predictions in two ways:

- During rocking, more energy is absorbed in hysteresis.
- Post-peak softening (and subsequent removal of fully crushed elements) represents toe-crushing damage and ejection of fragments of masonry. This leads to the possibility of collapse of specimens when the vertical load can no longer be supported.

The stress-strain curve for CaSi masonry as an example is presented in Figure 2. The curve is taken from compression test on masonry wallettes by EUC [2] up to

the peak stress. The softening slope may be regarded as an artificial modelling parameter and was determined by trial and error. It controls the drift at which collapse occurs in rocking mode. Elements are deleted from the analysis automatically when the compressive strength reaches zero. A stress-strain curve for clay masonry has also been developed similarly.

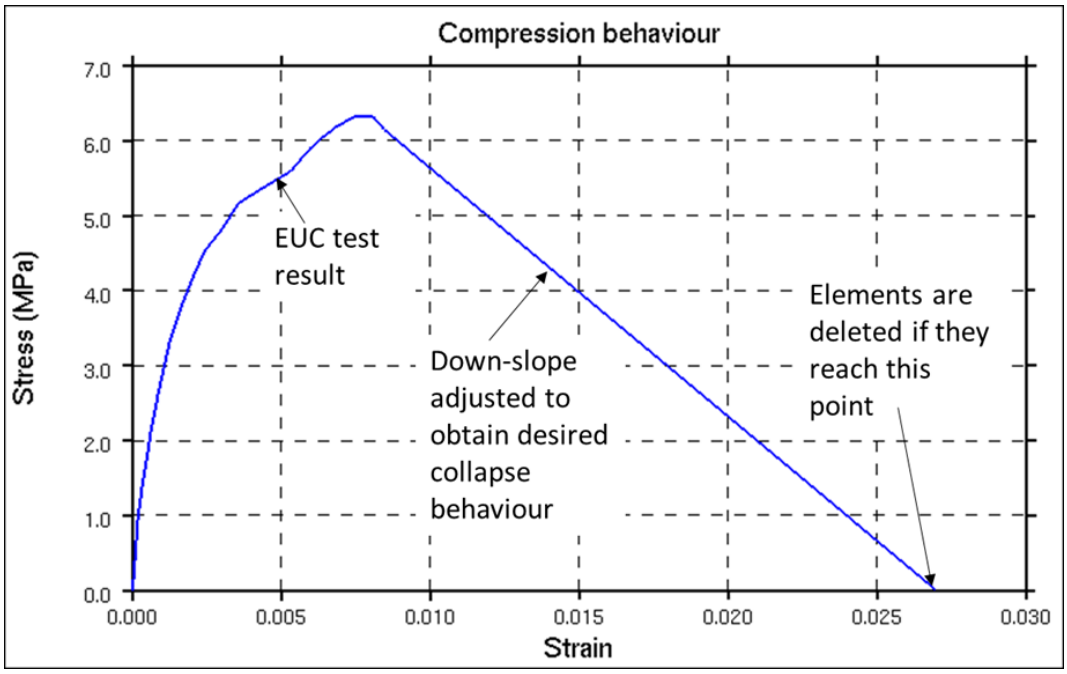

Figure 2: Compressive stress-strain input data for post-test LS-DYNA analyses of CaSi components

3.2.1.3 Boundary conditions to match the laboratory tests

The overburden loads and applied displacement protocols in all models were adjusted to match those applied in the laboratory tests.

3.2.1.4 Extended protocols and collapse assessment

For all the post-test in-plane analyses, larger displacement cycles were added after the cycles applied in the laboratory tests, in order to find the drift at which the model specimen collapsed. This is illustrated in Figure 3.

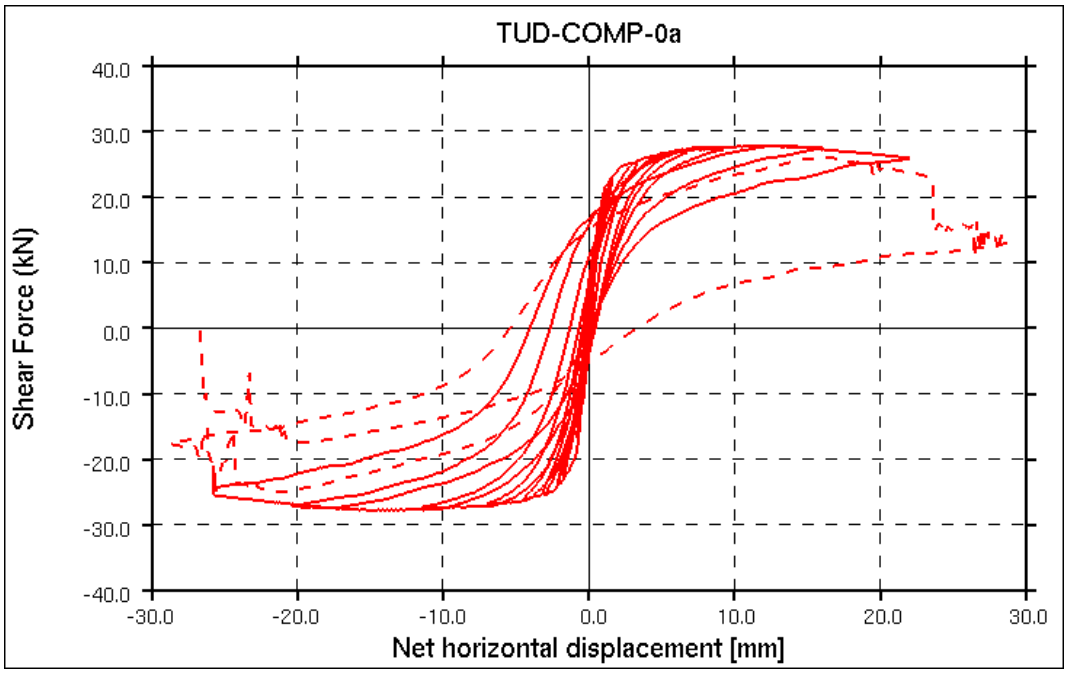

Figure 3 - Example LS-DYNA result from displacement protocol applied in the laboratory (continuous line) and additional larger cycles (dashed line)

The hysteresis graphs in this report show the LS-DYNA result only up to the point when the test was stopped, i.e. the continuous line in Figure 3 above, to enable like-for-like comparisons with the test result. However, the assessment of drift to collapse was made considering the whole of the hysteresis response including the larger cycles (continuous and dashed lines).

The assessment of collapse was carried out in the following manner. In most cases, the laboratory tests were stopped because of damage implying a near-collapse condition, but the specimen did not actually collapse. There is a lack of precision in defining “near-collapse”; some specimens might have tolerated larger drifts without collapsing, while others might have collapsed if only slightly larger drifts were applied. Comparisons with LS-DYNA predictions of collapse must therefore be treated with caution. In this report, the drift to achieve a near-collapse condition is given as a range. The lower bound is defined by the first element being deleted due to toe-crushing. The upper bound is defined by a drop of resistance of 30% or more, as seen at 25mm drift in Figure 3 above. In this example the lower and upper bounds form a narrow range and total collapse occurs shortly after (at -27mm), but in other tests the range defined in this way is much wider.

3.2.2 EUCENTRE changes to TREMURI models for in-plane post-test predictions

The main differences compared to the blind prediction models are:

- Some of the blind prediction TREMURI models were run before the material properties were measured and used material properties from NAM's Basis for Design (Appendix A). The post-test models all used the material properties of masonry measured at EUC and TUD.
- The loads and displacements were changed to reflect those actually applied during the tests.
- A new constitutive relationship has been implemented in the macroelement model and used for the post-test simulations of the TUD tests only. The improved model (identified hereafter as "new model") is characterized by a different hysteretic behaviour in compression that allows an increased energy dissipation in bending-rocking mechanisms.

3.2.2.1 Material properties

The calcium silicate and clay properties measured at EUC [2] differed somewhat from those measured at TUD [5]. TREMURI models of tests performed by EUC used the material properties measured at EUC, while the models of tests performed by TUD used material properties measured at TUD. In all other respects, the same consistent set of material properties was used for all the post-test analyses reported here. The key differences in the material properties are summarised in Table 4 and Table 5 below.

Table 4: Calcium silicate material properties used in TREMURI blind predictions and post-test refined predictions

	NAM Basis for Design (used in blind prediction models unless noted otherwise)	**Measured properties (used in post-test models)**	
		EUC	TUD
Young's Modulus	3500 MPa	4182 MPa	5091 MPa
Compressive strength	6.0 MPa	6.2 MPa	5.9 MPa
Shear modulus	1450 MPa	1673 MPa	2036 MPa
Bed joint shear strength (f_{v0})	300 kPa	210 kPa	140 kPa
Bed joint friction coefficient (μ)	0.75	0.42	0.43

Table 5: Clay material properties used in TREMURI blind predictions and post-test refined predictions

	NAM Basis for Design (used in blind prediction models unless noted otherwise)	**Measured properties (used in post-test models)**	
		EUC	TUD
Young's Modulus	6000 MPa	6033 MPa	6921 MPa
Compressive strength	8.0 MPa	11.3 MPa	14.7 MPa
Bed joint shear strength (f_{v0})	300 kPa	150 kPa (+)	150 kPa
Bed joint friction coefficient (μ)	0.75	0.87 (+)	0.87

(+) Properties not reported by EUC – data from TUD used.

3.2.2.2 Boundary conditions to match the laboratory tests

The overburden loads and applied displacement protocols in all models were adjusted to match those applied in the laboratory tests.

3.2.3 TU-Delft changes to DIANA models for in-plane post-test predictions

Compared to the blind predictions, the main differences are:

- The material properties have been changed from those of the NAM's Basis for Design (Appendix A), which had been used for the blind predictions. The post-test refined models used the material properties measured by EUC and TUD.
- The loads and displacements were changed to reflect those actually applied during the tests.
- A new orthotropic constitutive model has been implemented and adopted to provide a better representation of the failure modes and to evaluate more accurately the dissipated energy, especially for shear failure of long walls. The new constitutive model is presented in Section 3.2.3.2.

3.2.3.1 Material properties

DIANA in-plane component models used material properties reported in Table 6 for calcium silicate masonry.

Table 6: Calcium silicate material properties used in DIANA blind predictions and post-test refined predictions of in-plane component tests

	NAM Basis for Design (used in blind prediction models unless noted otherwise)	**Measured properties (used in post-test models)**	
		EUC	TUD
Young's Modulus in direction perpendicular to bed joints (E_{m-2})	3500 MPa	4182 MPa	5091 MPa
Compressive strength in direction perpendicular to bed joints (f_m)	6.0 MPa	6.2 MPa	5.9 MPa
Young's Modulus in direction parallel to bed joints ($E_{m,h-2}$)	---	3583 MPa (+)	3583 MPa
Compressive strength in direction parallel to bed joints ($f_{m,h}$)	---	7.55 MPa (+)	7.55 MPa
Compressive behaviour	Elastic-perfectly-plastic	Stress-strain curve with softening	
Masonry flexural strength with moment vector parallel to bed joint and in plane of wall (f_{x1})	150 kPa (*)	238 kPa (*)	210 kPa
Masonry flexural strength with moment vector orthogonal to bed joint and in plane of wall (f_{x2})	150 kPa (*)	238 kPa (*)	760 kPa
Bed joint shear strength (f_{v0})	300 kPa	210 kPa	140 kPa
Bed joint friction coefficient (μ)	0.75	0.42	0.43

(*) Assumed reported f_w properties

(+) Properties not reported by EUC – data from TUD used.

3.2.3.2 Orthotropic constitutive model for masonry material properties

The adopted constitutive model is characterised by the following main features:

- The material is anisotropic: two pre-defined crack/crush directions (aligned to the bed- and head-joints, referenced as x- and y- direction, respectively) are defined in the plane of the model;
- Three elastic parameters: the Young's moduli in the x- and y- directions, and the elastic shear modulus.
- Five possible failure modes are possible (tensile failures in the x- and y-directions; crushing in the x- and y-directions; shear failure);
- Brittle cracking with linear unloading based on fracture energy. A secant unloading/reloading is assumed (Figure 4a);
- Multilinear crushing, with bi-linear (non-secant) unloading-reloading behaviour (Figure 4b);
- Coulomb friction model to determine the maximum shear, with elastic unloading and reloading (Figure 4c).

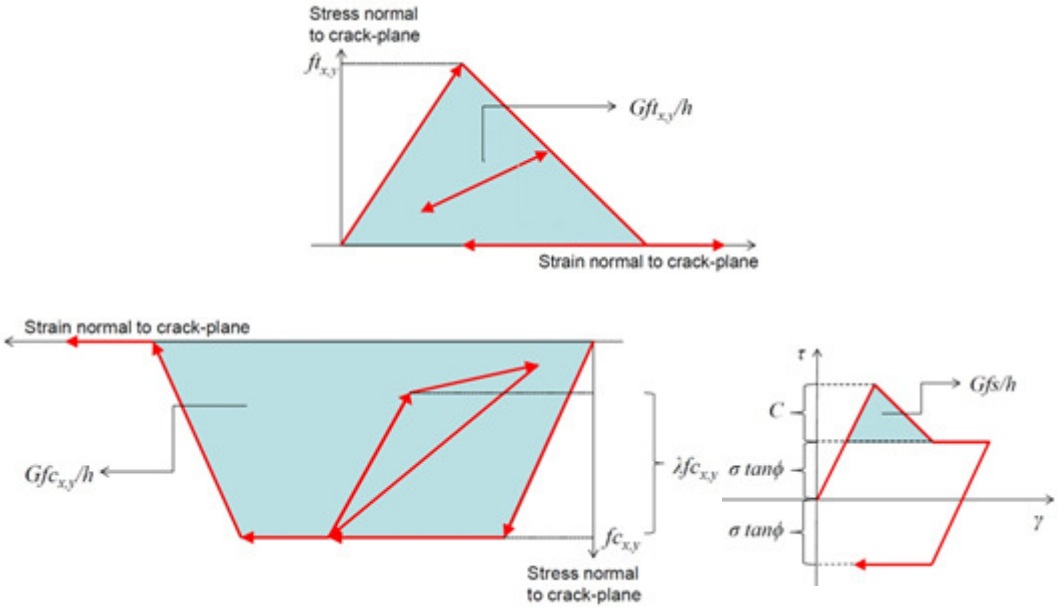

Figure 4: DIANA contitutive model stress-strain inputs for (a) cracking, (b) crushing and (c) shear

3.3 Comparison of Post-Test Refined Predictions

After receipt of the laboratory test results, the analyses were updated and re-run. This section reports the results of those analyses.

3.3.1 TUD-COMP-0a

3.3.1.1 Test Description

TUD-COMP-0a was the first of a series of quasi-static in-plane tests administered by TU-Delft. This specimen was a single-wythe wall constructed of calcium silicate units 102 mm thick. It was 1.1 m long and 2.76 m high. The applied overburden stress was 0.7 MPa. The wall was tested under double clamped boundary conditions.

Upon cyclically loading specimen TUD-COMP-0a, a gradual reduction of the initial stiffness occurred at very low drifts. First cracks appeared at the top right corner for positive displacements during the fourth loading cycle (circled in red in Figure 5). The failure mode combined rocking, sliding and crushing. More specifically, the wall underwent a rocking mechanism at first, followed by bed-joint sliding. Toe-crushing only occurred at the end of the test.

The specimen showed asymmetric mechanical behaviour. This can be explained by the fact that the cracks at the left bottom and top right occurred at a different height than those at the right bottom and top left.

The wall was tested up to a peak drift of 0.9%. The test was stopped after a large reduction of resistance for negative imposed displacements because the integrity of the wall could have been compromised.

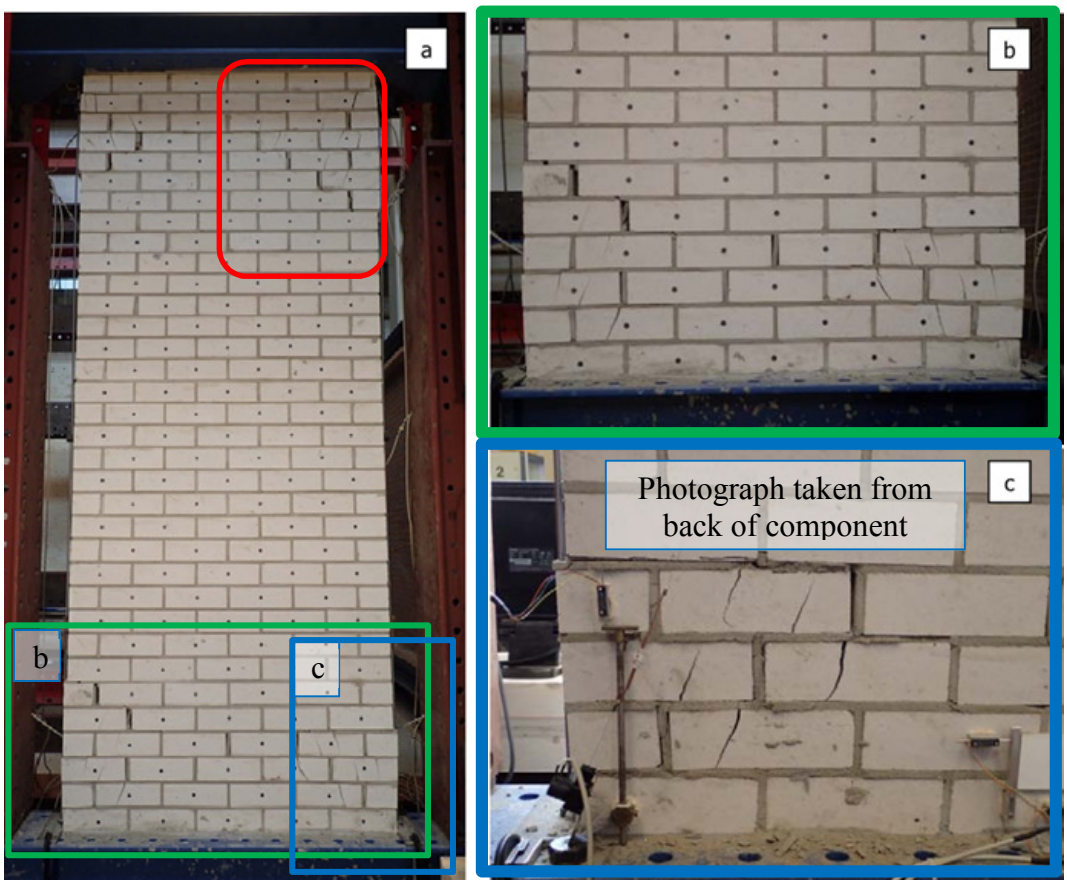

Figure 5: TUD-COMP-0a: Crack pattern at failure; general overview. Cracks in areas highlighted in red (a); detail of the bottom part of the wall (b) and of the toe crushing (c).

The measured hysteresis is shown in Figure 6.

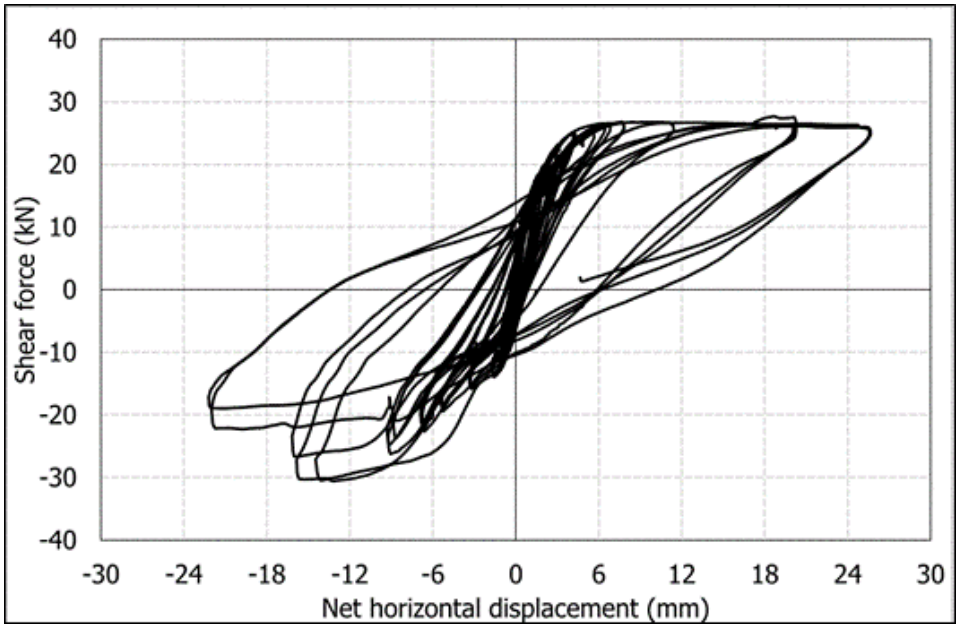

Figure 6: TUD-COMP-0a: Lab test result – Shear force-displacement curve

3.3.1.2 Arup Post-Test Refined Prediction

The LS-DYNA model of TUD-COMP-0a correctly predicted rocking behaviour with toe crushing as shown in Figure 7.

The lateral-force-versus-displacement relationship is shown in Figure 8. The predicted ultimate load was approximately 28 kN at a drift of 0.9%, compared with 30kN in the test. The predicted initial stiffness was approximately 29.7 kN/mm. Although more energy dissipation was captured in the post-test refined model in comparison to the blind prediction model, the amount of energy dissipation was still under-predicted.

In the laboratory, the test was stopped at 0.9% drift due to toe-crushing damage suggesting a near-collapse state. The analysis indicated near-collapse at 0.9 – 1.0% drift.

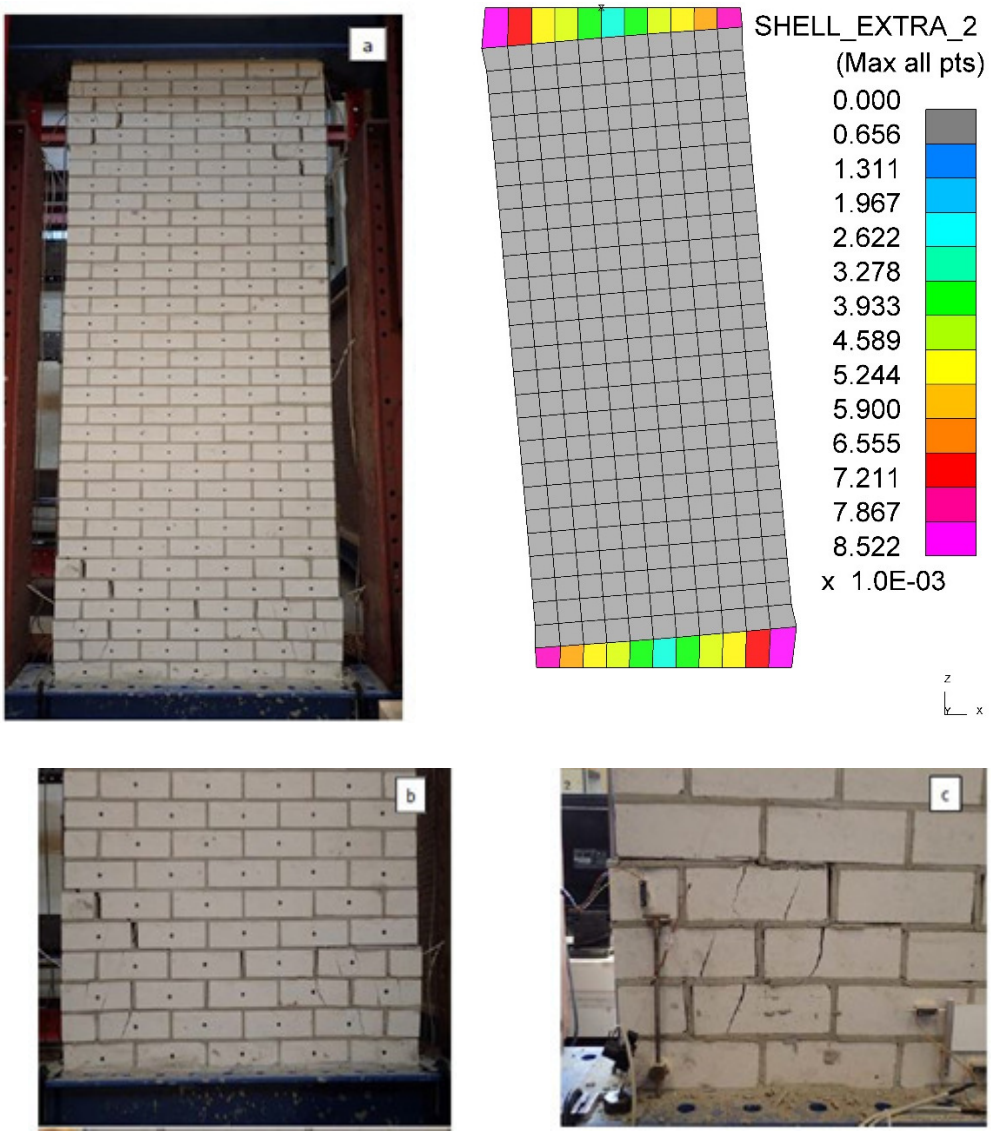

Figure 7: TUD-COMP-0a: LS-DYNA post-test refined prediction - Damage plot at end of analysis (top right) compared to observed damage in laboratory

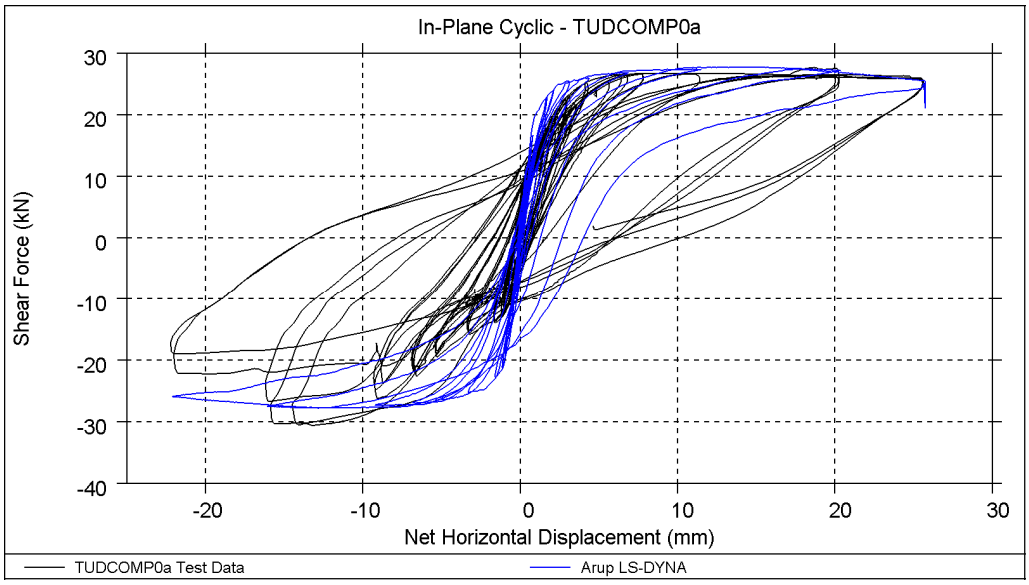

Figure 8: TUD-COMP-0a: LS-DYNA post-test refined prediction - Shear force-displacement curve

Table 7: TUD-COMP-0a: LS-DYNA post-test refined prediction - Summary table

Consultant	**Predominant Failure Mechanism Predicted**	**Initial Stiffness [kN/mm]**	**Peak Strength [kN]**	**Maximum Achieved Drift**	
LS-DYNA	Rocking behaviour / toe crushing	29.7	28	0.9% to 1.0%	Near collapse
Test Result	Rocking behaviour / toe crushing	25.8	30	0.9 %	Near collapse

3.3.1.3 EUCENTRE Post-Test Refined Prediction

- The shear force -displacement relationships are shown in Figure 9. The ultimate strength as well as the initial stiffness are well predicted by the TREMURI model. Although more energy dissipation is captured in the post-test refined "new model", the amount of energy dissipation is still under-predicted (Figure 10).

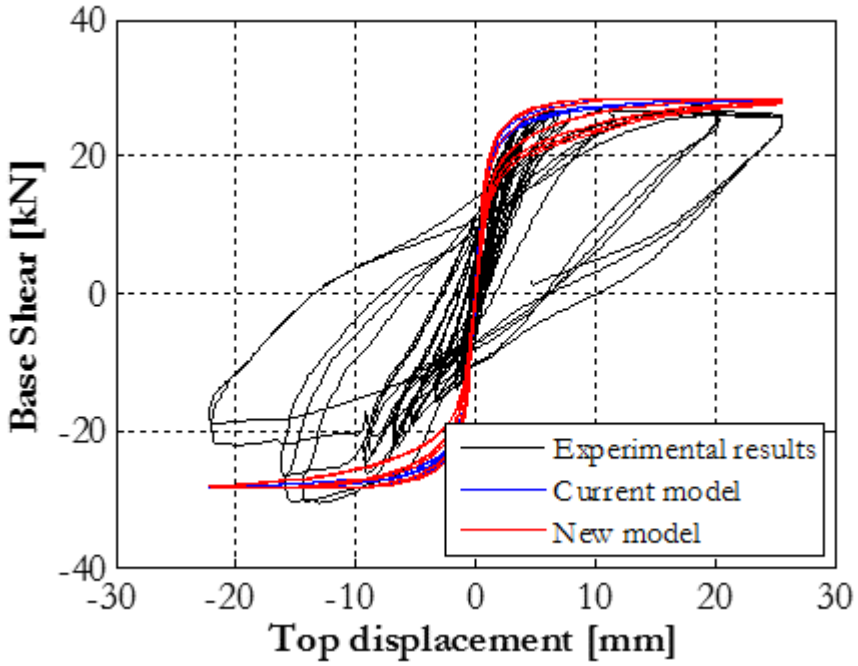

Figure 9: TUD-COMP-0a: TREMURI post-test refined prediction - Shear force-displacement curve

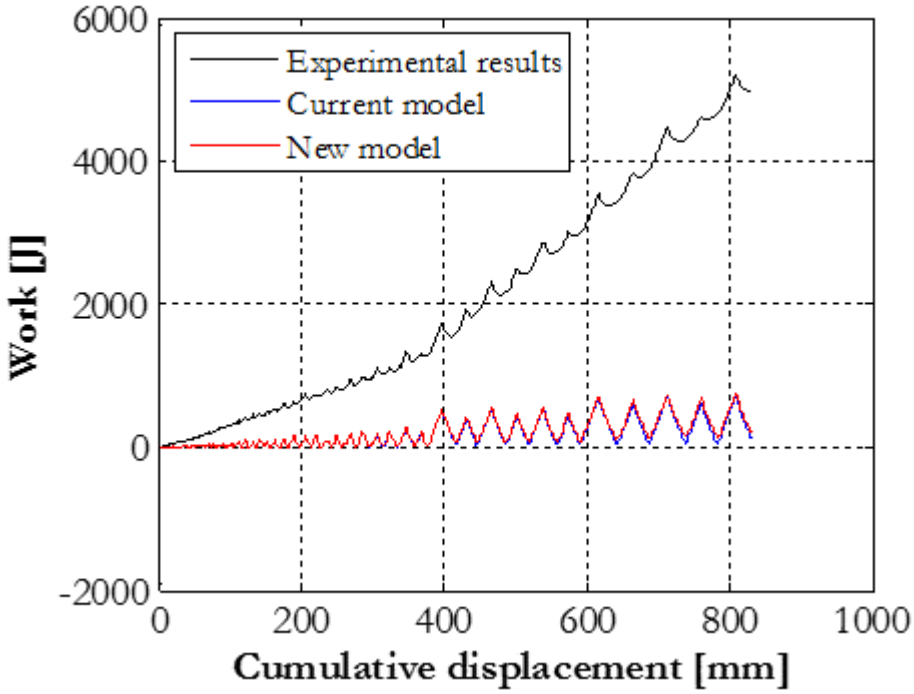

Figure 10: TUD-COMP-0a: TREMURI post-test refined prediction – Work and dissipated energy

Table 8: TUD-COMP-0a: TREMURI post-test refined prediction - Summary table

Consultant	**Predominant Failure Mechanism Predicted**	**Initial Stiffness [kN/mm]**	**Peak Strength [kN]**	**Maximum Achieved Drift**	
TREMURI new model	Rocking behaviour / toe crushing	23	28.4	0.93%	
Test Result	Rocking behaviour / toe crushing	25.8	30	0.9 %	Near collapse

3.3.1.4 TU-Delft Post-Test Refined Prediction

The DIANA model of TUD-COMP-0a, with the application of the new material model, noticeably improved the prediction of the experimental behaviour of the panel. The real loading protocol has been applied with no convergence problems until larger displacements.

The numerical damage pattern is more extensive with respect to the experiment (Figure 11). A rocking behaviour is detected with cracks at the base and top of the panel spreading also along the height, with some horizontal cracks at the two lateral edges of the panel. In the last stages of the test, some additional cracks in the middle of the panel also occur.

The shear-displacement history is reported in Figure 12. The numerical peak shear capacity is 28.2 kN and the initial stiffness is approximately 21 kN/mm, both slightly lower than the experimental values.

With respect to the blind prediction, a larger energy dissipation is recorded with the new material model, similar to what was recorded in the experiment. With respect to the test, some more degradation of the ultimate capacity is observed with increasing applied displacements.

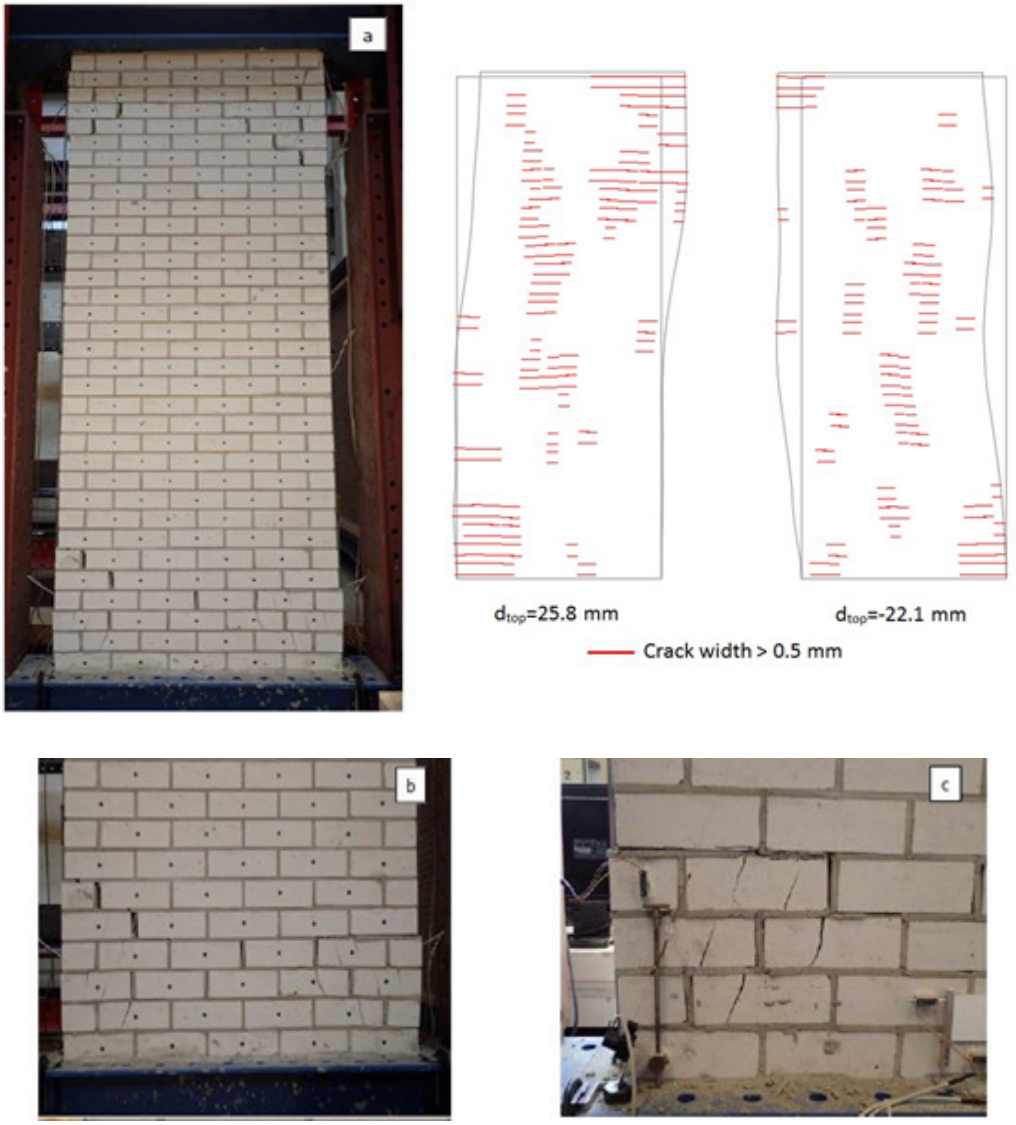

Figure 11: TUD-COMP-0a: DIANA post-test refined prediction - Damage plot at end of analysis (top right) compared to observed damage in laboratory

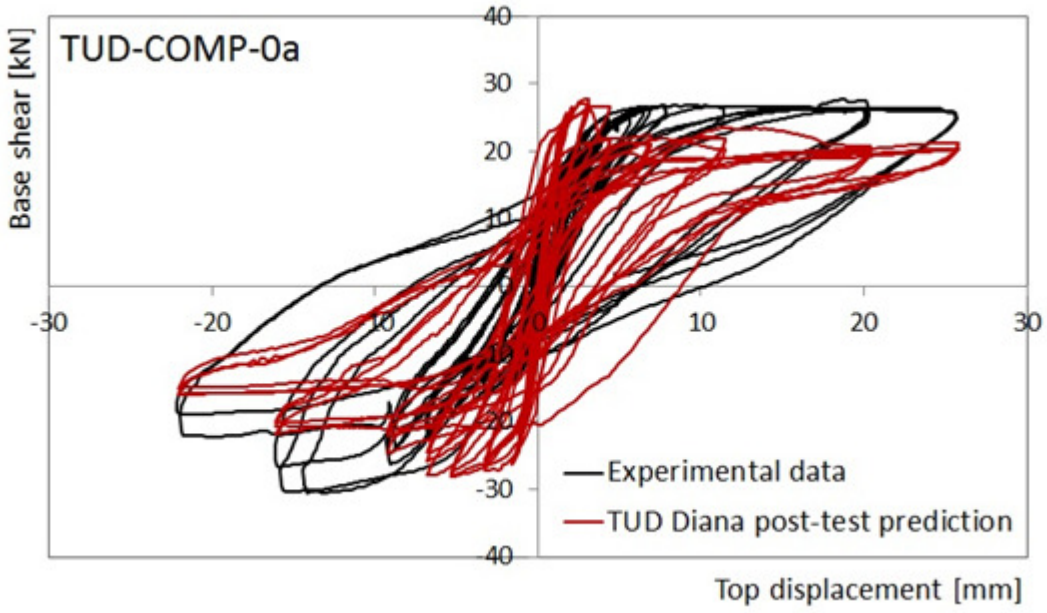

Figure 12: TUD-COMP-0a: DIANA post-test refined prediction - Shear force-displacement curve

Table 9: TUD-COMP-0a: DIANA post-test refined prediction - Summary table

Consultant	**Predominant Failure Mechanism Predicted**	**Initial Stiffness [kN/mm]**	**Peak Strength [kN]**	**Maximum Achieved Drift**	
DIANA	Rocking / cracks in middle of panel	21	28.2	0.9%	End of test protocol / extensive damage
Test Result	Rocking behaviour / toe crushing	25.8	30	0.9 %	Near collapse

3.3.2 TUD-COMP-1

3.3.2.1 Test Description

TUD-COMP-1 was the second quasi-static in-plane test administered by TU-Delft. This specimen was a single-wythe wall constructed of calcium silicate units, 102 mm thick. It was 1.1 m long and 2.76 m high. The applied overburden stress was 0.52 MPa. The wall was tested under cantilever boundary conditions.

Upon cyclically loading specimen TUD-COMP-1, a gradual reduction of the initial stiffness occurred at very low drifts. First cracks appeared at the bottom left corner for negative displacements during the fifth cycle (approximately 0.8% drift). The failure mode was mainly governed by rocking with diagonal crack patterns at the bottom of the wall as mentioned. The specimen showed asymmetric mechanical behaviour. The test was stopped at a net drift of 1.6%.

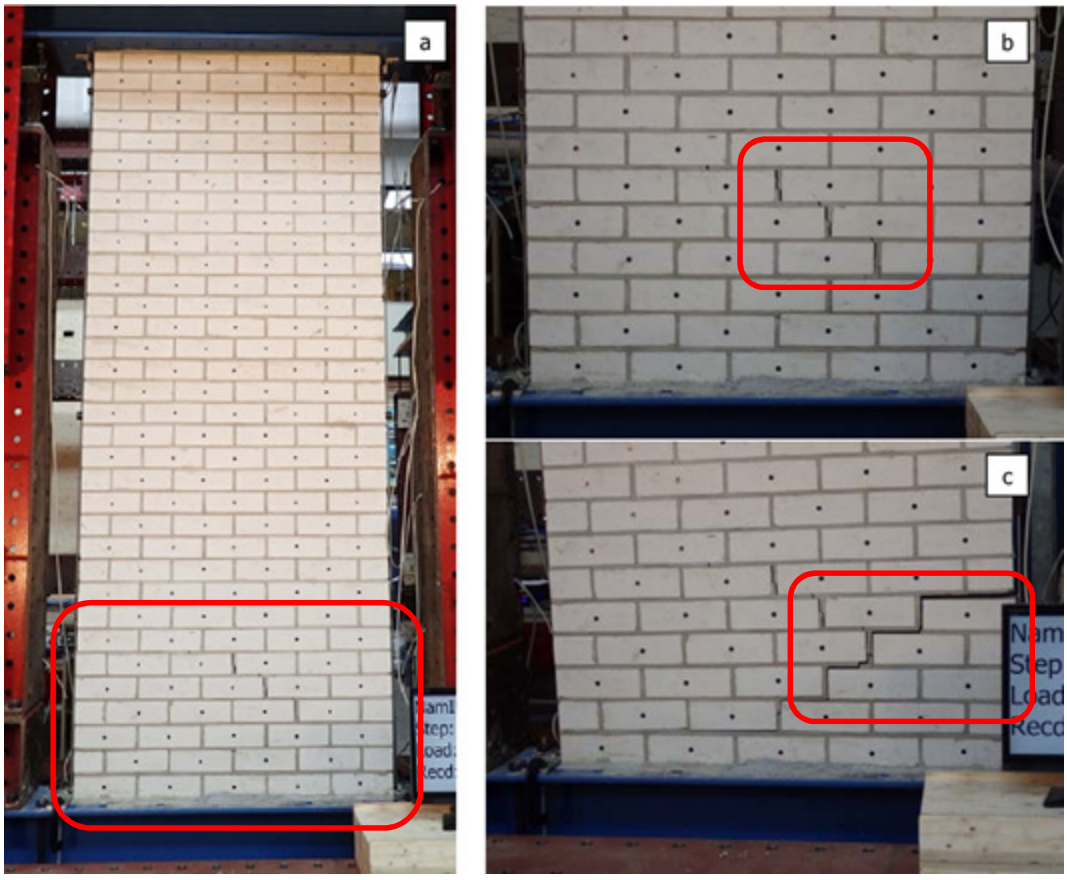

Figure 13: TUD-COMP-1: Crack pattern at failure; general overview (a); detail of the bottom part of the wall for positive (b) and negative (c) peak top displacements.

The measured hysteresis is shown in Figure 14. Some readings of the load cell were compromised and thus rendered some sections of the test response unreliable for comparison purposes. These sections are highlighted in Figure 14.

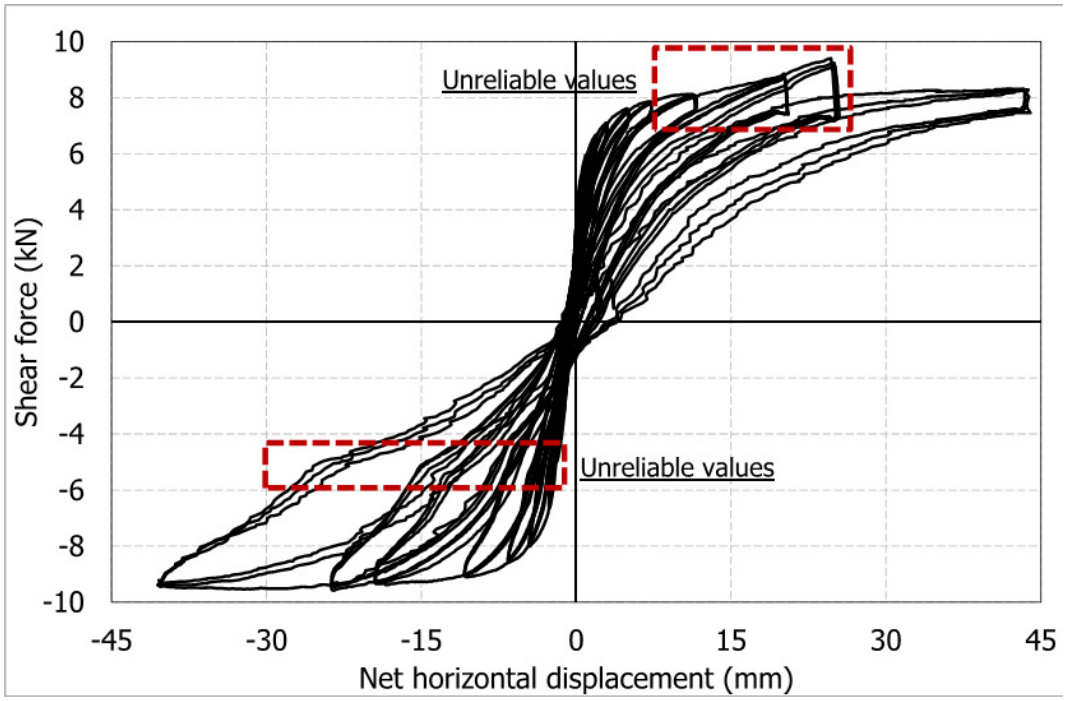

Figure 14: TUD-COMP-1: Lab test result – Shear force-displacement curve

3.3.2.2 Arup Post-Test Refined Prediction

The LS-DYNA model of TUD-COMP-1 correctly predicted rocking behaviour with toe crushing as shown in Figure 15. However, while the analysis predicted a horizontal failure plane, in the lab test the failure plane was stepped.

The lateral-force-versus-displacement relationship is shown in Figure 16. The predicted initial stiffness was approximately 7.8 kN/mm and the predicted ultimate load was approximately 10.9 kN at a drift of 1.6%.. The lab test gave a maximum load of 9.5 kN for negative drift but only about 8kN for positive drift. The reason for the asymmetry of response is not clear, but may be related to the asymmetrical stepped failure plane. Although more energy dissipation was captured in the post-test refined model in comparison to the blind prediction model, the amount of energy dissipation was still under-predicted.

In the laboratory, the test was stopped at 1.6% drift. The test report does not state the reason for stopping. The photographs do not appear to indicate a near-collapse state. The analysis indicated near-collapse at 1.6 – 1.8% drift.

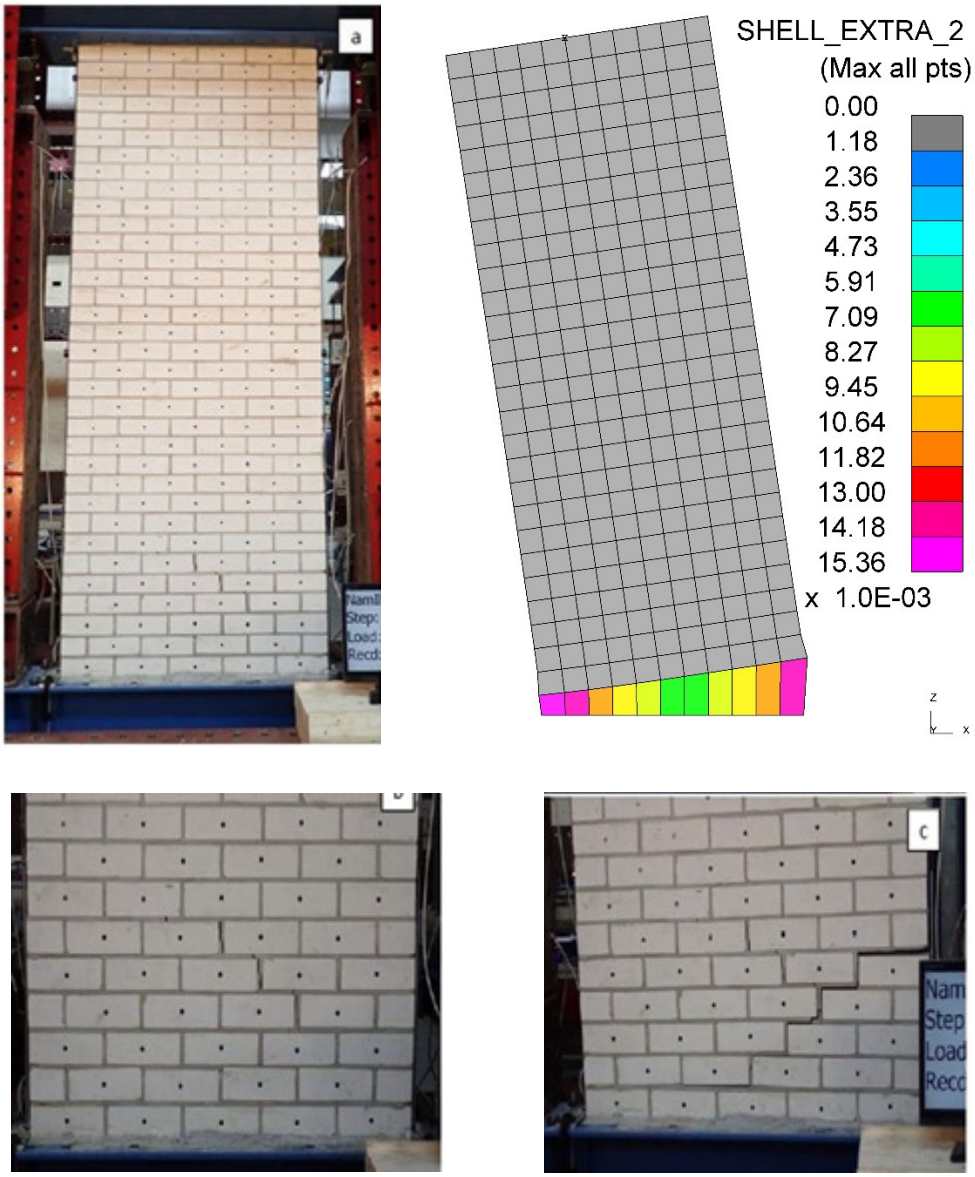

Figure 15: TUD-COMP-1: LS-DYNA post-test refined prediction - Damage plot at end of analysis (top right) compared to observed damage in laboratory

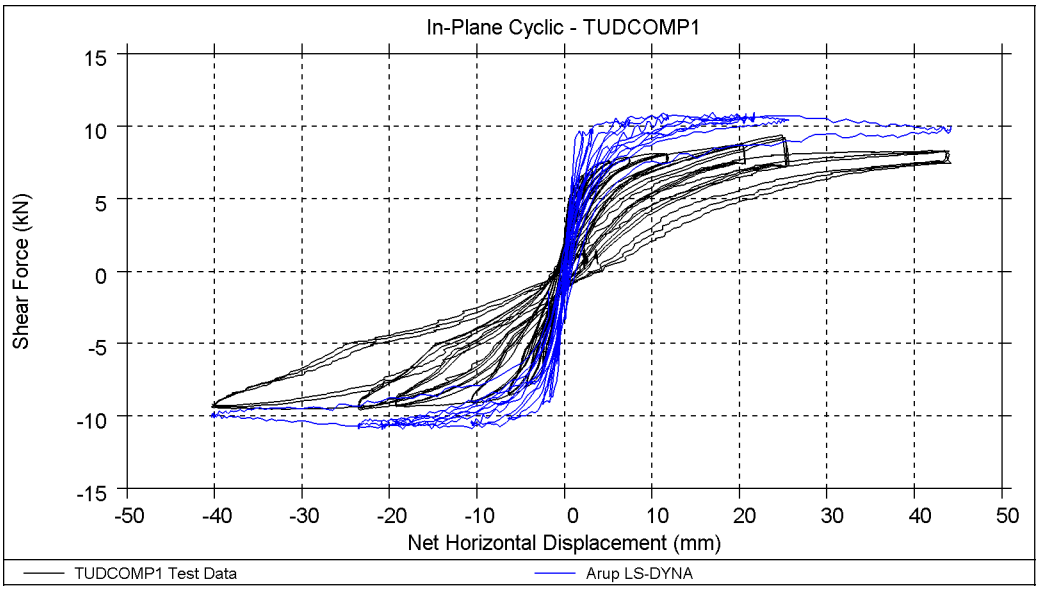

Figure 16: TUD-COMP-1: LS-DYNA post-test refined prediction - Shear force-displacement curve

Table 10: TUD-COMP-1: LS-DYNA post-test refined prediction - Summary table

Consultant	**Predominant Failure Mechanism Predicted**	**Initial Stiffness [kN/mm]**	**Peak Strength [kN]**	**Maximum Achieved Drift**	
LS-DYNA	Rocking behaviour / toe crushing	7.8	10.9	1.6% to 1.8%	Near collapse
Test Result	Rocking behaviour / toe crushing	7.7	9.5	1.6%	Reason for stopping not known

3.3.2.3 EUCENTRE Post-Test Refined Prediction

The shear force-displacement relationships are shown in Figure 17. The TREMURI models tend to overestimate the ultimate strength as well as the initial stiffness (in particular in the positive direction of loading). Although more energy dissipation is captured in the post-test refined "new model", the amount of energy dissipation is still under-predicted (Figure 18).

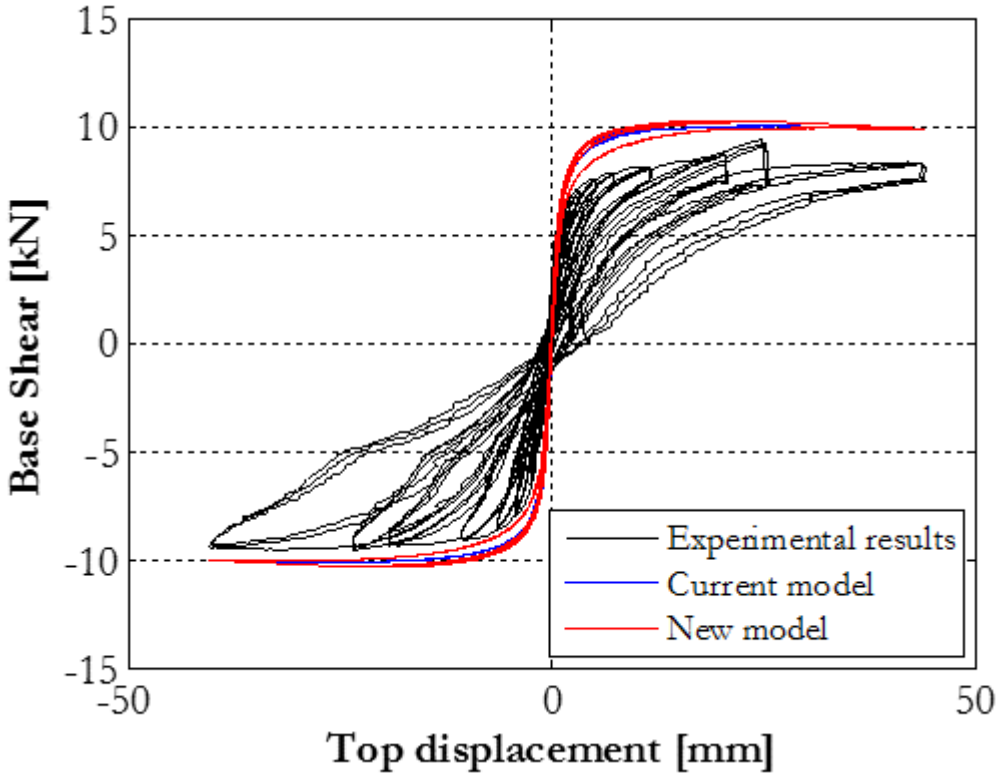

Figure 17: TUD-COMP-1: TREMURI post-test refined prediction - Shear force-displacement curve

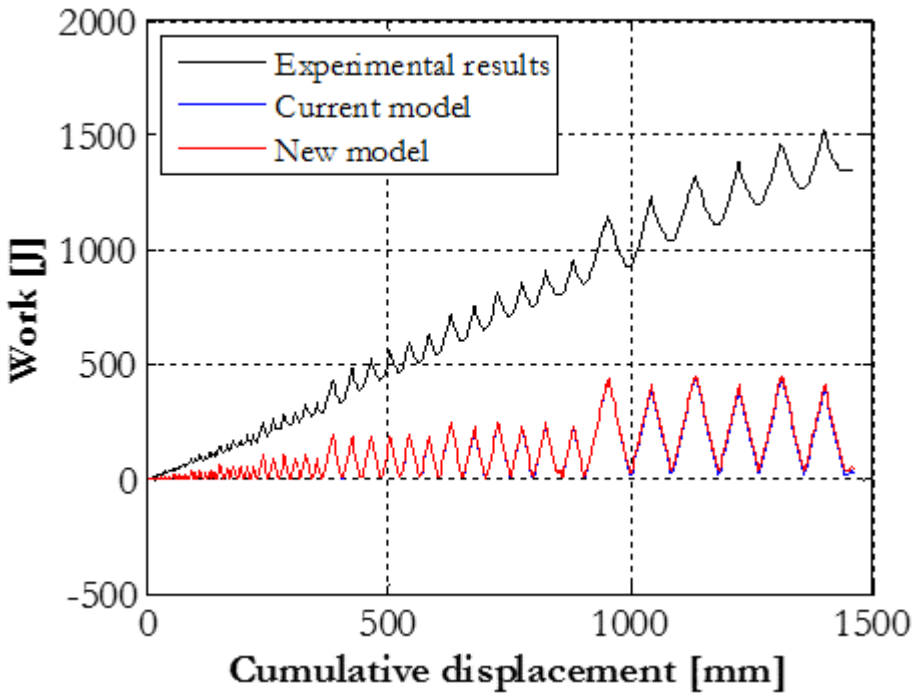

Figure 18: TUD-COMP-1: TREMURI post-test refined prediction – Work and dissipated energy

Table 11: TUD-COMP-1: TREMURI post-test refined prediction - Summary table

Consultant	**Predominant Failure Mechanism Predicted**	**Initial Stiffness [kN/mm]**	**Peak Strength [kN]**	**Maximum Achieved Drift**	
TREMURI new model	Rocking	7.9	10.3	1.6%	
Test Result	Rocking behaviour / toe crushing	7.7	9.5	1.6%	Reason for stopping not known

3.3.2.4 TU-Delft Post-Test Refined Prediction

The DIANA model of TUD-COMP-1, with the application of the new material model, noticeably improved the prediction of the experimental behaviour of the panel. The real loading protocol has been applied with no convergence problems until larger displacements.

The numerical damage pattern shows a rocking behaviour with damage at the base of the panel (Figure 19).

The shear-displacement history is reported in Figure 20. The numerical model predicted a higher peak shear capacity, equal to 11.8 kN, against the 9.5 kN detected in the experiment. The initial stiffness is very close to experiment.

Although a larger energy dissipation is recorded with the new material model with respect to the blind prediction, it is still under-predicted since the model is dominated by pure rocking behaviour in this case.

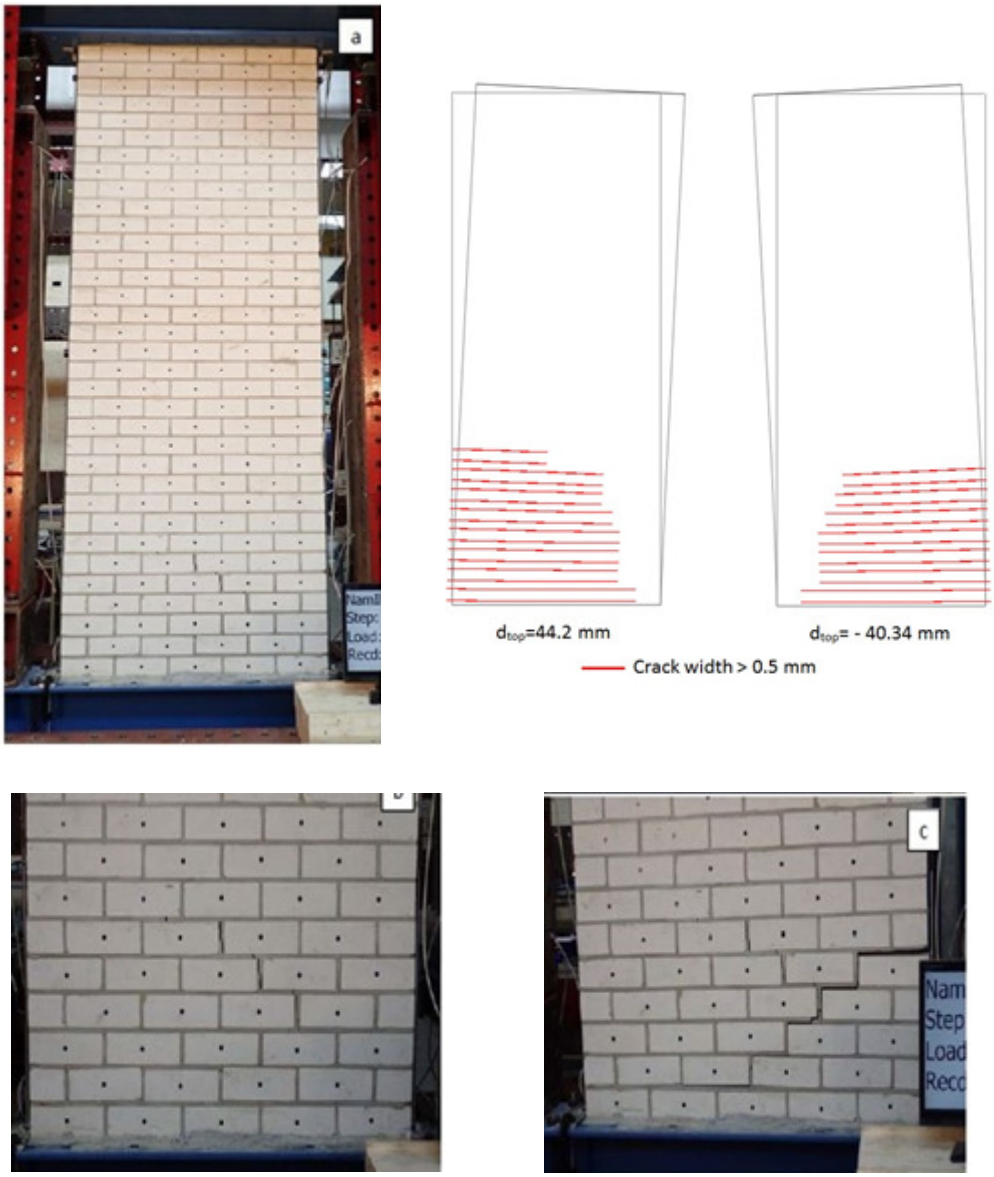

Figure 19: TUD-COMP-1: DIANA post-test refined prediction - Damage plot at end of analysis (top right) compared to observed damage in laboratory

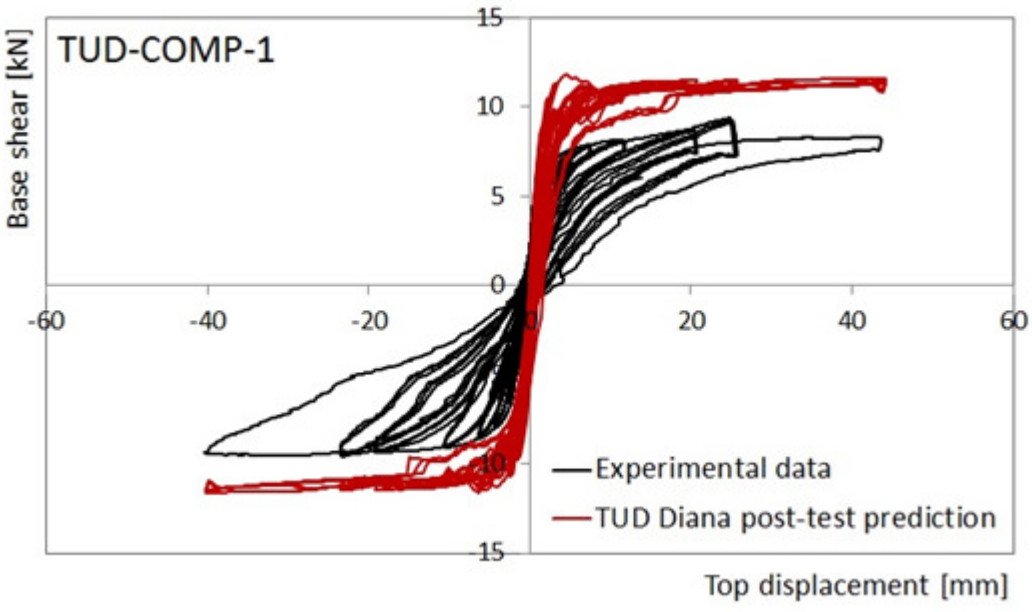

Figure 20: TUD-COMP-1: DIANA post-test refined prediction - Shear force-displacement curve

Table 12: TUD-COMP-1: DIANA post-test refined prediction - Summary table

Consultant	**Predominant Failure Mechanism Predicted**	**Initial Stiffness [kN/mm]**	**Peak Strength [kN]**	**Maximum Achieved Drift**	
DIANA	Rocking behaviour	7.4	11.8	1.6%	End of test protocol
Test Result	Rocking behaviour / toe crushing	7.7	9.5	1.6%	Reason for stopping not known

3.3.3 TUD-COMP-2

3.3.3.1 Test Description

TUD-COMP-2 was the third quasi-static in-plane test administered by TU-Delft. This specimen was a single-wythe wall constructed of calcium silicate units 102 mm thick. It was 1.1 m long and 2.76 m high. The applied overburden stress was 0.7 MPa. The wall was tested under cantilever boundary conditions.

Upon cyclically loading specimen TUD-COMP-2, a gradual reduction of the initial stiffness occurred after the second cycle. First cracks appeared at the bottom corners during the sixth cycle. During the twelfth cycle, new flexural cracks opened, starting from the sixth or seventh mortar bed joints. The cracks developed along the mortar joint for approximately half of the length of the wall, and then were diagonally oriented pointing to the opposite bottom corner of the wall.

At the end stage, crushing of the toes and sliding along the flexural cracks were observed. The failure mode was mainly governed by rocking and diagonally oriented damage, followed by toe-crushing and sliding. The specimen showed symmetric mechanical behaviour. The test was stopped at a net drift of 1%, when an extensive cracking at the base of the wall was detected.

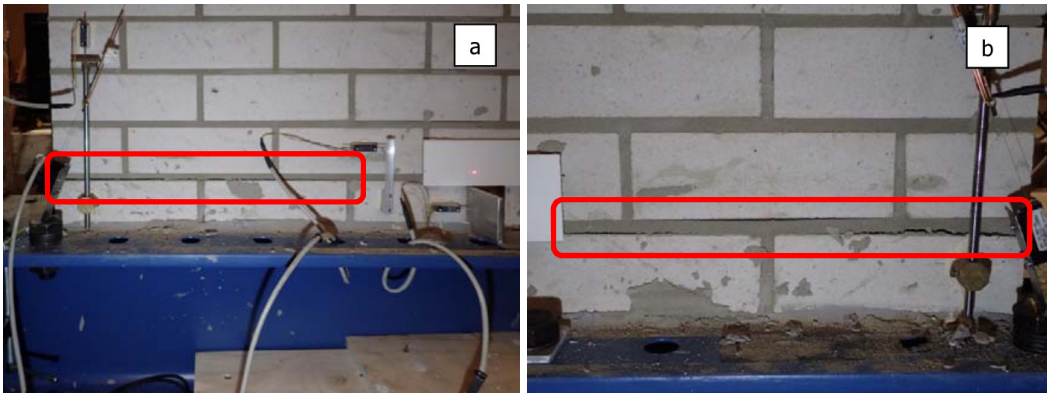

Figure 21: TUD-COMP-2: Rocking cracks (highlighted in red) at the base of the wall: details of the left (a) and right (b) toes

Figure 22: TUD-COMP-2: Crack pattern at failure for positive (a) and negative (b) drifts; details of the toe crushing (c) and sliding (d) at end stage.

The measured hysteresis is shown in Figure 23.

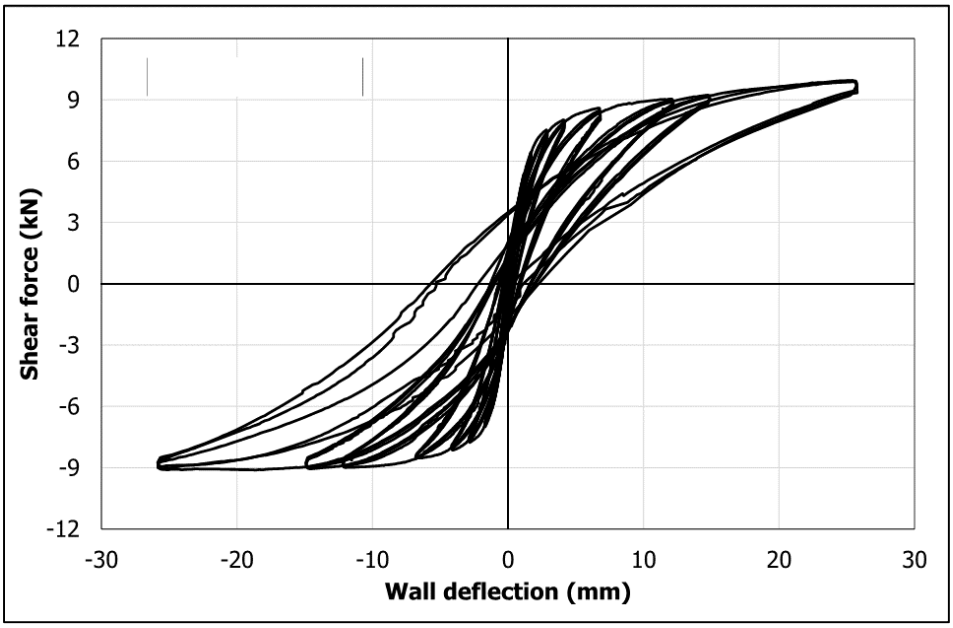

Figure 23: TUD-COMP-2: Lab test result – Shear force-displacement curve

3.3.3.2 Arup Post-Test Refined Prediction

The LS-DYNA model of TUD-COMP-2 correctly predicted rocking behaviour with toe crushing as shown in Figure 24, but failed to predict the stepped diagonal line of failure.

The lateral-force-versus-displacement relationship is shown in Figure 25. The simulated peak strength (14 kN) significantly exceeds the lab test value (10 kN). It is noted, however, that the resistance reported for tests TUD-COMP-1 and TUD-COMP-2 are both surprisingly low given the specimen dimensions and overburden, and unexpectedly similar to each other despite the 40% difference of overburden load.

In the laboratory, the test was stopped at 0.9% drift due to “extensive cracking at the base of the wall”. The analysis indicated near-collapse at 1.2 – 1.5% drift.

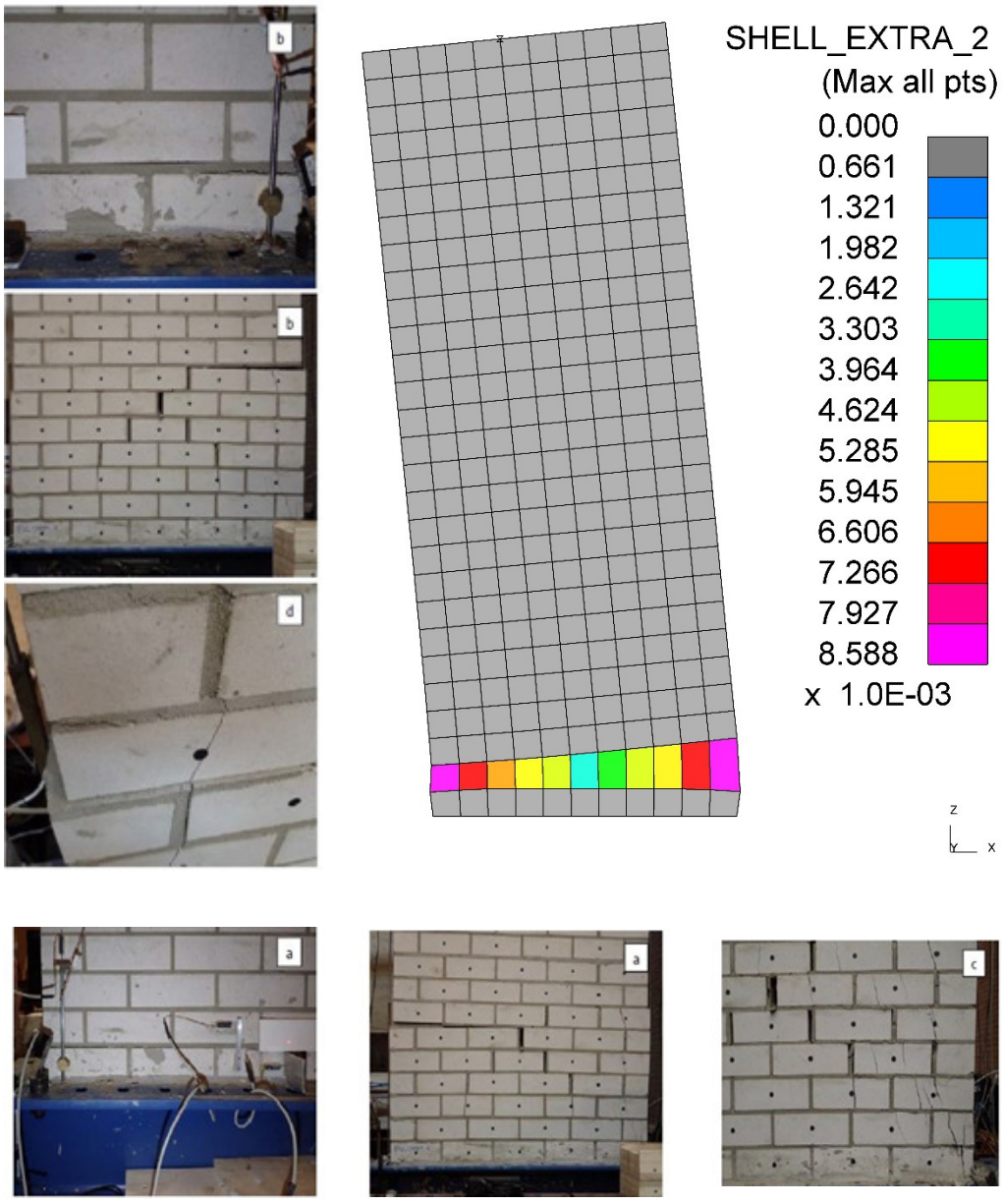

Figure 24: TUD-COMP-2: LS-DYNA post-test refined prediction - Damage plot at end of analysis (top right) compared to observed damage in laboratory

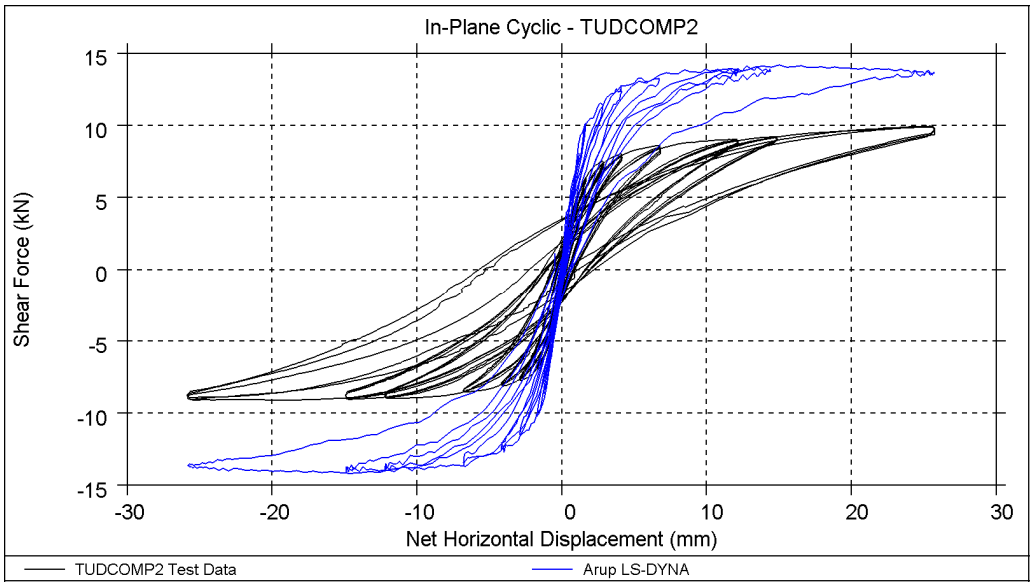

Figure 25: TUD-COMP-2: LS-DYNA post-test refined prediction - Shear force-displacement curve

Table 13: TUD-COMP-2: LS-DYNA post-test refined prediction - Summary table

Consultant	**Predominant Failure Mechanism Predicted**	**Initial Stiffness [kN/mm]**	**Peak Strength [kN]**	**Maximum Achieved Drift**	
LS-DYNA	Rocking behaviour / toe crushing	7.3	14.2	1.2% to 1.5%	Near collapse
Test Result	Rocking behaviour / toe crushing	7.23	10	0.9%	Extensive cracking

3.3.3.3 EUCENTRE Post-Test Refined Prediction

The post-test analysis was not conducted by EUCENTRE since the laboratory records for this test resulted to be far from theoretical calculation (from which the TREMURI algorithm is developed).

In particular, assuming a vertical compression of 0.7 MPa, a cantilever boundary condition and a compressive strength of the masonry equal to 5.93 MPa (according to material tests), the ultimate shear capacity considering a flexural behaviour is around 14 kN according to

$$M_u = \frac{l \cdot N}{2}\left(1 - \frac{N}{l \cdot t \cdot \kappa \cdot f_m}\right)$$

This is somehow confirmed comparing the experimental result of TUD-COMP-1 (0.5 MPa) and TUD-COMP-2 (0.7 MPa), which exhibited a very similar ultimate shear capacity despite the different vertical compressive loads.

If the lab results and assumptions will be confirmed (e.g. mechanical properties, homogeneity of the masonry, value of vertical load, etc.), even the theoretical calculation would not be able to predict such an ultimate shear capacity. Conversely, a reduction of the axial force value would allow producing numerical and analytical simulations consistent with the experimental results.

3.3.3.4 TU-Delft Post-Test Refined Prediction

The DIANA model of TUD-COMP-2, with the application of the new material model, noticeably improved the prediction of the experimental behaviour of the panel. The real loading protocol has been applied with no convergence problems until larger displacements.

The numerical damage pattern shows a rocking behaviour with damage at the base of the panel (Figure 26).

The shear-displacement history is reported in Figure 27. The numerical model predicted a higher peak shear capacity, equal to 15.8 kN against the 10 kN detected in the experiment. The initial stiffness is very close to the experiment. Although a larger energy dissipation is recorded with the new material model with respect to the blind prediction, it is still under-predicted since the model is dominated by pure rocking behaviour in this case.

Figure 26: TUD-COMP-2: DIANA post-test refined prediction - Damage plot at end of analysis (top right) compared to observed damage in laboratory

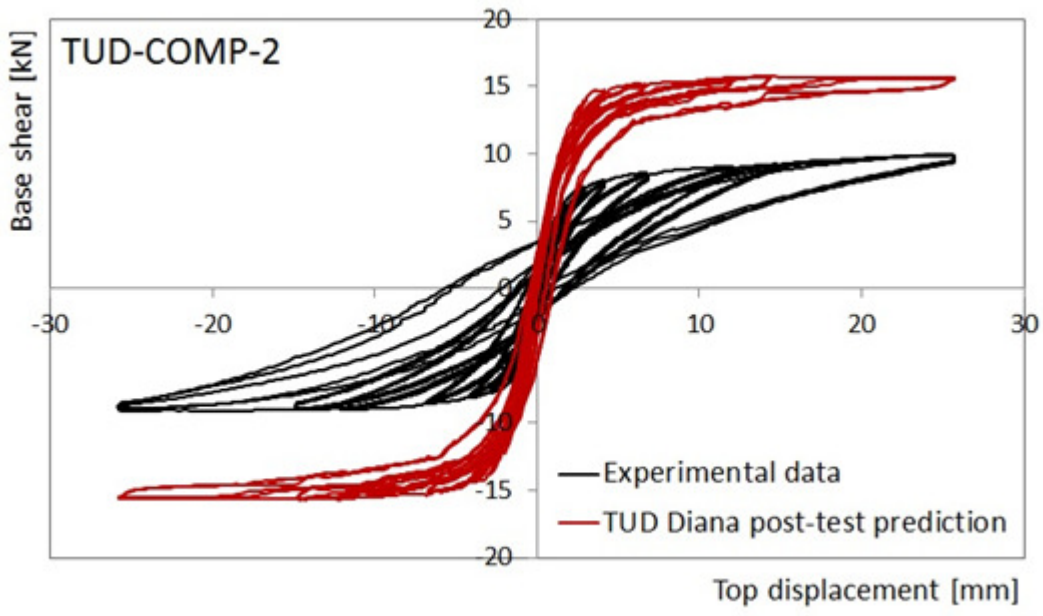

Figure 27: TUD-COMP-2: DIANA post-test refined prediction - Shear force-displacement curve

Table 14: TUD-COMP-2: DIANA post-test refined prediction - Summary table

Consultant	Predominant Failure Mechanism Predicted	Initial Stiffness [kN/mm]	Peak Strength [kN]	Maximum Achieved Drift	
DIANA	Rocking behaviour	7.4	15.8	0.9%	End of loading protocol / Extensive cracking
Test Result	Rocking behaviour / toe crushing	7.23	10	0.9%	Extensive cracking

3.3.3.5 Comment on Test Results

Further investigation into the test measurements is recommended. All three predict parties predicted substantially higher resistance than was measured. Until a conclusion is reached about the validity of the test result, it is proposed that this test is not used for validation purposes.

3.3.4 TUD-COMP-3

3.3.4.1 Test Description

TUD-COMP-3 was the fourth quasi-static in-plane test administered by TU-Delft. This specimen was a single-wythe wall constructed of calcium silicate units 102 mm thick. It was 1.1 m long and 2.76 m high. The originally planned overburden stress was 0.3 MPa. The wall was tested under double clamped boundary conditions.

In the actual test, the applied overburden stress was 0.3 MPa initially, but the due to potential instability of the test system, the test was stopped in the elastic phase. The test was restarted with an increase in overburden to 0.4 MPa.

Upon cyclically loading specimen TUD-COMP-3 initially under 0.3 MPa overburden stress, a gradual reduction of the initial stiffness occurred after the second cycle (0.01% drift). The test was stopped at a drift of 0.012%. No cracks were reported during this initial phase of the test.

The overburden stress was increased to 0.4 MPa and the test re-began. A gradual reduction of the initial stiffness of this test phase occurred after the second cycle (0.01% drift). Horizontal cracks first appeared along the first top and bottom head joints at the bottom left corner during the fifth cycle (0.065% drift) followed by cracks at the opposite corners during the sixth cycle (0.11% drift). Diagonally-oriented cracks appeared during the 11^{th} cycle (0.9% drift). The failure mode was mainly governed by flexure, associated with toe crushing and bed joint sliding. The test was stopped at a net drift of 1.3% when severe damage was experienced at the top portion of the wall.

Figure 28: TUD-COMP-3: Rocking cracks at the top & bottom left corners (a) and top & bottom right corners (b)

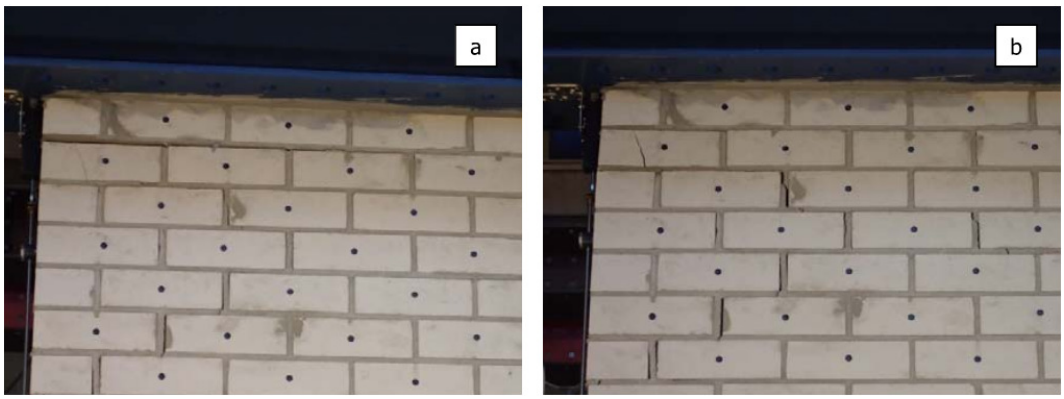

Figure 29: TUD-COMP-3: Progression of diagonal crack at the top of the wall for positive drifts after 0.49% drift (a) and after 0.89% drift (b)

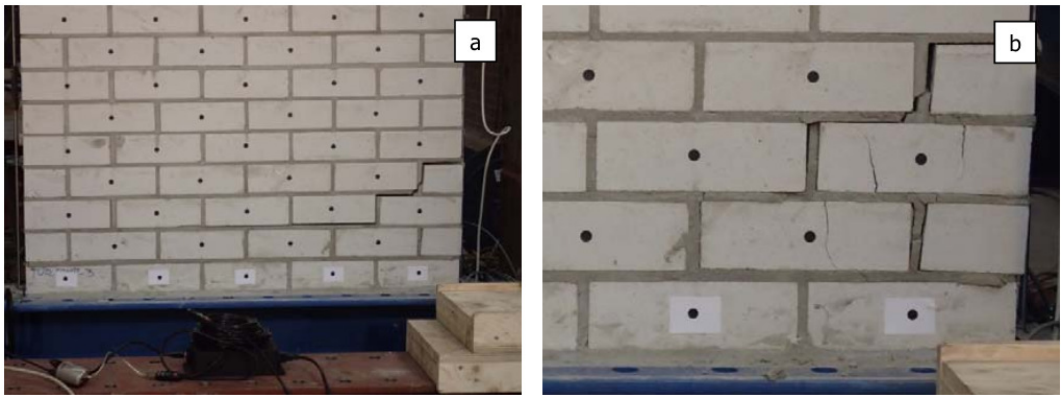

Figure 30: TUD-COMP-3: Crack pattern at the end of the test--diagonal cracks & toe crushing

The measured hysteresis during the first phase and second phase of the test is shown in Figure 31 and in Figure 32, respectively.

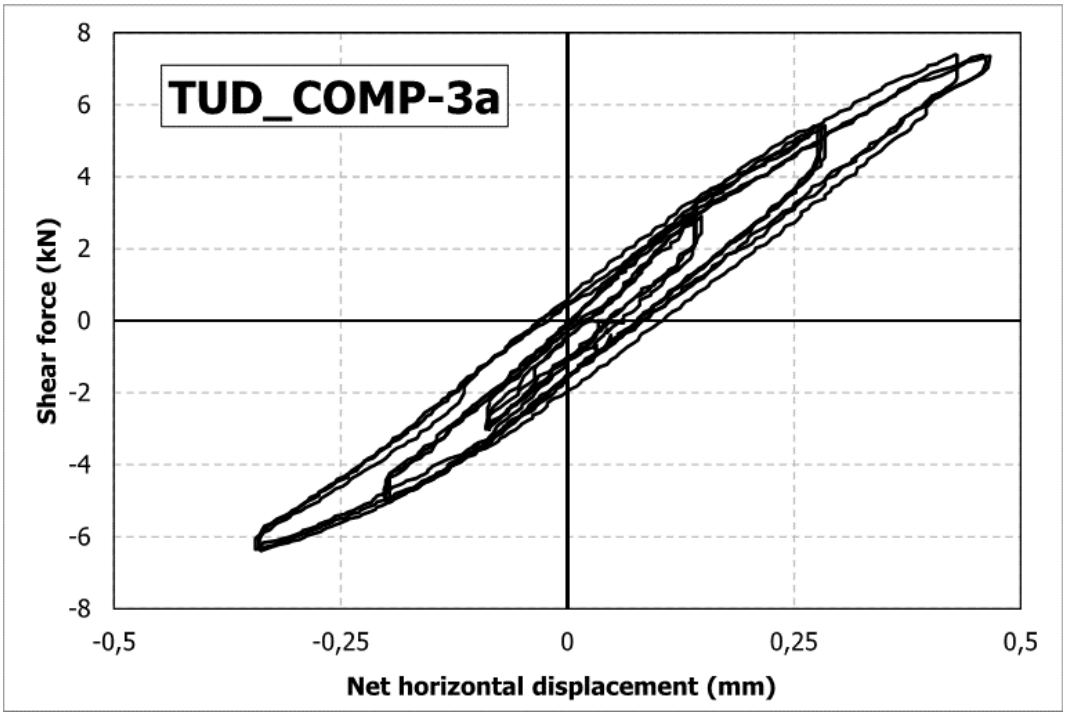

Figure 31: TUD-COMP-3a: Lab test result with 0.3 MPa overburden – Shear force-displacement curve

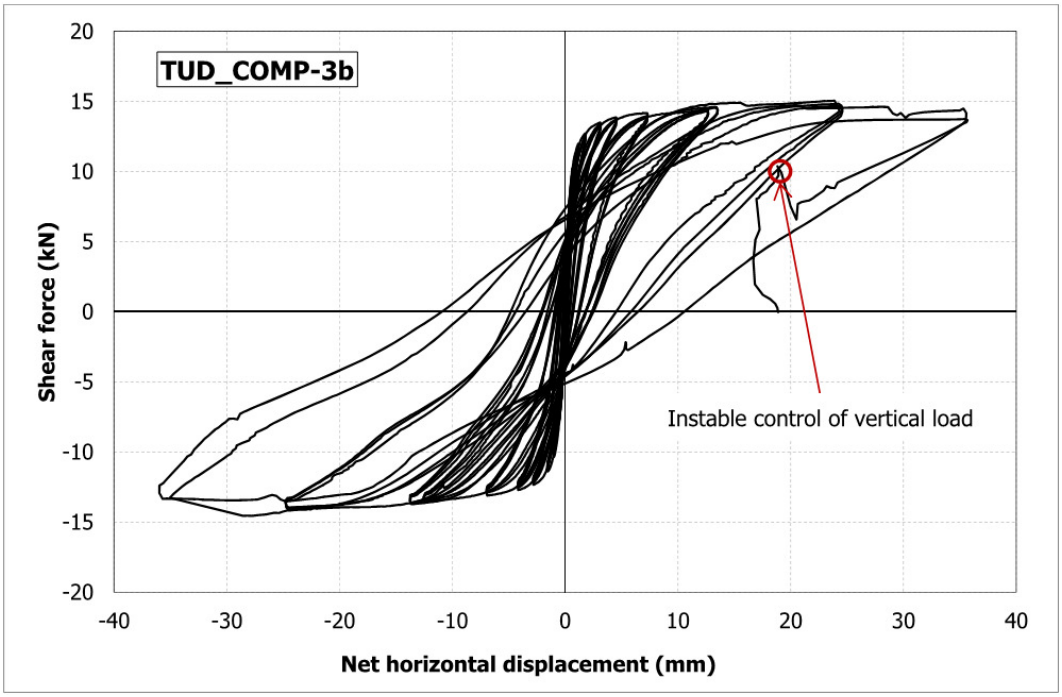

Figure 32: TUD-COMP-3b: Lab test result with 0.4 MPa overburden – Shear force-displacement curve

3.3.4.2 Arup Post-Test Refined Prediction

The LS-DYNA model of TUD-COMP-3b correctly predicted rocking behaviour with toe crushing as shown in Figure 33. However, while the analysis predicted a horizontal failure plane, in the lab test the failure planes were stepped.

The lateral-force-versus-displacement relationship is shown in Figure 34. The predicted ultimate load was approximately 18 kN at a drift of 0.9%, compared with 15 kN in the test. Although more energy dissipation was captured in the post-test refined model in comparison to the blind prediction model, the amount of energy dissipation was still under-predicted.

In the laboratory, the test was stopped at 1.3% drift, due to instability of the loading mechanism indicating severe damage in the specimen. It is unclear from the photographs whether the specimen was in a near-collapse state. The analysis indicated near-collapse at 1.7 – 1.8% drift.

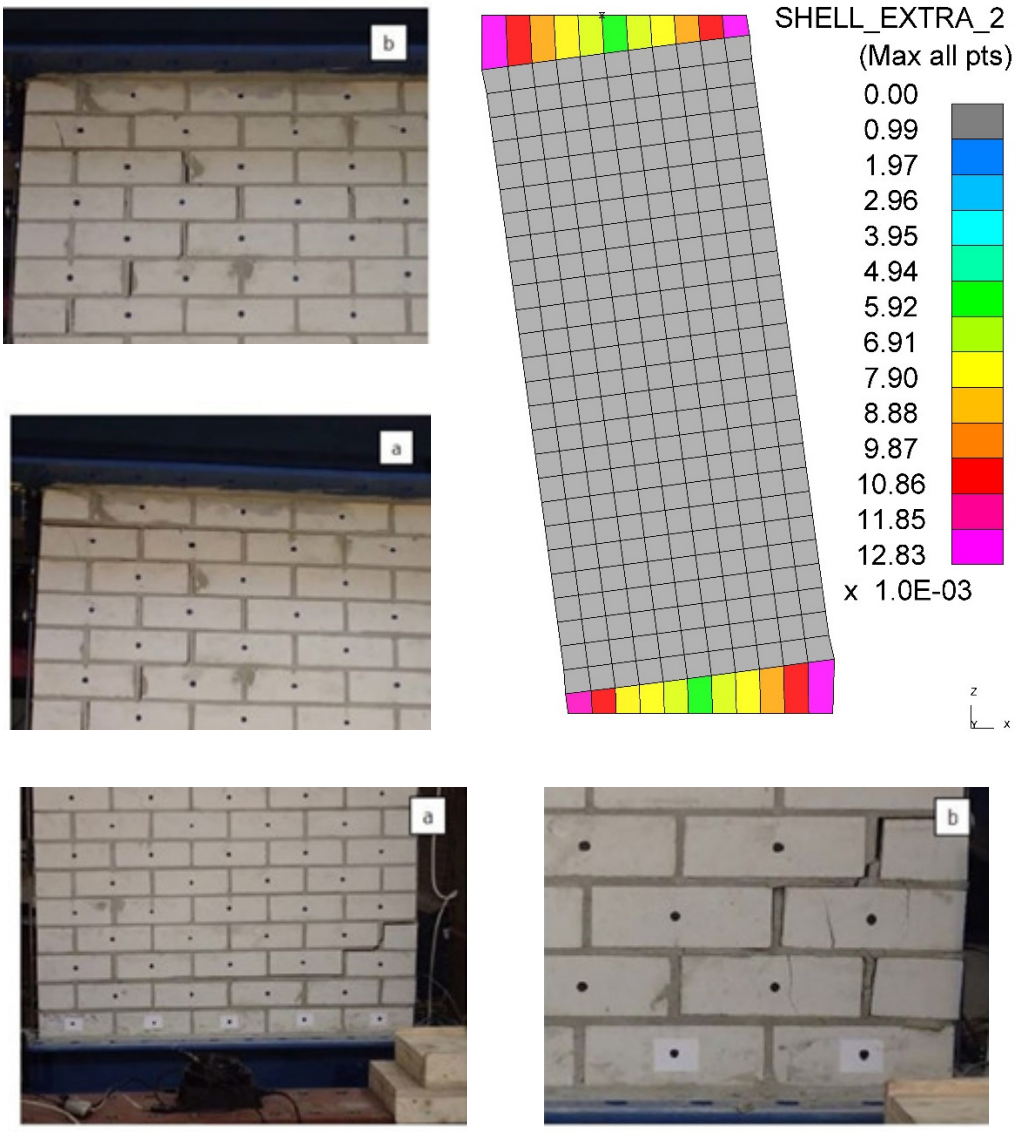

Figure 33: TUD-COMP-3: LS-DYNA post-test refined prediction - Damage plot at end of analysis (top right) compared to observed damage in laboratory

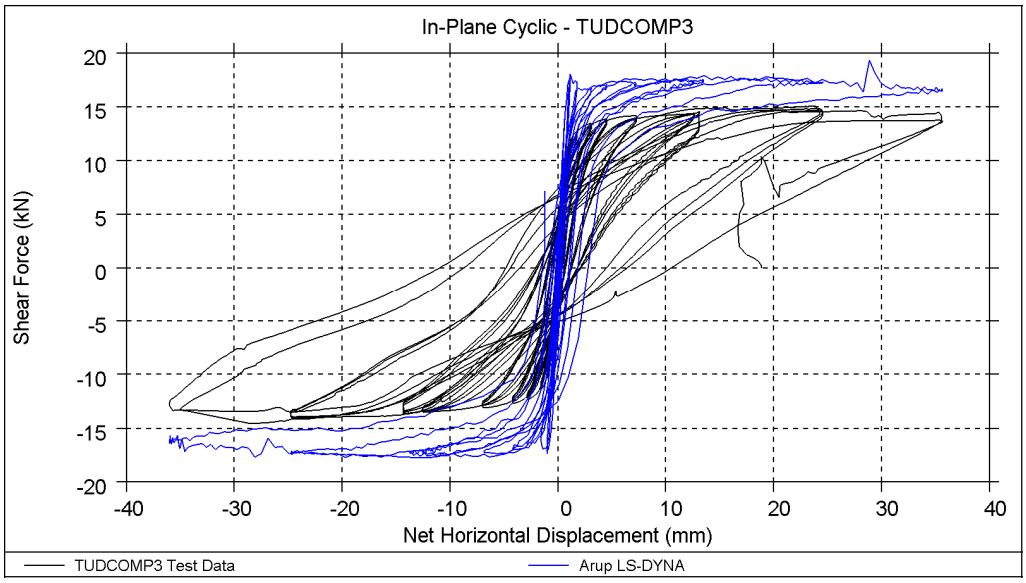

Figure 34: TUD-COMP-3: LS-DYNA post-test refined prediction - Shear force-displacement curve

Table 15: TUD-COMP-3: LS-DYNA post-test refined prediction - Summary table

Consultant	**Predominant Failure Mechanism Predicted**	**Initial Stiffness [kN/mm]**	**Peak Strength [kN]**	**Maximum Achieved Drift**	
LS-DYNA	Rocking behaviour / toe crushing	26.9	18	1.7% to 1.8%	Near collapse
Test Result (2nd phase)	Rocking behaviour / toe crushing	22.4	15	1.3%	Test system instability / severe damage

3.3.4.3 EUCENTRE Post-Test Refined Prediction

The shear force -displacement relationships are shown in Figure 35.

The TREMURI model performed with a vertical compression of 0.4 MPa, double fixed boundary condition and compressive strength of the masonry equal to 5.93 MPa (according to material tests) overestimates the shear capacity of the wall (see also the discussion reported for TUD-COMP-2). Although more energy dissipation is captured in the post-test refined "new model", the amount of energy dissipation is still under-predicted (Figure 36).

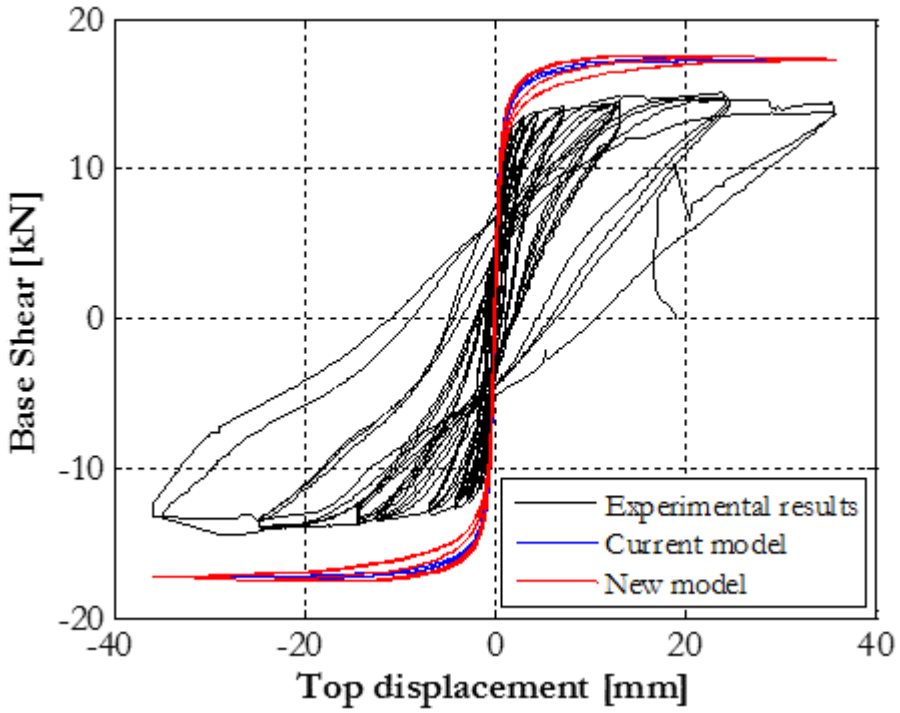

Figure 35: TUD-COMP-3: TREMURI post-test refined prediction - Shear force-displacement curve

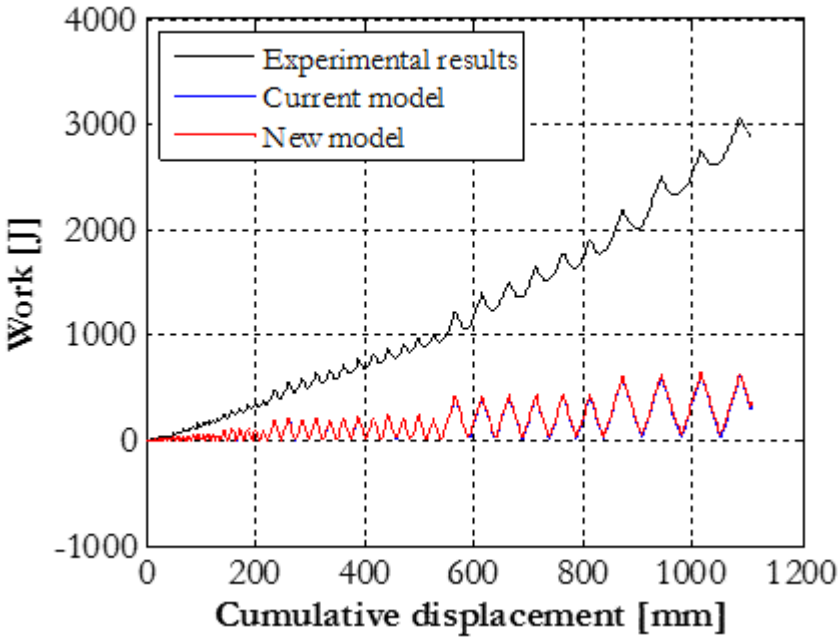

Figure 36: TUD-COMP-3: TREMURI post-test refined prediction – Work and dissipated energy

Table 16: TUD-COMP-3: TREMURI post-test refined prediction - Summary table

Consultant	**Predominant Failure Mechanism Predicted**	**Initial Stiffness [kN/mm]**	**Peak Strength [kN]**	**Maximum Achieved Drift**	
TREMURI new model	Rocking	24	17.6	1.3%	
Test Result (2nd phase)	Rocking behaviour / toe crushing	22.4	15	1.3%	Test system instability / severe damage

3.3.4.4 TU-Delft Post-Test Refined Prediction

The DIANA model of TUD-COMP-3, with the application of the new material model, noticeably improved the prediction of the experimental behaviour of the panel. The real loading protocol has been applied with no convergence problems until larger displacements.

The numerical damage pattern is more extensive with respect to the experiment (Figure 37). A rocking behaviour is detected with cracks at the base and top of the panel, spreading also along the height. In the last stages of the test, some additional cracks in the middle of the panel also occur.

The shear-displacement history is reported in Figure 38. The numerical peak shear capacity is 18.3 kN, which is somewhat higher than the experiment. The shear-displacement loops are very close to the test, with quite large energy dissipation.

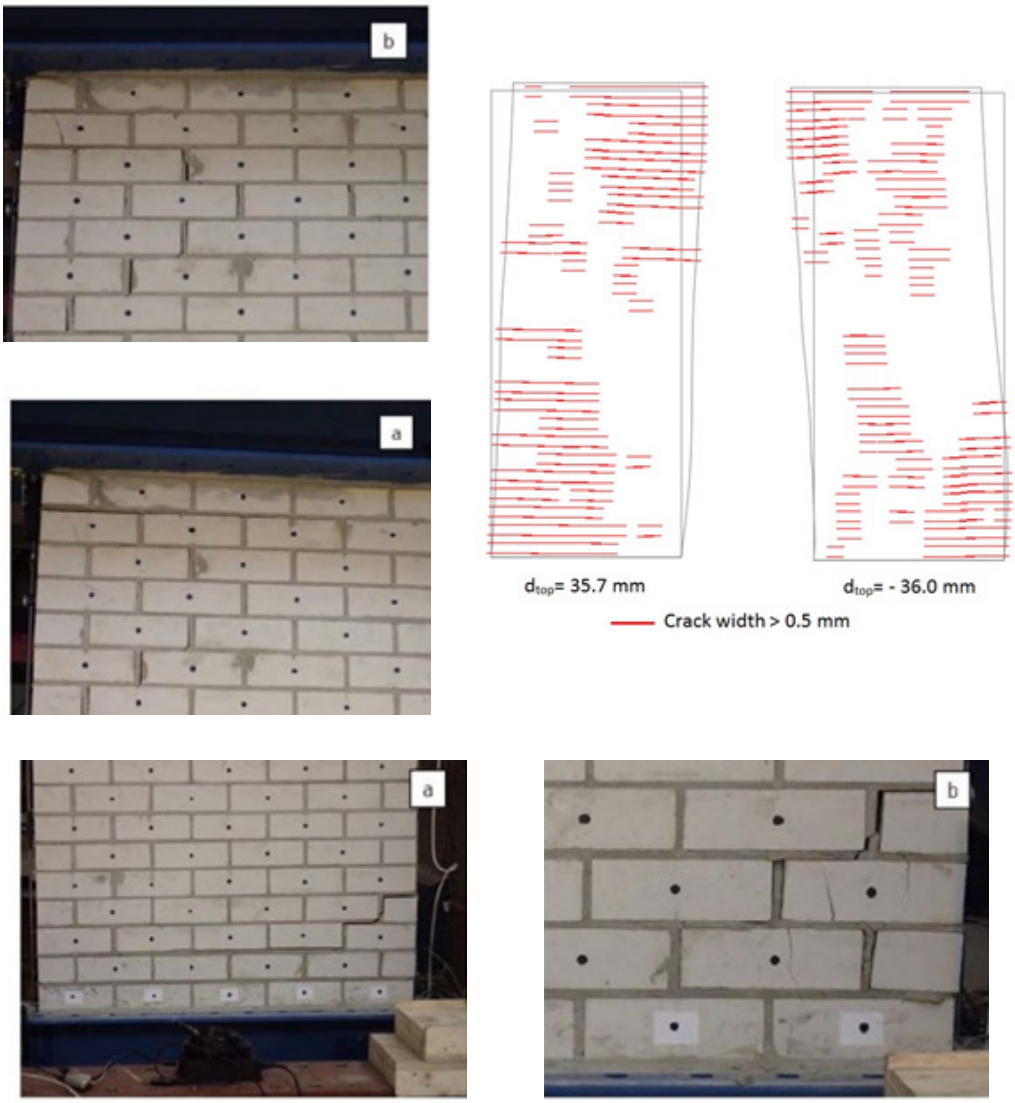

Figure 37: TUD-COMP-3: DIANA post-test refined prediction - Damage plot at end of analysis (top right) compared to observed damage in laboratory

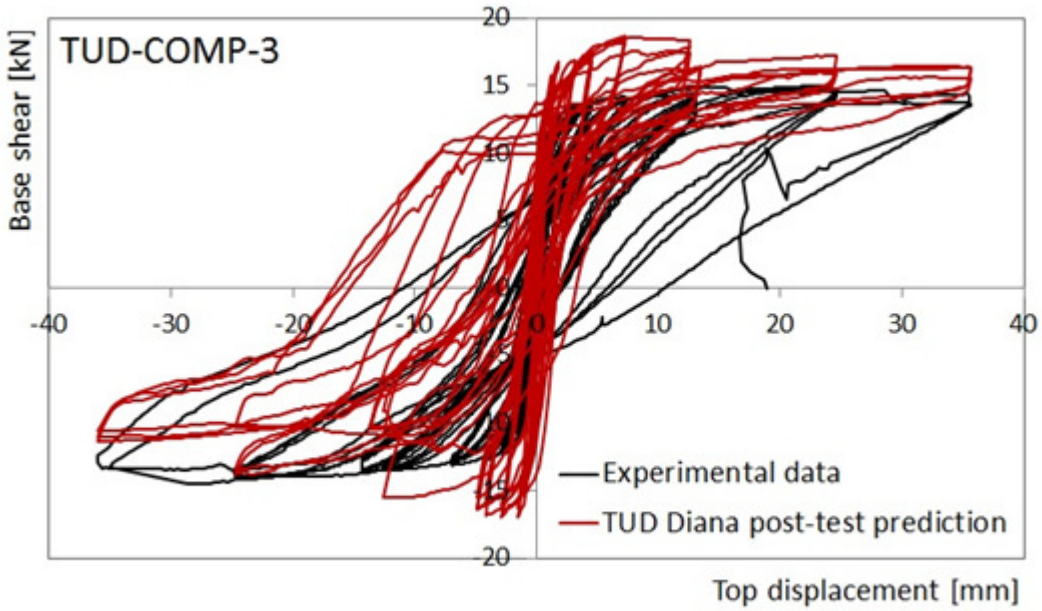

Figure 38: TUD-COMP-3: DIANA post-test refined prediction - Shear force-displacement curve

Table 17: TUD-COMP-3: DIANA post-test refined prediction - Summary table

Consultant	**Predominant Failure Mechanism Predicted**	**Initial Stiffness [kN/mm]**	**Peak Strength [kN]**	**Maximum Achieved Drift**	
DIANA	Rocking / cracks in middle of panel	21	18.3	1.3%	End of loading protocol / extensive damage
Test Result (2nd phase)	Rocking behaviour / toe crushing	22.4	15	1.3%	Test system instability / severe damage

3.3.5 TUD-COMP-4

3.3.5.1 Test Description

TUD-COMP-4 was the fifth quasi-static in-plane test administered by TU-Delft. This specimen was a single-wythe wall constructed of calcium silicate units 102 mm thick. It was 4 m long and 2.75 m high. The applied overburden stress was 0.5 MPa. The wall was tested under double clamped boundary conditions.

During the pre-test calibration phase, a horizontal crack formed between the first and second brick layer from the top. The crack was repaired. However, as a consequence, the specimen became in effect one brick-height shorter. This was not taken into account in the blind prediction model.

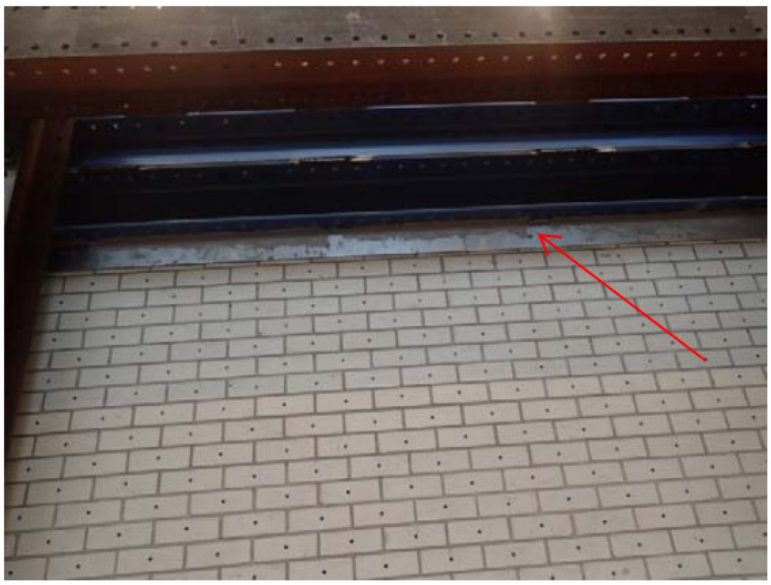

Figure 39: TUD-COMP-4: repair of the horizontal crack during the pre-test phase

First cracks appeared during the sixth cycle (0.04% drift). These were diagonally oriented cracks, which progressively increased in width during the duration of the test. At the end of the test, maximum crack widths of 40 mm were measured. The failure mode was mainly governed by diagonally oriented damage. The test was stopped at a net drift of 0.2% drift due to the near collapse of the wall.

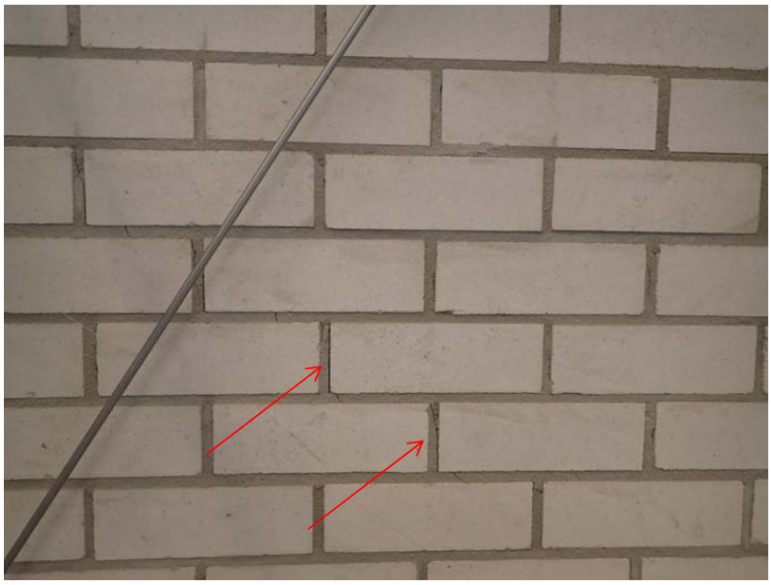

Figure 40: TUD-COMP-4: First cracks visible after 0.04% drift

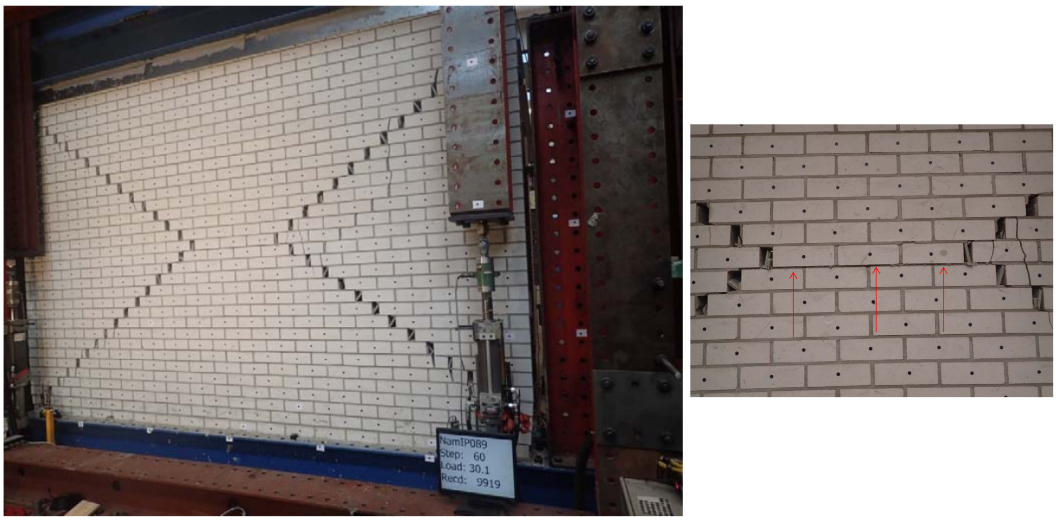

Figure 41: TUD-COMP-4: Crack pattern at the end of the test

The measured hysteresis is shown in Figure 42.

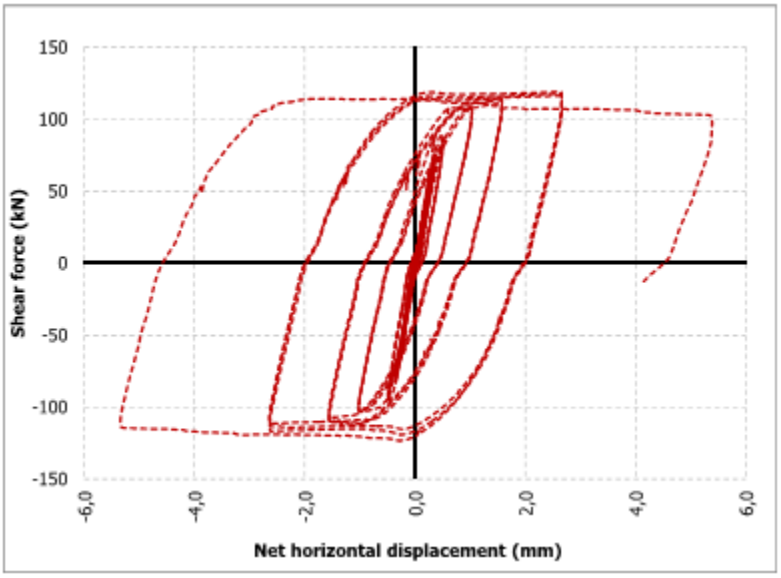

Figure 42: TUD-COMP-4: Lab test result – Shear force-displacement curve

3.3.5.2 Arup Post-Test Refined Prediction

The LS-DYNA model of TUD-COMP-4 correctly predicted a diagonal tensile failure mode as shown in Figure 43. However, the envelope-shape of the cracks was not matched exactly by the analysis, and the final head joint gap widths in the test (up to 40 mm) were very much larger than those predicted by the analysis (around 2 mm). This is because, in the analysis, the gaps opened and closed with the positive and negative parts of each displacement cycle, while in the test the head joints opened in the positive half and jammed open in the negative half of the cycle, producing a gap that increased with each cycle.

The lateral-force-versus-displacement relationship is shown in Figure 44. The ultimate load was well predicted, at 120 kN. The hysteresis and energy absorption were also reasonably well predicted.

In the laboratory, the test was stopped at 0.2% drift because the specimen was close to collapse. Bricks were cracked in the corners of the specimen (suggesting toe-crushing) and above and below the open head joints (perhaps suggesting a shear failure of those bricks). The analysis did not predict the onset of collapse, even at drift of 1.6%. It appears that the mechanisms leading to collapse of squat walls are complex, and further development of the material model would be needed in order to capture these.

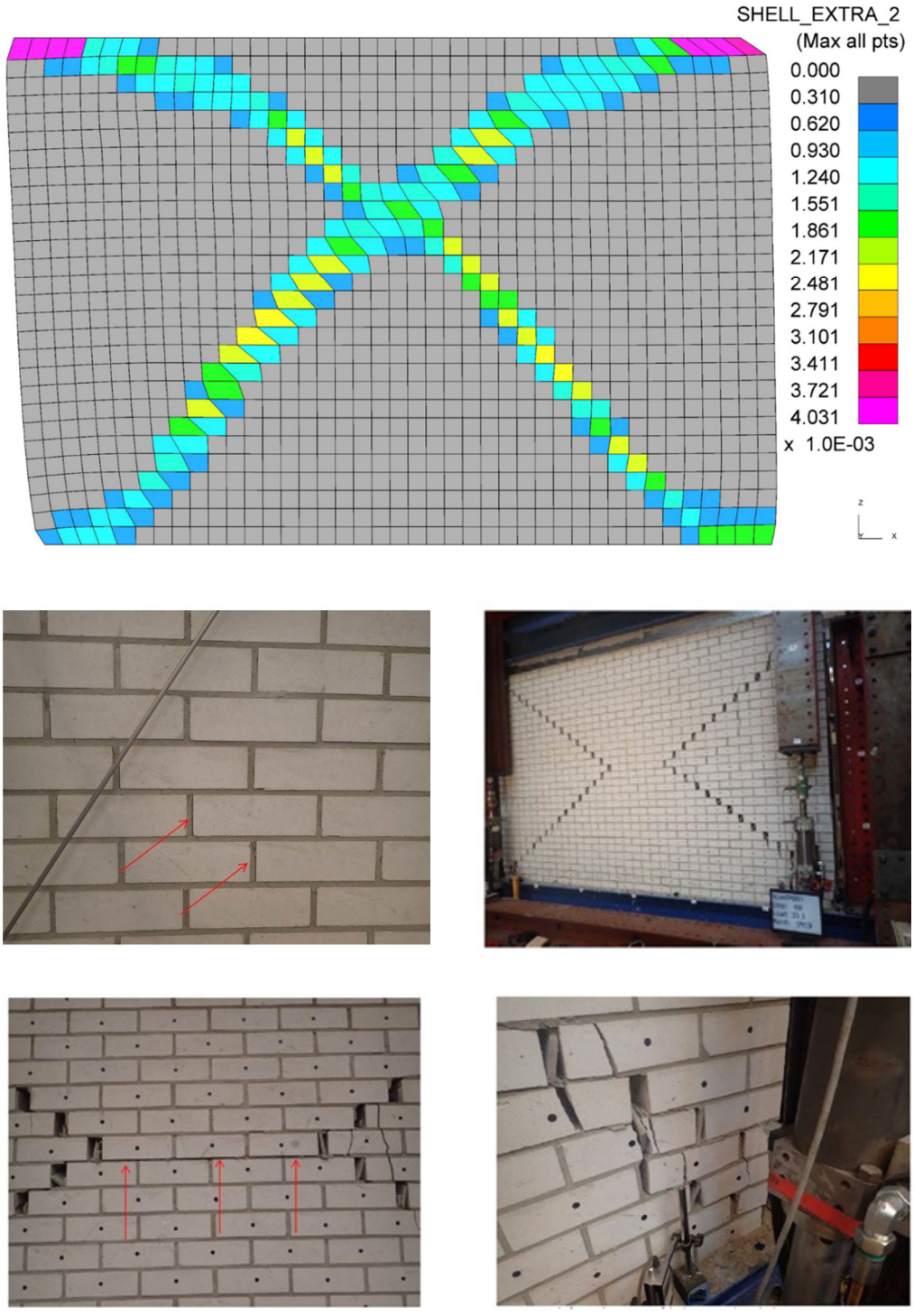

Figure 43: TUD-COMP-4: LS-DYNA post-test refined prediction - Damage plot at end of analysis (top right) compared to observed damage in laboratory

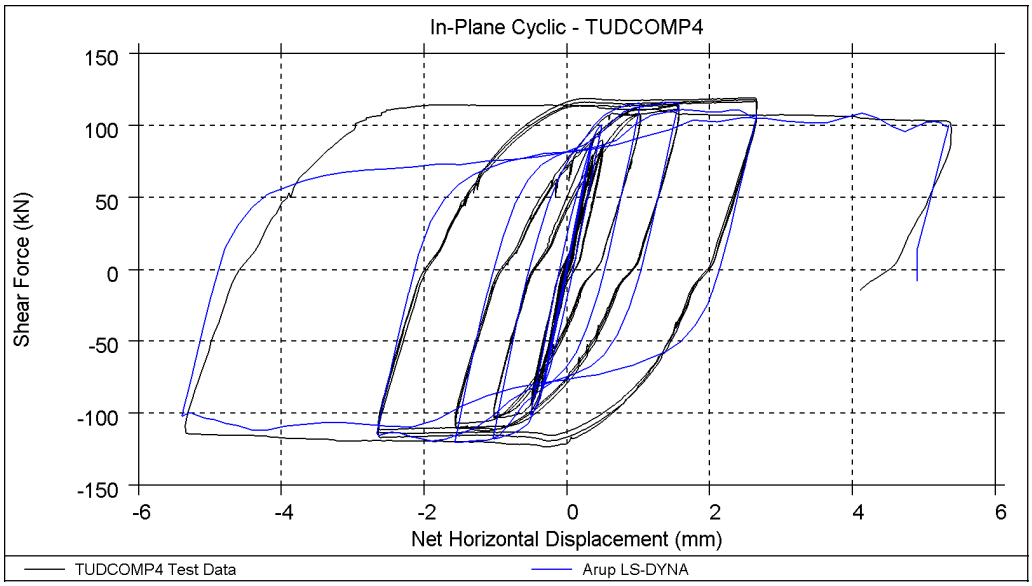

Figure 44: TUD-COMP-4: LS-DYNA post-test refined prediction - Shear force-displacement curve

Table 18: TUD-COMP-4: LS-DYNA post-test refined prediction - Summary table

Consultant	**Predominant Failure Mechanism Predicted**	**Initial Stiffness [kN/mm]**	**Peak Strength [kN]**	**Maximum Achieved Drift**	
LS-DYNA	Diagonal cracks / bed joint sliding	263	120	0.5% to 1.6%	End of analysis – no collapse
Test Result	Diagonal cracks / toe crushing	> 223	119	0.2%	Near collapse

3.3.5.3 EUCENTRE Post-Test Refined Prediction

The shear force -displacement relationships are shown in Figure 45. The ultimate strength as well as the initial stiffness are well predicted by the TREMURI model. The hysteresis and energy dissipation are also well predicted. (Figure 46).

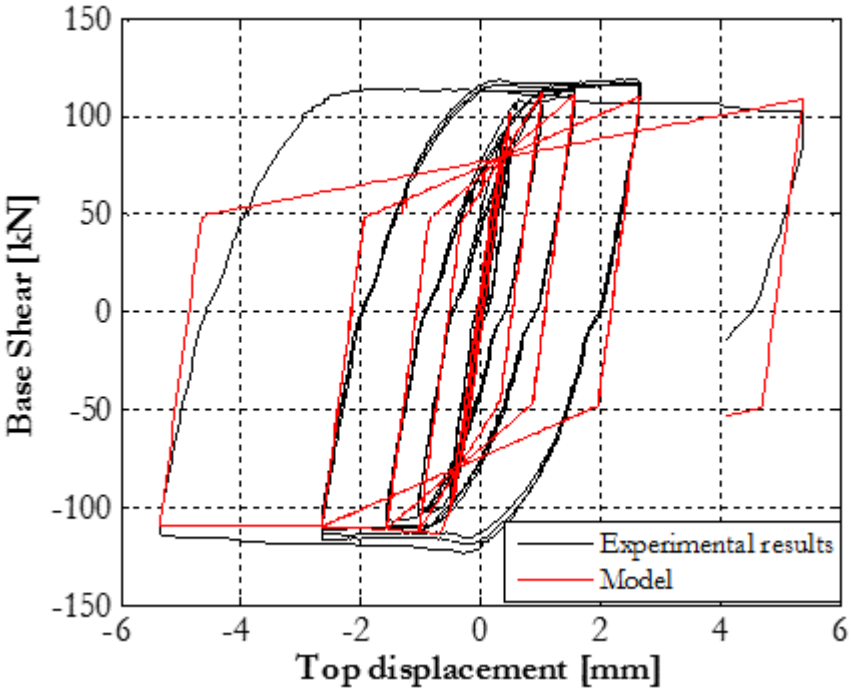

Figure 45: TUD-COMP-4: TREMURI post-test refined prediction - Shear force-displacement curve

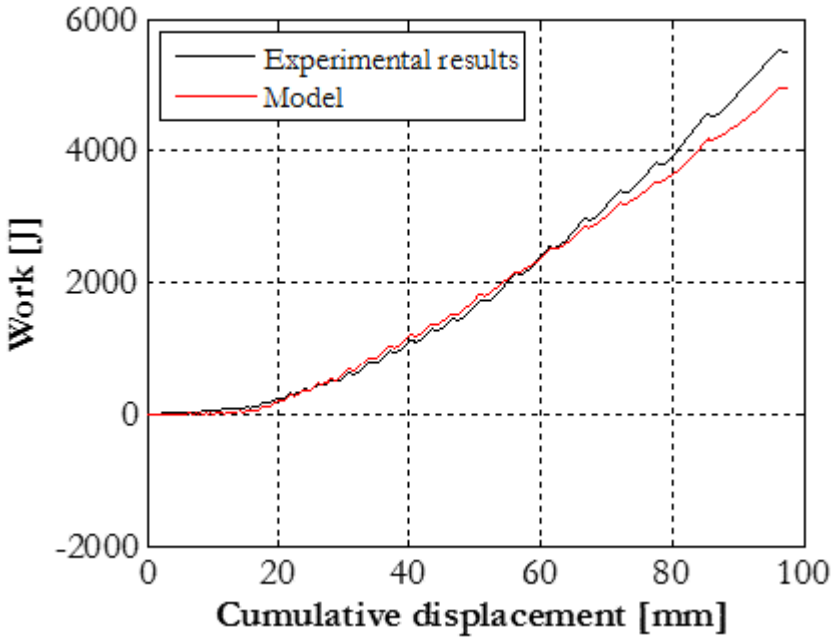

Figure 46: TUD-COMP-4: TREMURI post-test refined prediction – Work and dissipated energy

Table 19: TUD-COMP-4: TREMURI post-test refined prediction - Summary table

Consultant	**Predominant Failure Mechanism Predicted**	**Initial Stiffness [kN/mm]**	**Peak Strength [kN]**	**Maximum Achieved Drift**	
TREMURI new model	Shear	230	114.1	0.2%	
Test Result	Diagonal cracks / toe crushing	> 223	119	0.2%	Near collapse

3.3.5.4 TU-Delft Post-Test Refined Prediction

The DIANA model of TUD-COMP-4, with the application of the new material model, noticeably improved the prediction of the experimental behaviour of the panel. The real loading protocol has been applied with no convergence problems until larger displacements.

The numerical damage pattern is more extensive with respect to the experiment (Figure 47). Most of the damage is in the middle of the panel, characterized by several diagonal cracks, but it is not possible to completely identify the typical X-shaped cracks observed in the experiment.

The shear-displacement history is reported in Figure 48. The numerical peak shear capacity is 121.7 kN, very close to the experimental value, which is equal to 119 kN.

With respect to the blind prediction, a larger energy dissipation is recorded with the new material model, although still lower than the experiment. With respect to the test, a degradation of the ultimate capacity is observed with increasing applied displacements. There is no horizontal plateau, but the shear capacity gradually decreases for larger drifts.

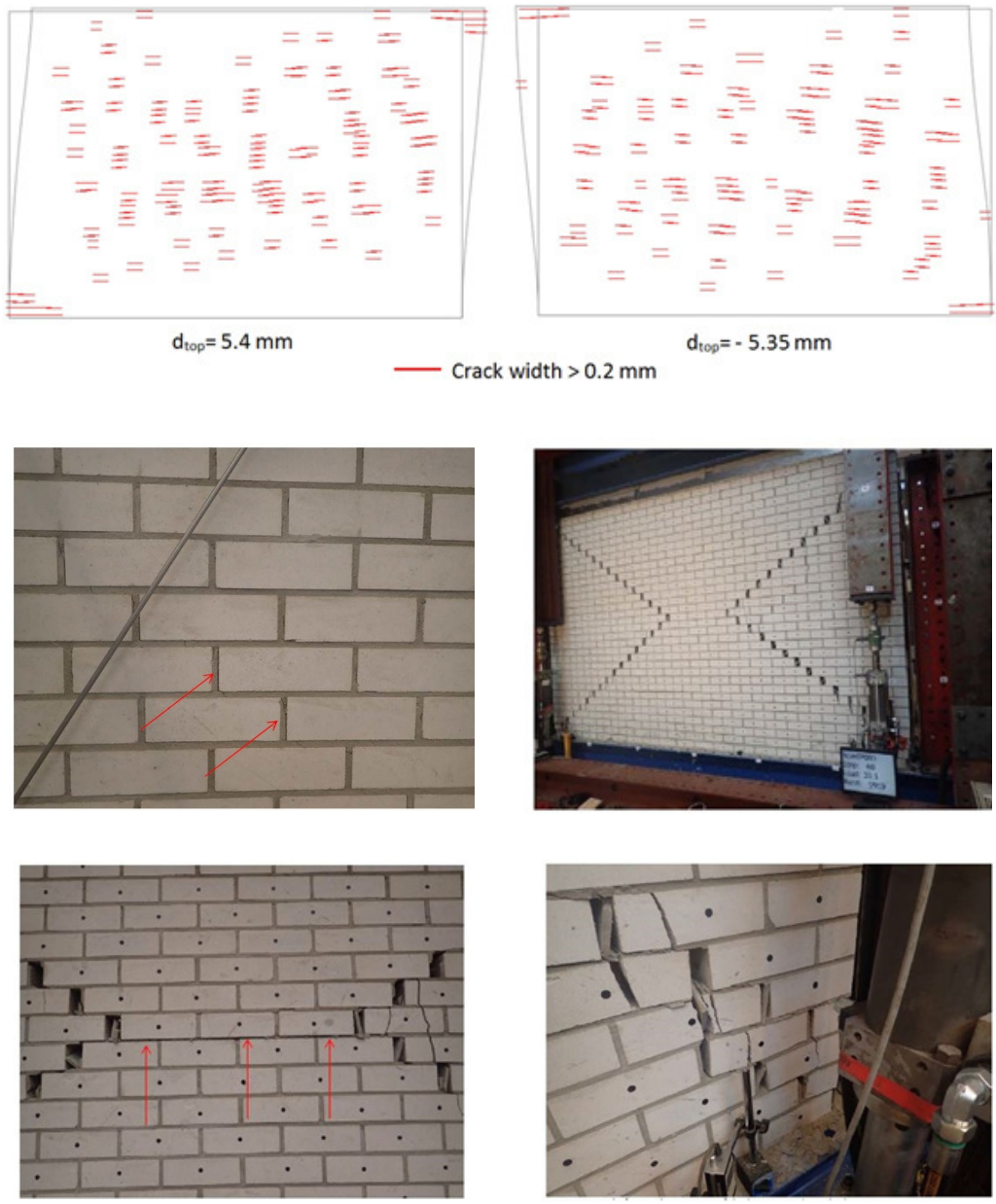

Figure 47: TUD-COMP-4: DIANA post-test refined prediction - Damage plot at end of analysis (top) compared to observed damage in laboratory

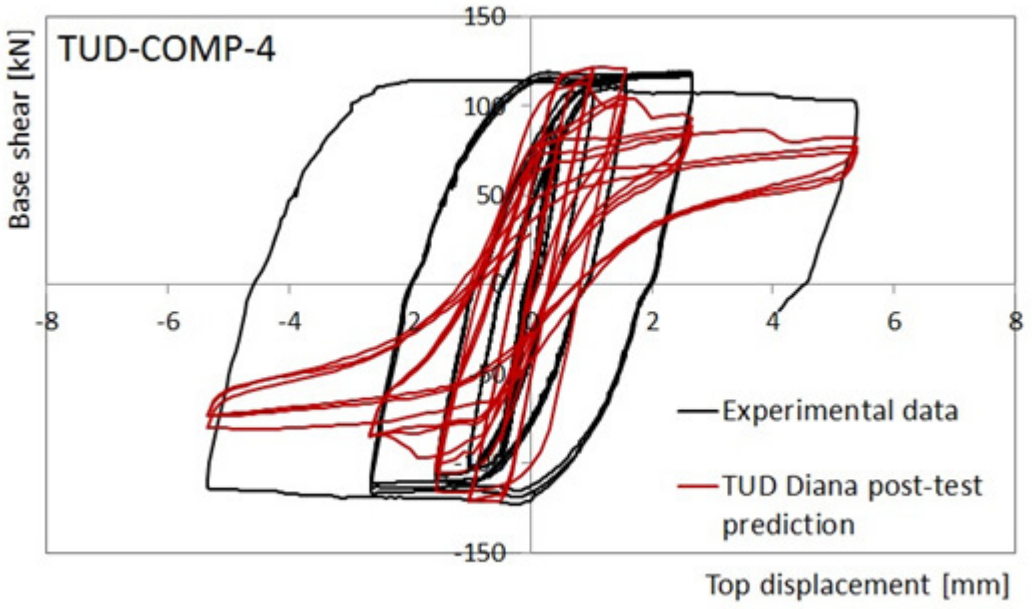

Figure 48: TUD-COMP-4: DIANA post-test refined prediction - Shear force-displacement curve

Table 20: TUD-COMP-4: DIANA post-test refined prediction - Summary table

Consultant	**Predominant Failure Mechanism Predicted**	**Initial Stiffness [kN/mm]**	**Peak Strength [kN]**	**Maximum Achieved Drift**	
DIANA	Diagonal cracks	180	121.7	0.2%	End of loading protocol / extensive damage
Test Result	Diagonal cracks / toe crushing	> 223	119	0.2%	Near collapse

3.3.6 TUD-COMP-5

3.3.6.1 Test Description

TUD-COMP-5 was the sixth quasi-static in-plane test administered by TU-Delft. This specimen was a single-wythe wall constructed of calcium silicate units 102 mm thick. It was 4 m long and 2.75 m high. The applied overburden stress was 0.3 MPa. The wall was tested under double clamped boundary conditions.

First cracks, which were a combination of diagonally oriented cracks and horizontal cracks in the bed joints, appeared during the sixth cycle (0.5% drift). These cracks progressively increased during the duration of the test. In addition, vertical cracks through bricks as well as bed-joint sliding near the bottom of the wall occurred. At the end of the test, maximum crack widths of 30 mm were measured. The failure mode was mainly governed by diagonally oriented damage. The test was stopped at a net drift of 0.5% drift in the negative direction only because the asymmetry in the actuator loads did not allow further cycling.

Similar to TUD-COMP-4, during the pre-test calibration phase, a horizontal crack formed between the first and second brick layer from the top. The crack was repaired. However, as a consequence, the specimen became in effect one brick-height shorter. This was not taken into account in the blind prediction model.

Throughout the test, the wall experienced asymmetrical damage, which caused a redistribution of forces in the actuators. In order to ensure that the proper boundary conditions were maintained, during the last three cycles of the test, the wall was only able to be pushed in one direction. Thus the test result may be compromised in some way. Even though the displacement input in the analysis was modified to match that actually applied in the test, any comparison with these test results should be treated with caution.

Figure 49: TUD-COMP-5: Crack pattern at the end of the test

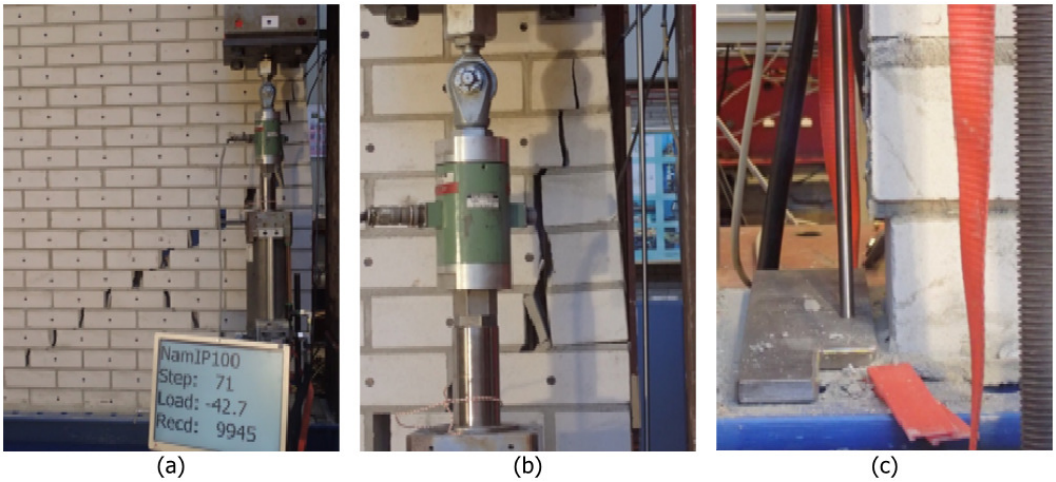

Figure 50: TUD-COMP-5: Details of final crack patterns: diagonal cracks at the bottom-right corner (a), vertical cracks through bricks (b), residual sliding at the bottom left corner (c)

The measured hysteresis is shown in Figure 51.

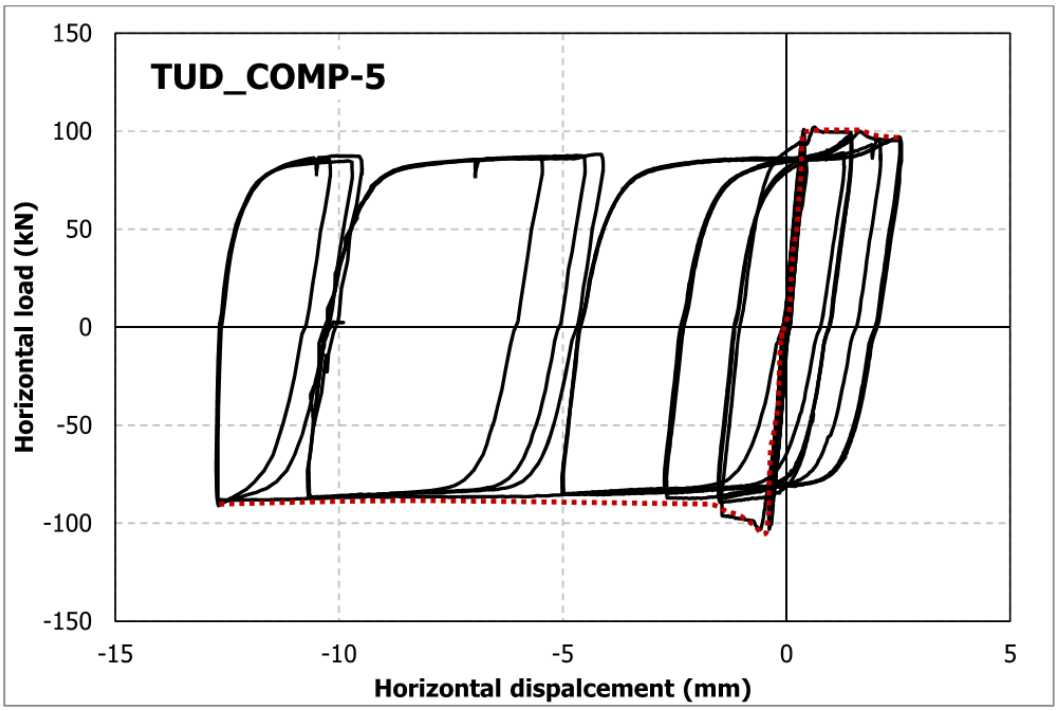

Figure 51: TUD-COMP-5: Lab test result – Shear force-displacement curve

3.3.6.2 Arup Post-Test Refined Prediction

The LS-DYNA model of TUD-COMP-5 correctly predicted a diagonal tensile failure mode as shown in Figure 52. However, the location of the cracks did not match the test (in the lab test the cracks were near the bottom-right corner of the specimen).

In the test, it became necessary to apply displacement in the negative direction only due to difficulty in maintaining the double-clamped boundary condition. The test was eventually stopped for that reason, so it is not possible to infer the onset of collapse. The behaviour of the specimen that caused these difficulties may also have compromised the test result in other ways, so data and conclusions from this specimen should be treated cautiously.

The lateral-force-versus-displacement relationship is shown in Figure 53. The ultimate load was under-predicted (84 kN versus 103 kN in the test) and the resistance at large negative drift values was also under-predicted.

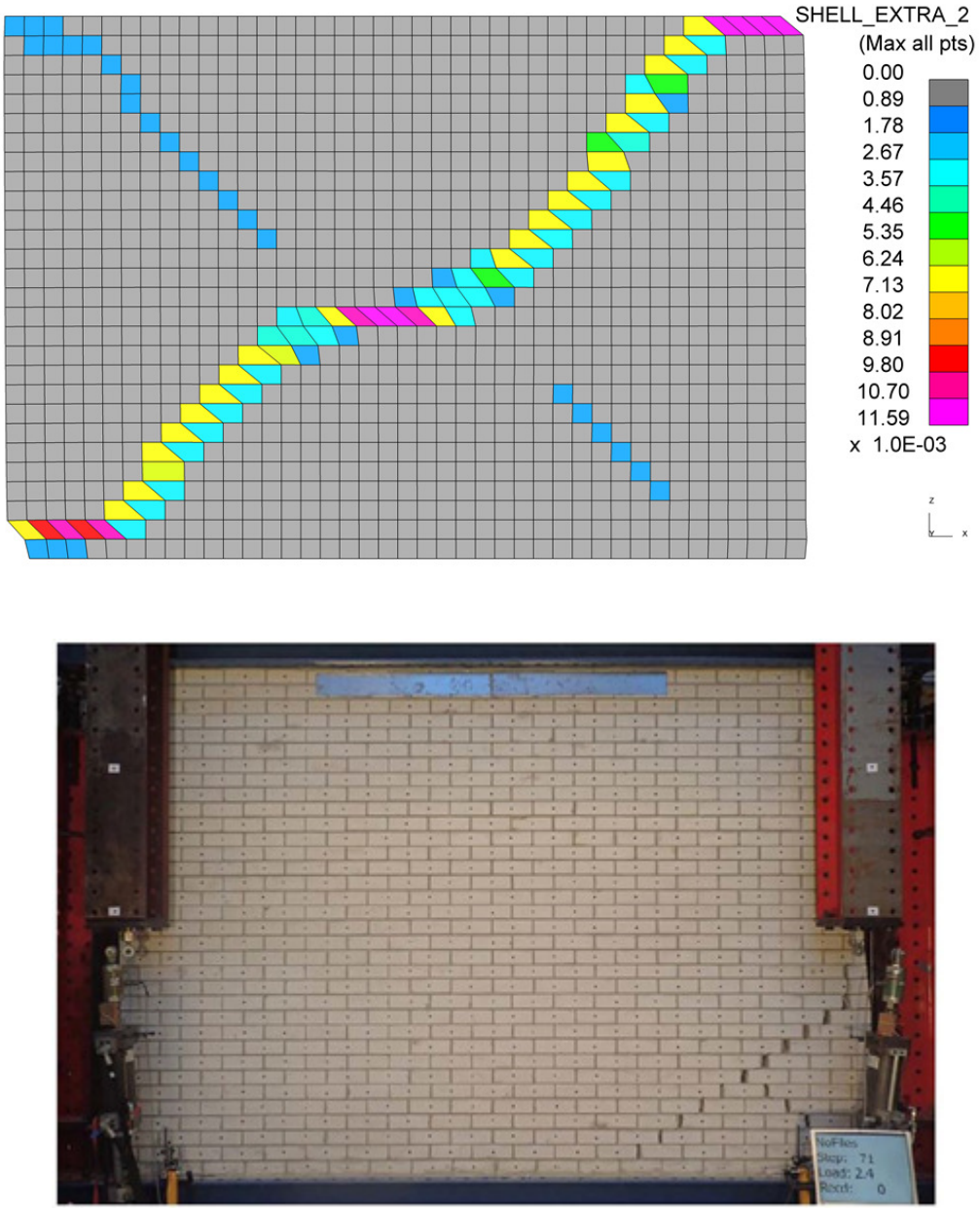

Figure 52: TUD-COMP-5: LS-DYNA post-test refined prediction - Damage plot at end of analysis

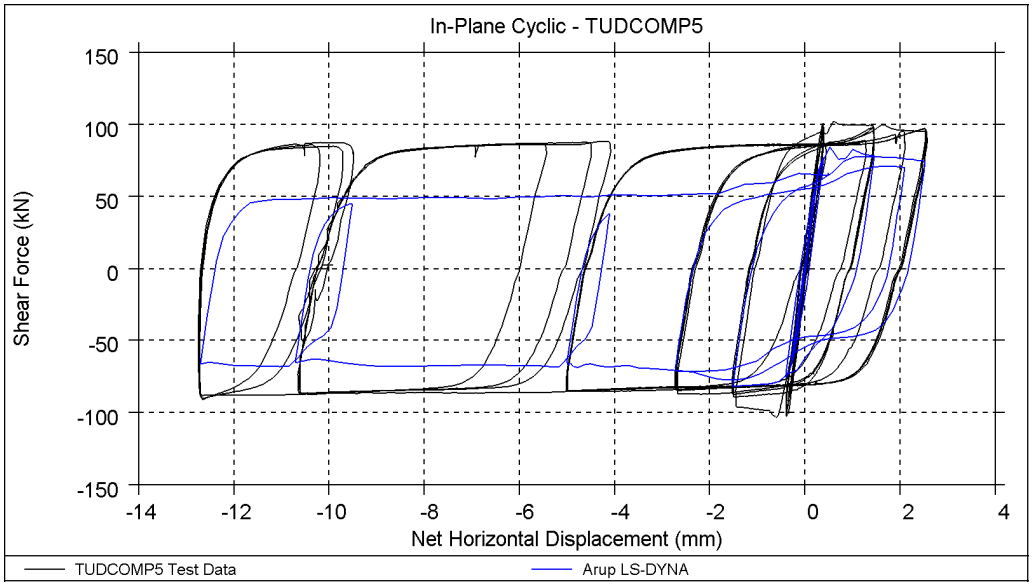

Figure 53: TUD-COMP-5: LS-DYNA post-test refined prediction - Shear force-displacement curve

Table 21: TUD-COMP-5: LS-DYNA post-test refined prediction - Summary table

Consultant	**Predominant Failure Mechanism Predicted**	**Initial Stiffness [kN/mm]**	**Peak Strength [kN]**	**Maximum Achieved Drift**	
LS-DYNA	Diagonal cracks / bed joint sliding	279	84	1.0%	End of analysis – no collapse
Test Result	Diagonal cracks / bed joint sliding / toe crushing	> 288	103	0.5%	Stopped – no collapse (*)

(*) The test stopped due to inability to maintain the double-clamped boundary condition, not due to imminent collapse.

3.3.6.3 EUCENTRE Post-Test Refined Prediction

The shear force -displacement relationships are shown in Figure 54. The ultimate strength as well as the initial stiffness are well predicted by the TREMURI model. The hysteresis and energy dissipation are also well captured (Figure 55).

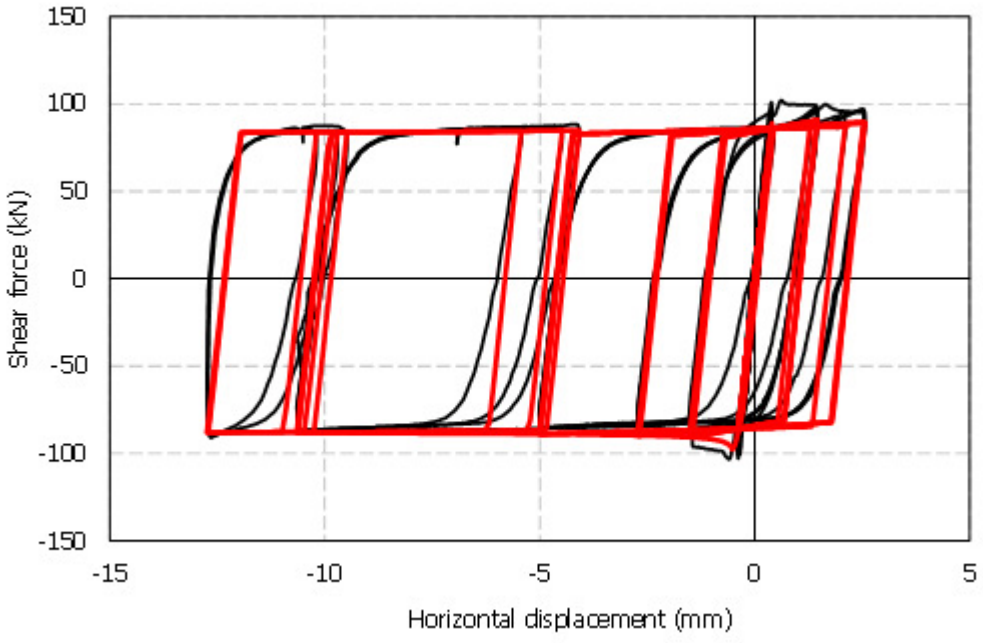

Figure 54: TUD-COMP-5: TREMURI post-test refined prediction - Shear force-displacement curve

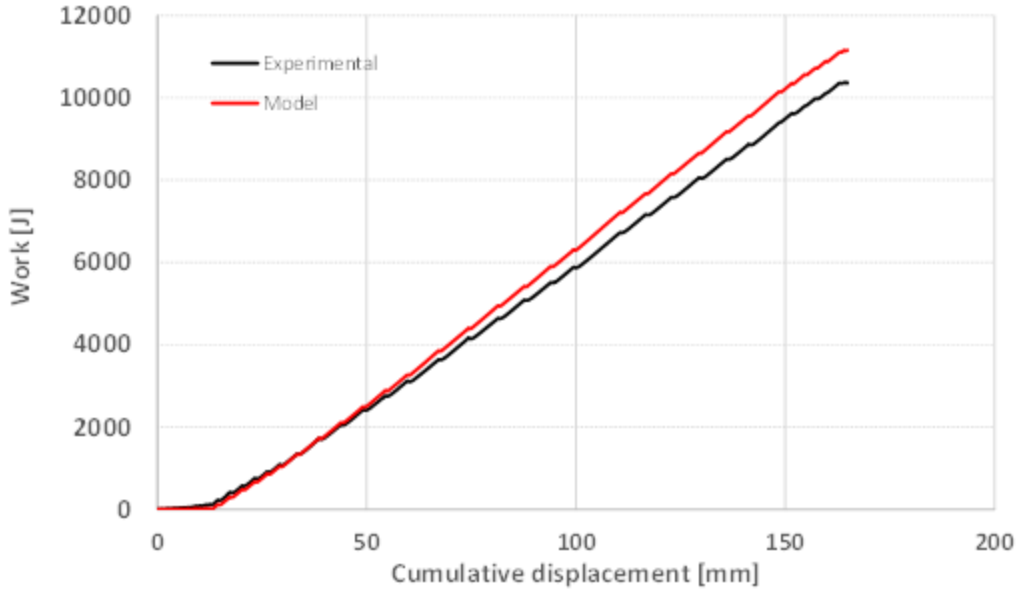

Figure 55: TUD-COMP-5: TREMURI post-test refined prediction – Work and dissipated energy

Table 22: TUD -COMP-5: TREMURI post-test refined prediction - Summary table

Consultant	**Predominant Failure Mechanism Predicted**	**Initial Stiffness [kN/mm]**	**Peak Strength [kN]**	**Maximum Achieved Drift**	
TREMURI new model	Shear / sliding	225.5	103.3	0.46%	
Test Result	Diagonal cracks / bed joint sliding / toe crushing	> 288	103	0.5%	Stopped – no collapse (*)

(*) The test stopped due to inability to maintain the double-clamped boundary condition, not due to imminent collapse.

3.3.6.4 TU-Delft Post-Test Refined Prediction

The DIANA model of TUD-COMP-5, with the application of the new material model, noticeably improved the prediction of the experimental behaviour of the panel. The real loading protocol has been applied with no convergence problems until larger displacements.

The numerical damage pattern is more extensive and does not really match the experiment (Figure 56). Most of the damage is in the middle of the panel characterized by several diagonal cracks, more developed in one direction since the loading history increases in displacement in the negative direction only.

The shear-displacement history is reported in Figure 57. The numerical peak shear capacity is 90.6 kN, which is reasonably close to the experiment.

With respect to the blind prediction, a larger energy dissipation is recorded with the new material model, although still lower than the experiment. With respect to the test, a degradation of the ultimate capacity is observed with increasing applied displacements. There is no horizontal plateau, but the shear capacity gradually decreases for larger drifts.

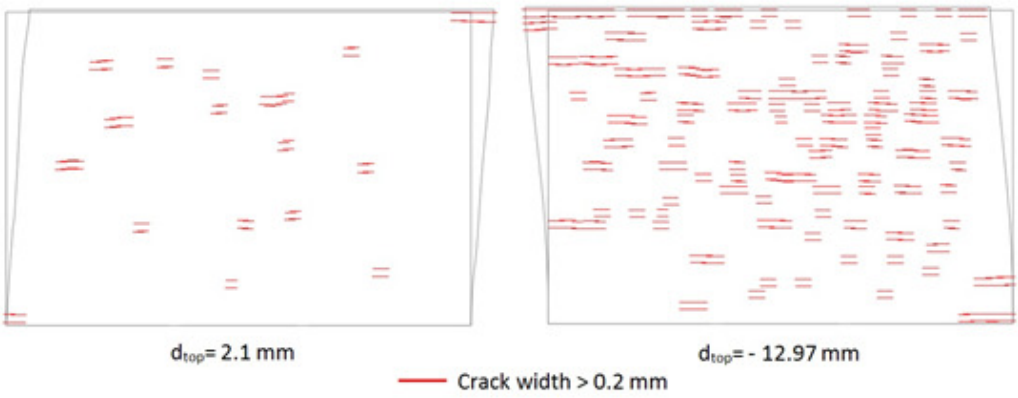

Figure 56: TUD-COMP-5: DIANA post-test refined prediction - Damage plot at end of analysis

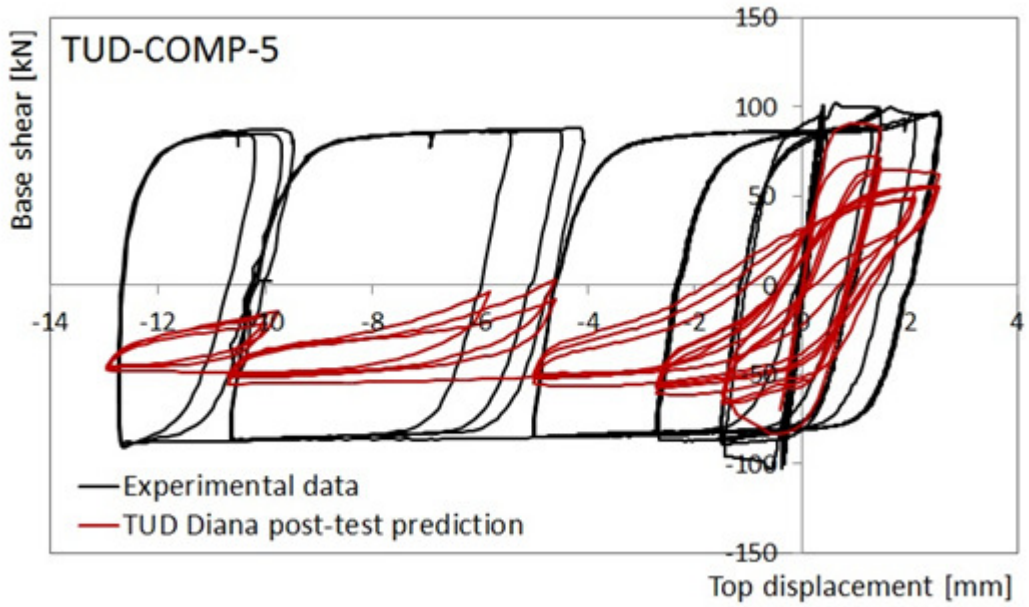

Figure 57: TUD-COMP-5: DIANA post-test refined prediction - Shear force-displacement curve

Table 23: TUD-COMP-5: DIANA post-test refined prediction - Summary table

Consultant	**Predominant Failure Mechanism Predicted**	**Initial Stiffness [kN/mm]**	**Peak Strength [kN]**	**Maximum Achieved Drift**	
DIANA	Diagonal cracks	180	90.6	0.5%	End of loading protocol
Test Result	Diagonal cracks / bed joint sliding / toe crushing	> 288	103	0.5%	Stopped – no collapse (*)

(*) The test stopped due to inability to maintain the double-clamped boundary condition, not due to imminent collapse.

3.3.7 TUD-COMP-6

3.3.7.1 Test Description

TUD-COMP-6 was the seventh quasi-static in-plane test administered by TU-Delft. This specimen was a single-wythe wall constructed of calcium silicate units 102 mm thick. It was 4 m long and 2.75 m high. The applied overburden stress was 0.5 MPa. The wall was tested under cantilever boundary conditions.

First cracks along the main diagonal of the wall appeared during the fifth cycle (0.02% drift). Similar cracks along the opposite diagonal also formed. These cracks progressively increased during the duration of the test and penetrated brick as well as mortar. In addition, bed-joint sliding near the bottom of the wall occurred after the ninth cycle (0.37% drift). After the tenth cycle (0.47% drift), significant brick crushing occurred. The test was stopped at a net drift of 0.56% drift due to potential near partial collapse of the wall.

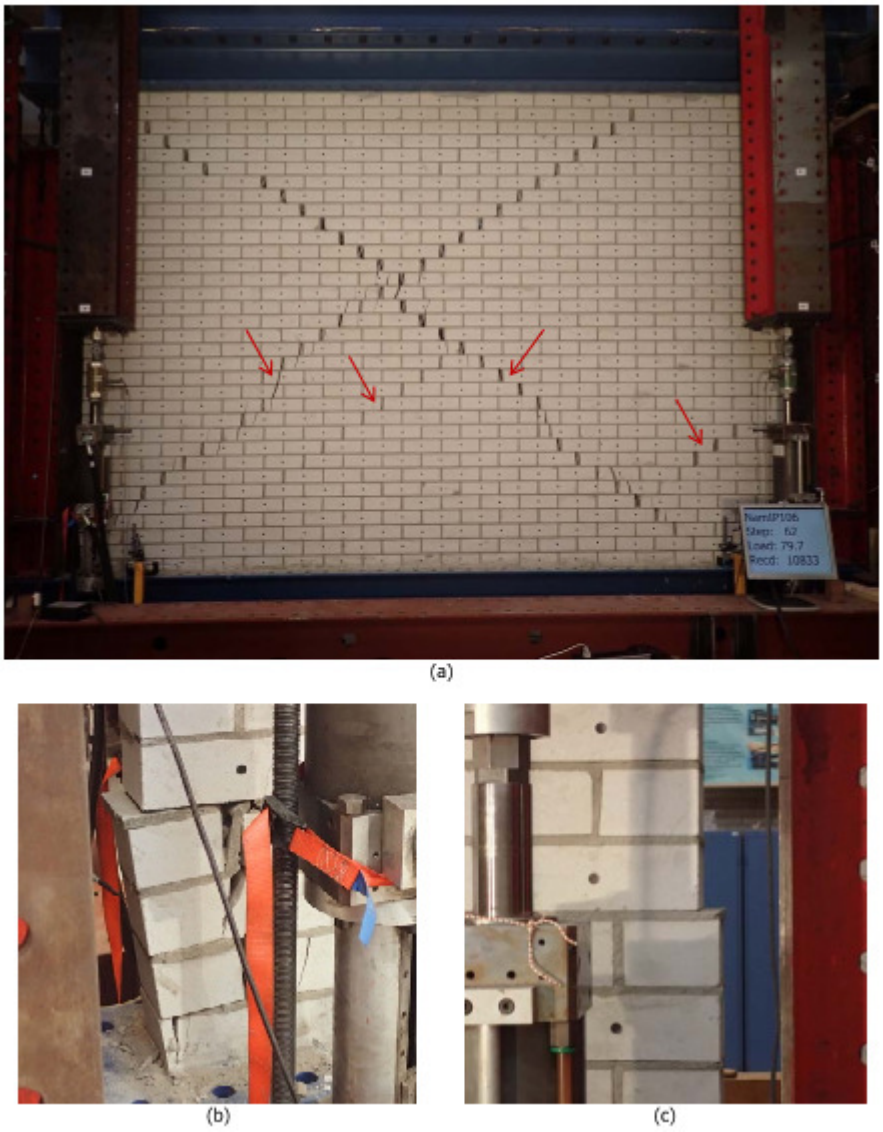

Figure 58: TUD-COMP-6: Crack pattern after 0.37% drift--general overview (a) and bottom left (b) and right (c) corners

Figure 59: TUD-COMP-6: Crack pattern after 0.47% drift--central portion (a) and bottom right corner (b)

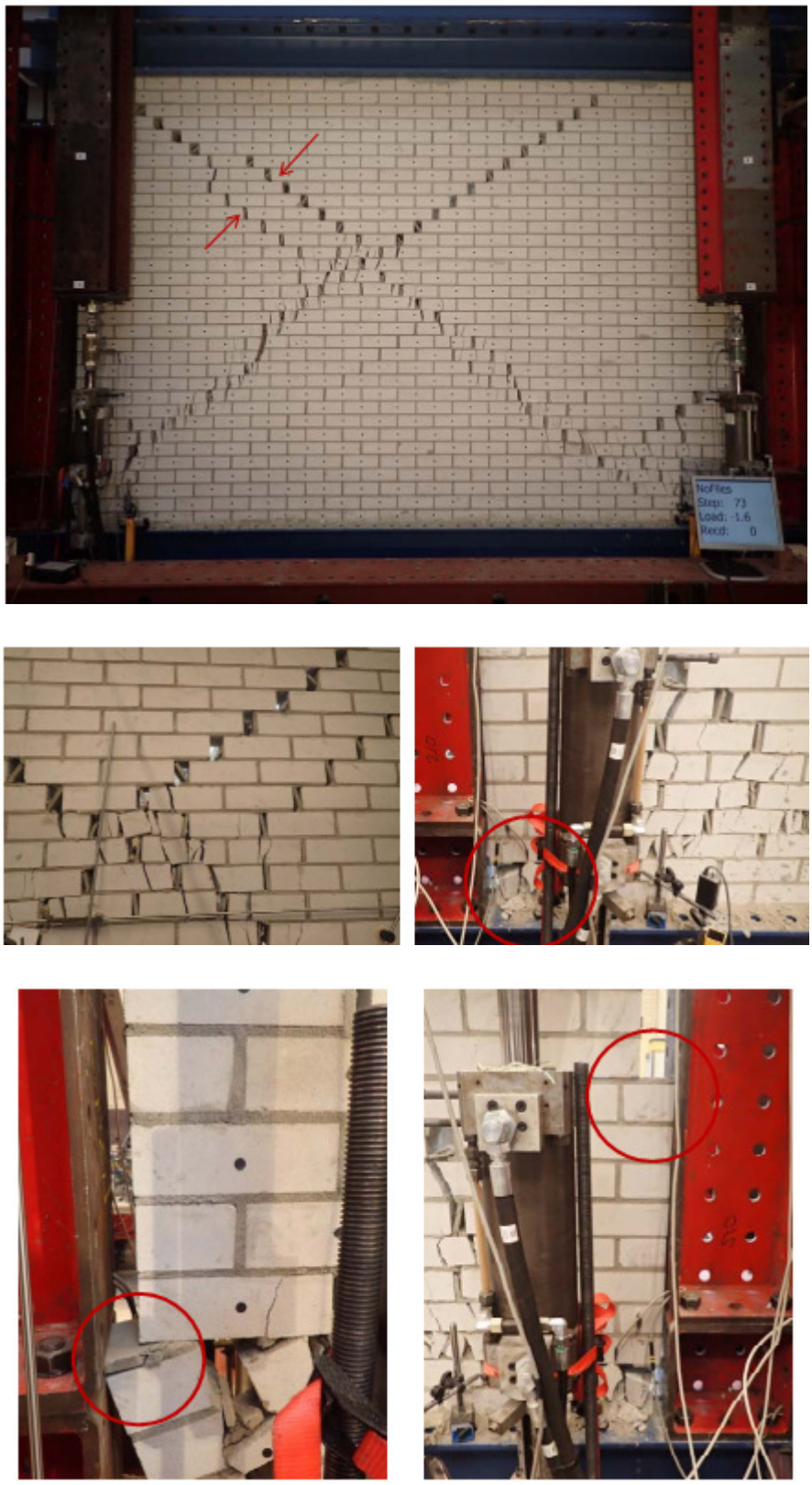

Figure 60: TUD-COMP-6: Final crack pattern

The measured hysteresis is shown in Figure 61.

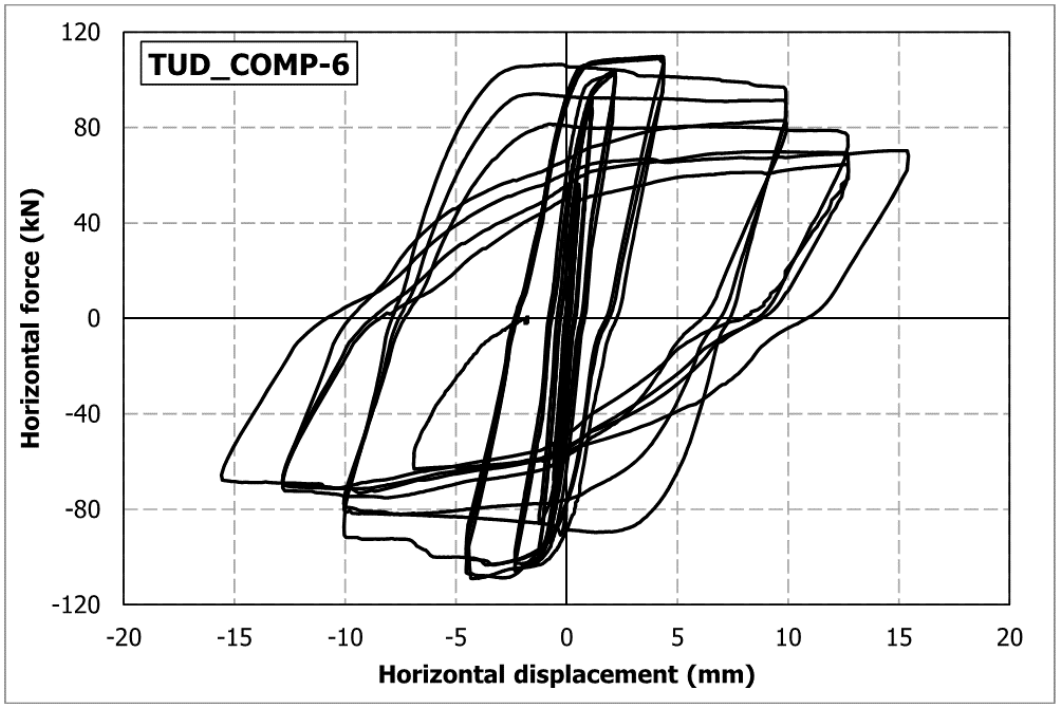

Figure 61: TUD-COMP-6: Lab test result – Shear force-displacement curve

3.3.7.2 Arup Post-Test Refined Prediction

The LS-DYNA model of TUD-COMP-6 correctly predicted a diagonal tensile failure mode as shown in Figure 62. However, the location of the cracks were not matched exactly by the analysis.

The lateral-force-versus-displacement relationship is shown in Figure 63. The ultimate load at around 110 kN was well predicted, as were the hysteresis and energy absorption.

In the laboratory, the test was stopped at 0.6% drift because the specimen was heavily damaged and close to collapse. There was extensive toe-crushing in the corners of the specimen, and cracking of bricks around the diagonal failure lines. The analysis also predicted near-collapse at a drift of 0.5 to 0.7%. The removal of elements in the corners of the model due to damage by toe-crushing can be seen in Figure 62.

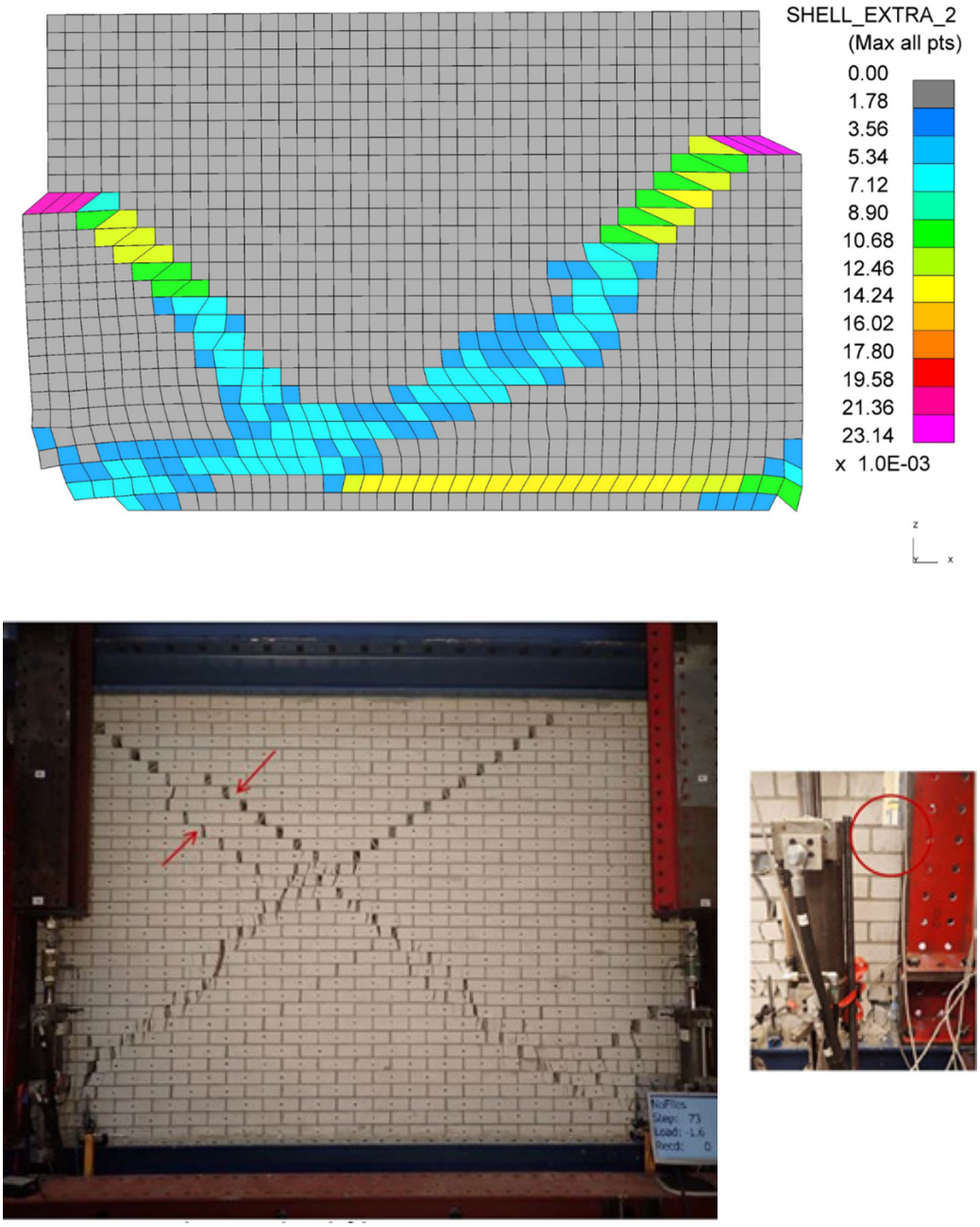

Figure 62: TUD-COMP-6: LS-DYNA post-test refined prediction - Damage plot at end of analysis (top) compared to observed damage in laboratory

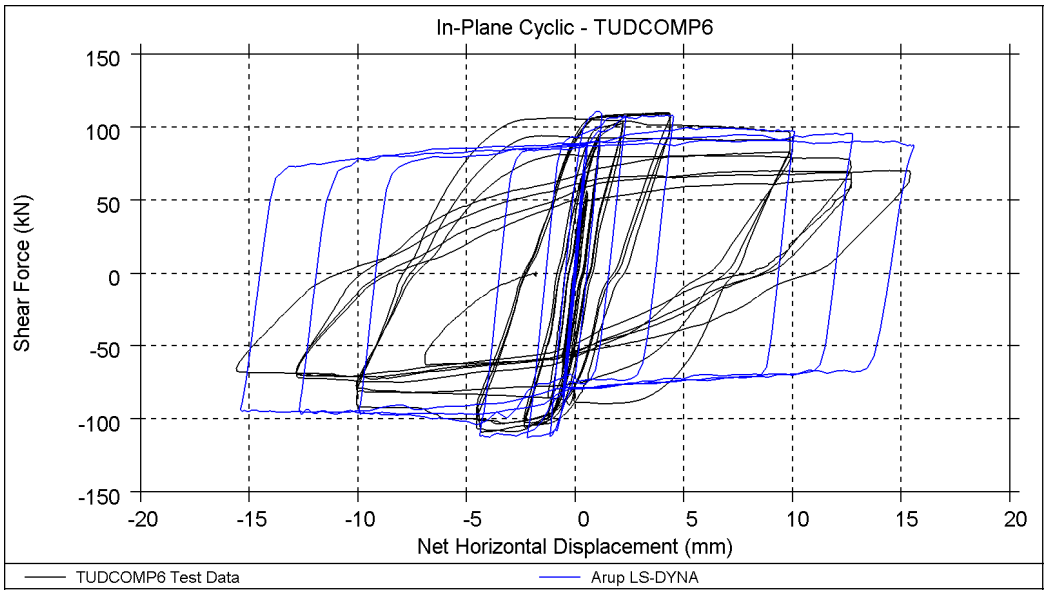

Figure 63: TUD-COMP-6: LS-DYNA post-test refined prediction - Shear force-displacement curve

Table 24: TUD-COMP-6: LS-DYNA post-test refined prediction - Summary table

Consultant	**Predominant Failure Mechanism Predicted**	**Initial Stiffness [kN/mm]**	**Peak Strength [kN]**	**Maximum Achieved Drift**	
LS-DYNA	Diagonal cracks / bed joint sliding	174	113	0.5% to 0.7%	Near collapse
Test Result	Diagonal cracks / toe crushing	125	110	0.6%	Near collapse

3.3.7.3 EUCENTRE Post-Test Refined Prediction

The shear force -displacement relationships are shown in Figure 64. The ultimate strength is under-predicted by the TREMURI model. While the hysteresis and energy dissipation as well as the initial stiffness are overestimated (Figure 65).

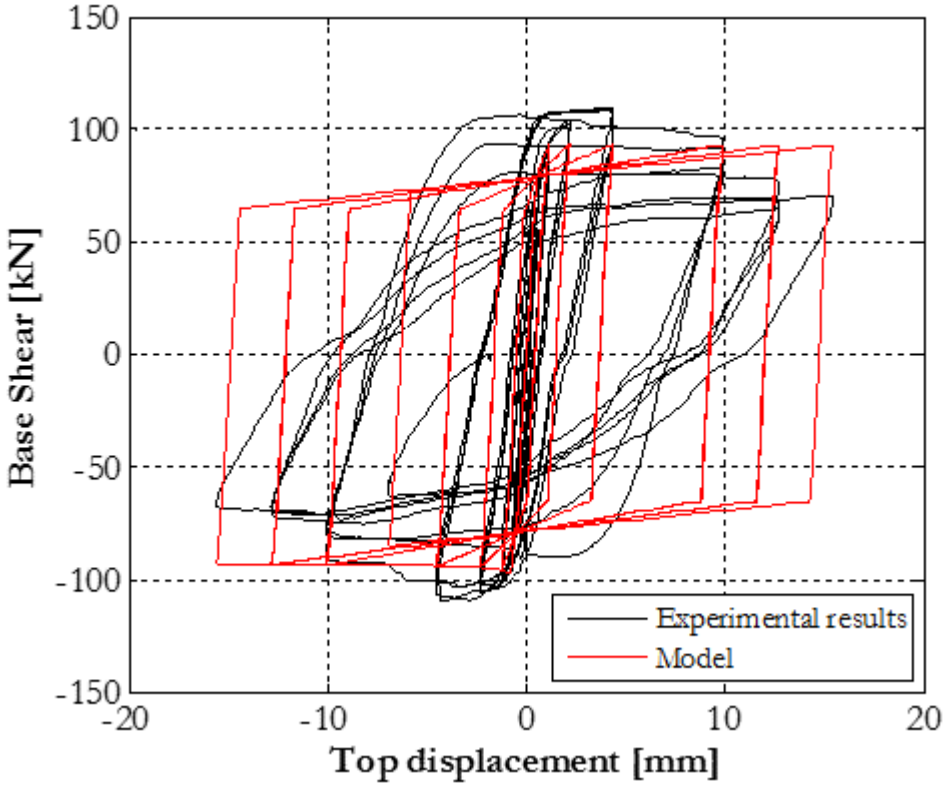

Figure 64: TUD-COMP-6: TREMURI post-test refined prediction - Shear force-displacement curve

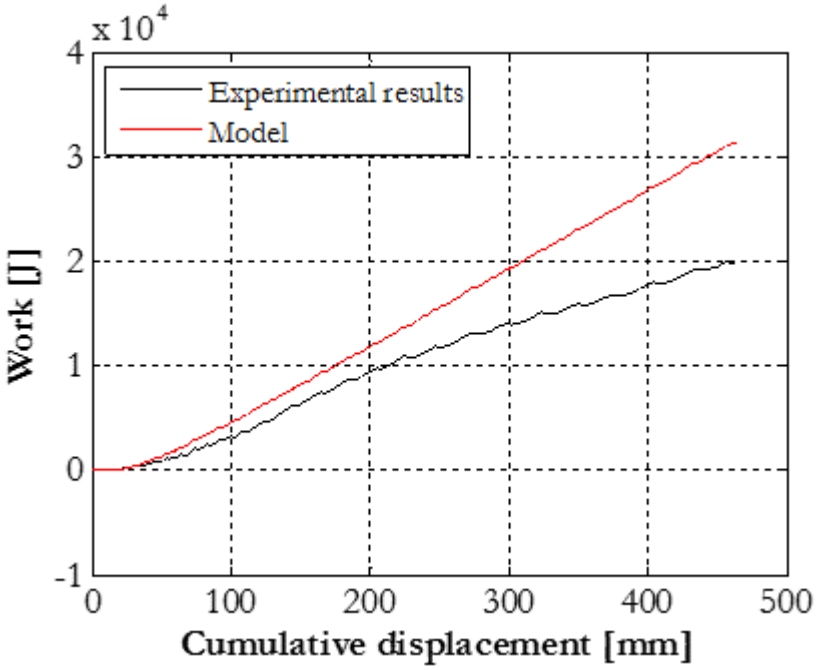

Figure 65: TUD-COMP-6: TREMURI post-test refined prediction – Work and dissipated energy

Table 25: TUD-COMP-6: TREMURI post-test refined prediction - Summary table

Consultant	**Predominant Failure Mechanism Predicted**	**Initial Stiffness [kN/mm]**	**Peak Strength [kN]**	**Maximum Achieved Drift**	
TREMURI new model	Shear	160	97.2	0.56%	
Test Result	Diagonal cracks / toe crushing	125	110	0.6%	Near collapse

3.3.7.4 TU-Delft Post-Test Refined Prediction

The DIANA model of TUD-COMP-4, with the application of the new material model, noticeably improved the prediction of the experimental behaviour of the panel. The real loading protocol has been applied with no convergence problems until larger displacements.

The numerical damage pattern is more extensive with respect to the experiment (Figure 66). Most of the damage is in the middle of the panel, characterized by several diagonal (almost vertical) cracks, but it is not possible to completely identify the typical X-shaped cracks observed in the experiment.

The shear-displacement history is reported in Figure 67. The numerical peak shear capacity is 104.6 kN, quite close to the experimental value, which is equal to 110 kN.

With respect to the blind prediction, a larger energy dissipation is recorded with the new material model, although still lower than the experiment. With respect to the test, some more degradation of the ultimate capacity is observed with increasing applied displacements.

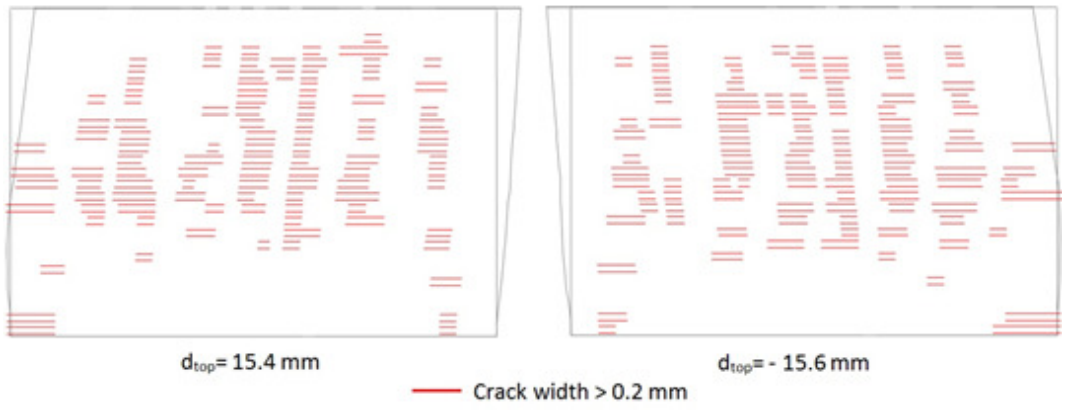

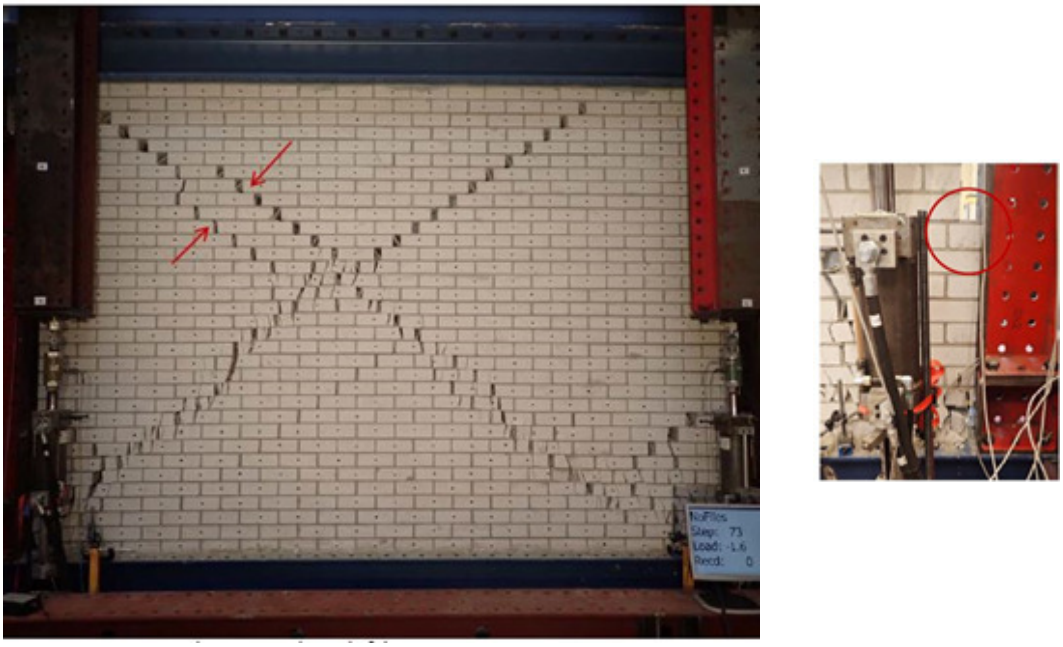

Figure 66: TUD-COMP-6: DIANA post-test refined prediction - Damage plot at end of analysis (top) compared to observed damage in laboratory

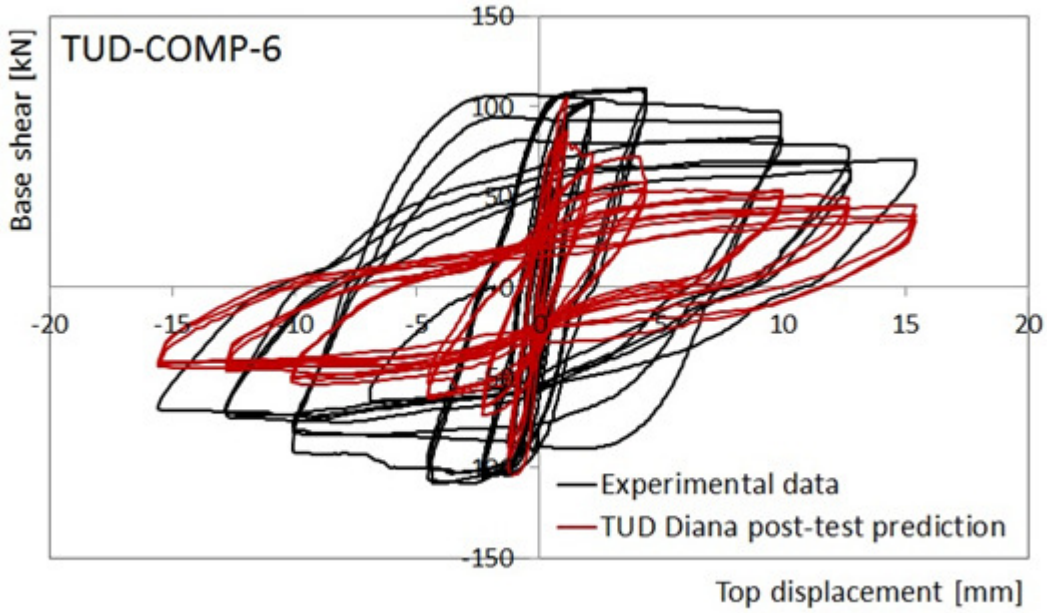

Figure 67: TUD-COMP-6: DIANA post-test refined prediction - Shear force-displacement curve

Table 26: TUD-COMP-6: DIANA post-test refined prediction - Summary table

Consultant	**Predominant Failure Mechanism Predicted**	**Initial Stiffness [kN/mm]**	**Peak Strength [kN]**	**Maximum Achieved Drift**	
DIANA	Diagonal cracks	133	104.6	0.6%	End of loading protocol / extensive damage
Test Result	Diagonal cracks / toe crushing	125	110	0.6%	Near collapse

3.3.8 EUC-COMP-1

3.3.8.1 Test Description

EUC-COMP-1 was one of the three quasi-static in-plane tests administered by EUCENTRE. This specimen was a single-wythe wall constructed of calcium silicate units 102 mm thick. It was 1.1 m long and 2.75 m high. The applied overburden is 0.5 MPa. The wall was tested under double clamped boundary conditions.

As expected, specimen EUC-COMP-1 initially exhibited a pure rocking behaviour with cracks opening at the edges upon cyclically loading the specimen. A migration of the horizontal crack at the bottom was observed. At a drift of 0.6%, the location of the horizontal crack was at the interface. At a drift of 1.5%, the horizontal crack migrated above the first course of bricks and above the second course of bricks during last cycle with 2% drift.

The end of the test was reached for the inability of the pier to sustain the imposed vertical load at a drift of 2% drift. A toe crushing mechanism was exhibited.

Figure 68: EUC-COMP-1: Toe-crushing damage at end of test (a) bottom right; (b) top left corner; (c) top right corner

See Figure 69 below for the shear force-displacement plot of the lab test result of EUC-COMP-1.

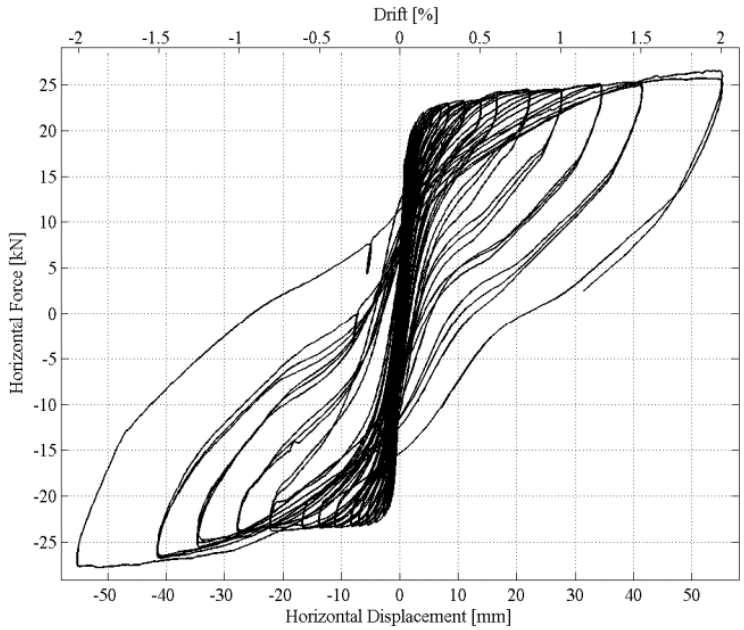

Figure 69: EUC-COMP-1: Lab test result – Shear force-displacement curve

3.3.8.2 Arup Post-Test Refined Prediction

The LS-DYNA model of EUC-COMP-1 correctly predicted rocking behaviour with toe crushing as shown in Figure 70.

The lateral-force-versus-displacement relationship is shown in Figure 71. The initial strength of the specimen, around 22 kN, was well predicted but as the drift increased the specimen in the lab apparently became stronger, with resistance up to 28kN at the largest negative drift values. The reason for the increase of strength in the test is not clear, and was not predicted by the analysis. As with the other tall specimens, the amount of energy dissipation during hysteresis was under-predicted.

In the laboratory, the test was stopped at 2% drift, due to extensive toe-crushing damage indicating a near-collapse state. In comparison, the tests on tall double-clamped specimens at TUD, TUD-COMP-0a and TUD-COMP-3, were stopped at 0.9 and 1.3% drift. The photos suggest that the EUC-COMP-1 was continued to a greater level of damage, and possibly the TUD-COMP-0a and TUD-COMP-3 specimens could have tolerated greater levels of drift. However, some random test-to-test variability in the drift to collapse is expected. Therefore, the analysis prediction for EUC-COMP-1 of near-collapse at 1.1% and complete collapse at 1.2% drift is within the expected range.

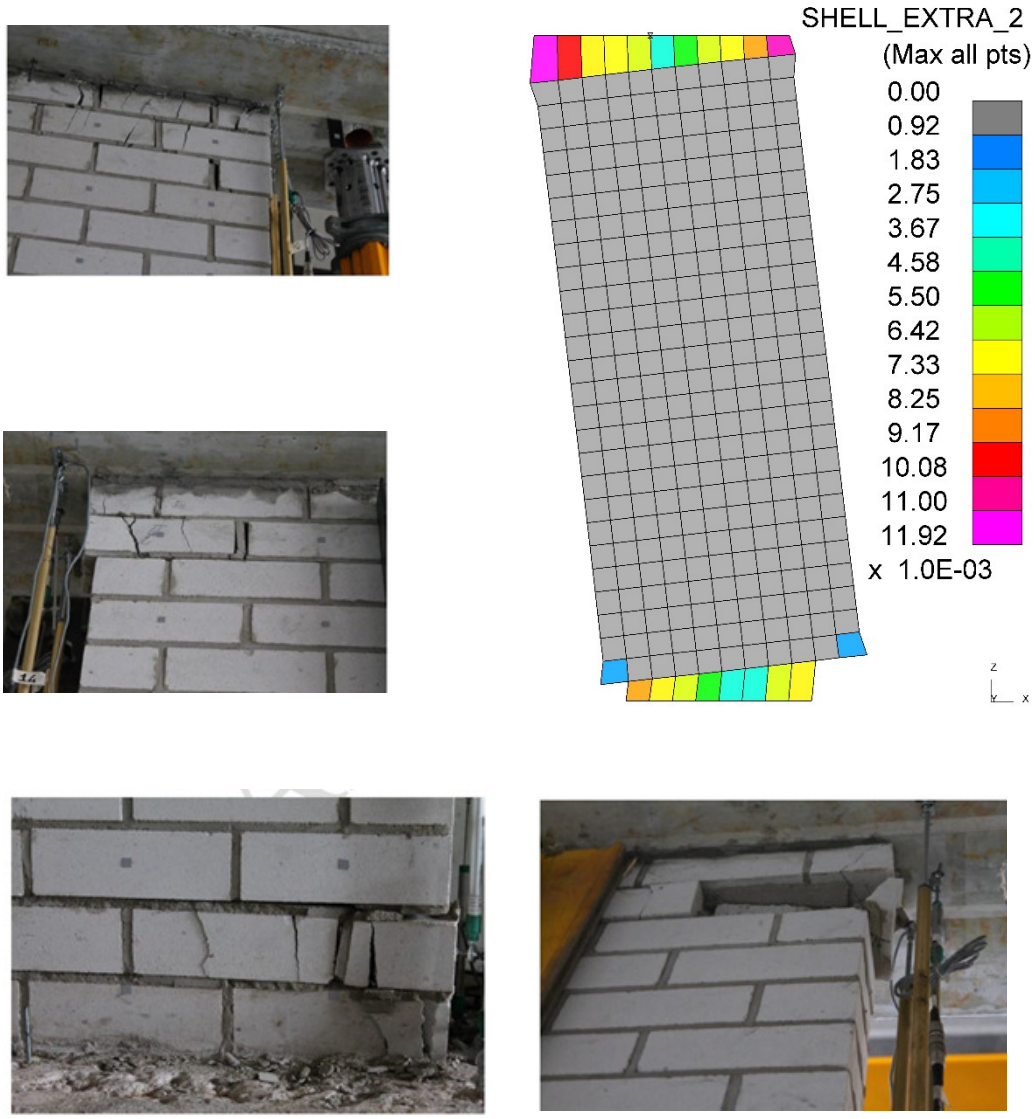

Figure 70: EUC-COMP-1: LS-DYNA post-test refined prediction - Damage plot at end of analysis (top right) compared to observed damage in laboratory

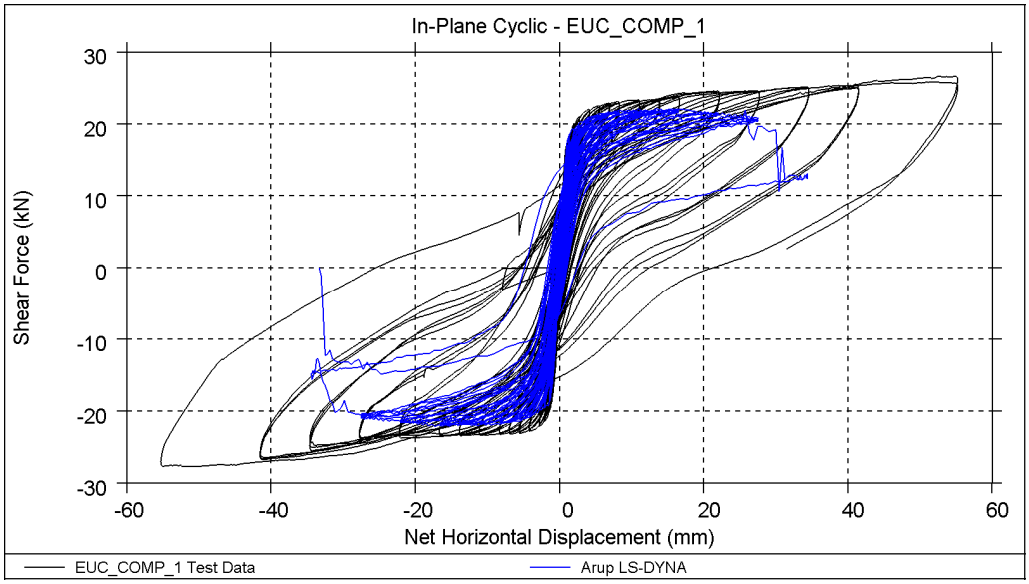

Figure 71: EUC-COMP-1: LS-DYNA post-test refined prediction - Shear force-displacement curve

Table 27: EUC-COMP-1: LS-DYNA post-test refined prediction - Summary table

Consultant	**Predominant Failure Mechanism Predicted**	**Initial Stiffness [kN/mm]**	**Peak Strength [kN]**	**Maximum Achieved Drift**	
LS-DYNA	Rocking behaviour / toe crushing	20	22	1.1% to 1.2%	Near collapse
Test Result	Rocking behaviour / toe crushing	22.9	28	2%	Near collapse

3.3.8.3 EUCENTRE Post-Test Refined Prediction

Since during the test a migration of the horizontal (flexural) cracks was observed from the top and bottom towards the centre of the specimen, an additional TREMURI model with reduced macro-element effective height (one layer at the top and one at the base were removed) was analysed. The main results are reported below.

The increase of the vertical overburden led to an increase of the shear capacity now closer to the one observed experimentally. As reported in the energy plots, the numerical results underestimated the energy dissipated during the hysteretic loops.

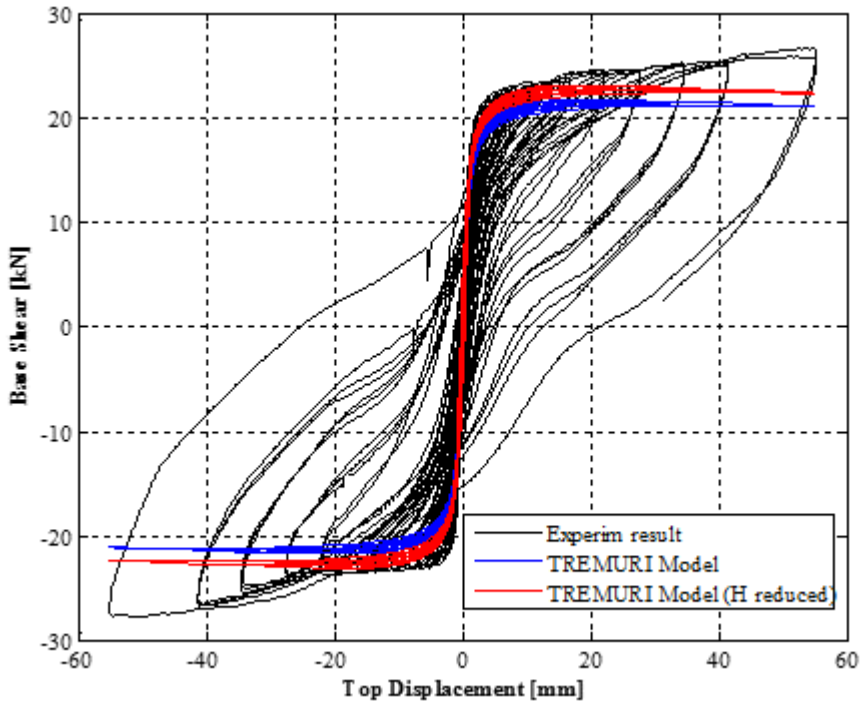

Figure 72: EUC-COMP-1: TREMURI post-test refined prediction - Shear force-displacement curve

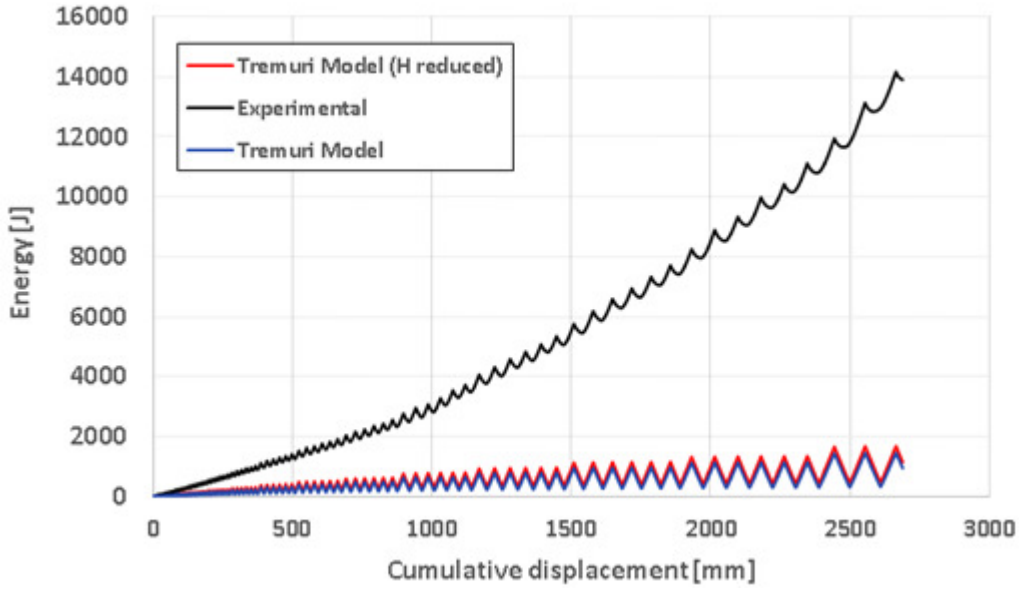

Figure 73: EUC-COMP-1: TREMURI post-test refined prediction – Work and dissipated energy

Table 28: EUC-COMP-1: TREMURI post-test refined prediction - Summary table

Consultant	**Predominant Failure Mechanism Predicted**	**Initial Stiffness [kN/mm]**	**Peak Strength [kN]**	**Maximum Achieved Drift**	
TREMURI H-reduced	Rocking	14	23.0	2.5%	
Test Result	Rocking behaviour / toe crushing	22.9	28	2%	Near collapse

Additional sensitivity studies on the adopted value for friction and cohesion coefficient were carried out. The reduced values implemented in the TREMURI model are summarised in Table 29.

Results were sensitive to small variations in the adopted shear strength parameters, which, in some cases, led to a switch in the failure mechanism predicted by the model.

Table 29: EUC-COMP-1: TREMURI post-test refined simulation sensitivity analysis – variation of friction and cohesion coefficient

μ	**c [MPa]**	**Description**
0.75	0.3	Blind prediction values
0.5	0.3	Intermediate values
0.45	0.2	From material characterisation tests

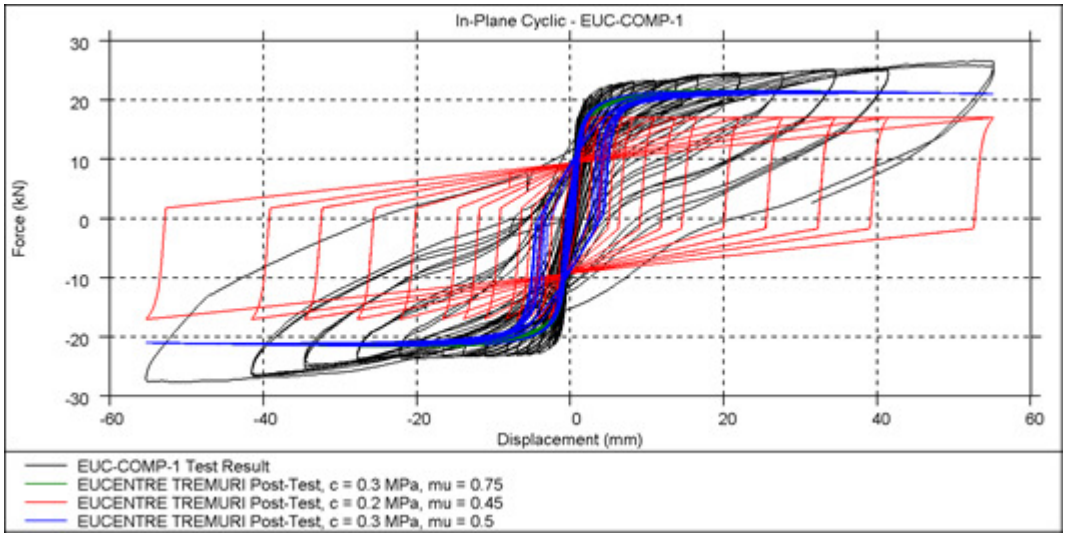

Figure 74: EUC-COMP-1: TREMURI post-test refined simulation sensitivity analysis – shear force-displacement curve

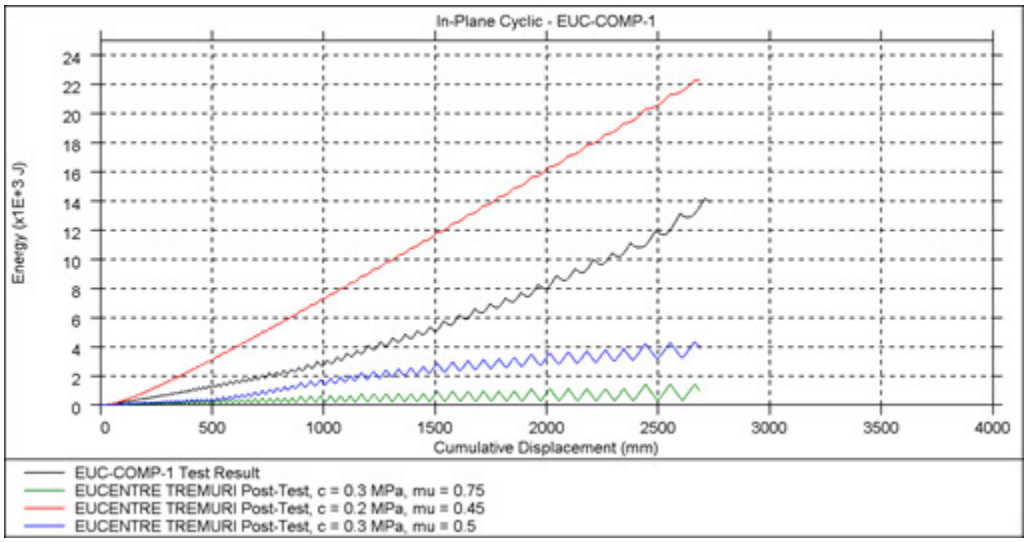

Figure 75: EUC-COMP-1: TREMURI post-test refined simulation sensitivity analysis – energy dissipation plot

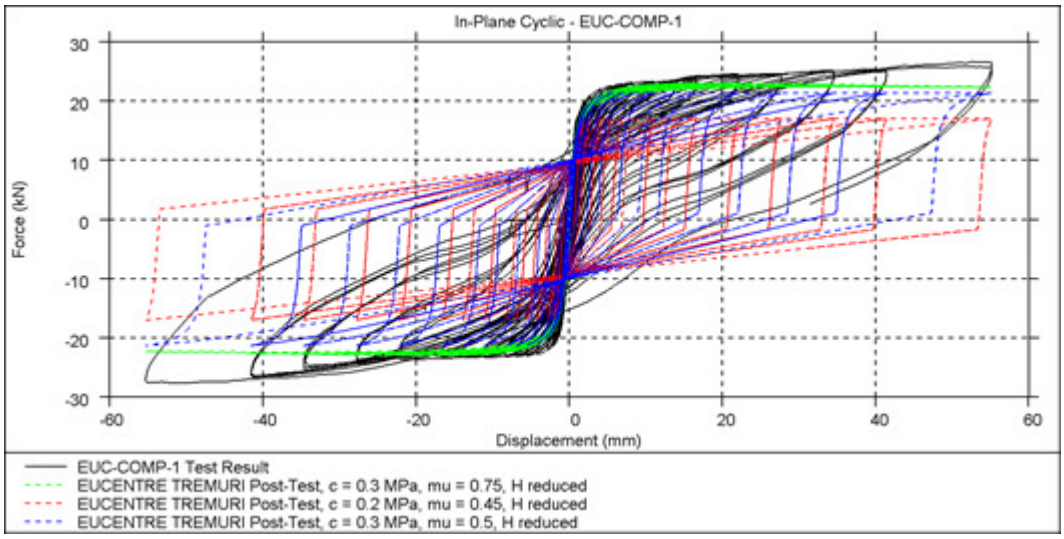

Figure 76: EUC-COMP-1: TREMURI post-test refined simulation sensitivity analysis – shear force-displacement curve with H reduced

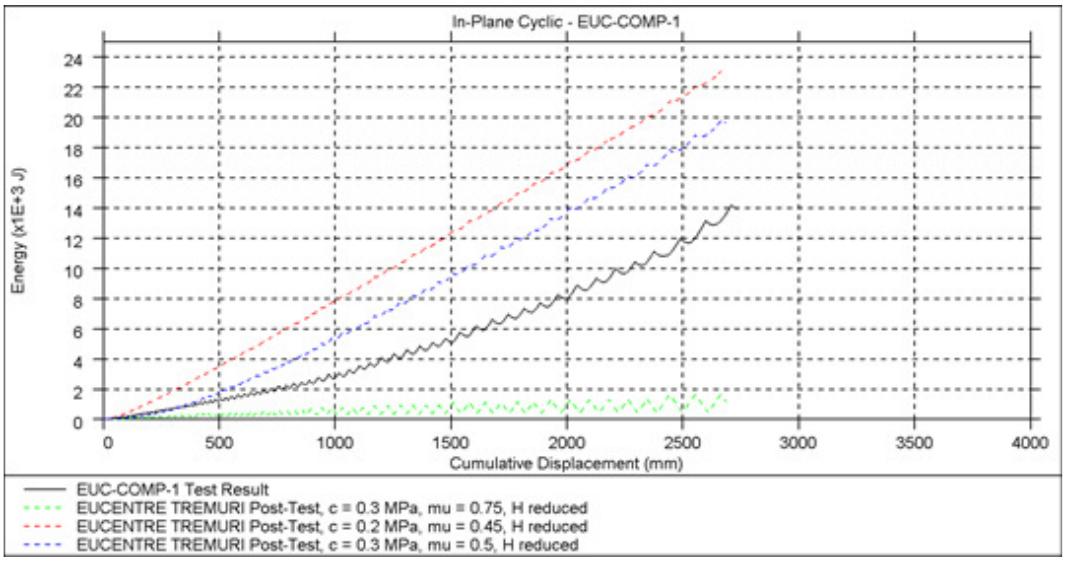

Figure 77: EUC-COMP-1: TREMURI post-test refined simulation sensitivity analysis – energy dissipation plot with H reduced

3.3.8.4 TU-Delft Post-Test Refined Prediction

The application of the new material to DIANA model of EUC-COMP-1 noticeably improved the stability of the numerical solution since the real loading protocol has been applied with no convergence problems until larger displacements.

The numerical damage pattern is more extensive with respect to the experimental one (Figure 78). A rocking behaviour is detected with cracks at the base and top of the panel spreading also along the height with some horizontal cracks at the two lateral edges of the panel. In the last stages of the test, some additional cracks in the middle of the panel also occur.

The shear-displacement history is reported in Figure 79. The numerical peak shear capacity is 21.8 kN and the initial stiffness is approximately 17.5 kN/mm, both reasonably close to the experiment.

With respect to the blind prediction, a larger energy dissipation is observed with the new material model, similar to what was recorded in the experiment. With respect to the test, a degradation of the ultimate capacity is observed with increasing applied displacements, whereas in the experiment an unexpected hardening phenomenon is noticed.

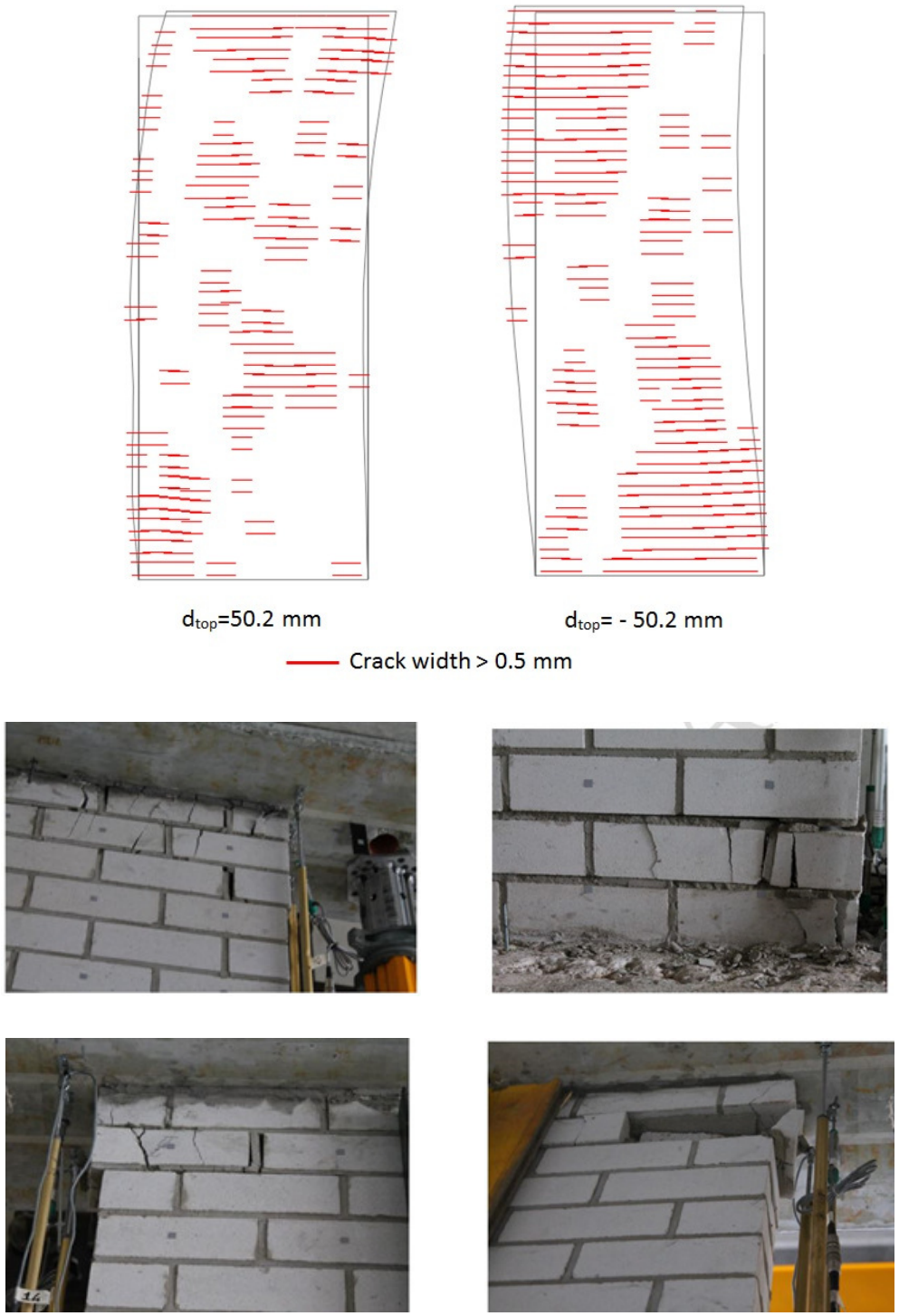

Figure 78: EUC-COMP-1: DIANA post-test refined prediction - Damage plot at end of analysis (top) compared to observed damage in laboratory

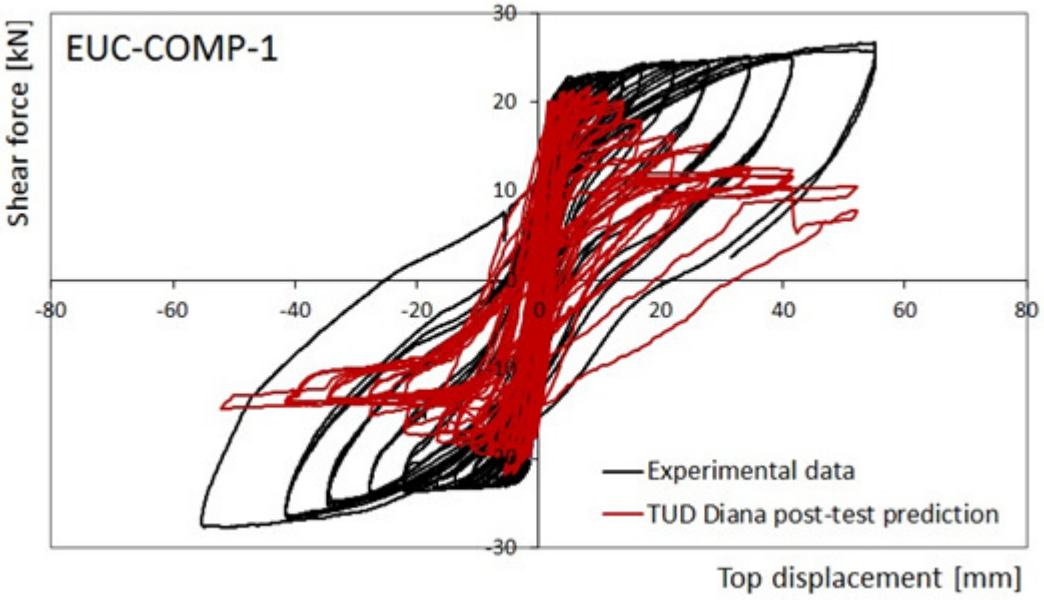

Figure 79: EUC-COMP-1: DIANA post-test refined prediction - Shear force-displacement curve

Table 30: EUC-COMP-1: DIANA post-test refined prediction - Summary table

Consultant	**Predominant Failure Mechanism Predicted**	**Initial Stiffness [kN/mm]**	**Peak Strength [kN]**	**Maximum Achieved Drift**	
DIANA	Rocking / cracks in middle of panel	17.5	21.8	2%	End of loading protocol / Extensive damage
Test Result	Rocking behaviour / toe crushing	22.9	28	2%	Near collapse

3.3.9 EUC-COMP-2

3.3.9.1 Test Description

EUC-COMP-2 was one of the three quasi-static in-plane tests administered by EUCENTRE. This specimen was a single-wythe wall constructed of calcium silicate units 102 mm thick. It was 1.1 m long and 2.75 m high. The applied overburden during the test is 0.7 MPa.

Initially, specimen EUC-COMP-2 exhibited a pure rocking behaviour with cracks opening at the edges upon cyclically loading the specimen. No other damage was observed in the masonry panel.

The top restraint condition did not behave in the expected fixed-fixed manner and began to rotate out of plane after 0.15% drift. The test was therefore stopped early (at 0.22% drift) due to out-of-plane wall failure.

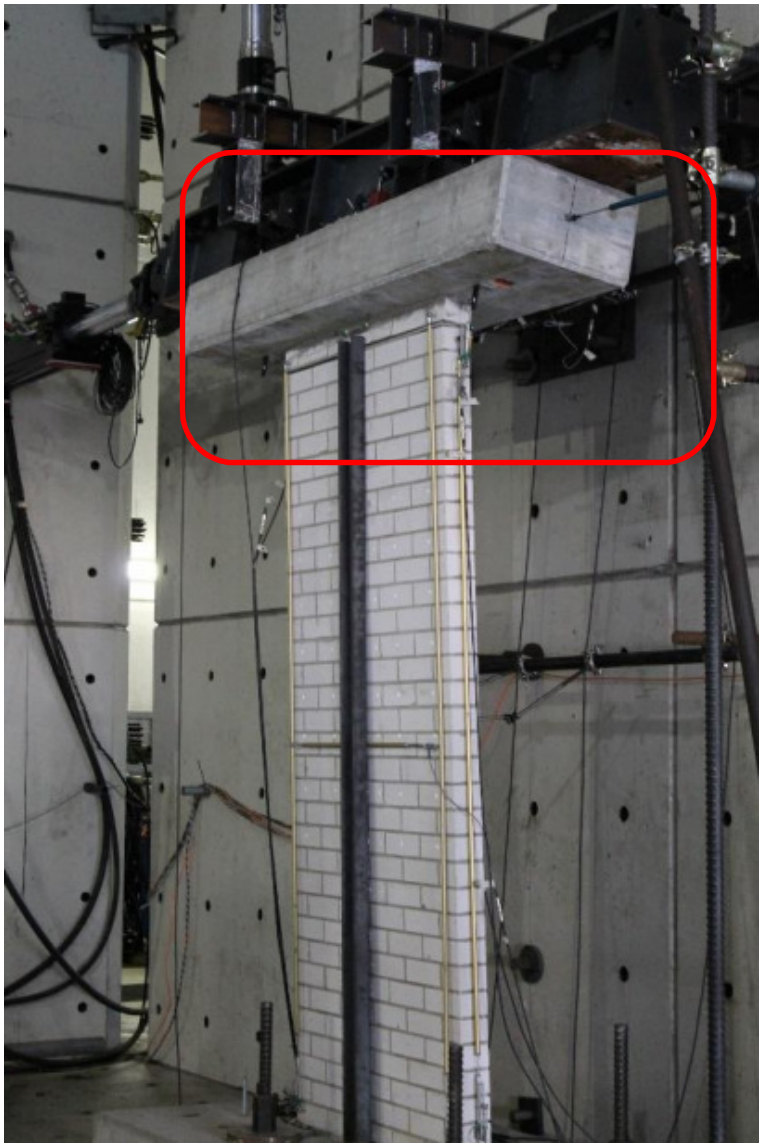

Figure 80: EUC-COMP-2: Out of plane failure mechanism at 0.22% drift

See Figure 81 below for the shear force-displacement plot of the lab test result of EUC-COMP-2 up to the point that the test was stopped.

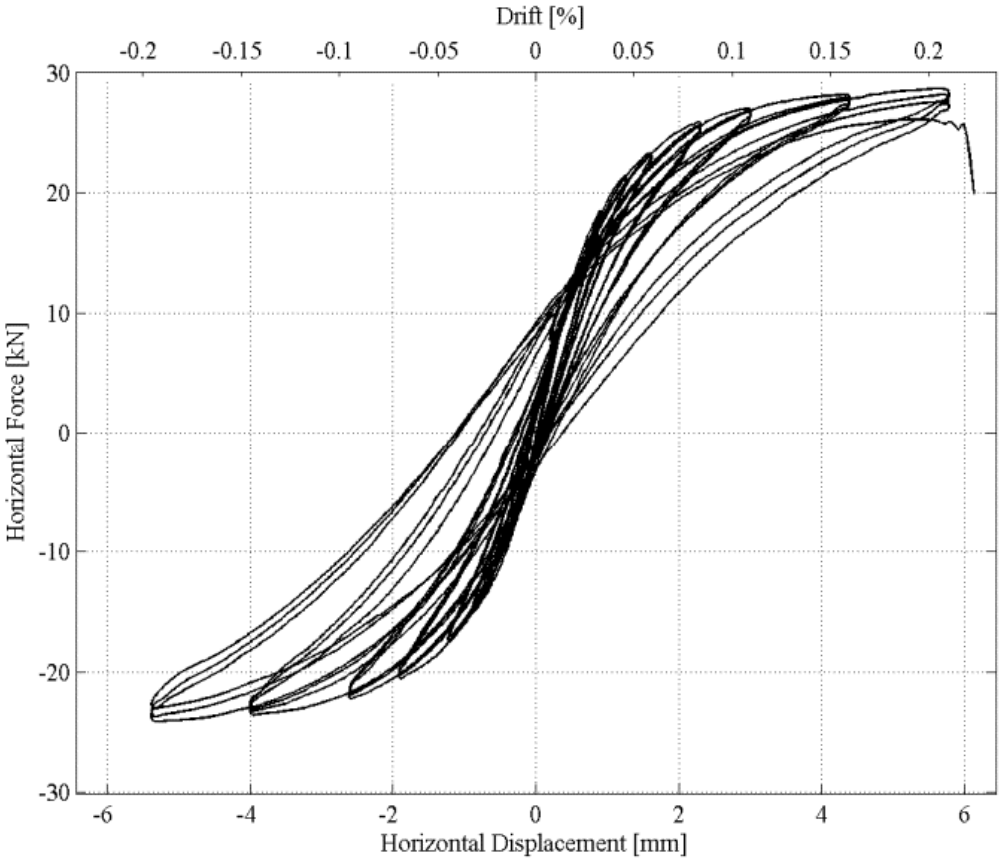

Figure 81: EUC-COMP-2: Lab test result – Shear force-displacement curve

3.3.9.2 Arup Post-Test Refined Prediction

The LS-DYNA model of EUC-COMP-2 correctly predicted rocking behaviour as shown in Figure 82.

The lateral-force-versus-displacement relationship is shown in Figure 83. The strength and backbone curve are well predicted, although as with the other tall specimens, the amount of energy dissipation during hysteresis was under-predicted. Due to the premature termination of the test, no conclusions can be drawn about the prediction of in-plane damage or collapse.

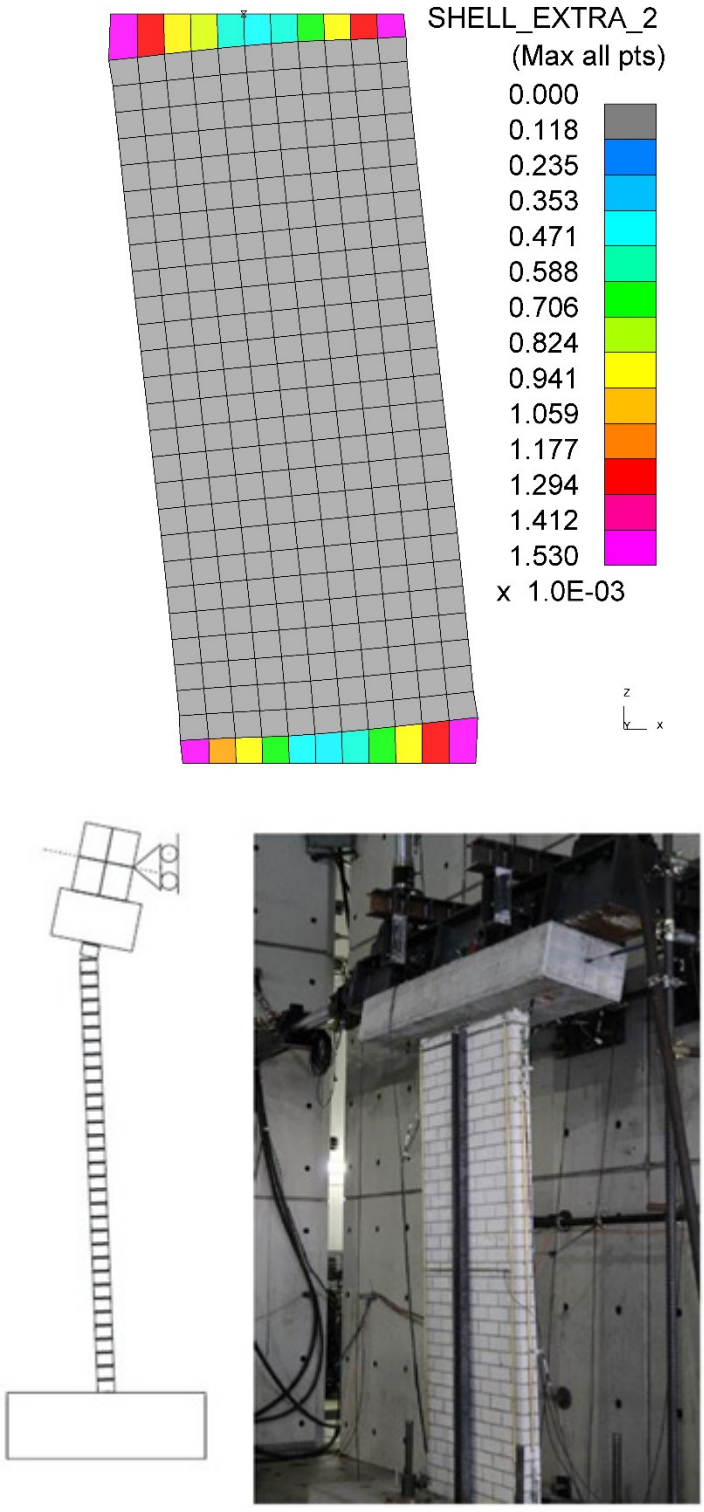

Figure 82: EUC-COMP-2: LS-DYNA post-test refined prediction - Damage plot at end of analysis

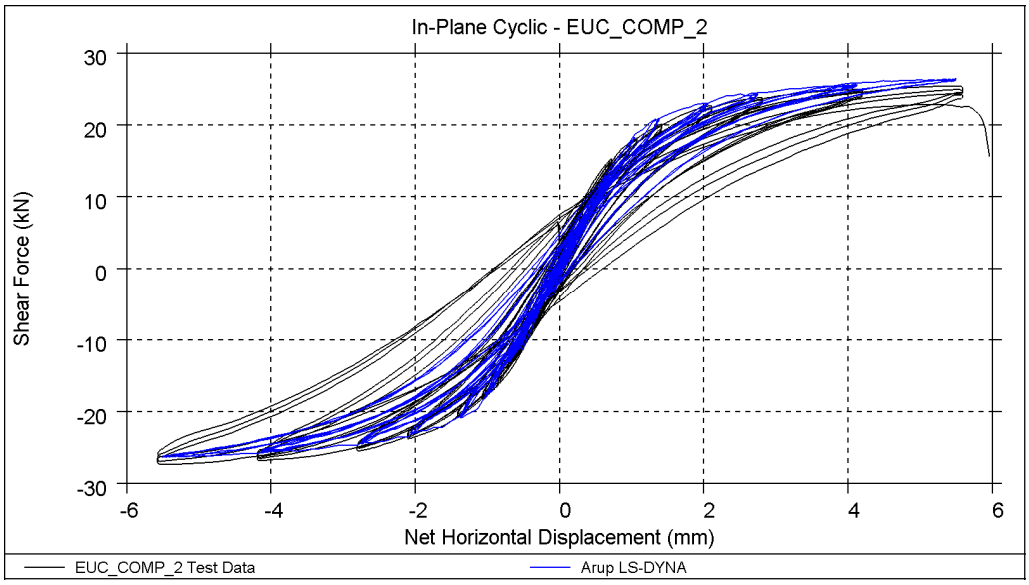

Figure 83: EUC-COMP-2: LS-DYNA post-test refined prediction - Shear force-displacement curve

Table 31: EUC-COMP-2: LS-DYNA post-test refined prediction - Summary table

Consultant	**Predominant Failure Mechanism Predicted**	**Initial Stiffness [kN/mm]**	**Peak Strength [kN]**	**Maximum Achieved Drift**	
LS-DYNA	Rocking behaviour	21	27	0.2%	End of analysis – no collapse
Test Result	Out of plane instability	24	27	0.2%	Premature out-of-plane failure

3.3.9.3 EUCENTRE Post-Test Refined Prediction

The shear force -displacement relationships are shown in Figure 84. The ultimate strength is well predicted by the TREMURI model. The hysteresis and energy dissipation as well as the initial stiffness are under-predicted (Figure 85).

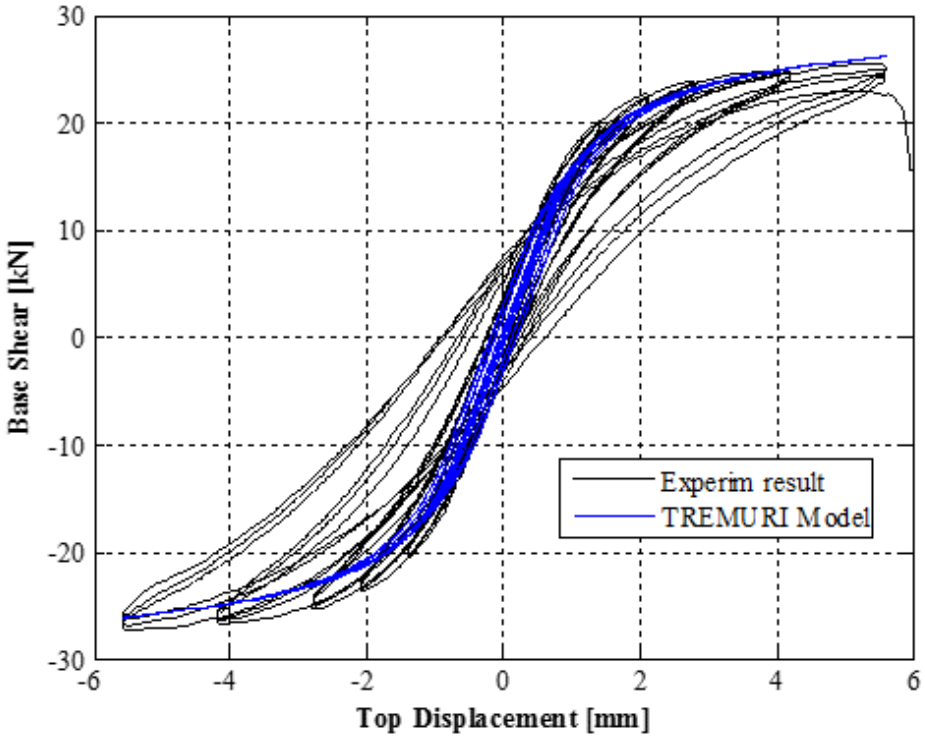

Figure 84: EUC-COMP-2: TREMURI post-test refined prediction - Shear force-displacement curve

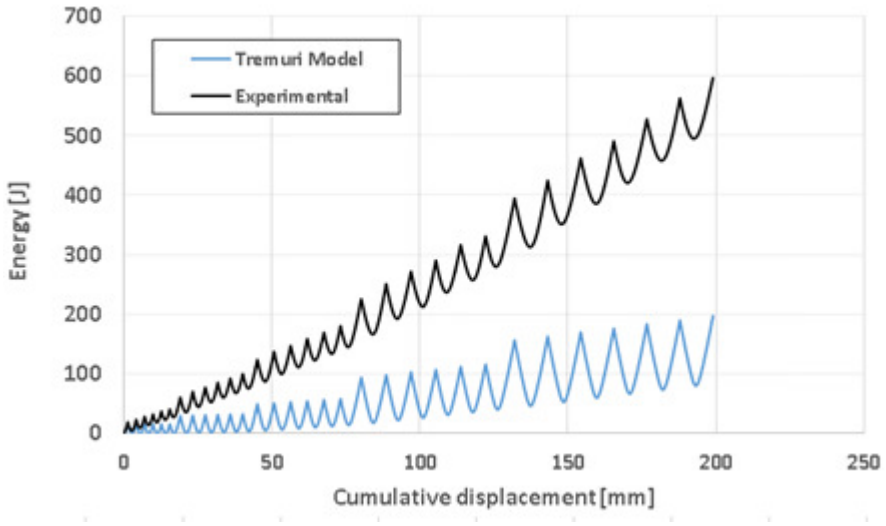

Figure 85: EUC-COMP-2: TREMURI post-test refined prediction – Work and dissipated energy

Table 32: EUC-COMP-2: TREMURI post-test refined prediction - Summary table

Consultant	**Predominant Failure Mechanism Predicted**	**Initial Stiffness [kN/mm]**	**Peak Strength [kN]**	**Maximum Achieved Drift**	
TREMURI	Rocking	17	26.1	0.2%	
Test Result	Out of plane instability	24	27	0.2%	Premature out-of-plane failure

3.3.9.4 TU-Delft Post-Test Refined Prediction

The DIANA model of EUC-COMP-2 correctly predicted rocking behaviour as shown in the experiment (Figure 86). The test was stopped at only 0.22% drift due to unexpected out-of-plane instability of the specimen, therefore the behaviour for higher levels of drifts could not be explored.

The shear-displacement history is reported in Figure 87. The numerical loops almost overlap the experimental ones, also correctly reproducing the energy dissipation.

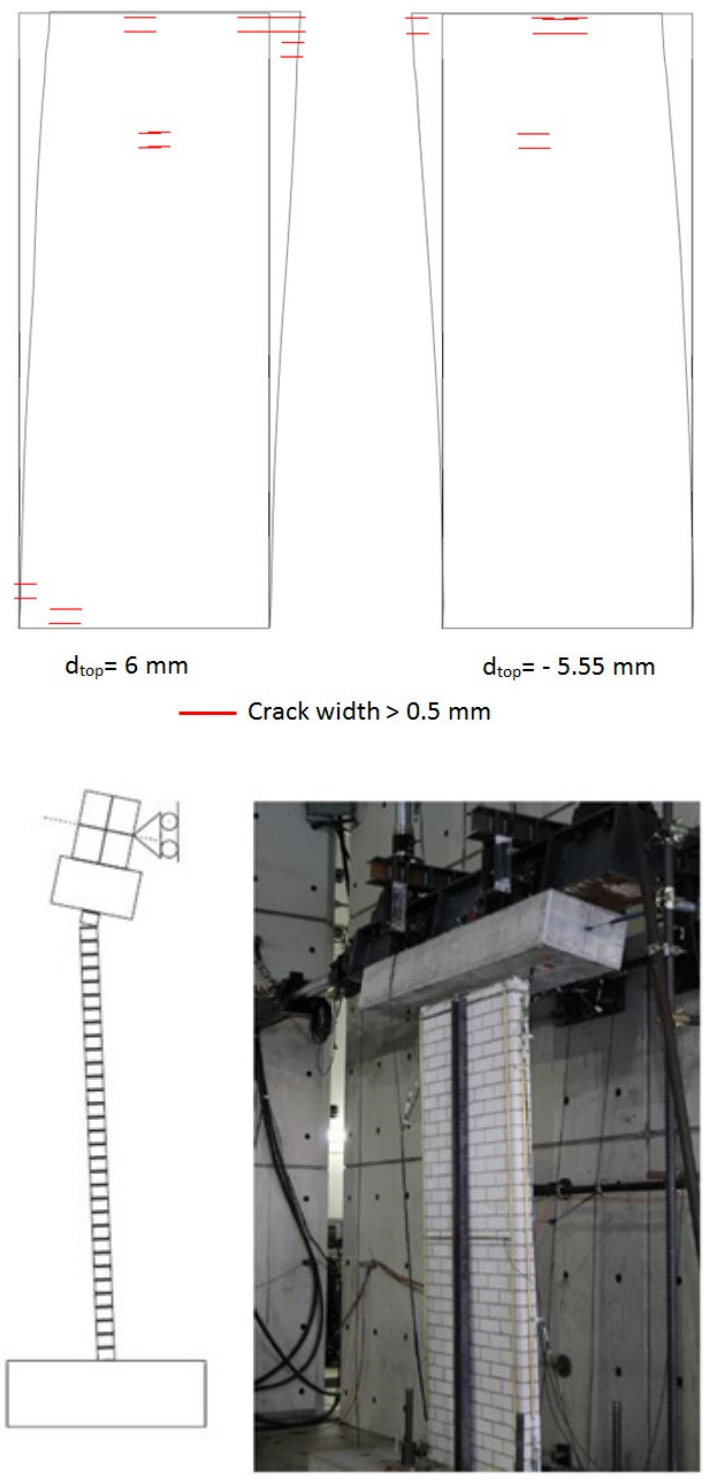

Figure 86: EUC-COMP-2: DIANA post-test refined prediction - Damage plot at end of analysis

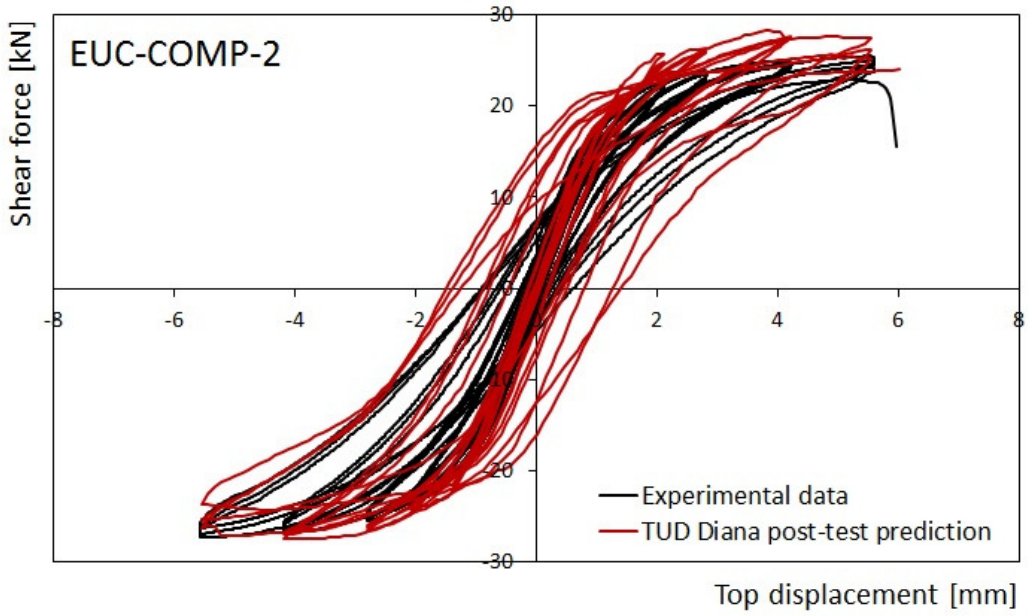

Figure 87: EUC-COMP-2: DIANA post-test refined prediction - Shear force-displacement curve

Table 33: EUC-COMP-2: DIANA post-test refined prediction - Summary table

Consultant	**Predominant Failure Mechanism Predicted**	**Initial Stiffness [kN/mm]**	**Peak Strength [kN]**	**Maximum Achieved Drift**	
DIANA	Rocking behaviour	17.5	28	0.2%	End of loading protocol
Test Result	Out of plane instability	24	27	0.2%	Premature out-of-plane failure

3.3.10 EUC-COMP-3

3.3.10.1 Test Description

EUC-COMP-3 was one of the three quasi-static in-plane tests administered by EUCENTRE. This specimen was a single-wythe wall constructed of calcium silicate units 102 mm thick. It was 4 m long and 2.75 m high. The applied overburden stress is 0.3 MPa. The wall was tested under cantilever boundary conditions.

As expected, specimen EUC-COMP-3 exhibited shear behaviour with diagonally oriented cracks. First cracks appeared after 0.05% drift.. These cracks progressively increased during the duration of the test. The test was stopped at a net drift of 0.3% due to partial collapse of the left side of the specimen.

0.05% drift

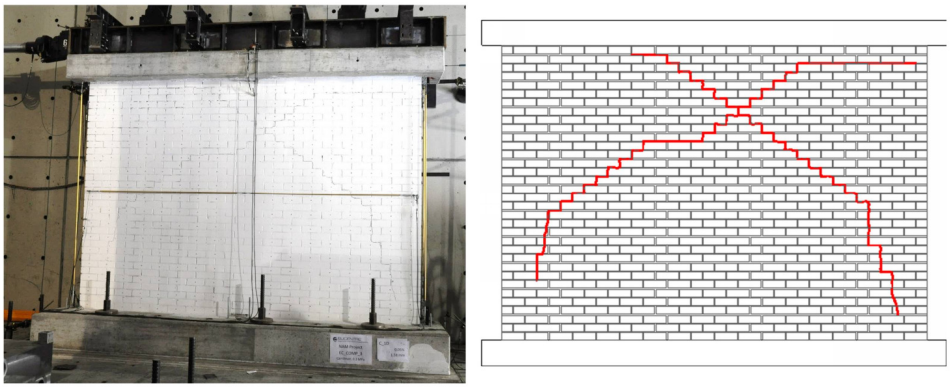

0.075% drift

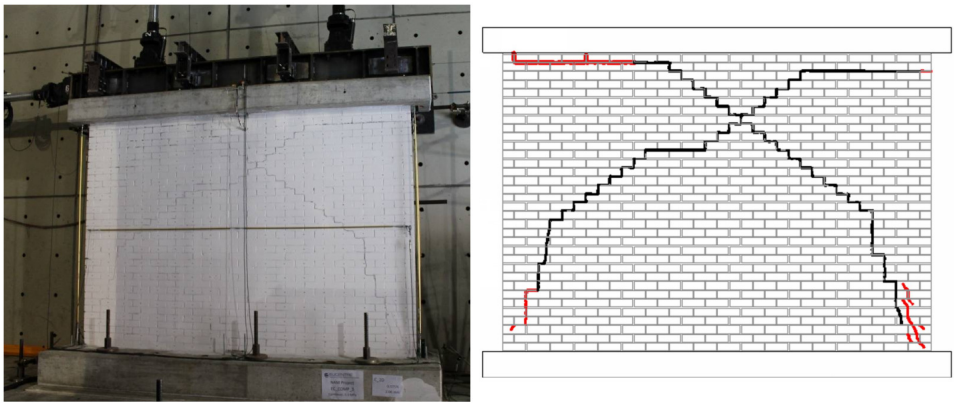

0.15% drift

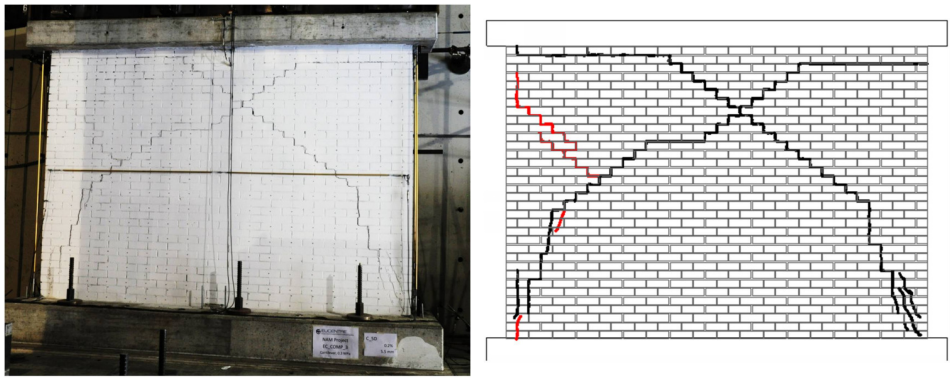

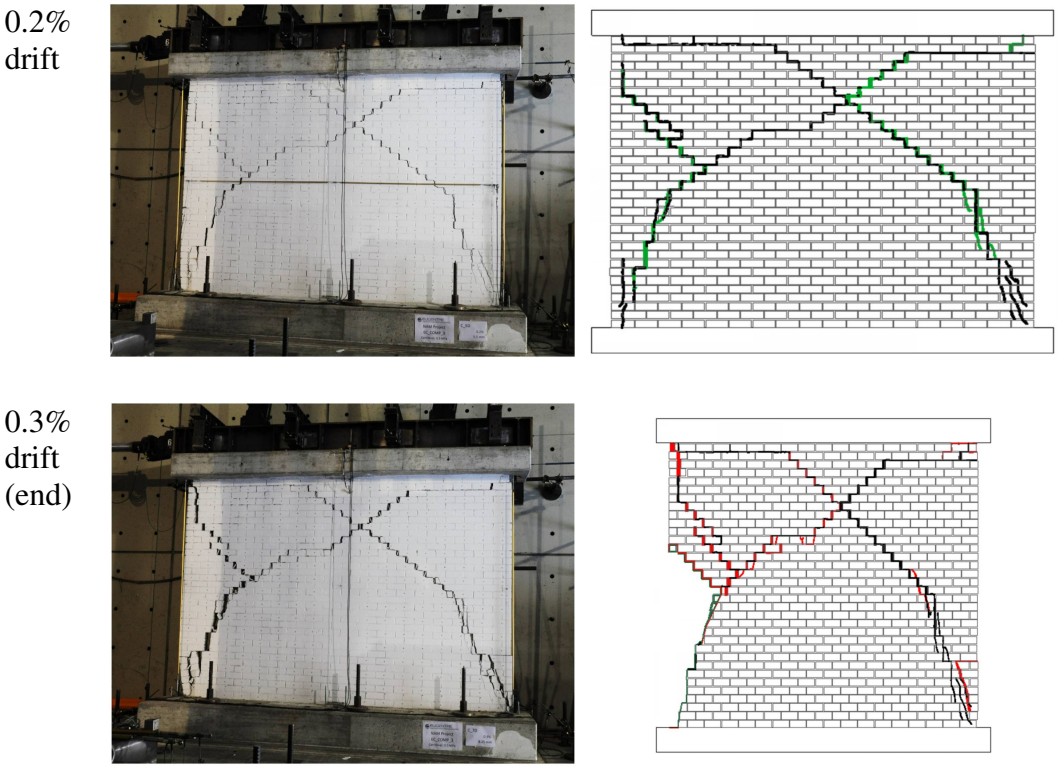

Figure 88: EUC-COMP-3: Progression of damage

See Figure 89 below for the shear force-displacement plot of the lab test result of EUC-COMP-3.

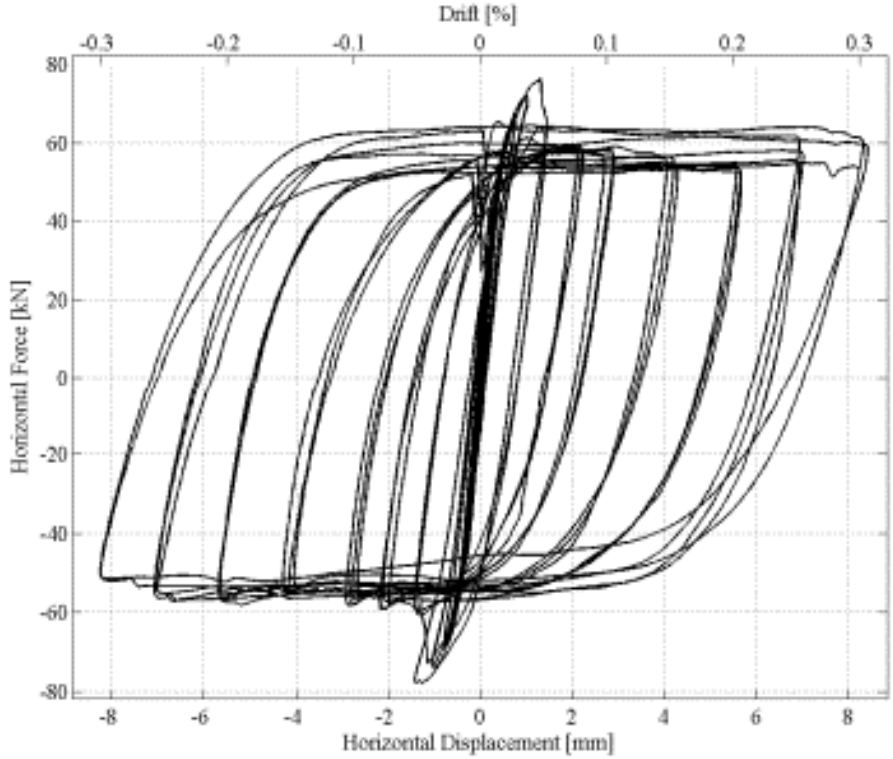

Figure 89: EUC-COMP-3: Lab test result – Shear force-displacement curve

3.3.10.2 Arup Post-Test Refined Prediction

The LS-DYNA model of EUC-COMP-3 correctly predicted a diagonal tensile initial failure mode as shown in Figure 90. However, at higher drift levels the failure mode in the analysis changed to bed joint sliding, and the analysis failed to predict the severe toe-crushing which occurred in corners of the specimen in the lab test. As with the other in-plane tests on squat walls the head joint gap sizes were much greater in the lab test than predicted by the analysis.

The lateral-force-versus-displacement relationship is shown in Figure 91. The ultimate load was slightly over-predicted (87 kN compared to 78 kN in the lab test). The hysteresis and energy absorption were reasonably well predicted.

In the laboratory, the test was stopped at 0.3% drift because the specimen was heavily damaged by toe-crushing and close to collapse. The analysis predicted that a near-collapse condition would not be reached until much higher drifts of 0.5 to 0.8% drift. It appears that diagonal tensile deformation is more damaging than assumed by the analysis. The mechanisms by which diagonal tensile deformation promotes progressively increasing opening of head joints, toe-crushing and cracking of bricks need to be understood and implemented in the material model.

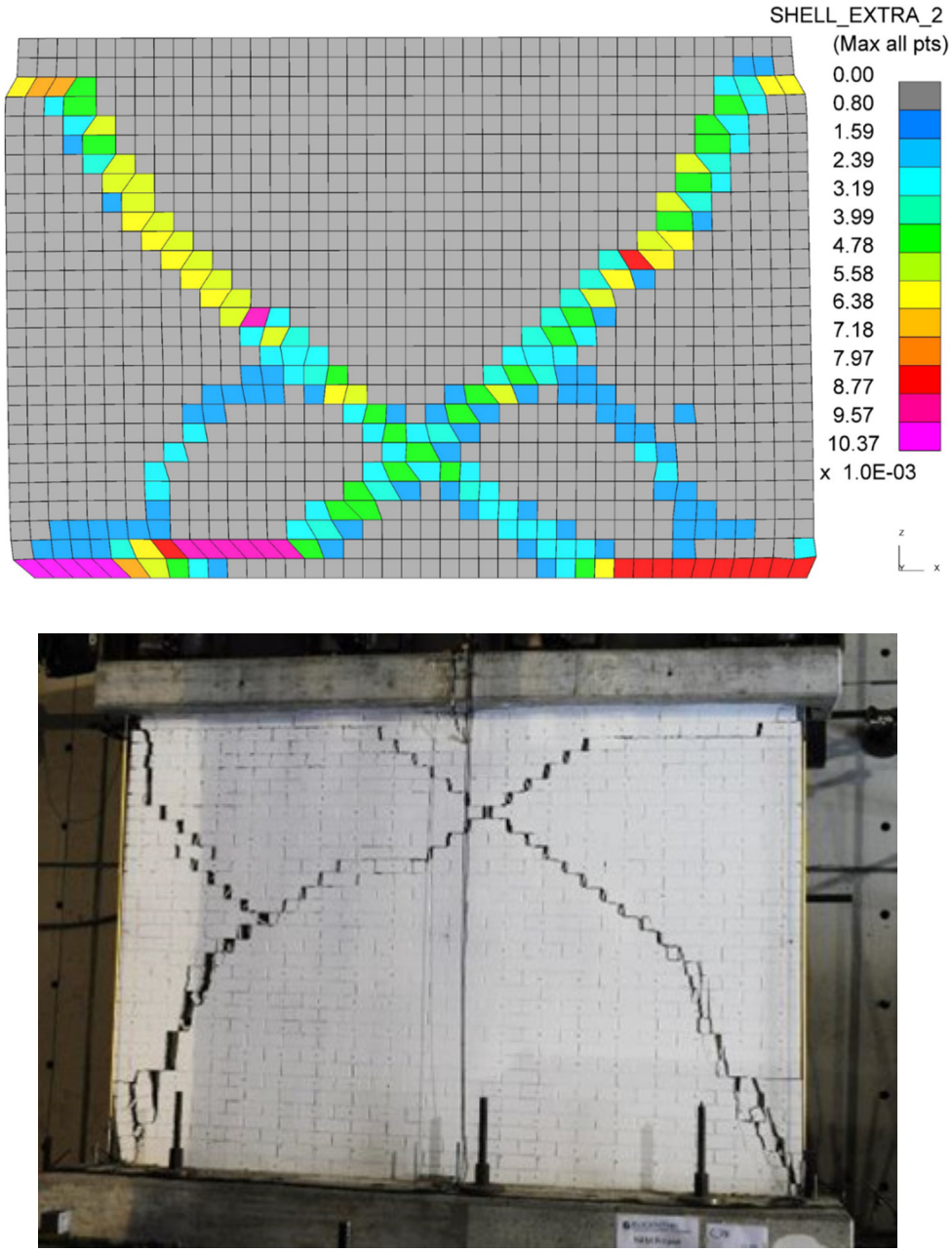

Figure 90: EUC-COMP-3: LS-DYNA post-test refined prediction - Damage plot at end of analysis

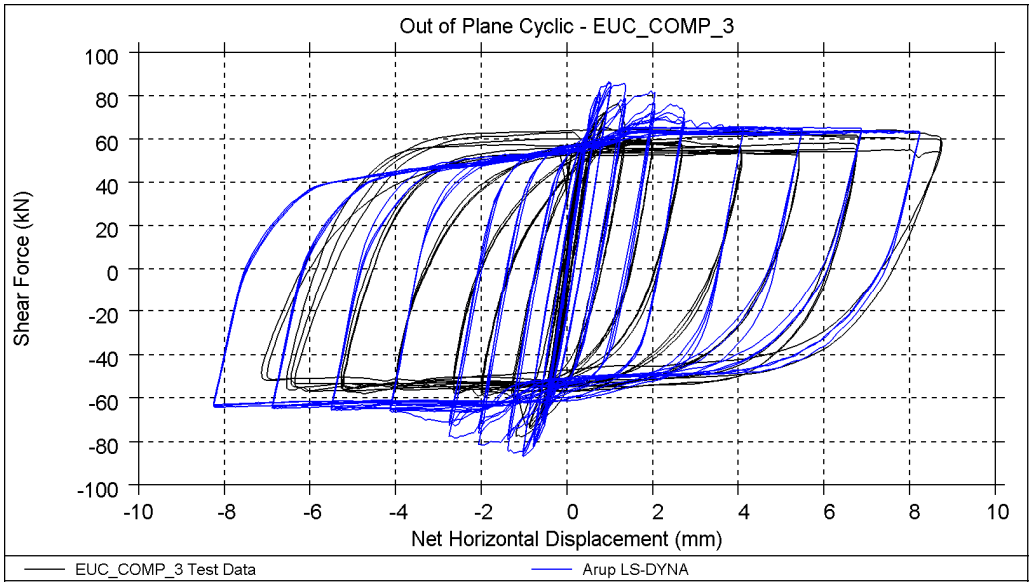

Figure 91: EUC-COMP-3: LS-DYNA post-test refined prediction - Shear force-displacement curve

Table 34: EUC-COMP-3: LS-DYNA post-test refined prediction - Summary table

Consultant	**Predominant Failure Mechanism Predicted**	**Initial Stiffness [kN/mm]**	**Peak Strength [kN]**	**Maximum Achieved Drift**	
LS-DYNA	Diagonal cracks / bed joint sliding	159	87	0.5% to 0.8%	Near collapse
Test Result	Diagonal cracks / toe crushing	152	78	0.3%	Near collapse

3.3.10.3 EUCENTRE Post-Test Refined Prediction

The shear force -displacement relationships are shown in Figure 92. The ultimate strength as well as the initial stiffness are well predicted by the TREMURI model. The hysteresis and energy dissipation are also well captured. (Figure 93).

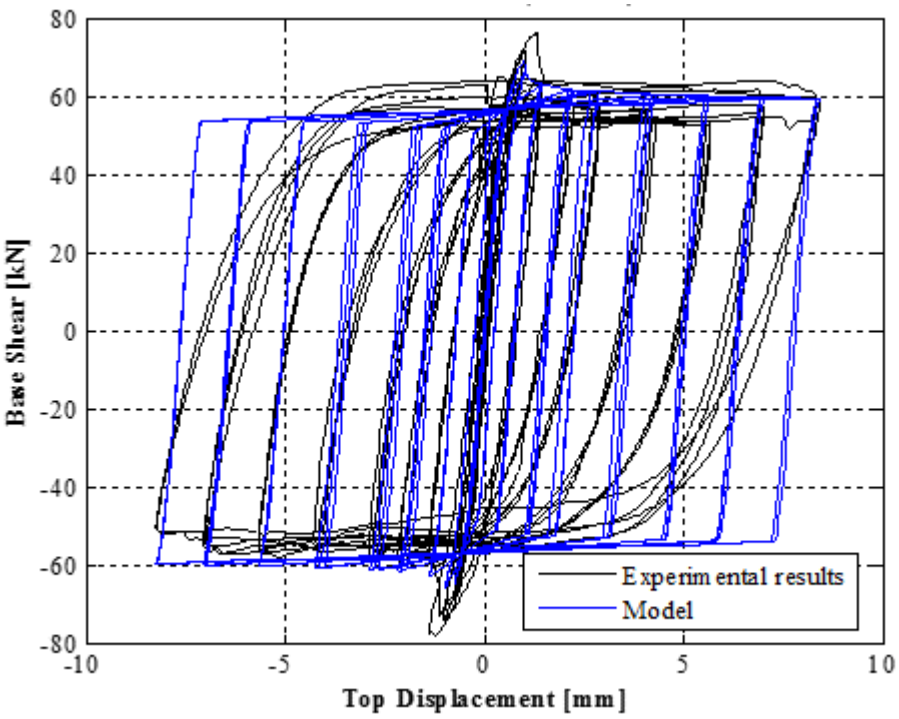

Figure 92: EUC-COMP-3: TREMURI post-test refined prediction - Shear force-displacement curve

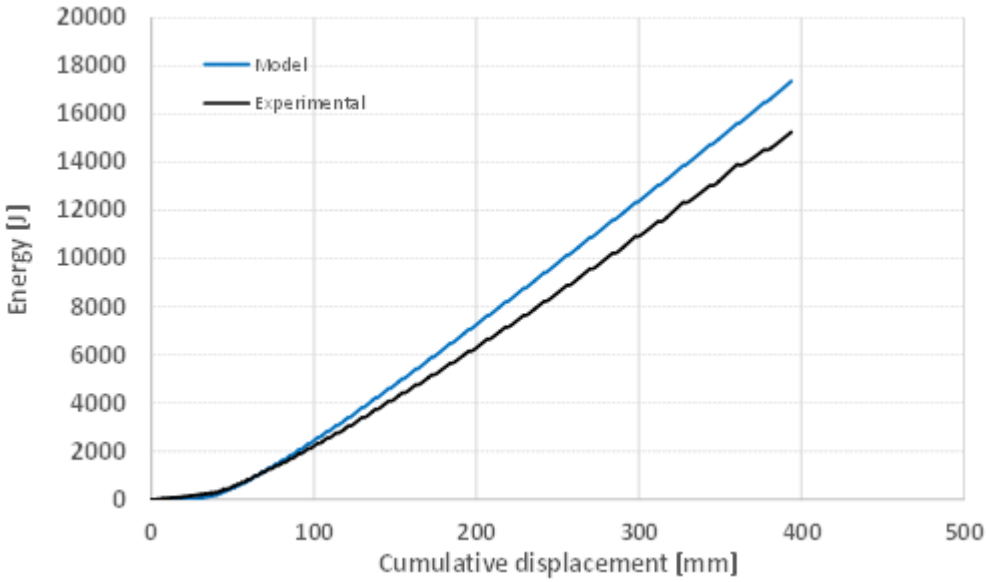

Figure 93: EUC-COMP-3: TREMURI post-test refined prediction – Work and dissipated energy

Table 35: EUC-COMP-3: TREMURI post-test refined prediction - Summary table

Consultant	**Predominant Failure Mechanism Predicted**	**Initial Stiffness [kN/mm]**	**Peak Strength [kN]**	**Maximum Achieved Drift**	
TREMURI	Shear	124	69.5	0.26%	
Test Result	Diagonal cracks / toe crushing	152	78	0.3%	Near collapse

3.3.10.4 TU-Delft Post-Test Refined Prediction

The DIANA model of EUC-COMP-3, with the application of the new material model, noticeably improved the prediction of the experimental behaviour of the panel. The real loading protocol has been applied with no convergence problems until larger displacements.

The numerical damage pattern is more extensive with respect to the experimental one (Figure 94). Most of the damage is in the middle of the panel, characterized by several diagonal (almost vertical) cracks, but it is not possible to completely identify the typical X-shaped cracks observed in the experiment.

The shear-displacement history is reported in Figure 95. The numerical peak shear capacity is 83 kN, quite close to the experimental value, which is equal to 78 kN.

With respect to the blind prediction, a larger energy dissipation is recorded with the new material model. The shear-displacement loops almost overlap the experiment curve for part of the test (top displacements < 4 mm), whereas in the last cycles a degradation of the ultimate capacity and a lower energy dissipation are observed.

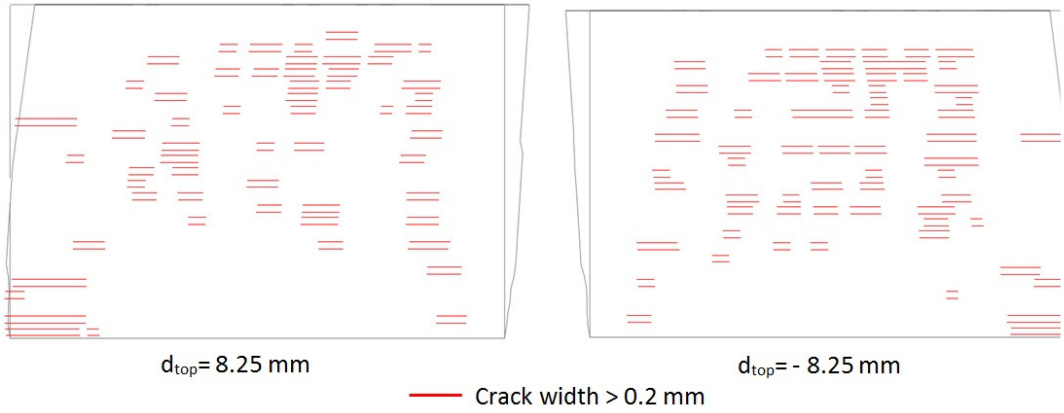

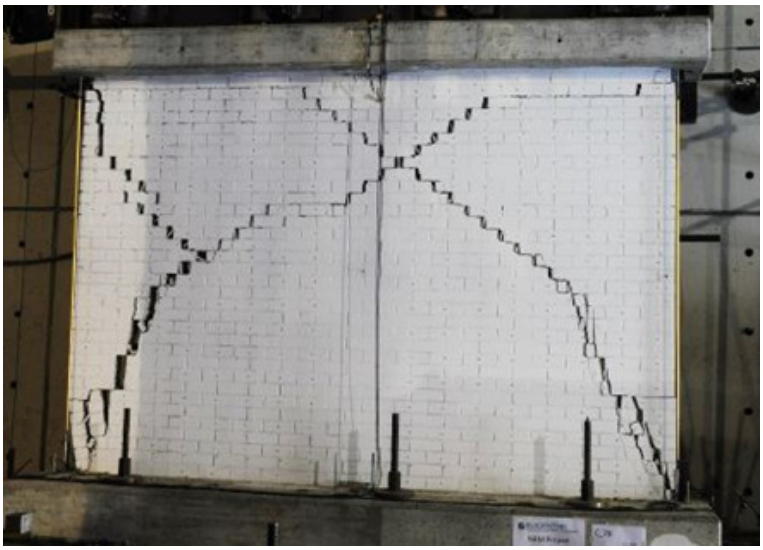

Figure 94: EUC-COMP-3: DIANA post-test refined prediction - Damage plot at end of analysis

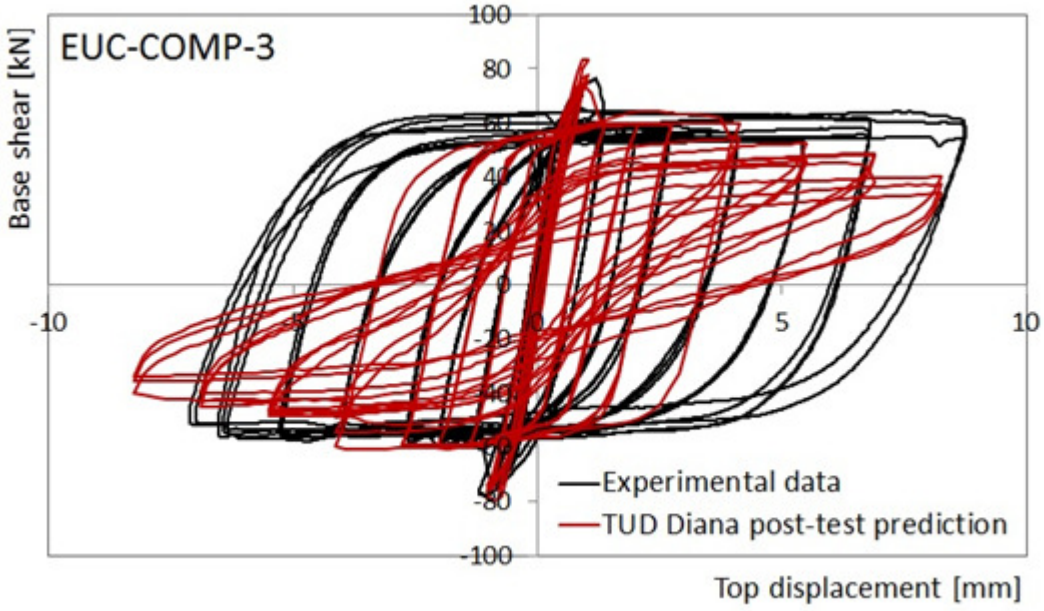

Figure 95: EUC-COMP-3: DIANA post-test refined prediction - Shear force-displacement curve

Table 36: EUC-COMP-3: DIANA post-test refined prediction - Summary table

Consultant	**Predominant Failure Mechanism Predicted**	**Initial Stiffness [kN/mm]**	**Peak Strength [kN]**	**Maximum Achieved Drift**	
DIANA	Diagonal cracks	110	83	0.3%	End of loading protocol / Extensive damage
Test Result	Diagonal cracks / toe crushing	152	78	0.3%	Near collapse

3.3.11 Summary

Table 37: Summary of post-test analyses of in-plane component tests

Component	LS-DYNA			TREMURI			DIANA			Test Result		
	Failure Mechanism	Peak Strength [kN]	Max Achieved Drift [%]	Failure Mechanism	Peak Strength [kN]	Max Achieved Drift [%]	Failure Mechanism	Peak Strength [kN]	Max Achieved Drift [%]	Failure Mechanism	Peak Strength [kN]	Max Achieved Drift [%]
TUD-COMP-0a	Rocking behaviour / toe crushing	28	0.9 to 1.0	Rocking behaviour / toe crushing	28.4 (*)	0.93 (*)	Rocking / cracks the middle of panel	28.2	0.9	Rocking behaviour / toe crushing	30	0.9
TUD-COMP-1	Rocking behaviour / toe crushing	10.9	1.6 to 1.8	Rocking	10.3 (*)	1.6 (*)	Rocking behaviour	11.8	1.6	Rocking behaviour / toe crushing	9.5	1.6
TUD-COMP-2	Rocking behaviour / toe crushing	14.2	1.2 to 1.5	---	---	---	Rocking behaviour	15.8	0.9	Rocking behaviour / toe crushing	10	0.9
TUD-COMP-3	Rocking behaviour / toe crushing	18	1.7 to 1.8	Rocking	17.6 (*)	1.3 (*)	Rocking / cracks in middle of panel	18.3	1.3	Rocking behaviour / toe crushing	15	1.3
TUD-COMP-4	Diagonal cracks / bed joint sliding	120	> 1.6 (no collapse))	Shear	114.1 (*)	0.2 (*)	Diagonal cracks	121.7	0.2	Diagonal cracks / toe crushing	119	0.2
TUD-COMP-5	Diagonal cracks / bed joint sliding	84	>1.0 (no collapse))	Shear/Sliding	103.3 (*)	0.46 (*)	Diagonal cracks	90.6	0.5	Diagonal cracks / bed joint sliding / toe crushing	103	0.5
TUD-COMP-6	Diagonal cracks / bed joint sliding	113	0.5 to 0.7	Shear	97.2 (*)	0.56 (*)	Diagonal cracks	104.6	0.6	Diagonal cracks / toe crushing	110	0.6
EUC-COMP-1	Rocking behaviour / toe crushing	22	1.1 to 1.2	Rocking	23.0 (**)	2.5 (**)	Rocking / cracks in middle of panel	21.8	2	Rocking behaviour / toe crushing	28	2
EUC-COMP-2	Rocking behaviour	27	>0.5 (no collapse)	Rocking	26.1	0.2	Rocking behaviour	28	0.2	Out of plane instability	27	0.2 (stopped due to instability
EUC-COMP-3	Diagonal cracks / bed joint sliding	87	0.5 to 0.8	Shear	69.5	0.26	Diagonal cracks	83	0.3	Diagonal cracks / toe crushing	78	0.3

(*) Value from the TREMURI “new model.” See section 3.2.2 for more information

(**) Value from TREMURI current model with reduction of effective height

4 Analysis Predictions of Out-of-Plane Component Tests

4.1 Blind Predictions for Out-of-Plane Component Tests

Blind prediction results are reported in a separate annex [13] to this report.

4.2 Changes to Analysis Models for Post-Test Refined Predictions of Out-of-Plane Component Tests

After receipt of the laboratory test results, the analysis models were updated. This section describes the changes made.

4.2.1 Arup changes to LS-DYNA models for out-of-plane post-test predictions

The out-of-plane models were updated to incorporate the most up-to-date input data. The differences compared to the blind prediction models are:

- The blind prediction LS-DYNA models used material properties from NAM's Basis for Design (Appendix A). The post-test models used the material properties of masonry measured by EUC and TUD. The material input data is identical to that used for the analyses of in-plane specimens - see Section 3.2.1.1 for more details.
- Material characteristics in the post-test analyses include better representation of non-linear behaviour in compression. This is described in Section 3.2.1.2.
- In the blind predictions, the wall ties were modelled as rigid links. In the post-test refined predictions they were modelled as deformable, using data from cyclic pull-out tests [6] and illustrated in Figure 96 below.
- The overburden loads, applied displacements (static tests) and applied ground motions (dynamic tests) were changed to reflect those actually applied during the tests.

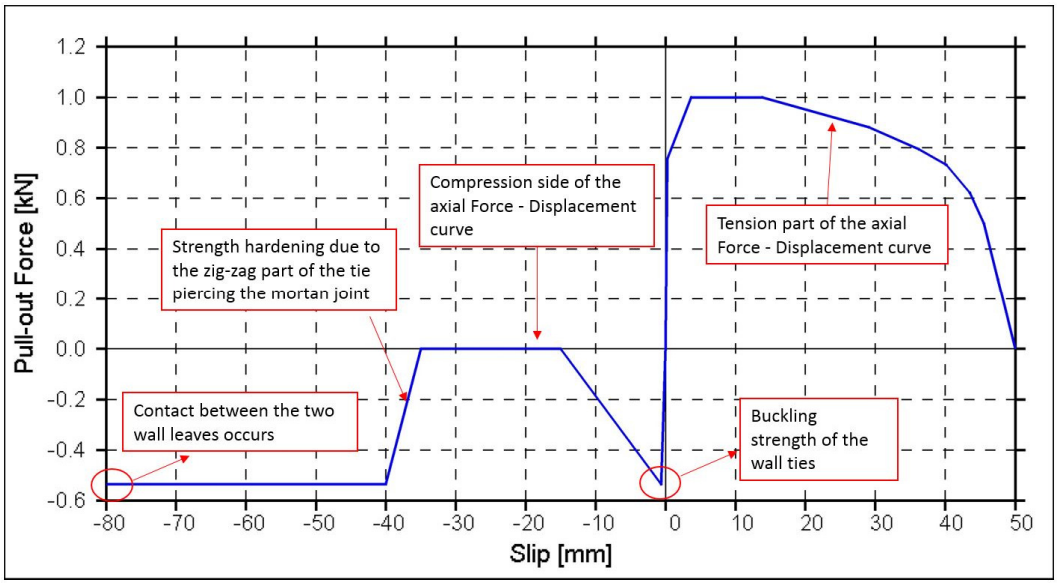

Figure 96: Force-vs-Slip constitutive relationship used to model the axial response of the wall ties in the LS-DYNA analysis

In the analyses of the dynamic tests, these assumptions were made:

- The motion was measured during the lab tests at different positions on the specimen and on the supporting structure. The acceleration time-histories measured at the foundation of the masonry specimens were used as input to the post-test refined LS-DYNA model. The only exception is component EUC-COMP-7 for which the accelerometer on the foundation was found not work properly during the test. It was suggested by EUCENTRE to use the shake table acceleration as an input motion for the simulation of that test.

  These motions were applied at both the top and the bottom of the specimen. Thus, it was assumed that deflection of the supporting frame was negligible.

- The dynamic tests consisted of three types of input motions:

  1. Ground Motion 1 (Gr_1) as from 'Groningen Record - Crowley et al'.
  2. Ground Motion 2 (Gr_2) as from the 'Floor Accelerograms (FA) obtained with TREMURI program (Gr_1 input, PGA 0.2g) assuming T1_STAR'.
  3. A 'Pulse Phase' consisting of a 'Ricker Wave Acceleration' signal, intended for calibration purposes.

  Ground motion 1 is sequentially applied with different scaling factors until the specimen is observed to crack.

  After cracking has occurred, an incremental dynamic input of the 'Ricker Wave Acceleration' is made and Gr_2 input accelerations are sequentially increased up to significant damage or collapse of the specimen.

- Only the Gr_1 and Gr_2 phases were modelled—it is assumed that the 'Ricker Wave Acceleration' signal phases has a negligible influence on the results of the Gr_1 and Gr_2 phases.
- The overburden load was applied as a constant force. The mass of the loading beam was ignored. In practice, vertical motion of the loading beam might have an influence on the response of the specimen.

All the post-test analyses were run using the October 2015 version of LS-DYNA's masonry material model.

4.2.2 EUCENTRE changes to TREMURI models for out-of-plane post-test predictions (dynamic only)

During the blind prediction exercise, a strong influence of damping model on the displacement demand was observed. Therefore, in order to first be able to accurately predict backbone curves, the attention was focused on the calibration of such static models. The proposed static models performed generally well.

4.2.3 TU Delft changes to DIANA models for out-of-plane post-test predictions

Differently from the in-plane models, the out-of-plane models adopted the same isotropic constitutive model already used during the blind-prediction analyses. The introduction of the constitutive model employed for the in-plane analyses should not determine any difference for the one-way bending tests, whereas it could allow a better prediction of the post-peak behaviour for the two-way bending tests.

Regarding all out-of-plane tests, the differences compared to the blind prediction models are:

- The blind prediction DIANA model used the material properties from NAM's Basis for Design (Appendix A). The post-test models used the material properties of masonry measured by EUC and TUD.
- The model has been changed from plane strain to shell element and the element type has been converted from discrete to continuum (smeared) crack model.

Regarding the dynamic out-of-plane tests, the main differences compared to the blind prediction model are:

- The time step is decreased from 0.0025 to 0.00125s. A ratio of 1/40 between the time step size and the period of the first out-of-plane mode is then achieved. Smaller time steps did not lead to any further significant improvement.
- A high number of sensitivity analyses suggested the choice of a small value for the shear retention factor ($\beta=10^{-4}$). Larger shear retention factors caused shear locking during the analyses and did not let the crack experience complete opening.

4.2.3.1 Material properties

DIANA out-of-plane component models used material properties reported in Table 38 and Table 39 for calcium silicate and clay masonry, respectively.

Table 38: Calcium silicate material properties used in DIANA blind predictions and post-test refined predictions of out-of-plane component tests

	NAM Basis for Design (used in blind prediction models unless noted otherwise)	**Measured properties (used in post-test models)**	
		EUC	TUD
Young's Modulus	3500 MPa	4182 MPa	5091 MPa
Compressive strength	6.0 MPa	6.2 MPa	5.9 MPa
Compressive behaviour	Elastic-perfectly-plastic	Stress-strain curve with softening	
Masonry flexural strength with moment vector parallel to bed joint and in plane of wall (f_{x1})	150 kPa (*)	238 kPa (*)	210 kPa
Bed joint shear strength (f_{v0})	300 kPa	210 kPa	140 kPa
Bed joint friction coefficient (μ)	0.75	0.42	0.43

(*) Assumed reported f_w properties

Table 39: Clay material properties used in DIANA blind predictions and post-test refined predictions of out-of-plane component tests

	NAM Basis for Design (used in blind prediction models unless noted otherwise)	**Measured properties (used in post-test models)**	
		EUC	TUD
Young's Modulus	6000 MPa	6033 MPa	6921 MPa
Compressive strength	8.0 MPa	11.3 MPa	14.7 MPa
Compressive behaviour	Elastic-perfectly-plastic	Stress-strain curve with softening	
Masonry flexural strength with moment vector parallel to bed joint and in plane of wall (f_{x1})	150 kPa (*)	158 kPa (*)	400 kPa
Bed joint shear strength (f_{v0})	300 kPa	150 kPa (+)	150 kPa
Bed joint friction coefficient (μ)	0.75	0.87 (+)	0.87

(*) Assumed reported f_w properties

(+) Properties not reported by EUC – data from TUD used.

4.3 Comparison of Post-Test Refined Predictions

4.3.1 TUD-COMP-0b

This test was stopped due to instability of the test system. It was repeated as TUD-COMP-7 with all the same boundary conditions. Therefore, analyses of TUD-COMP-0b are not reported.

4.3.2 TUD-COMP-7

4.3.2.1 Test Description

TUD-COMP-7 was the second quasi-static one-way out-of-plane test administered by TU-Delft. This specimen was a single-wythe wall constructed of calcium silicate units 102 mm thick. It was 1.4 metres long and 2.75 metres high. The applied overburden stress was 0.2MPa. The wall was tested under double clamped boundary conditions.

Loading was provided by airbags on either side of the specimen. The pressure in the airbags was controlled to provide the required displacement. The lateral load was measured via load cells attached to the reaction frame. See Figure 97 for a schematic of the test set-up.

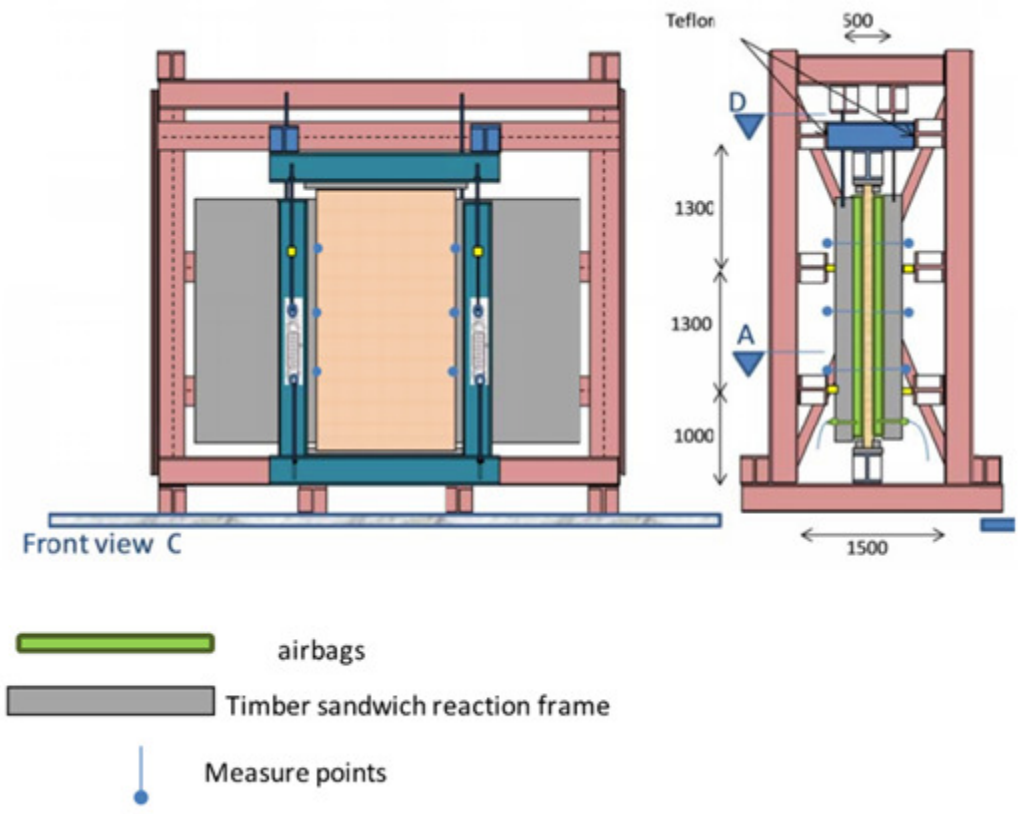

Figure 97: TUD-COMP-7: Schematic of test set-up

Figure 98: TUD-COMP-7: Final deflected shape of the (top) and cracks at top and bottom supports (bottom).

The measured hysteresis is shown in Figure 99.

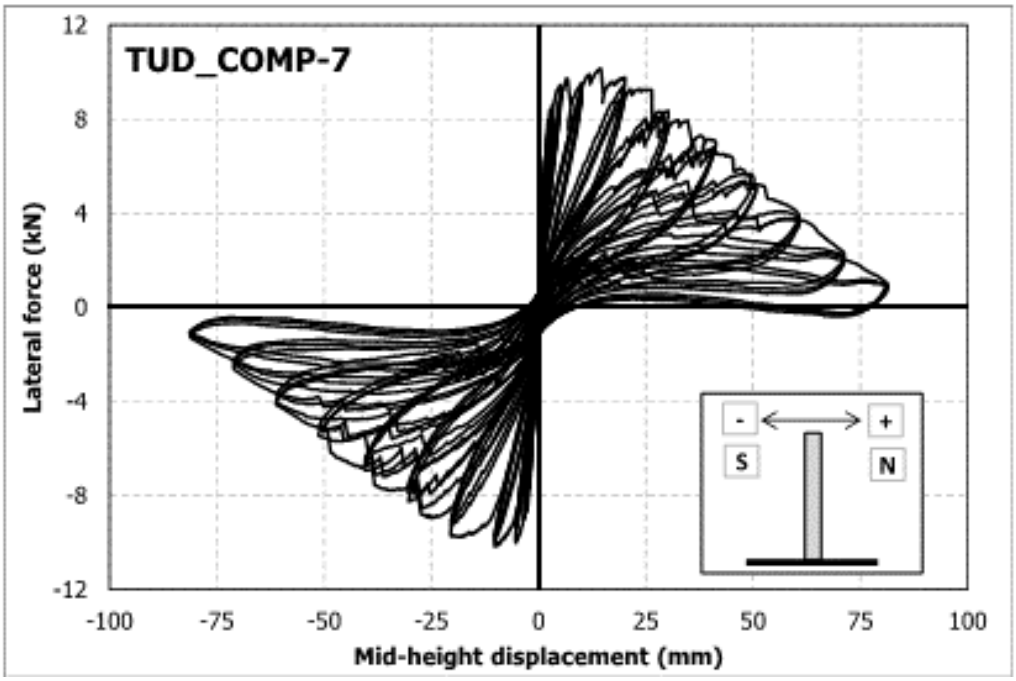

Figure 99: TUD-COMP-7: Lab test result – Applied force-mid-height displacement curve

4.3.2.2 Arup Post-Test Refined Prediction

The LS-DYNA analysis correctly predicts a three-point bending deformation mode with horizontal cracks at the top, bottom and mid-span as shown in Figure 100.

Compared with the lab test result, the initial resistance is over-predicted by 20%. The hysteresis curve from the analysis follows the form of the theoretical curve for out-of-plane rigid body rocking, with maximum lateral resistance being near-identical for all cycles and little energy absorbed in hysteresis. The test result, meanwhile, indicates a maximum lateral resistance that reduces with larger cycles and relatively large amounts of energy absorbed in hysteresis. Crushing of the mortar at the outer surfaces may explain the reduction of lateral resistance, i.e. the rectangular cross-section shape may become more rounded. Further study is needed to understand the mechanism by which the energy absorption occurs.

No conclusions can be drawn regarding predictions of collapse, because the specimen did not reach a near-collapse state in the lab test. Indeed, the test protocol was designed to exercise the specimen only within the theoretically-stable displacement limit for out-of-plane behaviour, which is equal to the thickness of the wall. Other analyses (not reported here) have confirmed that the LS-DYNA models do indeed collapse if out-of-plane displacement exceeds that limit.

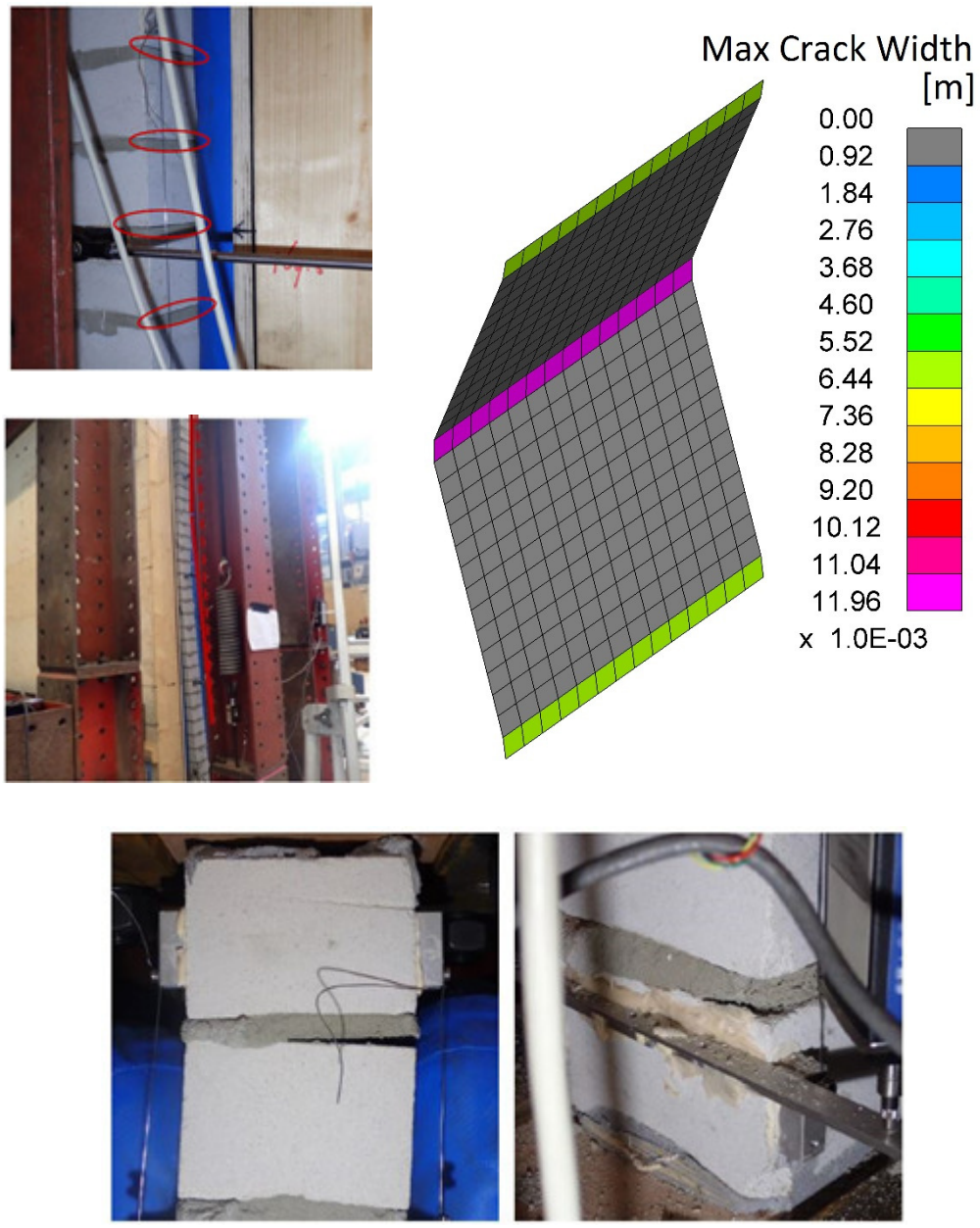

Figure 100: TUD-COMP-7: LS-DYNA post-test refined prediction - Damage plot at end of analysis

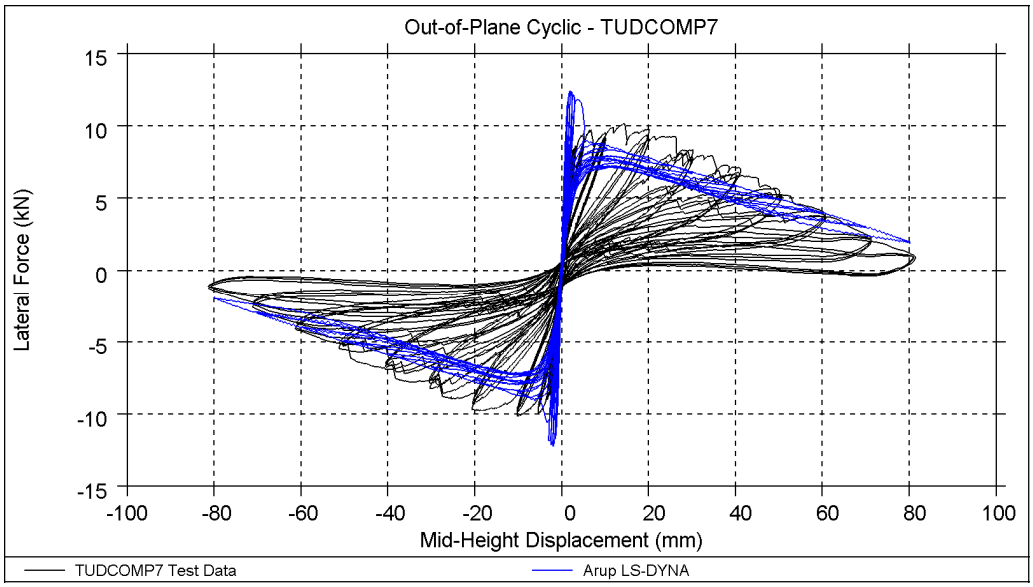

Figure 101: TUD-COMP-7: LS-DYNA post-test refined prediction - Shear force-displacement curve

Table 40: TUD-COMP-7: LS-DYNA post-test refined prediction - Summary table

Consultant	**Predominant Failure Mechanism Predicted**	**Initial Stiffness [kN/mm]**	**Peak Strength [kN]**	**Maximum Achieved Mid-Span Displacement [mm]**	
LS-DYNA	One-way out-of-plane failure	10	12.4	80	End of protocol
Test Result	One-way out-of-plane failure	4.5	10	80	End of protocol

4.3.2.3 EUCENTRE Post-Test Refined Prediction

As depicted in Figure 102, the red line represents the theoretical out-of-plane capacity of an infinitely strong rigid-body model, the green line is the TREMURI blind prediction, whereas the blue one is the theoretical estimate for the rigid-body model considering a limited compressive strength.

The blind prediction was not further refined because the experimental test results exceeded the theoretical upper bound (rigid block) in terms of force for displacement between 5 and 50 mm. This is probably due to an increase of the overburden load occurring when the wall was subjected to higher mid-height displacements.

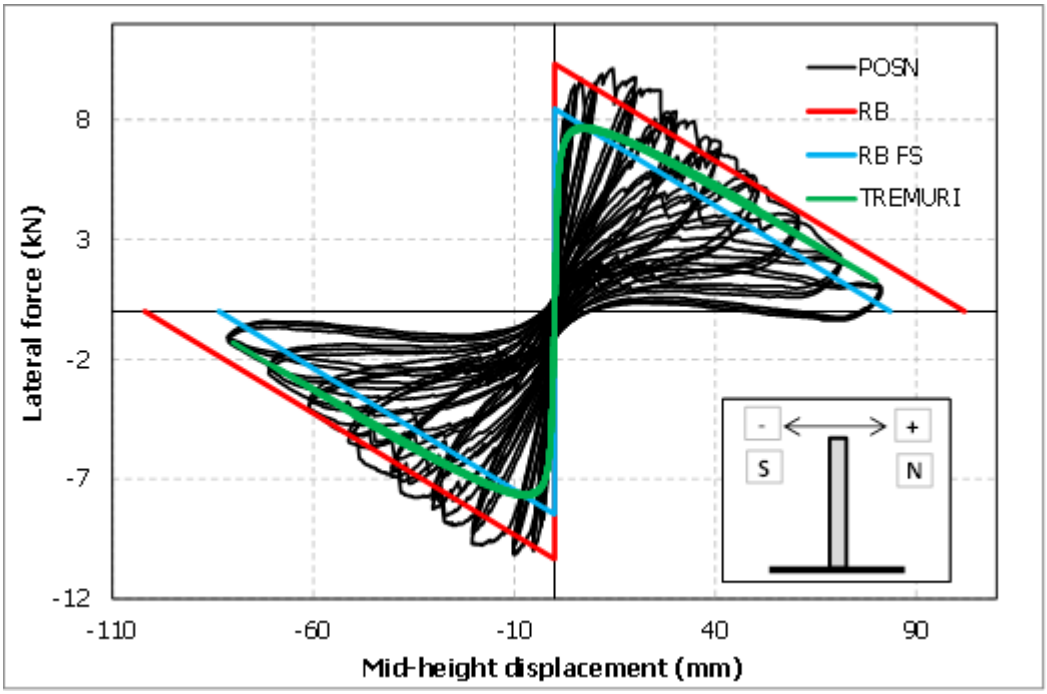

Figure 102: TUD-COMP-7: TREMURI post-test refined prediction - Shear force-displacement curve

4.3.2.4 TU-Delft Post-Test Refined Prediction

Given the symmetry of the test, a single vertical strip of the wall is modelled and subjected to monotonic pushover, as explained in section 4.2.3. The DIANA analysis correctly predicts a three-point out-of-plane rocking mechanism; cracks localise at the top, bottom and mid-span of the wall (Figure 103).

Compared with the lab test result, the initial resistance is correctly estimated. The post-peak phase is characterised by a gradual reduction of resistance for larger displacements that is mainly caused by second order effect and partially by the crushing of mortar at the level of the cracked elements that reduces the cross-section area.

The model could be pushed to the maximum displacement of 80 mm since the wall does not experience global instability during the entire loading history, which is also true of the tested specimen.

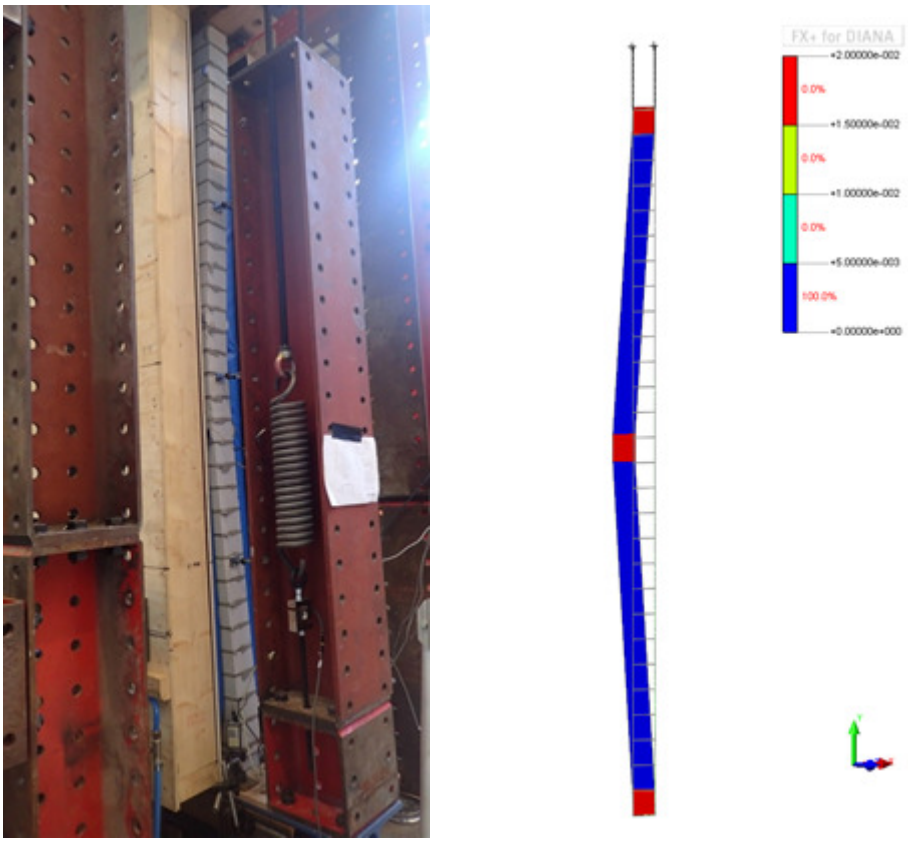

Figure 103: TUD-COMP-7: DIANA post-test refined prediction - Damage plot at end of analysis (tensile principal strains ε_1)

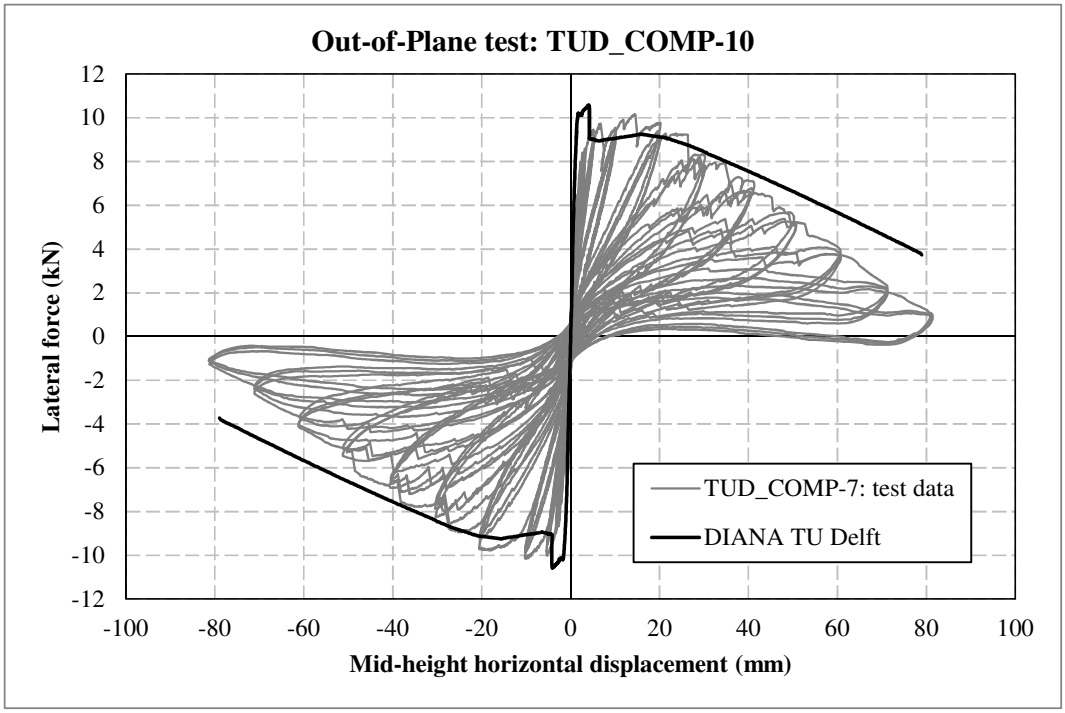

Figure 104: TUD-COMP-7: DIANA post-test refined prediction - Shear force-displacement curve

Table 41: TUD-COMP-7: DIANA post-test refined prediction - Summary table

Consultant	Predominant Failure Mechanism Predicted	Initial Stiffness [kN/mm]	Peak Strength [kN]	Maximum Achieved Mid-Span Displacement [mm]	
DIANA	One-way out-of-plane failure	8.3	10.5	80	End of protocol
Test Result	One-way out-of-plane failure	4.5	10	80	End of protocol

4.3.3 TUD-COMP-10

4.3.3.1 Test Description

TUD-COMP-10 was the fourth quasi-static out-of-plane test administered by TU-Delft. It was the second two-way out-of-plane test, in which rotation was fully fixed at the top and bottom but the wall was free to rotate in the out-of-plane direction along the vertical edges. The specimen was clamped at the bottom and top supports by gluing the top and bottom row of bricks to a plywood layer fixed to the top and bottom beam. The specimens were pinned on the vertical sides. This specimen was a single-wythe wall constructed of clay units 100 mm thick. It was approximately 4 metres long and 2.7 metres high. The top support to the specimen together with an applied vertical load give a uniform vertical overburden of 50 kPa.

Loading was provided by airbags on either side of the specimen. The pressure in the airbags was controlled to provide the required displacement. See

Figure 105 for a schematic of the test set-up.

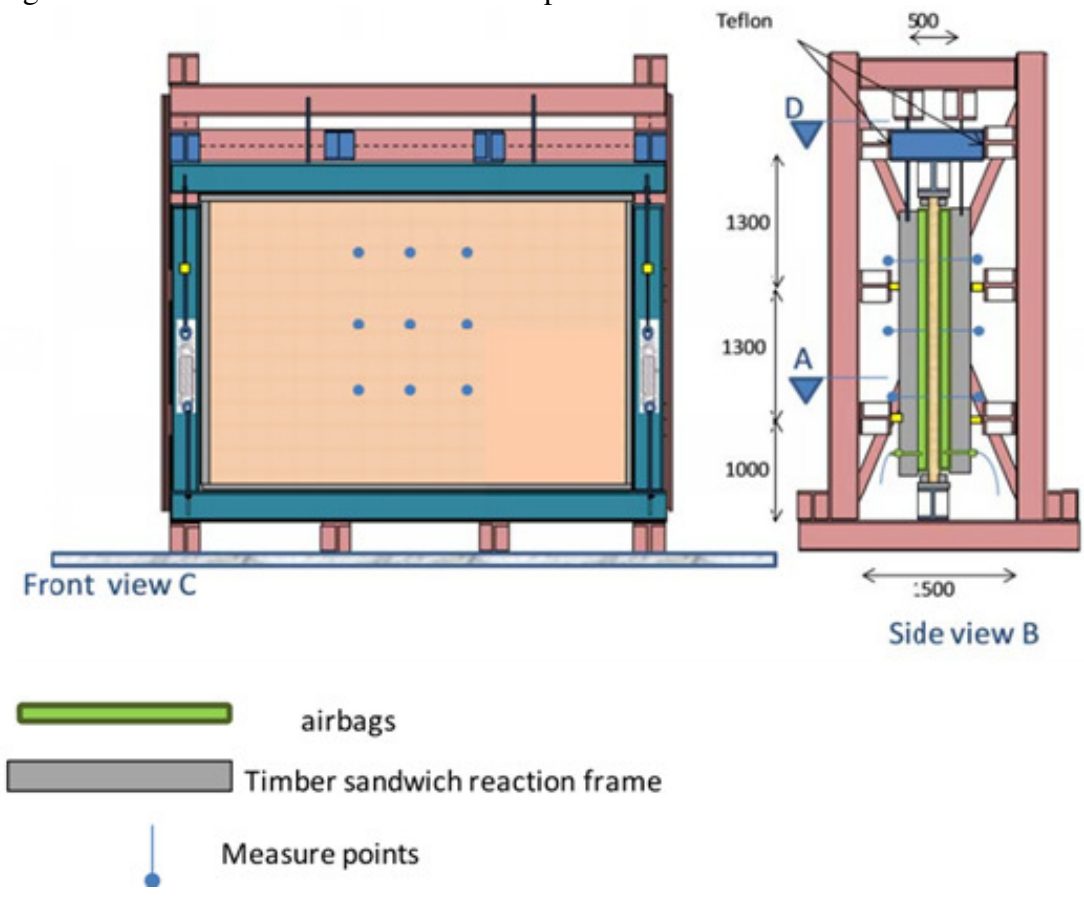

Figure 105: TUD-COMP-10: Schematic of test set-up

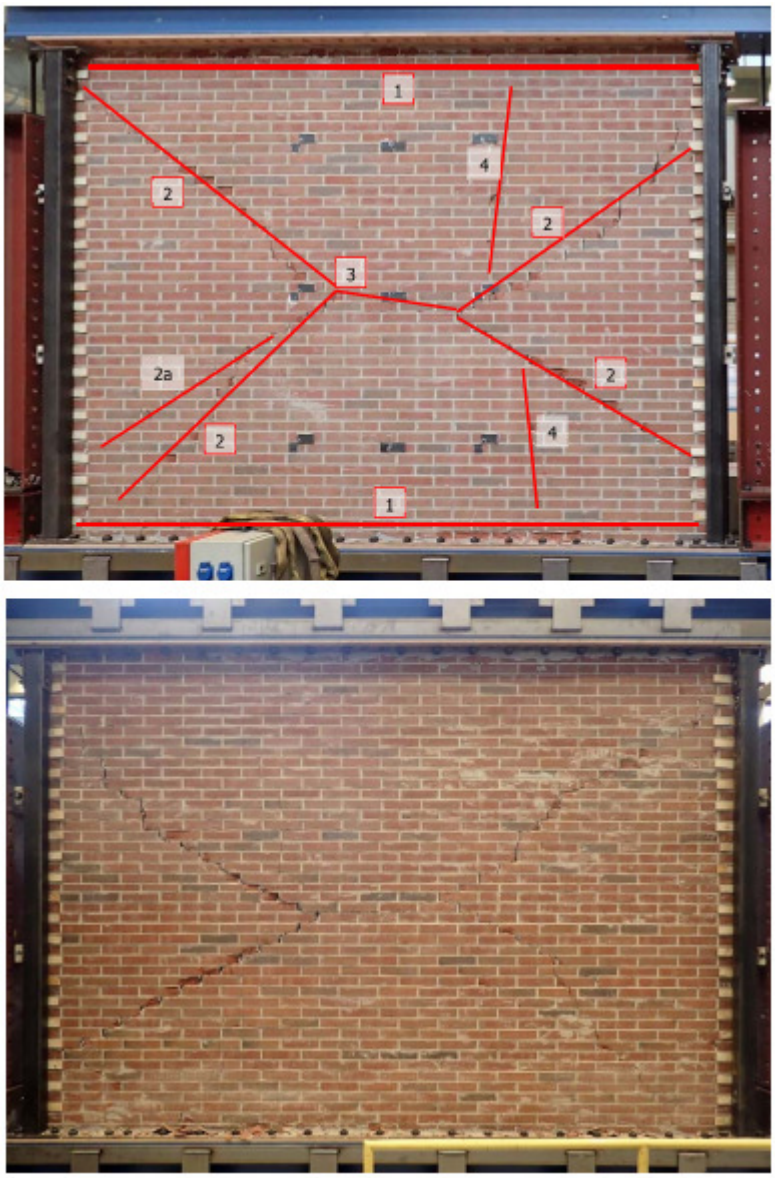

Figure 106: TUD-COMP-10: Final crack pattern of front side (top) and back side (bottom)

The measured hysteresis is shown in Figure 107.

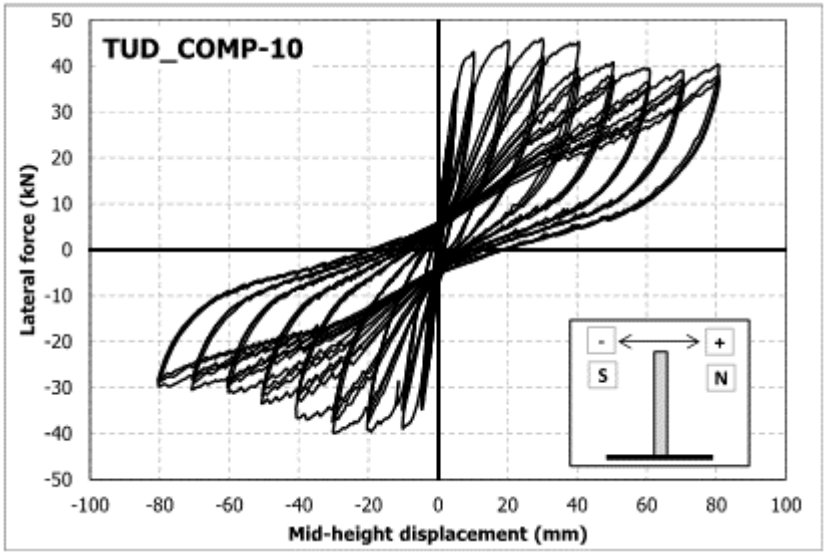

Figure 107: TUD-COMP-10: Lab test result – Applied force-mid-height displacement curve

4.3.3.2 Arup Post-Test Refined Prediction

The LS-DYNA prediction of two-way-spanning out-of-plane bending significantly under-estimates the resistance. The predicted strength (28 kN) is 60% of the measured value (46 kN) and the deformation mode fails to show the discrete diagonal and vertical cracks exhibited in the lab test. Resistance in two-way-spanning may be thought of as the total of resistance contributions from bending about horizontal and vertical axes. Although the LS-DYNA material model is reasonably accurate for bending about the horizontal axis, its bending response about the vertical axis is too weak.

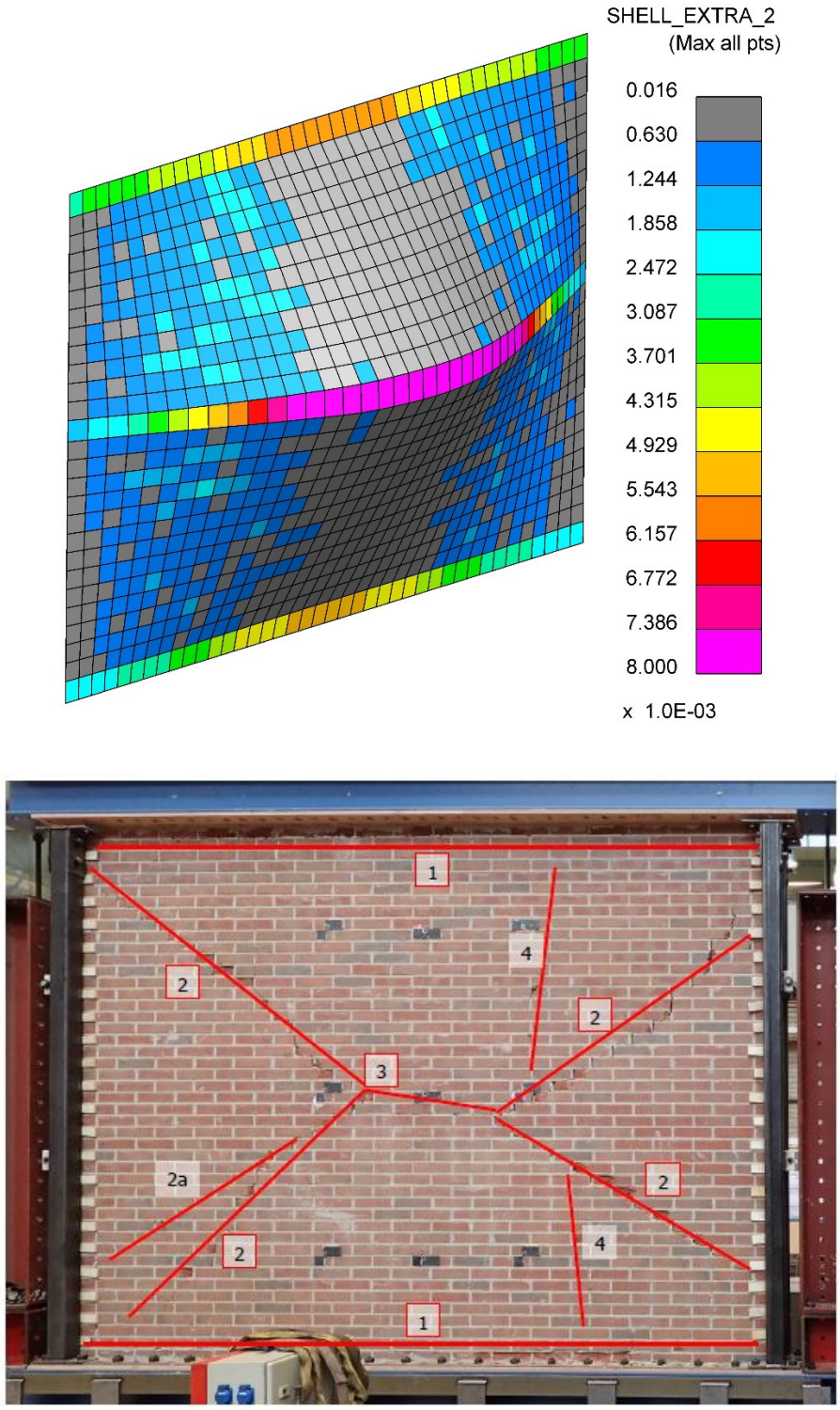

Figure 108: TUD-COMP-10: LS-DYNA post-test refined prediction - Damage plot at end of analysis

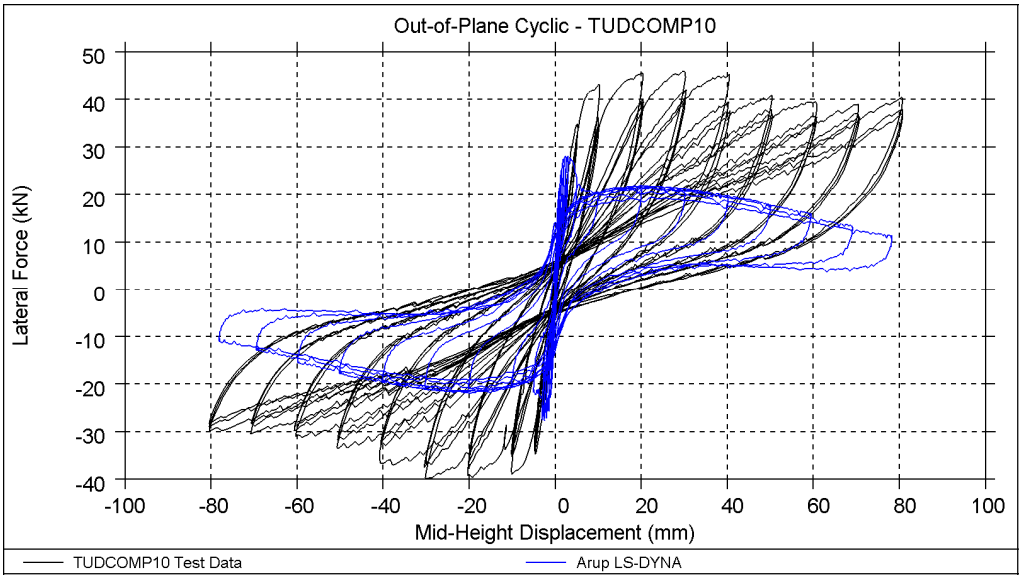

Figure 109: TUD-COMP-10: LS-DYNA post-test refined prediction - Shear force-displacement curve

Table 42: TUD-COMP-10: LS-DYNA post-test refined prediction - Summary table

Consultant	**Predominant Failure Mechanism Predicted**	**Initial Stiffness [kN/mm]**	**Peak Strength [kN]**	**Maximum Achieved Mid-Span Displacement [mm]**	
LS-DYNA	Two-way out-of plane failure	28.4	28	80	End of protocol
Test Result	Two-way out-of plane failure	12.9	46	80	End of protocol

4.3.3.3 EUCENTRE Post-Test Refined Prediction

Differently from what originally agreed, EUCENTRE provided some analytical calculations for specimens TUD-COMP-10 and TUD-COMP-11.

A calcium silicate (TUD-COMP-11) and clay (TUD-COMP-10) masonry solid walls were subject to quasi-static face load under a system of airbags. For each wall, Table 43 reports the main material properties, derived from characterisation tests [9]. In particular, the length, l_u, the height, h_u, and the thickness, t_u, of the units, the masonry weight density, γ, the flexural tensile strength, f_{mt}, and the lateral modulus of rupture, f_{ut}, are reported. The masonry Poisson's ratio resulted to be equal to 0.14 in the case of calcium silicate and 0.20 in the case of clay, respectively. Mortar joints were 10 mm thick.

Table 43: Main material properties

Wall	Type	l_u [mm]	h_u [mm]	t_u [mm]	γ [N/mm^3]	f_{mt} [MPa]	f_{ut} [MPa]
TUD-COMP-11	CS	214	71	102	$1.80 \cdot 10^{-5}$	0.36	2.74
TUD-COMP-10	Clay	210	50	100	$1.87 \cdot 10^{-5}$	0.14	4.78

Table 44 reports the dimensions (L_w, H_w) of each panel. The wall length, L_w, was taken from centre to centre of vertical supports. The wall height, H_w, was instead assumed as the distance between the bottom and top of the top and bottom rows of glued rows of bricks, respectively. The vertical pre-compression applied at the top, σ_v, is also reported. Figure 110 shows the geometry and support arrangement of the walls.

The AS 3700-Based and the Revised-Willis models were considered for predicting the ultimate strength. The degree of restraint of the vertical edges, Rf, was assumed equal to 0. Figure 111 compares the experimental strength values with the simulations obtained by Willis-based equations (red markers) and the Code-based equations (black markers). According to the Code, any moment contribution from vertical bending was initially ignored (Figure 111, left). It is observed that both the models underestimate the experimental values (Figure 111, left). The underestimation is more significant when the Revised-Willis model is exploited. As suggested by Vaculik [12], some residual moment capacity from horizontal cracks was then considered by assuming the crack to be opened together with idealised rigid rocking behaviour (Figure 111, right). Despite the inclusion of residual moment capacity of the horizontal cracks, the predictions still underestimate the experimental strength values. Such underestimation is higher in the case of the clay masonry specimen. Table 45 reports the ratio of the predicted and experimental ultimate strength, for each set of moment capacity equations.

Table 44: Dimensions and characteristics of the walls

Wall	Type	Wall dimensions		OBL
		Lw [mm]	Hw [mm]	σv [MPa]
TUD-COMP-11	CS	3920	2592	0.05
TUD-COMP-10	Clay	3960	2640	0.05

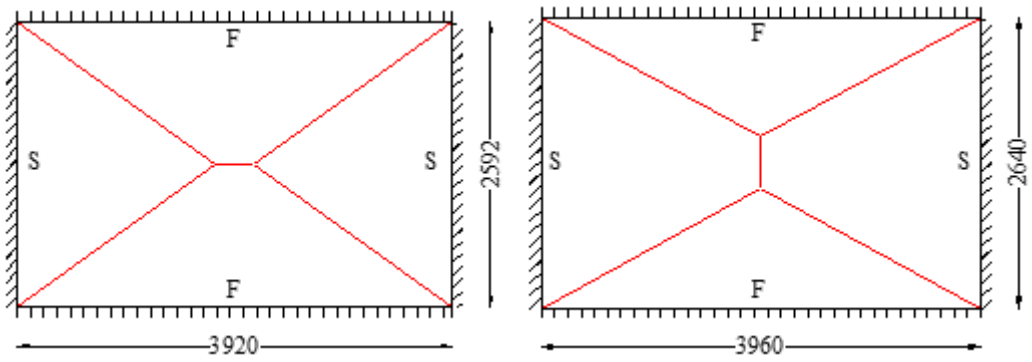

Figure 110: Wall dimensions, supports and superimposed crack pattern. Dimensions in mm. Calcium-silicate wall (left); Clay wall (right). S: simple support; F: fixed support.

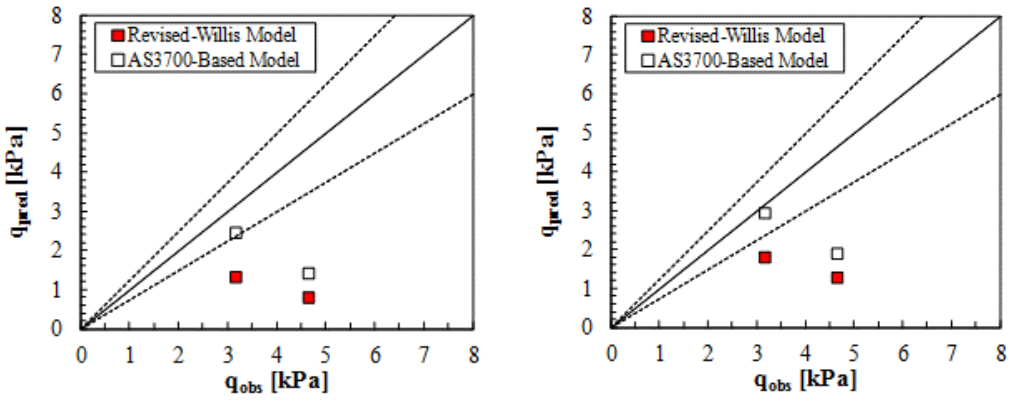

Figure 111: Experimental versus predicted ultimate strength. Moment contribution from horizontal cracks is ignored (left); residual capacity of horizontal cracks is accounted for (right).

Table 45: Ratios of the predicted and experimental ultimate strength

Wall	**q_{obs} [kPa]**	**Code-Based Model**		**Revised-Willis Model**	
		Horizontal cracks		Horizontal cracks	
		No contribution	Residual	No contribution	Residual
TUD-COMP-11	3.16	0.78	0.93	0.42	0.57
TUD-COMP-10	4.65	0.31	0.41	0.17	0.28

4.3.3.4 TU-Delft Post-Test Refined Prediction

This specimen is modelled and subjected to monotonic pushover, as explained in section 4.2.3. The DIANA analysis correctly predicts a two-way bending out-of-plane mechanism. As for the experimental crack pattern, the tensile principal strains highlight the localisation of cracks at the top and bottom of the wall, close to the clamped supports. Diagonal cracks develop from the corners to the centre of the panel with an angle of approximately 45°, and they are joined by a horizontal crack at mid-height of the wall (Figure 112). The predicted peak strength is underestimated (-13%) for positive loading, but very close to the measured value for the opposite direction (Figure 113).

A poor prediction of the post-peak behaviour is obtained: a sudden loss of resistance occurs immediately after the peak, followed by a more stable behaviour for larger displacements at approximately only half of the load measured for the experimental test. The isotropic model adopted in DIANA seems to not be able to properly represent the different cracking behaviour around horizontal and vertical axes. The development of an orthotropic material that allows to define different tensile strength and fracture energy in the vertical and horizontal directions is currently under investigation.

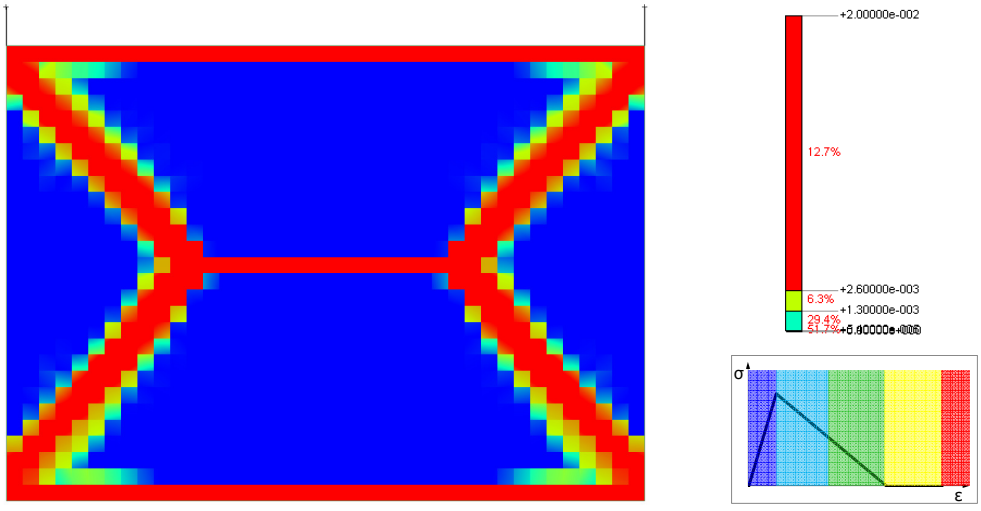

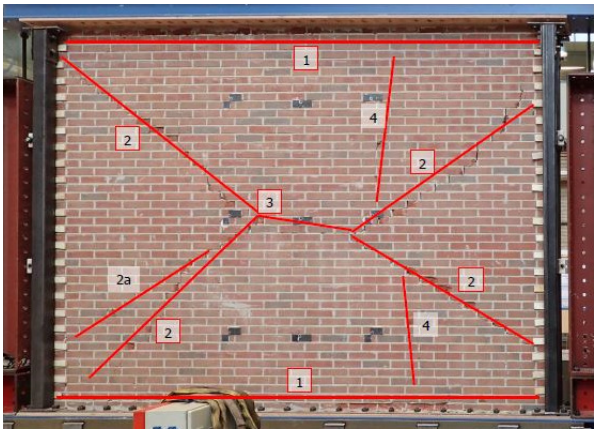

Figure 112: TUD-COMP-10: DIANA post-test refined prediction - Damage plot at end of analysis

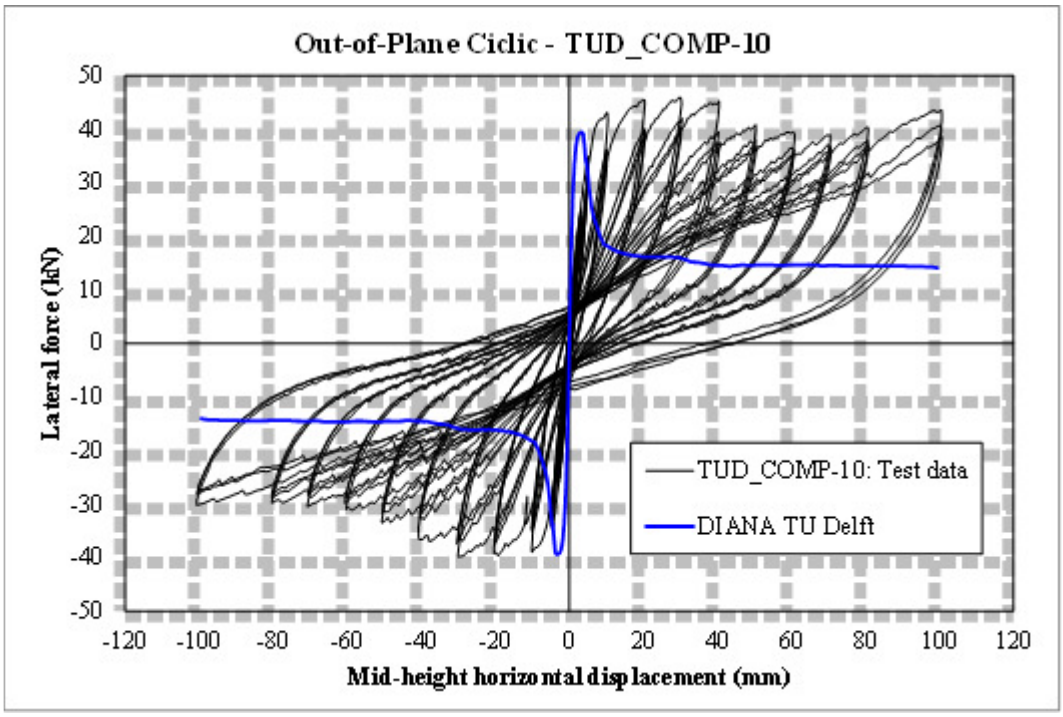

Figure 113: TUD-COMP-10: DIANA post-test refined prediction - Shear force-displacement curve

Table 46: TUD-COMP-10: DIANA post-test refined prediction - Summary table

Consultant	**Predominant Failure Mechanism Predicted**	**Initial Stiffness [kN/mm]**	**Peak Strength [kN]**	**Maximum Achieved Mid-Span Displacement [mm]**	
DIANA	Two-way out-of plane failure	35.8	39.5	100	End of protocol
Test Result	Two-way out-of plane failure	12.9	46	80	End of protocol

4.3.4 TUD-COMP-11

4.3.4.1 Test Description

TUD-COMP-11 was the third quasi-static out-of-plane test administered by TU-Delft. It was the first two-way out-of-plane test, in which rotation was fully fixed at the top and bottom but the wall was free to rotate in the out-of-plane direction along the vertical edges. This specimen was a single-wythe wall constructed of calcium silicate units 102 mm thick. It was approximately 4 metres long and 2.7 metres high. The top support to the specimen together with an applied vertical load give a uniform vertical overburden of 50 kPa.

Loading was provided by airbags on either side of the specimen, similar to TUD-COMP-10. The pressure in the airbags was controlled to provide the required displacement. See Figure 105 for a schematic of the test set-up.

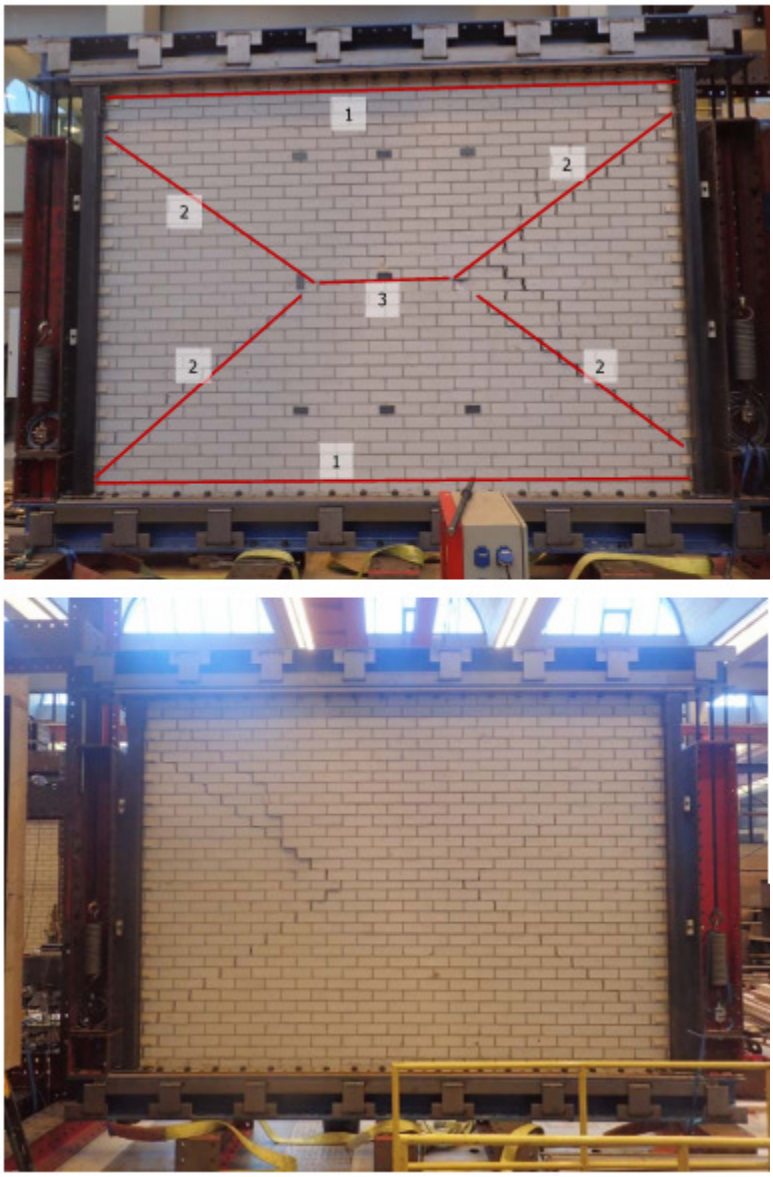

Figure 114: TUD-COMP-11: Final crack pattern of front side (top) and back side (bottom)

The measured hysteresis is shown in Figure 115.

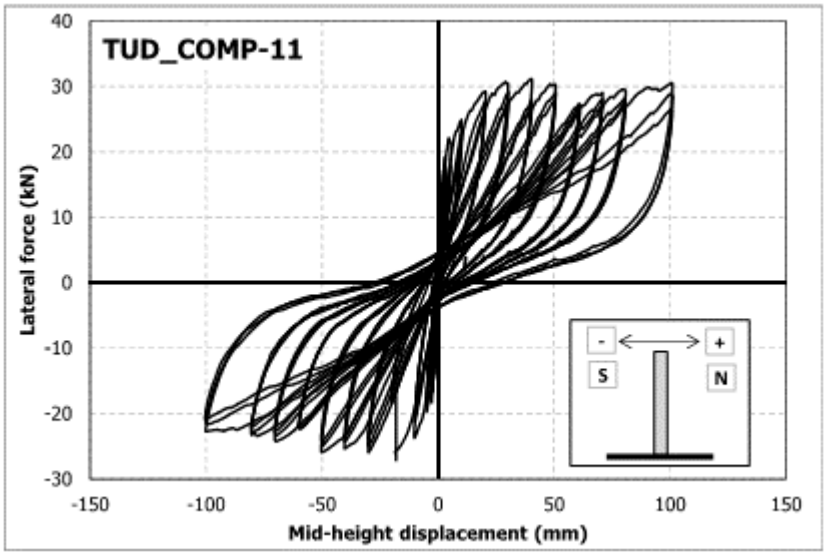

Figure 115: TUD-COMP-11: Lab test result – Applied force-mid-height displacement curve

4.3.4.2 Arup Post-Test Refined Prediction

As with TUD-COMP-10, the LS-DYNA prediction of two-way-spanning out-of-plane bending significantly under-estimates the resistance. The initial strength is predicted accurately but the subsequent hysteresis occurs at only around half the load measured in the laboratory. The deformation mode again fails to show the discrete diagonal cracks that were observed in the laboratory.

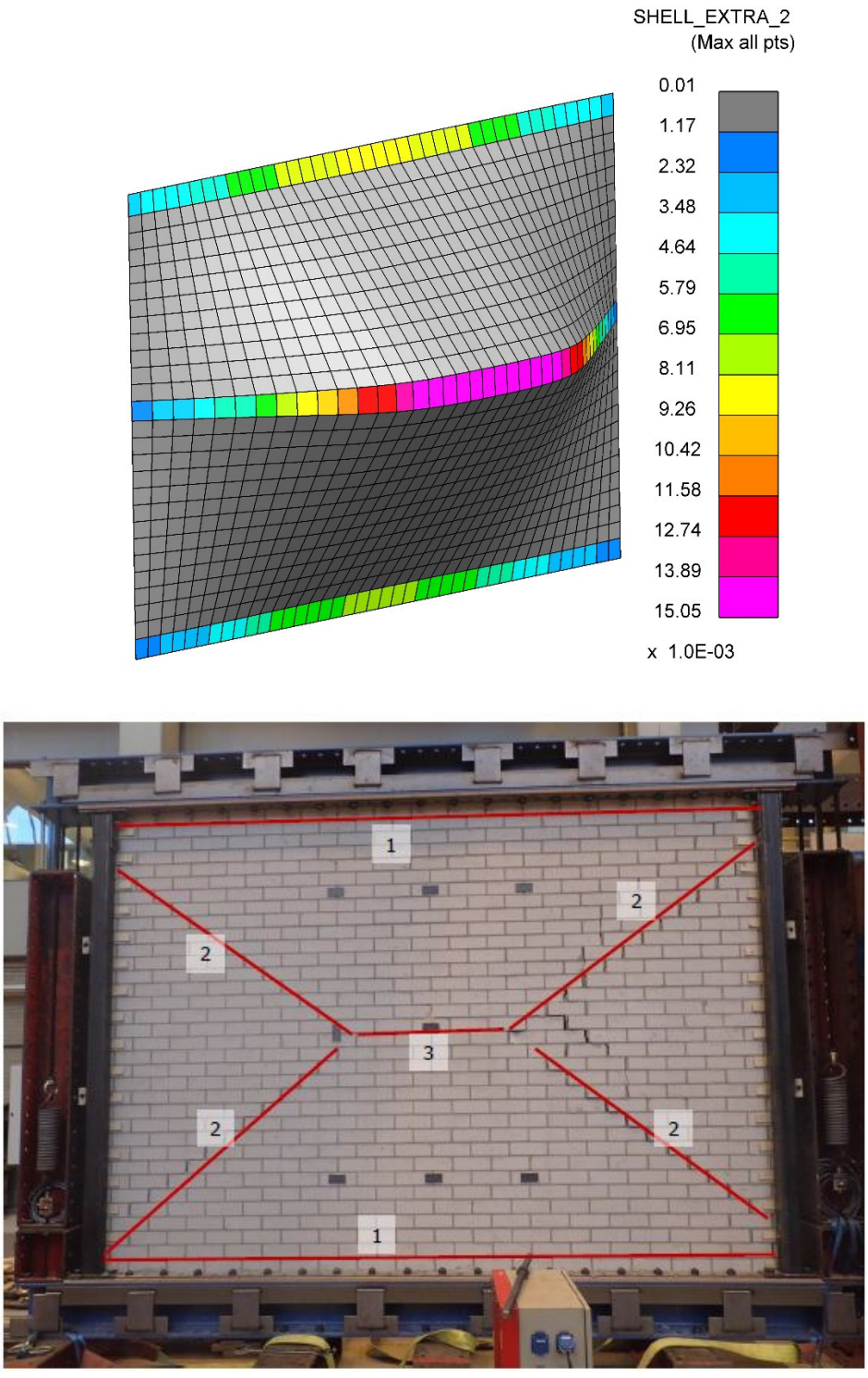

Figure 116: TUD-COMP-11: LS-DYNA post-test refined prediction - Damage plot at end of analysis

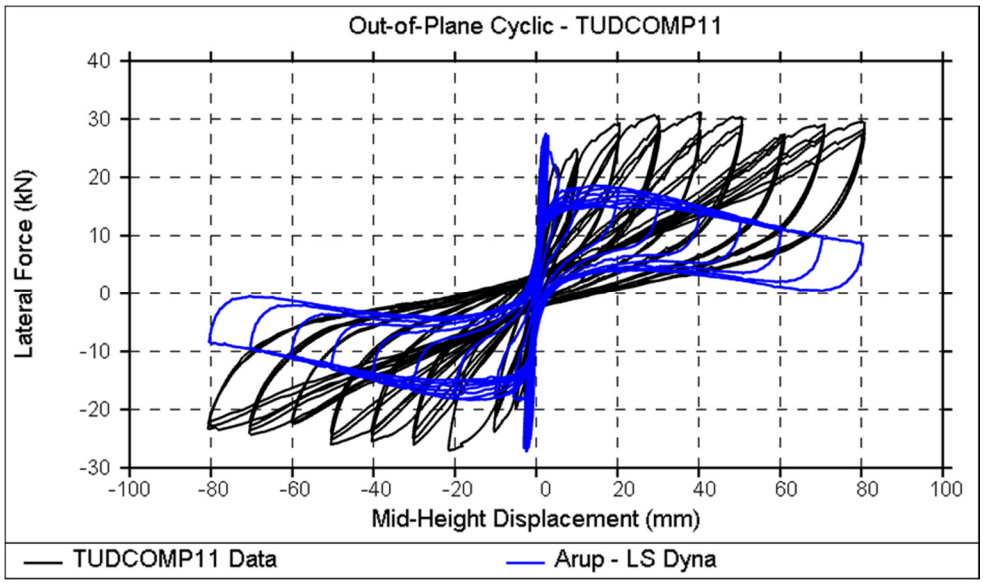

Figure 117: TUD-COMP-11: LS-DYNA post-test refined prediction - Shear force-displacement curve

Although the lab specimen was cycled up to a mid-height displacement of 100 mm, the measured hysteresis curve provided by TU-Delft only contains data up to a maximum mid-height displacement of 80 mm. This is also reflected in Table 47 below.

Table 47: TUD-COMP-11: LS-DYNA post-test refined prediction - Summary table

Consultant	**Predominant Failure Mechanism Predicted**	**Initial Stiffness [kN/mm]**	**Peak Strength [kN]**	**Maximum Achieved Mid-Span Displacement [mm]**	
LS-DYNA	Two-way out-of plane failure	27.8	28	80	End of provided protocol
Test Result	Two-way out-of plane failure	12	31	100	End of protocol

4.3.4.3 EUCENTRE Post-Test Refined Prediction

See Section 4.3.3.3 for TUD-COMP-10.

4.3.4.4 TU-Delft Post-Test Refined Prediction

This specimen is modelled and subjected to monotonic pushover, as explained in section 4.2.3. As for TUD-COMP-10, the DIANA analysis correctly predicts a two-way bending out-of-plane mechanism (Figure 118). The predicted strength is underestimated for both positive (-20%) and negative (-7%) loading directions (Figure 119). Again, a poor prediction of the post-peak behaviour is obtained: a sudden loss of resistance occurs immediately after the peak, followed by a more stable behaviour for larger displacements at approximately only a third of the load measured for the experimental test. As for TUD-COMP-10, the development of an orthotropic material that allows one to define different tensile strength and fracture energy in the vertical and horizontal directions is currently under investigation.

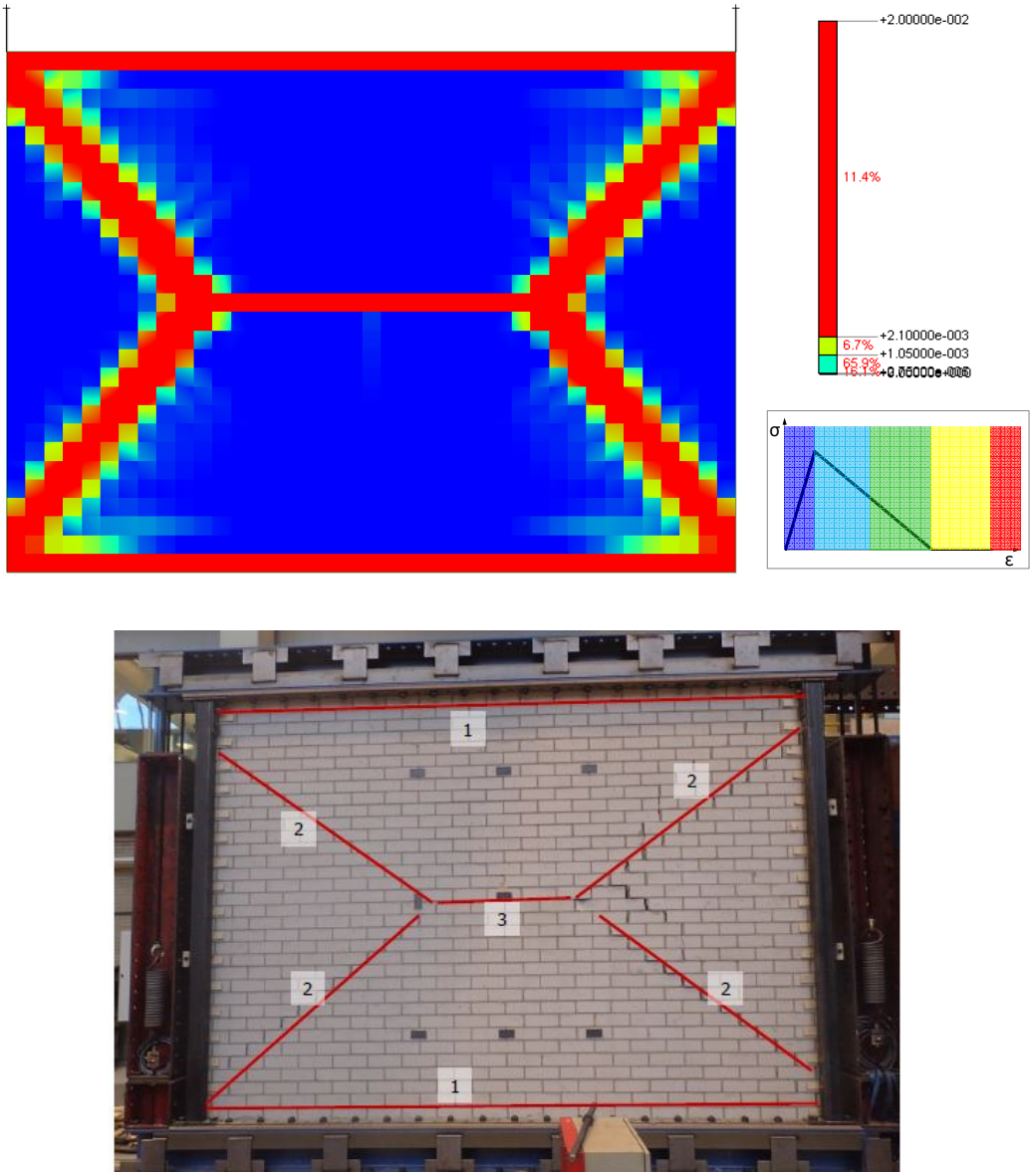

Figure 118: TUD-COMP-11: DIANA post-test refined prediction - Damage plot at end of analysis

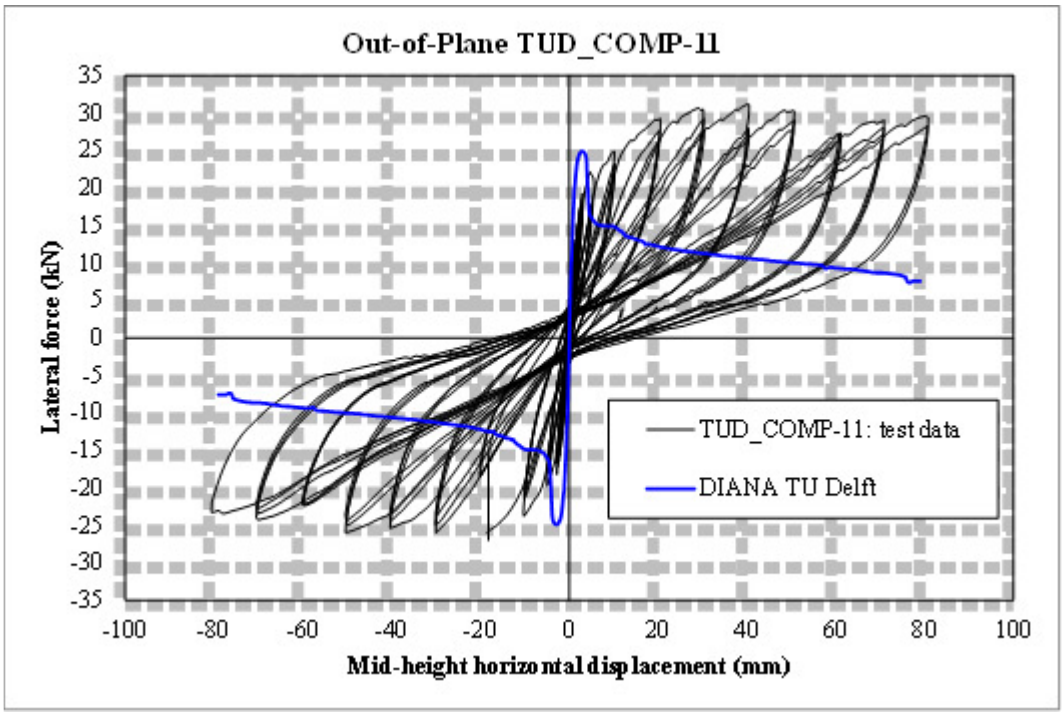

Figure 119: TUD-COMP-11: DIANA post-test refined prediction - Shear force-displacement curve

Table 48: TUD-COMP-11: DIANA post-test refined prediction - Summary table

Consultant	Predominant Failure Mechanism Predicted	Initial Stiffness [kN/mm]	Peak Strength [kN]	Maximum Achieved Mid-Span Displacement [mm]	
DIANA	Two-way out-of plane failure	23	25	100	End of protocol
Test Result	Two-way out-of plane failure	12	31	100	End of protocol

4.3.5 TUD-COMP-12

4.3.5.1 Test Description

TUD-COMP-12 was the fourth quasi-static out-of-plane test administered by TU-Delft. It was a two-way out-of-plane test, in which rotation was fully fixed at the top and bottom but the wall was free to rotate in the out-of-plane direction along the vertical edges. This specimen was a single-wythe wall constructed of calcium silicate units 102 mm thick. It was approximately 4 metres long and 2.75 metres high with a large single opening. The applied overburden was 50 kPa.

Loading was provided by airbags on either side of the specimen. The pressure in the airbags was controlled to provide the required displacement. The force on the wall was calculated from the difference in pressure of the airbags on either side. Therefore, the measured force includes an assumption concerning the area loaded by the airbags.

See Figure 120 for a schematic of the test set-up.

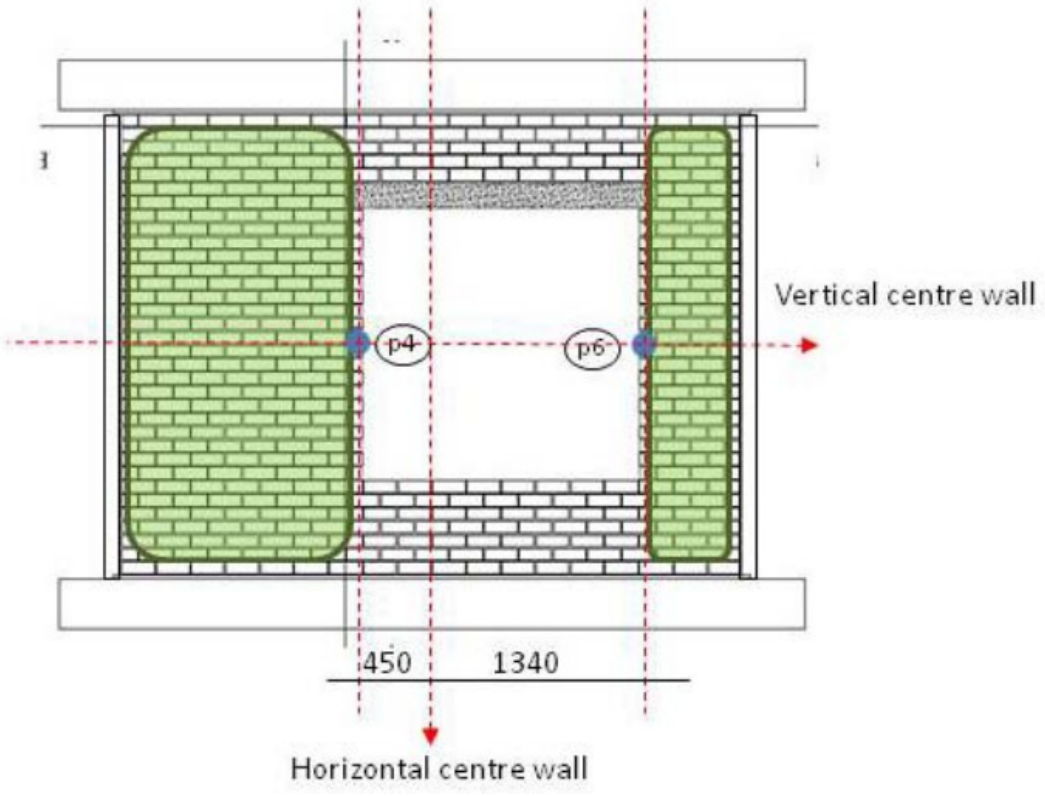

Figure 120: TUD-COMP-12: Schematic of test set-up

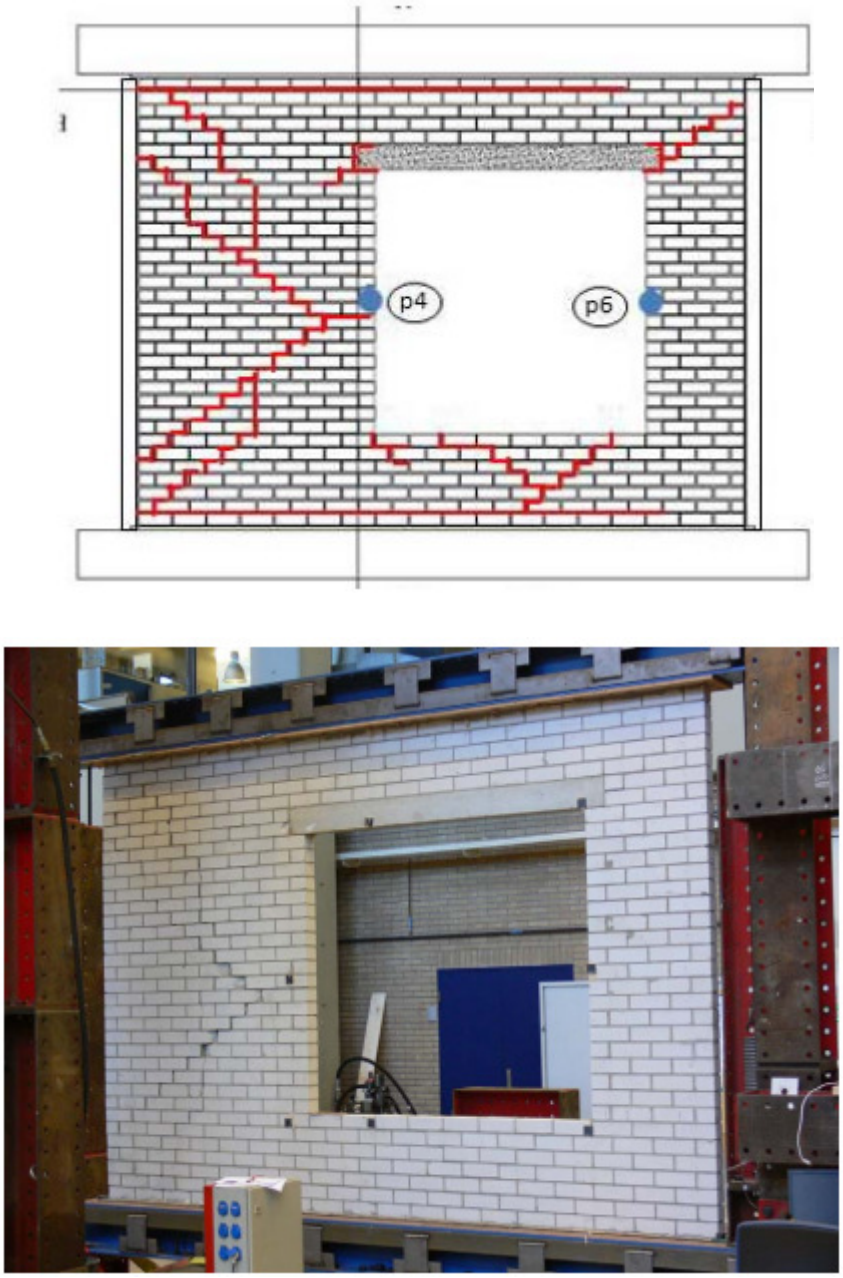

Figure 121: TUD-COMP-12: Final crack pattern

The measured hysteresis is shown in Figure 122.

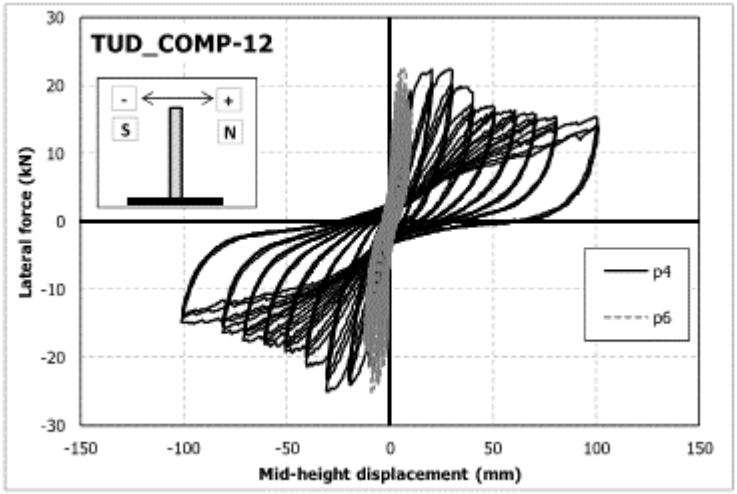

Figure 122: TUD-COMP-12: Lab test result – Applied force-(near) mid-height displacement curve

4.3.5.2 Arup Post-Test Refined Prediction

The LS-DYNA simulation does not clearly show the crack pattern exhibited by the test specimen, but the correct failure mechanism (two-way bending failure in both piers) is observed in Figure 123. The hysteresis curves are quite well predicted (Figure 124 and Figure 125). Compared to the blind prediction, the main difference was that the total force is measured and reported (as per the laboratory test), not only the forces on the top and bottom edges.

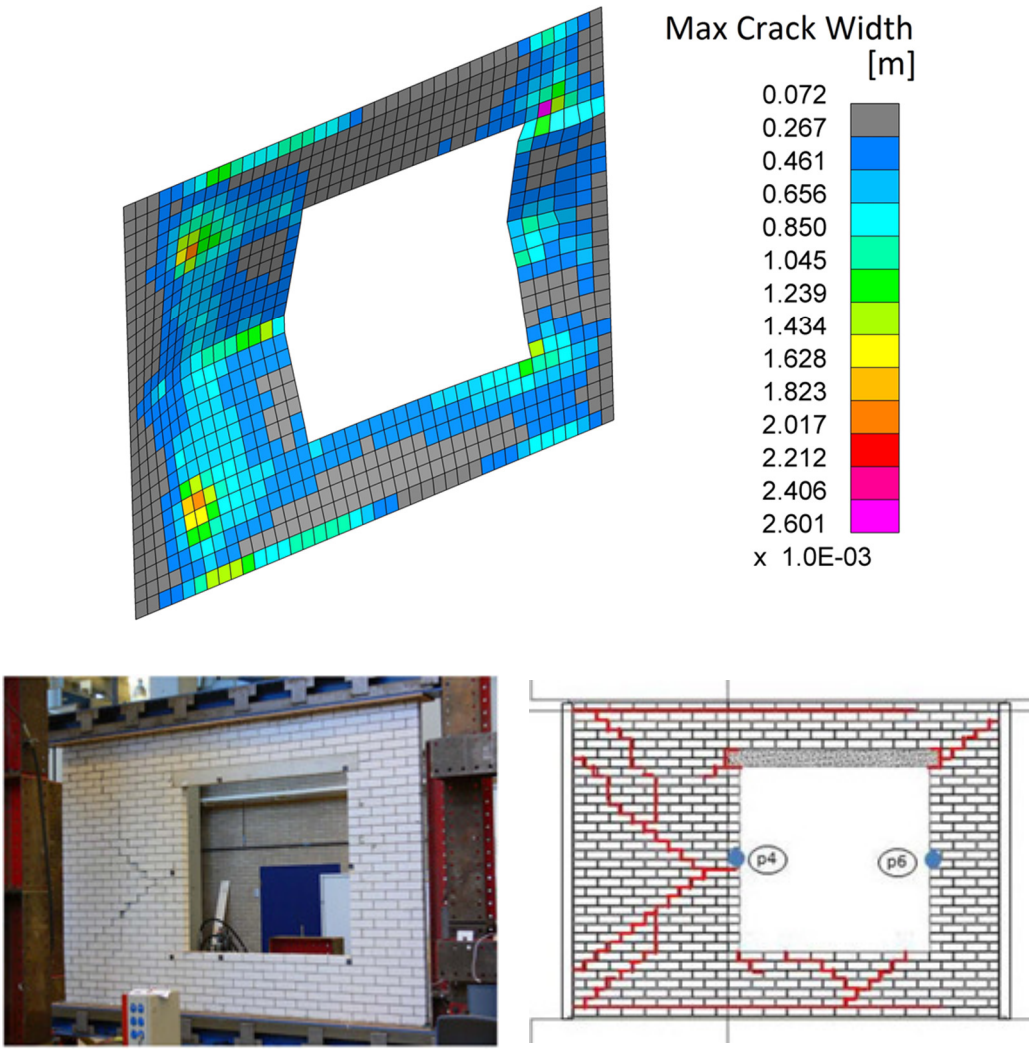

Figure 123: TUD-COMP-12: LS-DYNA post-test refined prediction

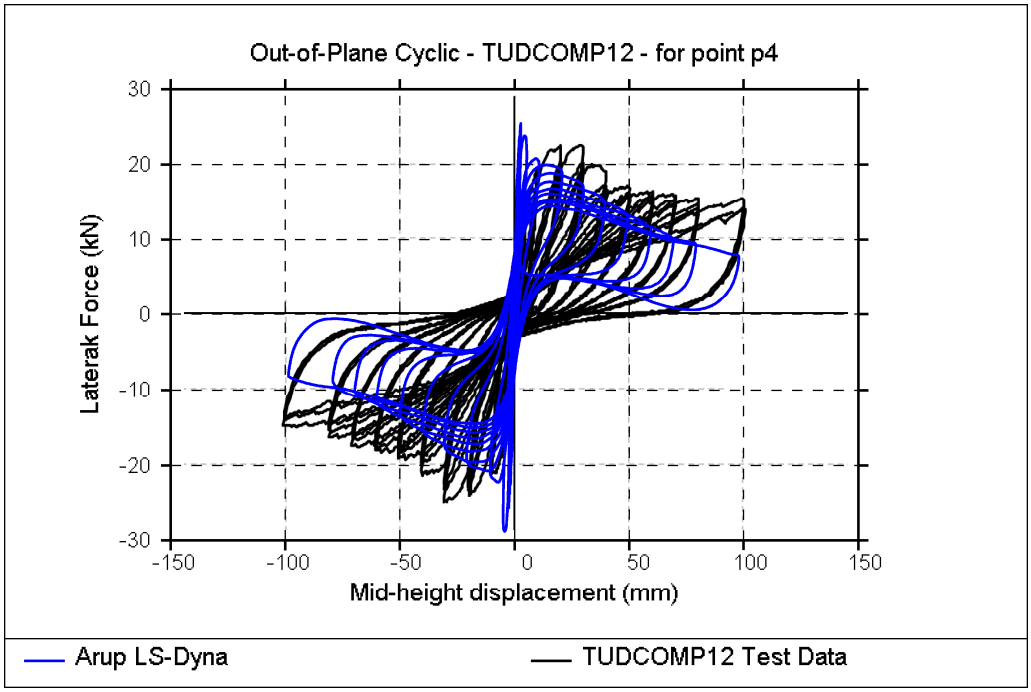

Figure 124: TUD-COMP-12: LS-DYNA post-test refined prediction – Total force versus displacement at reference point p4 (refer to Figure 120 for p4 location)

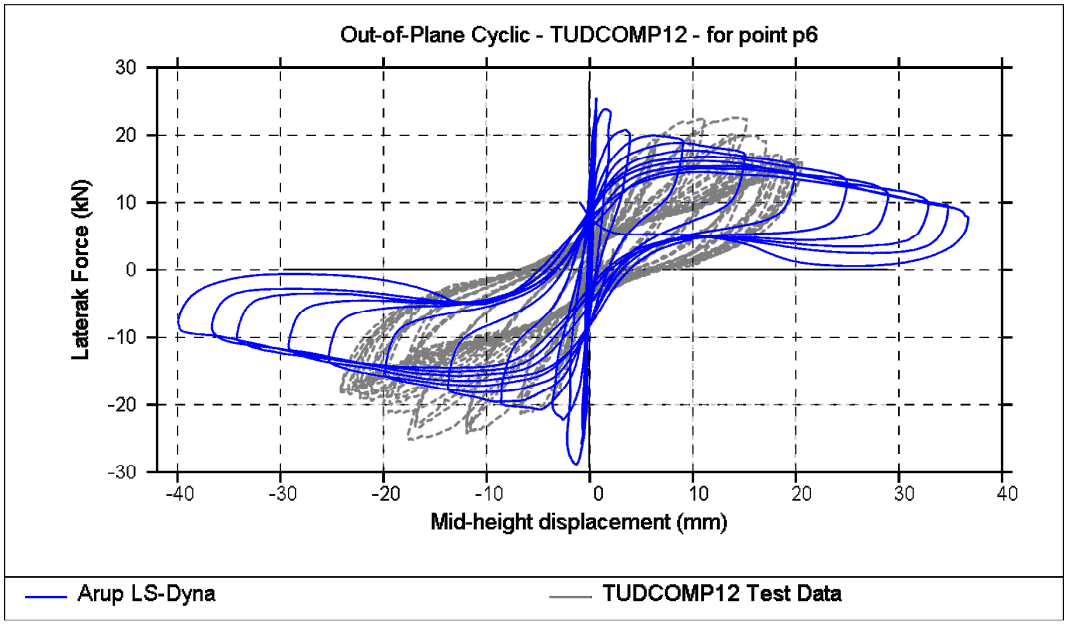

Figure 125: TUD-COMP-12: LS-DYNA post-test refined prediction – Total force versus displacement at reference point p6 (refer to Figure 120 for p6 location)

Table 49: TUD-COMP-12: LS-DYNA post-test refined prediction - Summary table

Consultant	**Predominant Failure Mechanism Predicted**	**Initial Stiffness [kN/mm]**	**Peak Strength [kN]**	**Maximum Achieved Mid-Span Displacement at ref. point 4 [mm]**	
LS-DYNA	Two-way out-of-plane failure	17	28	100	End of protocol
Test Result	Two-way out-of-plane failure	15.5	25	100	End of protocol

4.3.5.3 EUCENTRE Post-Test Refined Prediction

This post-test refined analysis of TUD-COMP-12 was not performed by EUCENTRE as it was originally agreed that EUCENTRE would not contribute to the modelling of the two-way tests.

4.3.5.4 TU-Delft Post-Test Refined Prediction

For TUD-COMP-12, no blind prediction had been submitted.

The DIANA simulation correctly predicts the principal cracks that define the failure mechanism. Only minor cracks on the top left corner above the short pier and in the inferior spandrel are not predicted by the model as shown in Figure 126. Two cyclic analyses have been performed: one according to the loading protocol—up to a maximum displacement of 30 mm—and a second with a reduced number of cycles—up to a maximum displacement of 100 mm. In addition, a monotonic analysis has been performed to provide an estimation of the resistance after that the cyclic analysis reached non-convergence. The three performed analyses provide similar values of initial stiffness and peak resistance with respect to the experimental data. The dissipated energy is underestimated, especially for large displacements (Figure 127 and Figure 128).

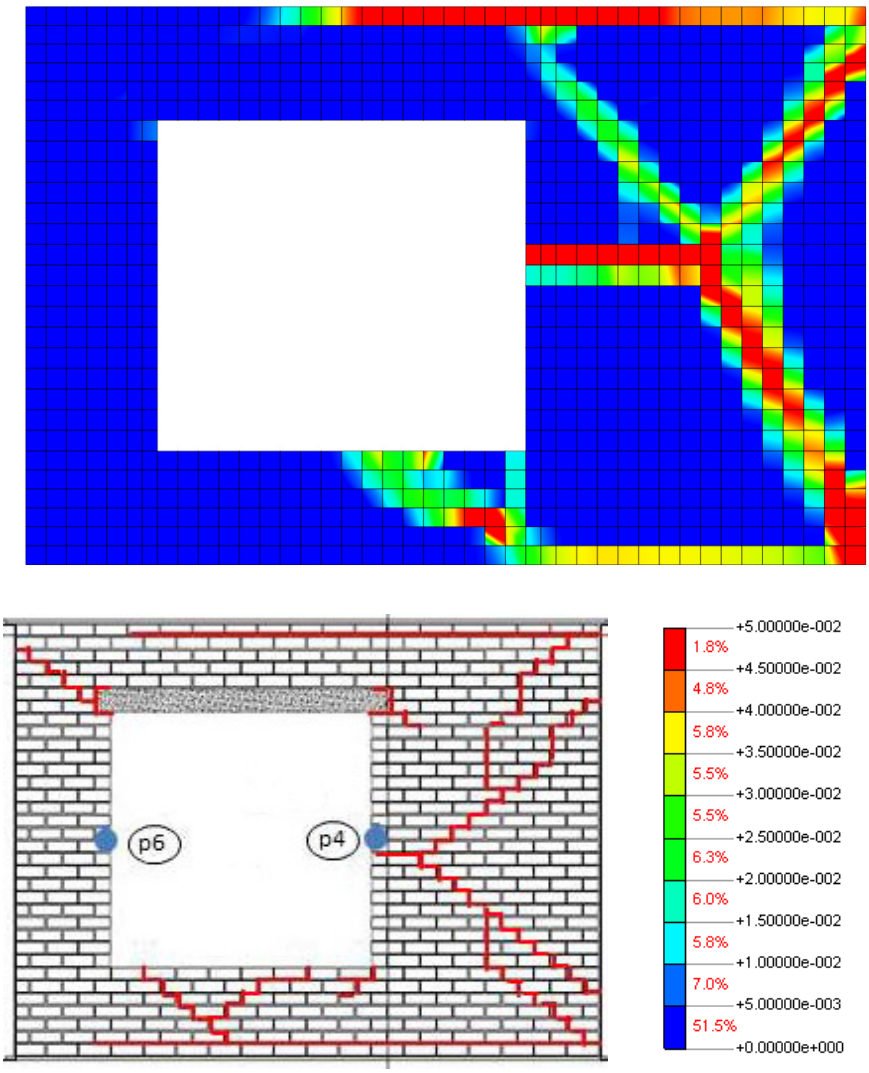

Figure 126: TUD-COMP-12: DIANA post-test refined prediction - Damage plot at end of analysis

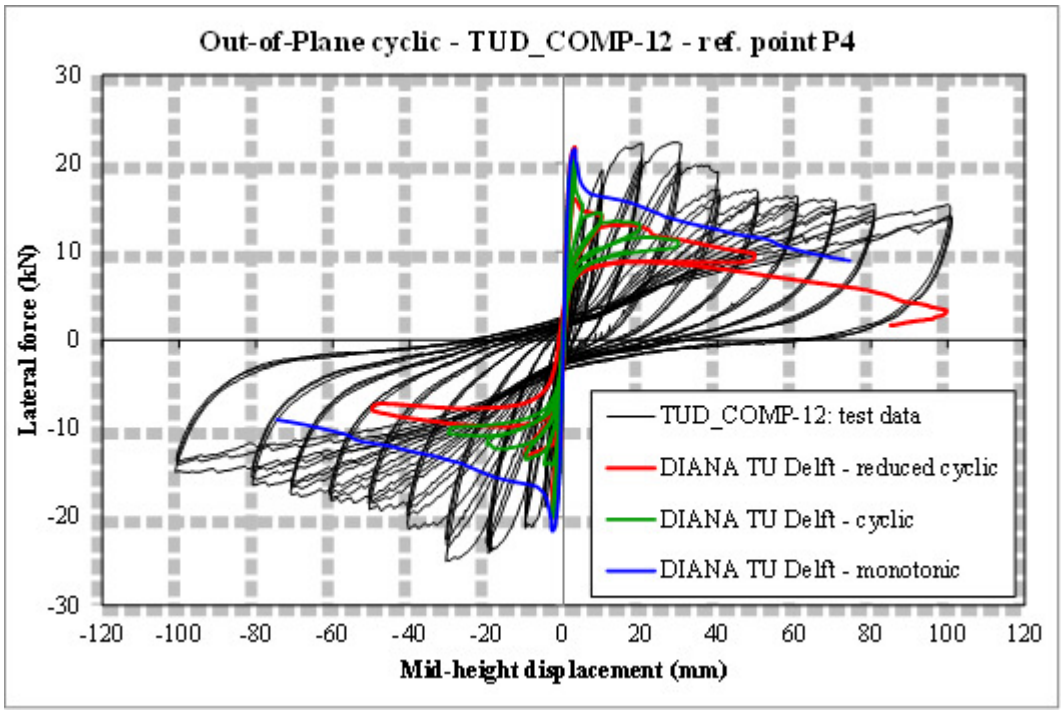

Figure 127: TUD-COMP-12: DIANA post-test refined prediction – Total force versus displacement at reference point p4 (refer to Figure 126 for p4 location)

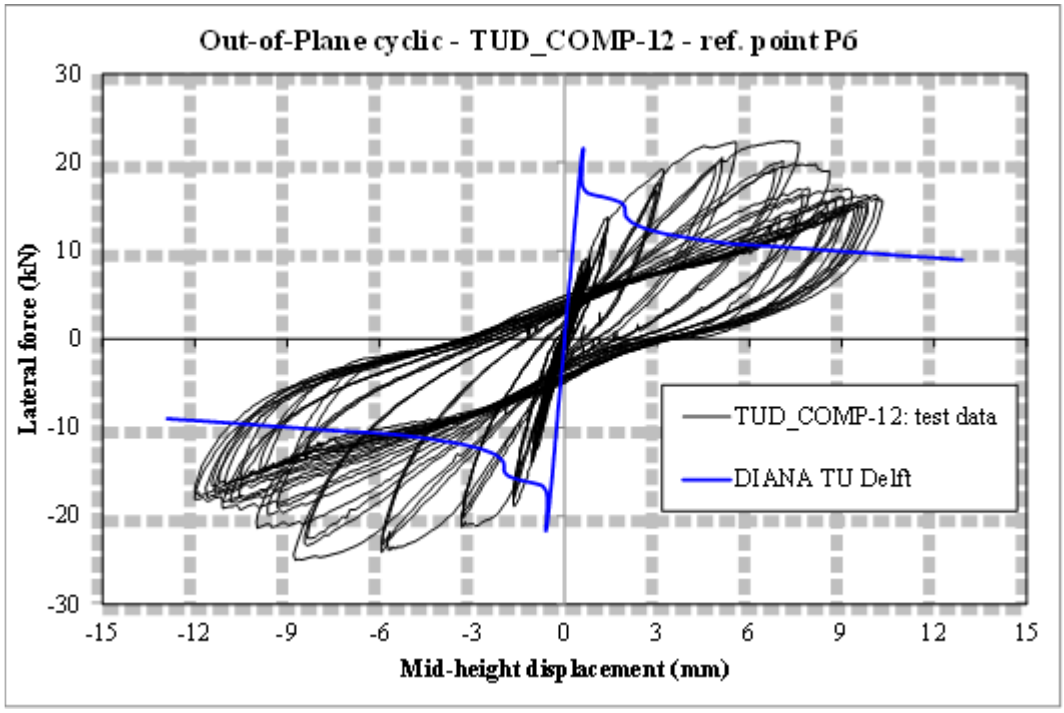

Figure 128: TUD-COMP-12: DIANA post-test refined prediction - Total force versus displacement at reference point p6 (refer to Figure 126 for p6 location)

Table 50: TUD-COMP-12: DIANA post-test refined prediction - Summary table

Consultant	**Predominant Failure Mechanism Predicted**	**Initial Stiffness [kN/mm]**	**Peak Strength [kN]**	**Maximum Achieved Mid-Span Displacement at ref. point 4 [mm]**	
DIANA	Two-way out-of-plane failure	17.5	22	100	End of protocol
Test Result	Two-way out-of-plane failure	15.5	25	100	End of protocol

4.3.6 EUC-COMP-4

4.3.6.1 Test Description

EUC-COMP-4 was the first dynamic out-of-plane test administered by EUCENTRE. This specimen was a single-wythe wall constructed of calcium silicate units 102 mm thick. It was 1.44 m long and 2.75 m high. The applied overburden stress was initially 0.3 MPa and later reduced to 0.1 MPa during the test. The wall was tested under double clamped boundary conditions. The testing sequence consisted of incremental dynamic testing with the following ground motions:

- Gr_1: Groningen record, PGA = 0.25g
- RWA: 4 Hz acceleration pulse input
- Gr_2: Floor accelerations obtained with TREMURI program assuming T1_STAR Model in the "weak" direction, PGA = 0.38g

Collapse of the wall occurred during the last test phase. The bottom crack appeared at the base, the "mid-height" crack between then 19th and 20th course of bricks, and the top crack between the 33rd and 34th course of bricks.

Table 51: EUC-COMP-4: Testing sequence

Specimen	Phase #	Test #	Dynamic Input	Input Scaling	PGA [g]
Imposed Overburden Pressure: 0.3 MPa					
EC_COMP_4	1	1.1	Gr_1	20%	+0.04
EC_COMP_4	1	1.2	Gr_1	40%	+0.09
EC_COMP_4	1	1.3	Gr_1	80%	+0.16
EC_COMP_4	1	1.4	Gr_1	100%	+0.20
EC_COMP_4	1	1.5	Gr_1	160%	+0.32
EC_COMP_4	1	1.6	Gr_1	200%	+0.42
EC_COMP_4	1	1.7	Gr_1	250%	+0.53
EC_COMP_4	1	1.8	Gr_1	350%	+0.74
EC_COMP_4	1	1.9	Gr_1	450%	+0.96
EC_COMP_4	2	2.1	RWA 2Hz	-	-1.11
EC_COMP_4	2	2.2	RWA 2Hz	-	-1.63
EC_COMP_4	2	2.3	RWA 2Hz	-	-1.04
EC_COMP_4	2	2.4	RWA 2Hz	-	-1.88
Imposed Overburden Pressure: 0.1 MPa					
EC_COMP_4	3	3.1	Gr_1	40%	+0.08
EC_COMP_4	3	3.2	Gr_1	80%	+0.17
EC_COMP_4	3	3.3	Gr_1	100%	+0.21
EC_COMP_4	3	3.4	Gr_1	160%	+0.34
EC_COMP_4	3	3.5	Gr_1	200%	+0.41
EC_COMP_4	3	3.6	Gr_1	250%	+0.51
EC_COMP_4	3	3.7	Gr_1	300%	+0.60
EC_COMP_4	3	3.8	Gr_1	350%	+0.73
EC_COMP_4	4	4.1	RWA 2Hz	-	-0.25
EC_COMP_4	4	4.2	RWA 2Hz	-	-0.48
EC_COMP_4	4	4.3	RWA 2Hz	-	-0.72
EC_COMP_4	4	4.4	RWA 2Hz	-	-0.96
EC_COMP_4	5	5.1	Gr_2	100%	+0.44
EC_COMP_4	5	5.2	Gr_2	150%	+0.64
EC_COMP_4	5	5.3	Gr_2	200%	+0.85

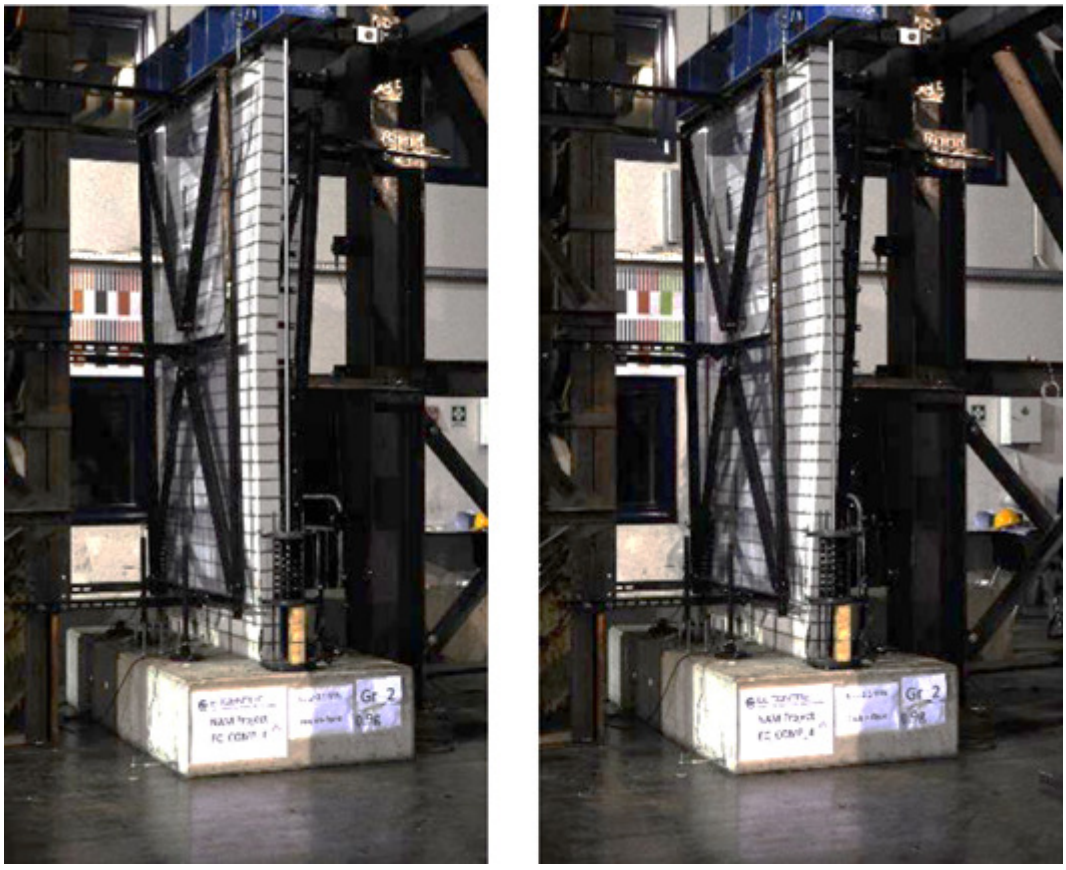

Figure 129: EUC-COMP-4: Deformed shape (left and right)

Figure 130: EUC-COMP-4: View of mid-height crack

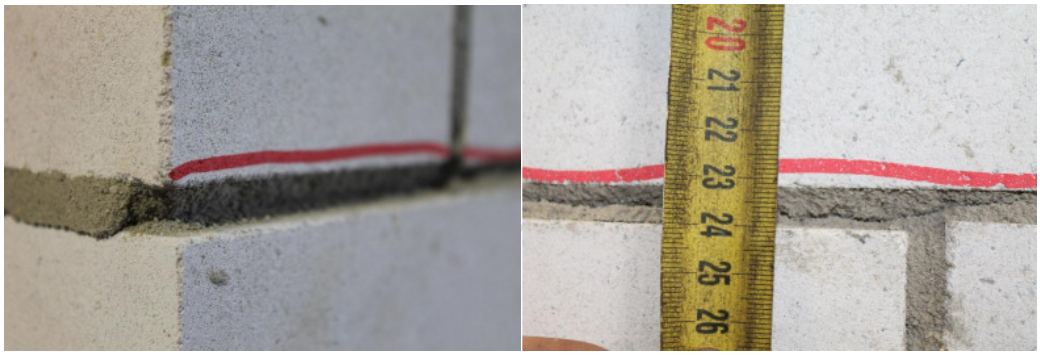

Figure 131: EUC-COMP-4: View of the cracked mortar bed-joint (left). Decrease in mortar bed-joint thickness (right)

4.3.6.2 Arup Post-Test Refined Prediction

In the test EUC-COMP-4 the specimen was subjected to ground motion Phases 1, 3 and 5 (see Table 51). Phases 2 and 4, consisting of the calibration Ricker Wave Acceleration signal, were not modelled.

Results for Phases 1, 3 and 5 are summarised in Figure 133 to Figure 135. The analysis results match the lab tests quite well. For the highly nonlinear responses (displacements above, say, 5-10mm) there is likely to be significant random variation of the peak displacement response, so an exact match with experiment is not expected. Of more importance is the prediction of the transition between small, quasi-linear response and larger nonlinear response. These transitions are fairly well predicted.

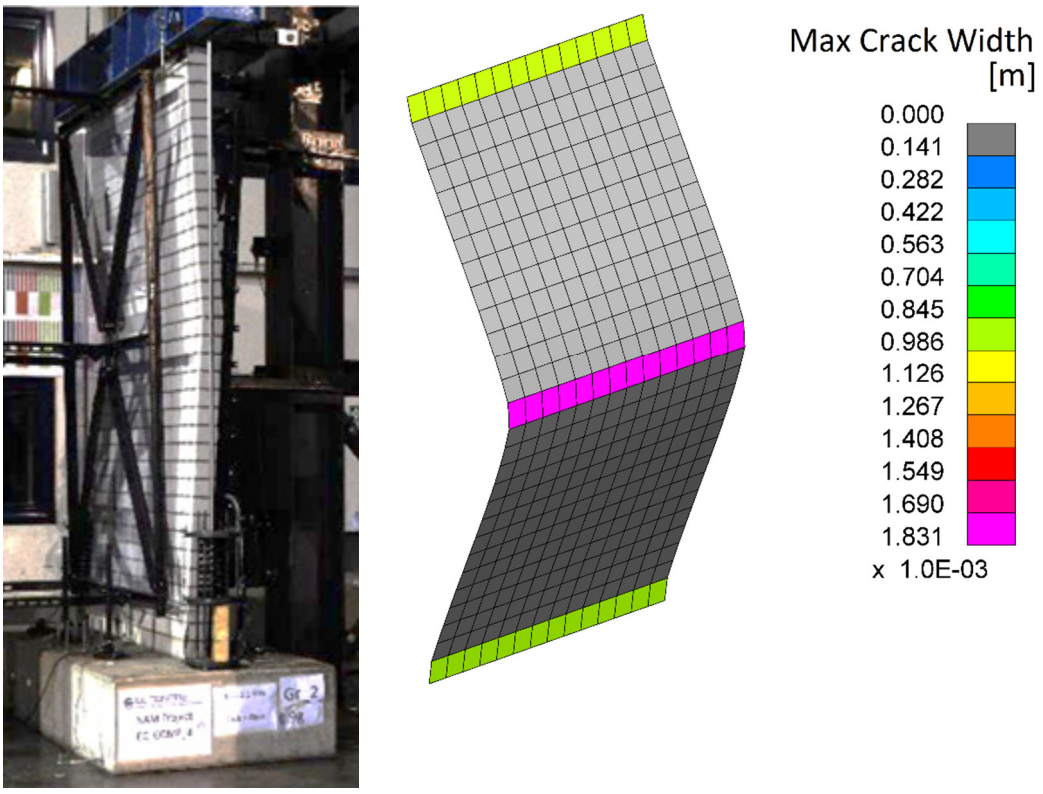

Figure 132: EUC-COMP-4: LS-DYNA post-test refined prediction - Damage plot at end of analysis

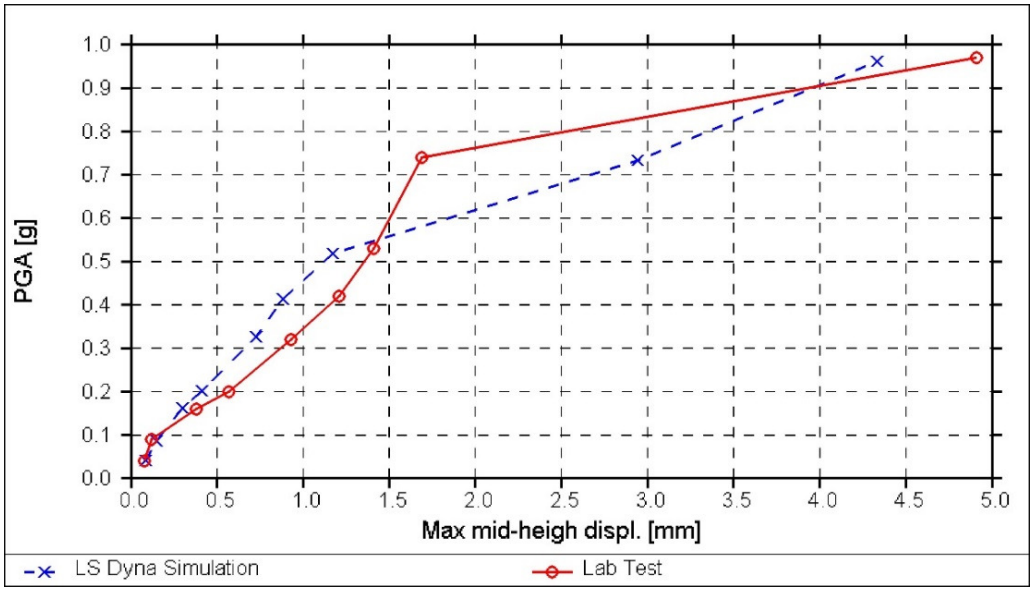

Figure 133: EUC-COMP-4: LS-DYNA post-test refined prediction – Relative mid-height response vs. PGA for 0.3 MPa overburden, under incremental dynamic testing procedure of ground motion Gr_1 (test phase #1)

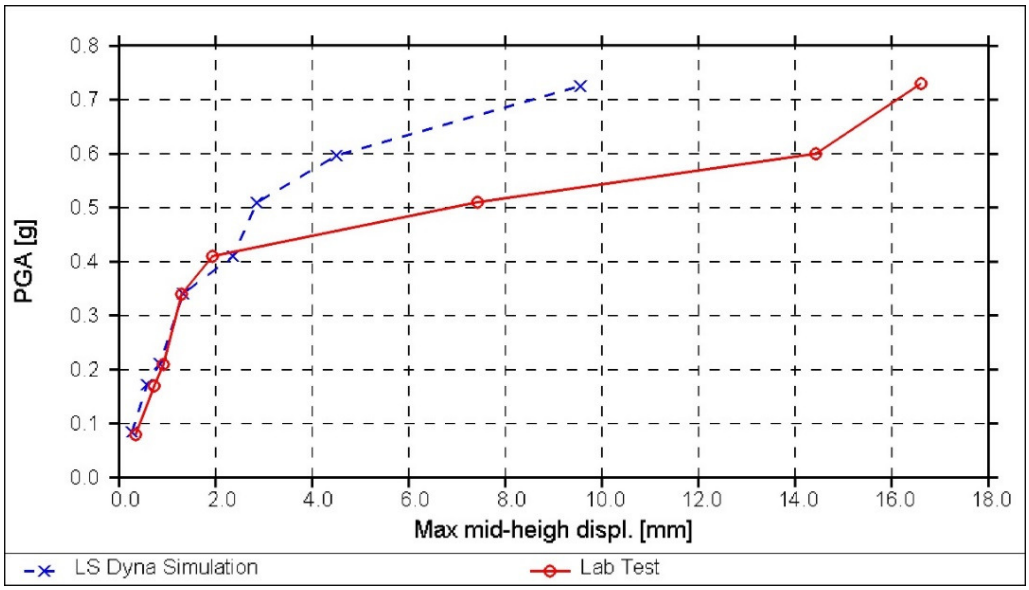

Figure 134: EUC-COMP-4: LS-DYNA post-test refined prediction – Relative mid-height response vs. PGA for 0.1 MPa overburden, under incremental dynamic testing procedure of ground motion Gr_1 (test phase #3)

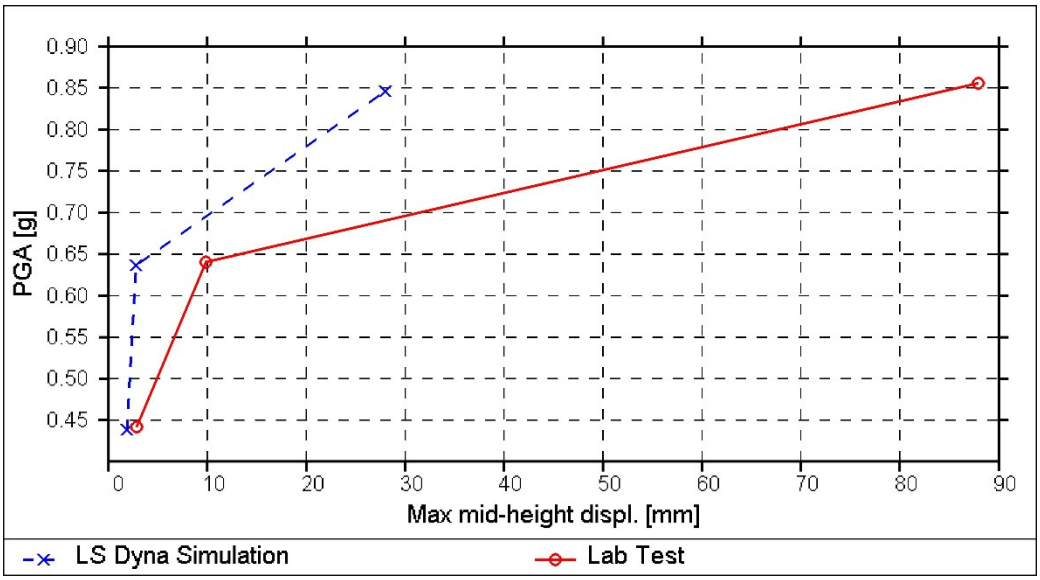

Figure 135: EUC-COMP-4: LS-DYNA post-test refined prediction – Relative mid-height response vs. PGA for 0.1 MPa overburden, under incremental dynamic testing procedure of ground motion Gr_2 (test phase #5)

4.3.6.3 EUCENTRE Post-Test Refined Prediction

For the reasons explained in Section 4.2.2, dynamic/cyclic analysis was not performed. Figure 136 compares the experimental results in terms of force-displacement curves with a pushover analysis performed in TREMURI. The pushover analysis was carried out using a distribution of force proportional to the distance from the considered mass and the nearer restraint (i.e. based on the expected deformed shape).

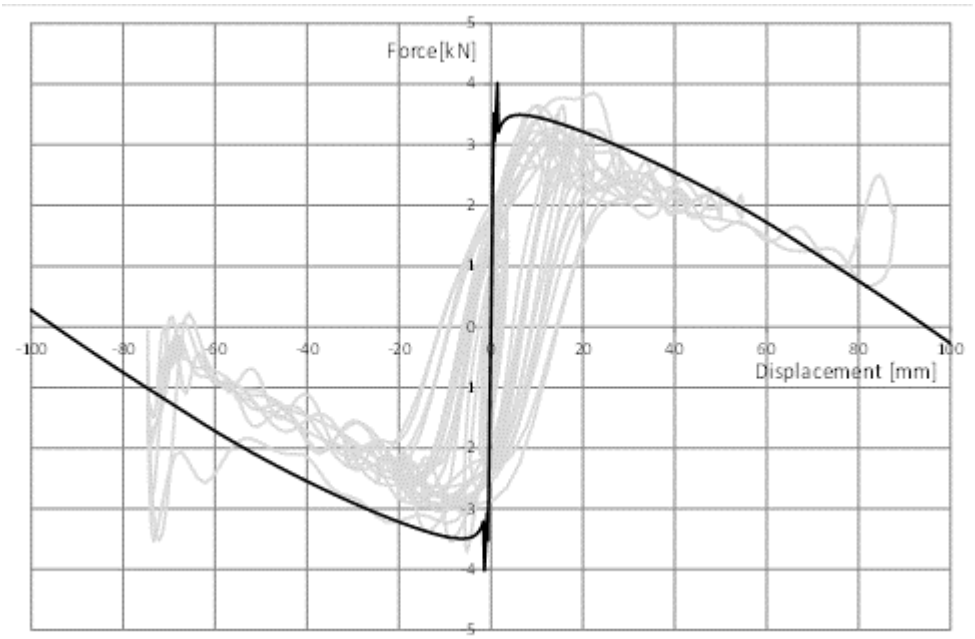

Figure 136: EUC-COMP-4: EUCENTRE post-test refined prediction – Force-displacement curve

Although the envelope force-displacement response is reasonably well captured, the pushover analysis, being a static analysis, is not capable of predicting the dynamic response of the wall to a given sequence of ground motion signals. A pushover analysis was performed instead in order to validate this method and develop a reliable reference for the backbone of a numerical SDOF system that EUCENTRE is calibrating. This tool is very useful if applied to compute the envelop response of walls with different ties density.

4.3.6.4 TU-Delft Post-Test Refined Prediction

In the test EUC-COMP-4, the specimen was subjected to ground motion Gr_1 and Gr_2 separately; consequently, no accumulated damage was considered. The individually applied ground motions were incrementally scaled similar but not identical to the reported scaling factors of Phases 1, 3 and 5 in the loading protocol as shown in Table 51. The results are summarised in Figure 137, Figure 138 and Figure 139.

The results show good agreement between the experimental and numerical outputs in terms of maximum drifts. The change of overburden does not affect the performance of the numerical model. The collapse of the numerical model occurred at 1.1g PGA, which is larger than that experimental collapse PGA (0.9g).

Significant improvements are seen with respect to the blind prediction analyses, which largely under-predicted the maximum drifts in any phase, especially for large PGAs.

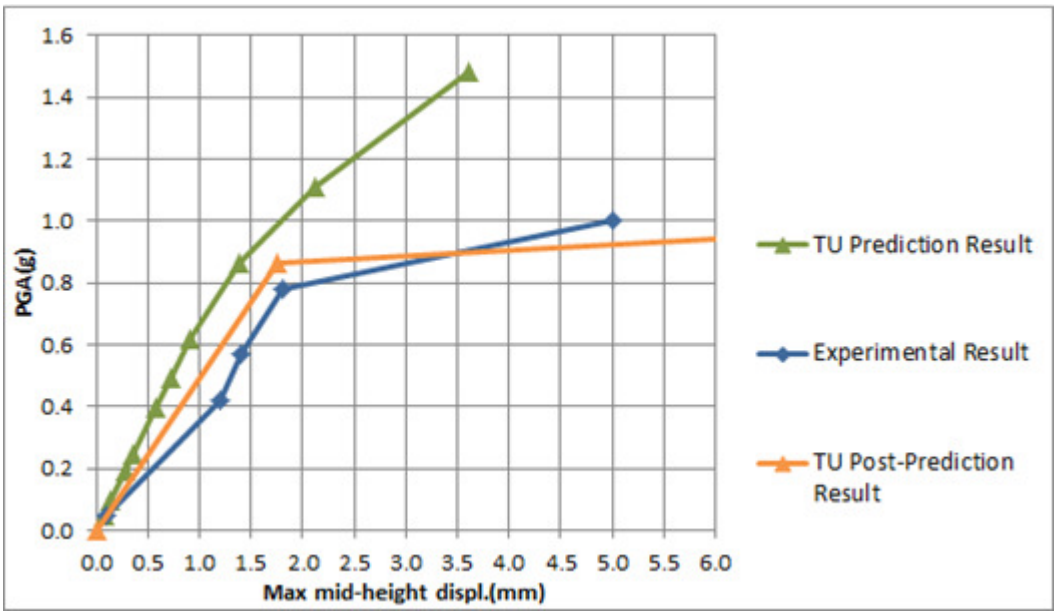

Figure 137: EUC-COMP-4: DIANA blind prediction – Relative mid-height response vs. PGA for 0.3 MPa overburden, under incremental dynamic testing procedure of ground motion Gr_1

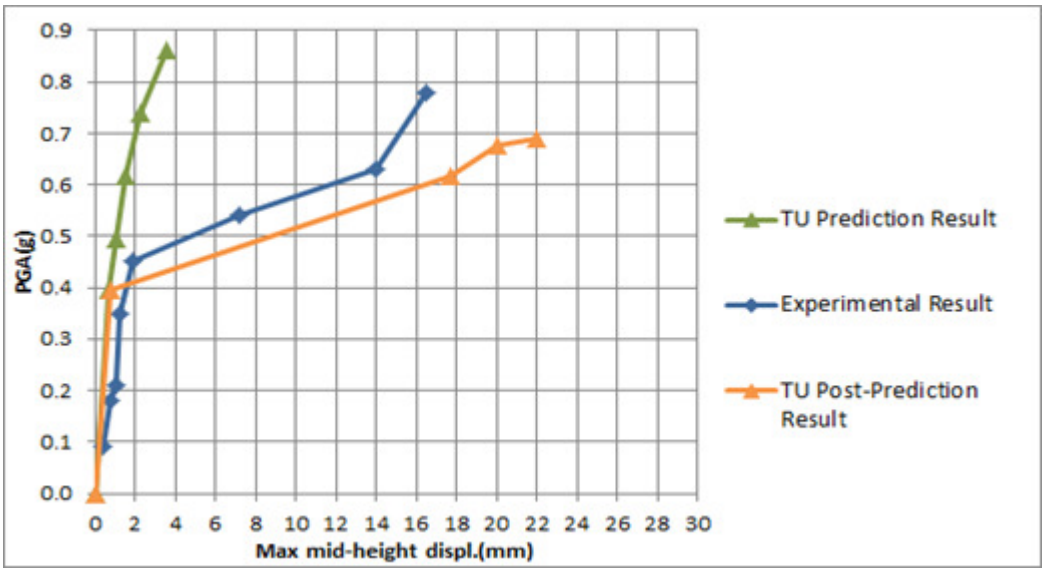

Figure 138: EUC-COMP-4: DIANA blind prediction – Relative mid-height response vs. PGA for 0.1 MPa overburden, under incremental dynamic testing procedure of ground motion Gr_1

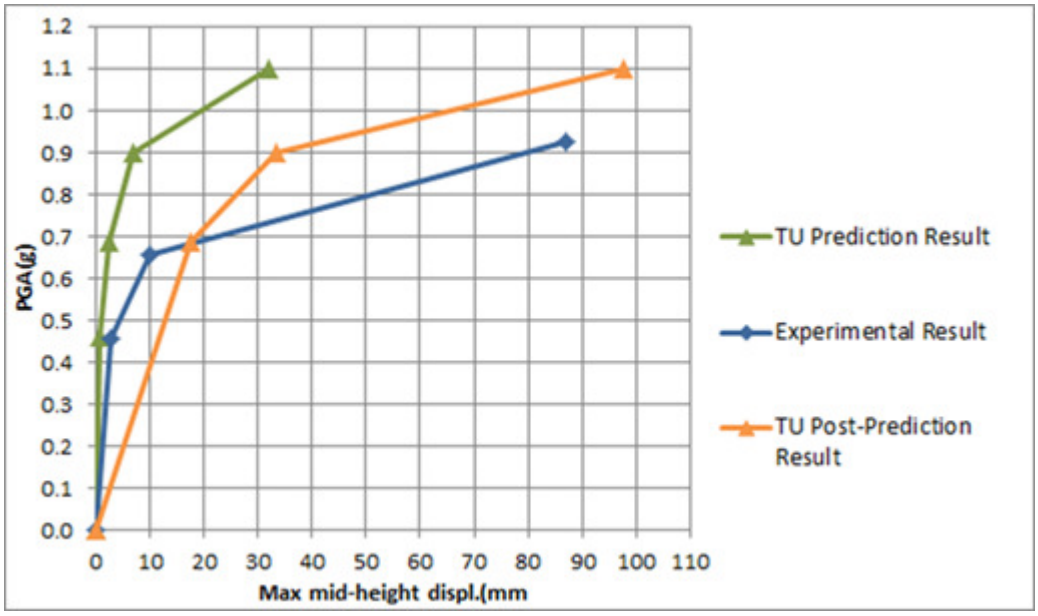

Figure 139: EUC-COMP-4: DIANA blind prediction – Relative mid-height response vs. PGA for 0.1 MPa overburden, under incremental dynamic testing procedure of ground motion Gr_2

4.3.7 EUC-COMP-5

4.3.7.1 Test Description

EUC-COMP-5 was the second dynamic out-of-plane test administered by EUC. This specimen was a single-wythe cavity wall. The inner (structural) leaf was constructed of calcium silicate units 102 mm thick and was 1.44 m long and 2.75 m high. The outer leaf was constructed of clay units 100 mm thick and was 1.44 m long and 2.7 m high. The inner and outer leaves are connected with 2 ties/m^2. The applied overburden stress, on the inner leaf only, was 0.1 MPa. The inner leaf was set up under double clamped boundary conditions and the outer leaf, cantilever boundary conditions. The testing sequence consisted of incremental dynamic testing procedure of the following ground motions:

- Gr_1: Groningen record, PGA = 0.25g
- RWA: 4 Hz acceleration pulse input
- Gr_2: Floor accelerations obtained with TREMURI program assuming T1_STAR Model in the "weak" direction, PGA = 0.38g

The test specimen reached global instability during test phase 6.

Table 52: EUC-COMP-5: Testing sequence

Specimen	Phase #	Test #	Dynamic Input	Input Scaling	PGA [g]
EC_COMP_5	0	0.1	Hammering	-	-
EC_COMP_5	0	0.2	White Noise	-	0.1
EC_COMP_5	1	1.1	Gr_1	+20%	+0.04
EC_COMP_5	1	1.2	Gr_1	+40%	+0.09
EC_COMP_5	1	1.3	Gr_1	-40%	-0.09
EC_COMP_5	1	1.4	Gr_1	+60%	+0.12
EC_COMP_5	1	1.5	Gr_1	+80%	+0.17
EC_COMP_5	1	1.6	Gr_1	+100%	+0.21
EC_COMP_5	1	1.7	Gr_1	-60%	-0.13
EC_COMP_5	1	1.8	Gr_1	-80%	-0.17
EC_COMP_5	1	1.9	Gr_1	-100%	-0.23
EC_COMP_5	2	2.1	RWA	-	-0.22
EC_COMP_5	2	2.2	RWA	-	-0.30
EC_COMP_5	3	3.1	Gr_2	+70%	+0.31
EC_COMP_5	3	3.2	Gr_2	+100%	+0.49
EC_COMP_5	3	3.3	Gr_2	+150%	+0.66
EC_COMP_5	4	4.1	Gr_1	+300%	+0.60
EC_COMP_5	5	5.1	RWA	-	-0.30
EC_COMP_5	5	5.2	RWA	-	-0.49
EC_COMP_5	6	6.1	Gr_2	+150%	+0.65

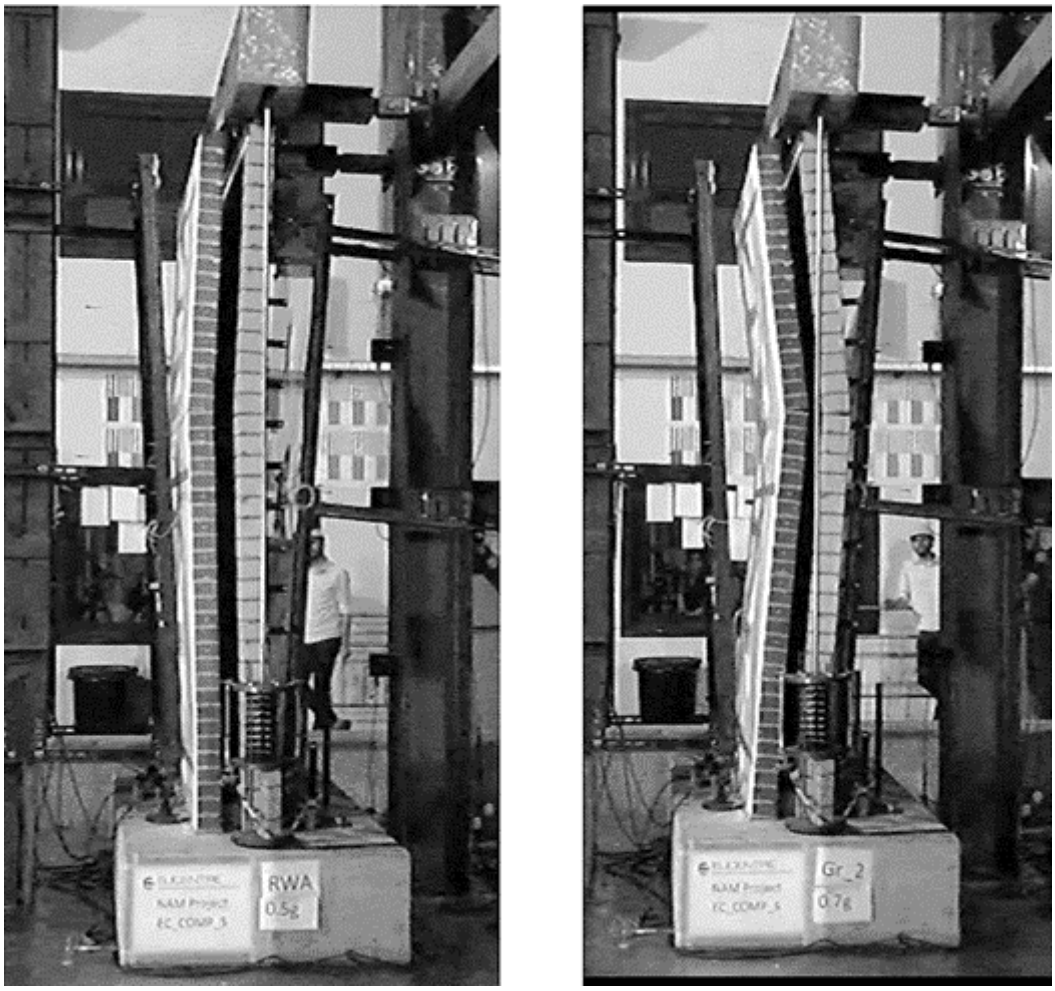

Figure 140: Deformed shape (left and right)

Figure 141: EUC-COMP-5: Formation of mid-height cracks at the tie location

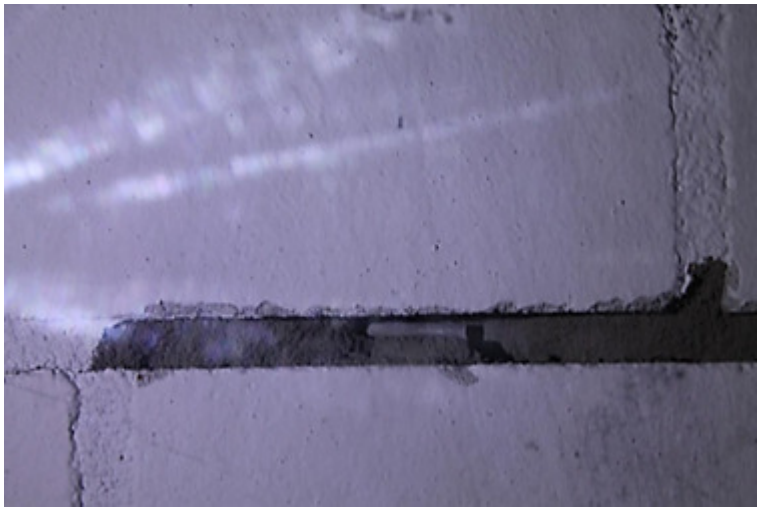

Figure 142: EUC-COMP-5: Expulsion of part of the mortar bed joint

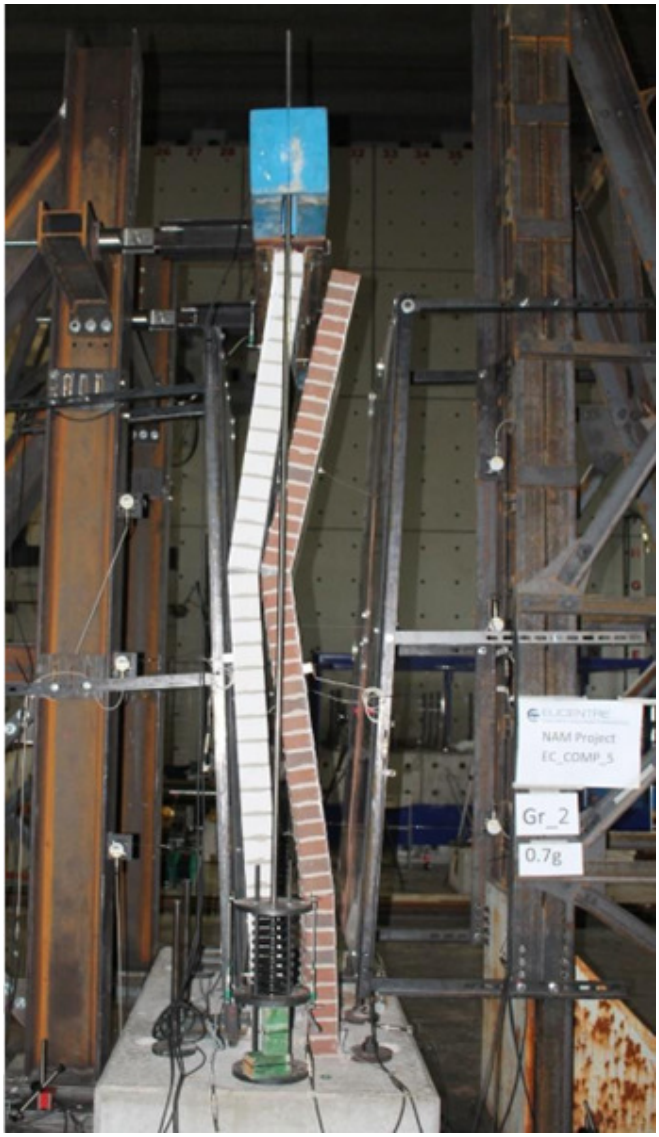

Figure 143: EUC-COMP-5: Collapse of specimen

4.3.7.2 Arup Post-Test Refined Prediction

In the test EUC-COMP-5 the specimen was subjected to ground motion Phases 1, 3, 4 and 6 (see Table 52). Phases 2 and 5, consisting of the calibration Ricker Wave Acceleration signal, were not modelled.

Results for the phases analysed are summarised in Figure 145 and Figure 146. At low PGA levels, the response of the calcium silicate load-bearing wall is represented quite accurately, but the clay wall exhibits a much greater deformation in the analysis than in the experiment. In the experiment, the two walls show little difference in their deflections. This suggests that the stiffness of the wall ties in dynamic tests is greater in reality than in the analysis, despite the input data being taken from cyclic tests on the wall ties.

In the analysis, the mid-height deflection of the clay wall reaches 20mm at 0.5g PGA, while in the lab test the deflection of both walls was small until the motion reached 0.6g PGA. The analysis predicted collapse at 0.6g PGA at Phase 4 for the clay wythe, initiated by pull-out of the top wall tie followed by unstable rocking of the upper portion of the clay wall (see Figure 144). In the laboratory the specimen collapsed at 0.68g PGA during Phase 6. Thus, the strength of the cavity wall system is under-predicted by around 10-20% in this experiment. In the laboratory, the collapse mode was by large displacement of both walls at mid-height with no indication of large pull-out or push-in of the uppermost wall tie. Significant uncertainties remain regarding wall tie behaviour at levels of response consistent with damage. It may be that the wall tie pull-out behaviour is stronger under dynamic conditions compared to the quasi-static cyclic tests from which the tie input data was derived. The effect of cracking of the bed joints (due to out-of-plane response of the walls) on wall tie performance is not currently understood. In addition there will be inherent variability in the actual response of individual wall ties (due to construction variability) that cannot be represented in an analysis.

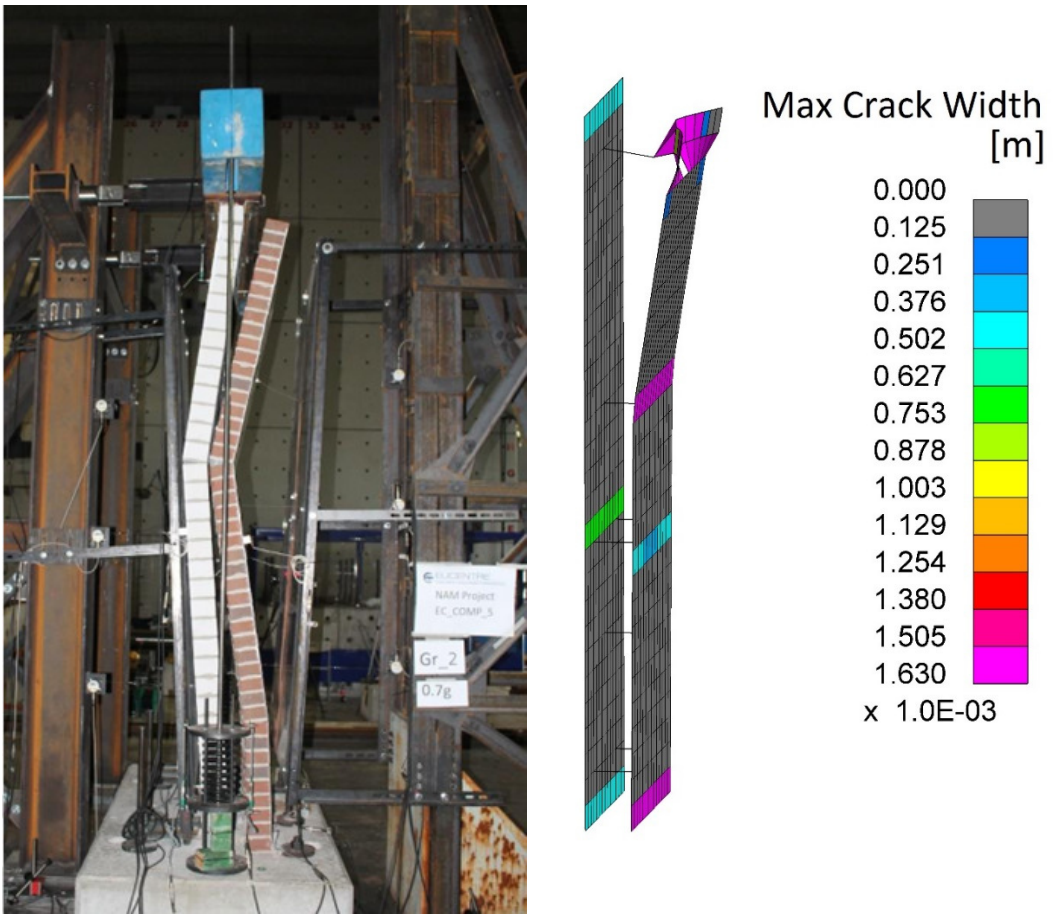

Figure 144: EUC-COMP-5: LS-DYNA post-test refined prediction - Damage plot at end of analysis

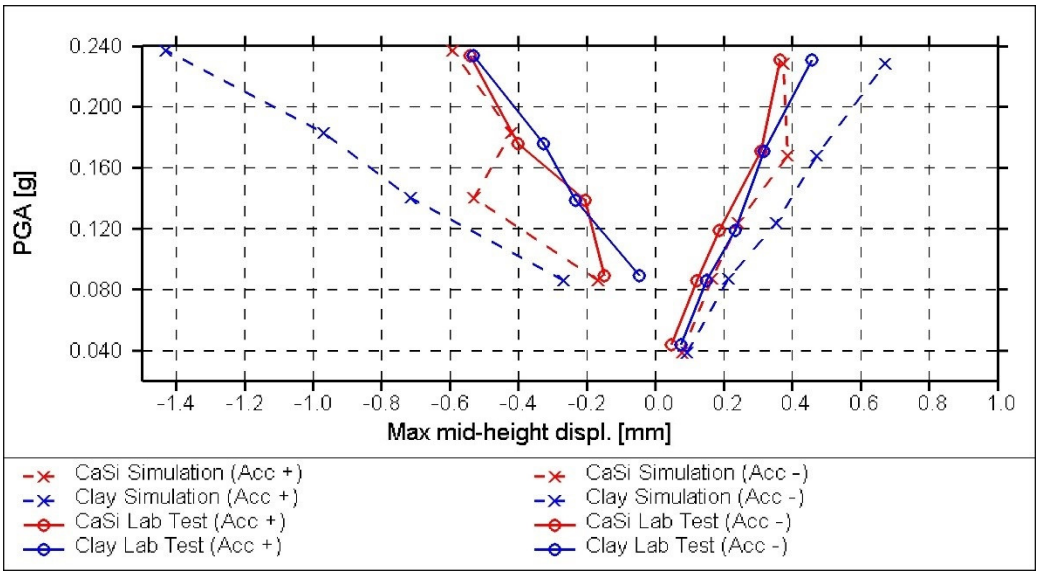

Figure 145: EUC-COMP-5: LS-DYNA post-test refined prediction – Relative mid-height response vs. PGA for model under incremental dynamic testing procedure of ground motion Gr_1 (test phases #1)

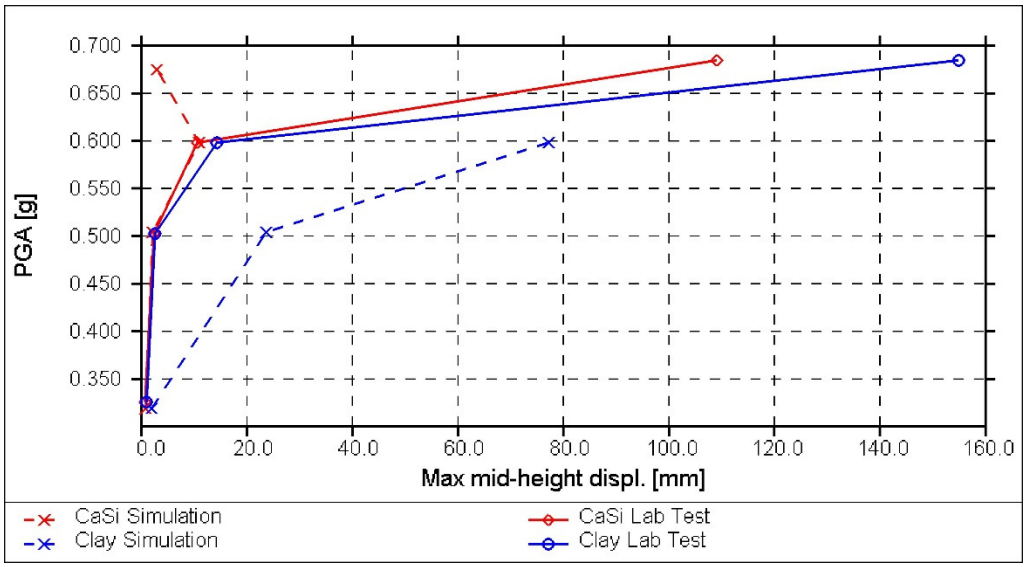

Figure 146: EUC-COMP-5: LS-DYNA post-test refined prediction – Relative mid-height response vs. PGA for model under incremental dynamic testing procedure of ground motion Gr_2 (test phases #3 & 6).

Note that the simulation reached a PGA of 0.68g with only the CaSi wythe acting, since the clay wythe becomes detached after the PGA reaches 0.65g. The corresponding peak displacement the CaSi wythe is smaller than the one at PGA=0.65g as the clay wythe is no longer connected.

A sensitivity study (Figure 147) demonstrated good correlation to the strong motion phase of the EUC-COMP-5 test results when the input force-deflection curve for the wall ties was scaled by 1.5. Meanwhile, if the wall ties were treated

as elastic, the possibility for collapse due to wall tie pull-out is eliminated, and therefore the capacity is limited only by the total strength of the two walls.

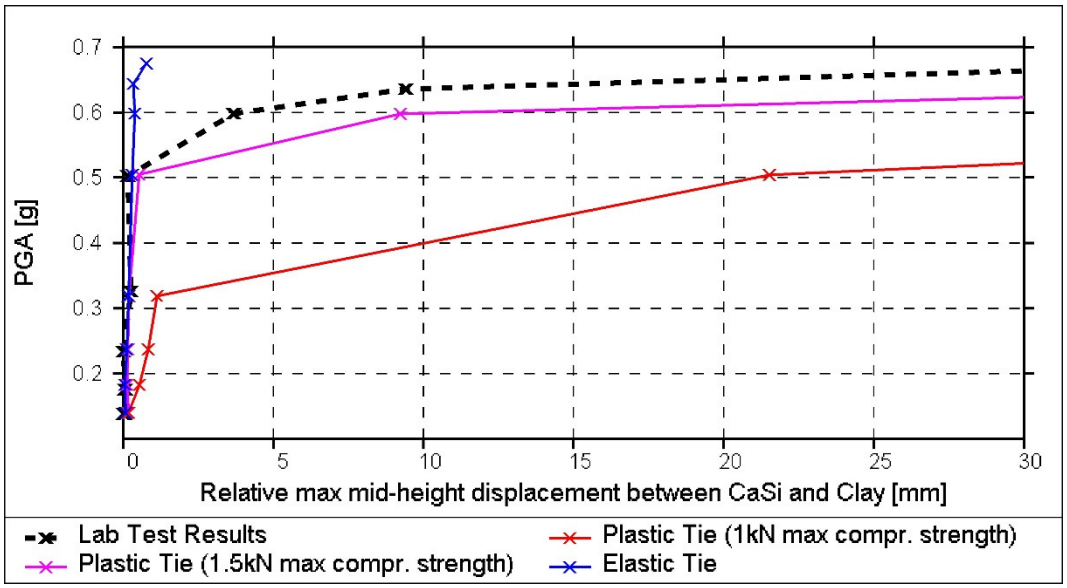

Figure 147: EUC-COMP-5: Effect of wall tie input data on LS-DYNA prediction – ground motion Gr_2 (test phases #3 & 6). Red curve: using result measured in cyclic wall tie test; Pink curve: using measured result scaled by 1.5; Blue curve: stiff elastic wall tie (no pull-out).

4.3.7.3 EUCENTRE Post-Test Refined Prediction

Figure 149 compares the experimental results in terms of force-displacement curves with a pushover analysis performed with TREMURI. The pushover analysis was carried out using a distribution of forces proportional to the distance from the considered mass and the nearer restraint (i.e. based on the expected deformed shape).

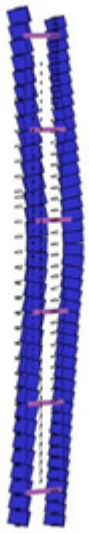

Figure 148: EUC-COMP-5: TREMURI model

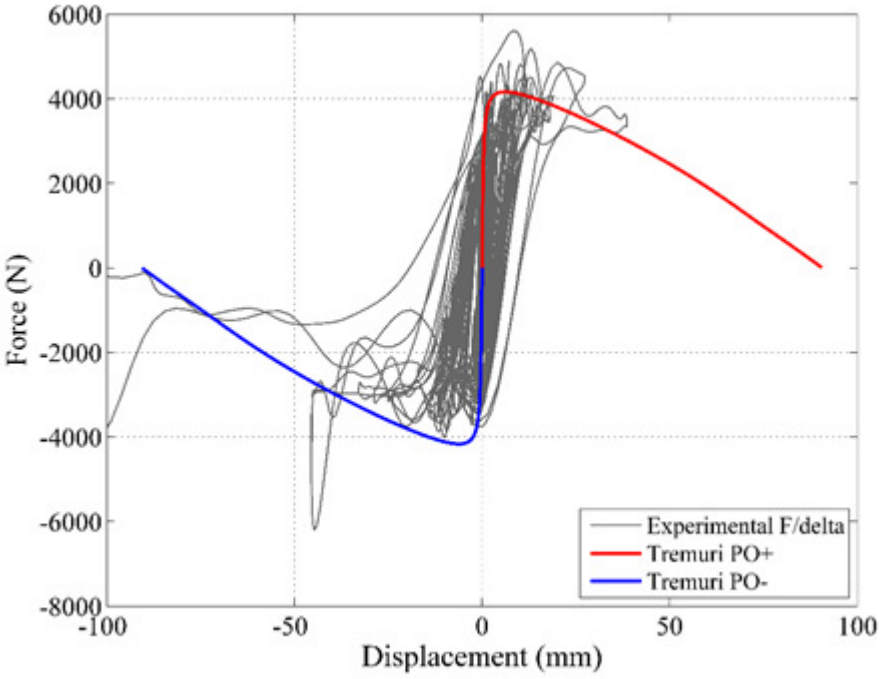

Figure 149: EUC-COMP-5: EUCENTRE post-test refined prediction – EUCENTRE post-test refined prediction – Force-displacement curve

Although the envelope force-displacement response is reasonably well captured, the pushover analysis, being a static analysis, is not capable of predicting the dynamic response of the wall to a given sequence of ground motion signals. A pushover analysis was performed instead in order to validate this method and develop a reliable reference for the backbone of a numerical SDOF system that EUCENTRE is calibrating. This tool is very useful if applied to compute the envelop response of walls with different ties density.

4.3.7.4 TU-Delft Post-Test Refined Prediction

In the test EUC-COMP-5, the specimen was subjected to ground motion Gr_1 and Gr_2 separately; consequently, no accumulated damage was considered. The individually applied ground motions were incrementally scaled similar but not identical to the reported scaling factors of Phases 1, 3, 4 and 6 in the loading protocol as shown in Table 52. The results are summarised in Figure 150 and Figure 151.

The results of the application of Gr_1 and Gr_2 up to 0.60 g PGA show good agreement between the experimental and numerical outputs in terms of maximum drifts.

During the application of Gr_2 beyond 0.60g PGA, the maximum drift is strongly underestimated (about 50%). Indeed, the model did not predict any collapse of the wall, whereas in the laboratory the specimen collapsed at 0.68g PGA. This may be partially a consequence of considering the separate analyses for each phase so that, in the last phase, the modelled wall is stiffer and more resistant than that which was actually tested.

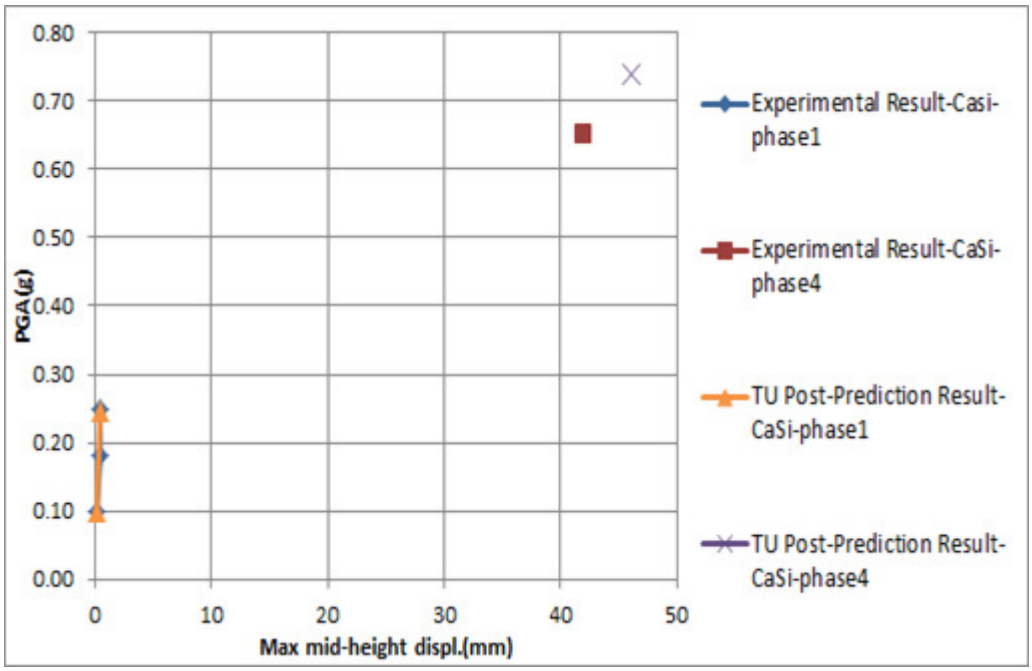

Figure 150: EUC-COMP-5: DIANA blind prediction – Relative mid-height response vs. PGA for model under incremental dynamic testing procedure of ground motion Gr_1

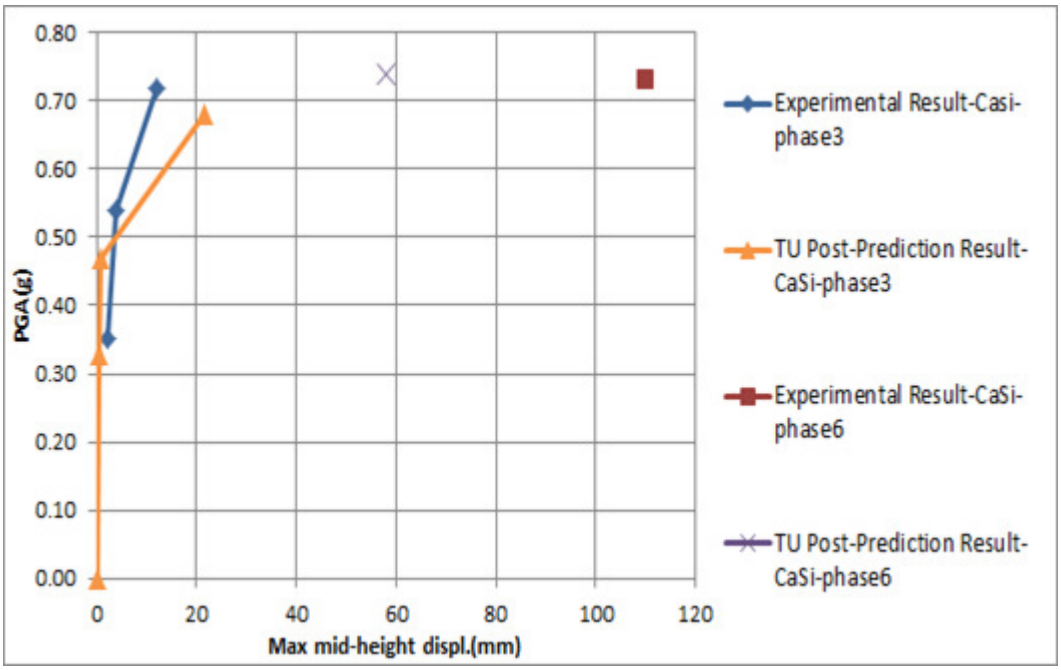

Figure 151: EUC-COMP-5: DIANA blind prediction – Relative mid-height response vs. PGA for model under incremental dynamic testing procedure of ground motion Gr_2.

4.3.8 EUC-COMP-6

4.3.8.1 Test Description

EUC-COMP-6 is the fourth dynamic out-of-plane test in the blind prediction program administered by EUCENTRE. This specimen is a single-wythe cavity wall. The inner (structural) leaf is constructed of calcium silicate units and is 1.44 metres long and 2.75 metres high. The outer leaf is constructed of clay units and is 1.44 metres long and 2.7 metres high. The inner and outer leaves are connected with 2 ties/m^2. The applied overburden stress on the inner leaf is 0.3 MPa. The testing sequence consisted of incremental dynamic testing procedure of the following ground motions:

- Gr_1: Groningen record, PGA = 0.25g
- RWA: 4 Hz acceleration pulse input
- Gr_2: Floor accelerations obtained with TREMURI program assuming T1_STAR Model in the “weak” direction, PGA = 0.38g

The test specimen reached global instability during test phase 6.

Table 53: EUC-COMP-6: Testing sequence

Specimen	Phase #	Test #	Dynamic Input	Input Scaling	PGA [g]
EC_COMP_6	0	0.1	Hammering	-	-
EC_COMP_6	0	0.2	White Noise	-	0.1
EC_COMP_6	1	1.1	Gr_1	+40%	-0.09
EC_COMP_6	1	1.2	Gr_1	-40%	+0.09
EC_COMP_6	1	1.3	Gr_1	+60%	-0.13
EC_COMP_6	1	1.4	Gr_1	+80%	-0.18
EC_COMP_6	1	1.5	Gr_1	+100%	-0.23
EC_COMP_6	1	1.6	Gr_1	-60%	+0.12
EC_COMP_6	1	1.7	Gr_1	-80%	+0.17
EC_COMP_6	1	1.8	Gr_1	-100%	+0.21
EC_COMP_6	2	2.1	RWA	-	-0.30
EC_COMP_6	2	2.2	RWA	-	+0.29
EC_COMP_6	3	3.1	Gr_2	+70%	-0.32
EC_COMP_6	3	3.2	Gr_2	+100%	-0.47
EC_COMP_6	3	3.3	Gr_2	+150%	-0.66
EC_COMP_6	3	3.4	Gr_2	+170%	-0.77
EC_COMP_6	4	4.1	RWA	-	-0.49
EC_COMP_6	4	4.2	RWA	-	+0.53
EC_COMP_6	5	5.1	Gr_2	+210%	-0.97
EC_COMP_6	5	5.2	Gr_2	+250%	-1.17

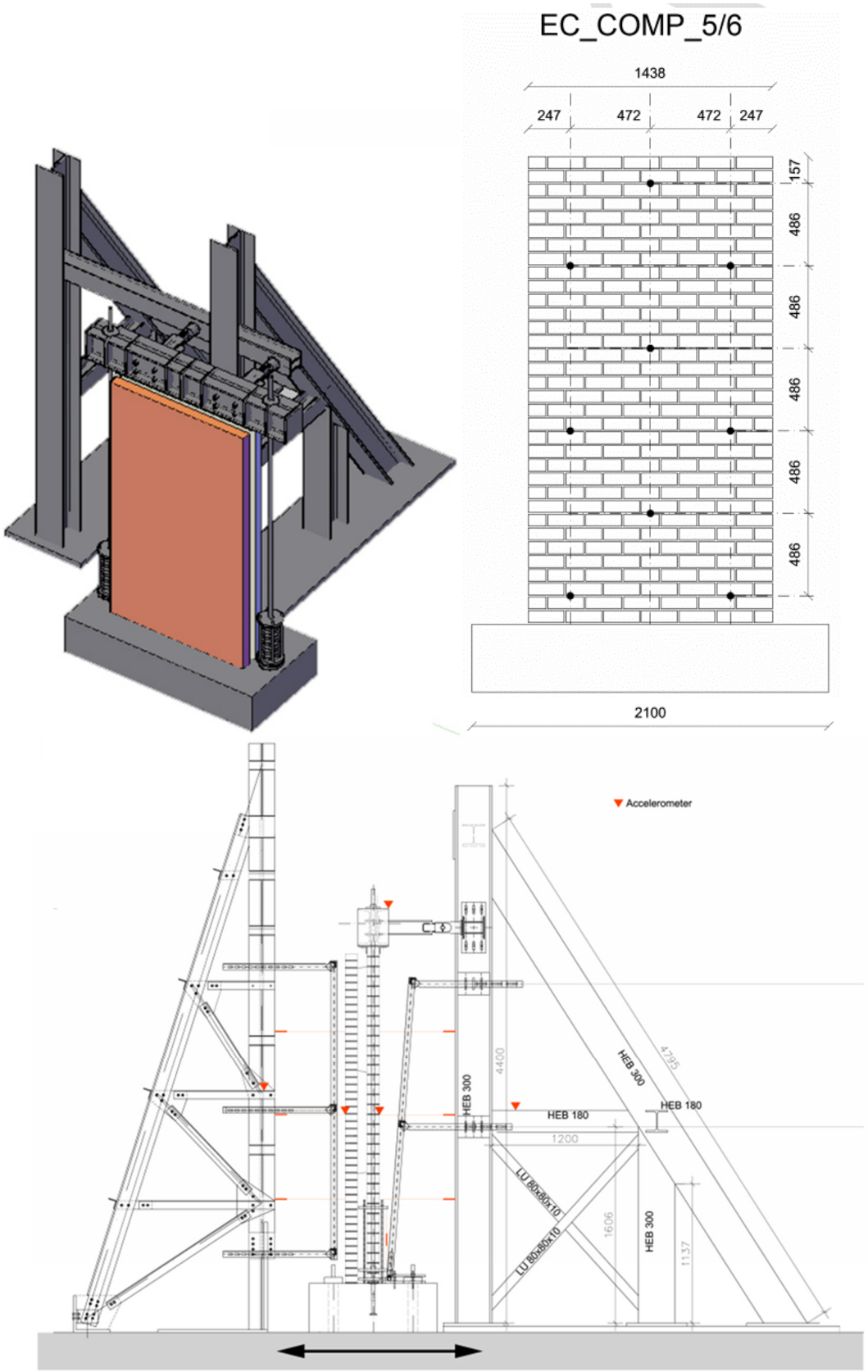

Figure 152: Test set-up images

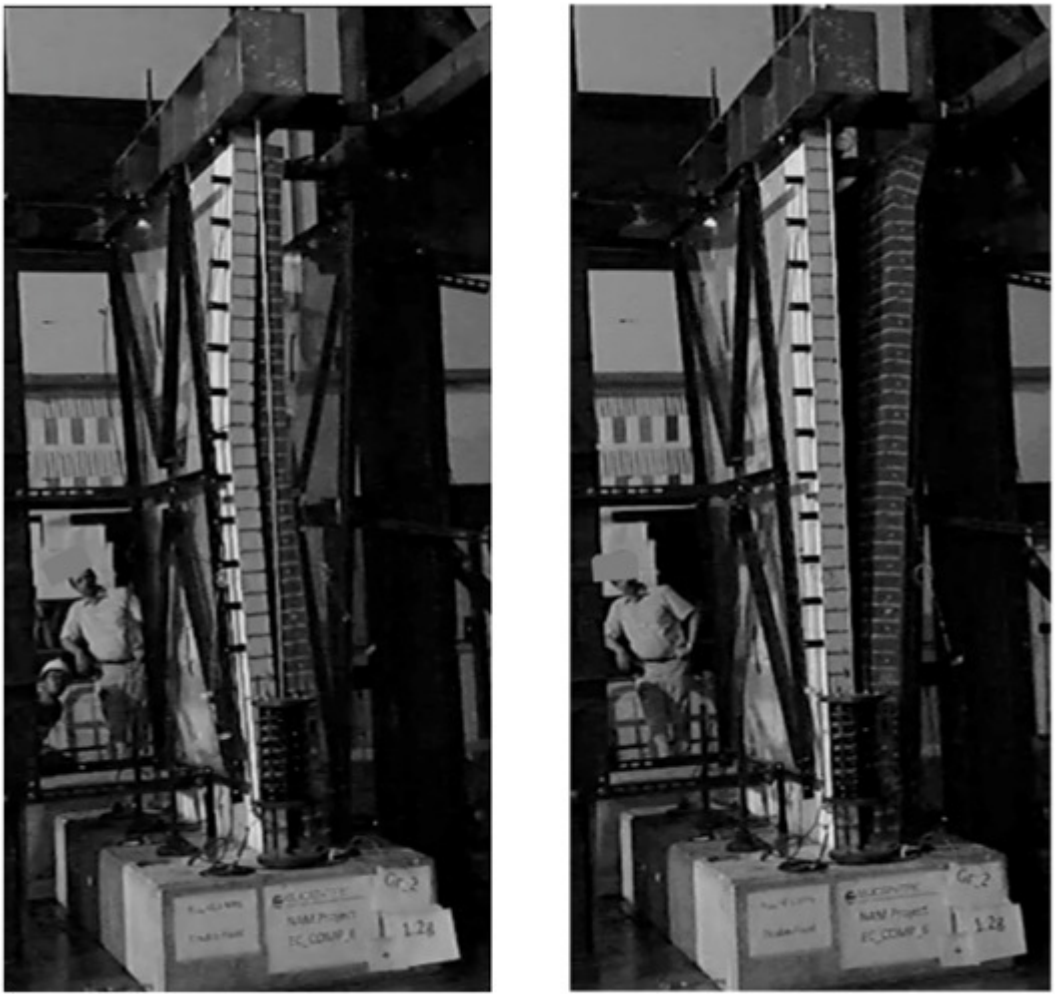

Figure 153: EUC-COMP-6: Final deformed shape / collapse

4.3.8.2 Arup Post-Test Refined Prediction

In the test EUC-COMP-6 the specimen was subjected to ground motion Phases 1, 3 and 5 (see Table 53). Phases 2 and 4, consisting of the calibration Ricker Wave Acceleration signal, were not modelled. The test is similar to EUC-COMP-5 except that the overburden on the calcium silicate wall is larger—0.3 MPa rather than 0.1 MPa.

Results for the phases analysed are summarised in Figure 155 and Figure 156. At low PGA levels, the response of the calcium silicate load-bearing wall is represented with acceptable accuracy, given the very small deflections.

In the analysis, the mid-height deflection of the clay wall shows a nonlinear response at 0.47g and collapses at 0.77g PGA. Collapse was initiated by pull-out of the top wall tie, after which the upper portion of the clay wall was free to rock out-of-plane. This deformation mode is similar to that exhibited in the analysis of EUC-COMP-5 – unsurprisingly, since neither the wall tie forces nor the strength of the clay wall are significantly influenced by the increased overburden. The response in the physical test was somewhat different: for PGA levels up to 0.96g, the two walls showed little separation and their deflections remained within 10 mm. Failure occurred at 1.17g PGA. The failure mode shown by the lab test (Figure 154) shows that large displacements are concentrated at the specimen mid-height. This is in contrast with the cantilevering deformation mode shown by the LS-DYNA simulation. The wall ties appear to be strong enough to mobilise the full strength of the calcium silicate wall, which is larger in EUC-COMP-6 than in EUC-COMP-5 because of the increased overburden.

The conclusion is similar to that reached for EUC-COMP-5: the dynamic behaviour of the wall ties is apparently stronger in these dynamic tests than assumed in the analysis. The prediction might be improved in future by adopting stronger input data for the wall ties.

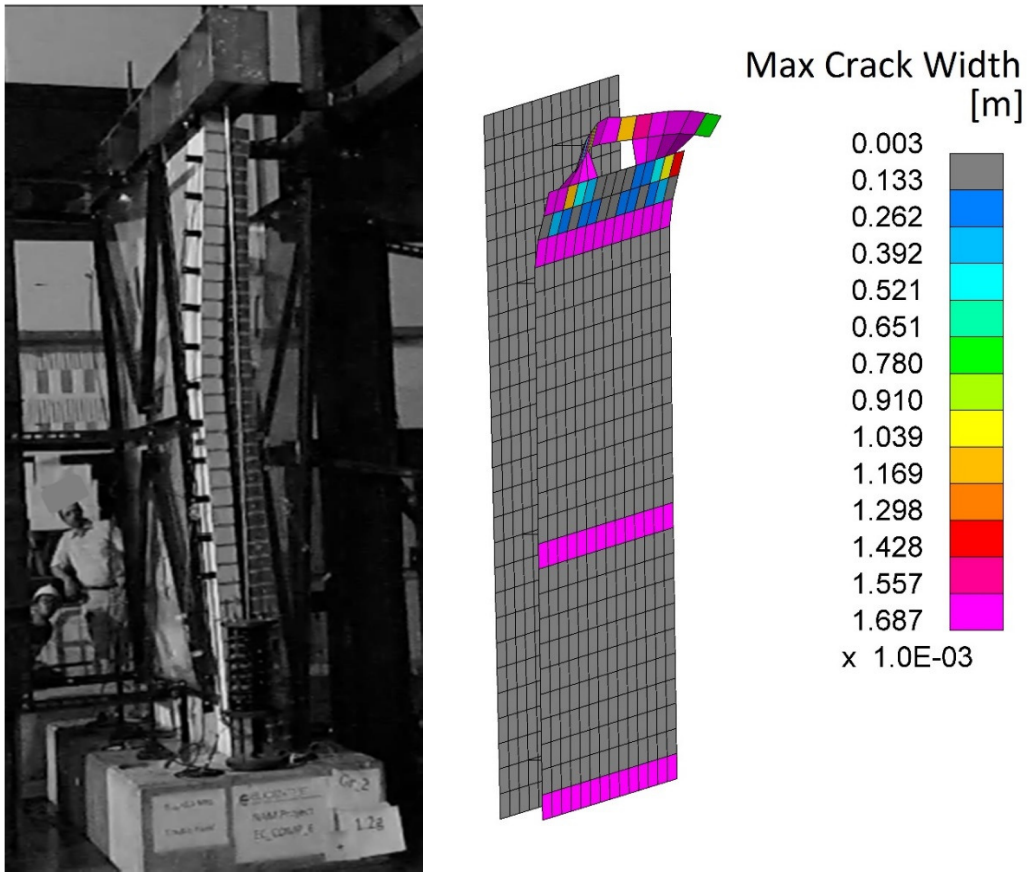

Figure 154: EUC-COMP-6: LS-DYNA post-test refined prediction - Damage plot at end of analysis

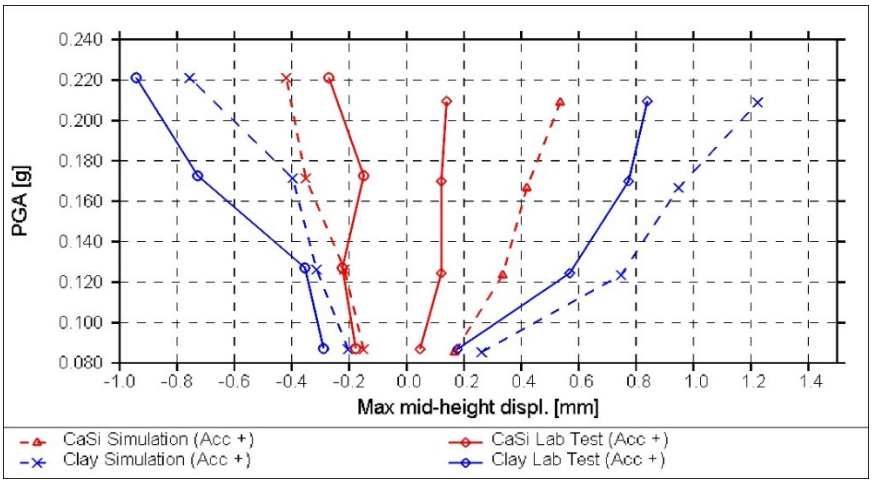

Figure 155: EUC-COMP-6: LS-DYNA post-test refined prediction – Relative mid-height response vs. PGA for model under incremental dynamic testing procedure of ground motion Gr_1 (test phase #1)

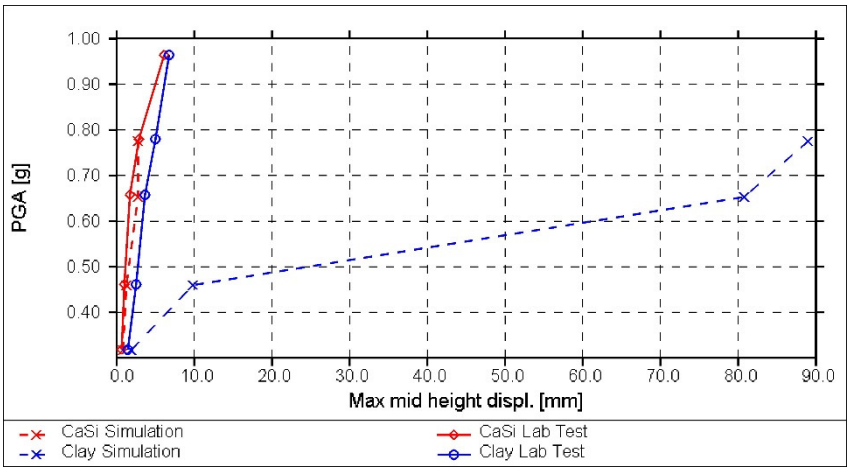

Figure 156: EUC-COMP-6: LS-DYNA post-test refined prediction – Relative mid-height response vs. PGA for model under incremental dynamic testing procedure of ground motion Gr_2 (test phases #3 & 5). Note that the lab result at test phase 5.2 is omitted since the maximum displacement of the clay leaf was not determined due to collapse in the lab.

4.3.8.3 EUCENTRE Post-Test Refined Prediction

Figure 157 compares the numerical results in terms of force-displacement curves with pushover analyses performed using TREMURI. The pushover analyses were performed adopting a distribution of forces proportional to the distance from the considered mass and the nearer restraint (i.e. based on the expected deformed shape).

In the presented plot, the results of the analyses carried out for EUC-COMP-5, EUC-COMP-6 and EUC-COMP-7 are plotted together.

According to the numerical model, the number of ties does not seem to significantly influence the out-of-plane capacity of the wall (blue and red lines superimposed in Figure 157).

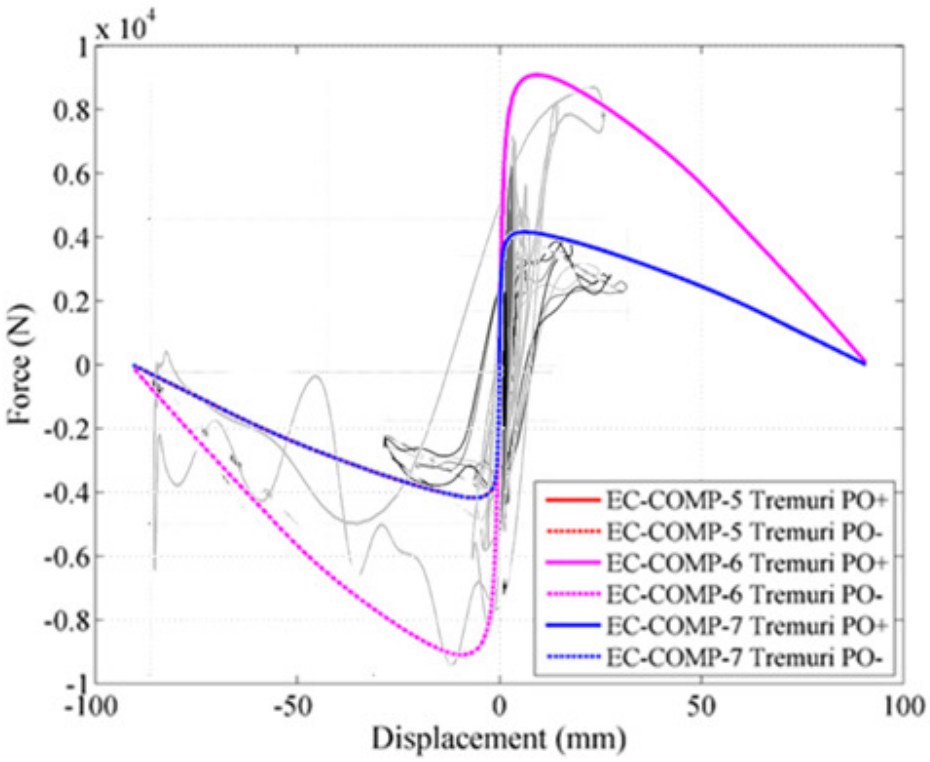

Figure 157: EUC-COMP-6 & EUC-COMP-7: EUCENTRE post-test refined prediction – Force-displacement curve

Although the envelope force-displacement response is reasonably well captured, the pushover analysis, being a static analysis, is not capable of predicting the dynamic response of the wall to a given sequence of ground motion signals. A pushover analysis was performed instead in order to validate this method and develop a reliable reference for the backbone of a numerical SDOF system that EUCENTRE is calibrating. This tool is very useful if applied to compute the envelop response of walls with different ties density.

4.3.8.4 TU-Delft Post-Test Refined Prediction

In the test EUC-COMP-6, the specimen was subjected to ground motion Gr_1 and Gr_2 separately; consequently, no accumulated damage was considered. The individually applied ground motions were incrementally scaled similar but not identical to the reported scaling factors of Phases 1, 3 and 5 in the loading protocol as shown in Table 53. The results are summarised in Figure 158 and Figure 159.

The results of the application of Gr_1 and Gr_2 up to 0.78g PGA show good agreement between the experimental and numerical outputs in terms of maximum drifts.

During the application of Gr_2 beyond 0.78g PGA, the maximum drift is strongly underestimated (about 80%). Indeed, the model did not predict any collapse of the wall, whereas in the laboratory the specimen collapsed at 1.16g PGA. This may be partially a consequence of considering the separate analyses for each phase so that, in the last phase, the modelled wall is stiffer and more resistant than that which was actually tested.

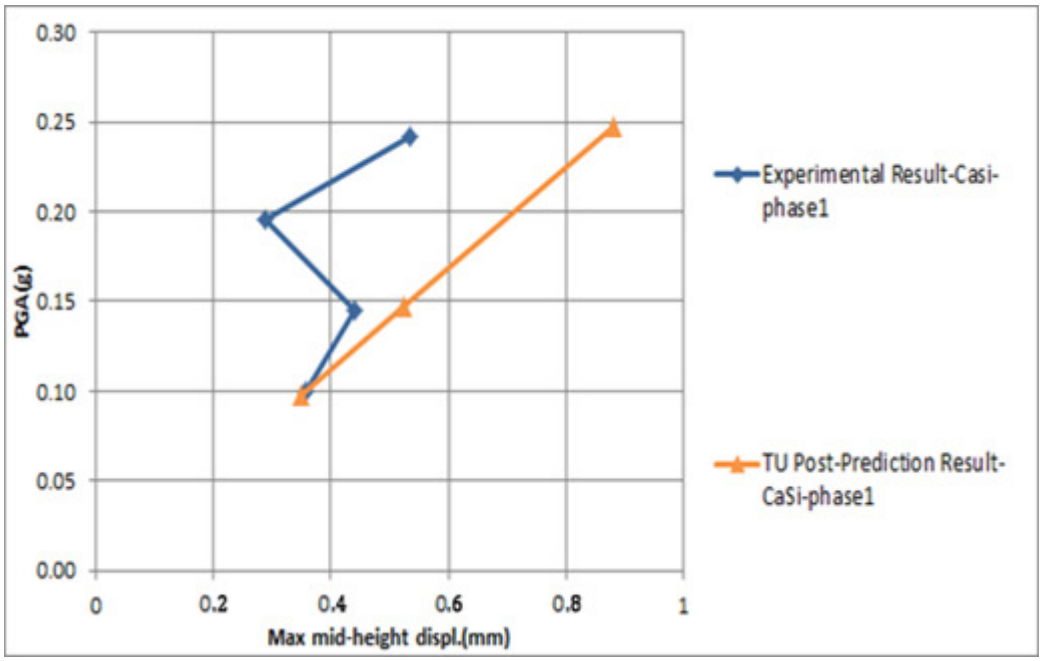

Figure 158: EUC-COMP-6: DIANA post-test refined prediction – Relative mid-height response vs. PGA for model under incremental dynamic testing procedure of ground motion Gr_1

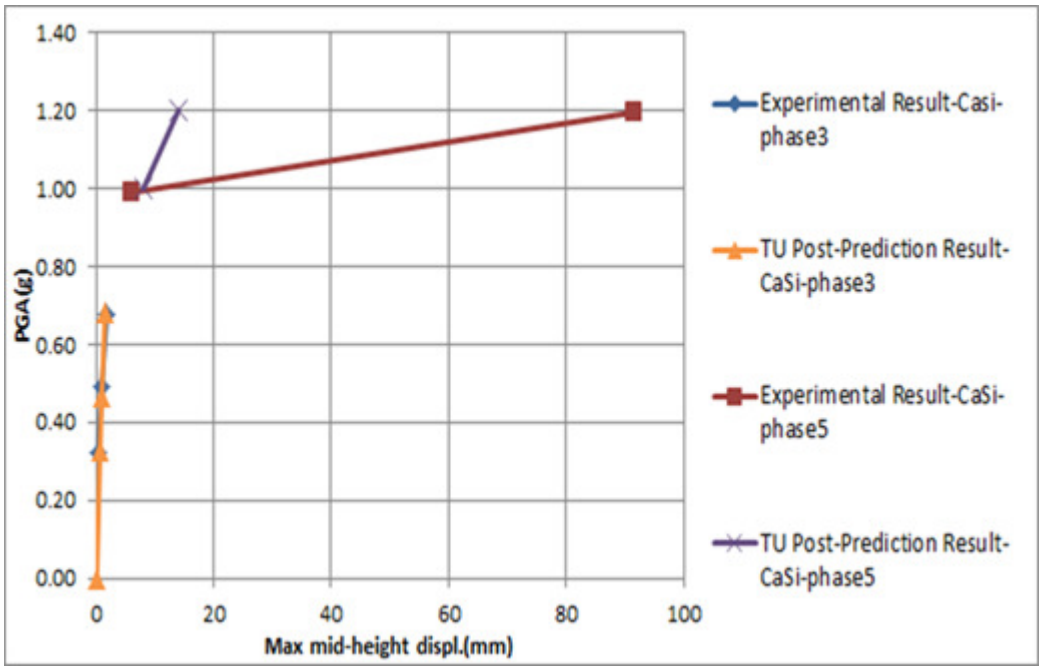

Figure 159: EUC-COMP-6: DIANA post-test refined prediction – Relative mid-height response vs. PGA for model under incremental dynamic testing procedure of ground motion Gr_2

4.3.9 EUC-COMP-7

4.3.9.1 Test Description

EUC-COMP-7 is the third dynamic out-of-plane test in the blind prediction program administered by EUCENTRE. This specimen is a single-wythe cavity wall. The inner (structural) leaf is constructed of calcium silicate units and is 1.44 metres long and 2.75 metres high. The outer leaf is constructed of clay units and is 1.44 metres long and 2.7 metres high. The inner and outer leaves are connected with 4 ties/m^2. The applied overburden stress on the inner leaf is 0.1 MPa.

Table 54: EUC-COMP-7: Testing sequence

Specimen	Phase #	Test #	Dynamic Input	Input Scaling	Expected PGA [g]
EC_COMP_7	0	0.1	Hammering	-	-
EC_COMP_7	0	0.2	White Noise	-	0.1
EC_COMP_7	1	1.1	Gr_1	+20%	-0.04
EC_COMP_7	1	1.2	Gr_1	+40%	-0.09
EC_COMP_7	1	1.4	Gr_1	+60%	-0.13
EC_COMP_7	1	1.5	Gr_1	+80%	-0.18
EC_COMP_7	1	1.6	Gr_1	+100%	-0.23
EC_COMP_7	2	2.1	RWA	-	-0.31
EC_COMP_7	2	2.2	RWA	-	+0.34
EC_COMP_7	3	3.1	Gr_2	+70%	-0.32
EC_COMP_7	3	3.2	Gr_2	+100%	-0.45
EC_COMP_7	3	3.3	Gr_2	+150%	-0.66
EC_COMP_7	3	3.4	Gr_2	+170%	-0.75
EC_COMP_7	4	4.1	RWA	-	+0.30
EC_COMP_7	4	4.2	RWA	-	-0.31
EC_COMP_7	4	4.3	Hammering	-	-
EC_COMP_7	4	4.4	White Noise	-	-
EC_COMP_7	4	4.5	RWA	-	-0.50
EC_COMP_7	4	4.6	RWA	-	+0.53
EC_COMP_7	5	5.1	Gr_2	+100%	-0.46
EC_COMP_7	5	5.2	Gr_2	+150%	-0.64
EC_COMP_7	5	5.3	Gr_2	-100%	+0.51
EC_COMP_7	5	5.4	Gr_2	-150%	+0.72

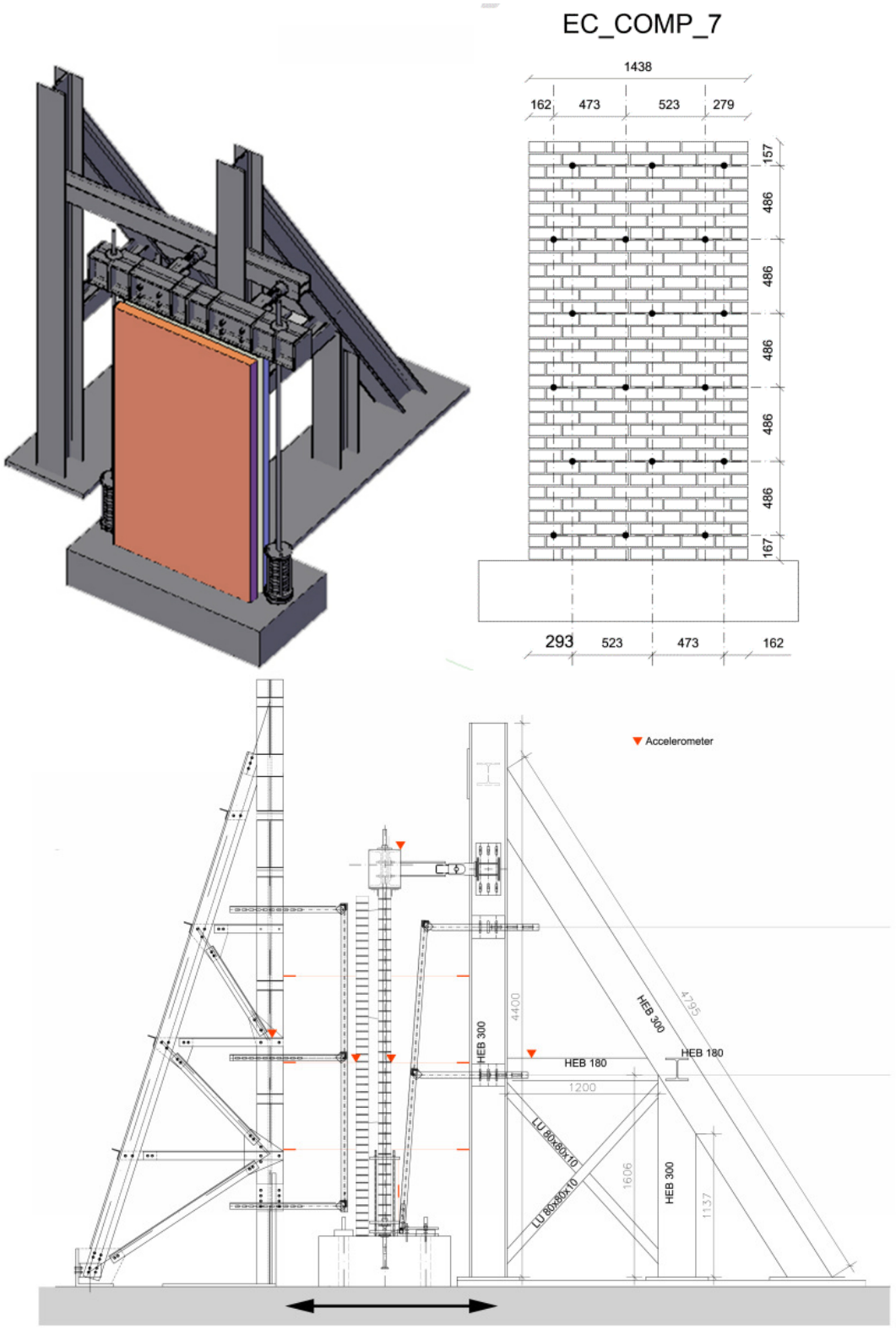

Figure 160: Test set-up images

Figure 161: EUC-COMP-7: collapse

4.3.9.2 Arup Post-Test Refined Prediction

In the test EUC-COMP-7 the specimen was subjected to ground motion Phases 1, 3 and 5 (see Table 54). Phases 2 and 4, consisting of the Ricker Wave Acceleration calibration signal, were not modelled.

Results for Phase 1 are shown in Figure 163. At low PGA levels, the analysis predicts greater displacements than the lab test. This may result from the model wall ties being under-stiff.

Results for Phase 3 are shown in Figure 164. Correlation with the lab test for the larger ground motions is good. Large deflections occur at 0.75g PGA, due to failure of the walls themselves in one-way bending (Figure 164). The greater density of wall ties ensures that they are not the weakest part of the system, and therefore potentially pessimistic representation of the properties of the wall ties in the analysis has less influence on results of this test. Results for Phase 5 are not shown since the model collapsed during the Test Phase 5.1.

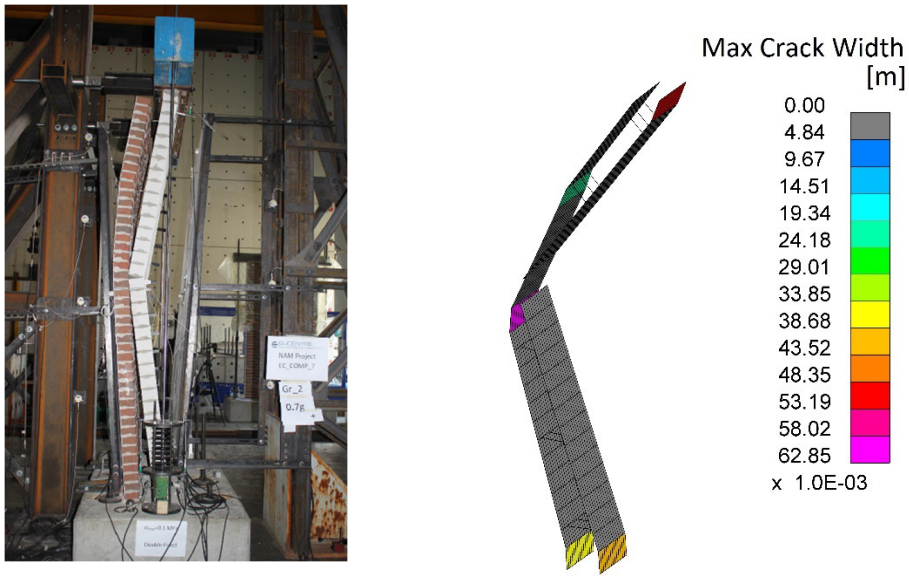

Figure 162: EUC-COMP-7: LS-DYNA post-test refined prediction - Damage plot at end of analysis

Figure

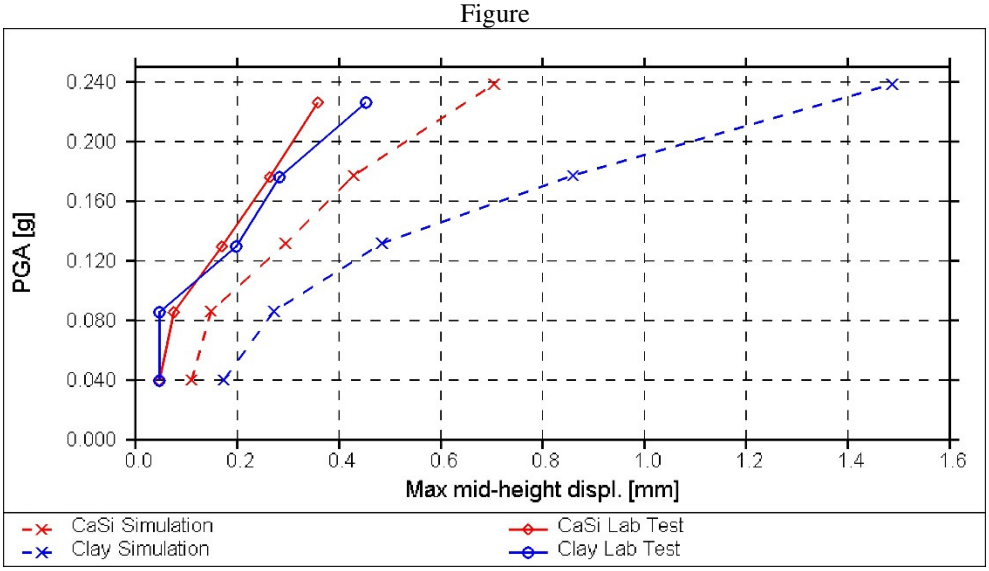

Figure 163: EUC-COMP-7: LS-DYNA post-test refined prediction – Relative mid-height response vs. PGA for model under incremental dynamic testing procedure of ground motion Gr_1 (test phases #1)

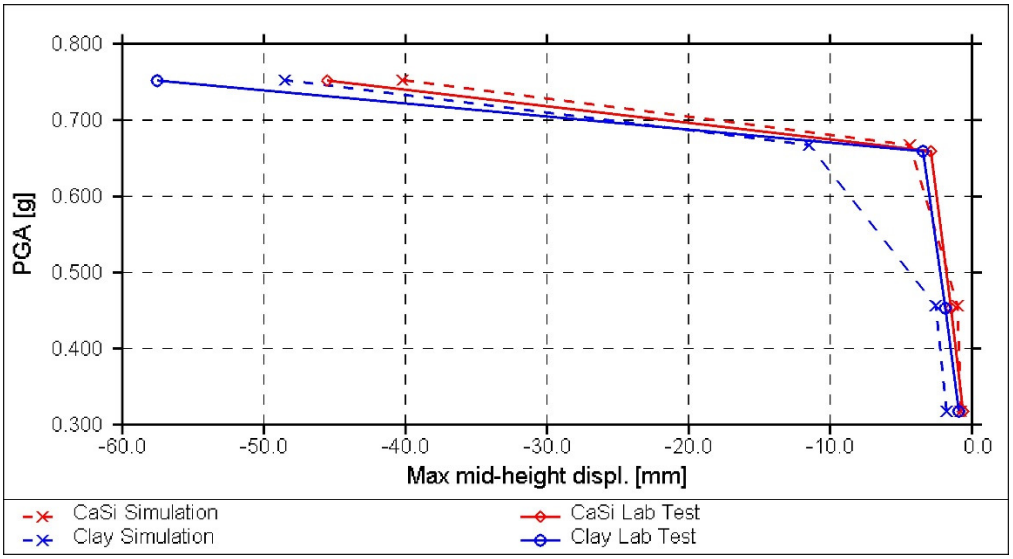

Figure 164: EUC-COMP-7: LS-DYNA post-test refined prediction – Relative mid-height response vs. PGA for model under incremental dynamic testing procedure of ground motion Gr_2 (test phases #3)

4.3.9.3 EUCENTRE Post-Test Refined Prediction

The simulation results are summarised in the comparison shown in Section 4.3.8.3, which also includes analysis results for EUC-COMP-5 and EUC-COMP-6.

4.3.9.4 TU-Delft Post-Test Refined Prediction

In the test EUC-COMP-7, the specimen was subjected to ground motion Gr_1 and Gr_2 separately; consequently, no accumulated damage was considered. The individually applied ground motions were incrementally scaled similar but not identical to the reported scaling factors of Phases 1, 3 and 5 in the loading protocol as shown in Table 54. The results are summarised in Figure 165 and Figure 166.

The results of the application of Gr_1 and Gr_2 up to 0.45g PGA show good agreement between the experimental and numerical outputs in terms of maximum drifts. The numerical model is in agreement with the experimental results up through 0.45g PGA of Gr_2 as it did not show any premature global collapse of the wall. This is also true of the experiment, in which the calcium silicate wall did not reach the limit displacement of 100 mm during Phase 3.

As a consequence, beyond 0.45g PGA of Gr_2, the maximum drift is strongly underestimated (about 70%). Indeed, the model predicted a displacement of 30 mm only at 0.72g PGA, whereas in the laboratory the specimen collapsed at that PGA. This may be partially due to performing separate analyses for each phase such that in the last phase, the modelled wall was stiffer and more resistant than that actually tested.

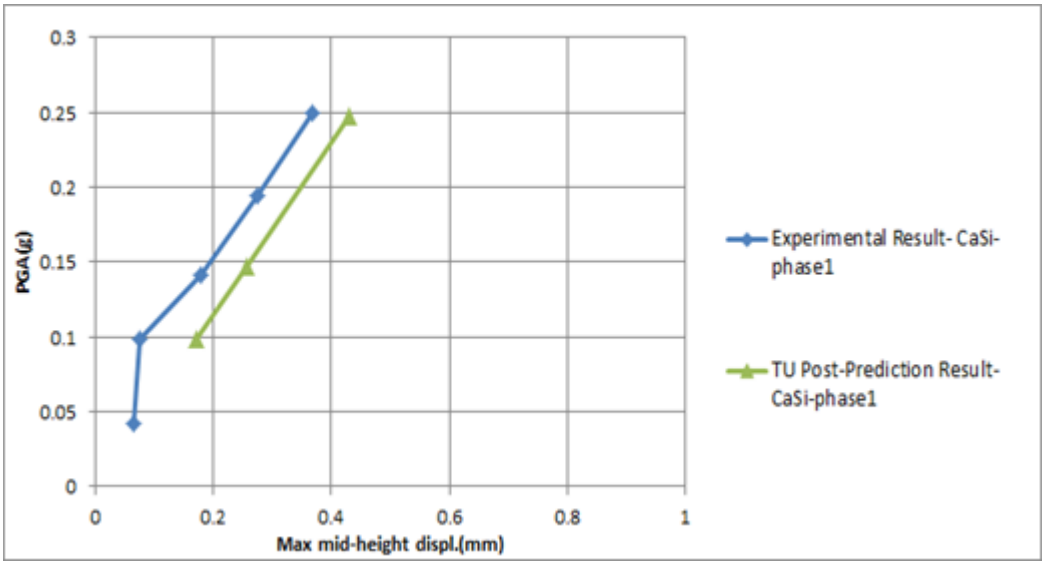

Figure 165: EUC-COMP-7: DIANA post-test refined prediction – Relative mid-height response vs. PGA for model under incremental dynamic testing procedure of ground motion Gr_1

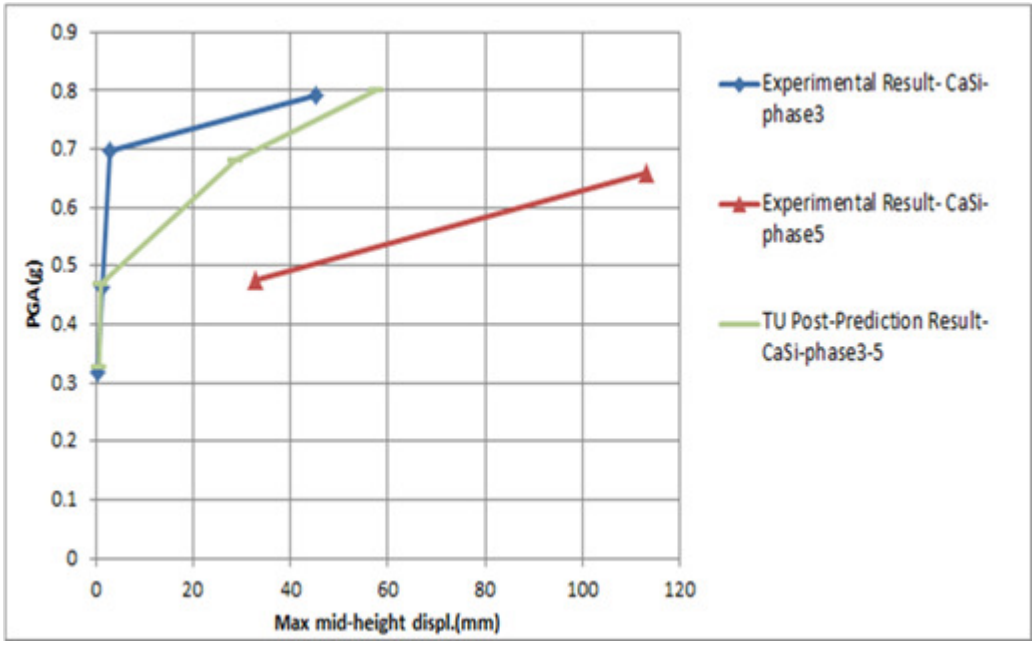

Figure 166: EUC-COMP-7: DIANA post-test refined prediction – Relative mid-height response vs. PGA for model under incremental dynamic testing procedure of ground motion Gr_2

4.3.10 Summary

A summary of the post-test refined prediction results for out-of-plane quasi-static and dynamic tests are summarised in Table 55 and Table 56 below.

Table 55: Summary of post-test analyses of out-of-plane quasi-static tests

Component	LS-DYNA		TREMURI		DIANA		Test Result	
	Peak Strength [kN]	**Max Achieved Drift (End of protocol) [mm]**	**Peak Strength [kN]**	**Max Achieved Drift (End of protocol) [mm]**	**Peak Strength [kN]**	**Max Achieved Drift (End of protocol) [mm]**	**Peak Strength [kN]**	**Max Achieved Drift (End of protocol) [mm]**
TUD-COMP-7	12.4	80	---	---	10.5 (**)	80	10	80
TUD-COMP-10	28	80	20.2 (*)	---	39.5 (**)	100	46	80
TUD-COMP-11	28	80	29.8 (*)	---	25 (**)	100	31	80
TUD-COMP-12	28	100	---	---	22 (**)	100	25	100

(*) Analytical calculation was performed in lieu of numerical analysis

(**) Pushover was performed in lieu of the applied cyclic loading protocol

Table 56: LS-DYNA post-test refined prediction results summary for out-of-plane dynamic tests

Component	LS-DYNA		TREMURI		DIANA		Test Result [1]	
	Max Achieved PGA [g]	Increment cycle at failure	Max Achieved PGA [g]	Increment cycle at failure	Max Achieved PGA [g]	Increment cycle at failure	Max Achieved PGA [g]	Increment cycle at failure
EUC-COMP-4	0.96 (no collapse)	5 [2]	--- [3]	--- [3]	1.1	--- [4]	0.96	5 [2]
EUC-COMP-5	0.60	4	--- [3]	--- [3]	0.7 (no collapse)	--- [4]	0.68	6
EUC-COMP-6	0.77	3	--- [3]	--- [3]	1.15 (no collapse)	--- [4]	1.16	5
EUC-COMP-7	0.75	5 [2]	--- [3]	--- [3]	0.8 (no collapse)	--- [4]	0.72	5 [2]

1. All lab tests resulted in collapse at the reported max achieved PGA

2. Increment cycles are defined as the first character of the 'Test #' in Table 51, Table 52, Table 53 and Table 54. This relates to the number of series of incremental ground motion which have been applied in order to reach failure. Note that for the simulations of components EUC-COMP-4 and EUC-COMP-7 the maximum PGA does not occur during the last series of incremental ground motion (increment cycle at failure) but at an earlier stage in the analysis.

3. Pushover (static) analysis method cannot predict this dynamic response

4. Each ground motion was applied separately. Since ground motions were not applied sequentially, increment cycle cannot be determined.

5 Conclusions

The post-test refined predictions presented in this report offer a snapshot of the current performance of the simulation methods and software used by the three consultants, using the best available input data. However, this report does not close out the analysis of the component tests. The tests have provided a rich source of information about the behaviour of masonry from which much can be learned and which should form the basis of future improvements in the simulation methods and software, leading to a greater ability to predict collapse of URM buildings in seismic events.

Table 57 below presents a summary of all of the component tests that summarizes whether or not each consultant modelled each component test as was performed in the laboratory and what software / material model version was used.

Table 57: Summary

Component	Description of Lab Test	Description of Analysis			Software / Material Model		
		Arup	EUCENTRE	TU-Delft	Arup	EUCENTRE	TU-Delft
TUD-COMP-0a	In-plane quasi-static (cyclic)	In-plane quasi-static (cyclic)	In-plane quasi-static (cyclic)	In-plane quasi-static (cyclic)	LS-DYNA [1]	TREMURI new model [3]	DIANA new in-plane model [5]
TUD-COMP-1	In-plane quasi-static (cyclic)	In-plane quasi-static (cyclic)	In-plane quasi-static (cyclic)	In-plane quasi-static (cyclic)	LS-DYNA [1]	TREMURI new model [3]	DIANA new in-plane model [5]
TUD-COMP-2	In-plane quasi-static (cyclic)	In-plane quasi-static (cyclic)	--- [6]	In-plane quasi-static (cyclic)	LS-DYNA [1]	---	DIANA new in-plane model [5]
TUD-COMP-3	In-plane quasi-static (cyclic)	In-plane quasi-static (cyclic)	In-plane quasi-static (cyclic)	In-plane quasi-static (cyclic)	LS-DYNA [1]	TREMURI new model [3]	DIANA new in-plane model [5]
TUD-COMP-4	In-plane quasi-static (cyclic)	In-plane quasi-static (cyclic)	In-plane quasi-static (cyclic)	In-plane quasi-static (cyclic)	LS-DYNA [1]	TREMURI new model [3]	DIANA new in-plane model [5]
TUD-COMP-5	In-plane quasi-static (cyclic)	In-plane quasi-static (cyclic)	In-plane quasi-static (cyclic)	In-plane quasi-static (cyclic)	LS-DYNA [1]	TREMURI new model [3]	DIANA new in-plane model [5]
TUD-COMP-6	In-plane quasi-static (cyclic)	In-plane quasi-static (cyclic)	In-plane quasi-static (cyclic)	In-plane quasi-static (cyclic)	LS-DYNA [1]	TREMURI new model [3]	DIANA new in-plane model [5]
EUC-COMP-1	In-plane quasi-static (cyclic)	In-plane quasi-static (cyclic)	In-plane quasi-static (cyclic)	In-plane quasi-static (cyclic)	LS-DYNA [1]	TREMURI current model [2] w/ reduced h_{eff}	DIANA new in-plane model [5]
EUC-COMP-2	In-plane quasi-static (cyclic)	In-plane quasi-static (cyclic)	In-plane quasi-static (cyclic)	In-plane quasi-static (cyclic)	LS-DYNA [1]	TREMURI current model [2]	DIANA new in-plane model [5]
EUC-COMP-3	In-plane quasi-static (cyclic)	In-plane quasi-static (cyclic)	In-plane quasi-static (cyclic)	In-plane quasi-static (cyclic)	LS-DYNA [1]	TREMURI current model [2]	DIANA new in-plane model [5]

Table 57 (continued): Summary

Component	Description of Lab Test	Description of Analysis			Software / Material Model		
		Arup	EUCENTRE	TU-Delft	Arup	EUCENTRE	TU-Delft
TUD-COMP-7	Out-of-plane quasi-static (cyclic)	Out-of-plane quasi-static (cyclic)	---	Out-of-plane static (pushover)	LS-DYNA [1]	---	DIANA out-of-plane model [4]
TUD-COMP-10	Out-of-plane quasi-static (cyclic)	Out-of-plane quasi-static (cyclic)	Analytical calculation	Out-of-plane static (pushover)	LS-DYNA [1]	---	DIANA out-of-plane model [4]
TUD-COMP-11	Out-of-plane quasi-static (cyclic)	Out-of-plane quasi-static (cyclic)	Analytical calculation	Out-of-plane static (pushover)	LS-DYNA [1]	---	DIANA out-of-plane model [4]
TUD-COMP-12	Out-of-plane quasi-static (cyclic)	Out-of-plane quasi-static (cyclic)	---	Out-of-plane static (pushover)	LS-DYNA [1]	---	DIANA out-of-plane model [4]
EUC-COMP-4	Out-of-plane dynamic	Out-of-plane dynamic	Out-of-plane static (pushover) [7]	Out-of-plane dynamic (separate models)	LS-DYNA [1]	TREMURI current model [2]	DIANA out-of-plane model [4]
EUC-COMP-5	Out-of-plane dynamic	Out-of-plane dynamic	Out-of-plane static (pushover) [7]	Out-of-plane dynamic (separate models)	LS-DYNA [1]	TREMURI current model [2]	DIANA out-of-plane model [4]
EUC-COMP-6	Out-of-plane dynamic	Out-of-plane dynamic	Out-of-plane static (pushover) [7]	Out-of-plane dynamic (separate models)	LS-DYNA [1]	TREMURI current model [2]	DIANA out-of-plane model [4]
EUC-COMP-7	Out-of-plane dynamic	Out-of-plane dynamic	Out-of-plane static (pushover) [7]	Out-of-plane dynamic (separate models)	LS-DYNA [1]	TREMURI current model [2]	DIANA out-of-plane model [4]

1. See Appendix B1.1

2. See Appendix B1.2

3. Different hysteretic behaviour in compression that allows an increased energy dissipation in bending-rocking mechanisms. See section 4.2.2.

4. Isotropic total strain fixed crack model, shell elements. See Appendix B1.3.

5. Orthotropic constitutive model, plane stress elements. See section 3.2.3.2 and Appendix B1.3.

6. The post-test analysis was not conducted by EUCENTRE since the laboratory records for this test resulted to be far from theoretical calculation (from which the TREMURI algorithm is developed)

7. This method does not predict the dynamic response of the walls to the applied ground motions. Pushover method performed instead to develop tool needed for a reliable SDOF calibration.

5.1 Arup Conclusions

General conclusions:

- The LS-DYNA models all ran robustly without abnormal termination, either completing the input protocol or predicting collapse of the specimen for physically plausible reasons.
- The peak strength of the in-plane specimens are in general well predicted.
- For the out-of-plane specimens, bending about the horizontal axis is predicted reasonably accurately, but bending about the vertical axis (which contributes to the resistance in two-way spanning) is weaker than indicated by the experiments.
- Results for the cavity wall dynamic test specimens are strongly influenced by the assumed behaviour of the wall-ties. Best results are obtained when the analysis assumed somewhat higher strength than was measured in quasi-static cyclic pull-out tests.
- In-plane and out-of-plane rocking modes absorb too little energy in the analyses compared to the tests.
- An important aspect of the analyses of existing buildings for the GESU project is to predict whether the building collapses or is in a near-collapse state. Predictions of the drift or dynamic loading to cause collapse of the specimens are in many cases reasonably good. Improvements are needed in respect of squat in-plane walls, some of which reach a near-collapse state at much lower drift levels in the laboratory than predicted by the analysis. Further work on wall tie behaviour is needed to enable reliable predictions of out-of-plane collapse of cavity walls.

Differences between blind predictions and post-test analyses, apart from those caused by differences of overburden or test protocol:

- In terms of strength and initial failure mode, there is little difference between the blind predictions and the post-test analyses.
- The most significant advance is the ability of the post-test refined analyses of in-plane tests to predict collapse or near-collapse conditions for in-plane loading.
- For the tall samples that exhibit a rocking mode, the post-test analyses show some increase in the energy absorbed in hysteresis compared with the blind predictions, but the absorbed energy is still under-predicted compared to the laboratory test results.

5.2 EUCENTRE Conclusions

The post-test simulation of the quasi-static tests on masonry walls (components) showed a general accuracy of the TREMURI models to replicate the backbone curves of in-plane and out-of-plane tests.

The new model developed for accounting for a different behaviour in compression associated with in-plane flexural response provided an increased energy dissipation but still smaller than the one reported in the test results.

For the squat walls failing in shear, the energy dissipation is well captured by the macro-element model.

The static simulation of the out-of-plane wall tests provided accurate backbone curves for single and cavity walls subject to quasi-static and dynamic loadings. This will allow future parametric studies to develop and validate appropriate damping models to be used in time history analyses of suitably defined SDOF and/or MDOF models.

Some remaining unclear issues in some of the test results limited the extension of post-test refined analyses and the validity of the comparisons to the specimens with results consistent with minimum physical checks.

5.3 TU Delft Conclusions

The results of the previously performed blind predictions highlighted the need for the definition of a direction dependent material model that is able to differentiate the nonlinear behaviour in pre-defined damage directions and, consequently, to capture the different failure modes that can occur. A new masonry material model has been recently developed and has been applied in the post-test refined prediction of the in-plane tests, giving promising improved results. The model is still under refinement and more improvements could be obtained in future. Extension to the out-of-plane tests is ongoing.

At the current stage of the post-test refined prediction process, the following conclusions can be drawn.

In-plane tests:

- The new material model is extremely beneficial in terms of stability of the solution. No convergence troubles have been encountered and the analyses have been all run for the whole loading protocol.
- The shear capacity of the panel is in general good agreement with the experiments
- A noticeable improvement in terms of energy dissipation is observed
- Larger degradation of lateral capacity compared to experimental results is observed in some cases
- Damage patterns tend to be too widespread compared to experiments. Damage localization should be improved.

Quasi-static out-of-plane tests:

- The model faced some convergence issues for large displacements. This is caused by the modality of application of the load (and, indeed, it did not occur for dynamic tests) which required the use of the arc-length control. For the same reason, only few cyclic analyses had been performed.
- The models can satisfactorily predict the resistance of the walls, and provide a consistent representation of the damage state at the end of the tests.
- The post-peak behaviour predictions are poor for two-way bending tests. In addition, the dissipated energy is underestimated, especially for large displacements. The application of an orthotropic constitutive law for masonry (which is currently under investigation and has already been applied in the analyses of in-plane tests) would allow to define different tensile strength and fracture energy in the vertical and horizontal directions so that a better representation of bending about the vertical axis could be provided.

Dynamic out-of-plane tests:

- The model is able to reproduce the main failure mechanism related to out-of-plane behaviour although the stiffness and strength at higher PGAs are often over-predicted
- The application of sequential analyses might improve the prediction of the final displacements for the last phases
- Refinement of the connections (wall ties), which are currently modelled as linear elements, would be advisable.

Appendix A

A1 Material Properties

A1.1 Basis for Design Material Properties

The NAM Basis for Design (BfD) revision 3 properties were used from [8], Table 7. These are not based on testing of the actual buildings under assessment. The table is reproduced below, for reference.

Table 58: NAM BfD rev 3 URM properties (extract from [8])

Symbol	Material Property	Clay Brickwork (pre 1945)	Clay Brickwork (post 1945)	Calcium-silicate brickwork (typical approx. 1960-1985)	Calcium-silicate blocks/ elements with thin layer joints (typical approx. 1985-present)
f'm	Masonry compressive strength	7.5	8.0	6.0	10
Em	Masonry Young's modulus	3500	6000	3500	7500
Gm	Masonry shear modulus	1450	2500	1450	3000
fx1	Masonry bending strength with the moment vector parallel to the bed joints and in the plane of the wall	0.15	0.2	0.2	0.6
fx2	Masonry bending strength with the moment vector orthogonal to the bed joint and in the plane of the wall	0.3	0.45	0.45	1.2
fx3	Masonry bending strength with the moment	0.3	0.45	0.45	1.2

Symbol	Material Property	Clay Brickwork (pre 1945)	Clay Brickwork (post 1945)	Calcium-silicate brickwork (typical approx. 1960-1985)	Calcium-silicate blocks/ elements with thin layer joints (typical approx. 1985-present)
	vector orthogonal to the plane of the wall				
fb	Masonry bond strength between brick and mortar	0.1	0.15	0.15	0.4
fv0	Masonry initial (bed joint) shear strength	0.2	0.3	0.3	0.6
tan φ	Masonry (bed joint) shear friction coefficient	0.75	0.75	0.75	0.75
Gf	Fracture energy in tension	35	35	15	15
Gc	Fracture energy in compression	5000	5000	5000	5000

Note that the input for LS-DYNA required certain masonry material parameters that were not provided in the BfD data. These values were calculated by Arup based on assumptions pertaining to the behaviour of the material.

Appendix B

B1 Modelling Approach

B1.1 Arup

Table 59: Arup general modelling notes

Component	Description
Analysis team	Arup
Analysis software and formulation	LS-DYNA – Explicit time integration scheme
Overview of modelling approach	Explicit time integration scheme is used for nonlinear pushover and response history analysis Masonry modelled with fully integrated shell elements with damage lumped at each integration point and crack plane directions are pre-defined to model mortar bonds Shell elements, beam elements, and discrete (spring) elements are used to model other components of the tests. Material properties are either defined based on the median material properties defined in the Basis for Design issued by NAM (blind predictions) or on available test data for masonry characterisation tests (post-test analyses), using a consistent methodology across all tests.
Model units	SI units (kg, m, sec)
Mesh size	0.1m x 0.1m
Assumptions	Applied overburden is uniformly distributed along the top of the wall using LOAD_RIGID_BODY Boundary condition at the top and bottom of the wall is continuous

Table 60: Arup model properties applicable for all blind prediction tests

Input	Description
Element formulation	2D, fully integrated shell elements. Two through-thickness integration points for models subjected strictly to in-plane action. Five through-thickness integration points for all other models.
Shell material type	MAT_SHELL_MASONRY*
Damping	DAMPING_PART_STIFFNESS, with damping coefficient 0.05, for numerical stability without affecting primary behaviours. DAMPING_FREQUENCY_RANGE_DEFORM, with damping coefficient 0.005 - 0.01 for frequency range 1-30 Hz for models subjected to out-of-plane dynamic action and damping coefficient 0.01 for frequency range 1-30 Hz for all other models.

*This material model is under development. For the post-test analyses reported in this document, the October 2015 version was used. This version offers bed joint sliding and opening capabilities, diagonal tensile failure, toe-crushing and compression failure.

B1.2 EUCENTRE

Table 61: EUCENTRE general modelling notes

Component	Description
Analysis team	EUC-Pavia
Analysis software and formulation	TREMURI – Equivalent-frame formulation based on a macro-element model
Overview of modelling approach	The adopted equivalent-frame modelling strategy implemented in the TREMURI program [Lagomarsino et al., 2013] [10] is based on the effective non-linear macro-element modelling approach. The macro-element model represents the cyclic non-linear behaviour associated with the two main in-plane masonry failure modes, bending-rocking and shear mechanisms, with a limited number of degrees of freedom (8 d.o.f) and internal variables which describe the damage evolution [Penna et al., 2014] [11]. The two-node macro-element, suitable for modelling piers and spandrel beams, can be ideally subdivided into three parts: a central body where only shear deformation can occur and two interfaces, where the external degrees of freedom are placed, which can have relative axial displacements and rotations with respect to those of the extremities of the central body. In the two interfaces, infinitely rigid in shear, the axial deformations are due to distributed system of zero-length springs with no-tension and limited compression behaviour. Due to the concentration of the axial and flexural deformations in the interfaces, the spring stiffness equal to $k = 2E'/h$, where E' is an effective elastic modulus and h is the element length (height in case of pier elements), is set differently as far as axial or lateral stiffness need to be more accurately reproduced. The following settings apply for E': $E' = E$ (masonry Young's modulus in compression) when axial stiffness in concerned; $E' = 1.5E$ when lateral stiffness is concerned in a cantilever wall; $E' = 3E$ when lateral stiffness is concerned in a double-fixed wall; E' is usually set to $2E$ when lateral stiffness is concerned in a building model with intermediate boundary conditions for the different structural elements. The macroscopic shear model is based on a combination of equivalent cohesion, $\bar{\bar{c}}$, and friction, $\bar{\bar{\mu}}$, parameters. The determination of the model parameters from the "local" mechanical parameters derived from characterisation tests depends on the adopted shear strength criterion: The TREMURI computer program performs several types of linear and nonlinear analyses: modal analysis, incremental static analyses (Newton-Raphson) with force or displacement control, 3D pushover analyses with fixed and adaptive load pattern and 3D time-history dynamic analysis (Newmark integration method; Rayleigh viscous damping). Floor and roof diaphragms are modelled by means of linear 3-node and 4-node orthotropic membrane elements.
Model units	SI units (kg, m, sec)

B1.3 TU-Delft

Table 62: TUD general modelling notes

Component	Description
Analysis team	TU-Delft
Analysis software and formulation	DIANA implicit solver
Overview of modelling approach	For in-plane test: new material model based on a total strain approach with two pre-defined crack/crush directions (aligned to the bed- and head-joints) and five possible failure mode (2 in tension, 2 in compression, shear). For more details see Section 3.2.3. For out-of-plane tests: total strain fixed crack model
Model units	SI units (kg, m, sec)
Mesh size	On average 0.1 m x 0.1 m for both in-plane and out-of-plane
Assumptions	Applied overburden is uniformly distributed along the top of the wall Boundary condition at the top and bottom of the wall is continuous

Table 63: Model properties applicable for all blind prediction tests

Input	Description
Element formulation	In-plane panels: Plane stress elements Out-of-plane panels: Shell elements
Shell material type	In-plane panels: New orthotropic material model Out-of-plane panels: Total strain fixed crack model
Damping	For dynamic tests, damping defined through Rayleigh parameters with damping coefficient equal to 1%.

References

[1] Arup, 229746_032.0_REP127, "Modelling and Analysis Cross-Validation – Arup, EUC, TU-Delft", July 2015, Rev A.01

[2] EUCENTRE, "Experimental campaign on cavity walls systems representative of the Groningen building stock", November 2015

[3] TU-Delft, "Preliminary test reports for in-plane tests on masonry walls at TU-Delft", October 2015

[4] TU-Delft, "Preliminary test reports for out-of-plane tests on masonry walls at TU-Delft", January 2016

[5] TU-Delft, "Tests for the characterisation of replicated masonry", October 2015

[6] TU-Delft, "Pull-out strength of wall ties", December 2015

[7] Tomassetti U., Graziotti F., Penna A., Magenes G. (2015). A single degree of freedom model for the simulation of the out-of-plane response of unreinforced masonry walls. Proc.Italian National Conference on Earthquake Engineering, L'Aquila, Italy.

[8] NAM, Basis for Design: Seismic Structural Upgrading of Existing Buildings in the Groningen Area, Rev 3, March 2015, Doc Ref: EP201403208456

[9] TU-Delft, "Tests for the characterisation of replicated masonry", August 2015, version 4

[10] Lagomarsino S., Penna A., Galasco A., Cattari S., (2013) "TREMURI Program: an equivalent frame model for the nonlinear seismic analysis of masonry buildings", ENGINEERING STRUCTURES, 56(11): 1787-1799.

[11] Penna A., Lagomarsino S., Galasco A., (2014) "A nonlinear macro-element model for the seismic analysis of masonry buildings", EARTHQUAKE ENGINEERING & STRUCTURAL DYNAMICS, 43(2): 159-179.

[12] Vaculik, J. [2012], "Unreinforced masonry walls subjected to out-of-plane seismic actions", PhD thesis, University of Adelaide

[13] Arup, 229746_031.0_REP1008, "Laboratory Component Testing Annex: Modelling Blind Predictions and Analysis Cross Validation", February 2016

Client: Nederlandse Aardolie Maatschappij

Arup Project Title: Groningen Earthquakes - Structural Upgrading

Laboratory Component Testing Annex: Modelling Blind Predictions and Analysis Cross Validation

229746_031.0_REP1008

Issue | 16 February 2016

Job number 229746

Arup bv
Naritaweg 118
1043 CA Amsterdam
PO box 57145
1040 BA Amsterdam
The Netherlands

ARUP

Contents

1 Introduction

This report annex presents the results of blind predictions carried out by Arup, EUCENTRE and TU-Delft prior to laboratory tests on unreinforced masonry walls during 2015. In practice, the actual loading applied in many of the tests differed from the planned protocol significantly (for example, in respect of the applied overburden). Comparisons between the blind predictions and the actual test results are therefore of limited value for those tests.

The background to the study, summary of the test campaign, and results of analyses in which the actual conditions of the test have been replicated ("post-test refined predictions") are given in the main report.

Figure 1: Collaboration partners of Arup

2 In-Plane Component Tests: Blind Predictions

2.1 Comparison of Blind Predictions

2.1.1 TUD-COMP-0a

2.1.1.1 Test Description

TUD-COMP-0a was the first of a series of quasi-static in-plane tests administered by TU-Delft. This specimen was a single-wythe wall constructed of calcium silicate units 102 mm thick. It was 1.1 m long and 2.76 m high. The applied overburden stress was 0.7 MPa. The wall was tested under double clamped boundary conditions.

Upon cyclically loading specimen TUD-COMP-0a, a gradual reduction of the initial stiffness occurred at very low drifts. First cracks appeared at the top right corner for positive displacements during the fourth loading cycle (circled in red in Figure 2). The failure mode combined rocking, sliding and crushing. More specifically, the wall underwent a rocking mechanism at first, followed by bed-joint sliding. Toe-crushing only occurred at the end of the test.

The specimen showed asymmetric mechanical behaviour. This can be explained by the fact that the cracks at the left bottom and top right occurred at a different height than those at the right bottom and top left.

The wall was tested up to a peak drift of 0.9%. The test was stopped after a large reduction of resistance for negative imposed displacements because the integrity of the wall could have been compromised.

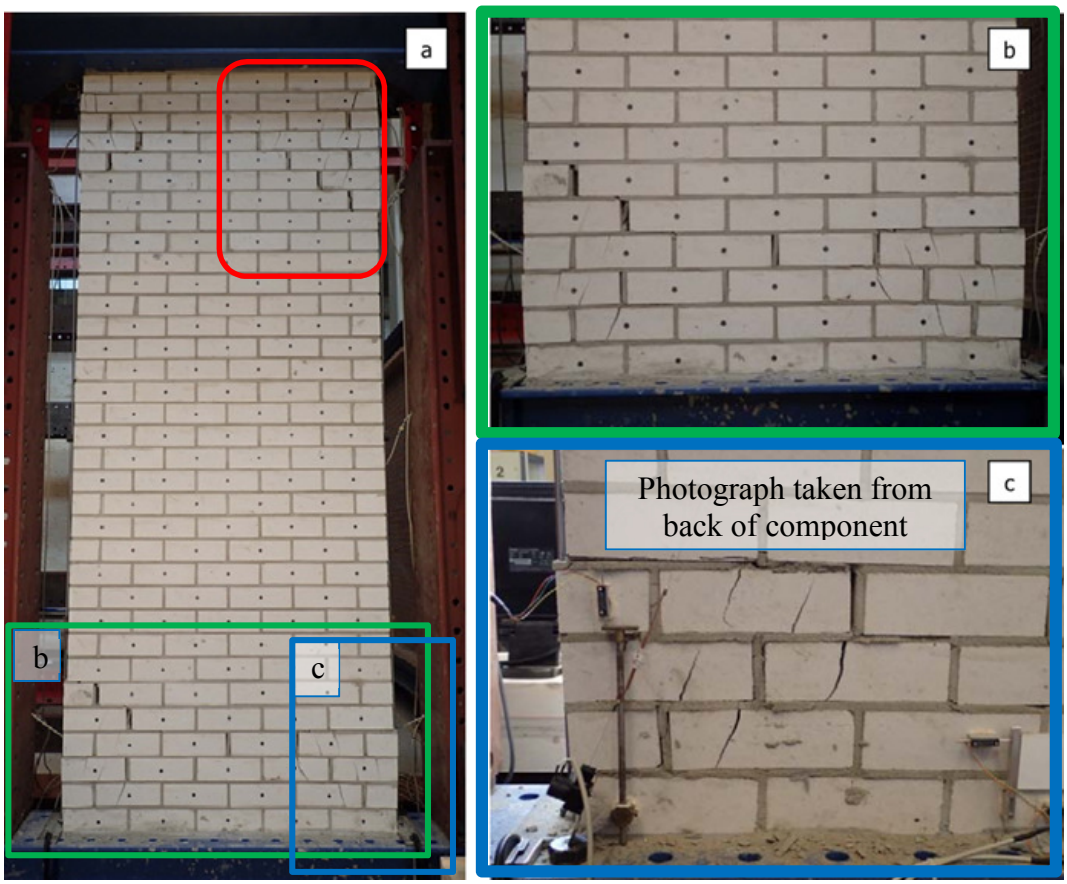

Figure 2: TUD-COMP-0a: Crack pattern at failure; general overview. Cracks in areas highlighted in red (a); detail of the bottom part of the wall (b) and of the toe crushing (c).

The actual loading regime of TUD-COMP-0a differed from that specified in the planned test protocol. The overburden matched the specified value.

The measured hysteresis is shown in Figure 3.

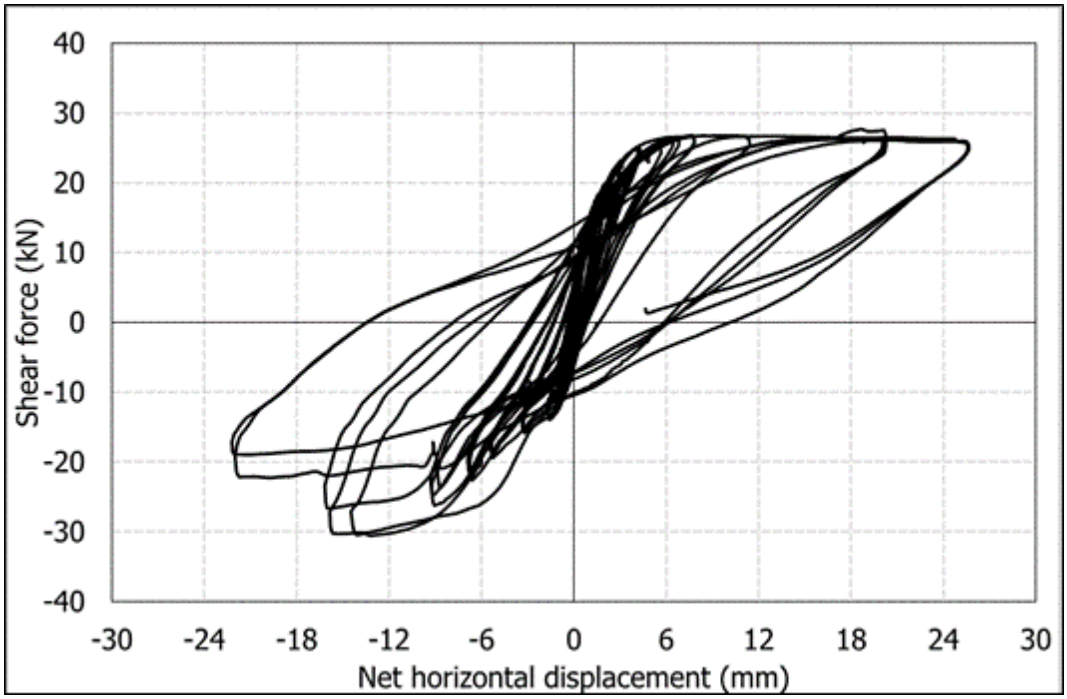

Figure 3: TUD-COMP-0a: Lab test result – Shear force-displacement curve

2.1.1.2 Arup Blind Prediction

The LS-DYNA model of TUD-COMP-0a predicted rocking behaviour and associated tensile bed joint failures at the top and bottom of the specimen as shown in Figure 4.

The lateral-force-versus-displacement relationship followed an S-shaped curve, as shown in Figure 5. The predicted ultimate load was approximately 28 kN at a drift of 0.9%. The predicted initial stiffness was approximately 16.4 kN/mm.

As illustrated by the hysteresis curve, there was little energy dissipated by the LS-DYNA model of the specimen.

The LS-DYNA model captured the rocking mechanism and backbone curve generated during the laboratory test but under-predicted the amount of energy dissipation. A considerable amount of the dissipated energy in the test was a product of the shear sliding and toe-crushing damage, which the LS-DYNA blind prediction model did not capture. The model did not predict collapse or a near-collapse state.

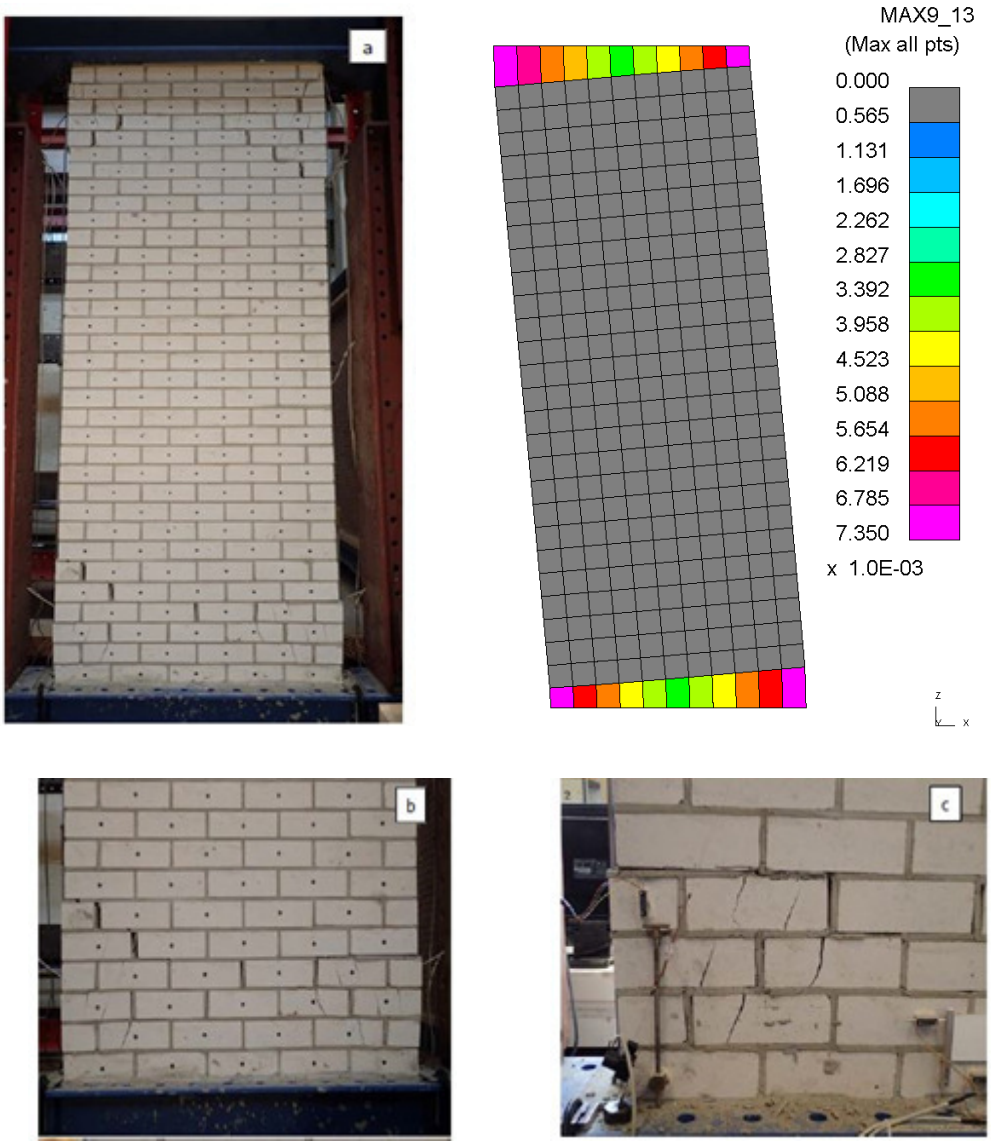

Figure 4: TUD-COMP-0a: LS-DYNA blind prediction - Damage plot at end of analysis (top right) compared to observed damage in laboratory

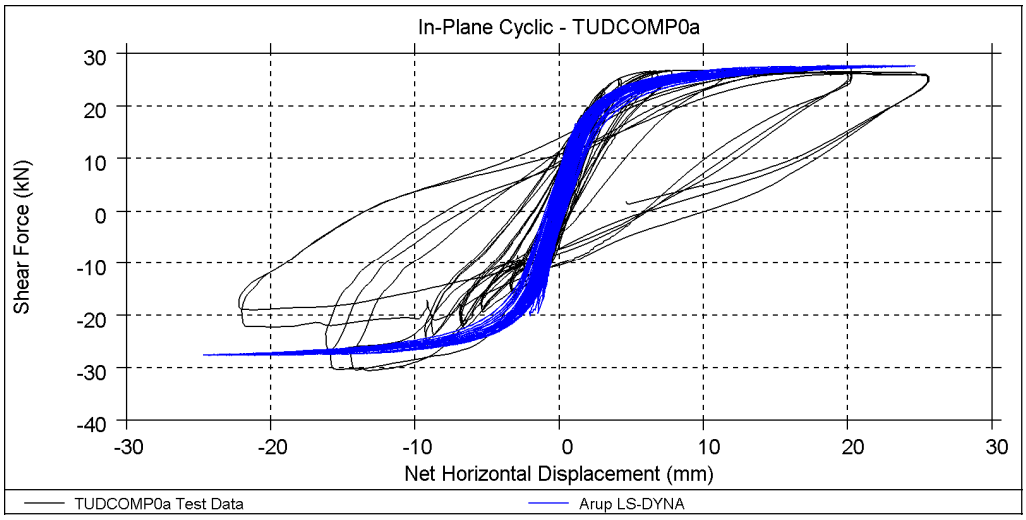

Figure 5: TUD-COMP-0a: LS-DYNA blind prediction - Shear force-displacement curve

Table 1: TUD-COMP-0a: LS-DYNA blind prediction - Summary table

	Predominant Failure Mechanism Predicted	**Initial Stiffness [kN/mm]**	**Peak Strength [kN]**	**Maximum Achieved Drift**	
LS-DYNA	Rocking	16.4	28	0.9%	End of protocol
Test Result	Rocking / toe crushing	25.8	30	0.9%	Near collapse

2.1.1.3 EUCENTRE Blind Prediction

The TREMURI macro-element model predicted a pure rocking behaviour and the resulting hysteresis curve (Figure 7) followed an S-shape curve with little energy dissipation (Figure 9).

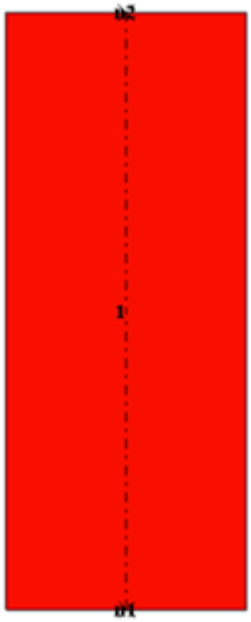

Figure 6: TUD-COMP-0a: TREMURI blind prediction model

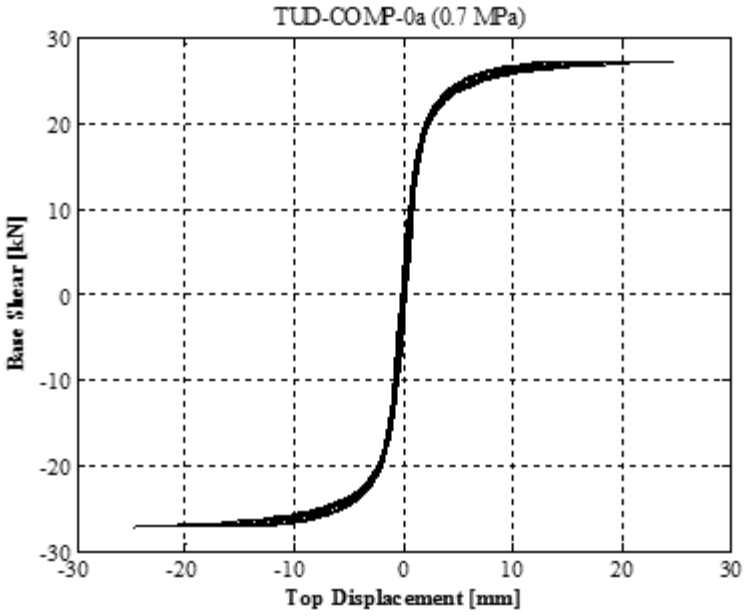

Figure 7: TUD-COMP-0a: TREMURI blind prediction - Shear force-displacement curve

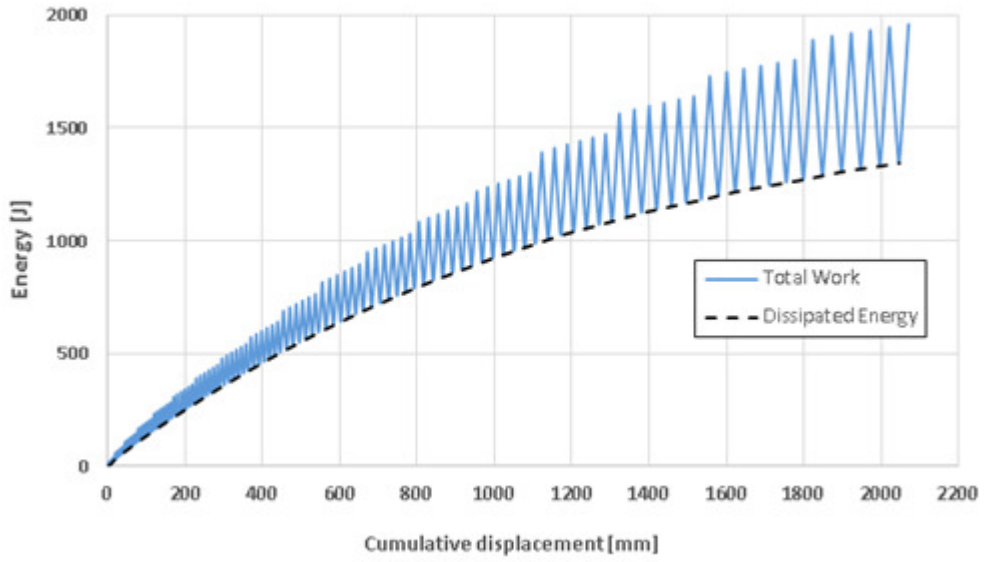

Figure 8: TUD-COMP-0a: TREMURI blind prediction - Work & energy dissipation

Table 2: TUD-COMP-0a: TREMURI blind prediction - Summary table

	Predominant Failure Mechanism Predicted	**Initial Stiffness [kN/mm]**	**Peak Strength [kN]**	**Maximum Achieved Drift**	
TREMURI	Rocking	15.3	27	0.9%	End of protocol
Test Result	Rocking / toe crushing	25.8	30	0.9%	Near collapse

2.1.1.4 TU-Delft Blind Prediction

The DIANA finite element model of the panel was divided in two areas—one at the boundaries where rocking occurs, characterised by a tensile strength equal to the bond strength between brick and mortar joints; and one in the middle of the panel characterised by a higher tensile strength related to a potential diagonal failure. This was done in order to take into account of different failure modes in the panel since, in principle, the total-strain approach provides an isotropic nonlinear behaviour in which the tensile strength is the same in all directions.

The predominant failure mode was rocking with an additional vertical splitting crack close to the upper right corner of the panel (Figure 9). The numerical base shear capacity was 27 kN and the maximum top displacement was 13.8 mm (Figure 10). The analysis could not be performed to larger displacement levels due to convergence issues. The dissipated energy was lower than the one experimentally observed.

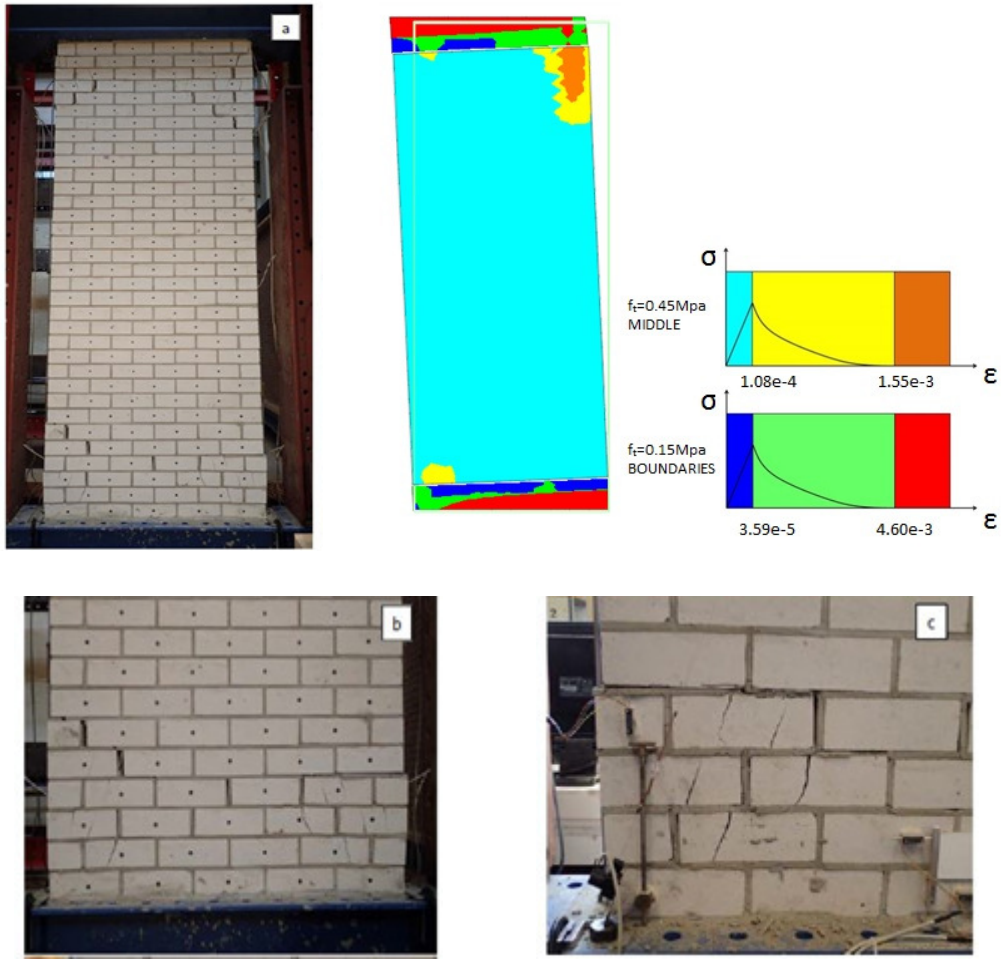

Figure 9: TUD-COMP-0a: DIANA blind prediction - Damage plot at end of analysis (top right) compared to observed damage in laboratory

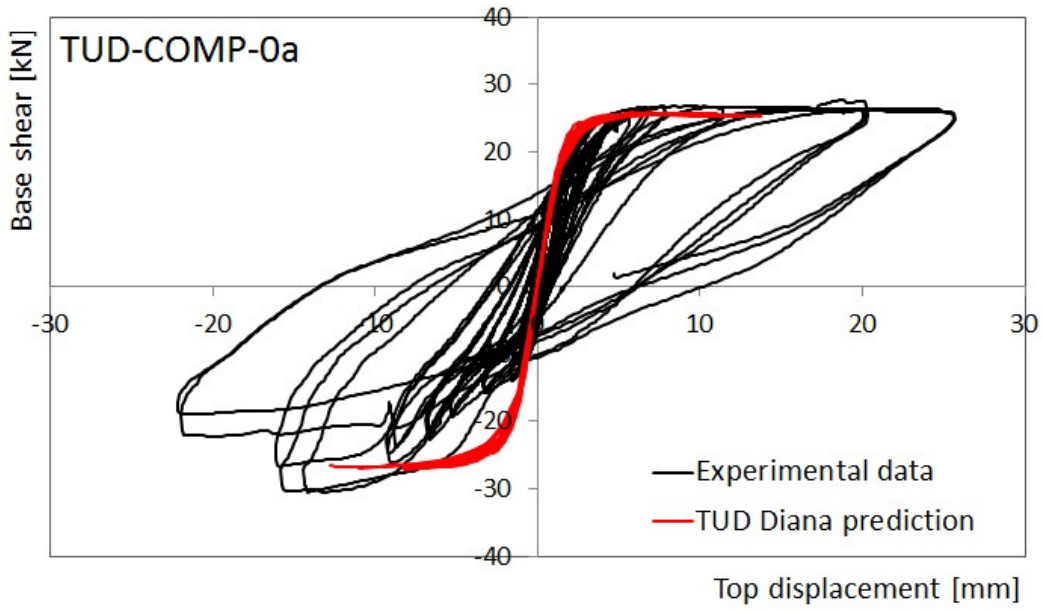

Figure 10: TUD-COMP-0a: DIANA blind prediction - Shear force-displacement curve

Table 3: TUD-COMP-0a: DIANA blind prediction - Summary table

	Predominant Failure Mechanism Predicted	**Initial Stiffness [kN/mm]**	**Peak Strength [kN]**	**Maximum Achieved Drift**	
DIANA	Rocking	15.9	27 (*)	0.5% (*)	(*)
Test Result	Rocking / toe crushing	25.8	30	0.9%	Near collapse

(*) Model not pushed up to 0.9% drift due to failure to converge

2.1.2 TUD-COMP-1

2.1.2.1 Test Description

TUD-COMP-1 was the second quasi-static in-plane test administered by TU-Delft. This specimen was a single-wythe wall constructed of calcium silicate units, 102 mm thick. It was 1.1 m long and 2.76 m high. The applied overburden stress was 0.52 MPa. The wall was tested under cantilever boundary conditions.

Upon cyclically loading specimen TUD-COMP-1, a gradual reduction of the initial stiffness occurred at very low drifts. First cracks appeared at the bottom left corner for negative displacements during the fifth cycle (approximately 0.8% drift). The failure mode was mainly governed by rocking with diagonal crack patterns at the bottom of the wall as mentioned. The specimen showed asymmetric mechanical behaviour. The test was stopped at a net drift of 1.6%.

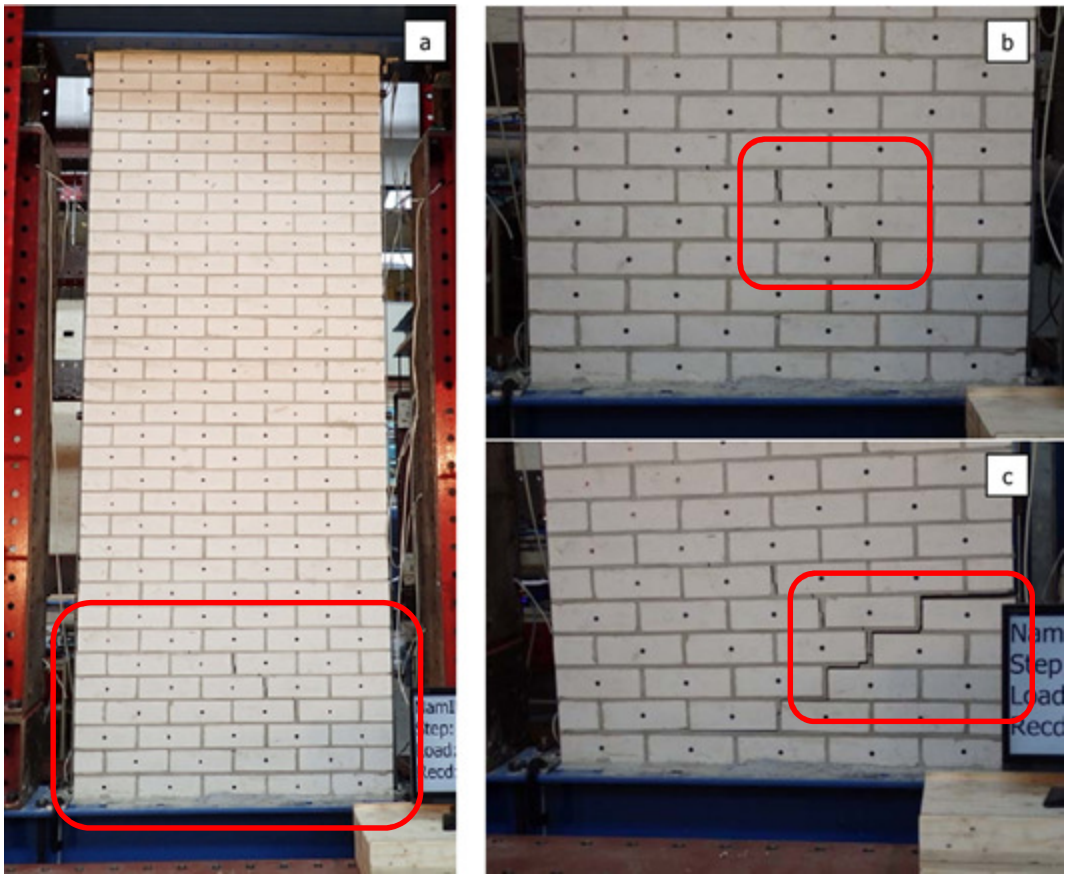

Figure 11: TUD-COMP-1: Crack pattern at failure; general overview (a); detail of the bottom part of the wall for positive (b) and negative (c) peak top displacements.

The actual loading regime of TUD-COMP-1 differed from that specified in the planned test protocol, which specified a maximum drift level of 0.9%. The overburden matched the specified value.

The measured hysteresis is shown in Figure 12. Some readings of the load cell were compromised and thus rendered some sections of the test response unreliable for comparison purposes. These sections are highlighted in Figure 12.

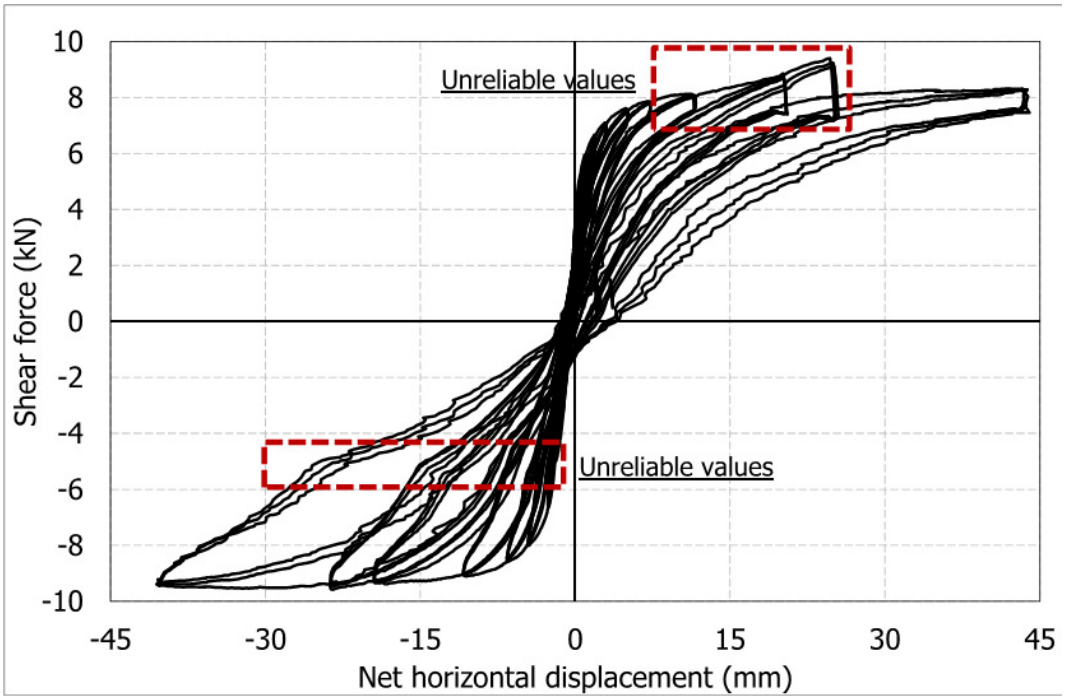

Figure 12: TUD-COMP-1: Lab test result – Shear force-displacement curve

2.1.2.2 Arup Blind Prediction

The LS-DYNA model of TUD-COMP-1 predicted rocking behaviour and associated tensile bed joint failures, predominantly at the bottom of the specimen. The model exhibited slight bed-joint damage in a few locations throughout the wall, due to the moment distribution in the wall, as it was cyclically loaded combined with the cantilever boundary conditions (see Figure 13).

The lateral force versus displacement relationship followed an S-shaped curve, as shown in Figure 14. The predicted ultimate load was approximately 11 kN at a drift of 0.9%. The predicted initial stiffness was approximately 4.9 kN/mm.

As illustrated by the hysteresis curve, there was little energy dissipation predicted. The maximum displacement of LS-DYNA simulation as shown in the hysteresis curve is smaller than that of the test since the planned loading protocol had been changed during the test.

The LS-DYNA model captured the rocking mechanism observed during the laboratory test but under-predicted the amount of energy dissipated. It is reasonable to conclude that a considerable amount of the dissipated energy was a product of the observed diagonal damage pattern observed at the bottom of the wall, which the LS-DYNA blind prediction model did not capture. The LS-DYNA model also over-predicted the initial lateral strength of the specimen. The model did not predict collapse or a near-collapse state.

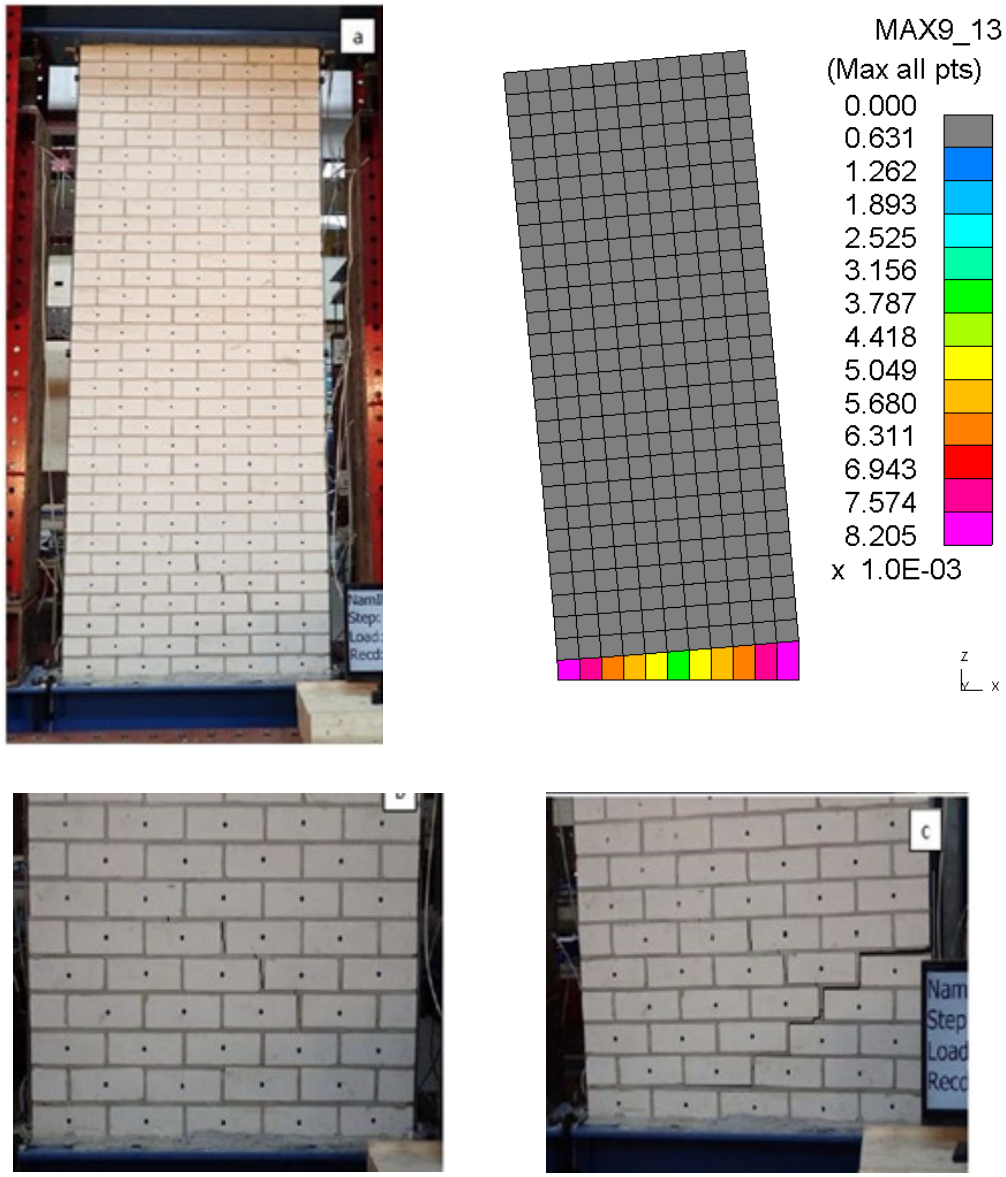

Figure 13: TUD-COMP-1: LS-DYNA blind prediction - Damage plot at end of analysis (top right) compared to observed damage in laboratory

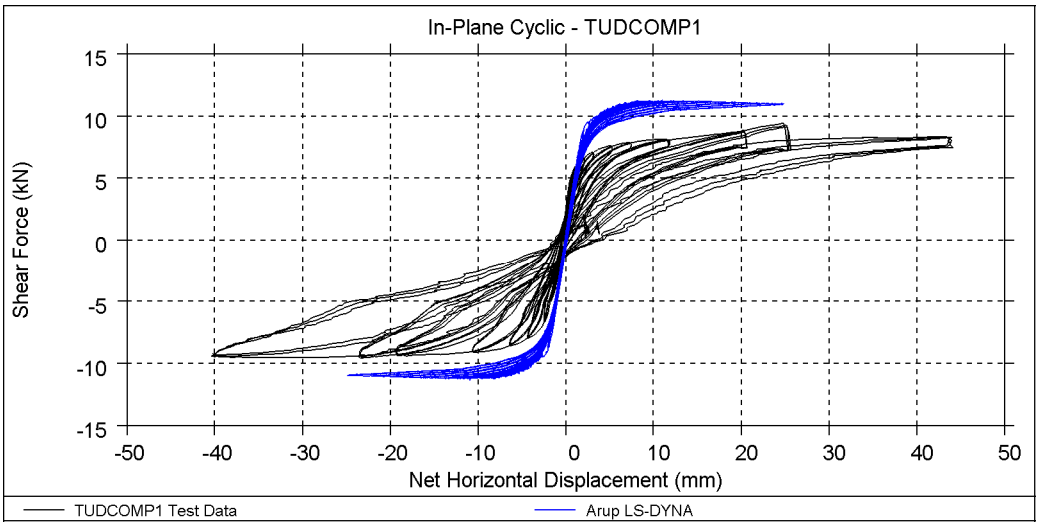

Figure 14: TUD-COMP-1: LS-DYNA blind prediction - Shear force-displacement curve

Table 4: TUD-COMP-1: LS-DYNA blind prediction - Summary table

	Predominant Failure Mechanism Predicted	**Initial Stiffness [kN/mm]**	**Peak Strength [kN]**	**Maximum Achieved Drift**	
LS-DYNA	Rocking	4.9	11	0.9%	End of protocol
Test Result	Rocking / toe crushing	7.7	9.5	1.6%	Reason for stopping not known

2.1.2.3 EUCENTRE Blind Prediction

The TREMURI macro-element model predicted a rocking dominated behaviour and the resulting hysteresis curve (Figure 16) followed an S-shape curve with moderate energy dissipation (Figure 17).

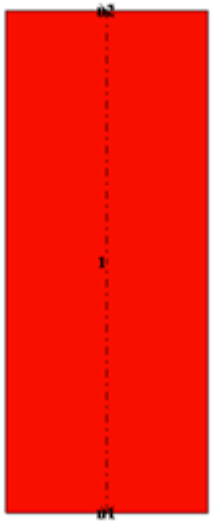

Figure 15: TUD-COMP-1: TREMURI blind prediction model

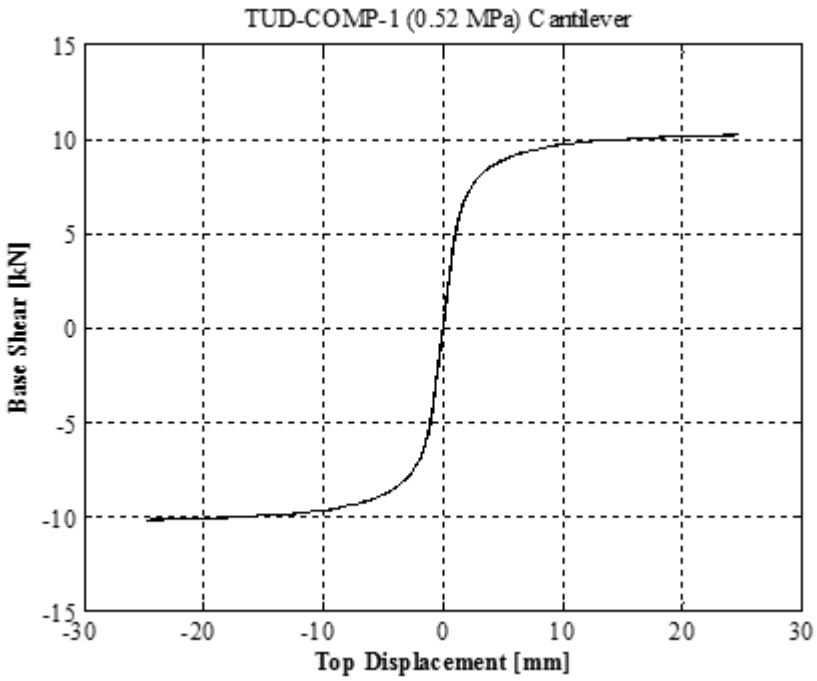

Figure 16: TUD-COMP-1: TREMURI blind prediction - Shear force-displacement curve

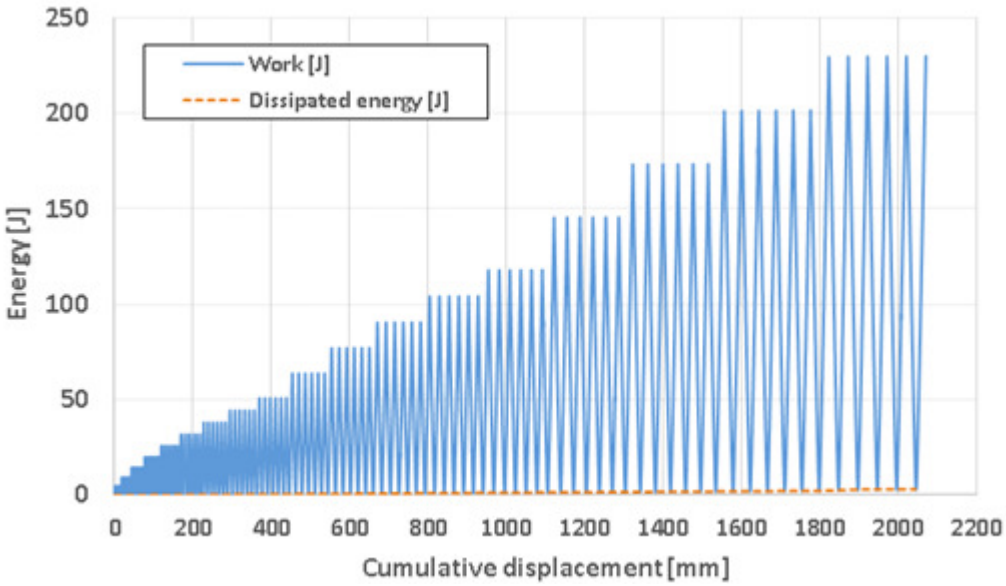

Figure 17: TUD-COMP-1: TREMURI blind prediction - Work & energy dissipation

Table 5: TUD-COMP-1: TREMURI blind prediction - Summary table

	Predominant Failure Mechanism Predicted	**Initial Stiffness [kN/mm]**	**Peak Strength [kN]**	**Maximum Achieved Drift**	
TREMURI	Rocking	5	10.2	0.9%	End of protocol
Test Result	Rocking / toe crushing	7.7	9.5	1.6%	Reason for stopping not known

2.1.2.4 TU-Delft Blind Prediction

Since TUD-COMP-1 is a cantilever panel, the expected failure mode was rocking at the base. Therefore, a uniform material model was applied to the whole panel, with a tensile strength equal to the bond strength between brick and mortar joints.

In the DIANA numerical model, the panel exhibited a rocking behaviour (Figure 18) with a numerical base shear capacity of 10 kN and a maximum top displacement of 4 mm (Figure 19). Larger displacement levels could not be reached due to failure to converge. In addition, to the rocking damage pattern, in the final stage of the analysis a vertical splitting crack was observed in the middle of the panel (Figure 18). A small amount of energy dissipation was predicted.

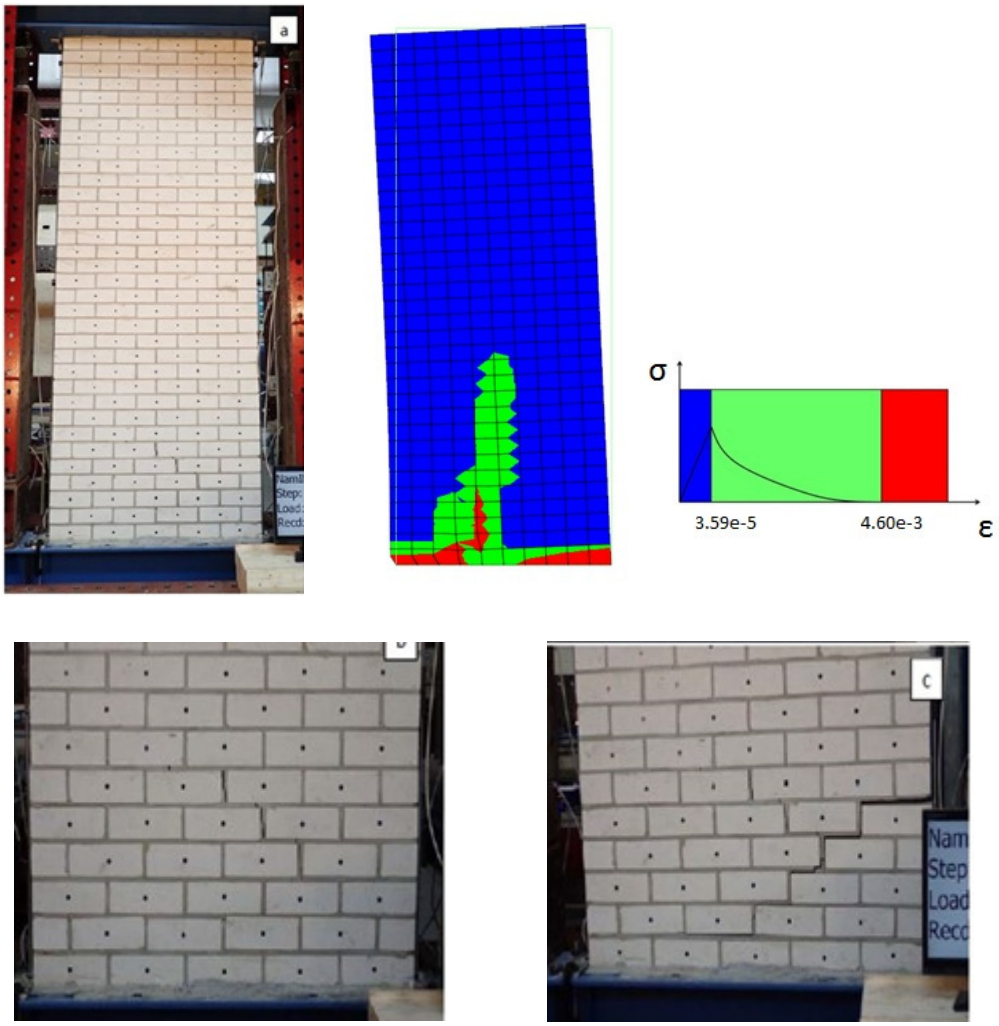

Figure 18: TUD-COMP-1: DIANA blind prediction - Damage plot at end of analysis (top right) compared to observed damage in laboratory

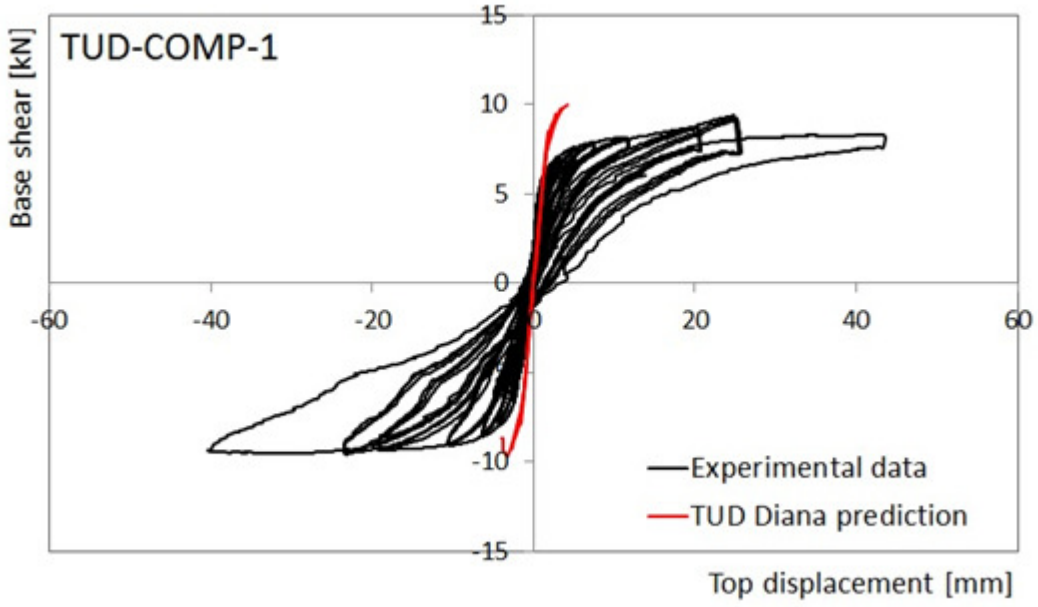

Figure 19: TUD-COMP-1: DIANA blind prediction - Shear force-displacement curve

Table 6: TUD-COMP-1: DIANA blind prediction - Summary table

	Predominant Failure Mechanism Predicted	**Initial Stiffness [kN/mm]**	**Peak Strength [kN]**	**Maximum Achieved Drift**	
DIANA	Rocking	5.1	10 (*)	0.15% (*)	(*)
Test Result	Rocking / toe crushing	7.7	9.5	1.6%	Reason for stopping not known

(*) Model not pushed up to 0.9% drift due to failure to converge

2.1.3 TUD-COMP-2

2.1.3.1 Test Description

TUD-COMP-2 was the third quasi-static in-plane test administered by TU-Delft. This specimen was a single-wythe wall constructed of calcium silicate units 102 mm thick. It was 1.1 m long and 2.76 m high. The applied overburden stress was 0.7 MPa. The wall was tested under cantilever boundary conditions.

Upon cyclically loading specimen TUD-COMP-2, a gradual reduction of the initial stiffness occurred after the second cycle. First cracks appeared at the bottom corners during the sixth cycle. During the twelfth cycle, new flexural cracks opened, starting from the sixth or seventh mortar bed joints. The cracks developed along the mortar joint for approximately half of the length of the wall, and then were diagonally oriented pointing to the opposite bottom corner of the wall.

At the end stage, crushing of the toes and sliding along the flexural cracks were observed. The failure mode was mainly governed by rocking and diagonally oriented damage, followed by toe-crushing and sliding. The specimen showed symmetric mechanical behaviour. The test was stopped at a net drift of 1%, when an extensive cracking at the base of the wall was detected.

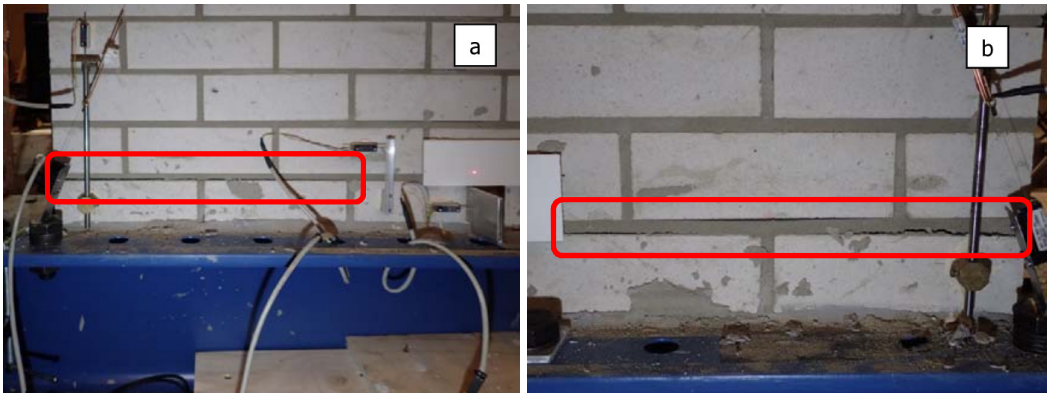

Figure 20: TUD-COMP-2: Rocking cracks (highlighted in red) at the base of the wall: details of the left (a) and right (b) toes

Figure 21: TUD-COMP-2: Crack pattern at failure for positive (a) and negative (b) drifts; details of the toe crushing (c) and sliding (d) at end stage.

The actual loading regime of TUD-COMP-2 differed from that specified in the planned test protocol, which specified a maximum drift level of 0.9%. The overburden matched the specified value.

The measured hysteresis is shown in Figure 22.

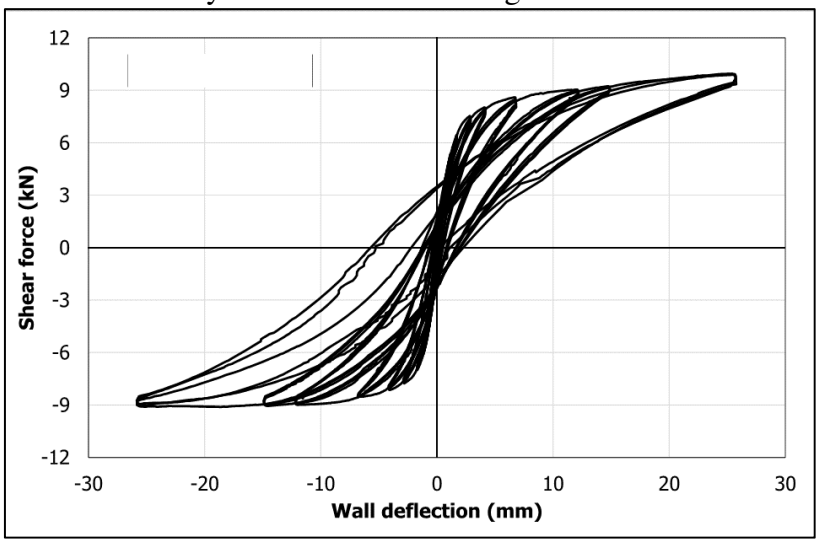

Figure 22: TUD-COMP-2: Lab test result – Shear force-displacement curve

2.1.3.2 Arup Blind Prediction

The LS-DYNA model of TUD-COMP-2 predicted rocking behaviour and associated tensile bed joint failures predominantly at the bottom of the specimen. The model exhibited bed-joint damage in a few locations throughout the height of the wall, due to the moment distribution in the wall, as it was cyclically loaded combined with the cantilever boundary conditions (see Figure 23). This bed-joint damage was also observed in the lab (see Figure 23, a & b).

The lateral-force-versus-displacement relationship followed an S-shaped curve, as shown in Figure 24. The predicted ultimate load was approximately 14 kN at a drift of 0.9%. The predicted initial stiffness was approximately 5 kN/mm.

As illustrated by the hysteresis curve, there was little dissipated energy predicted.

The LS-DYNA model captured the rocking mechanism observed during the laboratory test but under-predicted the amount of energy dissipated. A considerable amount of the dissipated energy was a product of the shear sliding (diagonal damage) and toe-crushing damage, which the LS-DYNA blind prediction model did not capture. The model did not predict collapse or a near-collapse state. The LS-DYNA model also over-predicted the initial lateral strength of the specimen. The test result shows a lateral strength significantly lower than the theoretical rocking strength for the given dimensions and overburden. The reasons for this are not clear.

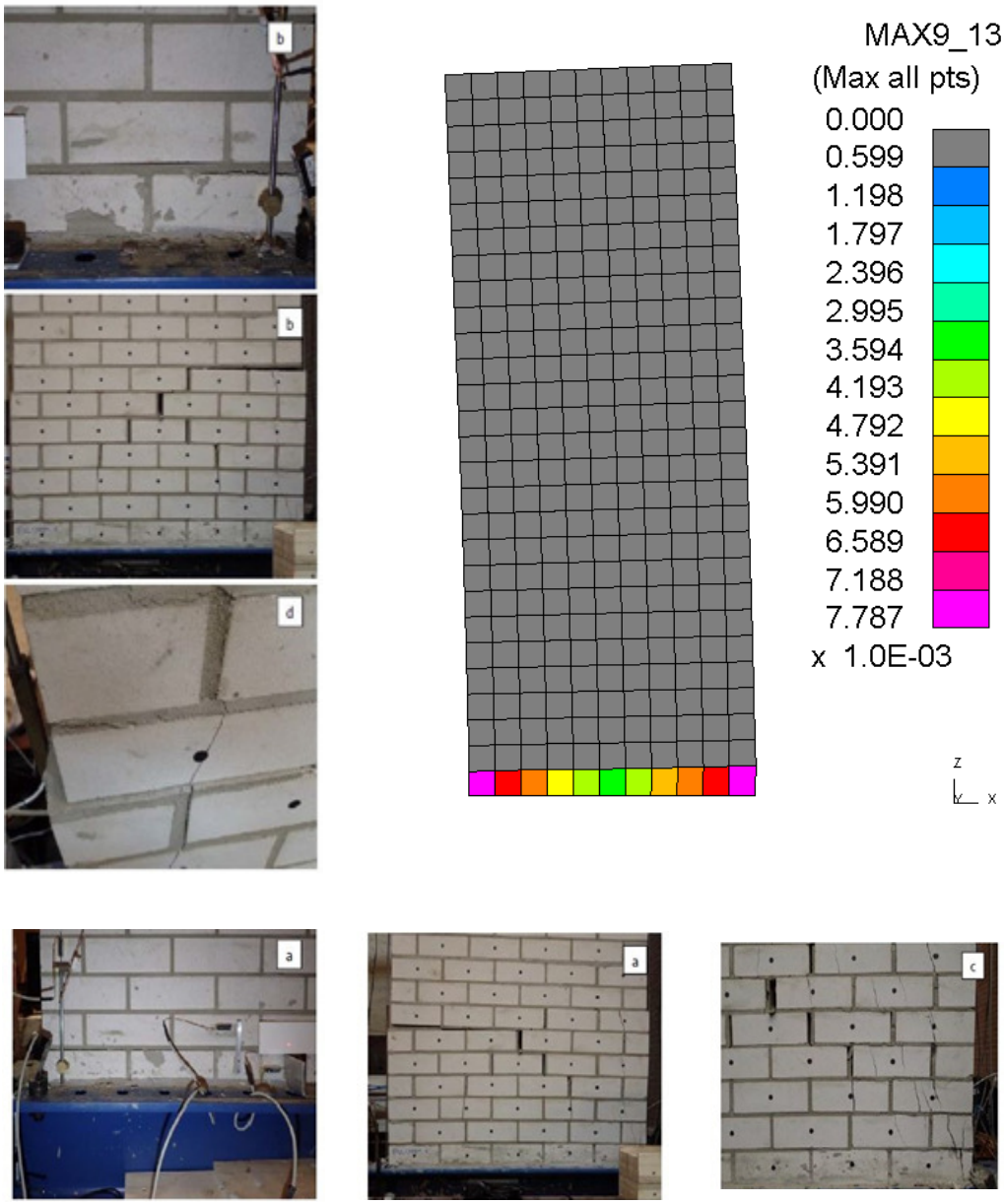

Figure 23: TUD-COMP-2: LS-DYNA blind prediction - Damage plot at end of analysis (top right) compared to observed damage in laboratory

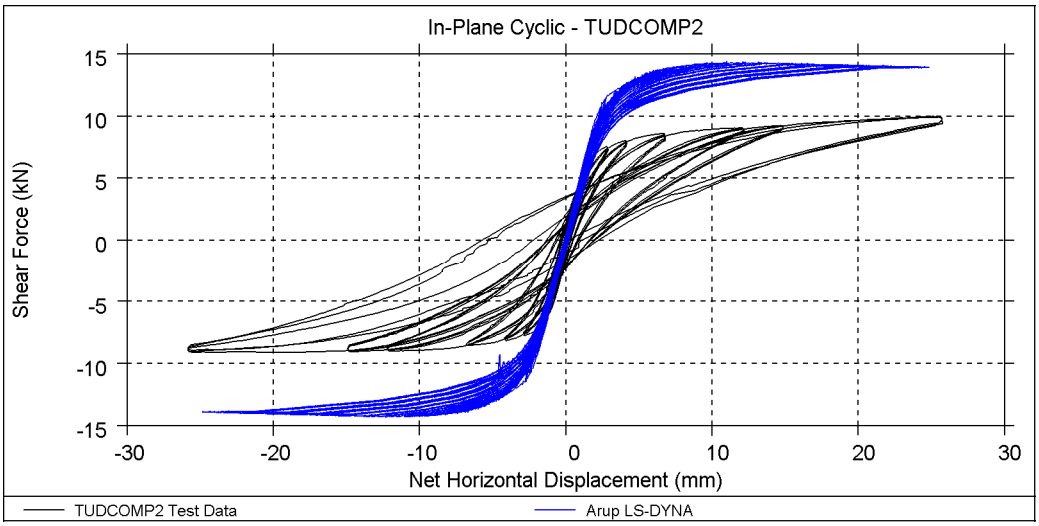

Figure 24: TUD-COMP-2: LS-DYNA blind prediction - Shear force-displacement curve

Table 7: TUD-COMP-2: LS-DYNA blind prediction - Summary table

	Predominant Failure Mechanism Predicted	**Initial Stiffness [kN/mm]**	**Peak Strength [kN]**	**Maximum Achieved Drift**	
LS-DYNA	Rocking	5	14	0.9%	End of protocol
Test Result	Rocking / toe crushing	7.2	10	0.9%	Near collapse

2.1.3.3 EUCENTRE Blind Prediction

The TREMURI macro-element model predicted a mainly rocking behaviour and the resulting hysteresis curve (Figure 26) followed an S-shape curve with moderate energy dissipation (Figure 27).

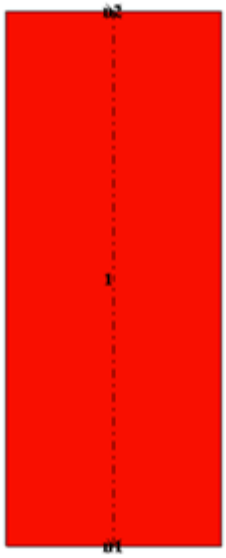

Figure 25: TUD-COMP-2: TREMURI blind prediction model

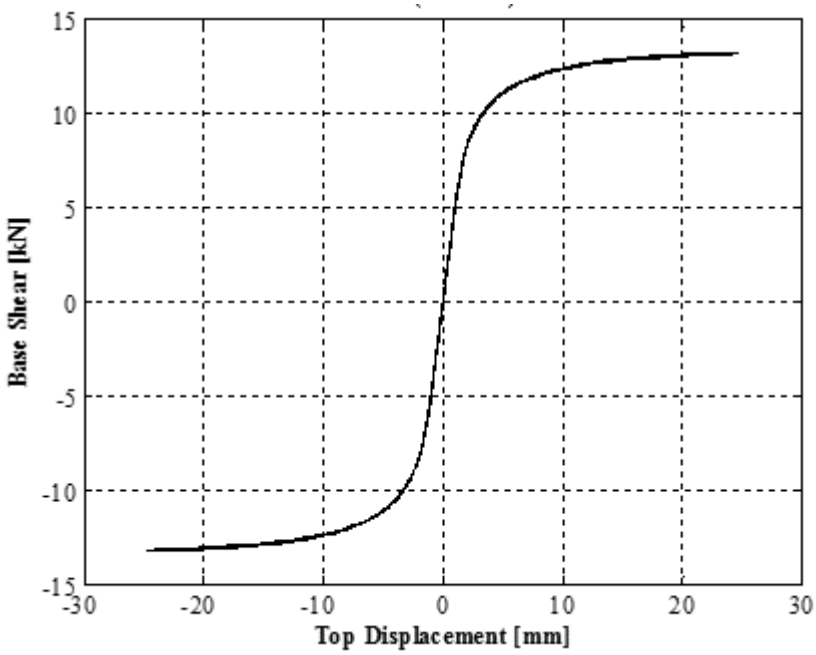

Figure 26: TUD-COMP-2: TREMURI blind prediction - Shear force-displacement curve

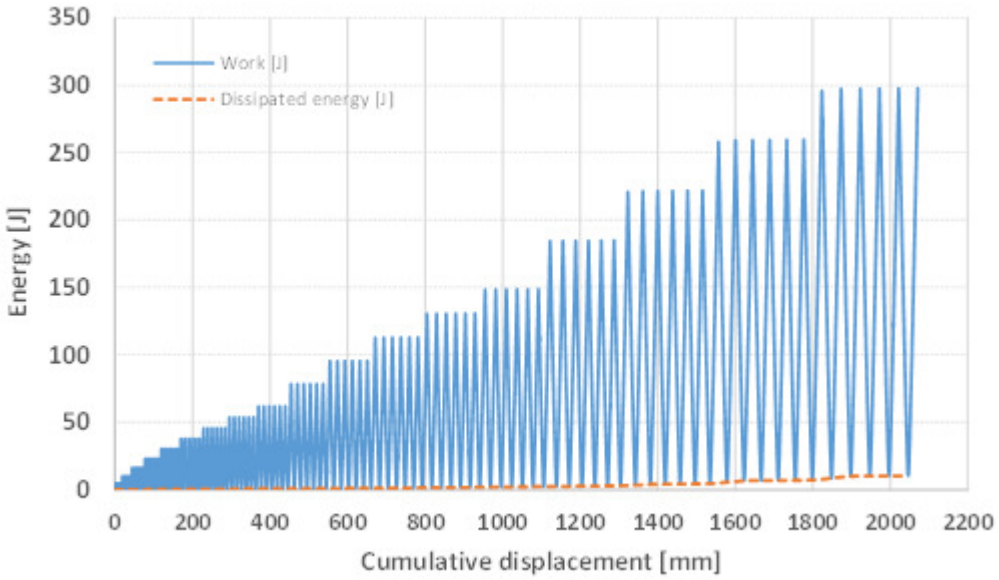

Figure 27: TUD-COMP-2: TREMURI blind prediction - Work & energy dissipation

Table 8: TUD-COMP-2: TREMURI blind prediction - Summary table

	Predominant Failure Mechanism Predicted	**Initial Stiffness [kN/mm]**	**Peak Strength [kN]**	**Maximum Achieved Drift**	
TREMURI	Rocking	5	13.1	0.9%	End of protocol
Test Result	Rocking / toe crushing	7.2	10	0.9%	Near collapse

2.1.3.4 TU-Delft Blind Prediction

TUD-COMP-2 had the same features as EUC-COMP-2 except for the upper boundary conditions that were free to displace and rotate in this case. The expected failure mode was rocking at the base, therefore a uniform material model was applied to the whole panel, with a tensile strength equal to the bond strength between brick and mortar joints.

In the DIANA numerical model, the panel exhibited a predominant rocking behaviour with an additional almost vertical splitting crack in the last stage of the analysis (Figure 28). The numerical base shear capacity was 13 kN and the maximum top displacement was 6.88 mm (Figure 29). Larger displacement levels could not be explored due to failure to converge. A small amount of energy dissipation was predicted.

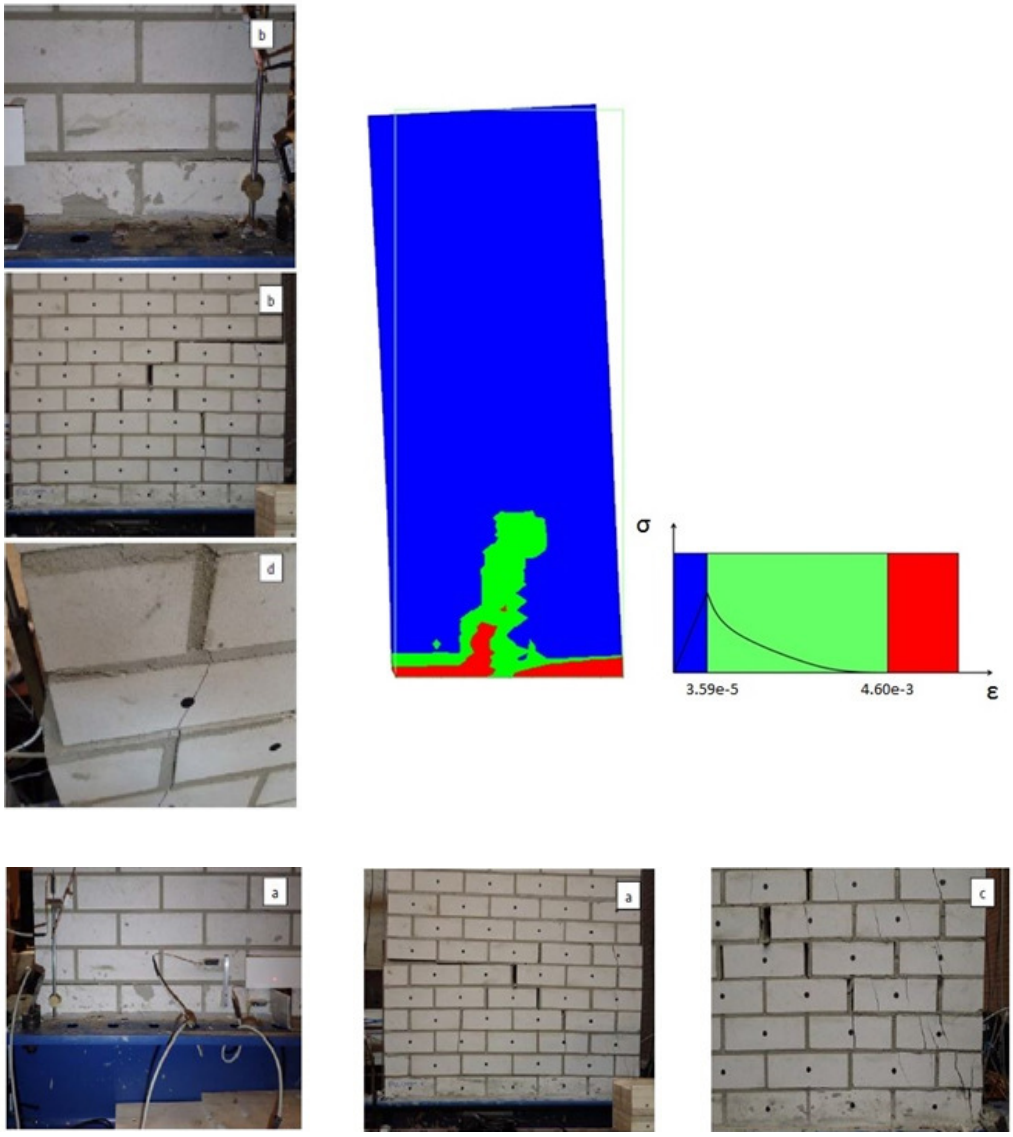

Figure 28: TUD-COMP-2: DIANA blind prediction - Damage plot at end of analysis (top right) compared to observed damage in laboratory

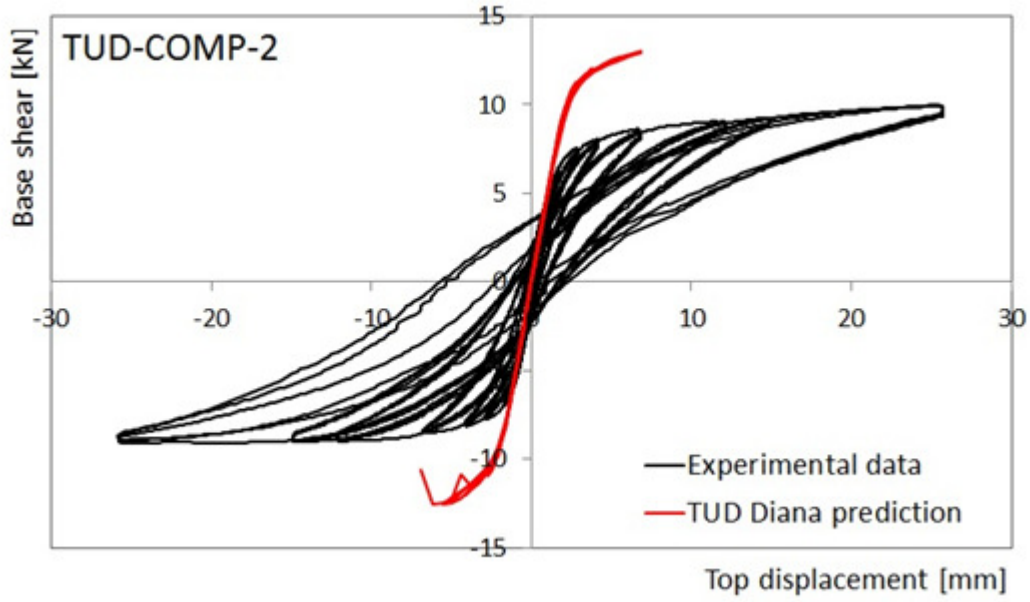

Figure 29: TUD-COMP-2: DIANA blind prediction - Shear force-displacement curve

Table 9: TUD-COMP-2: DIANA blind prediction - Summary table

	Predominant Failure Mechanism Predicted	**Initial Stiffness [kN/mm]**	**Peak Strength [kN]**	**Maximum Achieved Drift**	
DIANA	Rocking	5.1	13 (*)	0.25% (*)	(*)
Test Result	Rocking / toe crushing	7.2	10	0.9%	Near collapse

(*) Model not pushed up to 0.9% drift due to failure to converge

2.1.4 TUD-COMP-3

2.1.4.1 Test Description

TUD-COMP-3 was the fourth quasi-static in-plane test administered by TU-Delft. This specimen was a single-wythe wall constructed of calcium silicate units 102 mm thick. It was 1.1 m long and 2.76 m high. The originally planned overburden stress was 0.3 MPa. The wall was tested under double clamped boundary conditions.

In the actual test, the applied overburden stress was 0.3 MPa initially, but the due to potential instability of the test system, the test was stopped in the elastic phase. The test was restarted with an increase in overburden to 0.4 MPa.

Upon cyclically loading specimen TUD-COMP-3 initially under 0.3 MPa overburden stress, a gradual reduction of the initial stiffness occurred after the second cycle (0.01% drift). The test was stopped at a drift of 0.012%. No cracks were reported during this initial phase of the test.

The overburden stress was increased to 0.4 MPa and the test re-began. A gradual reduction of the initial stiffness of this test phase occurred after the second cycle (0.01% drift). Horizontal cracks first appeared along the first top and bottom head joints at the bottom left corner during the fifth cycle (0.065% drift) followed by cracks at the opposite corners during the sixth cycle (0.11% drift). Diagonally-oriented cracks appeared during the 11^{th} cycle (0.9% drift). The failure mode was mainly governed by flexure, associated with toe crushing and bed joint sliding. The test was stopped at a net drift of 1.3% when severe damage was experienced at the top portion of the wall.

Figure 30: TUD-COMP-3: Rocking cracks at the top & bottom left corners (a) and top & bottom right corners (b)

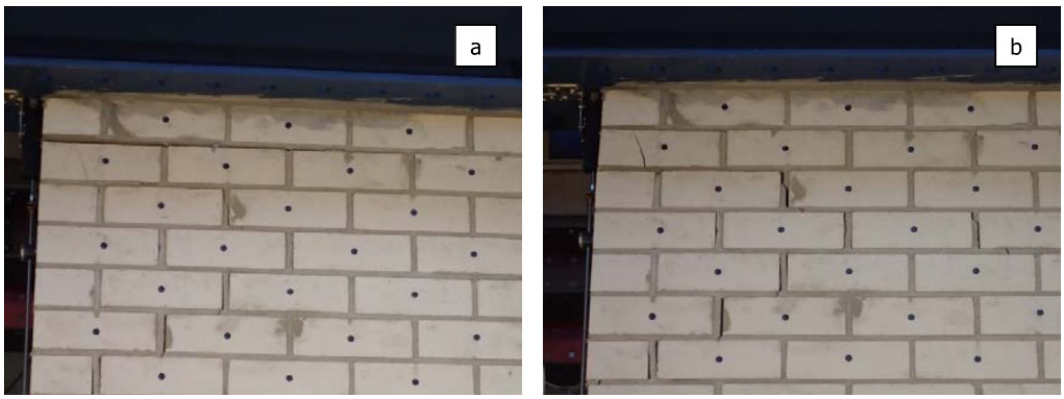

Figure 31: TUD-COMP-3: Progression of diagonal crack at the top of the wall for positive drifts after 0.49% drift (a) and after 0.89% drift (b)

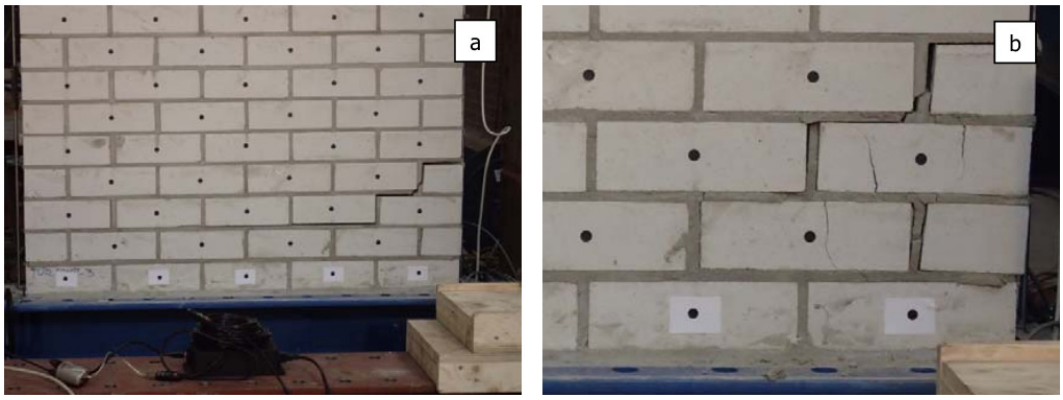

Figure 32: TUD-COMP-3: Crack pattern at the end of the test--diagonal cracks & toe crushing

The actual loading regime of TUD-COMP-3 differed from that specified in the planned test protocol, which specified a maximum drift level of 1.8%. In addition, as previously mentioned, the actual overburden applied during the test increased from 0.3 MPa to 0.4 MPa partly through the test.

The measured hysteresis during the first phase and second phase of the test is shown in Figure 33 and Figure 34, respectively.

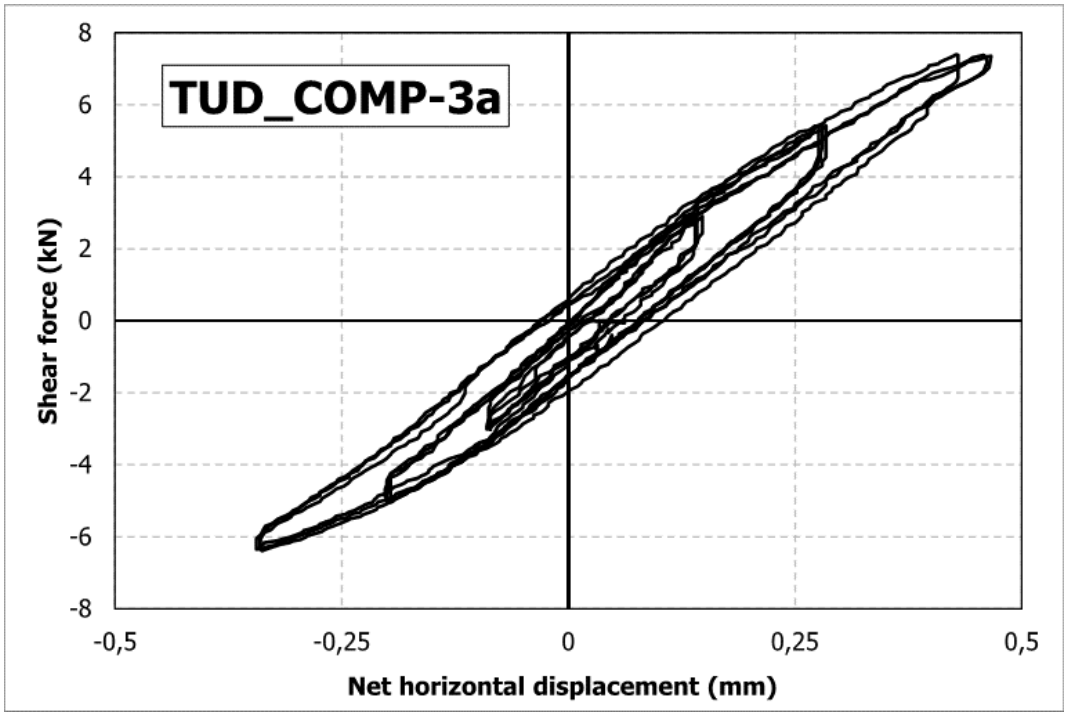

Figure 33: TUD-COMP-3a: Lab test result with 0.3 MPa overburden – Shear force-displacement curve

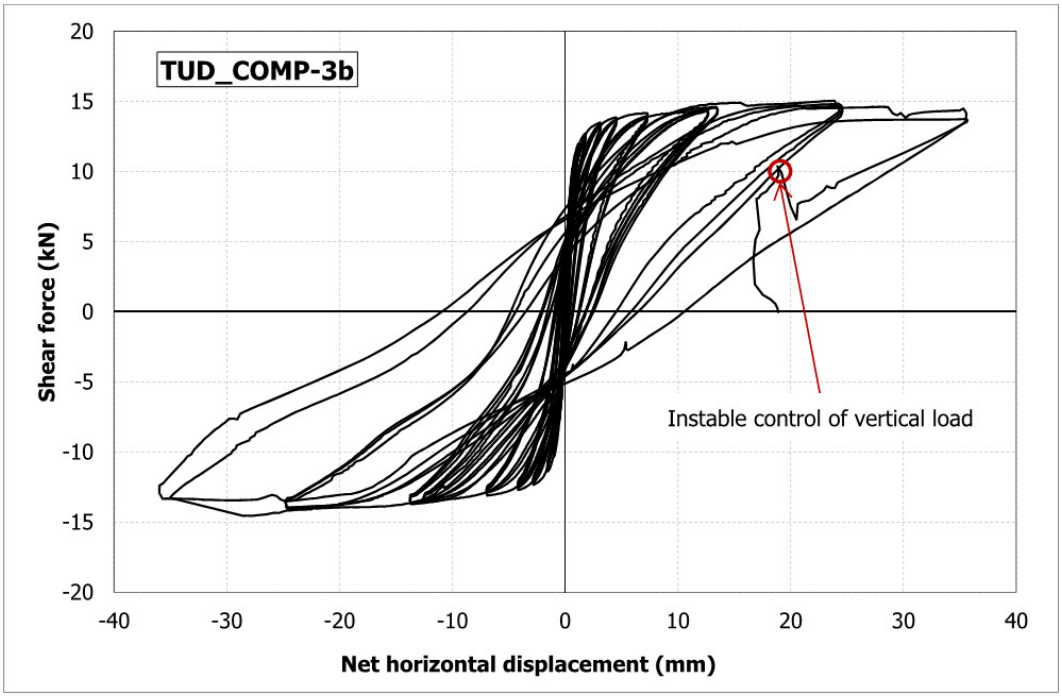

Figure 34: TUD-COMP-3b: Lab test result with 0.4 MPa overburden – Shear force-displacement curve

2.1.4.2 Arup Blind Prediction

The LS-DYNA model of TUD-COMP-3 predicted initial rocking behaviour and associated tensile bed joint failures at the top and bottom of the specimen. The behaviour was followed by a step-wise diagonal crack pattern that formed at the bottom of the specimen. This diagonal cracking led to an increase in energy dissipation.

The lateral-force-versus-displacement relationship followed an S-shaped curve, as shown in Figure 36. The predicted ultimate load was approximately 13.5 kN at a drift of 1.8%. The predicted initial stiffness was approximately 11.6 kN/mm. Note that the overburden was 0.3 MPa in the simulation, but 0.4MPa in the test.

As illustrated by the hysteresis curve, there was little energy dissipated predicted until the formation of the diagonal cracking at the bottom of the specimen, which slightly increased the amount of energy dissipated.

The LS-DYNA model captured the rocking mechanism and backbone curve generated during the laboratory test but under-predicted the amount of energy dissipated. A considerable amount of the dissipated energy was a product of the shear sliding (diagonal damage) and toe-crushing damage, which the LS-DYNA blind prediction model did not completely capture. The model did not predict collapse or a near-collapse state.

Note that the LS-DYNA blind prediction model of TUD-COMP-3 used material properties measured by TU-Delft as of August 2015 [9], not the NAM Basis for Design material properties.

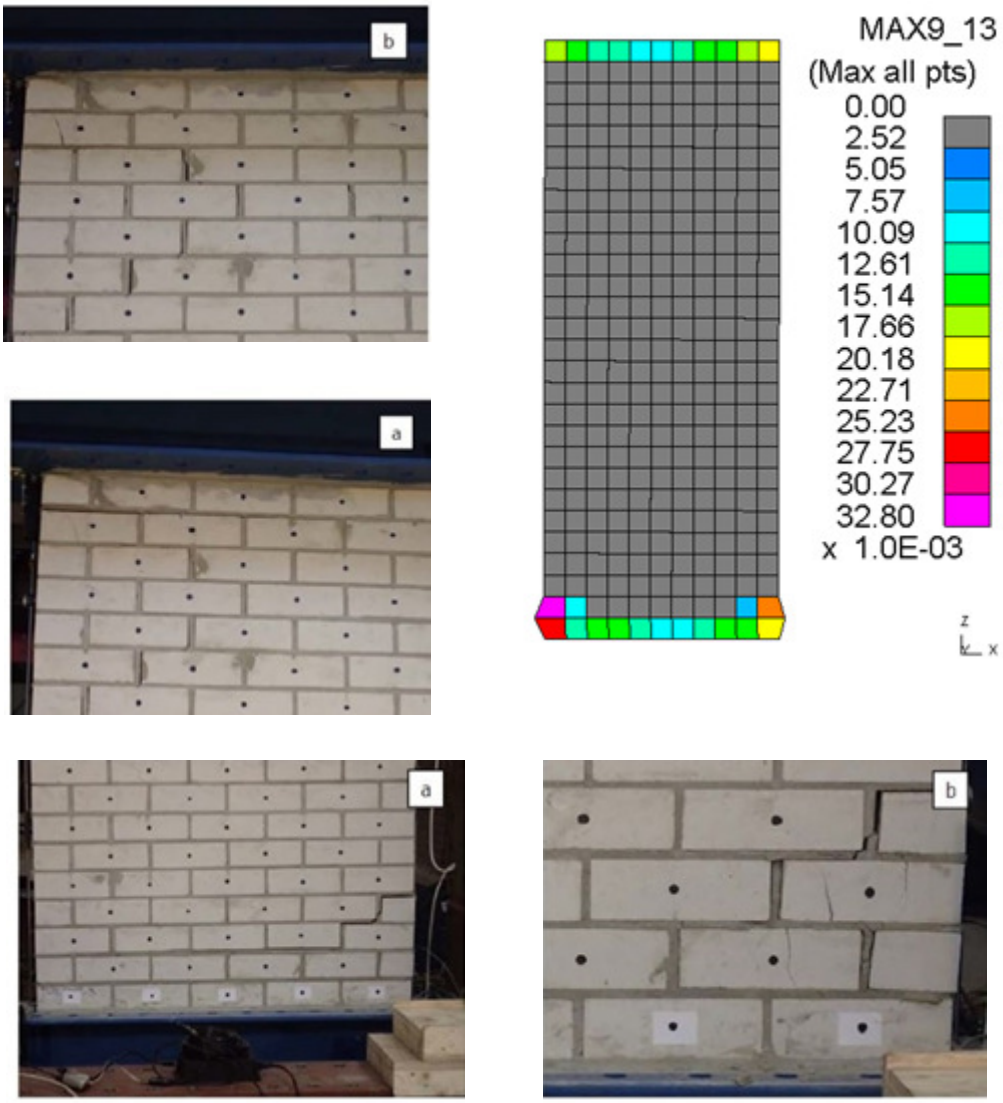

Figure 35: TUD-COMP-3: LS-DYNA blind prediction - Damage plot at end of analysis (top right) compared to observed damage in laboratory

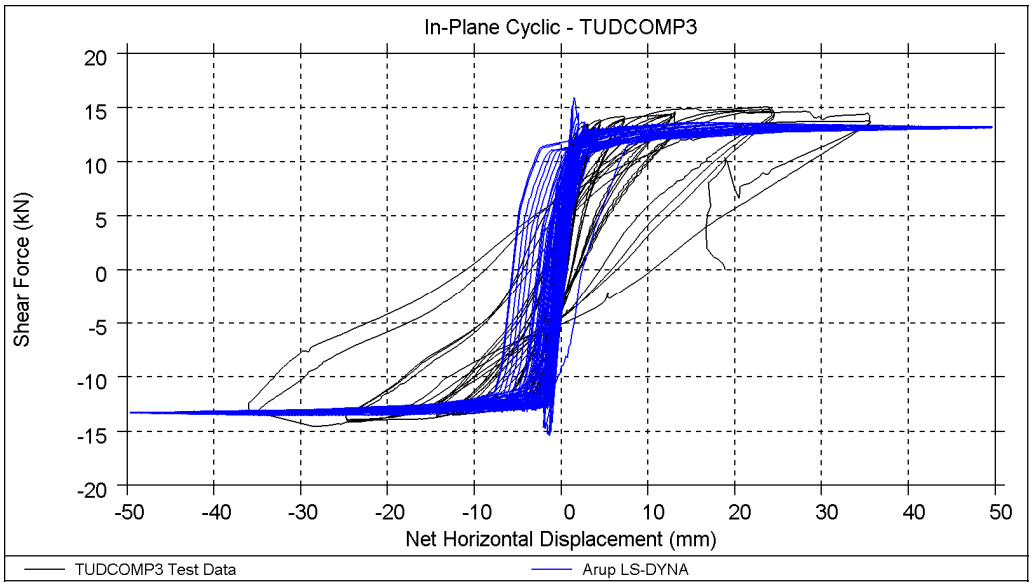

Figure 36: TUD-COMP-3: LS-DYNA blind prediction - Shear force-displacement curve

Table 10: TUD-COMP-3: LS-DYNA blind prediction - Summary table

	Predominant Failure Mechanism Predicted	**Initial Stiffness [kN/mm]**	**Peak Strength [kN]**	**Maximum Achieved Drift**	
LS-DYNA	Rocking / toe crushing	11.6 (*)	14 (*)	1.8%	End of protocol
Test Result (second phase)	Rocking / toe crushing	22.4	15	1.3%	Test system instability / severe damage

(*) LS-DYNA analysis performed under 0.3 MPa overburden stress as specified in the protocol

2.1.4.3 EUCENTRE Blind Prediction

The TREMURI macro-element model predicted a rocking behaviour and the resulting hysteresis curve (Figure 38) followed an S-shape curve with moderate energy dissipation (Figure 39). Note that the overburden was 0.3 MPa in the simulation, but 0.4 MPa in the test.

The TREMURI blind prediction model of TUD-COMP-3 used material properties measured by TU-Delft from mechanical characterization test, not the NAM Basis for Design material properties.

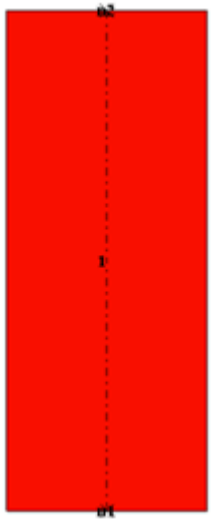

Figure 37: TUD-COMP-3: TREMURI blind prediction model

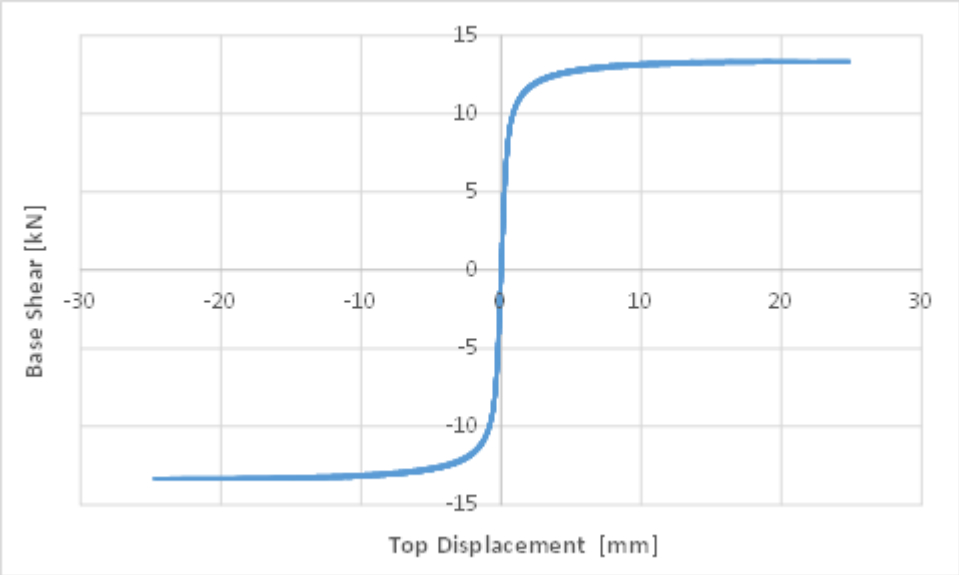

Figure 38: TUD-COMP-3: TREMURI blind prediction - Shear force-displacement curve

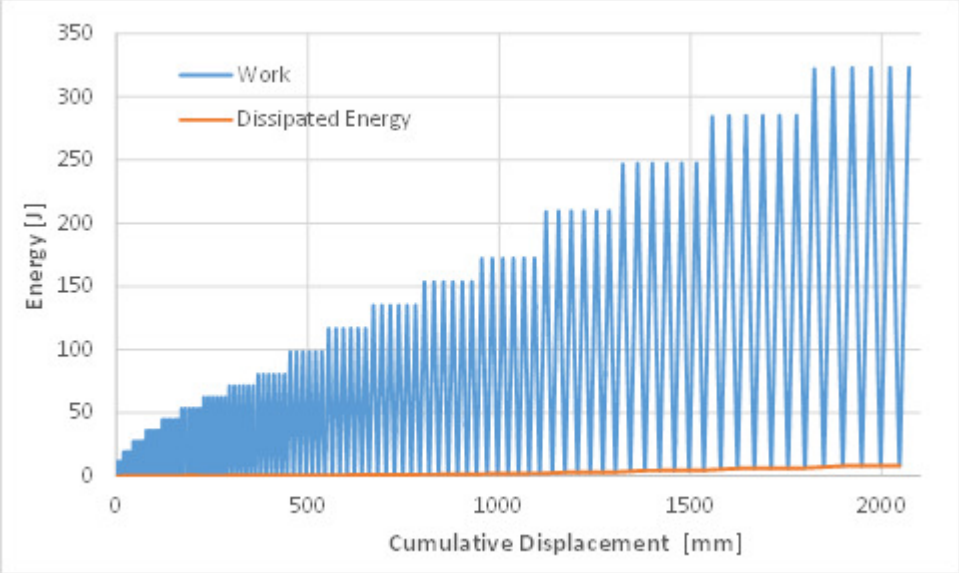

Figure 39: TUD-COMP-3: TREMURI blind prediction - Work & energy dissipation

Table 11: TUD-COMP-3: TREMURI blind prediction - Summary table

	Predominant Failure Mechanism Predicted	**Initial Stiffness [kN/mm]**	**Peak Strength [kN]**	**Maximum Achieved Drift**	
TREMURI	Rocking	21.5 (*)	13.4 (*)	0.9%	
Test Result (second phase)	Rocking / toe crushing	22.4	15	1.3%	Test system instability / severe damage

(*) TREMURI analysis performed under 0.3 MPa overburden stress as specified in the protocol

2.1.4.4 TU-Delft Blind Prediction

The DIANA finite element model of the panel was divided in two areas—one at the boundaries where rocking occurs, characterised by a tensile strength equal to the bond strength between brick and mortar joints; and one in the middle of the panel, characterised by a higher tensile strength related to a potential diagonal failure. This was done to take into account of different failure modes in the panel since, in principle, the total-strain approach provides an isotropic nonlinear behaviour in which the tensile strength is the same in all directions.

The panel exhibit a rocking behaviour (Figure 40) with a numerical base shear capacity of 14.4 kN and a maximum top displacement of 6.88 mm (Figure 41). The analysis could not be performed to larger displacement levels due to convergence issues. The dissipated energy was lower than the one experimentally observed.

TUD-COMP-3 is the first panel for which the material properties have been assigned according to the values obtained in the experimental campaign performed at TU-Delft laboratories [9].

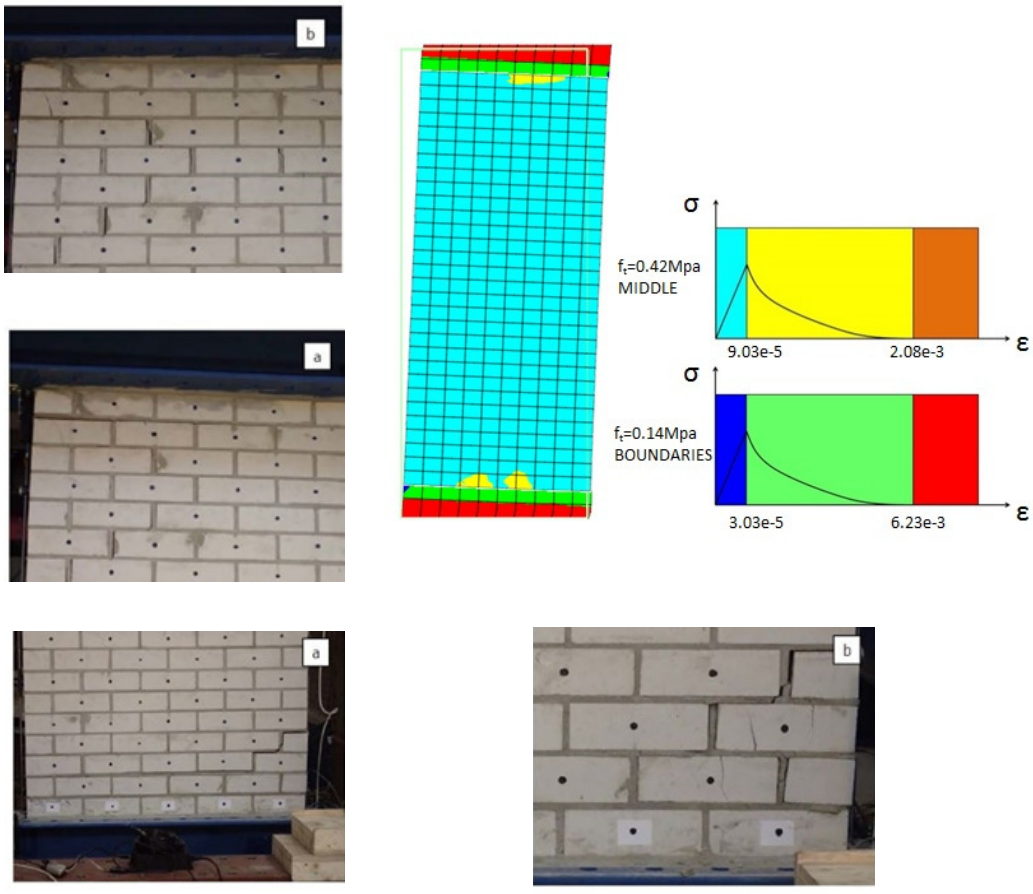

Figure 40: TUD-COMP-3: DIANA blind prediction - Damage plot at end of analysis (top right) compared to observed damage in laboratory

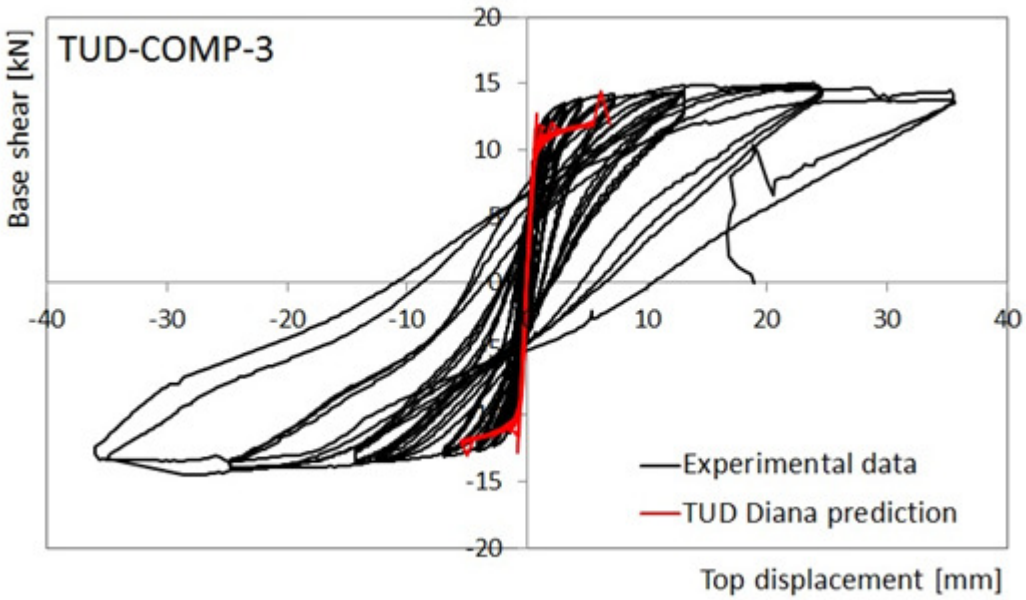

Figure 41: TUD-COMP-3: DIANA blind prediction - Shear force-displacement curve

Table 12: TUD-COMP-3: DIANA blind prediction - Summary table

	Predominant Failure Mechanism Predicted	**Initial Stiffness [kN/mm]**	**Peak Strength [kN]**	**Maximum Achieved Drift**	
DIANA	Rocking	20.5 [1]	14.4 [1,2]	0.25% [2]	[2]
Test Result (second phase)	Rocking / toe crushing	22.4	15	1.3%	Test system instability / severe damage

1. DIANA analysis performed under 0.3 MPa overburden stress as specified in the protocol

2. Model not pushed up to 1.3% drift due to failure to converge

2.1.5 TUD-COMP-4

2.1.5.1 Test Description

TUD-COMP-4 was the fifth quasi-static in-plane test administered by TU-Delft. This specimen was a single-wythe wall constructed of calcium silicate units 102 mm thick. It was 4 m long and 2.75 m high. The applied overburden stress was 0.5 MPa. The wall was tested under double clamped boundary conditions.

During the pre-test calibration phase, a horizontal crack formed between the first and second brick layer from the top. The crack was repaired. However, as a consequence, the specimen became in effect one brick-height shorter. This was not taken into account in the blind prediction model.

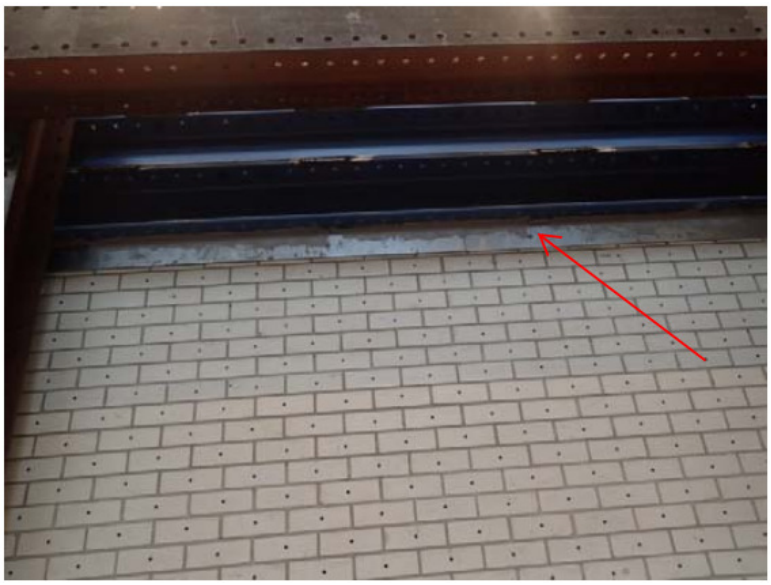

Figure 42: TUD-COMP-4: repair of the horizontal crack during the pre-test phase

First cracks appeared during the sixth cycle (0.04% drift). These were diagonally oriented cracks, which progressively increased in width during the duration of the test. At the end of the test, maximum crack widths of 40 mm were measured. The failure mode was mainly governed by diagonally oriented damage. The test was stopped at a net drift of 0.2% drift due to the near collapse of the wall.

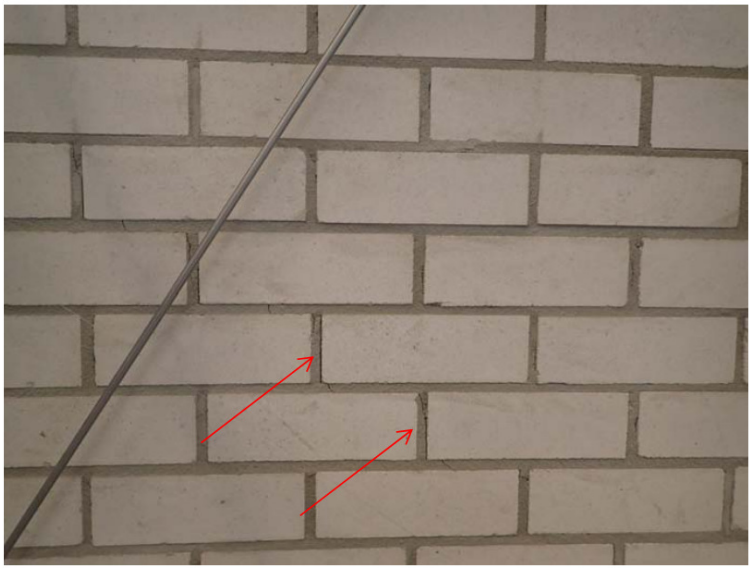

Figure 43: TUD-COMP-4: First cracks visible after 0.04% drift

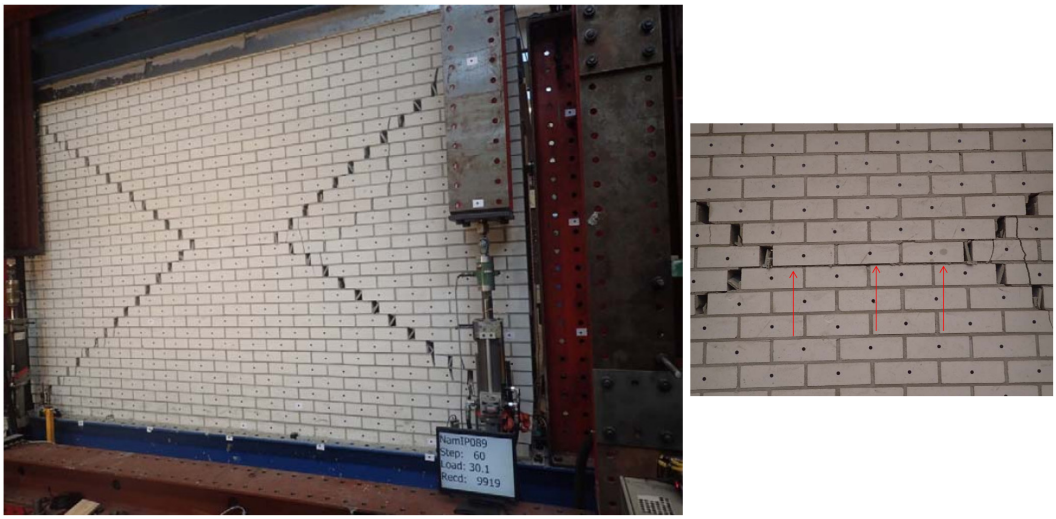

Figure 44: TUD-COMP-4: Crack pattern at the end of the test

The measured hysteresis is shown in Figure 45

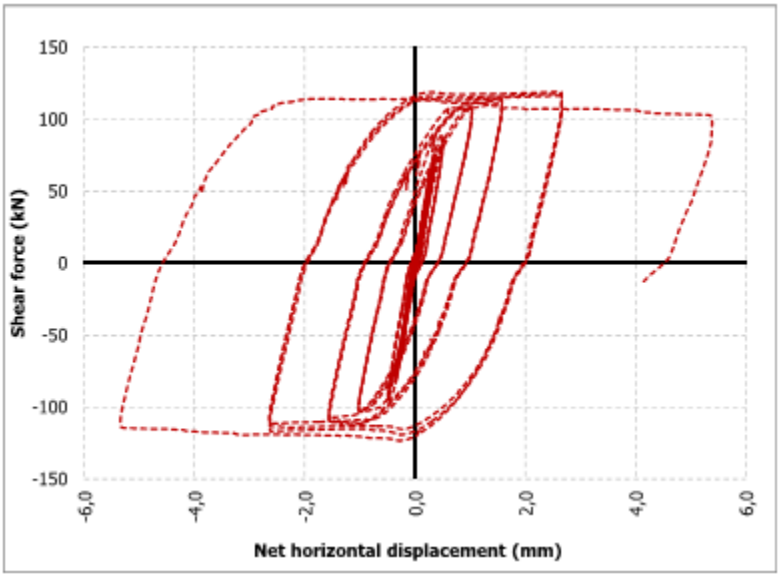

Figure 45: TUD-COMP-4: Lab test result – Shear force-displacement curve

2.1.5.2 Arup Blind Prediction

The LS-DYNA model of TUD-COMP-4 predicted failure governed by the formation of diagonal crack pattern through the specimen associated with bed joint sliding and head joint opening.

The lateral-force-versus-displacement relationship followed typical shear behaviour as shown in Figure 47. The predicted ultimate load initially peaked at approximately 104 kN and gradually decayed to a load of approximately 86 kN. The predicted initial stiffness was approximately 140 kN/mm.

The LS-DYNA model captured the shear mechanism and general loading / unloading pattern generated during the laboratory test but under-predicted the lateral strength of the wall. The model did not predict collapse or a near-collapse state.

Note that the LS-DYNA blind prediction model of TUD-COMP-4 used material properties measured by TU-Delft as of August 2015 [9], not the NAM Basis for Design material properties.

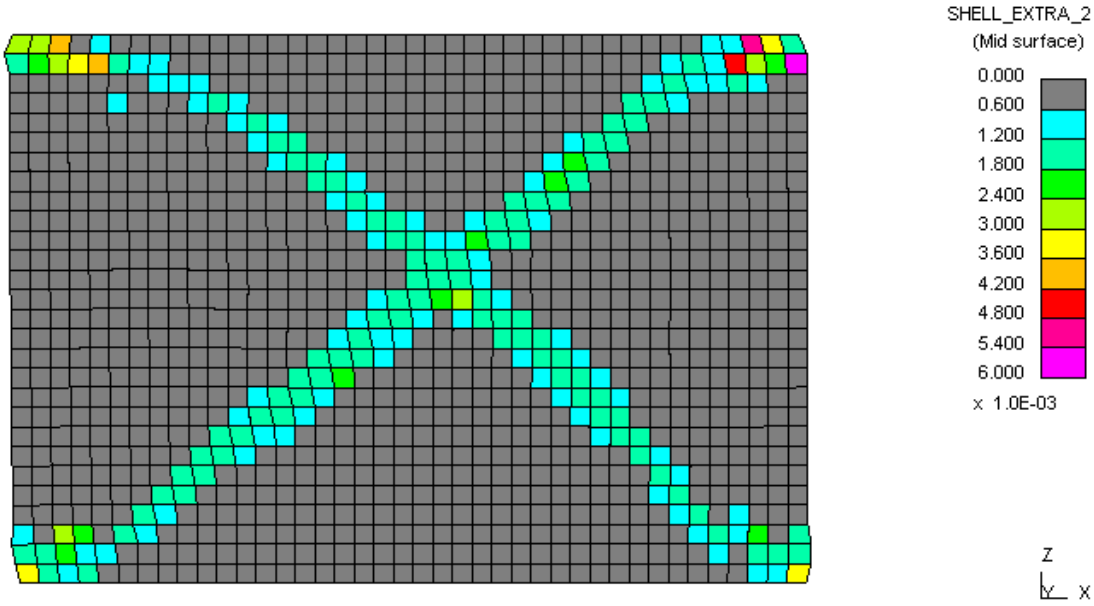

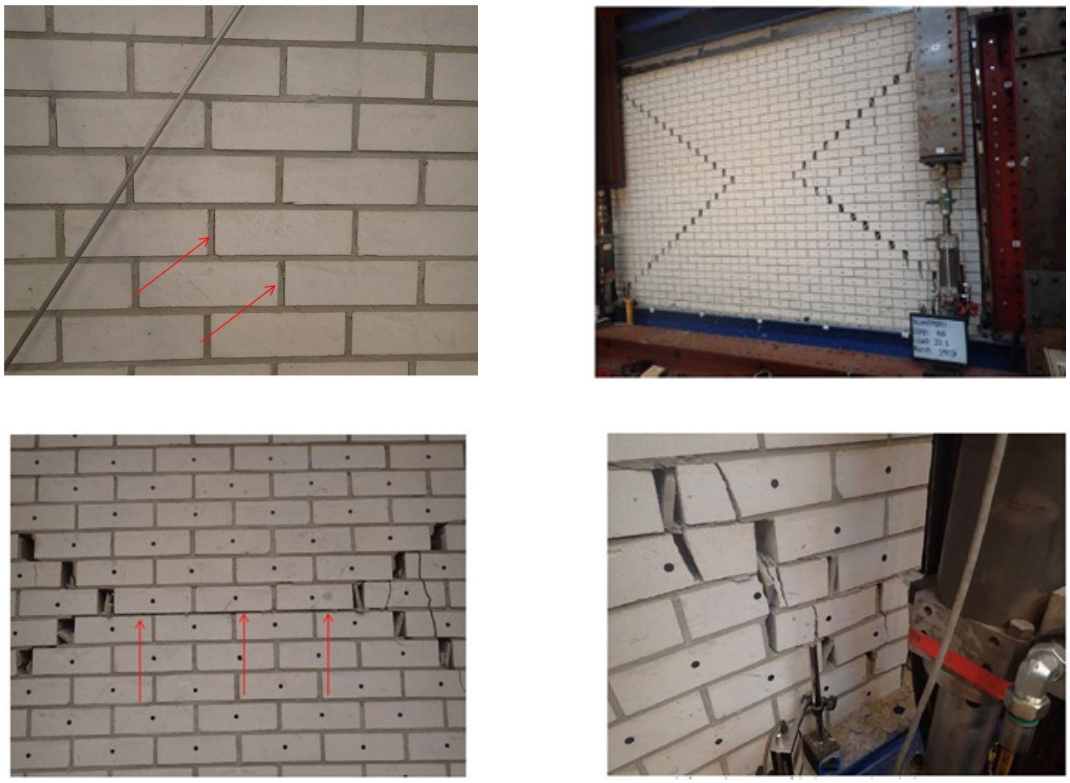

Figure 46: TUD-COMP-4: LS-DYNA blind prediction - Damage plot at end of analysis (top right) compared to observed damage in laboratory

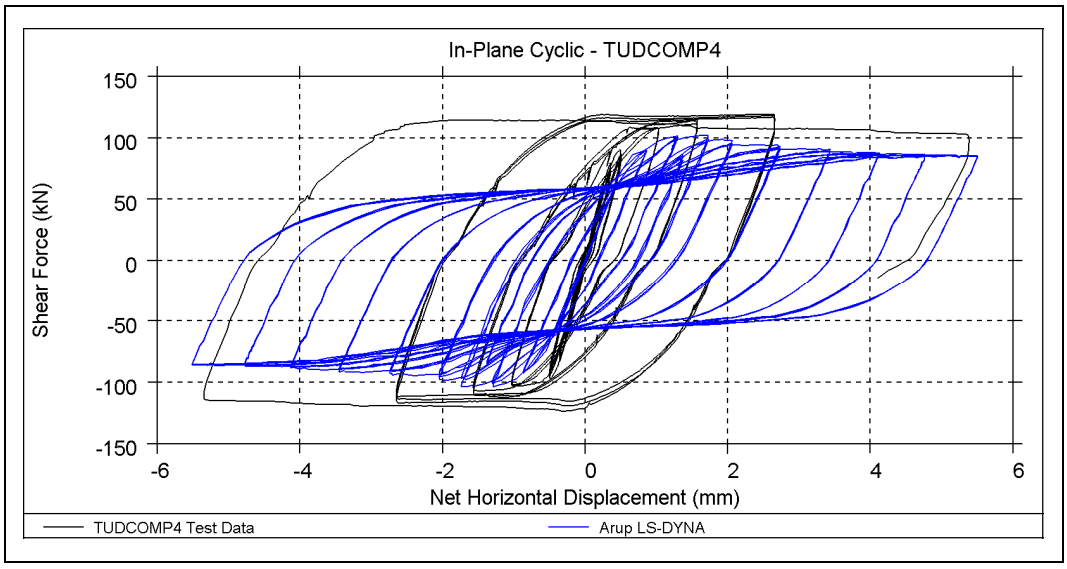

Figure 47: TUD-COMP-4: LS-DYNA blind prediction - Shear force-displacement curve

Table 13: TUD-COMP-4: LS-DYNA blind prediction - Summary table

	Predominant Failure Mechanism Predicted	**Initial Stiffness [kN/mm]**	**Peak Strength [kN]**	**Maximum Achieved Drift**	
LS-DYNA	Diagonal cracks / bed joint sliding	140	104	0.2%	End of protocol
Test Result	Diagonal cracks / toe crushing	> 223	119	0.2%	Near collapse

2.1.5.3 EUCENTRE Blind Prediction

The TREMURI macro-element model predicted a shear behaviour as shown by the hysteresis curve (Figure 49) with high energy dissipation (Figure 50).

The TREMURI blind prediction model of TUD-COMP-4 used material properties measured by TU-Delft from mechanical characterization test, not the NAM Basis for Design material properties.

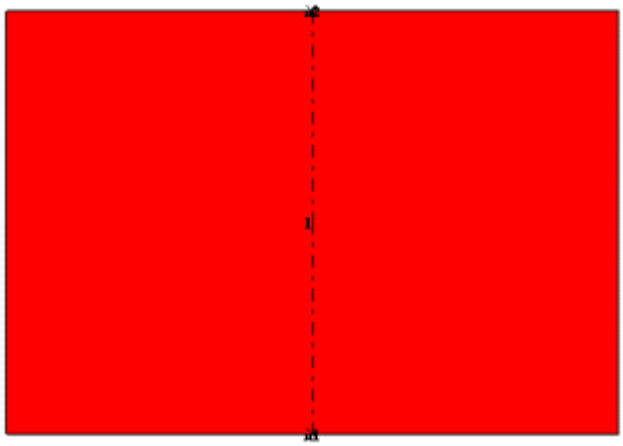

Figure 48: TUD-COMP-4: TREMURI blind prediction - Damage plot at end of analysis

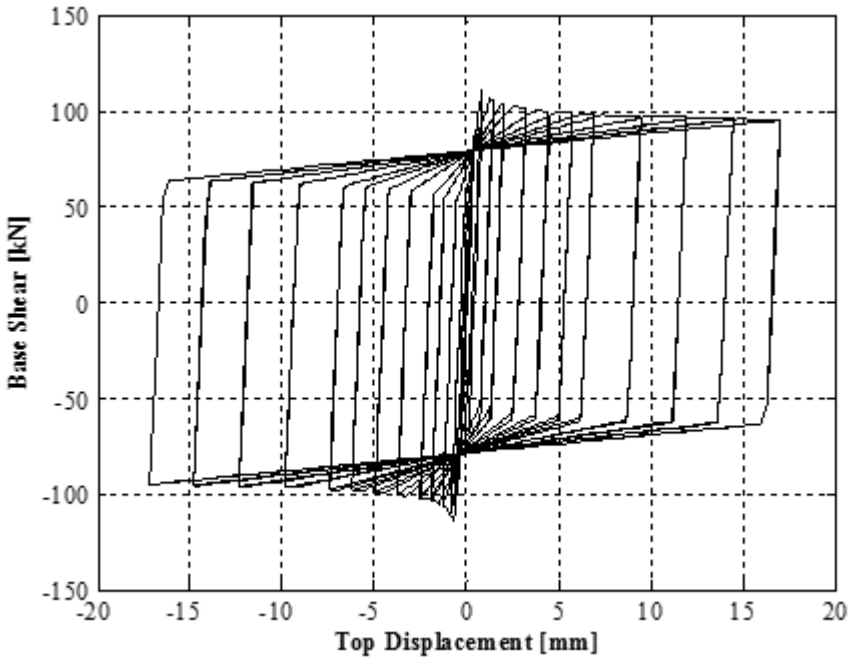

Figure 49: TUD-COMP-4: TREMURI blind prediction - Shear force-displacement curve

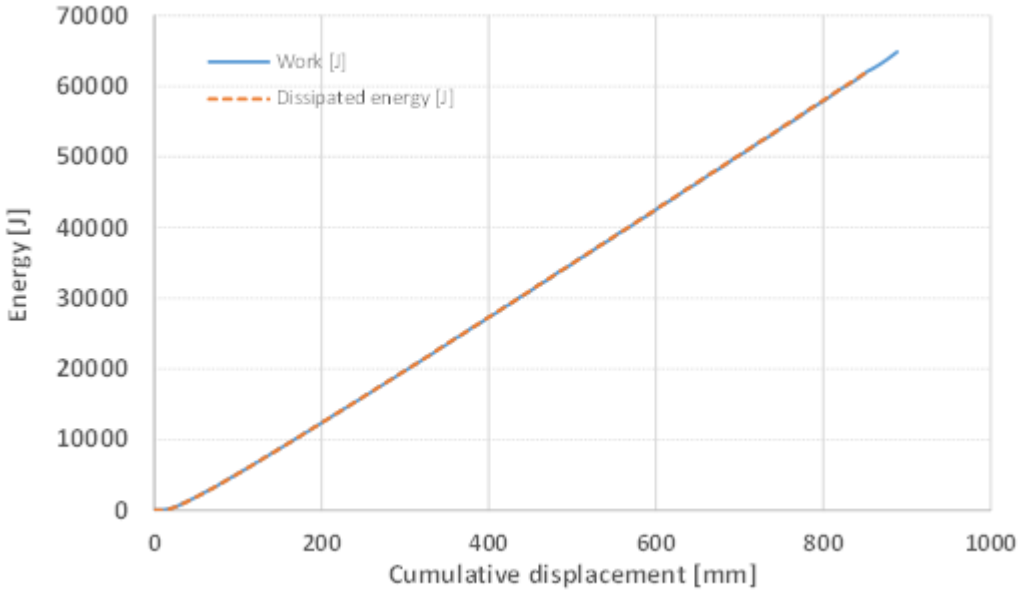

Figure 50: TUD-COMP-4: TREMURI blind prediction - Work & energy dissipation

Table 14: TUD-COMP-4: TREMURI blind prediction - Summary table

	Predominant Failure Mechanism Predicted	**Initial Stiffness [kN/mm]**	**Peak Strength [kN]**	**Maximum Achieved Drift**	
TREMURI	Shear	217	113.7	0.62%	
Test Result	Diagonal cracks / toe crushing	> 223	119	0.2%	Near collapse

2.1.5.4 TU-Delft Blind Prediction

The DIANA finite element model of TUD-COMP-4 exhibits a wide crack pattern even for low displacement levels. The failure occurs with the formation of several diagonal cracks in both directions, similar to what observed in the experiment, even though the damage pattern appears to be more widespread.

The numerical peak shear capacity resulted equal to 135 kN with a maximum top displacement equal to 2.1 mm. The analysis could not be performed to larger displacement levels due to convergence issues. The dissipated energy was lower than that observed in the experiment.

In the DIANA finite element model of TUD-COMP-4 the material properties have been assigned according to the values obtained in the experimental campaign performed at TU-Delft laboratories, as by report of August 2015 [9].

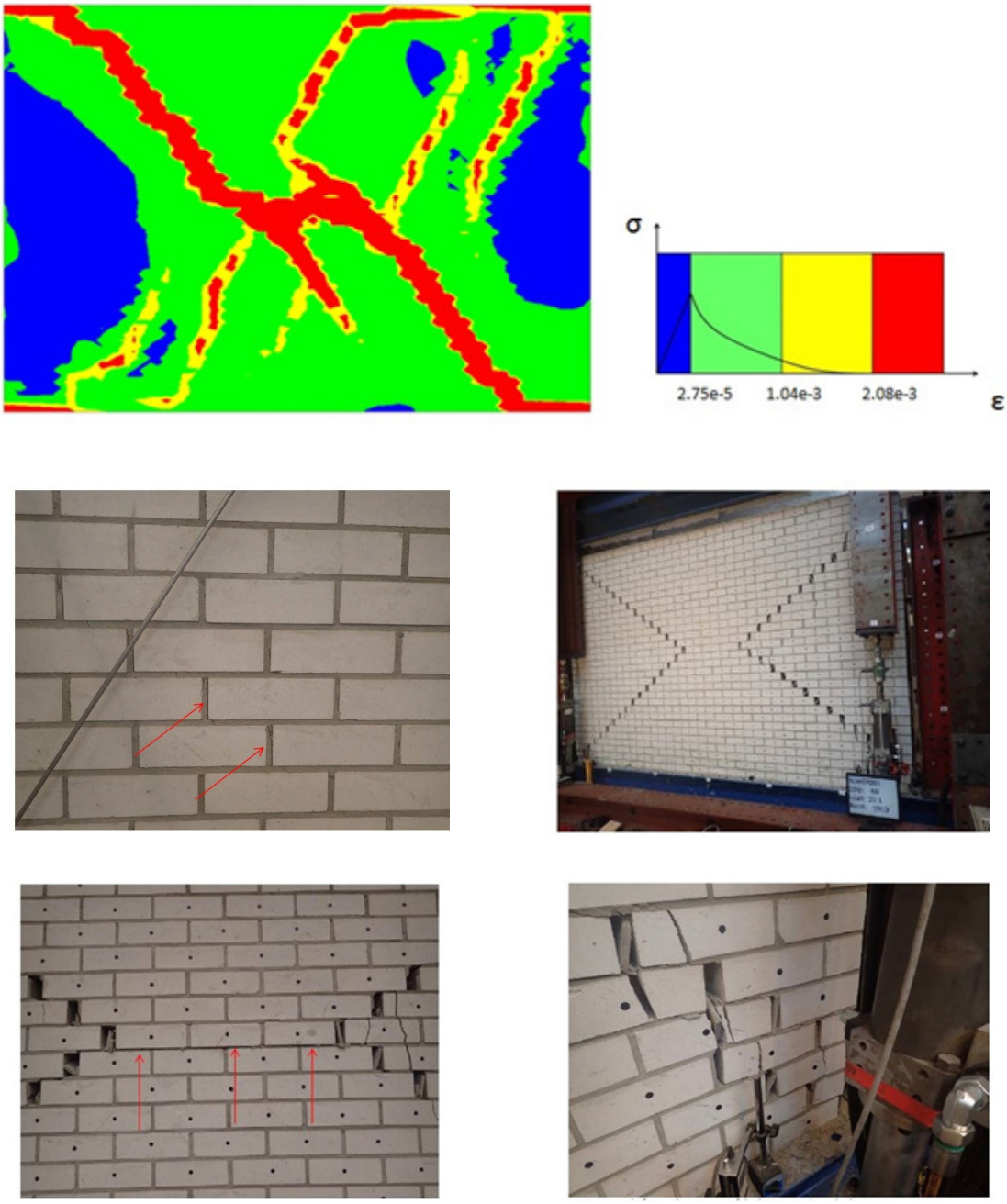

Figure 51: TUD-COMP-4: DIANA blind prediction - Damage plot at end of analysis (top right) compared to observed damage in laboratory

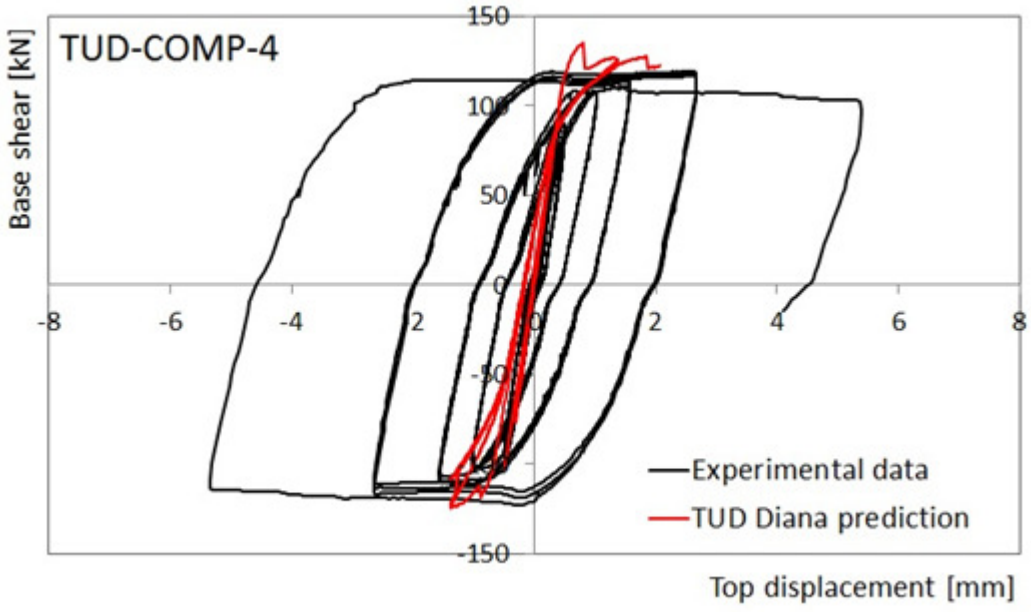

Figure 52: TUD-COMP-4: DIANA blind prediction - Shear force-displacement curve

Table 15: TUD-COMP-4: DIANA blind prediction - Summary table

	Predominant Failure Mechanism Predicted	**Initial Stiffness [kN/mm]**	**Peak Strength [kN]**	**Maximum Achieved Drift**	
DIANA	Diagonal cracks	243	135 (*)	0.08% (*)	(*)
Test Result	Diagonal cracks / toe crushing	> 223	119	0.2%	Near collapse

(*) Model not pushed up to 0.2% drift due to failure to converge

2.1.6 TUD-COMP-5

2.1.6.1 Test Description

TUD-COMP-5 was the sixth quasi-static in-plane test administered by TU-Delft. This specimen was a single-wythe wall constructed of calcium silicate units 102 mm thick. It was 4 m long and 2.75 m high. The applied overburden stress was 0.3 MPa. The wall was tested under double clamped boundary conditions.

First cracks, which were a combination of diagonally oriented cracks and horizontal cracks in the bed joints, appeared during the sixth cycle (0.05% drift). These cracks progressively increased during the duration of the test. In addition, vertical cracks through bricks as well as bed-joint sliding near the bottom of the wall occurred. At the end of the test, maximum crack widths of 30 mm were measured. The failure mode was mainly governed by diagonally oriented damage. The test was stopped at a net drift of 0.46% drift in the negative direction only because the asymmetry in the actuator loads did not allow further cycling.

Similar to TUD-COMP-4, during the pre-test calibration phase, a horizontal crack formed between the first and second brick layer from the top. The crack was repaired. However, as a consequence, the specimen became in effect one brick-height shorter. This was not taken into account in the blind prediction model.

Throughout the test, the wall experienced asymmetrical damage, which caused a redistribution of forces in the actuators. In order to ensure that the proper boundary conditions were maintained, during the last three cycles of the test, the wall was only able to be pushed in one direction. Thus the test result may be compromised in some way.

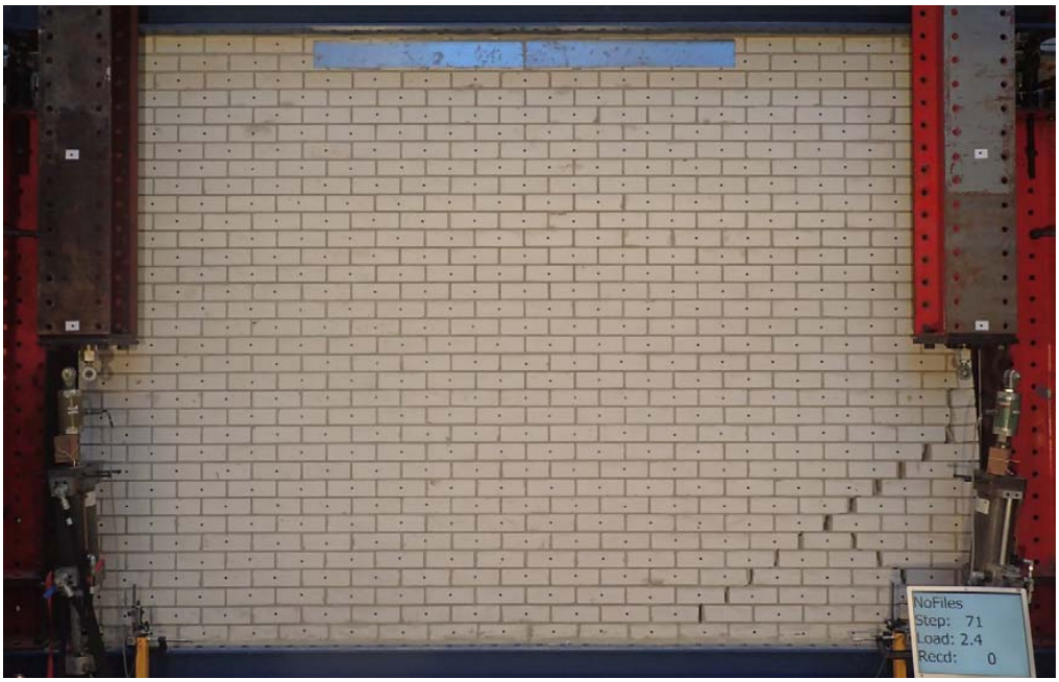

Figure 53: TUD-COMP-5: Crack pattern at the end of the test

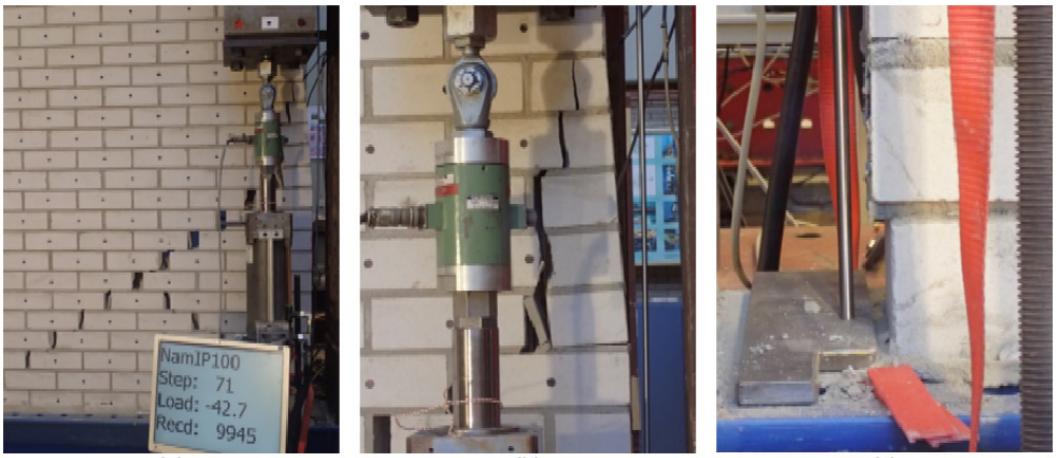

Figure 54: TUD-COMP-5: Details of final crack patterns: diagonal cracks at the bottom-right corner (a), vertical cracks through bricks (b), residual sliding at the bottom left corner (c)

The actual loading regime of TUD-COMP-5 differed from that specified in the planned test protocol, which specified a maximum drift level of 0.2%. The protocol greatly differed after a drift of 0.11% was reached, as was previously explained above. The overburden matched the specified value.

The measured hysteresis is shown in Figure 55.

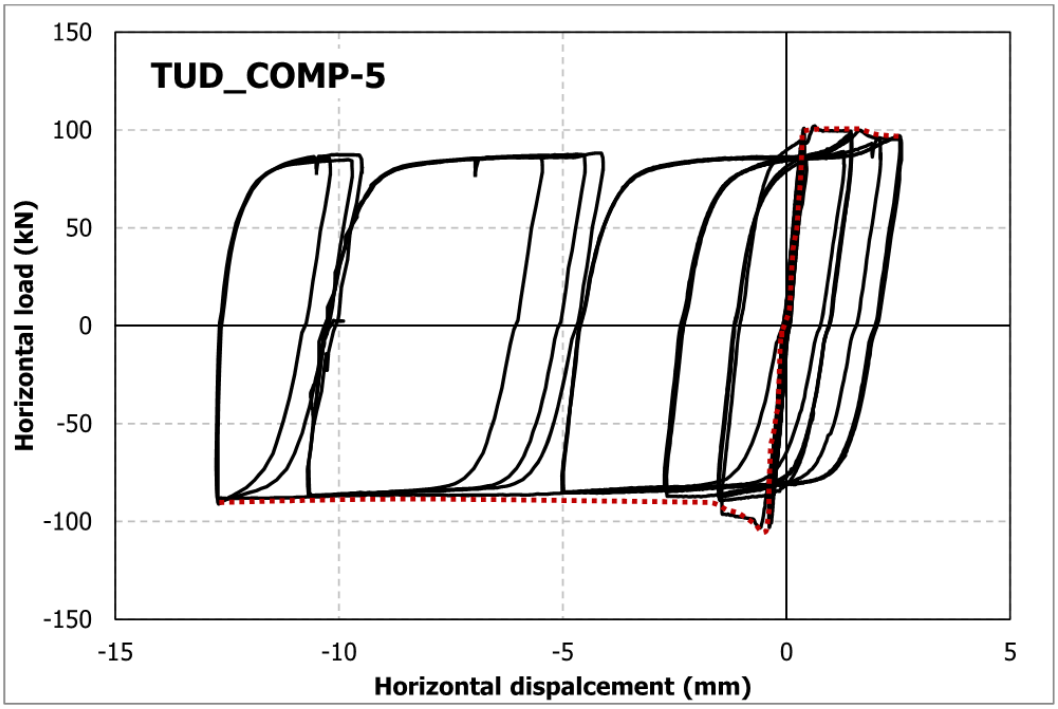

Figure 55: TUD-COMP-5: Lab test result – Shear force-displacement curve

2.1.6.2 Arup Blind Prediction

The LS-DYNA model of TUD-COMP-5 predicted failure governed by the formation of diagonal crack pattern through the specimen associated with bed joint sliding and head joint opening. Up to 0.2% drift, no collapse occurred. The simulation did not predict any excessive deformations.

The lateral-force-versus-displacement relationship followed typical shear behaviour as shown in Figure 57. The predicted ultimate load initially peaked at approximately 76 kN and gradually decayed to a load of approximately 54 kN. The predicted initial stiffness was approximately 160 kN/mm.

Because of the difficulties encountered during the physical test and resulting change of protocol, there is some doubt surrounding the reliability of the test result. Comparisons between the lab test result and the simulation are of limited value.

Note that the LS-DYNA blind prediction model of TUD-COMP-5 used material properties measured by TU-Delft as of August 2015 [9], not the NAM Basis for Design material properties.

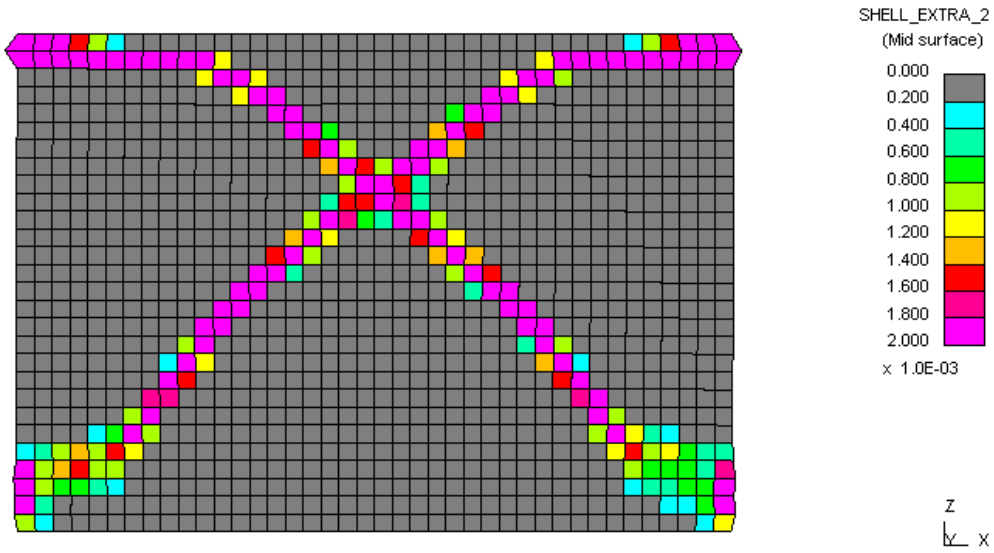

Figure 56: TUD-COMP-5: LS-DYNA blind prediction - Damage plot at end of analysis

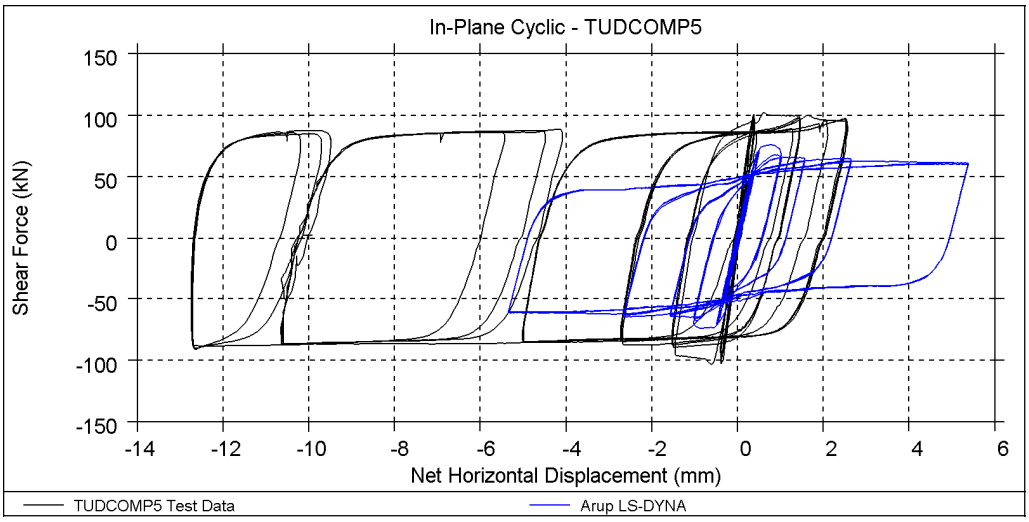

Figure 57: TUD-COMP-5: LS-DYNA blind prediction - Shear force-displacement curve

Table 16: TUD-COMP-5: LS-DYNA blind prediction - Summary table

	Predominant Failure Mechanism Predicted	**Initial Stiffness [kN/mm]**	**Peak Strength [kN]**	**Maximum Achieved Drift**	
LS-DYNA	Diagonal cracks / bed joint sliding	160	76	0.2%	End of protocol
Test Result	Diagonal cracks / toe crushing	> 288	103	0.5%	Stopped – no collapse (*)

(*) The test stopped due to inability to maintain the double-clamped boundary condition, not due to imminent collapse.

2.1.6.3 EUCENTRE Blind Prediction

The TREMURI macro-element model predicted a shear behaviour as shown by the hysteresis curve (Figure 59) with high energy dissipation (Figure 60).

Note that the overburden was 0.6 MPa in the simulation but 0.3 MPa in the test.

The TREMURI blind prediction model of TUD-COMP-5 used material properties measured by TU-Delft from mechanical characterization test, not the NAM Basis for Design material properties.

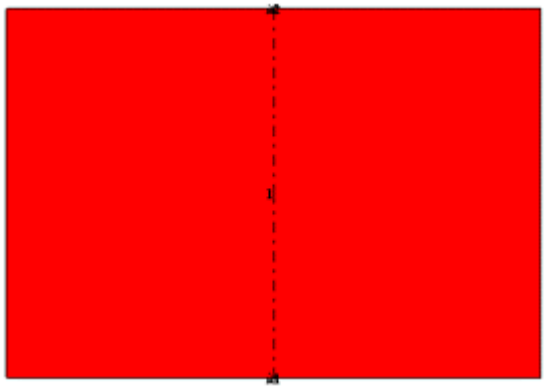

Figure 58: TUD-COMP-5: TREMURI blind prediction model

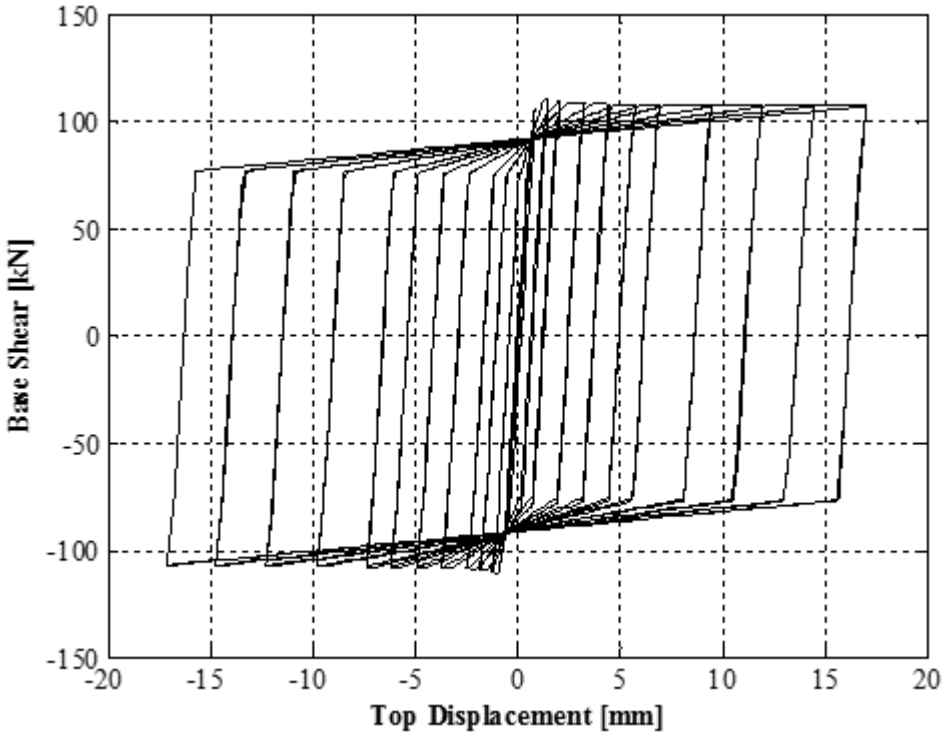

Figure 59: TUD-COMP-5: TREMURI blind prediction - Shear force-displacement curve

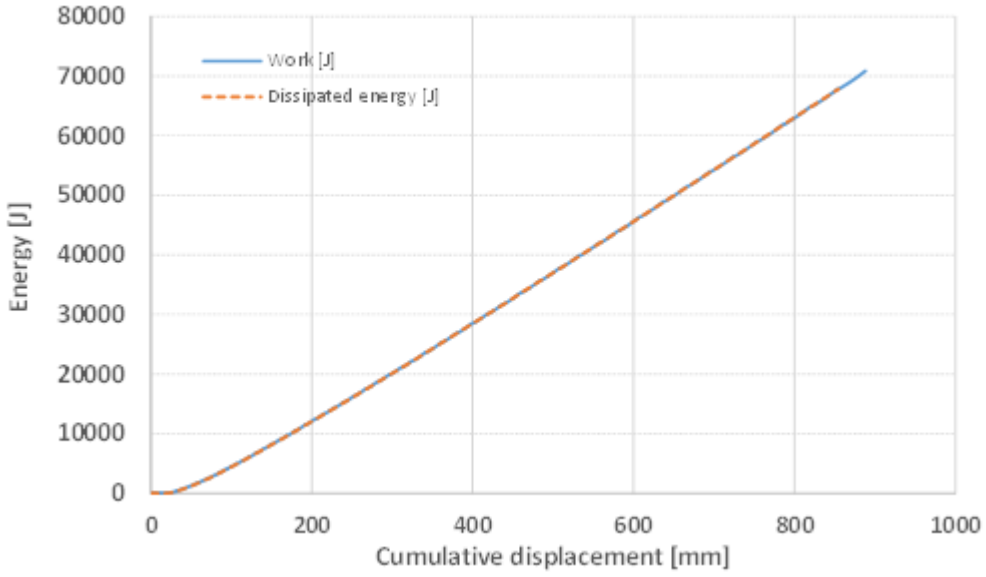

Figure 60: TUD-COMP-5: TREMURI blind prediction - Work & energy dissipation

Table 17: TUD-COMP-5: TREMURI blind prediction - Summary table

	Predominant Failure Mechanism Predicted	**Initial Stiffness [kN/mm]**	**Peak Strength [kN]**	**Maximum Achieved Drift**	
TREMURI	Shear	154 [1]	111.4 [1]	0.62%	
Test Result	Diagonal cracks / toe crushing	> 288	103	0.5%	Stopped – no collapse [2]

1. For 0.6 MPa overburden

2. The test stopped due to inability to maintain the double-clamped boundary condition, not due to imminent collapse.

2.1.6.4 TU-Delft Blind Prediction

The DIANA finite element model of TUD-COMP-5 exhibits a wide crack pattern even for low displacement levels. The failure occurs with the formation of multiple diagonal cracks in both directions, different to what was observed in the experiment. Moreover, differences between experimental and numerical results are increased by the change in the applied horizontal loading protocol, which substantially diverged from the initial planned one, because of difficulties encountered during the physical test.

The numerical peak shear capacity resulted equal to 109 kN with a maximum top displacement equal to 2.75 mm. The analysis could not be performed to larger displacement levels due to convergence issues. The dissipated energy was lower than that observed in the experiment.

In the DIANA finite element model of TUD-COMP-5 the material properties have been assigned according to the values obtained in the experimental campaign performed at TU-Delft laboratories, as by report of August 2015 [9].

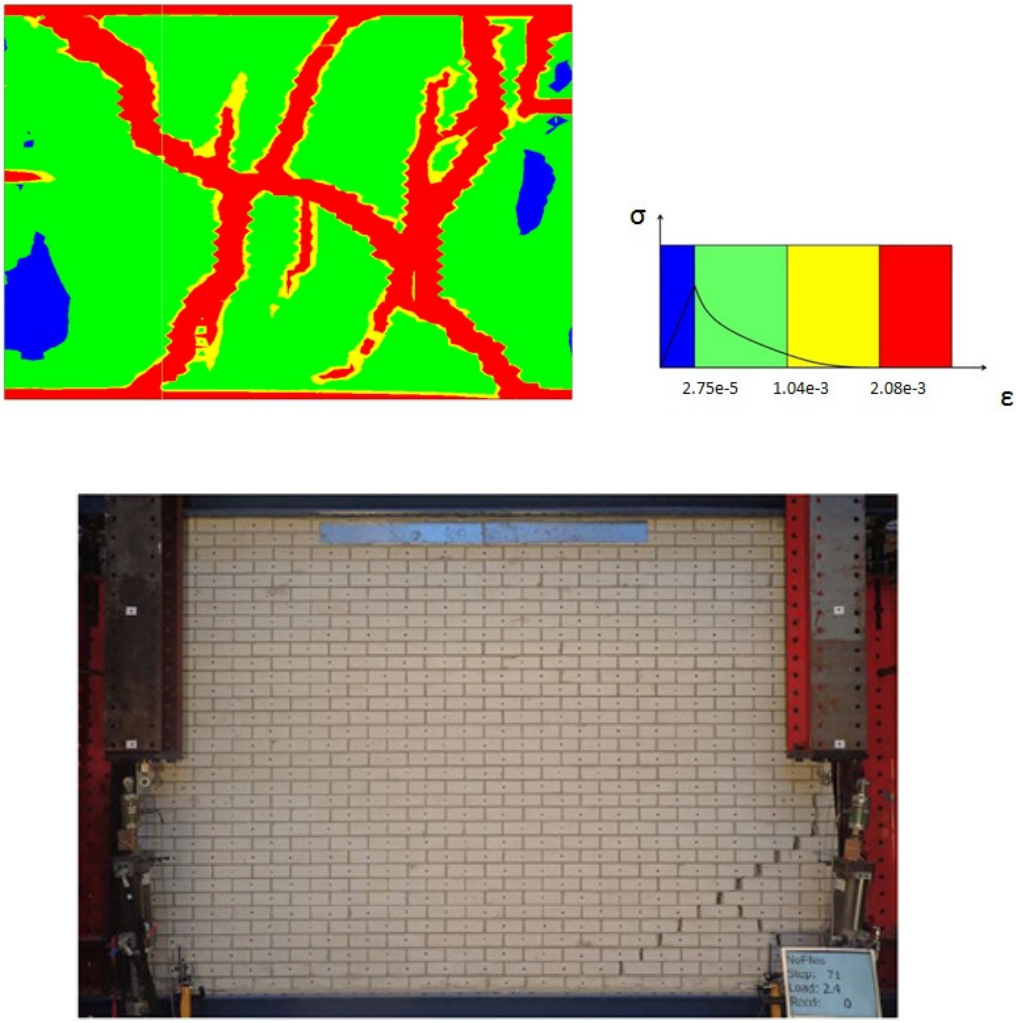

Figure 61: TUD-COMP-5: DIANA blind prediction - Damage plot at end of analysis

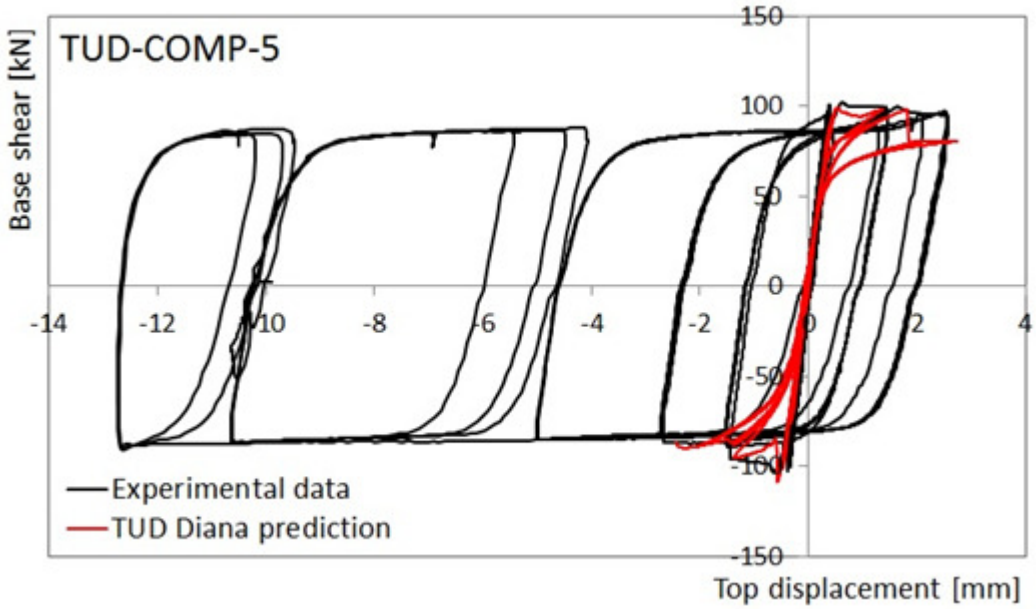

Figure 62: TUD-COMP-5: DIANA blind prediction - Shear force-displacement curve

Table 18: TUD-COMP-5: DIANA blind prediction - Summary table

	Predominant Failure Mechanism Predicted	**Initial Stiffness [kN/mm]**	**Peak Strength [kN]**	**Maximum Achieved Drift**	
DIANA	Diagonal cracks	243	109 [1]	0.1% [1]	[1]
Test Result	Diagonal cracks / toe crushing	> 288	103	0.5%	Stopped – no collapse [2]

1. Model not pushed up to 0.5% drift due to failure to converge

2. The test stopped due to inability to maintain the double-clamped boundary condition, not due to imminent collapse.

2.1.7 TUD-COMP-6

2.1.7.1 Test Description

TUD-COMP-6 was the seventh quasi-static in-plane test administered by TU-Delft. This specimen was a single-wythe wall constructed of calcium silicate units 102 mm thick. It was 4 m long and 2.75 m high. The applied overburden stress was 0.5 MPa. The wall was tested under cantilever boundary conditions.

First cracks along the main diagonal of the wall, appeared during the fifth cycle (0.02% drift). Similar cracks along the opposite diagonal also formed. These cracks progressively increased during the duration of the test and penetrated brick as well as mortar. In addition, bed-joint sliding near the bottom of the wall occurred after the ninth cycle (0.37% drift). After the tenth cycle (0.47% drift), significant brick crushing occurred. The test was stopped at a net drift of 0.56% drift due to potential collapse of the wall.

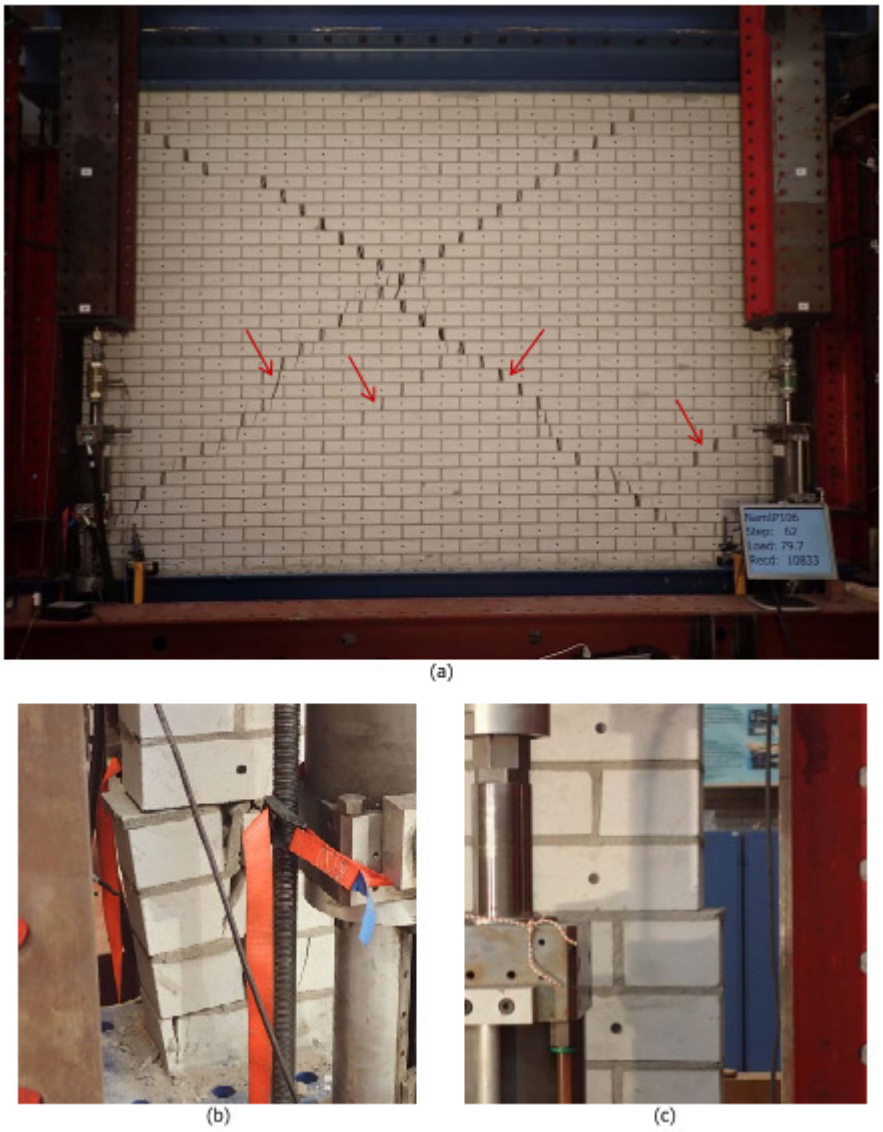

Figure 63: TUD-COMP-6: Crack pattern after 0.37% drift--general overview (a) and bottom left (b) and right (c) corners

Figure 64: TUD-COMP-6: Crack pattern after 0.47% drift--central portion (a) and bottom right corner (b)

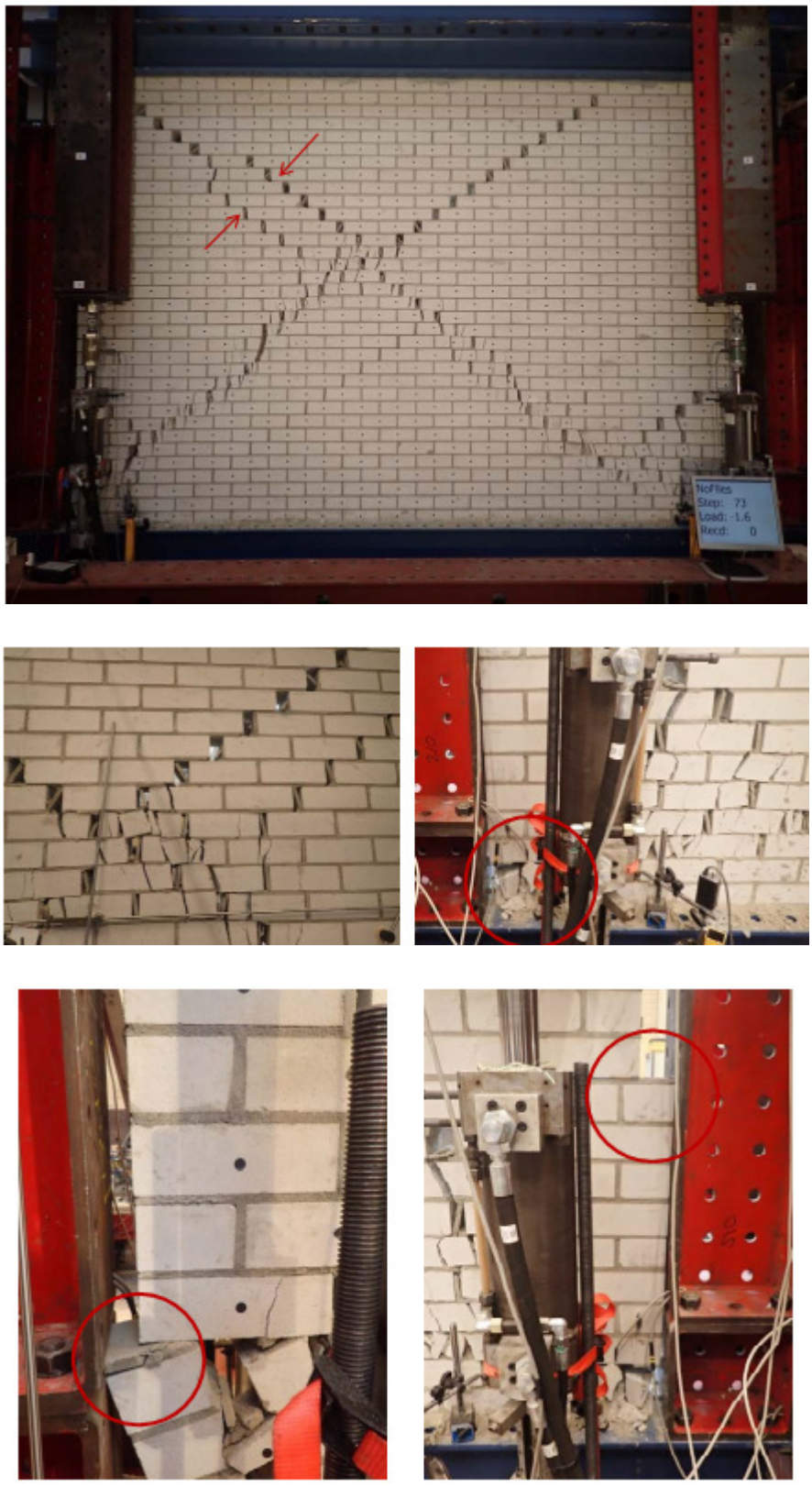

Figure 65: TUD-COMP-6: Final crack pattern

The measured hysteresis is shown in Figure 66:

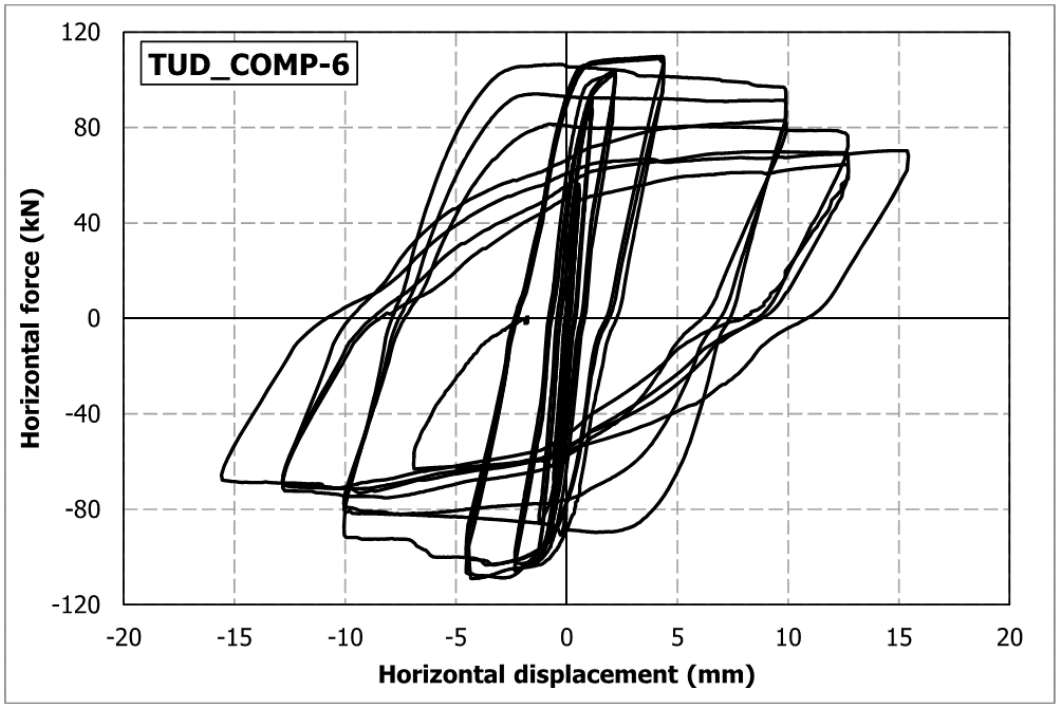

Figure 66: TUD-COMP-6: Lab test result – Shear force-displacement curve

2.1.7.2 Arup Blind Prediction

The LS-DYNA blind prediction analysis of TUD-COMP-6 assumed an overburden of 0.3 MPa rather than 0.5 MPa. Thus, the peak strength is under-predicted in comparison to the results obtained in the laboratory.

The LS-DYNA model of TUD-COMP-6 predicted failure governed by bed joint sliding at the base of the wall as well as near mid-height of the wall and the formation of diagonal cracks between the two locations of sliding. Up to 2% drift, no collapse occurred. The simulation did not predict any excessive deformations.

The lateral-force-versus-displacement relationship followed typical shear behaviour as shown in Figure 68. The predicted ultimate load initially peaked at approximately 76 kN and gradually decayed to a load of approximately 61 kN. The predicted initial stiffness was approximately 105 kN/mm.

The LS-DYNA model captured the shear mechanism generated during the laboratory test but under-predicted the lateral strength of the wall and over predicted the residual stiffness. This is largely due to the incorrect overburden stress. This has been corrected in the post-test refined prediction. Furthermore, in the LS-DYNA simulation, the maximum displacement is smaller than the test one as the planned loading protocol has been changed during the test.

Note that the LS-DYNA blind prediction model of TUD-COMP-6 used material properties measured by TU-Delft as of August 2015 [9].

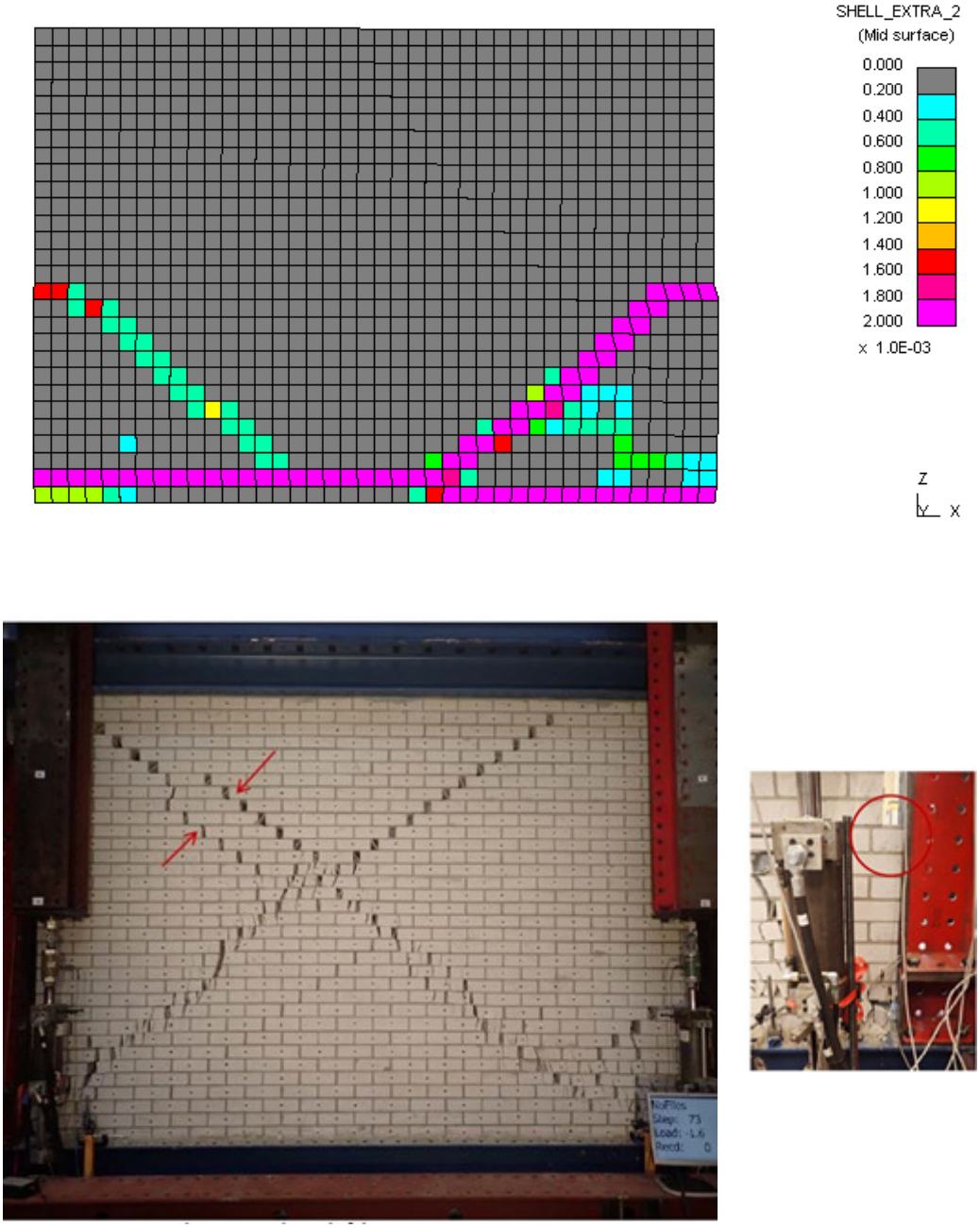

Figure 67: TUD-COMP-6: LS-DYNA blind prediction - Damage plot at end of analysis (top) compared to observed damage in laboratory

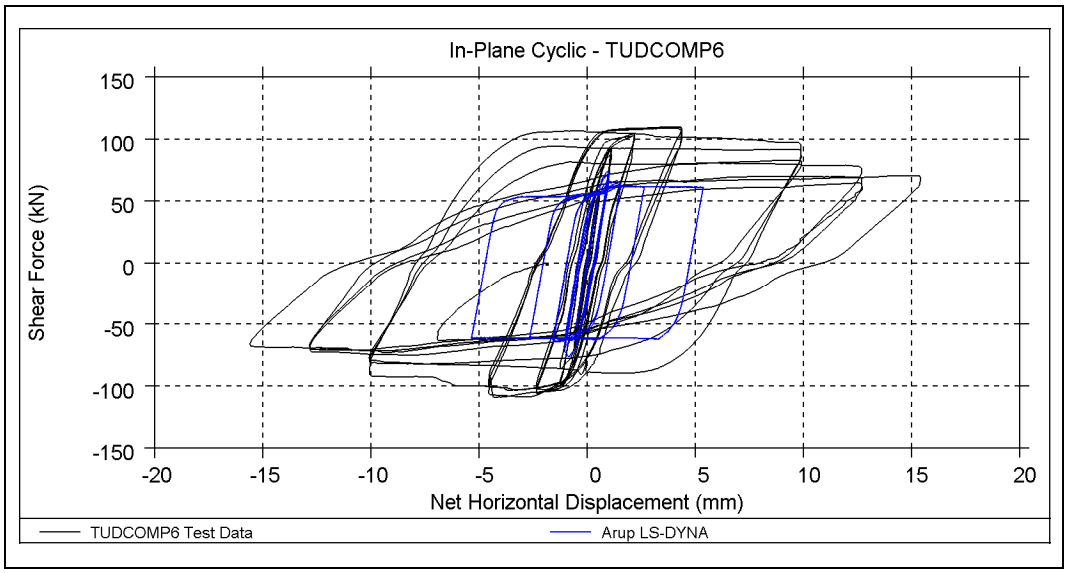

Figure 68: TUD-COMP-6: LS-DYNA blind prediction - Shear force-displacement curve

Table 19: TUD-COMP-6: LS-DYNA blind prediction - Summary table

	Predominant Failure Mechanism Predicted	**Initial Stiffness [kN/mm]**	**Peak Strength [kN]**	**Maximum Achieved Drift**	
LS-DYNA	Diagonal cracks / bed joint sliding	105 (*)	76 (*)	0.2%	End of protocol
Test Result	Diagonal cracks / toe crushing	125	110	0.6%	Near collapse

(*) For 0.3 MPa overburden

2.1.7.3 EUCENTRE Blind Prediction

The TREMURI macro-element model predicted a shear behaviour as shown by the hysteresis curve (Figure 70) with high energy dissipation (Figure 71).

Note that the overburden was 0.4 MPa in the simulation but 0.5 MPa in the test.

The TREMURI blind prediction model of TUD-COMP-6 used material properties measured by TU-Delft from mechanical characterization test, not the NAM Basis for Design material properties.

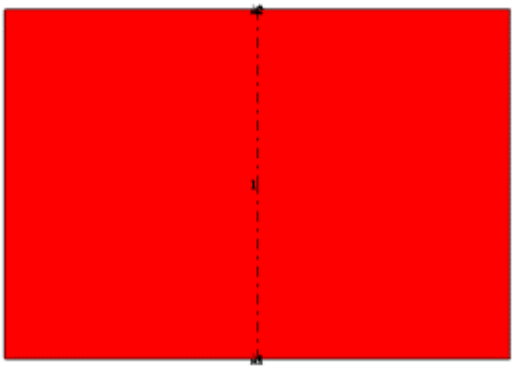

Figure 69: TUD-COMP-6: TREMURI blind prediction model

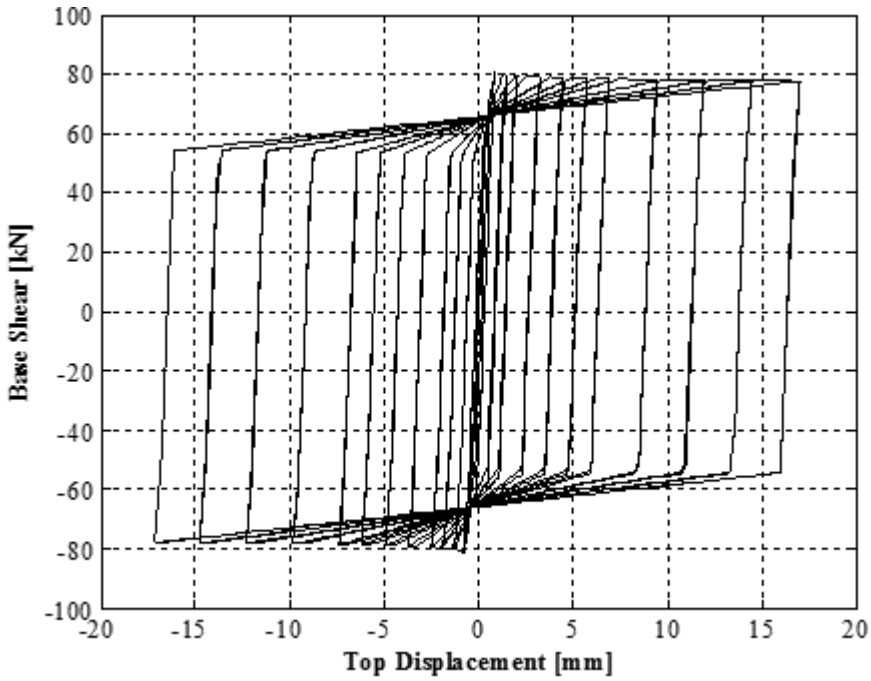

Figure 70: TUD-COMP-6: TREMURI blind prediction - Shear force-displacement curve

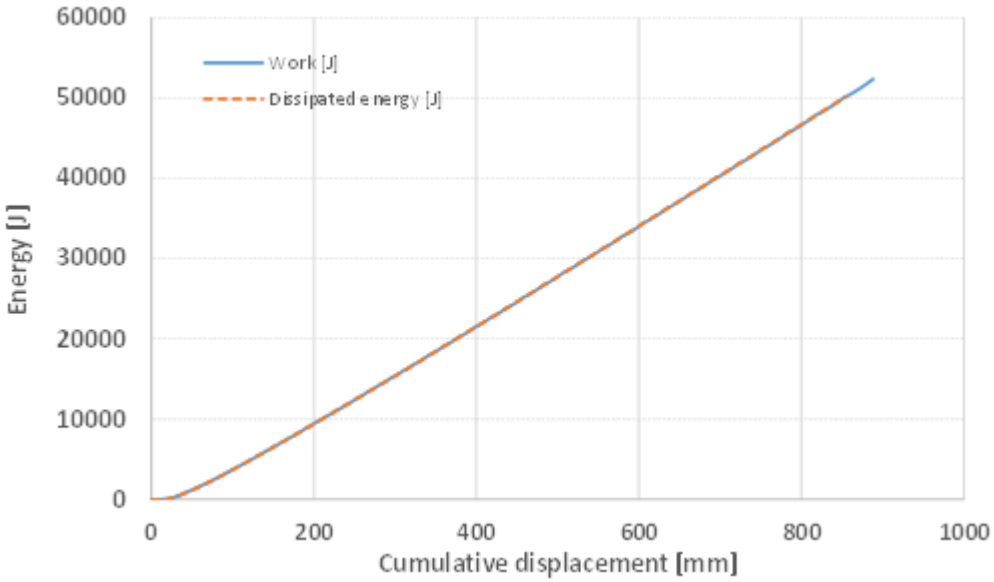

Figure 71: TUD-COMP-6: TREMURI blind prediction - Work & energy dissipation

Table 20: TUD-COMP-6: TREMURI blind prediction - Summary table

	Predominant Failure Mechanism Predicted	**Initial Stiffness [kN/mm]**	**Peak Strength [kN]**	**Maximum Achieved Drift**	
TREMURI	Shear	151 (*)	81.4 (*)	0.62%	
Test Result	Diagonal cracks / toe crushing	125	110	0.6%	Near collapse

(*) For 0.4 MPa overburden

2.1.7.4 TU-Delft Blind Prediction

The DIANA finite element model of TUD-COMP-6 exhibits a wide crack pattern even for low displacement levels. The failure occurs with the formation of several diagonal cracks in both directions, similar to what observed in the experiment, even though the damage pattern appears to be more widespread.

The numerical peak shear capacity resulted equal to 115.7 kN with a maximum top displacement equal to 2.3 mm. The analysis could not be performed to larger displacement levels due to convergence issues. The dissipated energy was lower than that observed in the experiment.

In the DIANA finite element model of TUD-COMP-6 the material properties have been assigned according to the values obtained in the experimental campaign performed at TU-Delft laboratories, as by report of August 2015 [9].

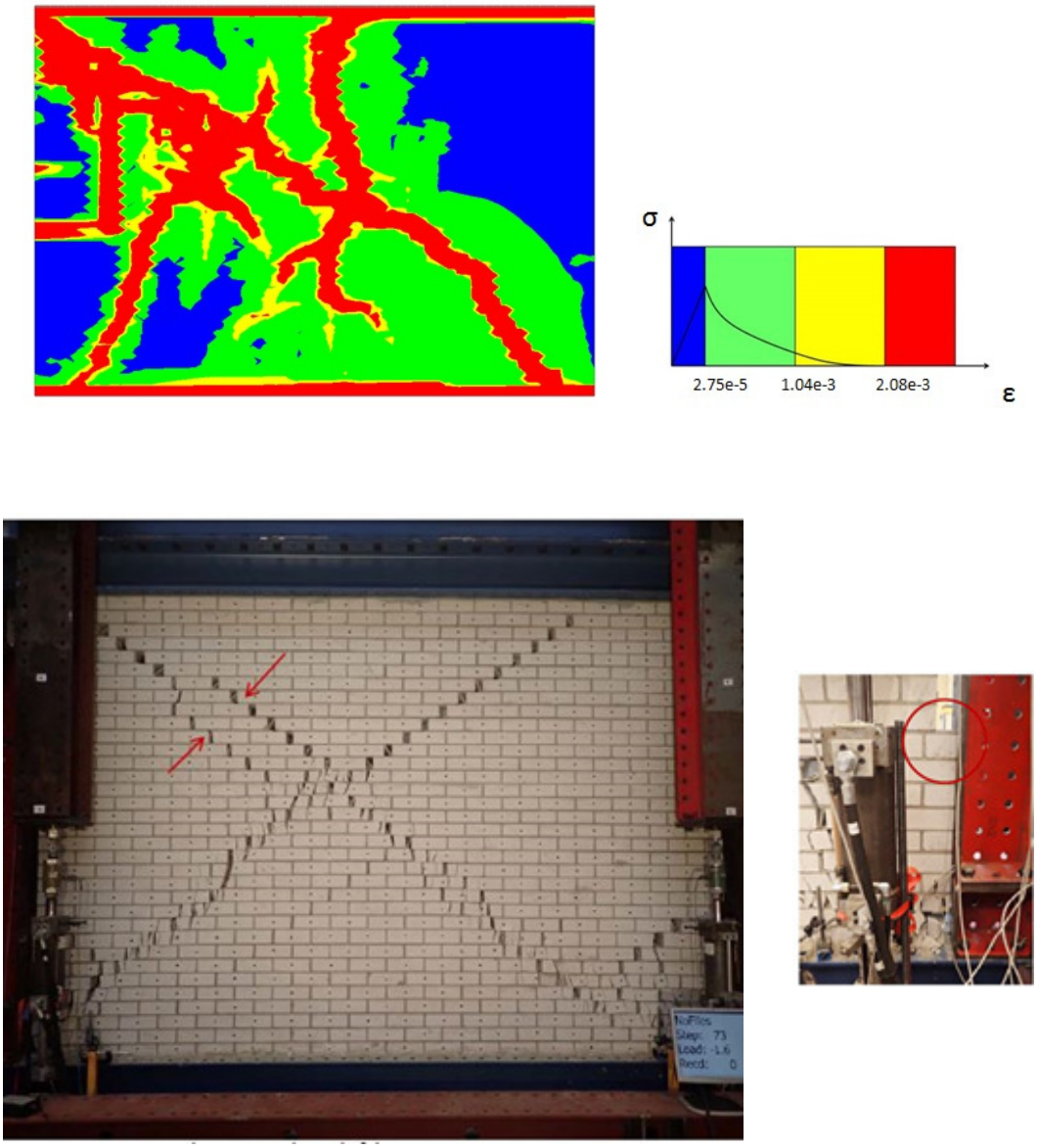

Figure 72: TUD-COMP-6: DIANA blind prediction - Damage plot at end of analysis (top) compared to observed damage in laboratory

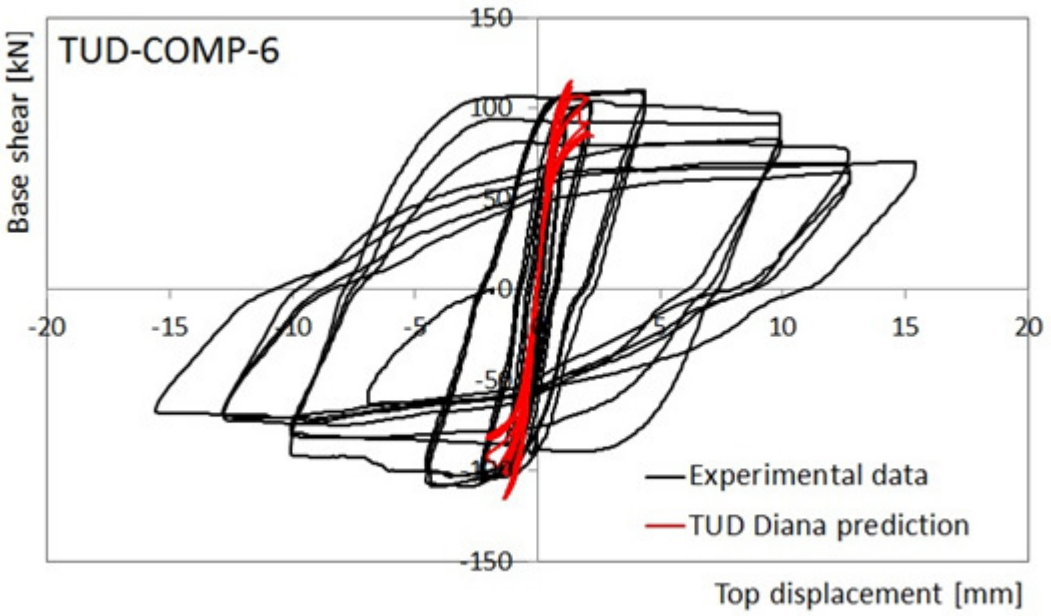

Figure 73: TUD-COMP-6: DIANA blind prediction - Shear force-displacement curve

Table 21: TUD-COMP-6: DIANA blind prediction - Summary table

	Predominant Failure Mechanism Predicted	**Initial Stiffness [kN/mm]**	**Peak Strength [kN]**	**Maximum Achieved Drift**	
DIANA	Diagonal cracks	163	115 (*)	0.08% (*)	(*)
Test Result	Diagonal cracks / toe crushing	125	110	0.6%	Near collapse

(*) Model not pushed up to 0.6% drift due to failure to converge

2.1.8 EUC-COMP-1

2.1.8.1 Test Description

EUC-COMP-1 was one of the three quasi-static in-plane tests administered by EUCENTRE Blind Prediction. This specimen was a single-wythe wall constructed of calcium silicate units 102 mm thick. It was 1.1 m long and 2.75 m high. The originally planned overburden stress was 0.4 MPa. The wall was tested under double clamped boundary conditions.

As expected, specimen EUC-COMP-1 initially exhibited a pure rocking behaviour with cracks opening at the edges upon cyclically loading the specimen. A migration of the horizontal crack at the bottom was observed. At a drift of 0.6%, the location of the horizontal crack was at the interface. At a drift of 1.5%, the horizontal crack migrated above the first course of bricks and above the second course of bricks during last cycle with 2% drift.

The test was stopped due to the inability of the pier to sustain the imposed vertical load at a drift of 2% drift. A toe crushing mechanism was exhibited.

Figure 74: EUC-COMP-1: Toe-crushing damage at end of test (a) bottom right; (b) top left corner; (c) top right corner

The actual test loading regime of EUC-COMP-1 matched the one specified in the planned protocol, which specified a maximum drift level of 2%. However, the actual overburden applied during the test was 0.52 MPa rather than 0.4 MPa. This was noted in the post-test refined predictions provided by all three consultants.

See Figure 75 below for the shear force-displacement plot of the lab test result of EUC-COMP-1.

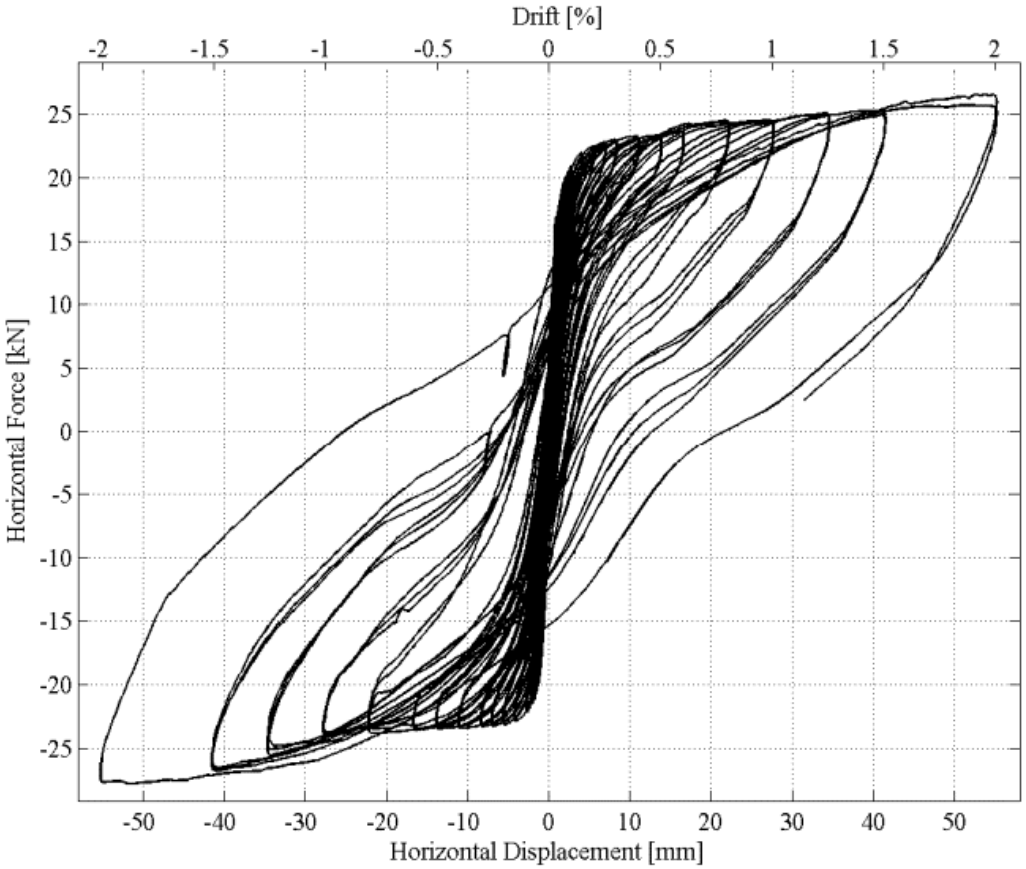

Figure 75: EUC-COMP-1: Lab test result – Shear force-displacement curve

2.1.8.2 Arup Blind Prediction

The LS-DYNA model of EUC-COMP-1 predicted rocking behaviour and associated tensile bed joint failures at the top and bottom of the specimen, as shown in Figure 76.

The lateral-force-versus-displacement relationship followed an S-shaped curve, as shown in Figure 77. The predicted ultimate load was approximately 17 kN at a drift of 2%. The lab test resulted in an ultimate load of 28 kN. As previously mentioned, the actual overburden applied during the test was 0.52 MPa rather than 0.4 MPa. This was noted in the post-test refined prediction. The predicted initial stiffness was approximately 12.7 kN/mm.

As illustrated by the hysteresis curve, there was little energy dissipated by the LS-DYNA model of the specimen. The model did not predict collapse or a near-collapse state.

The LS-DYNA model captured the rocking mechanism generated during the laboratory test. The lateral strength of the LS-DYNA model of the specimen did not match the lab results because the model assumed the overburden that was specified in the protocol (0.4 MPa) while the actual applied overburden applied during the test was 0.52 MPa.

The LS-DYNA model under-predicted the amount of energy dissipation. It is believed that the amount of the dissipated energy could partially be attributed to toe-crushing damage, which the LS-DYNA blind prediction model did not capture.

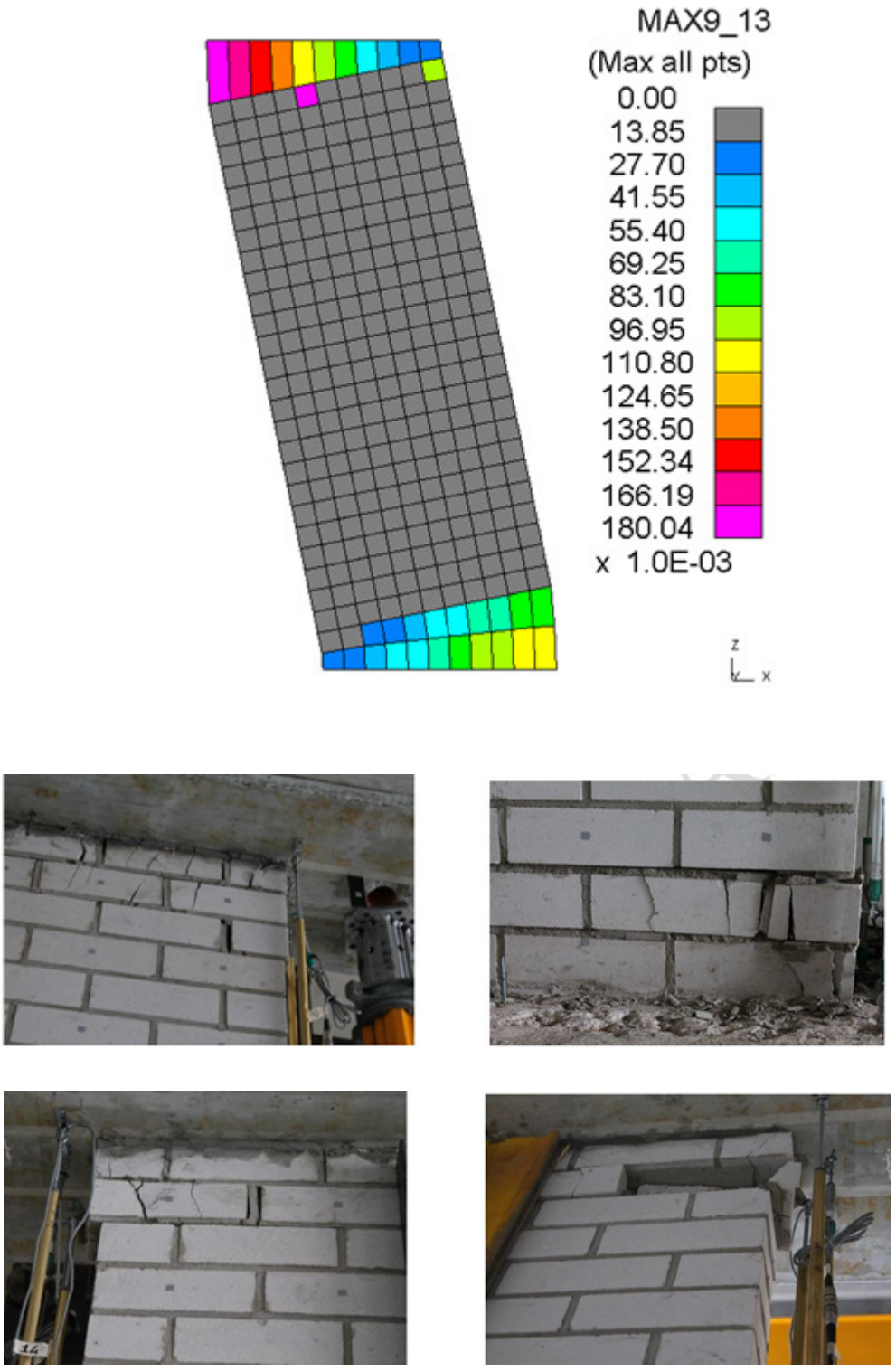

Figure 76: EUC-COMP-1: LS-DYNA blind prediction – Damage plot at end of analysis (top) compared to observed damage in laboratory

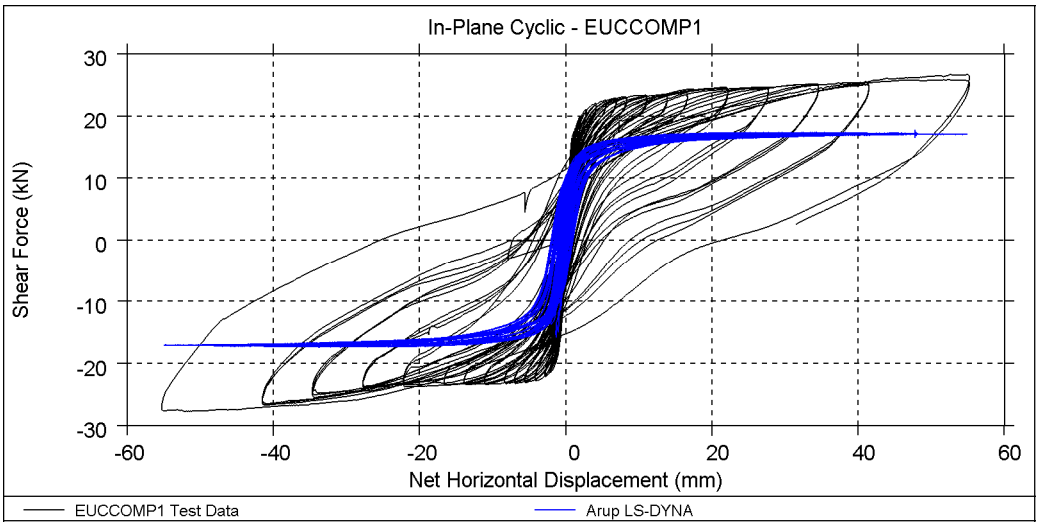

Figure 77: EUC-COMP-1: LS-DYNA blind prediction – Shear force-displacement curve

Table 22: EUC-COMP-1: LS-DYNA blind prediction – Summary table

	Predominant Failure Mechanism Predicted	**Initial Stiffness [kN/mm]**	**Peak Strength [kN]**	**Maximum Achieved Drift**	
LS-DYNA	Rocking	12.7 (*)	17 (*)	2%	End of protocol
Test Result	Rocking / diagonal cracks / toe crushing	22.9	28	2%	Near collapse

(*) LS-DYNA analysis performed under 0.4 MPa overburden stress as specified in the protocol

2.1.8.3 EUCENTRE Blind Prediction

The TREMURI macro-element model predicted a pure rocking behaviour and the resulting hysteresis curve (Figure 79) followed a classical S-shape curve with moderate energy dissipation (Figure 80).

The lateral strength of the TREMURI model of the specimen did not match the lab results because the model assumed the overburden that was specified in the protocol (0.4 MPa) while the actual applied overburden applied during the test was 0.52 MPa.

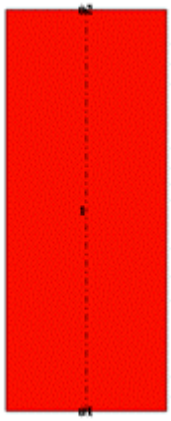

Figure 78: EUC-COMP-1: TREMURI blind prediction model

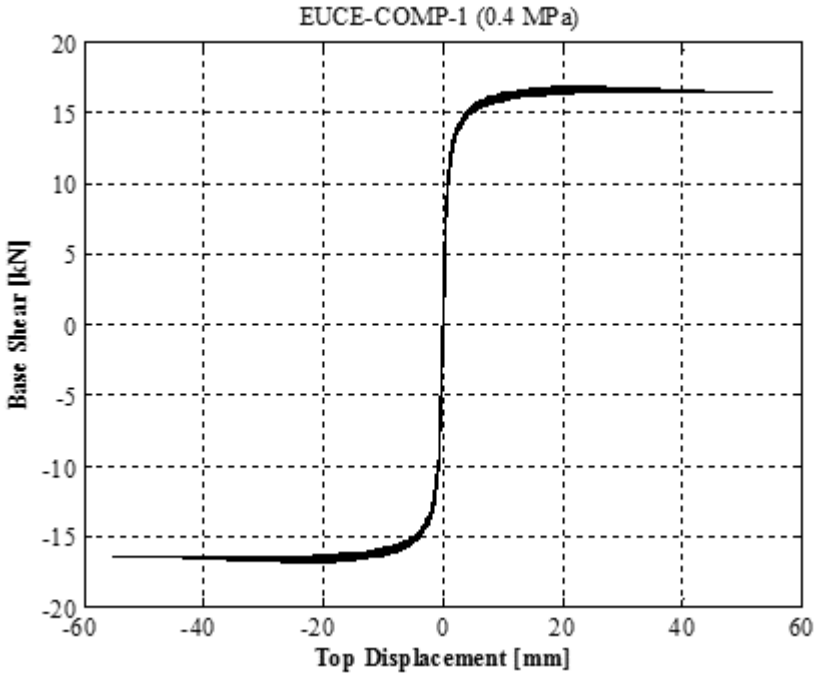

Figure 79: EUC-COMP-1: TREMURI blind prediction - Shear force-displacement curve

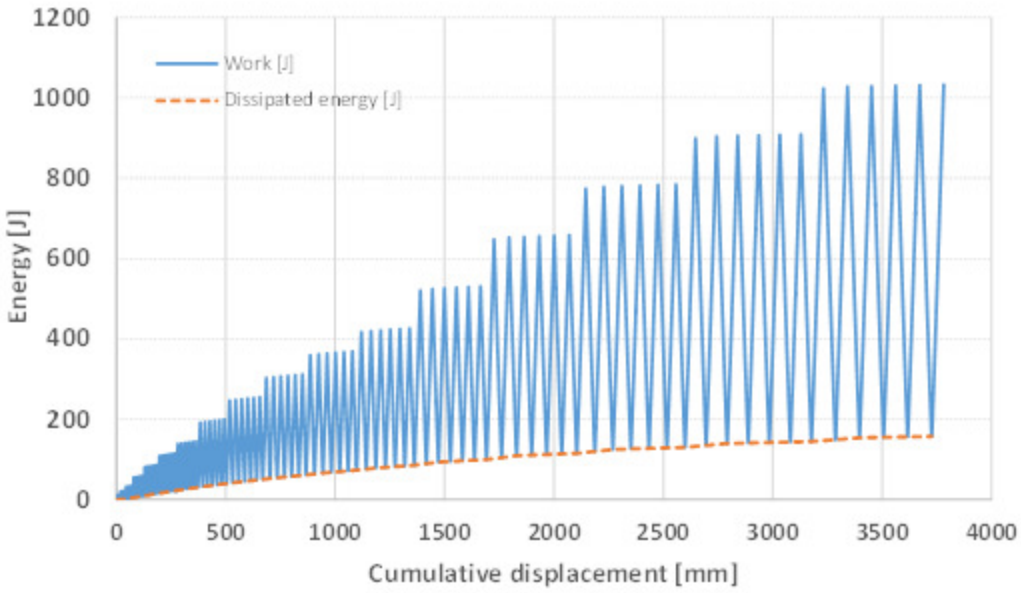

Figure 80: EUC-COMP-1: TREMURI blind prediction - Work & energy dissipation

Table 23: EUC-COMP-1: TREMURI blind prediction - Summary table

	Predominant Failure Mechanism Predicted	**Initial Stiffness [kN/mm]**	**Peak Strength [kN]**	**Maximum Achieved Drift**	
TREMURI	Rocking	15.1 (*)	16.8 (*)	2%	End of protocol
Test Result	Rocking / diagonal cracks / toe crushing	22.9	28	2%	Near collapse

(*) TREMURI analysis performed under 0.4 MPa overburden stress as specified in the protocol

2.1.8.4 TU-Delft Blind Prediction

In the DIANA model, the panel experienced rocking in the first stage of the numerical test. Later, failure occurred with a severe diagonal crack crossing the whole height of the panel. This behaviour was not observed during the experiment, where the panel exhibited a nearly pure rocking behaviour. The numerical base shear capacity was 15.6 kN with a maximum top displacement of 11 mm. The lab test resulted in an ultimate load of 28 kN. As previously mentioned, the actual overburden applied during the test was 0.52 MPa rather than 0.4 MPa. This was noted in the post-test refined prediction.

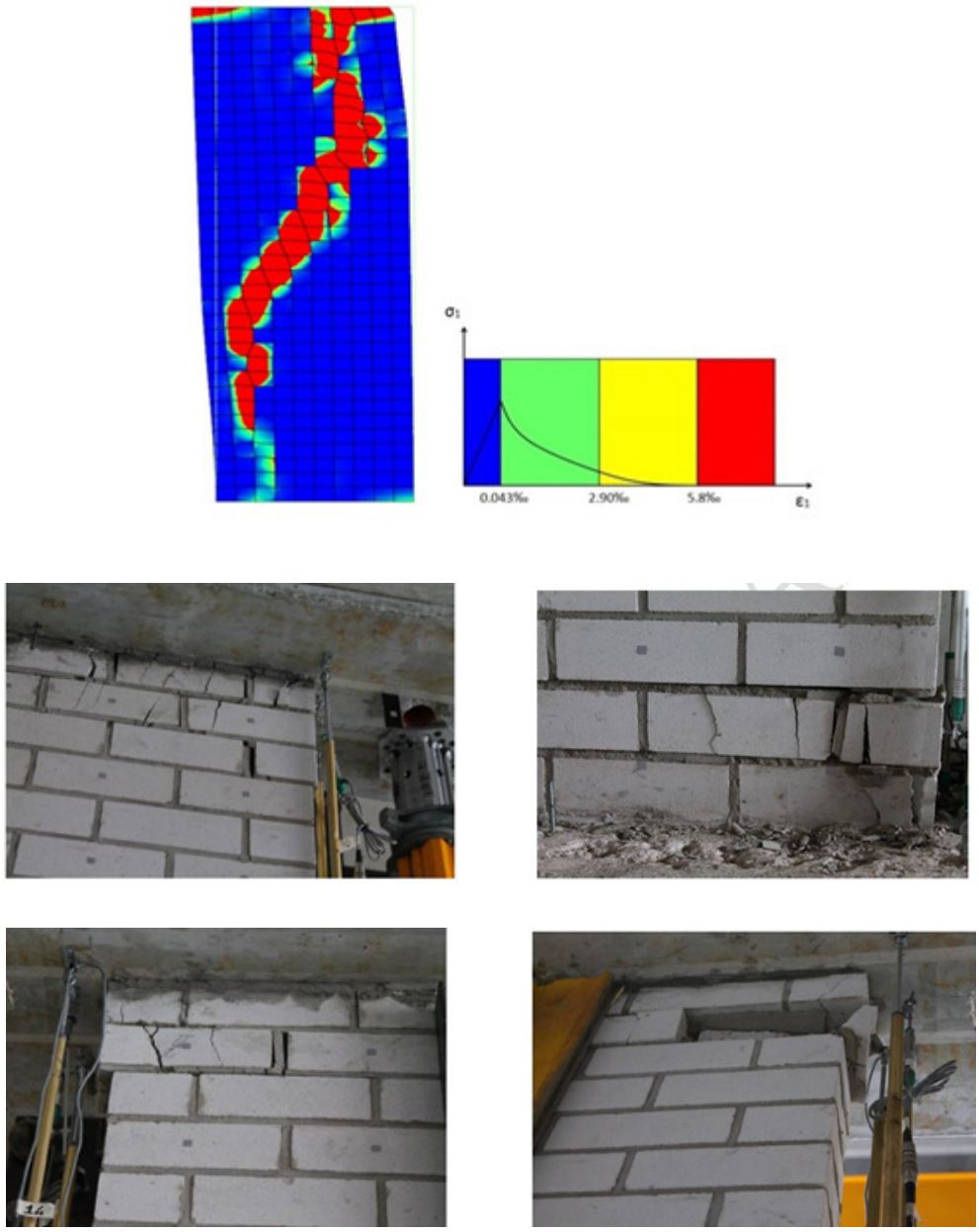

Figure 81: EUC-COMP-1: DIANA blind prediction – Damage plot at end of analysis (top) compared to observed damage in laboratory

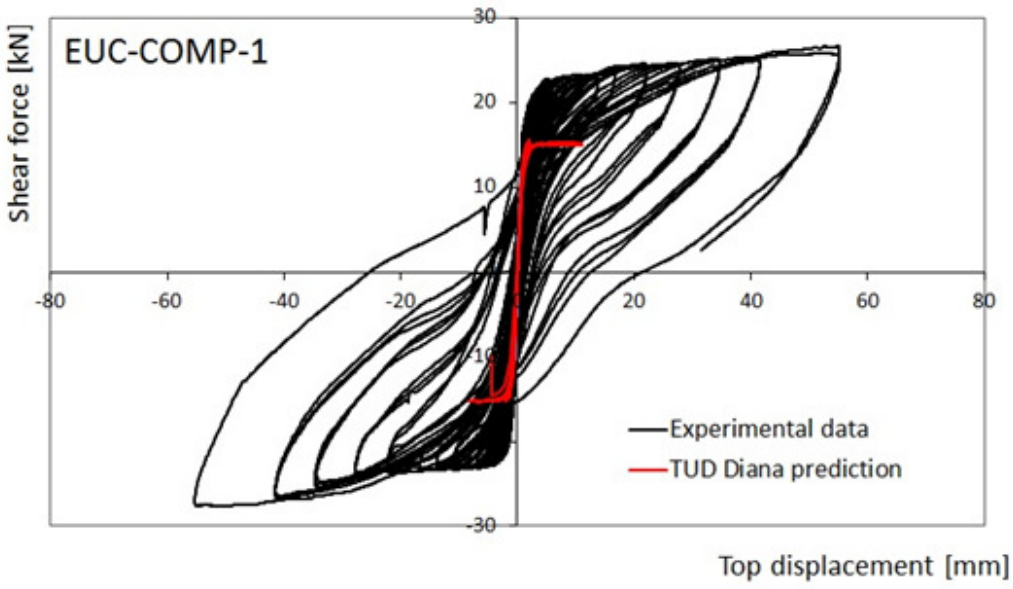

Figure 82: EUC-COMP-1: DIANA blind prediction – Shear force-displacement curve

Table 24: EUC-COMP-1: DIANA blind prediction – Summary table

	Predominant Failure Mechanism Predicted	**Initial Stiffness [kN/mm]**	**Peak Strength [kN]**	**Maximum Achieved Drift**	
DIANA	Rocking / diagonal crack	16 [1]	15.6 [1,2]	0.4% [2]	[2]
Test Result	Rocking / diagonal cracks / toe crushing	22.9	28	2%	Near collapse

1. DIANA analysis performed under 0.4 MPa overburden stress as specified in the protocol

2. Model not pushed up to 2% drift due to failure to converge

2.1.9 EUC-COMP-2

2.1.9.1 Test Description

EUC-COMP-2 was one of the three quasi-static in-plane tests administered by EUCENTRE Blind Prediction. This specimen was a single-wythe wall constructed of calcium silicate units 102 mm thick. It was 1.1 m long and 2.75 m high. The originally planned overburden stress was 0.6 MPa.

Initially, specimen EUC-COMP-2 exhibited a pure rocking behaviour with cracks opening at the edges upon cyclically loading the specimen. No other damage was observed in the masonry panel.

The top restraint condition did not behave in the expected fixed-fixed manner and began to rotate out of plane after 0.15% drift. The test was therefore stopped early (at 0.22% drift) due to out-of-plane wall failure.

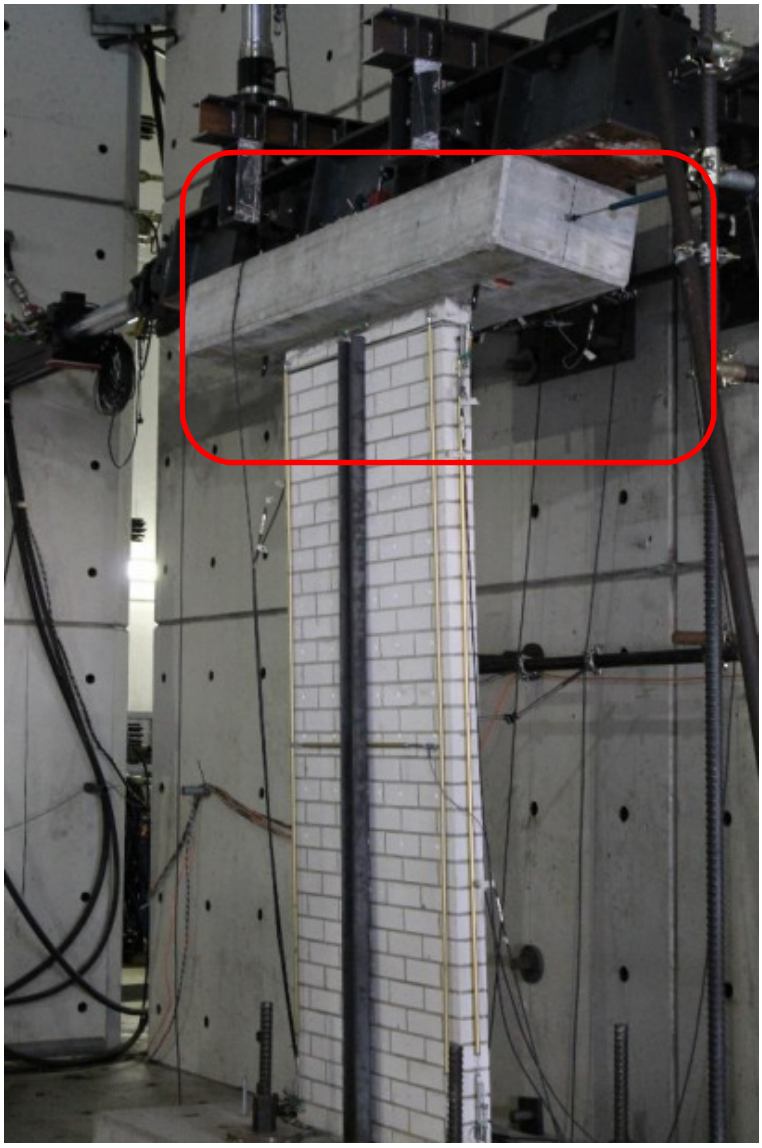

Figure 83: EUC-COMP-2: Out of plane failure mechanism at 0.25% drift

The actual test loading regime of EUC-COMP-2 matched the one specified in the planned protocol. However, the actual overburden applied during the test was 0.7 MPa rather than 0.6 MPa. This was noted in the post-test refined predictions provided by all three consultants.

As previously mentioned, the boundary conditions of the wall specimen provided by the test set-up did not match the specified boundary conditions. According to the protocol, out-of-plane rotational restraint was provided by the test set-up. However, the loading beam at the top of the wall was free to rotate during the test, which led to the observed out-of-plane failure.

See Figure 84 below for the shear force-displacement plot of the lab test result of EUC-COMP-2 up to the point that the test was stopped.

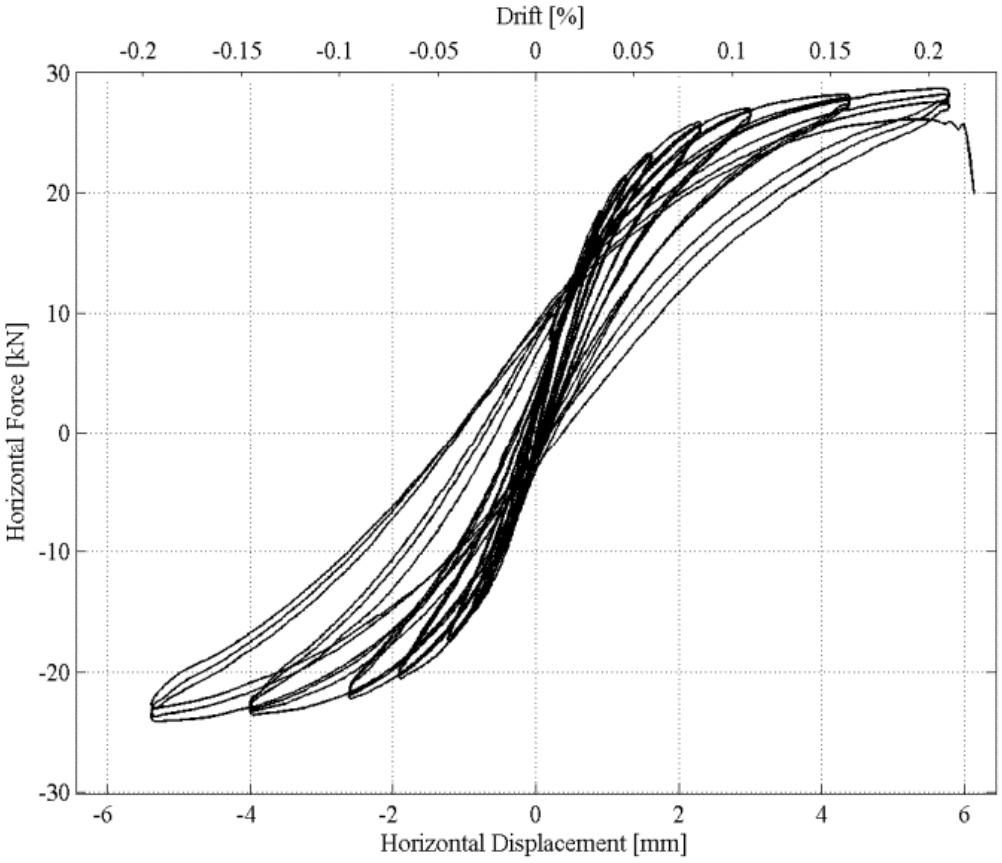

Figure 84: EUC-COMP-2: Lab test result – Shear force-displacement curve

2.1.9.2 Arup Blind Prediction

The LS-DYNA model of EUC-COMP-2 predicted rocking behaviour and associated tensile bed joint failures at the top and bottom of the specimen, as shown in Figure 85.

The lateral-force-versus-displacement relationship followed an S-shaped curve, as shown in Figure 86. The predicted ultimate load was approximately 22 kN at a drift of 2%. The lab test resulted in an ultimate load of 27 kN. As previously mentioned, the actual overburden applied during the test was 0.7 MPa rather than 0.6 MPa. This was noted in the post-test refined prediction. The predicted initial stiffness was approximately 14 kN/mm.

As illustrated by the hysteresis curve, there was little energy dissipated by the LS-DYNA model of the specimen.

The LS-DYNA model captured the rocking mechanism generated during the laboratory test up to the point of the out-of-plane failure. The lateral strength of the LS-DYNA model of the specimen did not match the lab results because the model assumed the overburden that was specified in the protocol (0.6 MPa) while the actual applied overburden applied during the test was 0.7 MPa.

The LS-DYNA model under-predicted the amount of energy dissipation during the test. It was unclear why a larger amount of energy was dissipated during the test. Due to the premature termination of the test, no conclusions can be drawn about the prediction of in-plane damage or collapse.

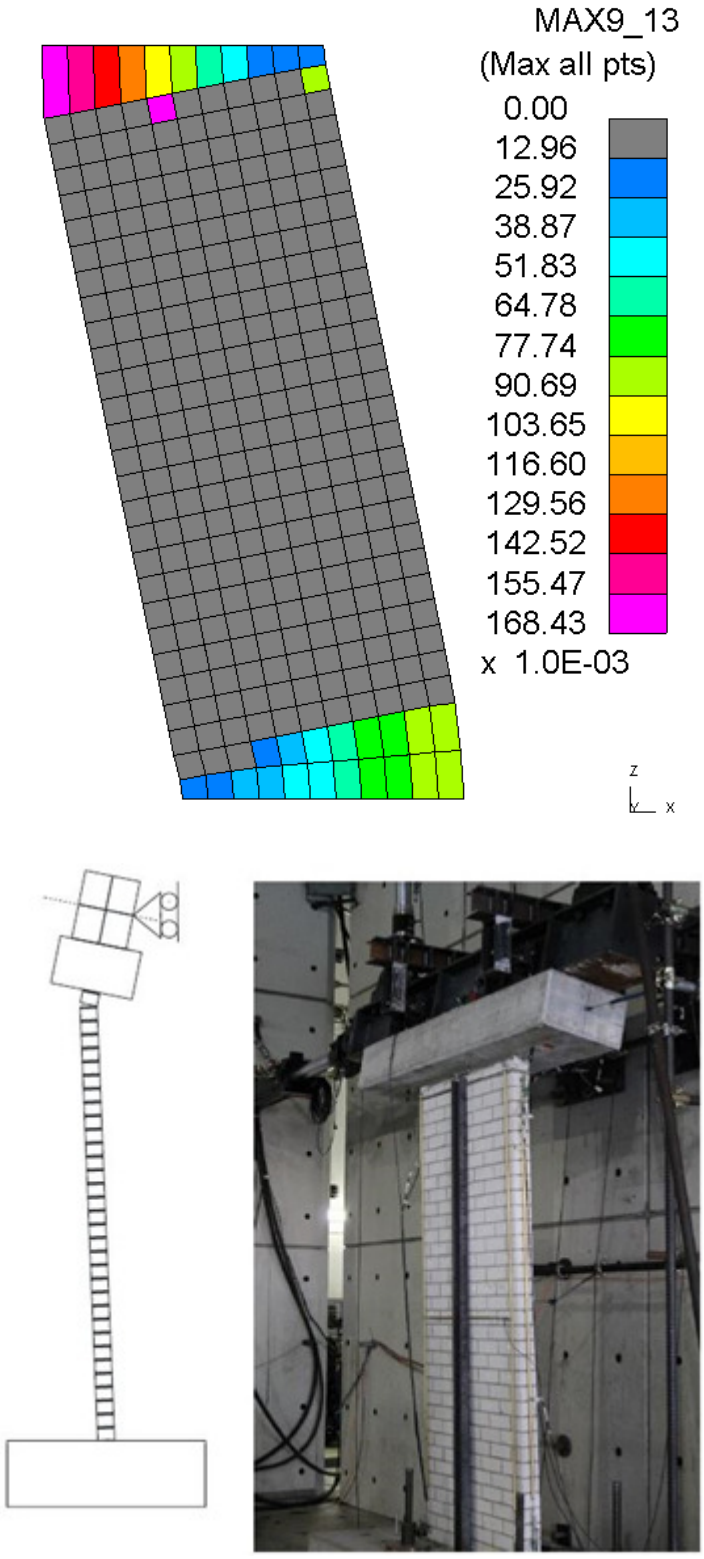

Figure 85: EUC-COMP-2: LS-DYNA blind prediction - Damage plot at end of analysis

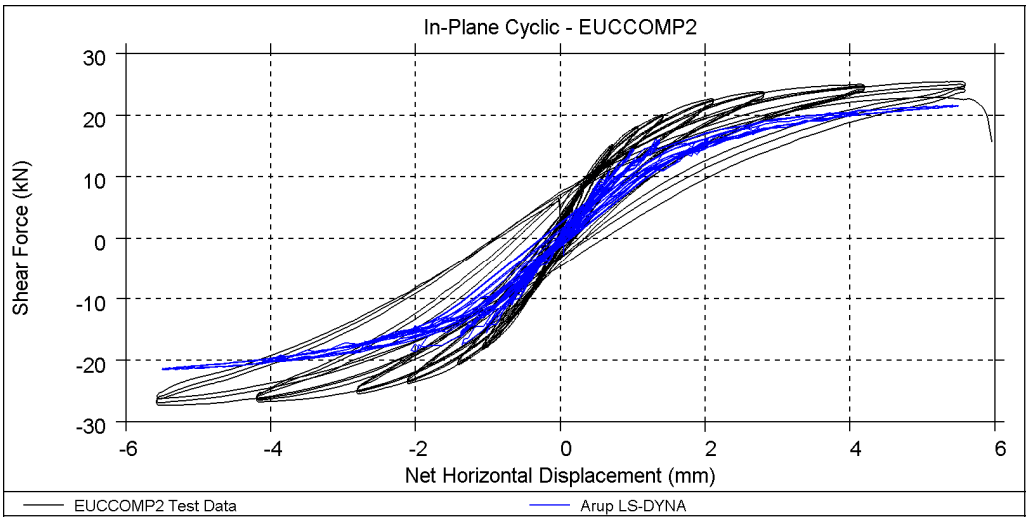

Figure 86: EUC-COMP-2: LS-DYNA blind prediction - Shear force-displacement curve

Table 25: EUC-COMP-2: LS-DYNA blind prediction - Summary table

	Predominant Failure Mechanism Predicted	**Initial Stiffness [kN/mm]**	**Peak Strength [kN]**	**Maximum Achieved Drift**	
LS-DYNA	Rocking	14 (*)	22 (*)	2%	End of protocol
Test Result	Out-of-plane instability	24	27	0.22%	Premature out-of-plane failure

(*) LS-DYNA analysis performed under 0.6 MPa overburden stress as specified in the protocol

2.1.9.3 EUCENTRE Blind Prediction

The TREMURI macro-element model (see Figure 87) predicted a rocking dominated behaviour with some toe-crushing and the resulting hysteresis curve (Figure 88) followed a classical S-shape curve with moderate energy dissipation (Figure 89). A flexure-dominated response was also observed in the test.

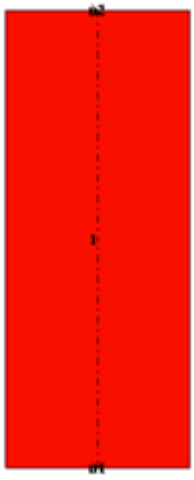

Figure 87: EUC-COMP-2: TREMURI blind prediction model

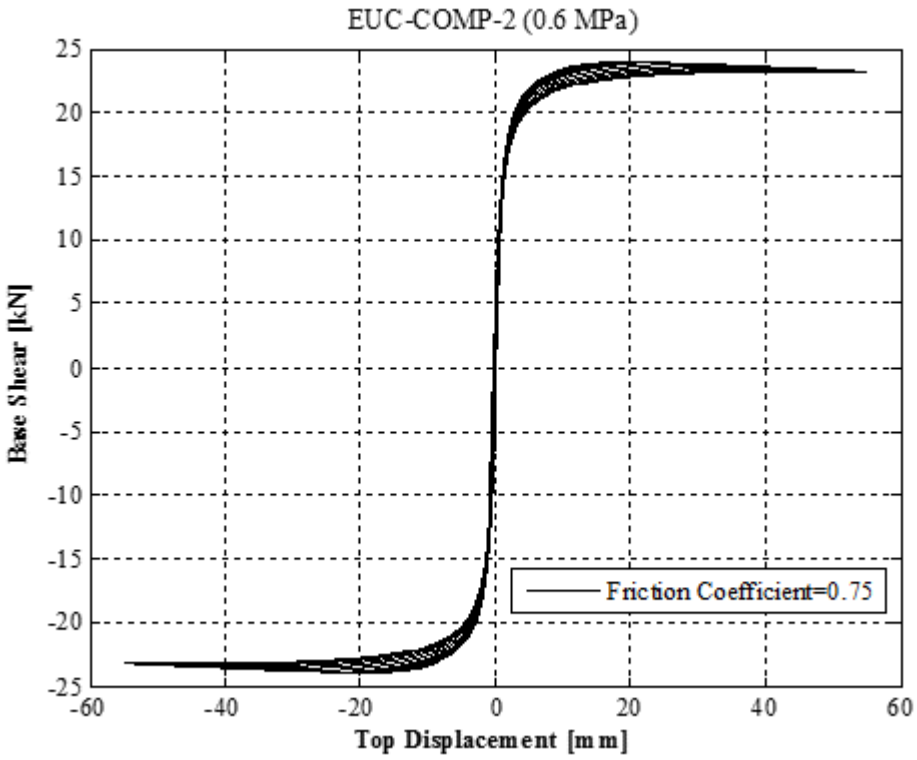

Figure 88: EUC-COMP-2: TREMURI blind prediction - Shear force-displacement curve

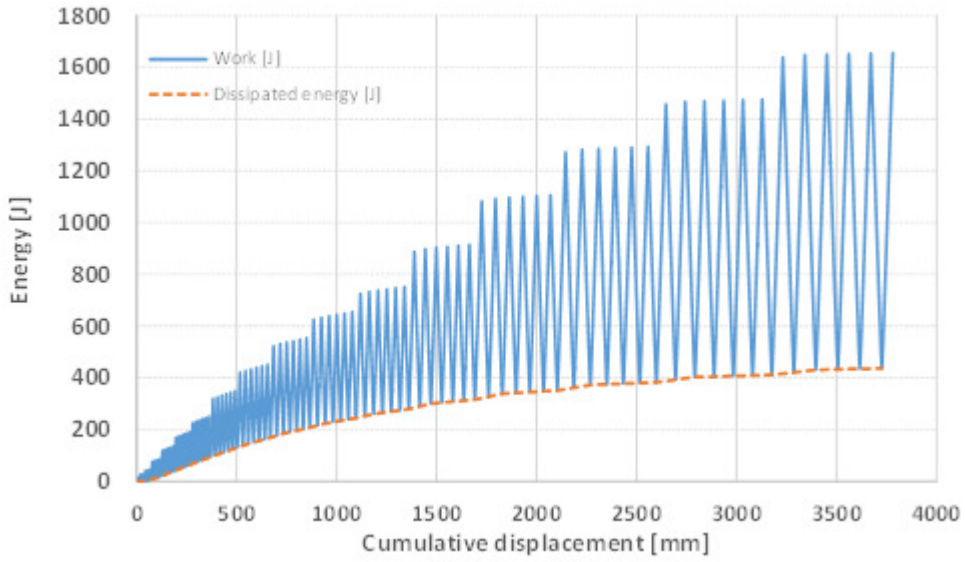

Figure 89: EUC-COMP-2: TREMURI blind prediction - Work & energy dissipation

Table 26: EUC-COMP-2: TREMURI blind prediction - Summary table

	Predominant Failure Mechanism Predicted	**Initial Stiffness [kN/mm]**	**Peak Strength [kN]**	**Maximum Achieved Drift**	
TREMURI	Rocking w/ toe crushing	15.3 (*)	23.9 (*)	2%	End of protocol
Test Result	Out-of-plane instability	24	27	0.22%	Premature out-of-plane failure

(*) TREMURI analysis performed under 0.6 MPa overburden stress as specified in the protocol

2.1.9.4 TU-Delft Blind Prediction

In the DIANA model, the failure of the panel occurred with a predominant rocking behaviour as observed in the experiment, followed by the propagation of a main crack from the lower-right corner toward the middle of the panel. The numerical base shear capacity was around 23 kN with a maximum top displacement of 11 mm. The lab test resulted in an ultimate load of 27 kN. As previously mentioned, the actual overburden applied during the test was 0.7 MPa rather than 0.6 MPa. This was noted in the post-test refined prediction.

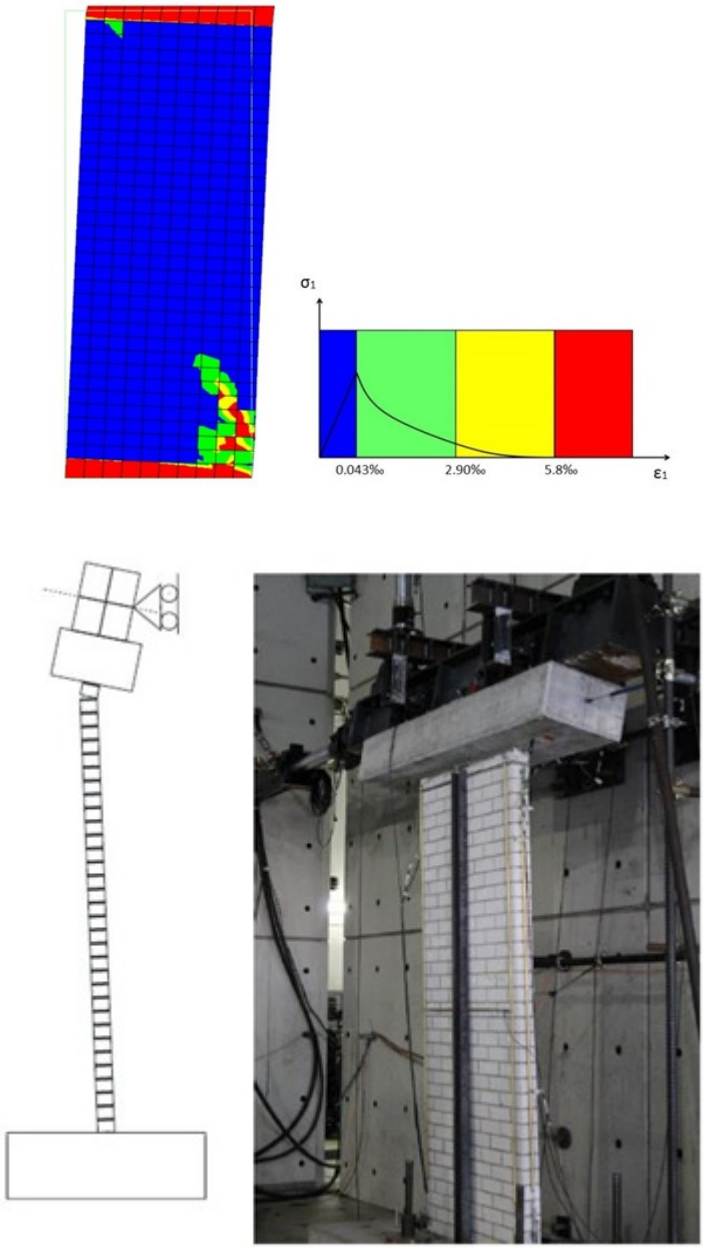

Figure 90: EUC-COMP-2: DIANA blind prediction - Damage plot at end of analysis

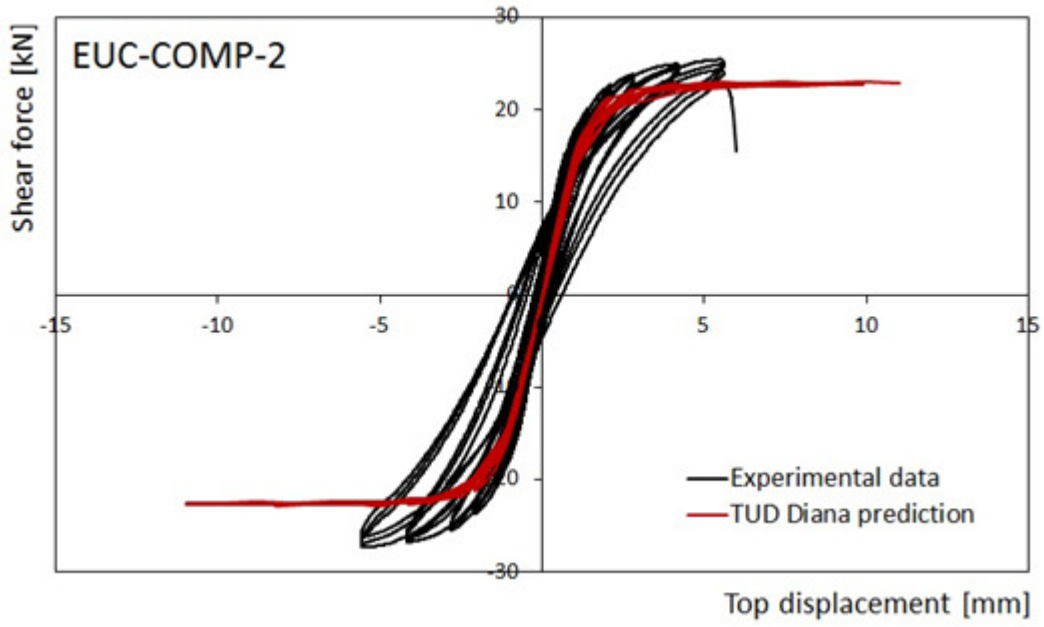

Figure 91: EUC-COMP-2: DIANA blind prediction - Shear force-displacement curve

Table 27: EUC-COMP-2: DIANA blind prediction - Summary table

	Predominant Failure Mechanism Predicted	**Initial Stiffness [kN/mm]**	**Peak Strength [kN]**	**Maximum Achieved Drift**	
DIANA	Rocking	16 [1]	23 [1,2]	0.4% [2]	[2]
Test Result	Out-of-plane instability	24	27	0.22%	Premature out-of-plane failure

1. DIANA analysis performed under 0.6 MPa overburden stress as specified in the protocol

2. Model not pushed up to 2% drift due to failure to converge

2.1.10 EUC-COMP-3

2.1.10.1 Test Description

EUC-COMP-3 was one of the three quasi-static in-plane tests administered by EUCENTRE. This specimen was a single-wythe wall constructed of calcium silicate units 102 mm thick. It was 4 m long and 2.75 m high. The originally planned overburden stress was 0.2 MPa. The wall was tested under cantilever boundary conditions.

As expected, specimen EUC-COMP-3 exhibited shear behaviour with diagonally oriented cracks. The first cracks appeared after 0.05% drift. These cracks progressively increased during the duration of the test. The test was stopped at a net drift of 0.3% due to partial collapse of the left side of the specimen.

0.05% drift

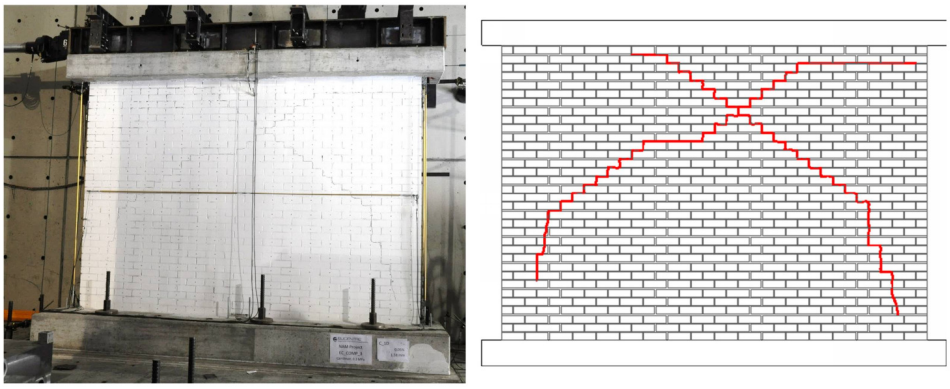

0.075% drift

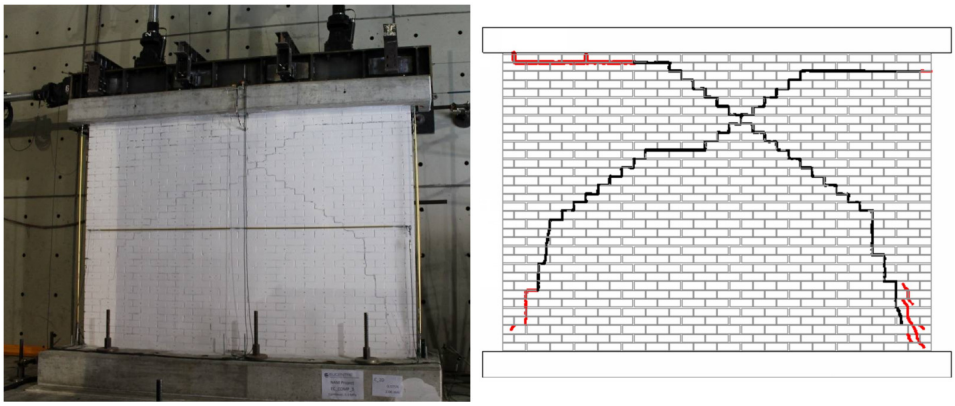

0.15% drift

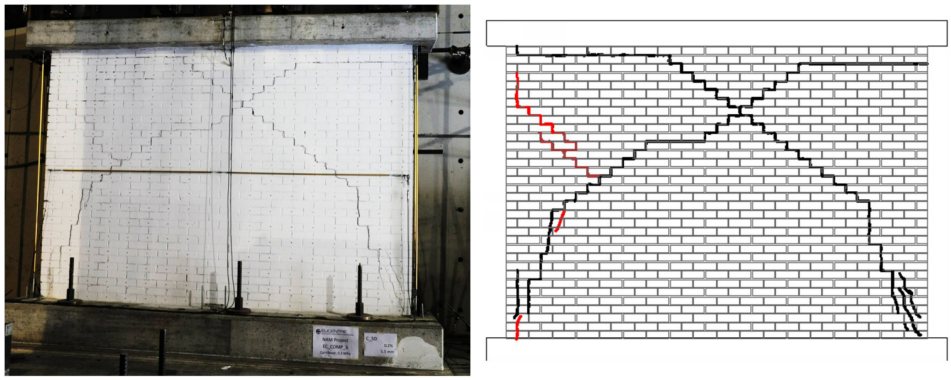

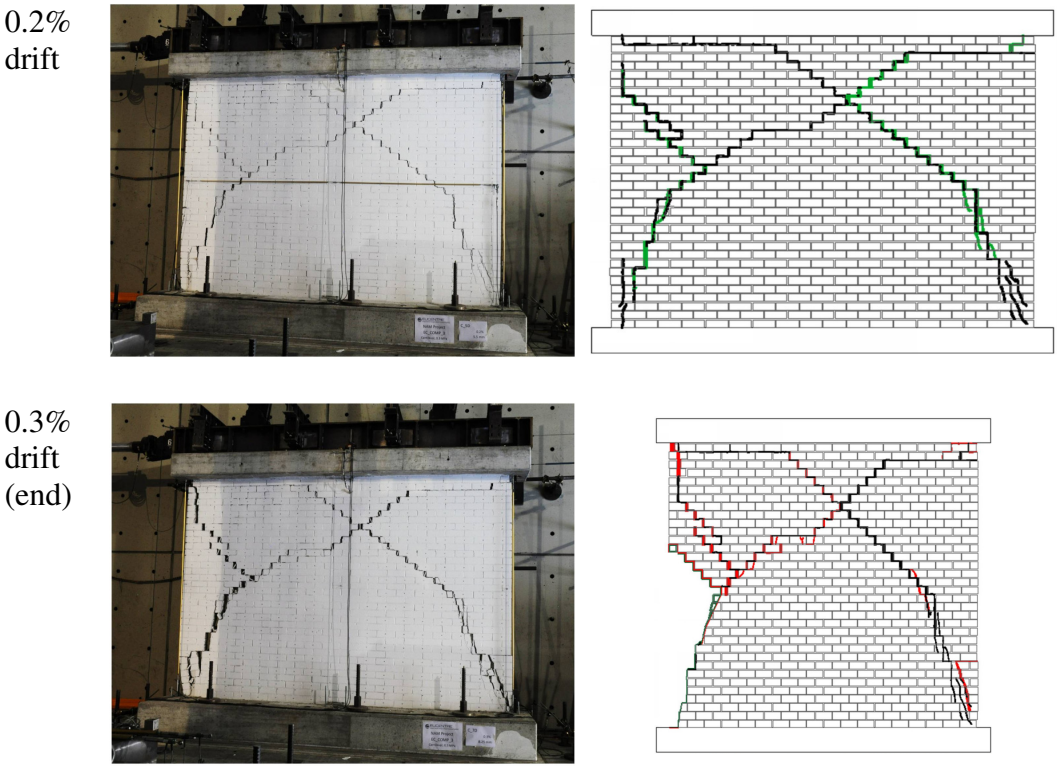

Figure 92: EUC-COMP-3: Progression of damage

The actual test loading regime of EUC-COMP-3 matched the one specified in the planned protocol. However, the actual overburden applied during the test was 0.3 MPa rather than 0.2 MPa. This was noted in the post-test refined predictions provided by all three consultants.

See Figure 93 below for the shear force-displacement plot of the lab test result of EUC-COMP-3.

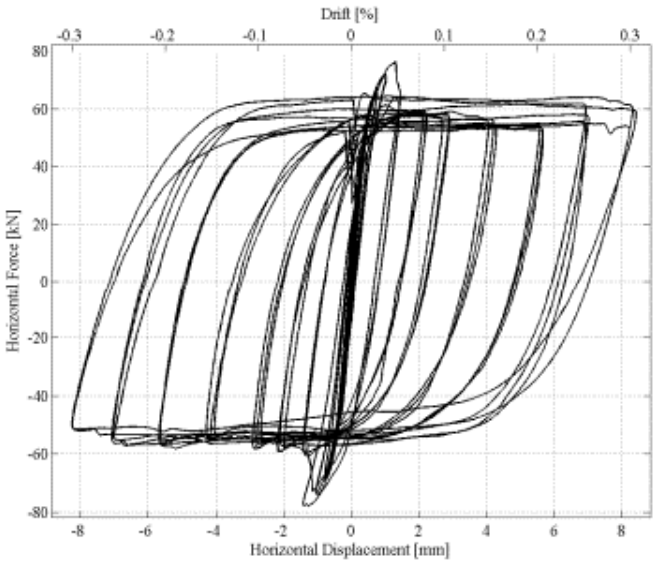

Figure 93: EUC-COMP-3: Lab test result – Shear force-displacement curve

2.1.10.2 Arup Blind Prediction

The LS-DYNA model of EUC-COMP-3 predicted failure due to bed joint sliding.

The lateral-force-versus-displacement relationship initially followed rocking behaviour but almost immediately transitioned to shear sliding behaviour as shown in Figure 94. The predicted ultimate load associated with bed-joint sliding was approximately 60 kN. As previously mentioned, the actual overburden applied during the test was 0.3 MPa rather than 0.2 MPa. This was noted in the post-test refined prediction. The predicted initial stiffness was approximately 160 kN/mm.

The LS-DYNA model captured shear-governing behaviour and backbone curve generated during the laboratory test but did not capture the correct shear mechanism with associated diagonal crack pattern. The model did not predict collapse or a near-collapse state.

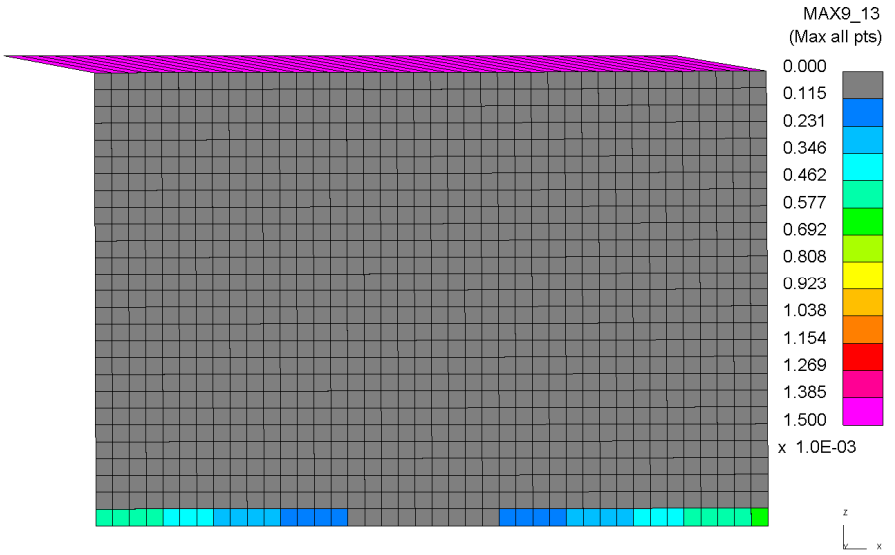

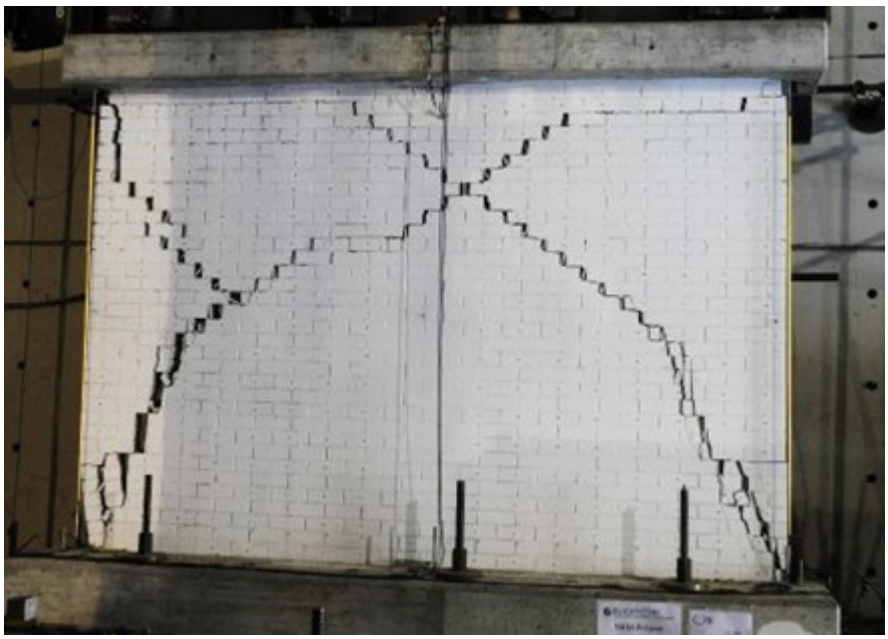

Figure 94: EUC-COMP-3: LS-DYNA blind prediction - Damage plot at end of analysis

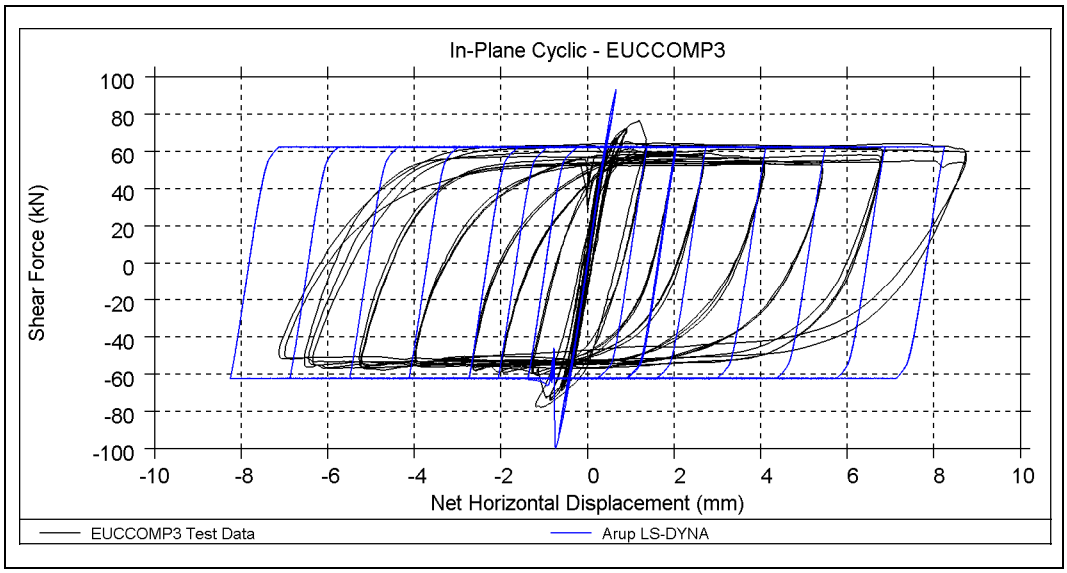

Figure 95: EUC-COMP-3: LS-DYNA blind prediction - Shear force-displacement curve

Table 28: EUC-COMP-3: LS-DYNA blind prediction - Summary table

	Predominant Failure Mechanism Predicted	**Initial Stiffness [kN/mm]**	**Peak Strength [kN]**	**Maximum Achieved Drift**	
LS-DYNA	Bed joint sliding	160 (*)	60 (*)	2%	End of protocol
Test Result	Diagonal cracks / toe crushing	152	78	0.3%	Near collapse

(*) LS-DYNA analysis performed under 0.2 MPa overburden stress as specified in the protocol

2.1.10.3 EUCENTRE Blind Prediction

Three blind predictions associated to three sets of mechanical parameters were conducted. At these stage, the first mechanical characterization test on CaSi masonry were conducted. It was noticed that the strength parameters were lower than the ones proposed (in particular $c \approx 0.2$MPa and $\mu \approx 0.45$). This resulted in three different hysteretic behaviours. The picture (Figure 97) shows all of them while Table 30 reports only the one performed with the updated material parameters (red in the Figure 97).

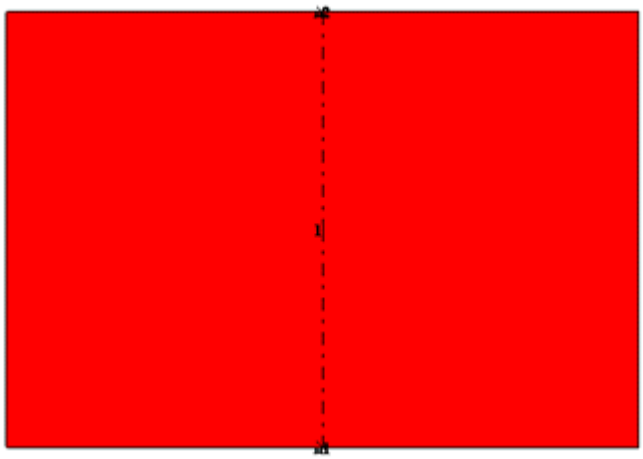

Figure 96: EUC-COMP-3: TREMURI blind prediction model

Table 29: Sensitivity analysis: Variation of friction and cohesion coefficient

μ	c [MPa]	
0.75	0.3	From blind prediction
0.5	0.3	Intermediate values
0.45	0.2	From material characterisation tests

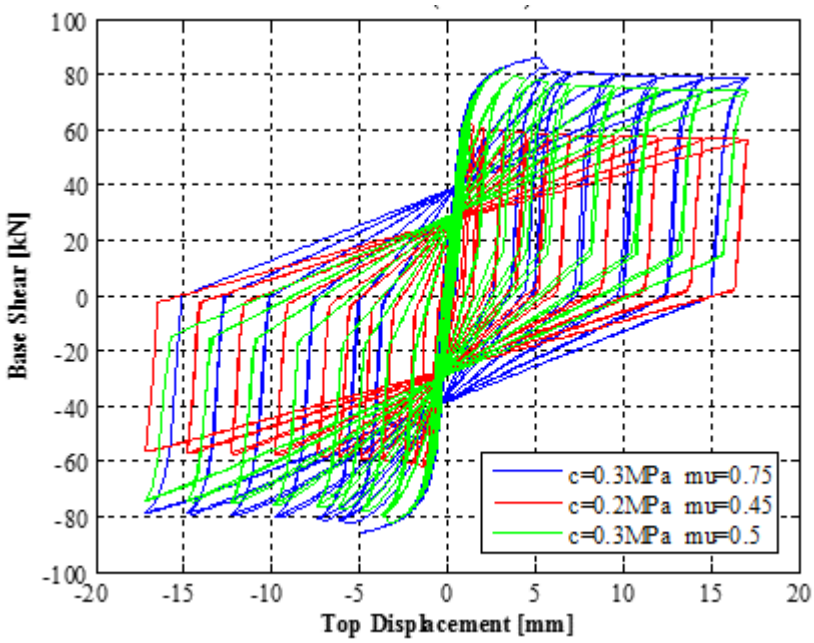

Figure 97: EUC-COMP-3: TREMURI blind prediction - Shear force-displacement curve

Table 30: EUC-COMP-3: TREMURI blind prediction - Summary table

	Predominant Failure Mechanism Predicted	**Initial Stiffness [kN/mm]**	**Peak Strength [kN]**	**Maximum Achieved Drift**	
TREMURI (w/ data from prev. charact. test)	Shear	103	63	0.62%	
Test Result	Diagonal cracks / toe crushing	152	78	0.3%	Near collapse

2.1.10.4 TU-Delft Blind Prediction

The DIANA finite element model of EUC-COMP-3 predicted a rocking behaviour follower by the formation of a wide crack through the panel, developing from the bottom left corner. Also some minor cracking in the middle of the top boundary is observed.

The numerical base shear capacity resulted equal to 76.3 kN with a maximum top displacement equal to 5.5 mm. Very little energy dissipation was detected in the analysis compared to the experiment.

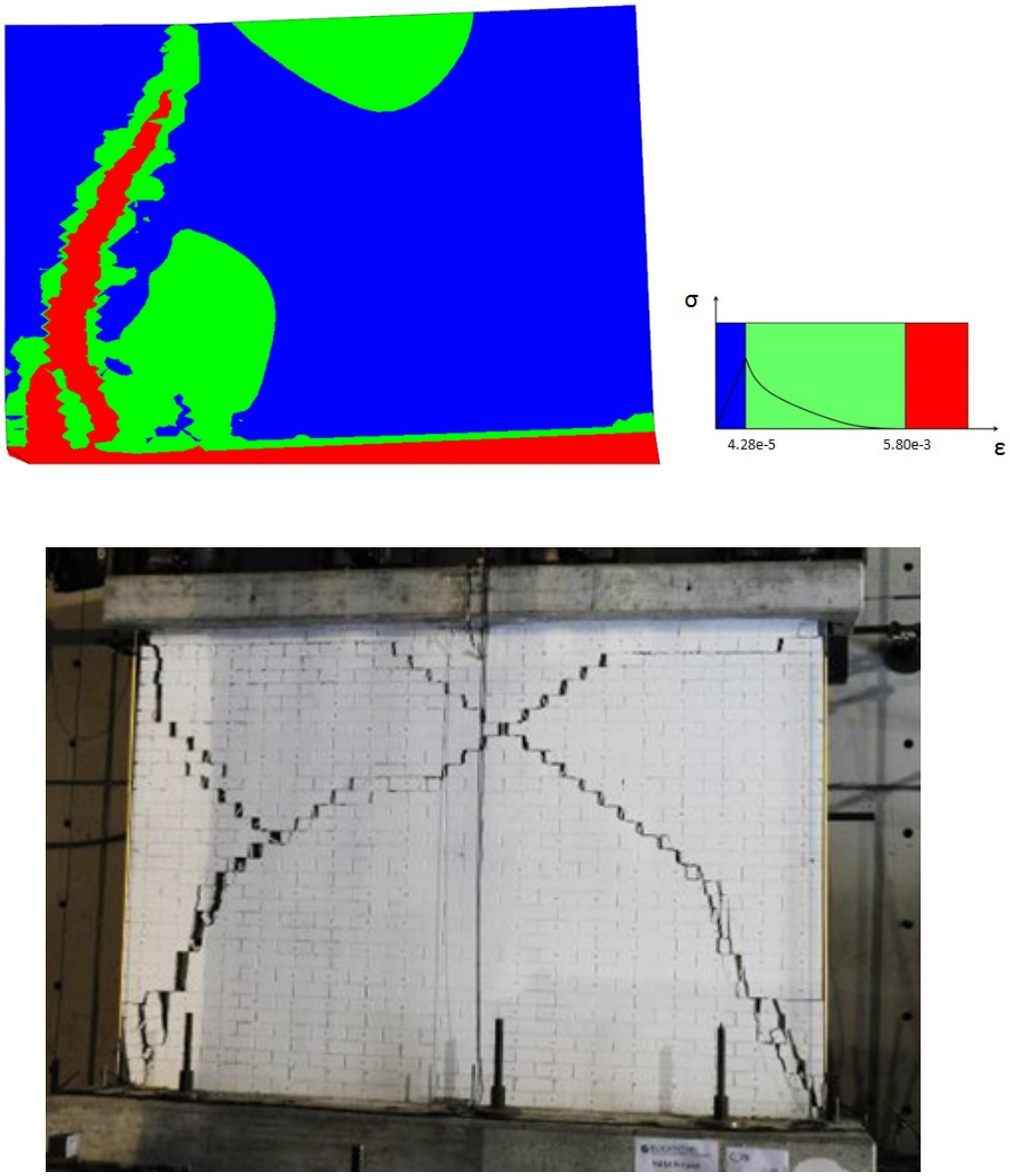

Figure 98: EUC-COMP-3: DIANA blind prediction - Damage plot at end of analysis

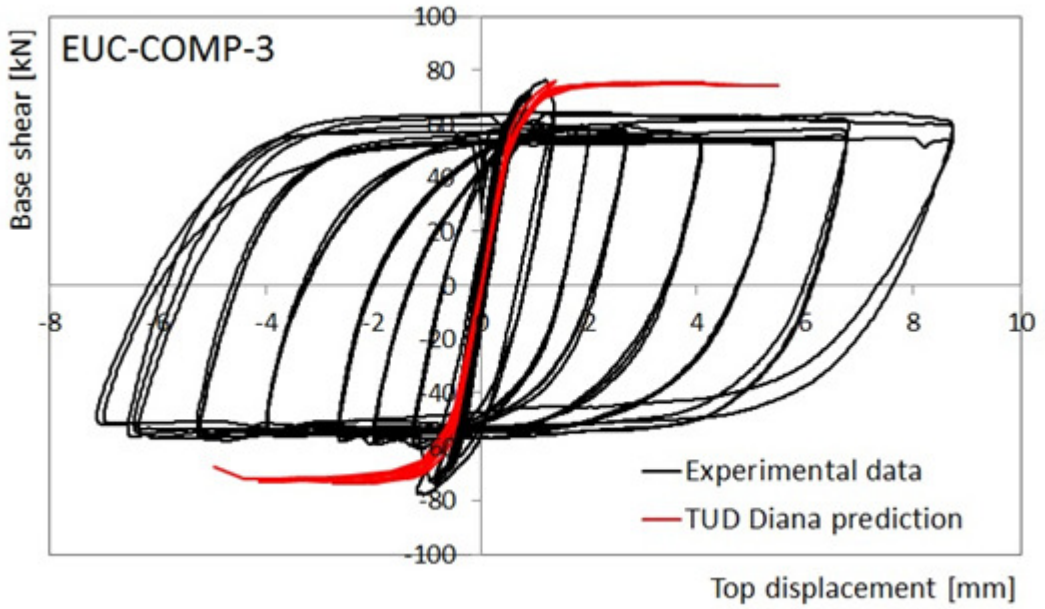

Figure 99: EUC-COMP-3: DIANA blind prediction - Shear force-displacement curve

Table 31: EUC-COMP-3: DIANA blind prediction - Summary table

	Predominant Failure Mechanism Predicted	**Initial Stiffness [kN/mm]**	**Peak Strength [kN]**	**Maximum Achieved Drift**	
DIANA	Rocking / Diagonal crack	113	76	0.2% (*)	(*)
Test Result	Diagonal cracks / toe crushing	152	78	0.3%	Near collapse

(*) Model not pushed up to 2% drift due to failure to converge

2.1.11 Summary

The blind prediction comparisons are of limited value for several of the tests, because the overburden and other conditions under which the test was performed differed from those assumed in the blind prediction analysis. Nevertheless, the results are summarised in Table 32 below.

Table 32: LS-DYNA blind prediction results summary

Component	LS-DYNA			TREMURI			DIANA (*)			Test Result		
	Failure Mechanism	Peak Strength [kN]	Max Achieved Drift (End of protocol) [%]	Failure Mechanism	Peak Strength [kN]	Max Achieved Drift [%]	Failure Mechanism	Peak Strength [kN]	Max Achieved Drift [%]	Failure Mechanism	Peak Strength [kN]	Max Achieved Drift (near collapse) [%]
TUD-COMP-0a	Rocking	28	0.9	Rocking	27	0.9	Rocking	27	0.5	Rocking / toe crushing	30	0.9
TUD-COMP-1	Rocking	11	0.9	Rocking	10	0.9	Rocking	10	0.15	Rocking / toe crushing	9.5	1.6
TUD-COMP-2	Rocking	14	0.9	Rocking	13	0.9	Rocking	13	0.25	Rocking / toe crushing	10	0.9
TUD-COMP-3	Rocking / toe crushing	14 (0.3MPa overburden)	1.8	Rocking	13 (0.3MPa overburden)	0.9	Rocking	14 (0.3MPa overburden)	0.25	Rocking / toe crushing	15 (0.4 MPa overburden)	1.3
TUD-COMP-4	Diagonal cracks / bed joint sliding	104	0.2	Shear	114	0.62	Diagonal cracks	135	0.08	Diagonal cracks / toe crushing	119	0.2
TUD-COMP-5	Diagonal cracks / bed joint sliding	76	0.2	Shear	111 (0.6MPa overburden)	0.62	Diagonal cracks	109	0.1	Diagonal cracks / toe crushing	103 (0.3MPa overburden)	0.5 (stopped due to instability

Table 32 (continued): LS-DYNA blind prediction results summary

Component	LS-DYNA			TREMURI			DIANA (*)			Test Result		
	Failure Mechanism	**Peak Strength [kN]**	**Max Achieved Drift (End of protocol) [%]**	**Failure Mechanism**	**Peak Strength [kN]**	**Max Achieved Drift [%]**	**Failure Mechanism**	**Peak Strength [kN]**	**Max Achieved Drift [%]**	**Failure Mechanism**	**Peak Strength [kN]**	**Max Achieved Drift (near collapse) [%]**
TUD-COMP-6	Diagonal cracks / bed joint sliding	76 (0.3MPa overburden)	0.2	Shear	81 (0.4MPa overburden)	0.62	Diagonal cracks	115	0.084	Diagonal cracks / toe crushing	110 (0.5MPa overburden)	0.6
EUC-COMP-1	Rocking	17 (0.4MPa overburden)	2	Rocking	17 (0.4MPa overburden)	2	Rocking / Diagonal cracks	16 (0.4MPa overburden)	0.4	Rocking behaviour / toe crushing	28 (0.52MPa overburden)	2
EUC-COMP-2	Rocking	22 (0.6MPa overburden)	2	Rocking	24 (0.6MPa overburden)	2	Diagonal cracks	23 (0.6MPa overburden)	0.4	Out of plane instability	27 (0.7MPa overburden)	0.2 (stopped due to instability
EUC-COMP-3	Bed joint sliding	60 (0.2MPa overburden)	2	Shear	63	0.62	Rocking / Diagonal cracks	76	0.2	Diagonal cracks / toe crushing	78 (0.3MPa overburden)	0.3

(*) All models failed to converge

3 Out-of-Plane Component Tests: Blind Predictions

3.1 Comparison of Blind Predictions

3.1.1 TUD-COMP-0b

This test was stopped due to instability of the test system. It was repeated as TUD-COMP-7 with all the same boundary conditions. Therefore, analyses of TUD-COMP-0b are not reported.

3.1.2 TUD-COMP-7

3.1.2.1 Test Description

TUD-COMP-7 was the second quasi-static one-way out-of-plane tests administered by TU-Delft. This specimen was a single-wythe wall constructed of calcium silicate units 102 mm thick. It was 1.4 metres long and 2.75 metres high. The applied overburden stress was 0.2MPa. The wall was tested under double clamped boundary conditions.

Loading was provided by airbags on either side of the specimen. The pressure in the airbags was controlled to provide the required displacement. The lateral load was measured via load cells attached to the reaction frame. See Figure 100 for a schematic of the test set-up.

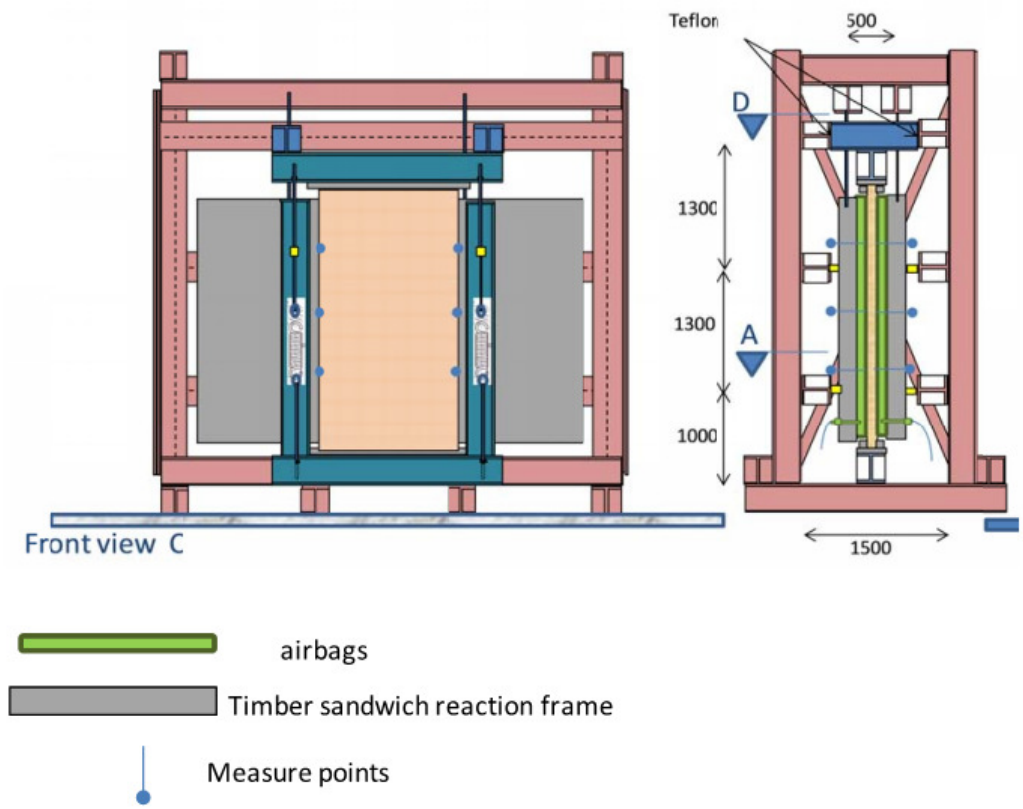

Figure 100: TUD-COMP-7: Schematic of test set-up

Figure 101: TUD-COMP-7: Final deflected shape of the (top) and cracks at top and bottom supports (bottom).

The measured hysteresis is shown in Figure 102.

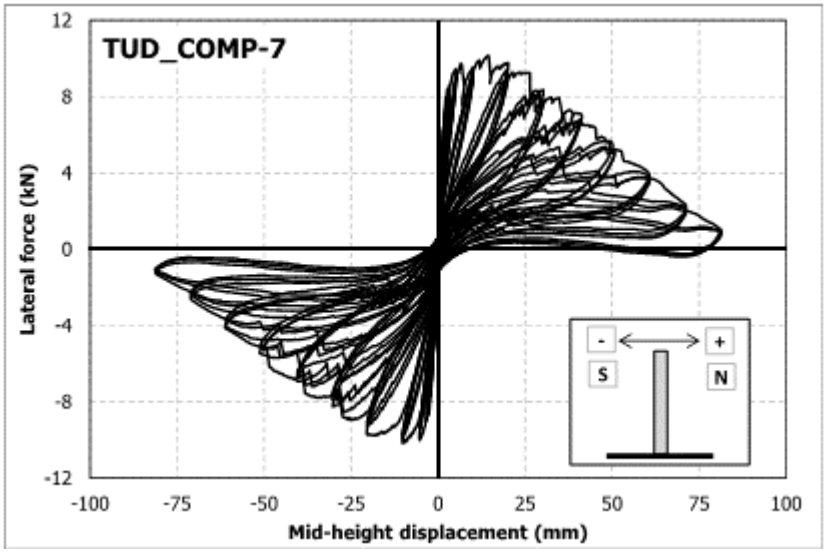

Figure 102: TUD-COMP-7: Lab test result – Applied force-mid-height displacement curve

3.1.2.2 Arup Blind Prediction

The analysis results predicted an out-of-plane rocking mechanism, which consisted of damage forming at the bed joints at the top and bottom of the wall as well as mid-height.

The predicted ultimate load before the formation of the out-of-plane mechanism was approximately 11 kN. The predicted initial stiffness was approximately 13 kN/mm. Upon the formation of the out-of-plane rigid-body rotation mechanism, the predicted stiffness reduced to approximately 5.6 kN/mm. The model did not reach global instability during the applied load protocol, which pushed the wall to a maximum displacement of 80 mm.

The hysteresis curve from the analysis follows the form of the theoretical curve for out-of-plane rigid body rocking, with lateral resistance being near-identical for all cycles and negligible energy absorbed in hysteresis. The test result, meanwhile, indicates a lateral resistance that reduces with larger cycles and relatively large amounts of energy absorbed in hysteresis. Crushing of the mortar at the outer surfaces may explain the reduction of lateral resistance, i.e. the rectangular cross-section shape becomes more rounded. Further study is needed to understand the mechanism by which the energy absorption occurs.

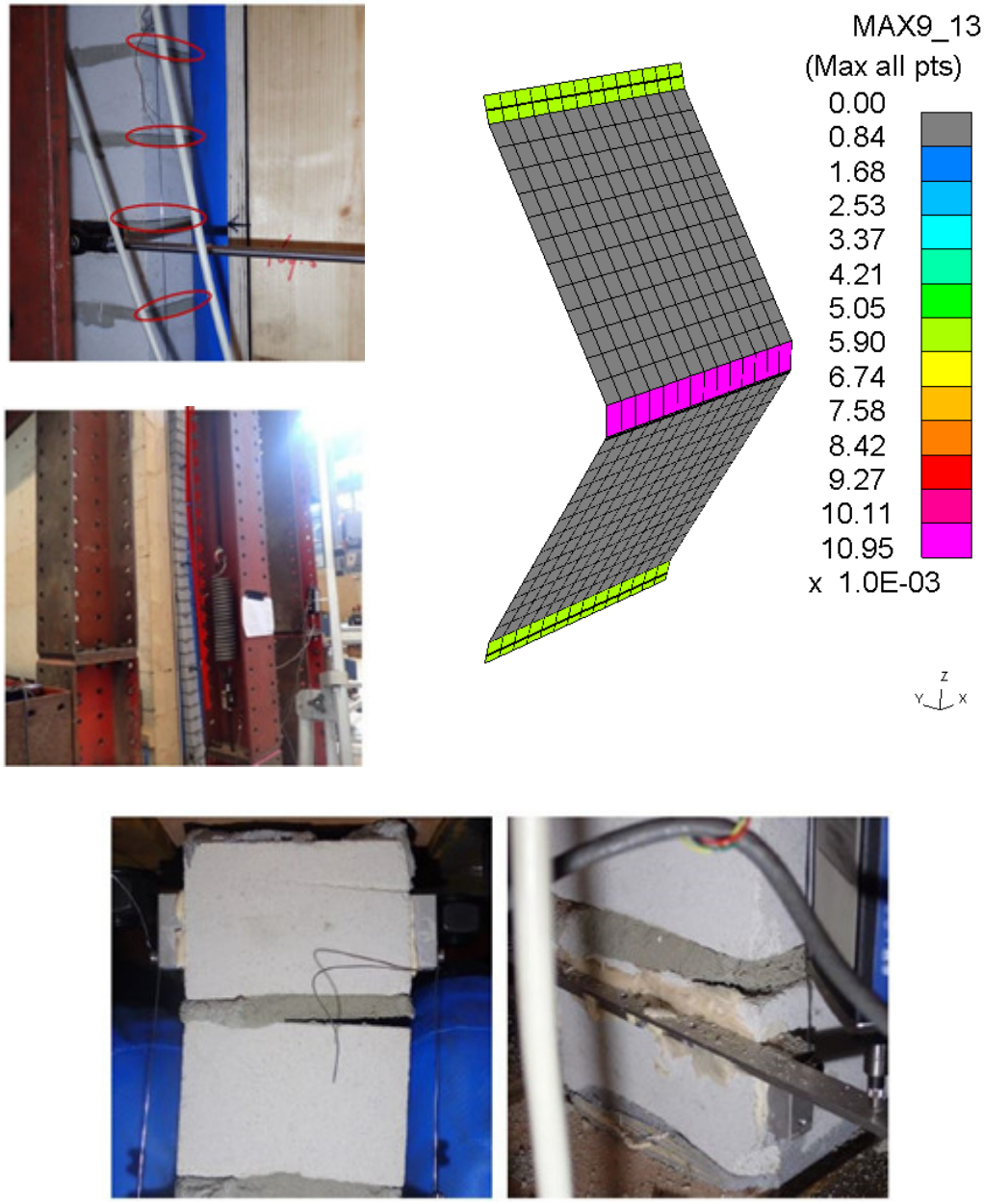

Figure 103: TUD-COMP-7: LS-DYNA blind prediction - Damage plot at end of analysis

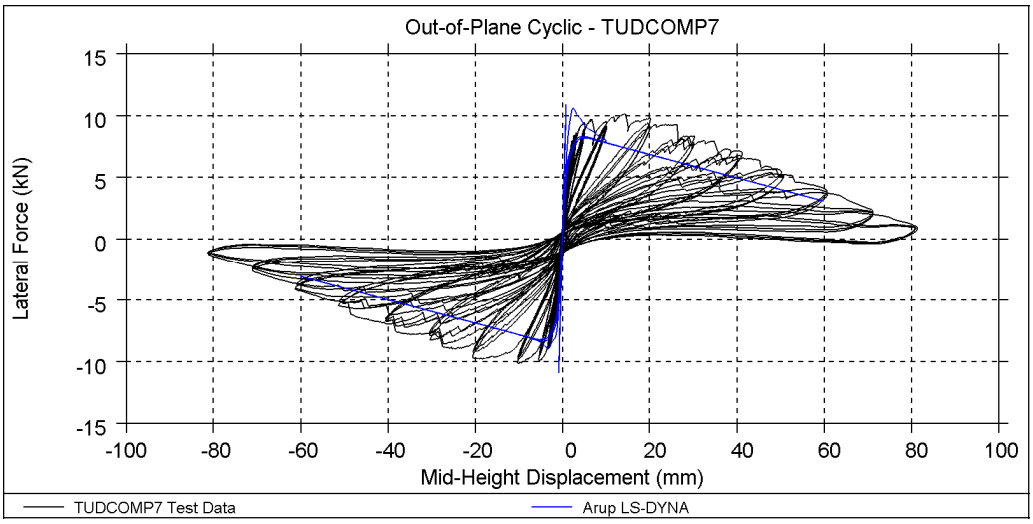

Figure 104: TUD-COMP-7: LS-DYNA blind prediction - Shear force-displacement curve

Table 33: TUD-COMP-7: LS-DYNA blind prediction - Summary table

	Predominant Failure Mechanism Predicted	**Initial Stiffness [kN/mm]**	**Peak Strength [kN]**	**Maximum Achieved Mid-Span Displacement [mm]**	
LS-DYNA	One-way out-of-plane failure	13	11	80	End of protocol
Test Result	One-way out-of-plane failure	4.5	10	80	End of protocol

3.1.2.3 EUCENTRE Blind Prediction

The hysteresis curve from the analysis is close to the shape of the theoretical curve for out-of-plane rigid body rocking, with negligible energy dissipated in hysteresis.

Figure 105: TUD-COMP-7: TREMURI model

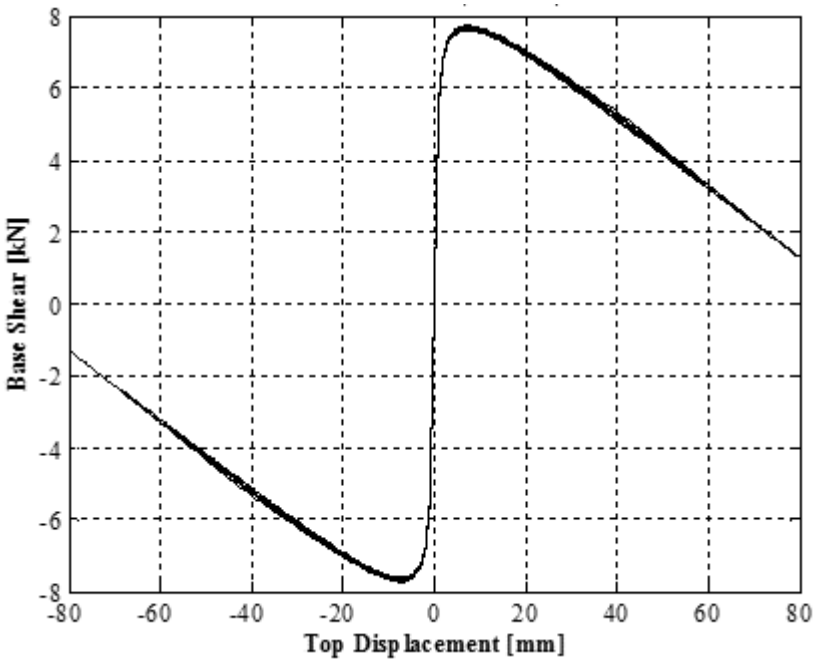

Figure 106: TUD-COMP-7: TREMURI blind prediction - Shear force-displacement curve

Table 34: TUD-COMP-7: TREMURI blind prediction - Summary table

	Predominant Failure Mechanism Predicted	**Initial Stiffness [kN/mm]**	**Peak Strength [kN]**	**Maximum Achieved Mid-Span Displacement [mm]**	
TREMURI	One-way out-of-plane failure	4.3	7.7	80	End of protocol
Test Result	One-way out-of-plane failure	4.5	10	80	End of protocol

3.1.2.4 TU-Delft Blind Prediction

TU-Delft did not perform a blind prediction of specimen TUD-COMP-7.

3.1.3 TUD-COMP-10

3.1.3.1 Test Description

TUD-COMP-10 was the fourth quasi-static out-of-plane test administered by TU-Delft. It was the second two-way out-of-plane test, in which rotation was fully fixed at the top and bottom but the wall was free to rotate in the out-of-plane direction along the vertical edges. The specimen was clamped at the bottom and top supports by gluing the top and bottom row of bricks to a plywood layer fixed to the top and bottom beam. The specimens were pinned on the vertical sides. This specimen was a single-wythe wall constructed of clay units 100 mm thick. It was approximately 4 metres long and 2.7 metres high. The top support to the specimen together with an applied vertical load give a uniform vertical overburden of 50 kPa.

Loading was provided by airbags on either side of the specimen. The pressure in the airbags was controlled to provide the required displacement. See Figure 107 for a schematic of the test set-up.

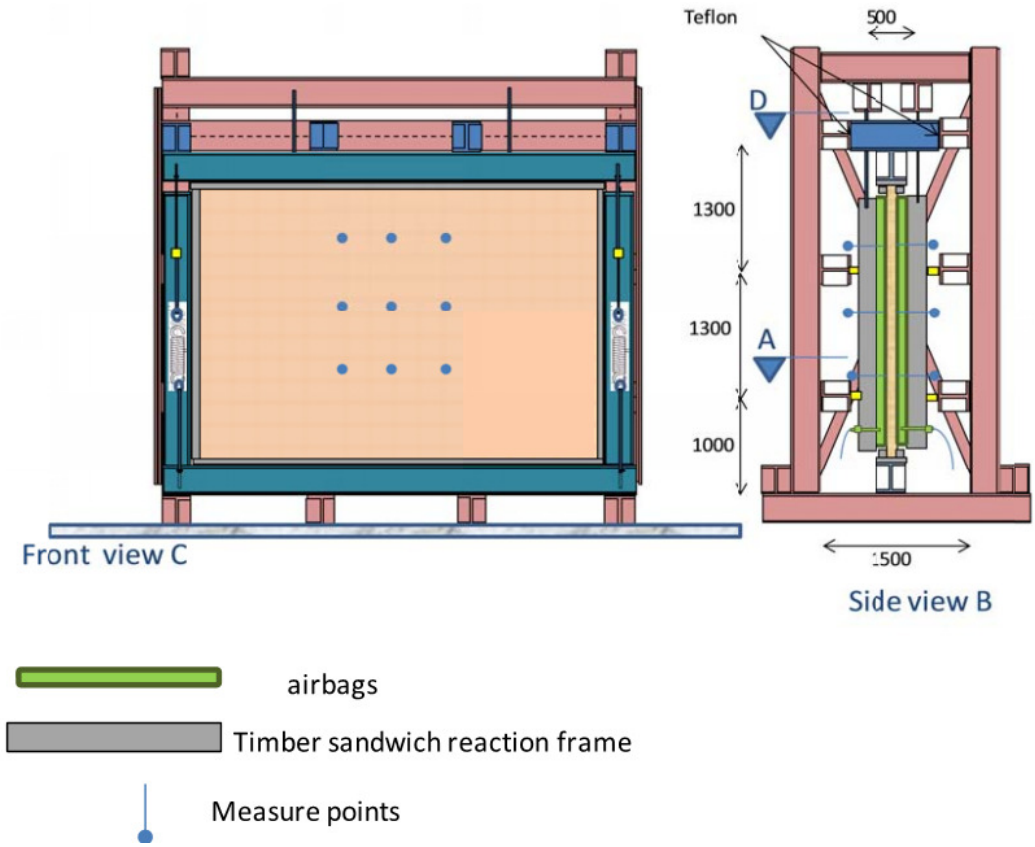

Figure 107: TUD-COMP-10: Schematic of test set-up

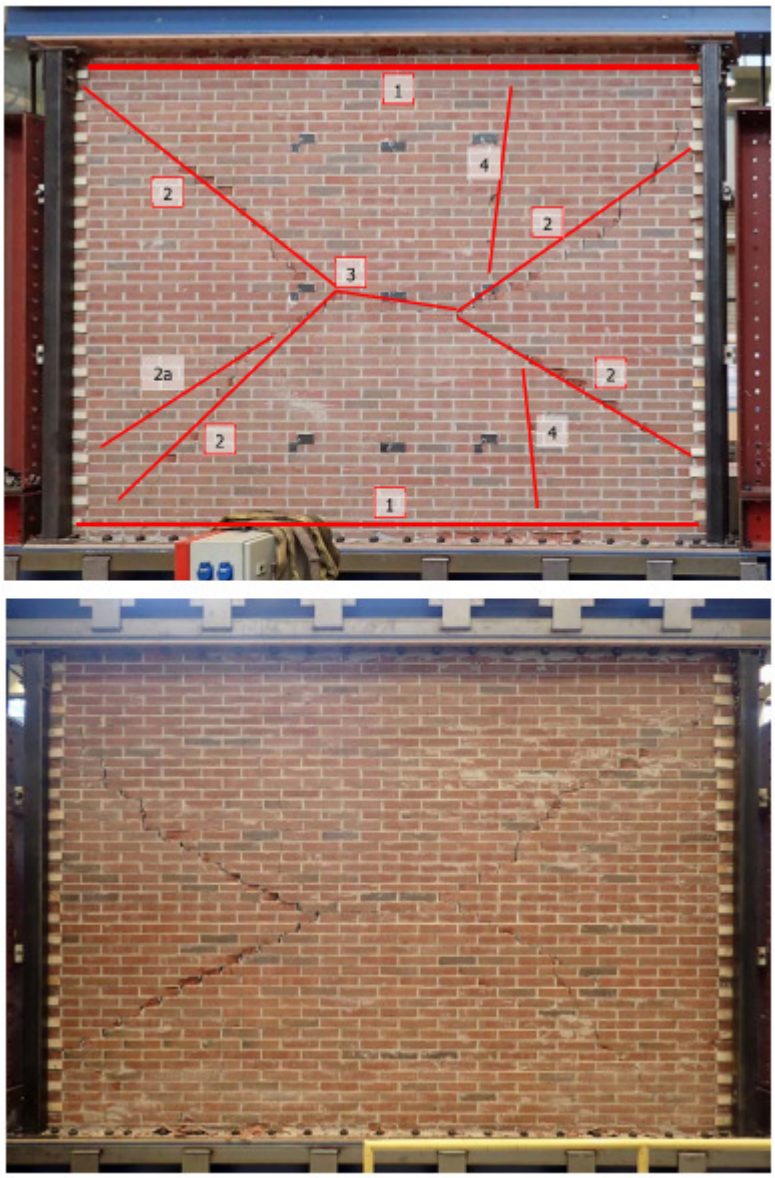

Figure 108: TUD-COMP-10: Final crack pattern of front side (top) and back side (bottom)

The measured hysteresis is shown in Figure 109.

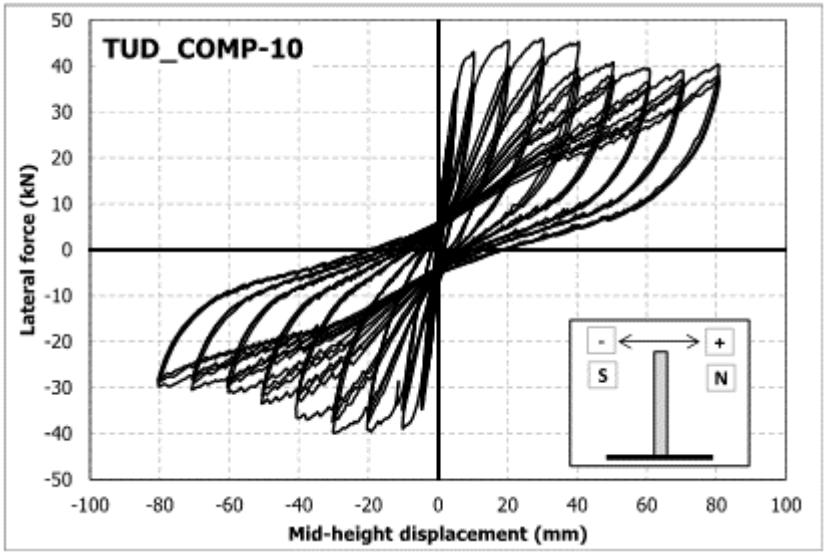

Figure 109: TUD-COMP-10: Lab test result – Applied force-mid-height displacement curve

3.1.3.2 Arup Blind Prediction

According to the test protocol issued before the test was carried out, the blind prediction simulation assumed no overburden.

LS-DYNA shell model of TUD-COMP-10 predicted an out-of-plane rocking mechanism, which consisted of damage forming at the bed joints at the top and bottom of the wall as well as mid-height.

It was understood that the net force that would be reported would be taken as the load transferred to the top and bottom timber reaction frames only. Therefore, the reported analysis net force was also only measured from the top and bottom edges of the blind prediction model, while the hysteresis from the test includes forces from all four edges. Thus, the curve comparison is of limited value.

The model did not reach global instability during the applied load protocol, which pushed the wall to a maximum displacement of 90 mm.

Note that the LS-DYNA blind prediction model of TUD-COMP-10 used material properties measured by TU-Delft as of August 2015 [9], not the NAM Basis for Design material properties.

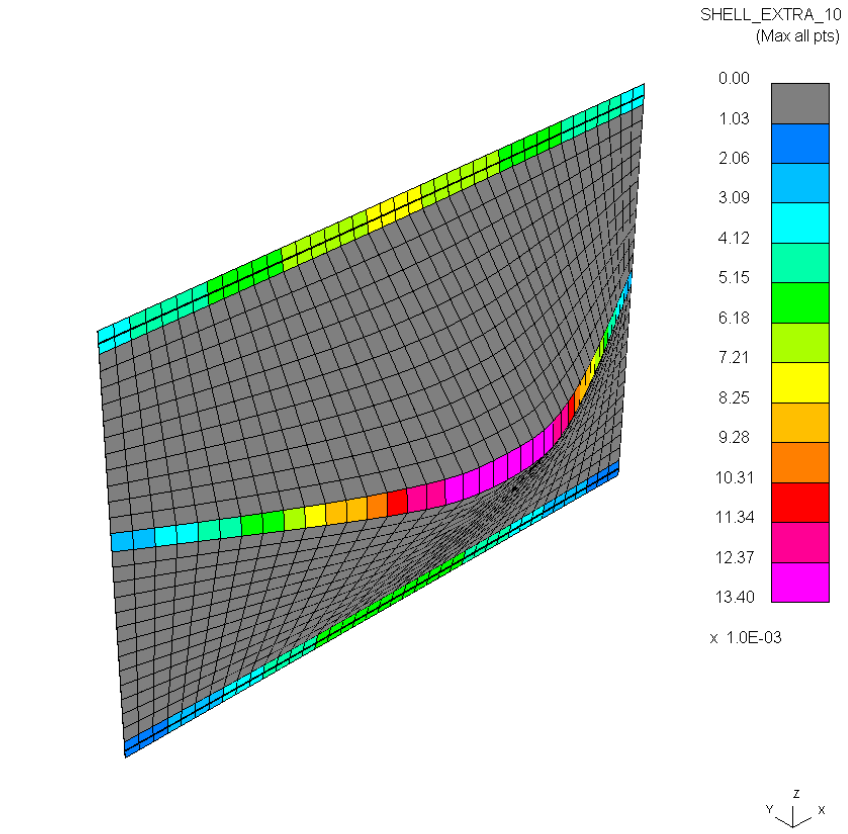

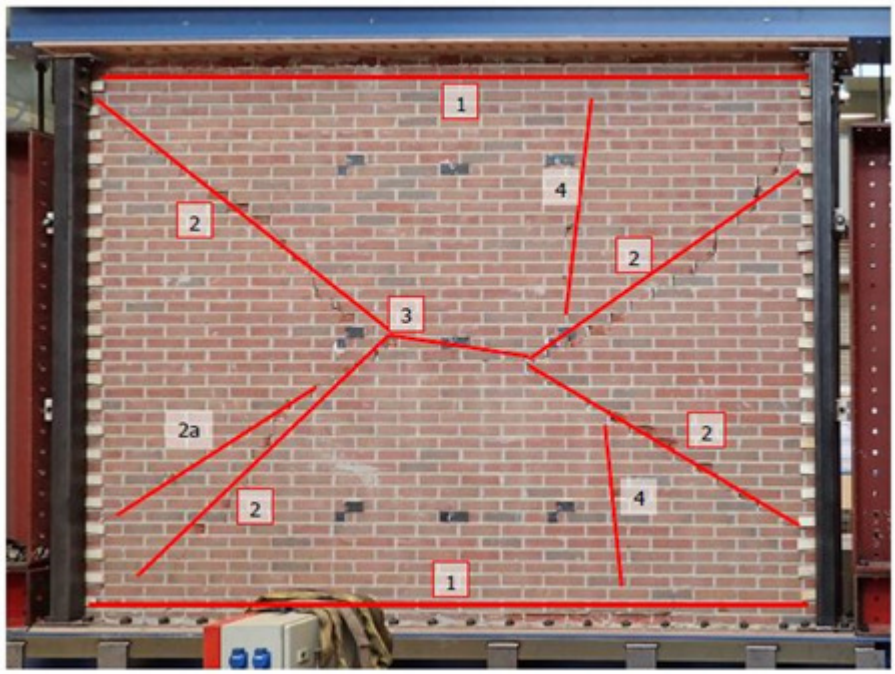

Figure 110: TUD-COMP-10: LS-DYNA blind prediction - Damage plot at end of analysis

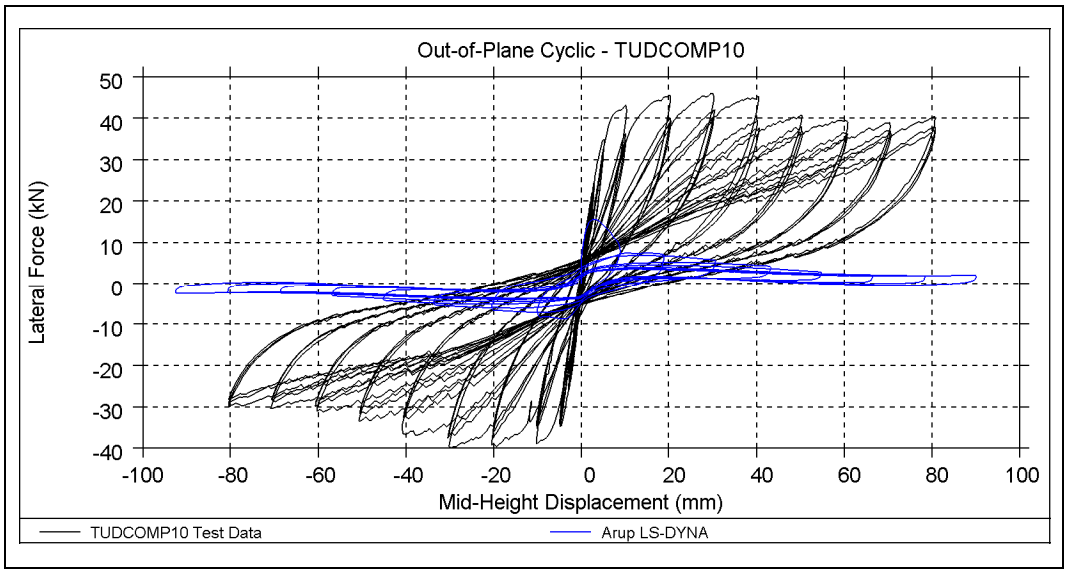

Figure 111: TUD-COMP-10: LS-DYNA blind prediction - Shear force-displacement curve (LS-DYNA result measured only along top and bottom edges - see text)

Table 35: TUD-COMP-10: LS-DYNA blind prediction - Summary table

	Predominant Failure Mechanism Predicted	**Initial Stiffness [kN/mm]**	**Peak Strength [kN]**	**Maximum Achieved Mid-Span Displacement [mm]**	
LS-DYNA	One-way out-of-plane failure	8.8	16	90	End of protocol
Test Result	Two-way out-of plane failure	12.9	46	80	End of protocol

3.1.3.3 EUCENTRE Blind Prediction

As initially agreed, EUCENTRE did not perform a blind prediction of specimen TUD-COMP-10.

3.1.3.4 TU-Delft Blind Prediction

The peak and last points of the lateral force-mid height displacement curves are selected to output maximum principal strain. The lateral force-mid height displacement curves can be seen in Figure 113. It is observed that the maximum load is 52.6 kN. It is also observed that the cracks first occur at the top and bottom supports. Next, a central horizontal crack occurs, followed by four corner cracks. The capacity meets the peak at around 3 mm mid height displacement when the top and bottom supports are heavily damaged and diagonal cracks start to develop. Finally, an envelope-shaped crack patterns results as the four corner cracks extend to the central crack. The FEM analysis terminates when the crack strains exceed the ultimate strain of the masonry tensile softening diagram. The mid height displacement increases dramatically after the envelope crack pattern was completed due to a rigid-body rotation mechanism. Besides, the minimum principal stress (4.13 MPa) is significantly smaller than the clay masonry strength (14 MPa).

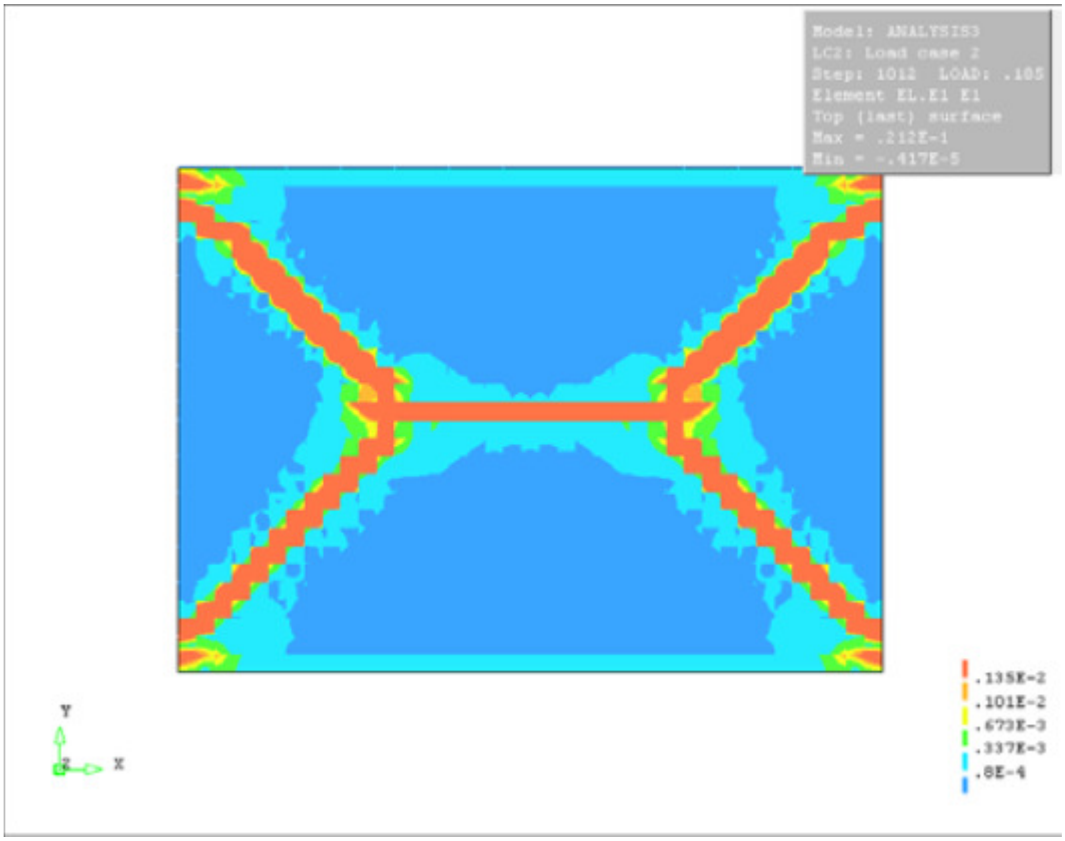

Figure 112: TUD-COMP-10: DIANA blind prediction - Damage plot at end of analysis—maximum principal strain contour

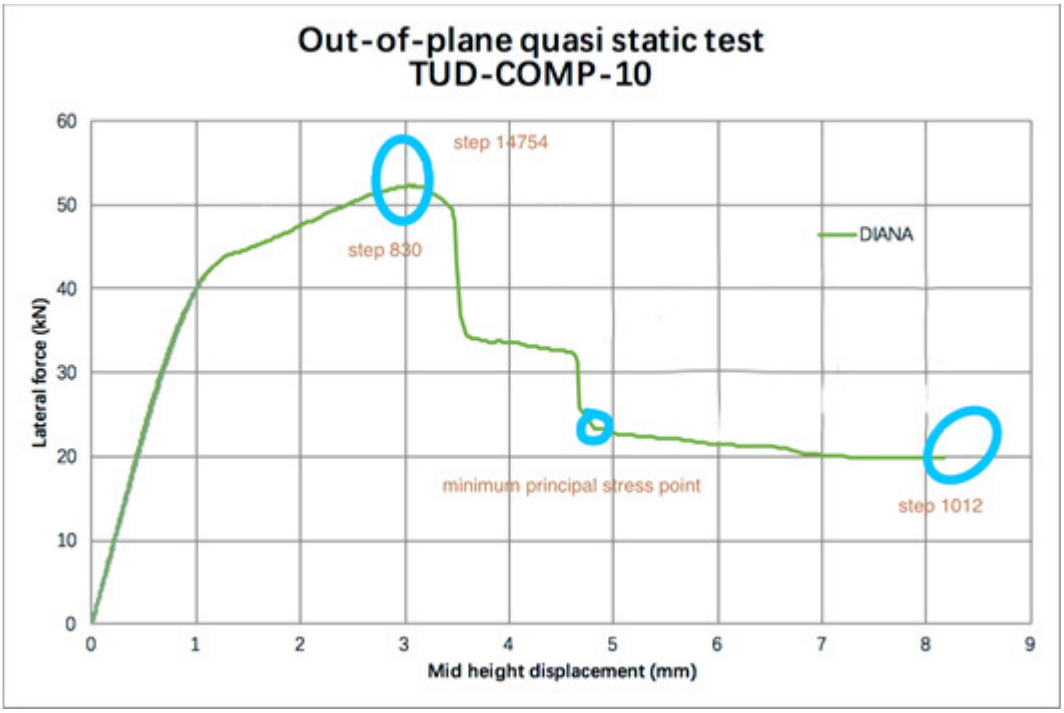

Figure 113: TUD-COMP-10: DIANA blind prediction - Shear force-displacement curve

Table 36: TUD-COMP-10: DIANA blind prediction - Summary table

	Predominant Failure Mechanism Predicted	**Initial Stiffness [kN/mm]**	**Peak Strength [kN]**	**Maximum Achieved Mid-Span Displacement [mm]**	
DIANA	Two-way out-of-plane failure	48	52.6	8 (*)	(*)
Test Result	Two-way out-of plane failure	12.9	46	80	End of protocol

(*) Model not pushed up to 80mm mid-span displacement due to failure to converge

3.1.4 TUD-COMP-11

3.1.4.1 Test Description

TUD-COMP-11 was the third quasi-static out-of-plane test administered by TU-Delft. It was the first two-way out-of-plane test, in which rotation was fully fixed at the top and bottom but the wall was free to rotate in the out-of-plane direction along the vertical edges. This specimen was a single-wythe wall constructed of calcium silicate units 102 mm thick. It was approximately 4 metres long and 2.7 metres high. The top support to the specimen together with an applied vertical load give a uniform vertical overburden of 50 kPa.

Loading was provided by airbags on either side of the specimen, similar to TUD-COMP-10. The pressure in the airbags was controlled to provide the required displacement. See Figure 114 for a schematic of the test set-up.

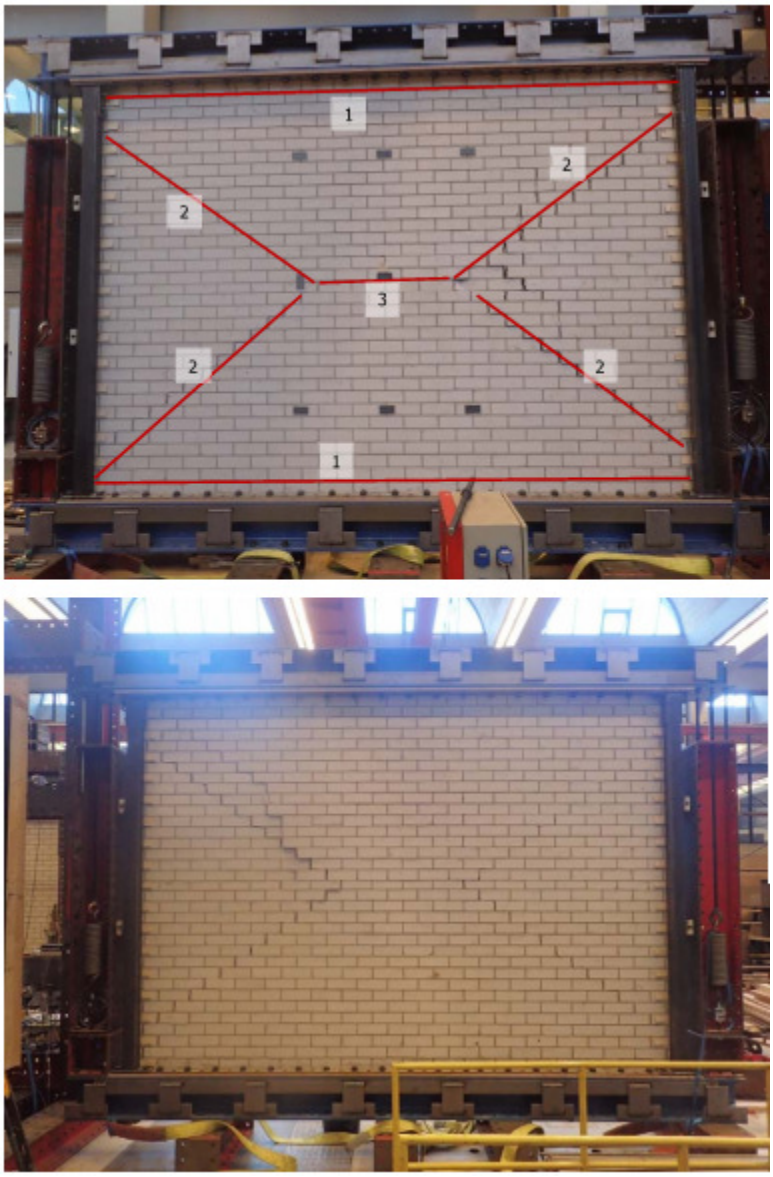

Figure 114: TUD-COMP-11: Final crack pattern of front side (top) and back side (bottom)

The measured hysteresis is shown in Figure 115.

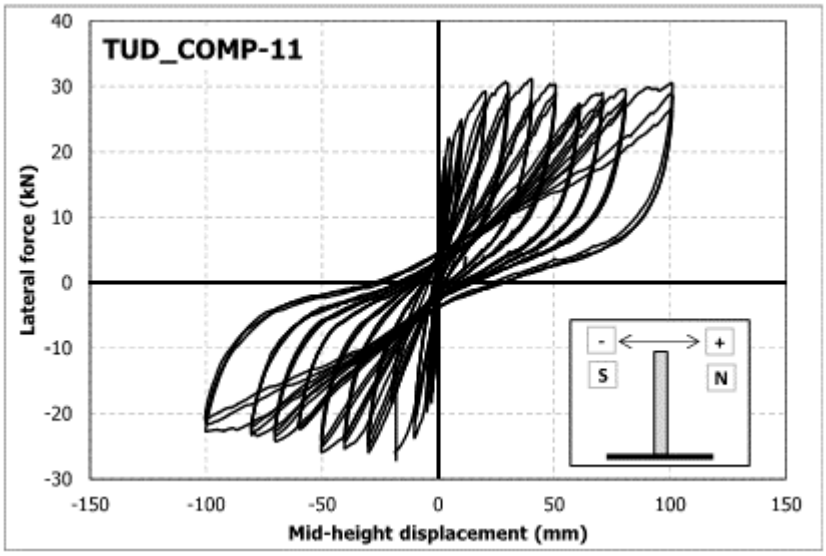

Figure 115: TUD-COMP-11: Lab test result – Applied force-mid-height displacement curve

3.1.4.2 Arup Blind Prediction

According to the test protocol issued before the test was carried out, the blind prediction simulation assumed no overburden.

LS-DYNA shell model of TUD-COMP-11 predicted an out-of-plane rocking mechanism, which consisted of damage forming at the bed joints at the top and bottom of the wall as well as throughout the wall in a diagonal pattern.

It was understood that the net force that would be reported would be taken as the load transferred to the top and bottom timber reaction frames only. Therefore, the reported analysis net force was also only measured from the top and bottom edges of the blind prediction model, while the hysteresis from the test includes forces from all four edges. Thus, the curve comparison is of limited value.

The model did not reach global instability during the applied load protocol, which pushed the wall to a maximum displacement of 73 mm.

Note that the LS-DYNA blind prediction model of TUD-COMP-11 used material properties measured by TU-Delft as of August 2015 [9], not the NAM Basis for Design material properties.

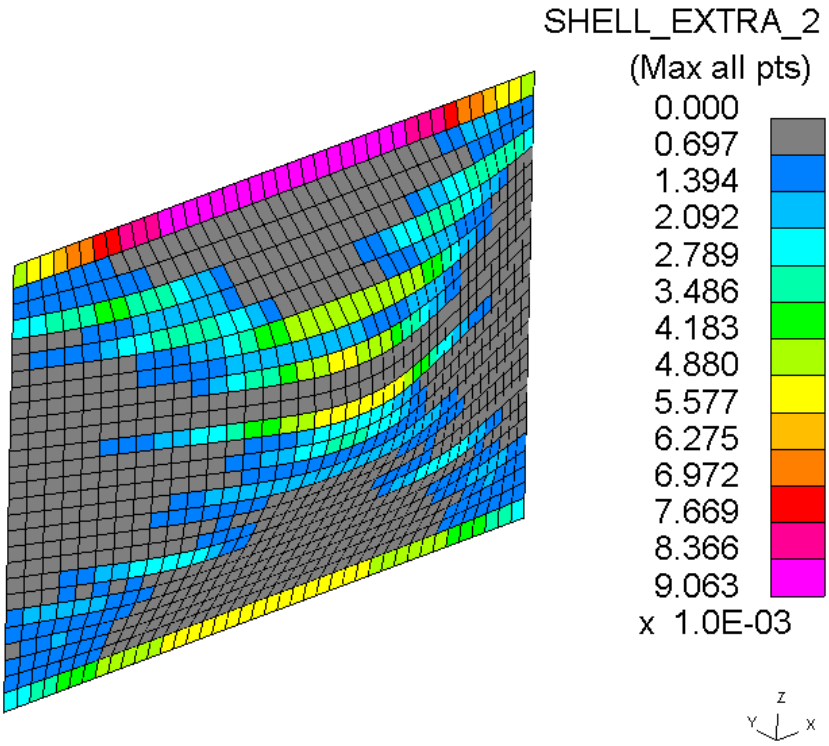

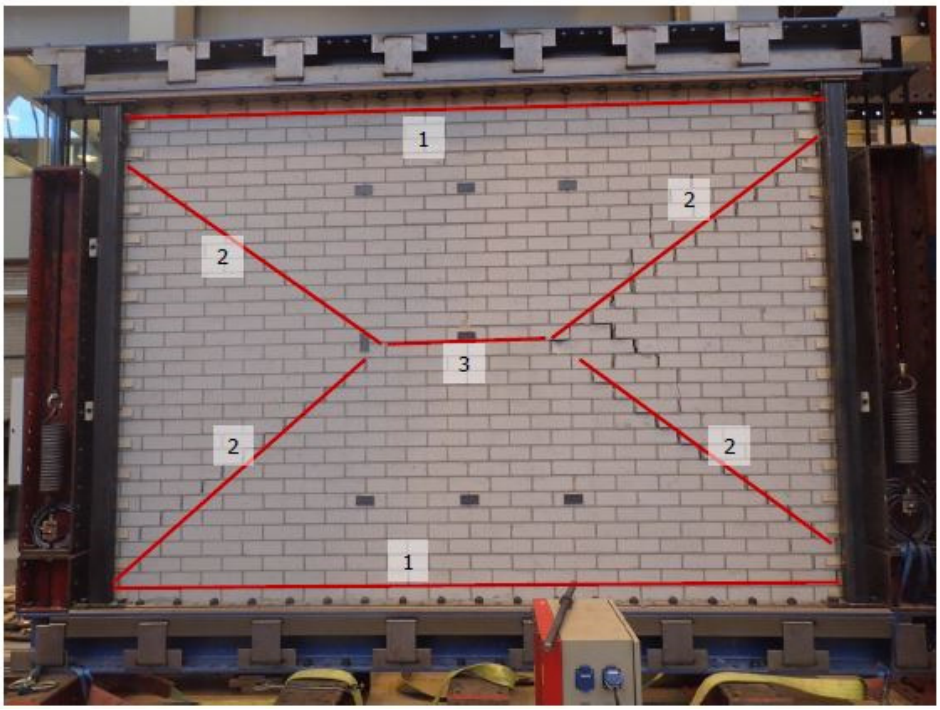

Figure 116: TUD-COMP-11: LS-DYNA blind prediction - Damage plot at end of analysis

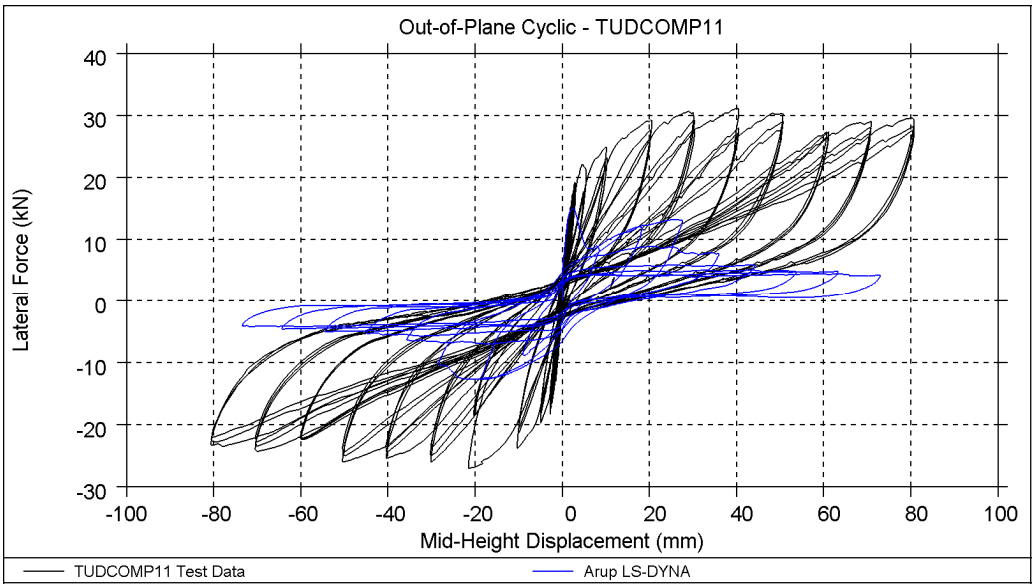

Figure 117: TUD-COMP-11: LS-DYNA blind prediction - Shear force-displacement curve. (LS-DYNA result measured along top and bottom edges only – see text)

Table 37: TUD-COMP-11: LS-DYNA blind prediction - Summary table

Consultant	**Predominant Failure Mechanism Predicted**	**Initial Stiffness [kN/mm]**	**Peak Strength [kN]**	**Maximum Achieved Mid-Span Displacement [mm]**	
LS-DYNA	Two-way out-of plane failure	12.3	15	73	End of protocol
Test Result	Two-way out-of plane failure	12	31	100	End of protocol

3.1.4.3 EUCENTRE Blind Prediction

As initially agreed, EUCENTRE did not perform a blind prediction of specimen TUD-COMP-11.

3.1.4.4 TU-Delft Blind Prediction

TU-Delft did not perform a blind prediction of specimen TUD-COMP-11.

3.1.5 TUD-COMP-12

3.1.5.1 Test Description

TUD-COMP-12 was the fourth quasi-static out-of-plane test administered by TU-Delft. It was a two-way out-of-plane test, in which rotation was fully fixed at the top and bottom but the wall was free to rotate in the out-of-plane direction along the vertical edges. This specimen was a single-wythe wall constructed of calcium silicate units 102 mm thick. It was approximately 4 metres long and 2.75 metres high with a large single opening. The applied overburden was 50 kPa.

Loading was provided by airbags on either side of the specimen. The pressure in the airbags was controlled to provide the required displacement. The force on the wall was calculated from the difference in pressure of the airbags on either side. Therefore, the measured force includes an assumption concerning the area loaded by the airbags. Nevertheless, it was understood from the test protocol that the net force that would be reported would be taken as the load transferred to the top and bottom timber reaction frames only.

See Figure 118 for a schematic of the test set-up.

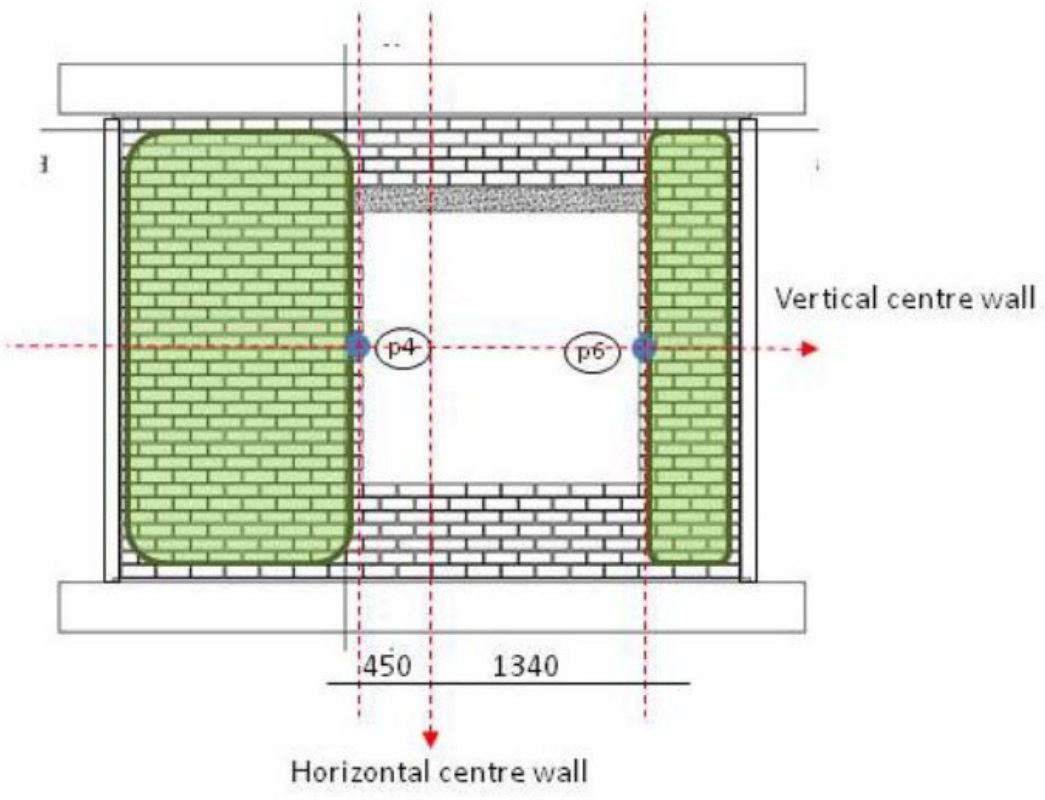

Figure 118: TUD-COMP-12: Schematic of test set-up

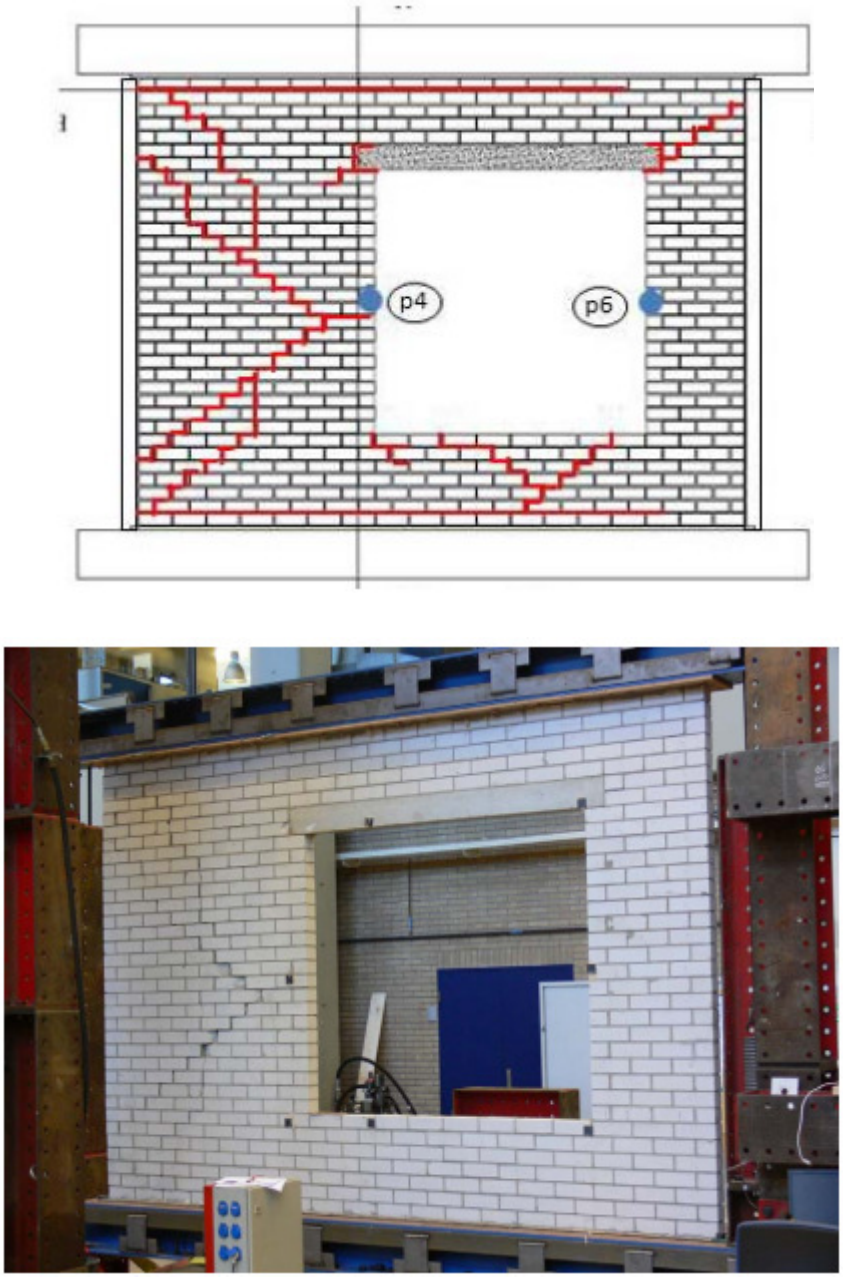

Figure 119: TUD-COMP-12: Final crack pattern

The actual loading regime of TUD-COMP-12 differed from that specified in the planned test protocol, which specified a maximum mid-height displacement level of 80 mm.

The measured hysteresis is shown in Figure 120.

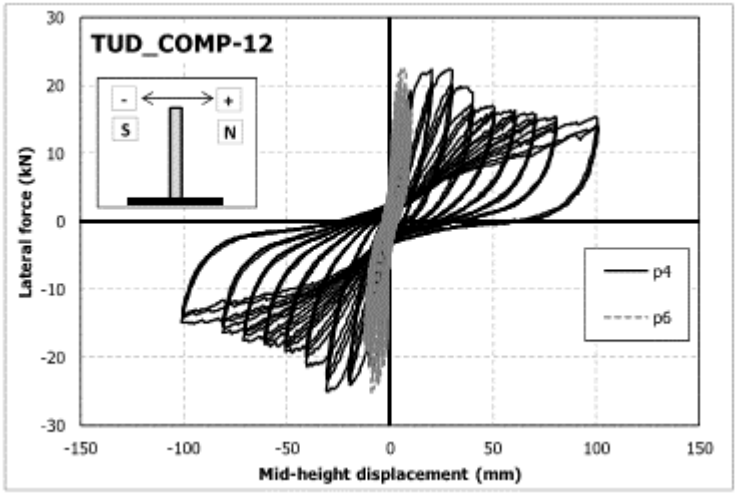

Figure 120: TUD-COMP-12: Lab test result – Applied force-(near) mid-height displacement curve

3.1.5.2 Arup Blind Prediction

LS-DYNA shell model of TUD-COMP-12 predicted an out-of-plane rocking mechanism. Damage occurred at the bed joints at the top and bottom of the wall. In the wider pier to the right of the opening, a horizontal crack occurred at mid-height of the wall as well as the formation of diagonal cracks. Damage is more spread out in the narrower pier to the left of the opening.

As previously mentioned, it was understood from the test protocol that the net force that would be reported would be taken as the load transferred to the top and bottom timber reaction frames only. Therefore, the reported analysis net force was also only measured from the top and bottom edges of the blind prediction model, while the hysteresis from the test includes forces from all four edges. Thus, the curve comparison is of limited value.

The model did not reach global instability during the applied load protocol, which pushed the wall to a maximum displacement of 80 mm.

Note that the LS-DYNA blind prediction model of TUD-COMP-12 used material properties measured by TU-Delft as of October 2015 [5].

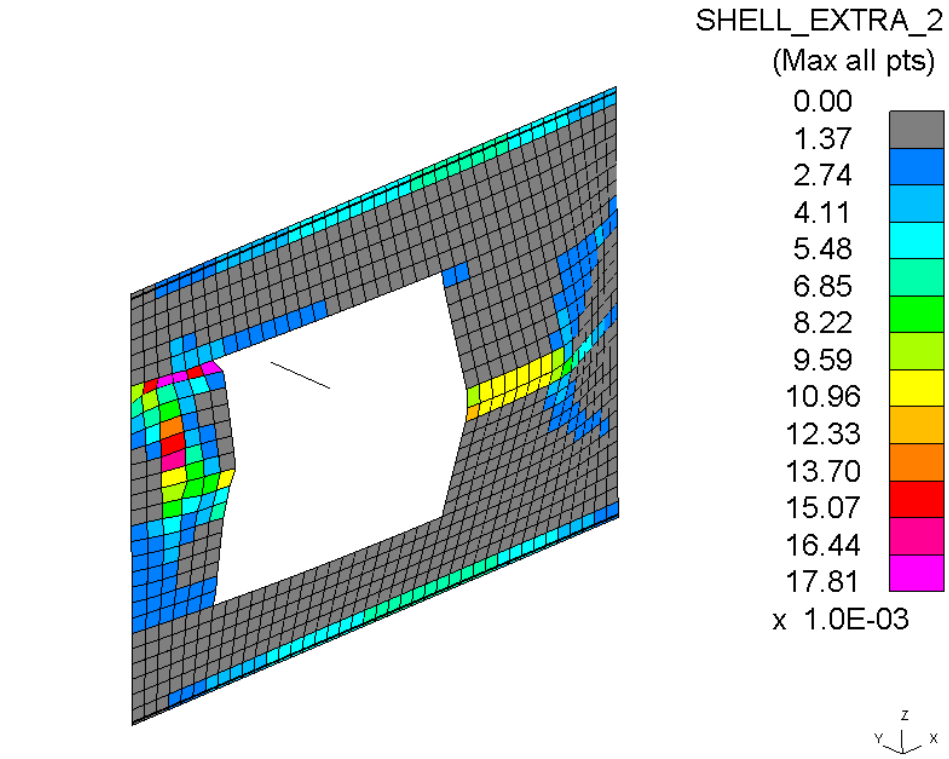

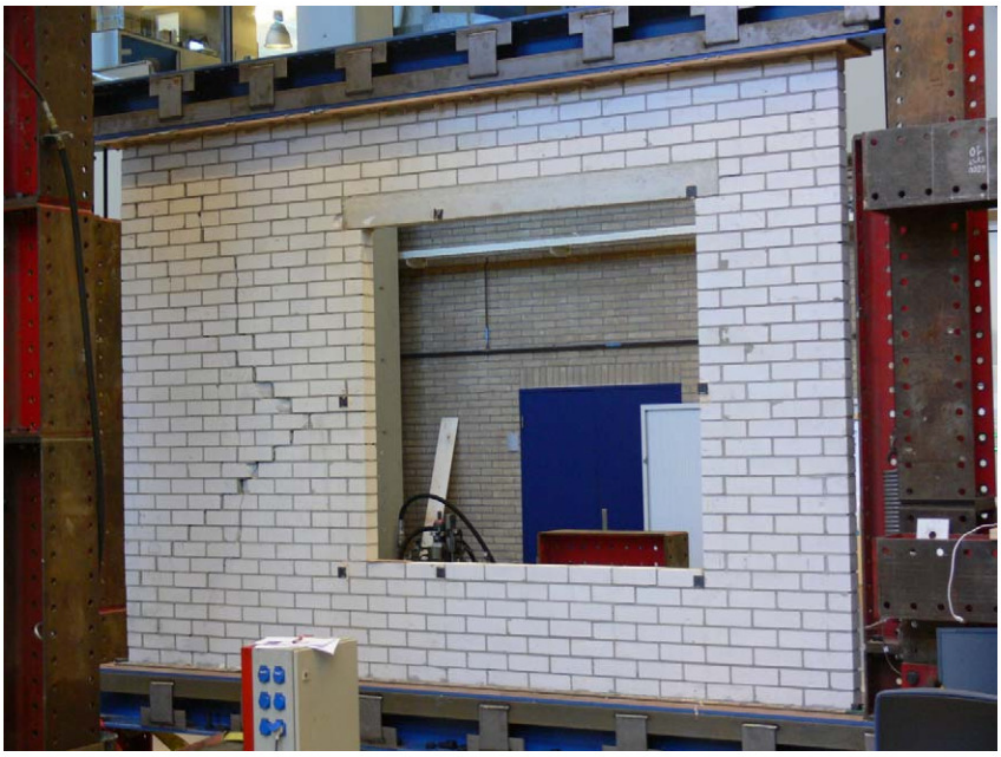

Figure 121: TUD-COMP-12: LS-DYNA blind prediction - Damage plot at end of analysis

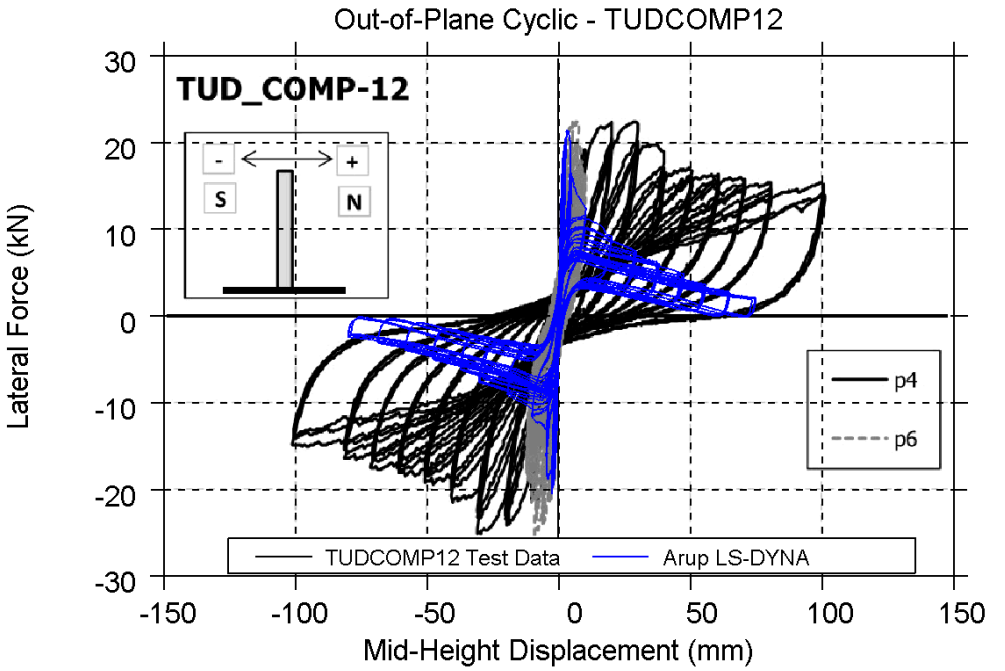

Figure 122: TUD-COMP-12: LS-DYNA blind prediction - Shear force-displacement curve at point p4. Test curve shows total force on wall, but analysis curve includes forces on top and bottom edges only.

Table 38: TUD-COMP-12: LS-DYNA blind prediction - Summary table

Consultant	**Predominant Failure Mechanism Predicted**	**Initial Stiffness [kN/mm]**	**Peak Strength [kN]**	**Maximum Achieved Mid-Span Displacement at ref. point 4 [mm]**	
LS-DYNA	Wide pier – two-way failure Narrow pier – one-way failure	15.4	22	80	End of protocol
Test Result	Two-way out-of-plane failure	15.5	25	100	End of protocol

3.1.5.3 EUCENTRE Blind Prediction

As initially agreed, EUCENTRE did not perform a blind prediction of specimen TUD-COMP-12.

3.1.5.4 TU-Delft Blind Prediction

TU-Delft did not perform a blind prediction of specimen TUD-COMP-12.

3.1.6 EUC-COMP-4

3.1.6.1 Test Description

EUC-COMP-4 was the first dynamic out-of-plane test administered by EUCENTRE. This specimen was a single-wythe wall constructed of calcium silicate units 102 mm thick. It was 1.44 m long and 2.75 m high. The applied overburden stress was initially 0.3 MPa and later reduced to 0.1 MPa during the test. The wall was tested under double clamped boundary conditions. The testing sequence consisted of incremental dynamic testing procedure of the following ground motions:

- Gr_1: Groningen record, PGA = 0.25g
- RWA: 4 Hz acceleration pulse input
- Gr_2: Floor accelerations obtained with TREMURI program assuming T1_STAR Model in the "weak" direction, PGA = 0.38g

Collapse of the wall occurred during the last test phase. The bottom crack appeared at the base, the "mid-height" crack between then 19th and 20th course of bricks, and the top crack between the 33rd and 34th course of bricks.

Table 39: EUC-COMP-4: Testing sequence

Specimen	Phase #	Test #	Dynamic Input	Input Scaling	PGA [g]
Imposed Overburden Pressure: 0.3 MPa					
EC_COMP_4	1	1.1	Gr_1	20%	+0.04
EC_COMP_4	1	1.2	Gr_1	40%	+0.09
EC_COMP_4	1	1.3	Gr_1	80%	+0.16
EC_COMP_4	1	1.4	Gr_1	100%	+0.20
EC_COMP_4	1	1.5	Gr_1	160%	+0.32
EC_COMP_4	1	1.6	Gr_1	200%	+0.42
EC_COMP_4	1	1.7	Gr_1	250%	+0.53
EC_COMP_4	1	1.8	Gr_1	350%	+0.74
EC_COMP_4	1	1.9	Gr_1	450%	+0.96
EC_COMP_4	2	2.1	RWA 2Hz	-	-1.11
EC_COMP_4	2	2.2	RWA 2Hz	-	-1.63
EC_COMP_4	2	2.3	RWA 2Hz	-	-1.04
EC_COMP_4	2	2.4	RWA 2Hz	-	-1.88
Imposed Overburden Pressure: 0.1 MPa					
EC_COMP_4	3	3.1	Gr_1	40%	+0.08
EC_COMP_4	3	3.2	Gr_1	80%	+0.17
EC_COMP_4	3	3.3	Gr_1	100%	+0.21
EC_COMP_4	3	3.4	Gr_1	160%	+0.34
EC_COMP_4	3	3.5	Gr_1	200%	+0.41
EC_COMP_4	3	3.6	Gr_1	250%	+0.51
EC_COMP_4	3	3.7	Gr_1	300%	+0.60
EC_COMP_4	3	3.8	Gr_1	350%	+0.73
EC_COMP_4	4	4.1	RWA 2Hz	-	-0.25
EC_COMP_4	4	4.2	RWA 2Hz	-	-0.48
EC_COMP_4	4	4.3	RWA 2Hz	-	-0.72
EC_COMP_4	4	4.4	RWA 2Hz	-	-0.96
EC_COMP_4	5	5.1	Gr_2	100%	+0.44
EC_COMP_4	5	5.2	Gr_2	150%	+0.64
EC_COMP_4	5	5.3	Gr_2	200%	+0.85

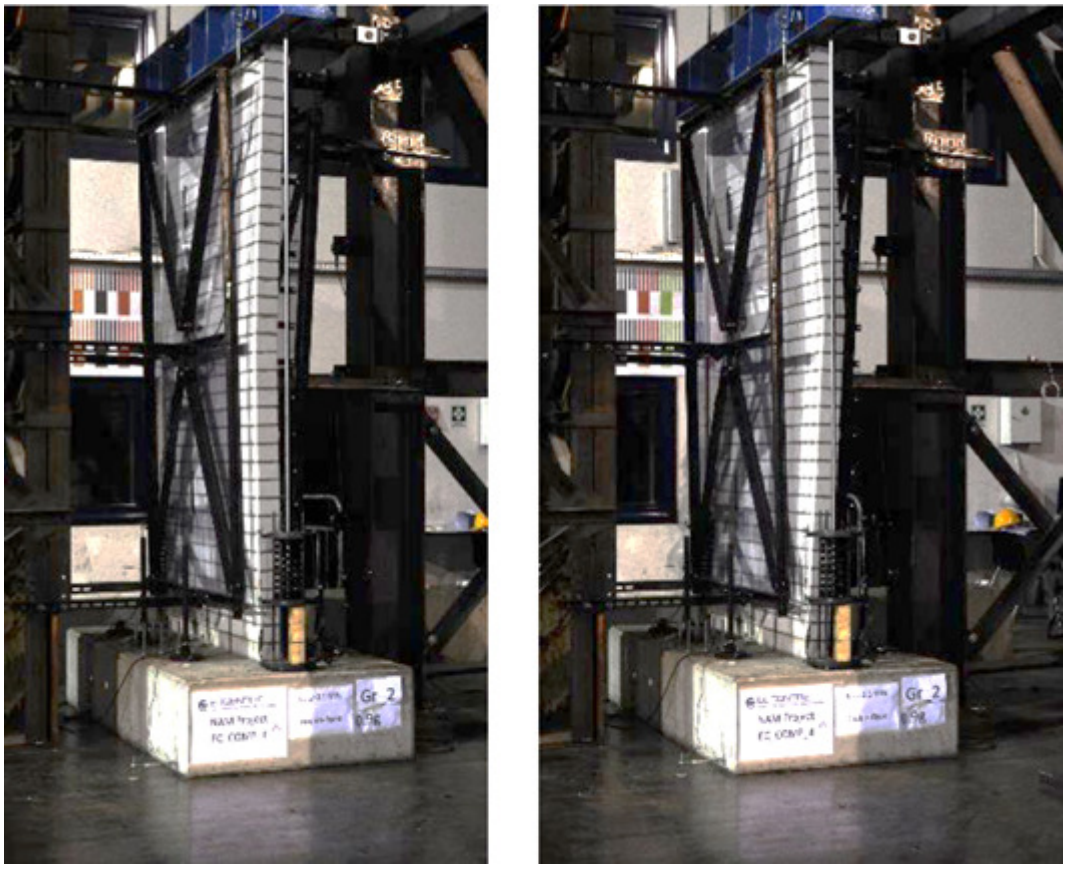

Figure 123: EUC-COMP-4: Deformed shape (left and right)

Figure 124: EUC-COMP-4: View of mid-height crack

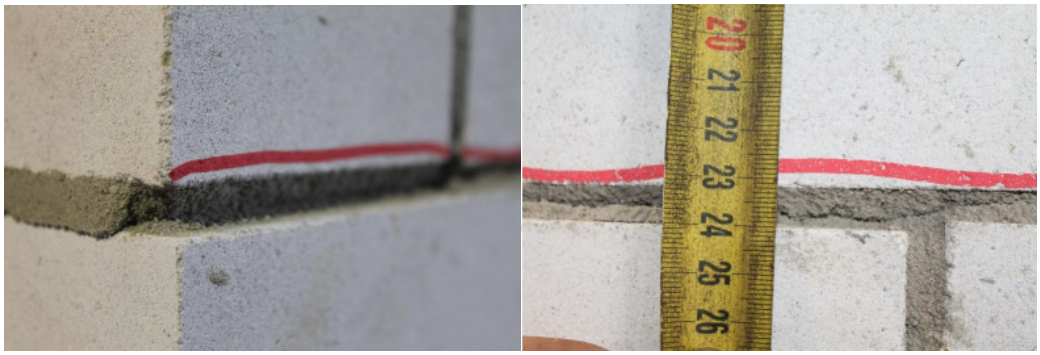

Figure 125: EUC-COMP-4: View of the cracked mortar bed-joint (left). Decrease in mortar bed-joint thickness (right)

3.1.6.2 Arup Blind Prediction

Analyses were performed on two separate LS-DYNA specimens, one with 0.1 MPa overburden and the other with 0.3 MPa overburden, by incrementally scaling ground motion Gr_1 and ground motion Gr_2.

The analysis results predicted an out-of-plane rocking mechanism, which consisted of damage forming at the bed joints at the top and bottom of the wall as well as mid-height. Global instability eventually occurred upon progressively increasing the acceleration demand.

Note that small discrepancies between the values for the PGA reported in Table 39 and the following curves for the Lab Test to LS-DYNA simulation comparison are due to baseline corrections applied to the measured accelerations.

Figure 126 through Figure 128 below plot the incremental dynamic response for the LS-DYNA models of EUC-COMP-4 that correlate to test phase #1, #3, and #5, respectively.

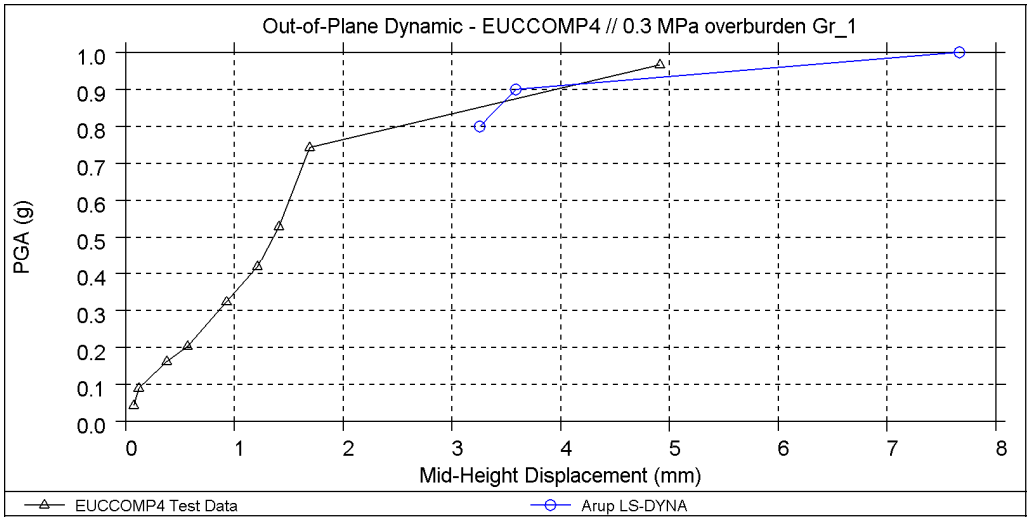

Figure 126: EUC-COMP-4: LS-DYNA blind prediction – Relative mid-height response vs. PGA for 0.3 MPa overburden, under incremental dynamic testing procedure of ground motion Gr_1 (test phase #1)

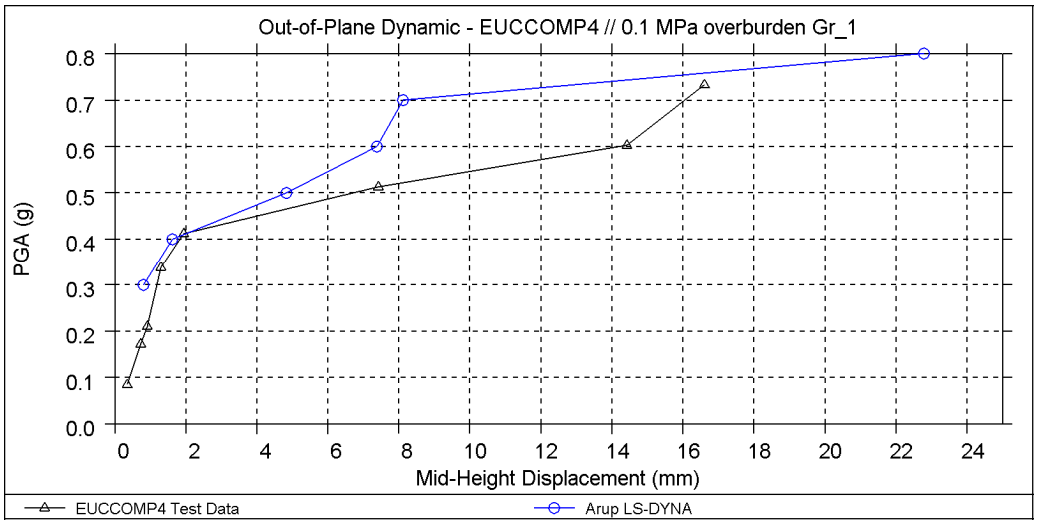

Figure 127: EUC-COMP-4: LS-DYNA blind prediction – Relative mid-height response vs. PGA for 0.1 MPa overburden, under incremental dynamic testing procedure of ground motion Gr_1 (test phase #3)

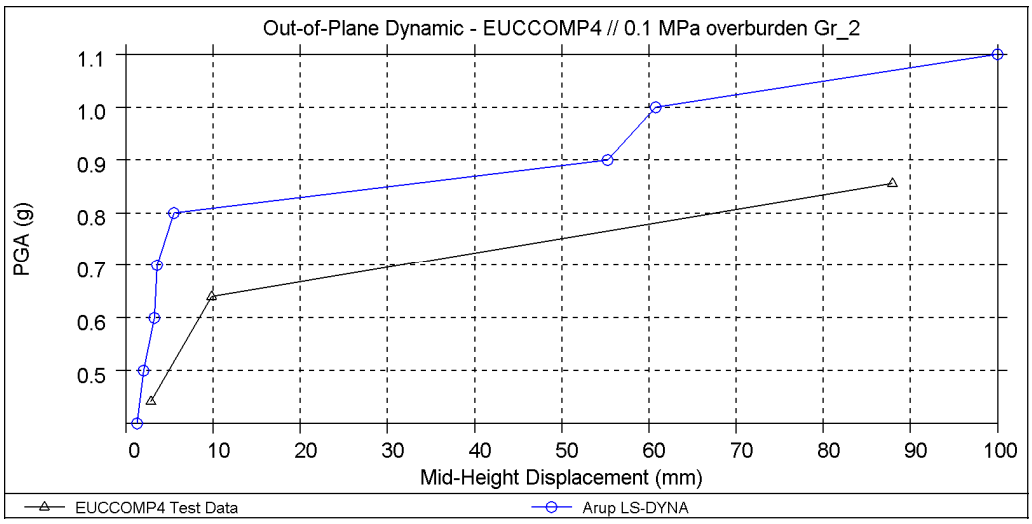

Figure 128: EUC-COMP-4: LS-DYNA blind prediction – Relative mid-height response vs. PGA for 0.1 MPa overburden, under incremental dynamic testing procedure of ground motion Gr_2 (test phase #5)

3.1.6.3 EUCENTRE Blind Prediction

The EUC blind predictions on the out-of-plane shake-table test of the EUC-COMP-4 specimen were based on a single degree of freedom SDOF numerical model which was able to reproduce the rocking response of URM walls. Such a model needed a realistic out-of-plane F-Δ relationship and a plausible damping model in order to successfully simulate the non-linear response. The F-Δ relationship of a wall pushed in the out-of-plane direction could be idealised as a tri-linear curve as proposed in several studies in the literature [7]. The damping model assumed was the Rayleigh damping model, proportional to current secant stiffness; the damping ratio was hence updated at each analysis time step according to the displacement level achieved by the system. The mass contribution component was set to zero; hence, the system was damped exclusively by the stiffness term with an initial 'elastic' damping ratio value equal to 14%. Since no experimental data on the F-Δ relationship of the tested walls was available, the F-Δ tri-linear curve was assumed by analogy to the static push tests present in the literature (Doherty, 2002) on similar specimens.

Figure 129 below shows the tri-linear curves assumed for the blind prediction.

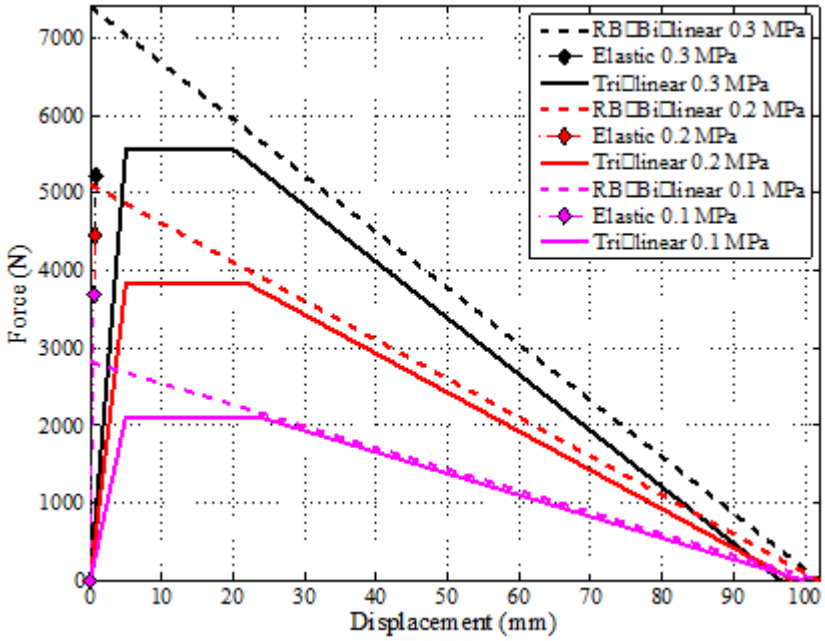

Figure 129: EUC-COMP-4: TREMURI blind prediction – input tri-linear curves assumed in model

Figure 130 through Figure 132 below plot the incremental dynamic response for the TREMURI model of EUC-COMP-4 that correlate to test phase #1, #3 and #5, respectively.

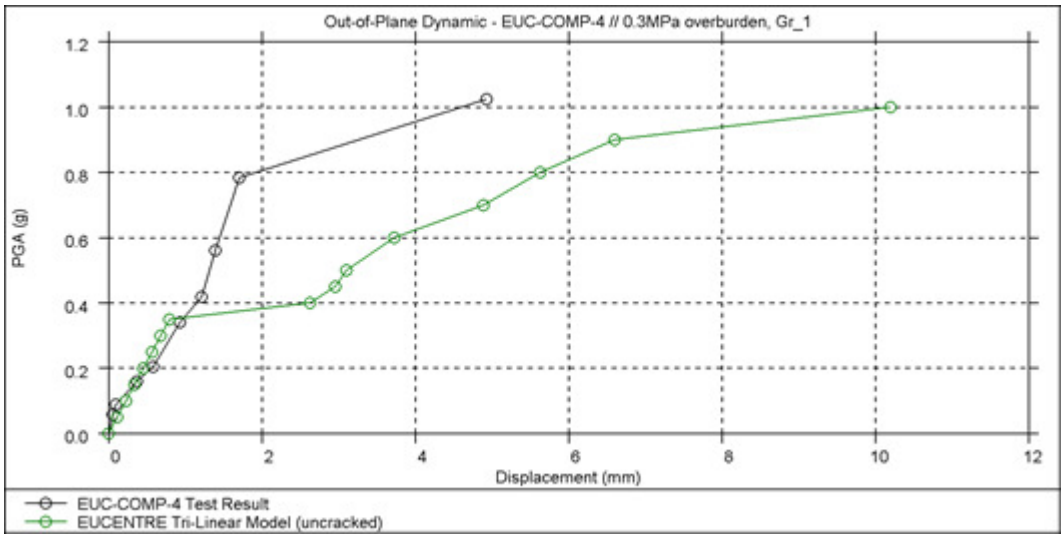

Figure 130: EUC-COMP-4: EUCENTRE blind prediction – Relative mid-height response vs. PGA of uncracked model for 0.3 MPa overburden, under incremental dynamic testing procedure of ground motion Gr_1 (test phase #1)

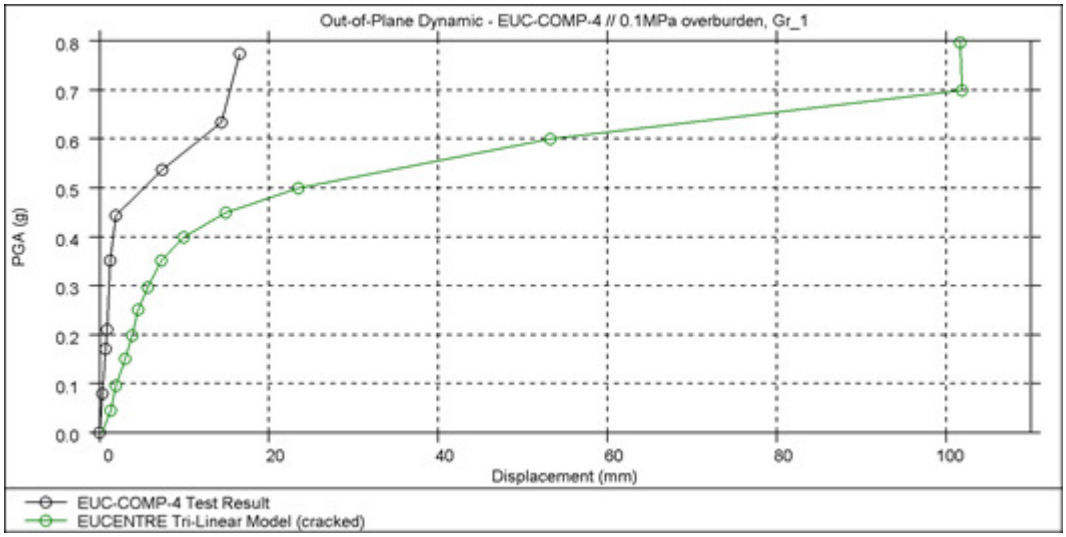

Figure 131: EUC-COMP-4: EUCENTRE blind prediction – Relative mid-height response vs. PGA of cracked model for 0.1 MPa overburden, under incremental dynamic testing procedure of ground motion Gr_1 (test phase #3)

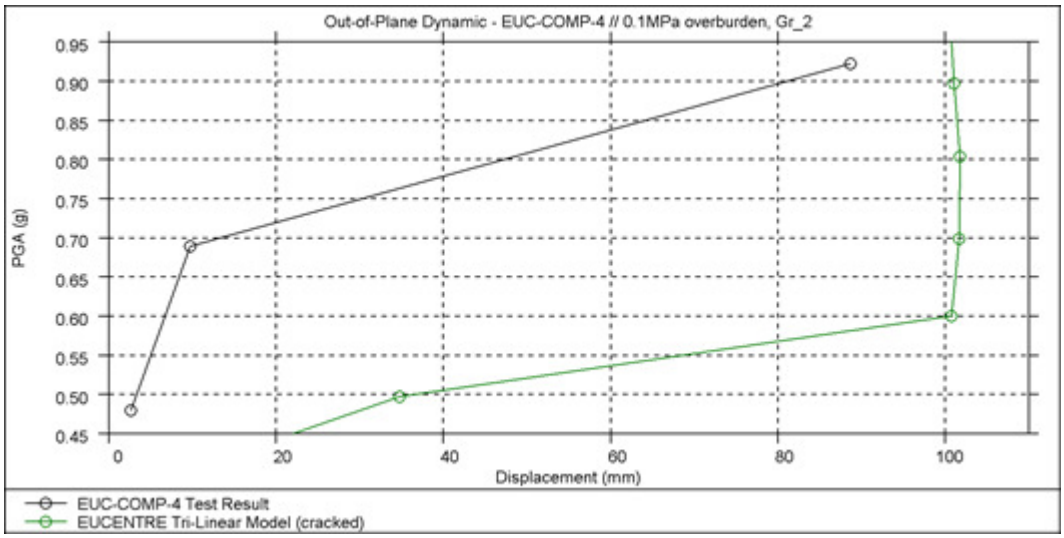

Figure 132: EUC-COMP-4: EUCENTRE blind prediction – Relative mid-height response vs. PGA of cracked model for 0.1 MPa overburden, under incremental dynamic testing procedure of ground motion Gr_2 (test phase #5)

3.1.6.4 TU-Delft Blind Prediction

The blind prediction of EUC-COMP-4 was done by applying separately the ground motions Gr_1 and Gr_2. In the protocol, the panel was assumed as cracked after test 1.1. Therefore the panel was analysed in the un-cracked and cracked conditions, for 0.3 and 0.1 MPa overburden.

The results of these analyses showed that a mechanism occurred due to cracking in the interfaces. For the 0.1 MPa overburden, a maximum PGA of 1.0 g was reached before global instability was observed. For the 0.3 MPa overburden, increasing PGA up to 2 g was analysed, and the mid-height displacement remained smaller than 10 mm. No global instability was observed for PGAs up to 2g.

The difference between the cracked and un-cracked assumption seemed to be rather small. The level of overburden had the most influence on the response of the wall. All the performed analyses showed a global behaviour stiffer and stronger with respect to the experimental results.

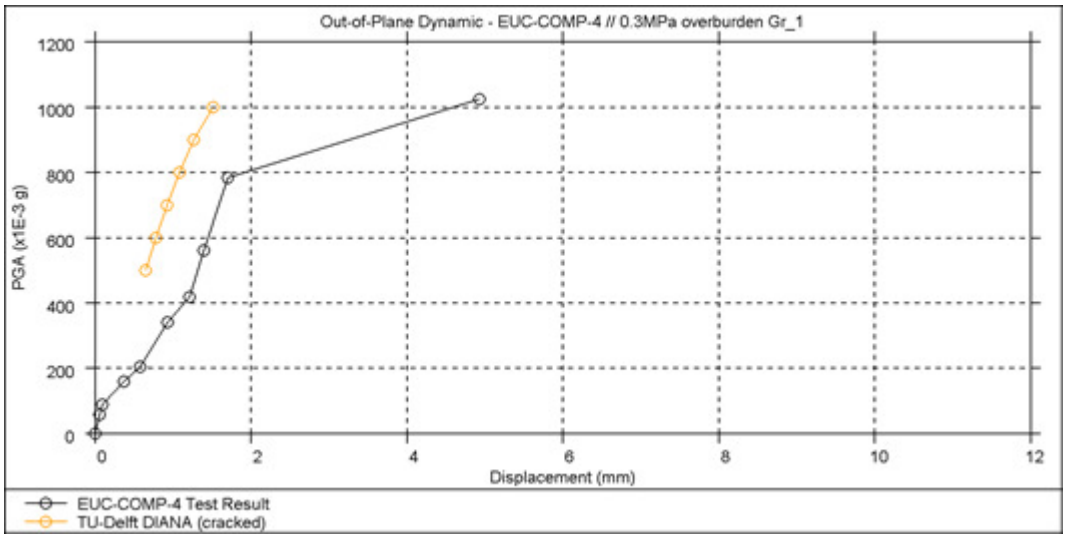

Figure 133: EUC-COMP-4: DIANA blind prediction – Relative mid-height response vs. PGA for 0.3 MPa overburden, under incremental dynamic testing procedure of ground motion Gr_1 (test phase #1)

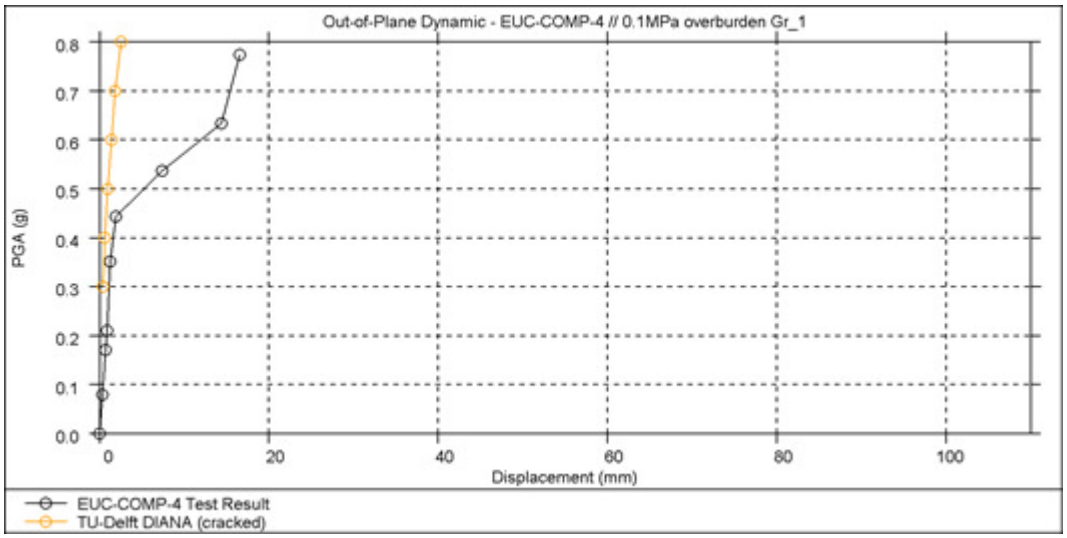

Figure 134: EUC-COMP-4: DIANA blind prediction – Relative mid-height response vs. PGA for 0.1 MPa overburden, under incremental dynamic testing procedure of ground motion Gr_1 (test phase #3)

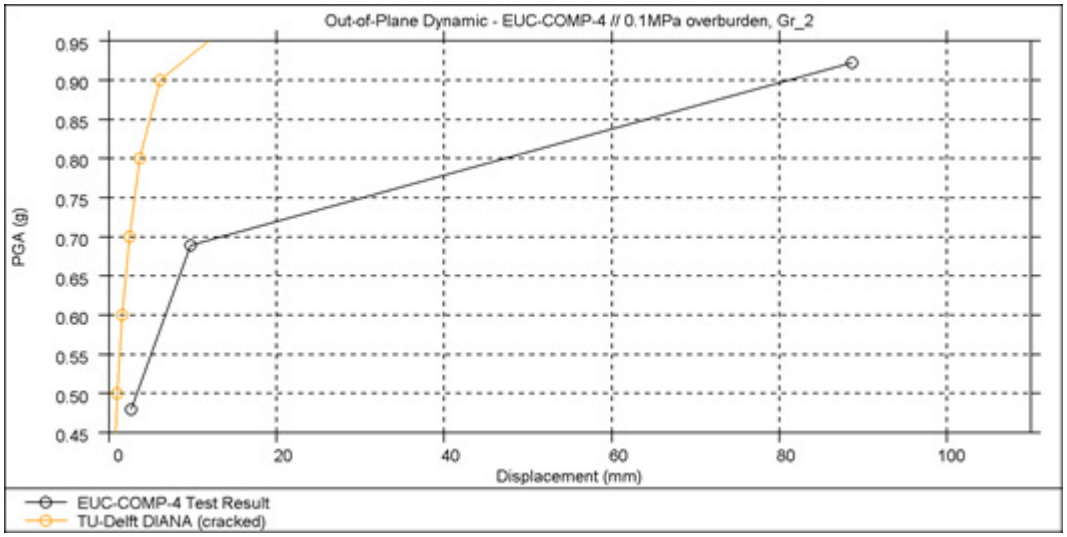

Figure 135: EUC-COMP-4: DIANA blind prediction – Relative mid-height response vs. PGA for 0.1 MPa overburden, under incremental dynamic testing procedure of ground motion Gr_2 (test phase #5)

3.1.7 EUC-COMP-5

3.1.7.1 Test description

EUC-COMP-5 was the second dynamic out-of-plane test administered by EUC. This specimen was a single-wythe cavity wall. The inner (structural) leaf was constructed of calcium silicate units 102 mm thick and was 1.44 m long and 2.75 m high. The outer leaf was constructed of clay units 100 mm thick and was 1.44 m long and 2.7 m high. The inner and outer leaves are connected with 2 ties/m^2. The applied overburden stress was 0.1 MPa. The inner leaf was set up under double clamped boundary conditions and the outer leaf, cantilever boundary conditions. The testing sequence consisted of incremental dynamic testing procedure of the following ground motions:

- Gr_1: Groningen record, PGA = 0.25g
- RWA: 4 Hz acceleration pulse input
- Gr_2: Floor accelerations obtained with TREMURI program assuming T1_STAR Model in the "weak" direction, PGA = 0.38g

The test specimen reached global instability during test phase 6.

Table 40: EUC-COMP-5: Testing sequence

Specimen	Phase #	Test #	Dynamic Input	Input Scaling	PGA [g]
EC_COMP_5	0	0.1	Hammering	-	-
EC_COMP_5	0	0.2	White Noise	-	0.1
EC_COMP_5	1	1.1	Gr_1	+20%	+0.04
EC_COMP_5	1	1.2	Gr_1	+40%	+0.09
EC_COMP_5	1	1.3	Gr_1	-40%	-0.09
EC_COMP_5	1	1.4	Gr_1	+60%	+0.12
EC_COMP_5	1	1.5	Gr_1	+80%	+0.17
EC_COMP_5	1	1.6	Gr_1	+100%	+0.21
EC_COMP_5	1	1.7	Gr_1	-60%	-0.13
EC_COMP_5	1	1.8	Gr_1	-80%	-0.17
EC_COMP_5	1	1.9	Gr_1	-100%	-0.23
EC_COMP_5	2	2.1	RWA	-	-0.22
EC_COMP_5	2	2.2	RWA	-	-0.30
EC_COMP_5	3	3.1	Gr_2	+70%	+0.31
EC_COMP_5	3	3.2	Gr_2	+100%	+0.49
EC_COMP_5	3	3.3	Gr_2	+150%	+0.66
EC_COMP_5	4	4.1	Gr_1	+300%	+0.60
EC_COMP_5	5	5.1	RWA	-	-0.30
EC_COMP_5	5	5.2	RWA	-	-0.49
EC_COMP_5	6	6.1	Gr_2	+150%	+0.65

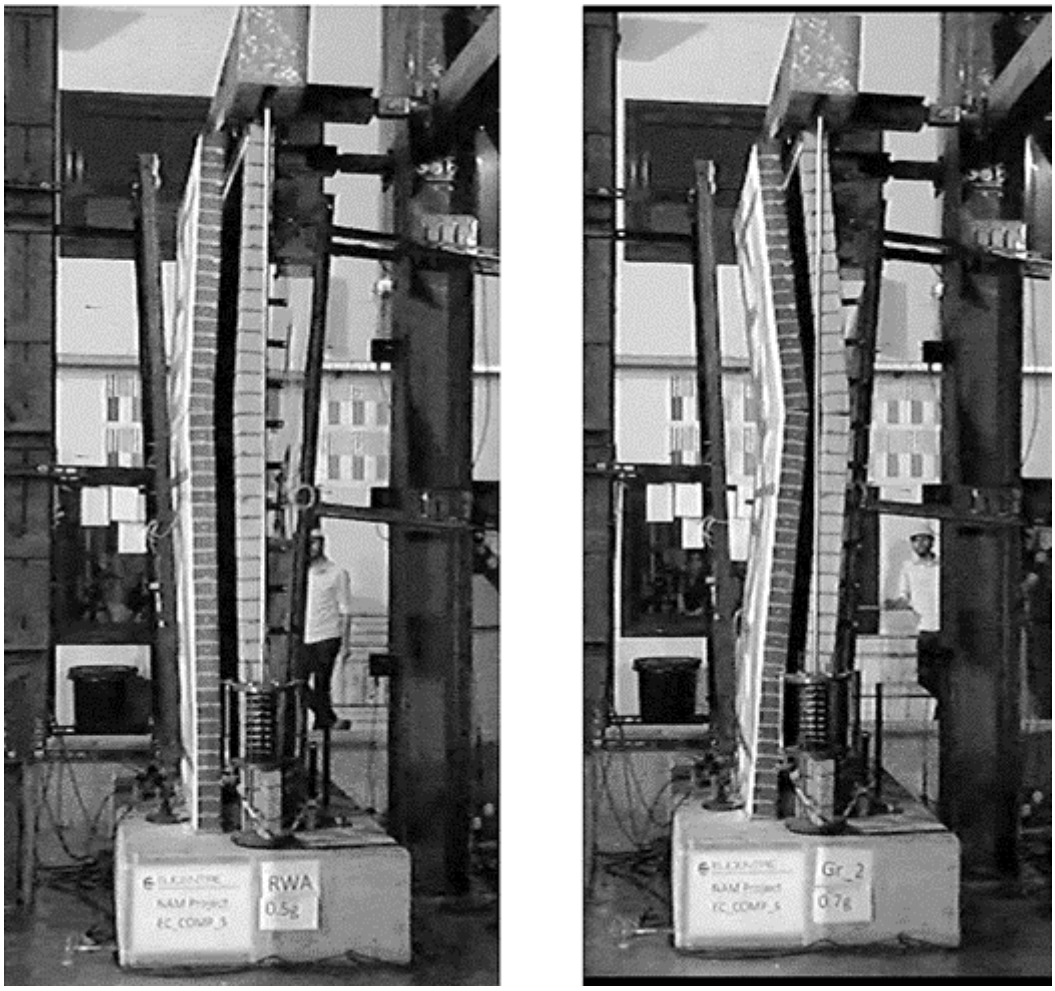

Figure 136: Deformed shape (left and right)

Figure 137: EUC-COMP-5: Formation of mid-height cracks at the tie location

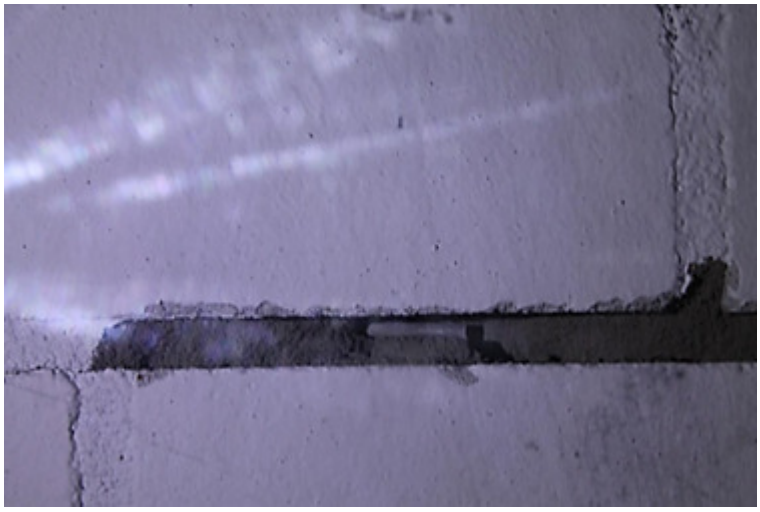

Figure 138: EUC-COMP-5: Expulsion of part of the mortar bed joint

Figure 139: EUC-COMP-5: Collapse of specimen

3.1.7.2 Arup Blind Prediction

In the LS-DYNA model, the inner and outer leaves were rigidly connected at the locations of the ties. Analyses were performed on one specimen with 0.1 MPa overburden by incrementally scaling ground motion Gr_1 and ground motion Gr_2.

The analysis results predicted an out-of-plane rocking mechanism for both leaves, which consisted of damage forming at the bed joints at the top and bottom of the wall as well as mid-height. Global instability eventually occurred at 0.7g peak ground acceleration. The test specimen continued beyond test phase 4 and reached collapse during test phase 6 (refer to Table 40).

Note that small discrepancies between the values for the PGA reported in Table 40 and the following curves for the Lab Test to LS-DYNA simulation comparison are due to baseline corrections applied to the measured PGA.

Figure 140 and Figure 141 below plot the incremental dynamic response for the LS-DYNA models of EUC-COMP-5 that correlate to test phase #1 & #4 and #3 & #6, respectively.

Note that Figure 140 and Figure 141 refer to displacement for the Ca-Si wall wythe.

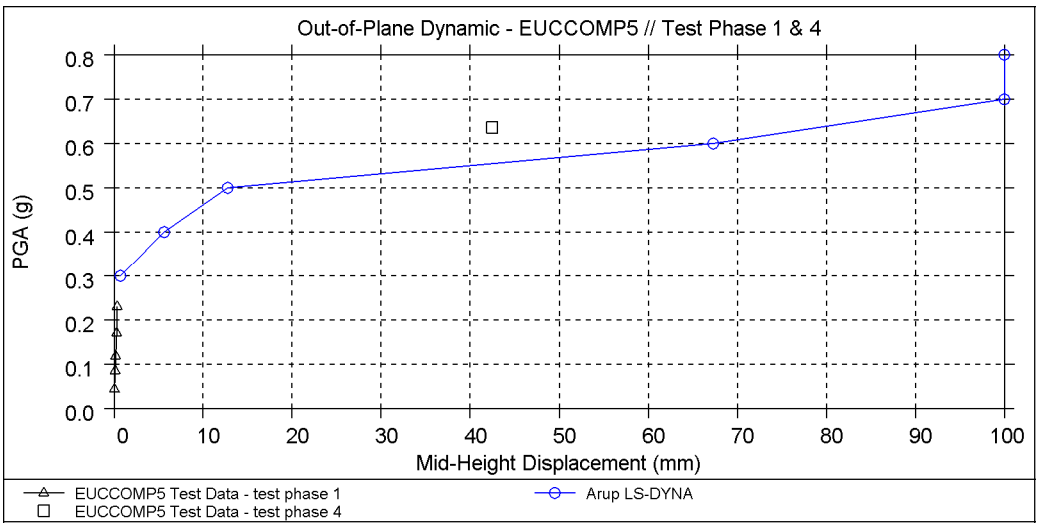

Figure 140: EUC-COMP-5: LS-DYNA blind prediction – Ca-Si wall wythe relative mid-height response vs. PGA for model under incremental dynamic testing procedure of ground motion Gr_1 (test phases #1 & 4)

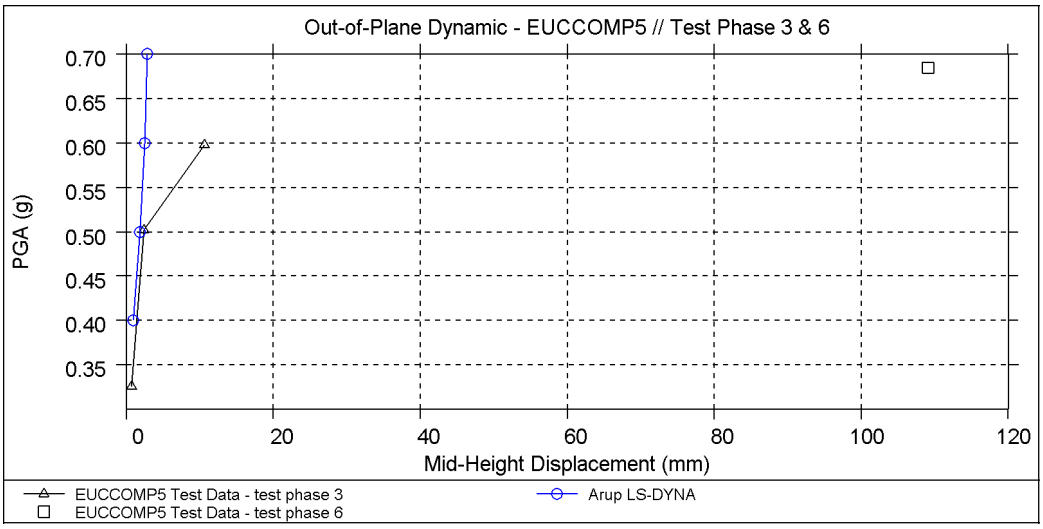

Figure 141: EUC-COMP-5: LS-DYNA blind prediction – Ca-Si wall wythe relative mid-height response vs. PGA for model under incremental dynamic testing procedure of ground motion Gr_2 (test phases #3 & 6)

3.1.7.3 EUCENTRE Blind Prediction

EUCENTRE did not perform a blind prediction of specimen EUC-COMP-5.

3.1.7.4 TU-Delft Blind Prediction

The blind prediction of EUC-COMP-5 was done by applying separately the ground motions Gr_1 and Gr_2. The panel was tested in the un-cracked and cracked conditions for 0.1 MPa overburden.

The results of these analyses showed that a mechanism occurred due to cracking in the interfaces. The maximum PGA before global instability occurred was 0.6g for the 0.1 MPa overburden. The difference between the cracked or uncracked assumption seemed to be rather small in all the analysed conditions and the level of overburden had the most influence on the response of the wall.

Figure 142 and Figure 143 plot the incremental dynamic response for the DIANA model of EUC-COMP-4 with 0.1 MPa overburden.

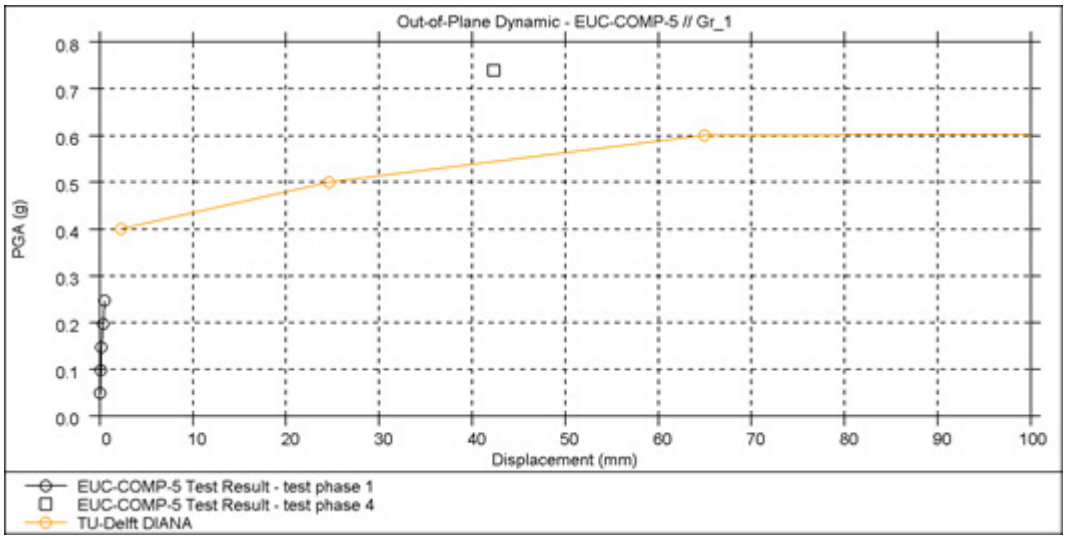

Figure 142: EUC-COMP-5: DIANA blind prediction – Ca-Si wall wythe relative mid-height response vs. PGA for model under incremental dynamic testing procedure of ground motion Gr_1 (test phases #1 & 4)

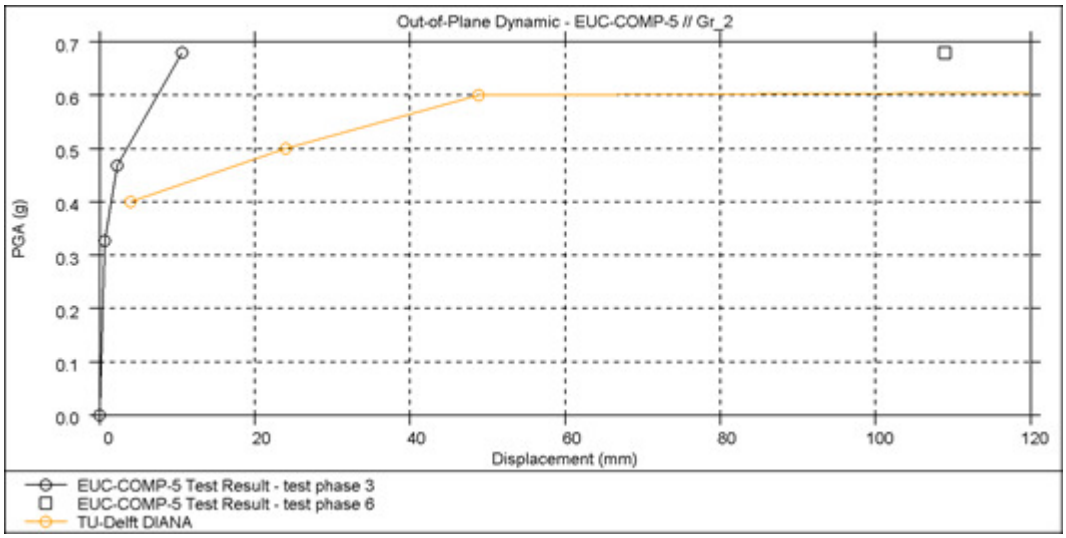

Figure 143: EUC-COMP-5: DIANA blind prediction – Ca-Si wall wythe relative mid-height response vs. PGA for model under incremental dynamic testing procedure of ground motion Gr_2 (test phases #3 & 6)

3.1.8 EUC-COMP-6

3.1.8.1 Test description

EUC-COMP-6 is the fourth dynamic out-of-plane test in the blind prediction program administered by EUCENTRE. This specimen is a single-wythe cavity wall. The inner (structural) leaf is constructed of calcium silicate units and is 1.44 metres long and 2.75 metres high. The outer leaf is constructed of clay units and is 1.44 metres long and 2.7 metres high. The inner and outer leaves are connected with 2 ties/m^2. The applied overburden stress on the inner leaf is 0.3 MPa. The testing sequence consisted of incremental dynamic testing procedure of the following ground motions:

- Gr_1: Groningen record, PGA = 0.25g
- RWA: 4 Hz acceleration pulse input
- Gr_2: Floor accelerations obtained with TREMURI program assuming T1_STAR Model in the “weak” direction, PGA = 0.38g

The test specimen reached global instability during test phase 6.

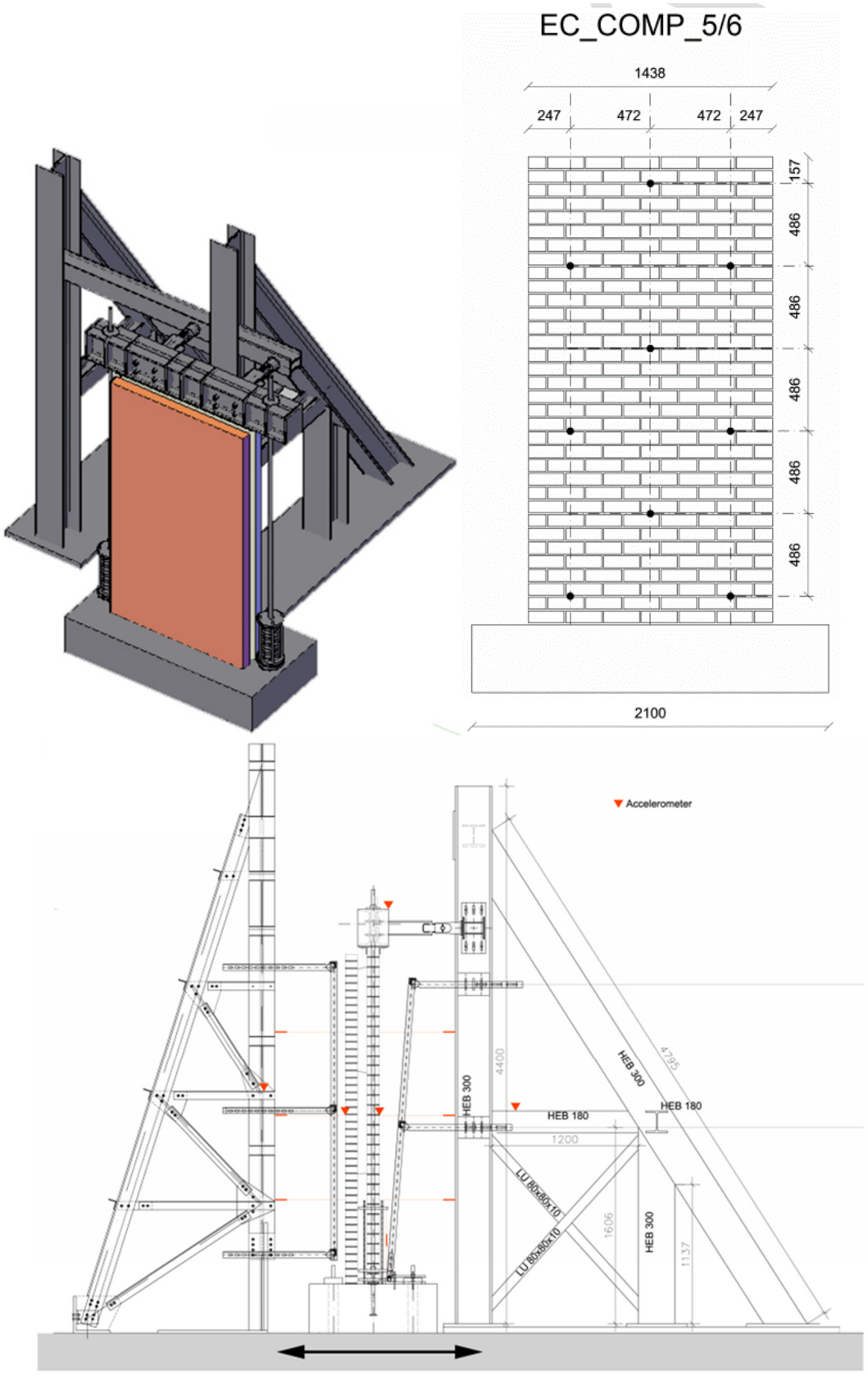

Figure 144: Test set-up images

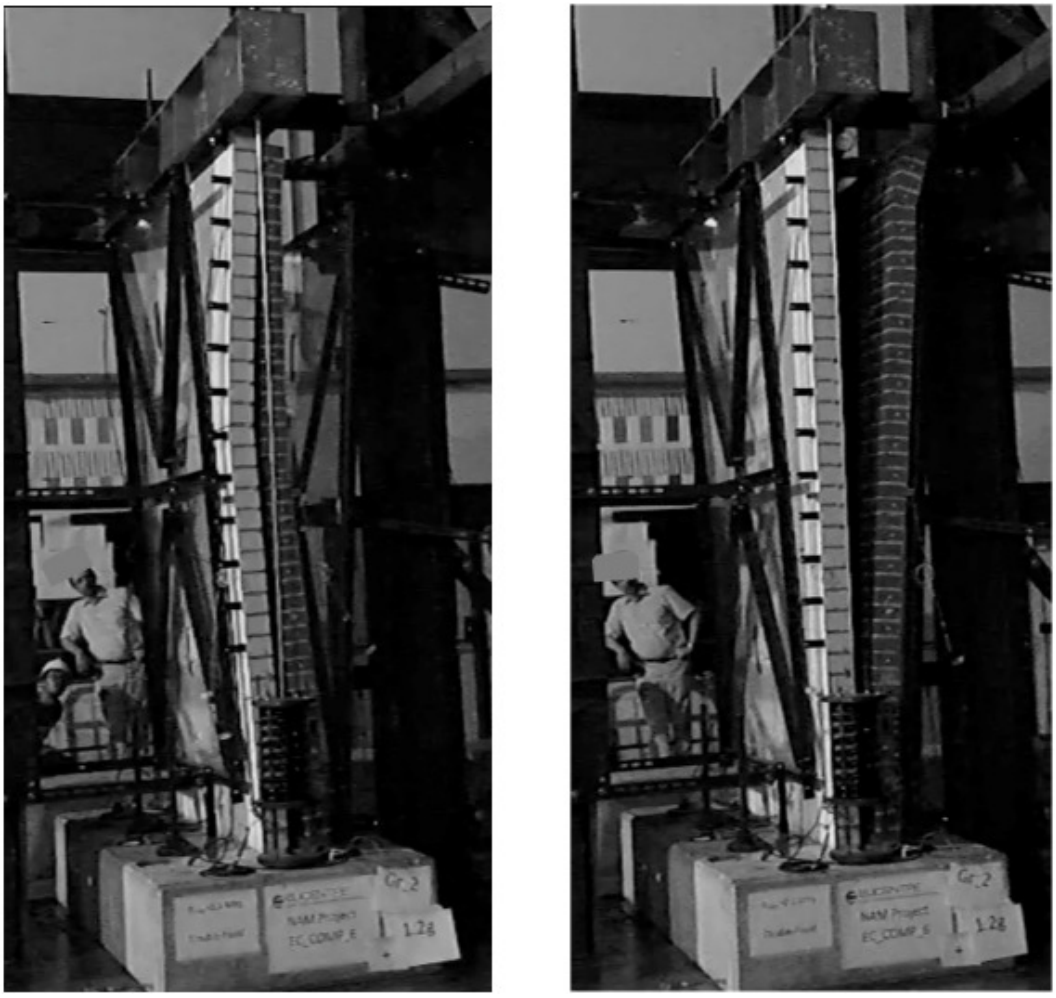

Figure 145: EUC-COMP-6: Final deformed shape / collapse

3.1.8.2 Arup Blind Prediction

The following loading protocol was applied to the blind prediction model of EUC-COMP-7 according to the provided test protocol at the time of analysis:

Table 41: EUC-COMP-6: Testing sequence

Phase #	Test #	Ground Motion	Input Scaling	PGA (g)
1	1.1	Gr_1	+0.20	0.049
1	1.2	Gr_1	+0.40	0.098
1	1.3	Gr_1	-0.40	0.098
1	1.4	Gr_1	+0.60	0.147
1	1.5	Gr_1	+0.80	0.197
1	1.6	Gr_1	+1.00	0.247
1	1.7	Gr_1	-0.60	0.147
1	1.8	Gr_1	-0.80	0.197
1	1.9	Gr_1	-1.00	0.247
2	2.1	RWA	2.0	0.20
2	2.2	RWA	3.0	0.30
3	3.1	Gr_2	+0.70	0.327
3	3.2	Gr_2	+1.00	0.468
3	3.3	Gr_2	+1.50	0.68
4	4.1	Gr_1	+3.00	0.739
5	5.1	RWA	3.0	0.30
5	5.1	RWA	5.0	0.50
6	6.1	Gr_2	+1.50	0.68

The LS-DYNA shell model of EUC-COMP-6 predicts out-of-plane rocking behavior and associated tensile bed joint failures at the top and bottom of the specimen as well as mid-height in both leaves.

The model predicts no collapse, assuming there is no failure in the ties as they have been modeled as rigid elements. For the specimen with 2 ties/m2, in the LS-DYNA model, the leaves deform uniformly during the applied ground motions. However, for the specimen with 1 tie/m2, in the LS-DYNA model, the leaves separate slightly more than the model with 2 ties/m^2 as a result of the reduction of number of ties.

Note that small discrepancies between the values for the PGA reported in Table 41 and the following curves for the Lab Test to LS-DYNA simulation comparison are due to baseline corrections applied to the measured PGA.

Figure 146 and Figure 147 below plot the incremental dynamic response for the LS-DYNA models of EUC-COMP-6 that correlate to test phase #1 and #3 & #5, respectively.

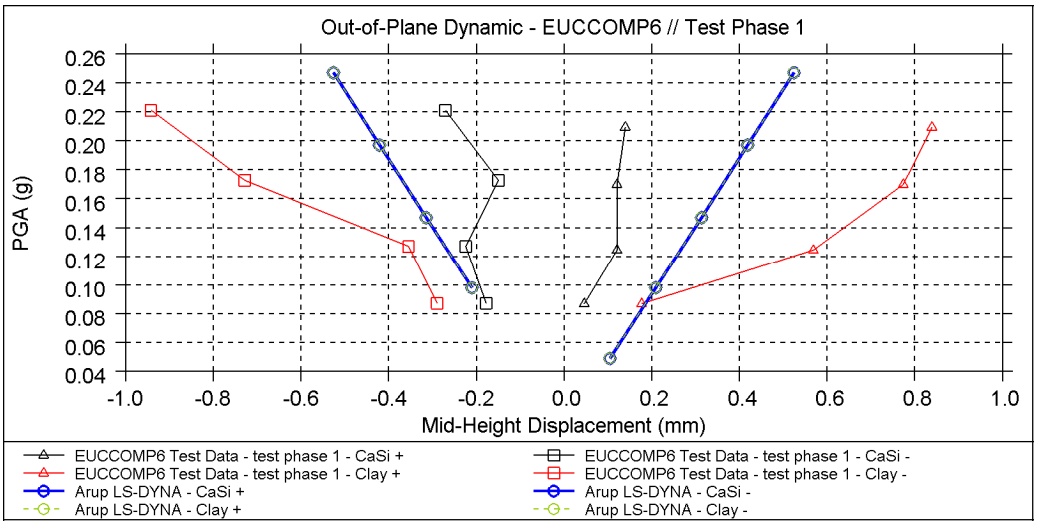

Figure 146: EUC-COMP-6: LS-DYNA blind prediction – Relative mid-height response vs. PGA for model under incremental dynamic testing procedure of ground motion Gr_1 (test phase #1)

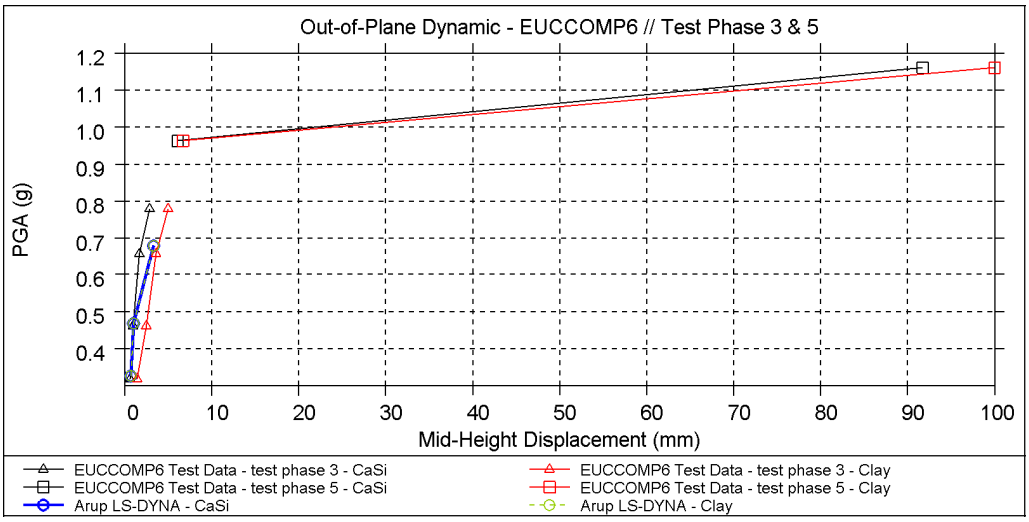

Figure 147: EUC-COMP-6: LS-DYNA blind prediction – Relative mid-height response vs. PGA for model under incremental dynamic testing procedure of ground motion Gr_2 (test phases #3 & 5)

3.1.8.3 EUCENTRE Blind Prediction

EUCENTRE did not perform a blind prediction of specimen EUC-COMP-6.

3.1.8.4 TU-Delft Blind Prediction

A plane strain finite element model was used. This model was validated using the experiment of Doherty on one-way out-of-plane bending URM walls. The plane strain elements are orientated in the thickness direction of the both inner and outer leafs and have an elastic material model applied to them. The strength properties of the masonry are lumped in the line interfaces which are located on the points where a crack is expected to occur. In Figure 148 the results from the analysis are presented. The blind prediction has been done by applying separately the ground motions Gr_1 and Gr_2. The panel has been tested in the un-cracked and cracked conditions. The difference between the cracked or un-cracked assumption seems to be rather small.

With an overburden of 0.3 MPa, global instability of the wall occurs at 1.1g.

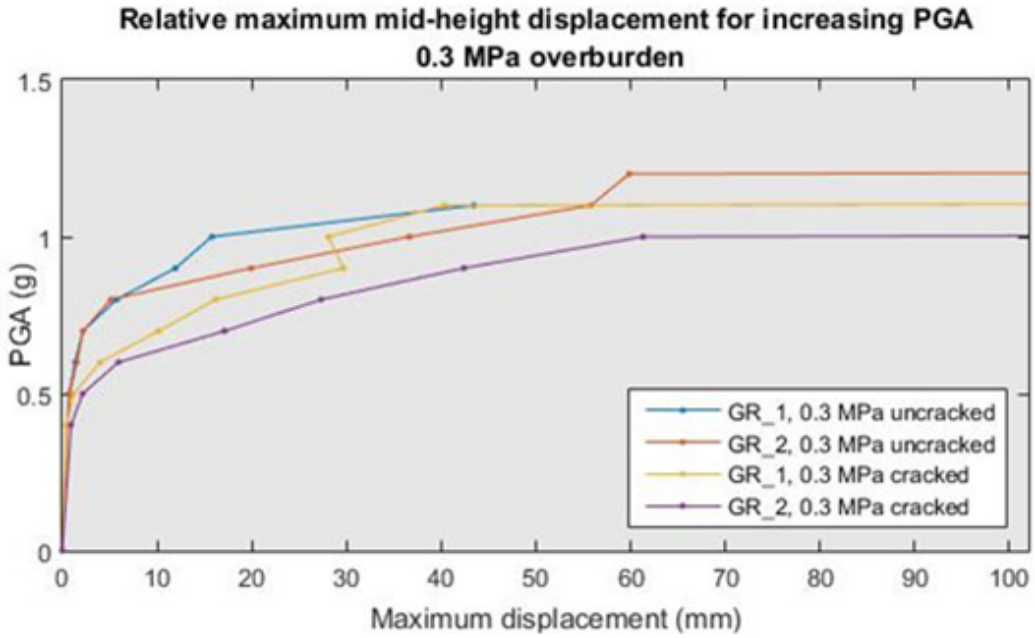

Figure 148: EUC-COMP-6: DIANA blind prediction – Relative mid-height response vs. PGA for 0.3 MPa overburden, under incremental dynamic testing procedure of ground motion Gr_1 (test phase #1) and Gr_2 (test phase #3 and #5)

3.1.9 EUC-COMP-7

3.1.9.1 Test description

EUC-COMP-7 is the third dynamic out-of-plane test in the blind prediction program administered by EUCENTRE. This specimen is a single-wythe cavity wall. The inner (structural) leaf is constructed of calcium silicate units and is 1.44 metres long and 2.75 metres high. The outer leaf is constructed of clay units and is 1.44 metres long and 2.7 metres high. The inner and outer leaves are connected with 4 ties/m^2. The applied overburden stress on the inner leaf is 0.1 MPa.

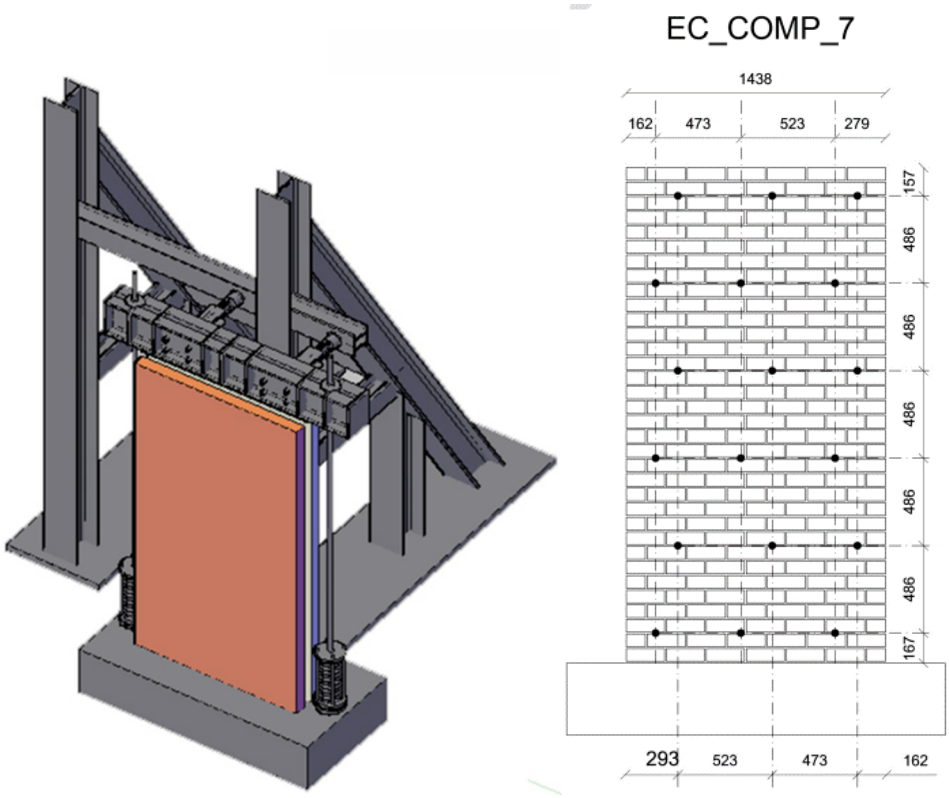

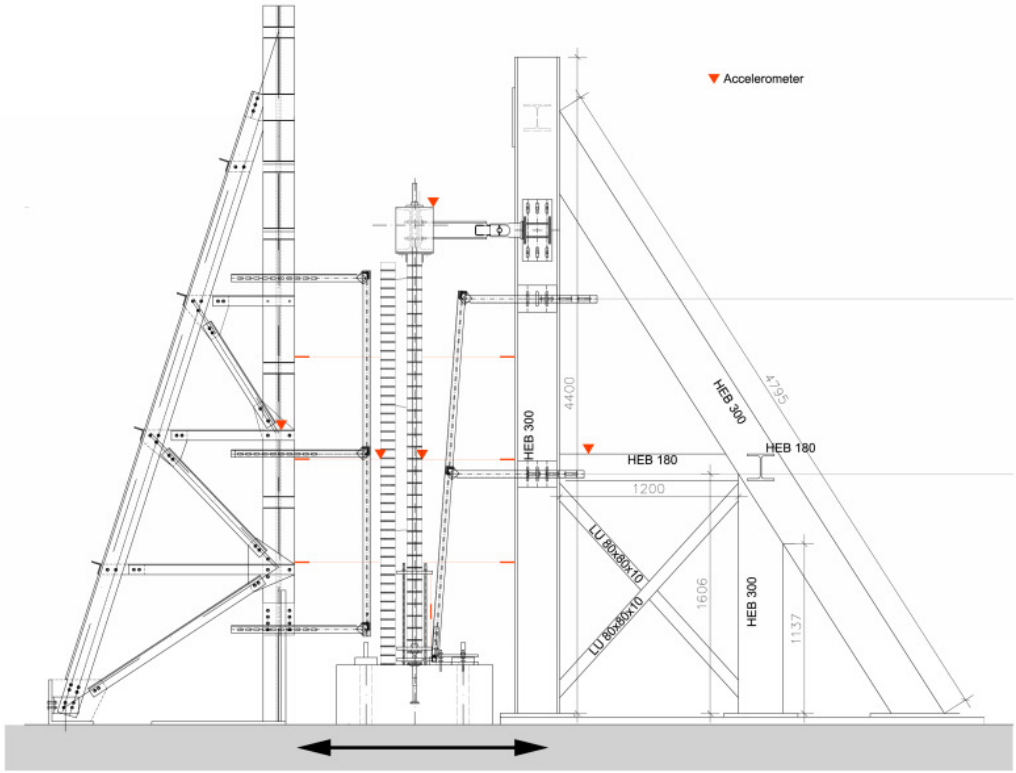

Figure 149: Test set-up images

Figure 150: EUC-COMP-7: collapse

3.1.9.2 Arup Blind Prediction

The following loading protocol was applied to the blind prediction model of EUC-COMP-7 according to the provided test protocol at the time of analysis:

Table 42: Assumed loading protocol for EUC-COMP-7

Phase #	Test #	Ground Motion	Input Scaling	PGA (g)
1	1.1	Gr_1	+0.20	0.049
1	1.2	Gr_1	+0.40	0.098
1	1.3	Gr_1	-0.40	0.098
1	1.4	Gr_1	+0.60	0.147
1	1.5	Gr_1	+0.80	0.197
1	1.6	Gr_1	+1.00	0.247
1	1.7	Gr_1	-0.60	0.147
1	1.8	Gr_1	-0.80	0.197
1	1.9	Gr_1	-1.00	0.247
2	2.1	RWA	2.0	0.20
2	2.2	RWA	3.0	0.30
3	3.1	Gr_2	+0.70	0.327
3	3.2	Gr_2	+1.00	0.468
3	3.3	Gr_2	+1.50	0.68
4	4.1	Gr_1	+3.00	0.739

The LS-DYNA shell model of EUC-COMP-7 predicts out-of-plane rocking behavior and associated tensile bed joint failures at the top and bottom of the specimen as well as mid-height in both leaves.

The model predicts collapse during test #4.1. In addition, due to the high density of ties and their rigidity in the LS-DYNA model, the deformation of the two leaves is identical. Hence, only the results of the calcium-silicate leaf are displayed. Figure 151 and Figure 152 below plot the incremental dynamic response for the LS-DYNA models of EUC-COMP-7 that correlate to test phases #1 and #3 & #5, respectively.

Note that small discrepancies between the values for the PGA reported in Table 42 and the following curves for the Lab Test to LS-DYNA simulation comparison are due to baseline corrections applied to the measured PGA.

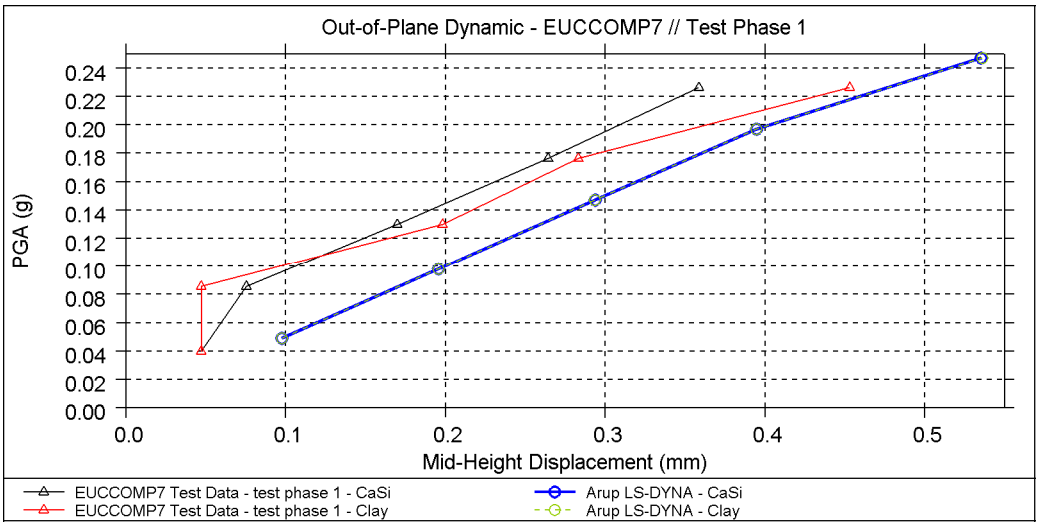

Figure 151: EUC-COMP-7: LS-DYNA blind prediction – Relative mid-height response vs. PGA for model under incremental dynamic testing procedure of ground motion Gr_1 (test phases #1)

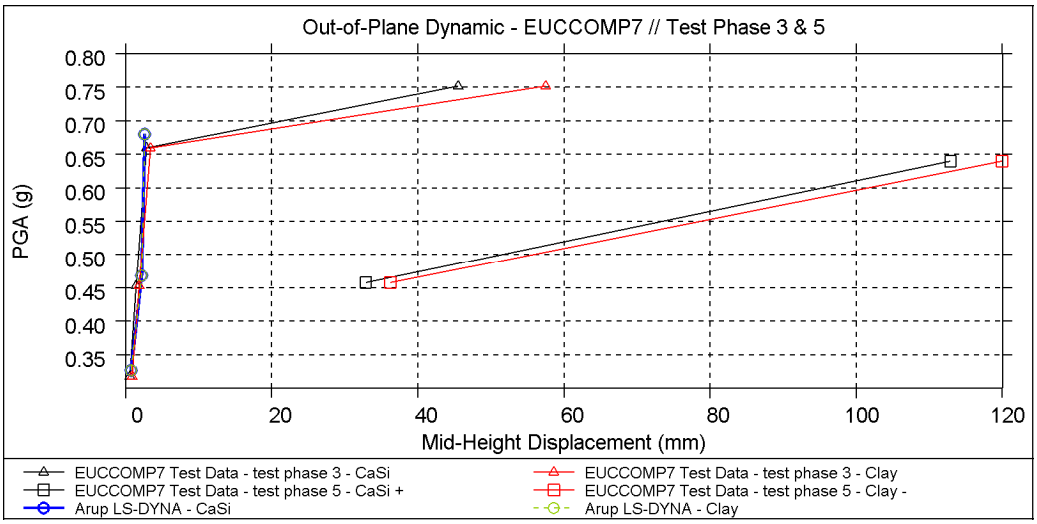

Figure 152: EUC-COMP-7: LS-DYNA blind prediction – Relative mid-height response vs. PGA for model under incremental dynamic testing procedure of ground motion Gr_2 (test phases #3 & 5)

3.1.9.3 EUCENTRE Blind Prediction

Figure 153 and Figure 154 plot the incremental dynamic response of the Tri-linear models for EUC-COMP-7

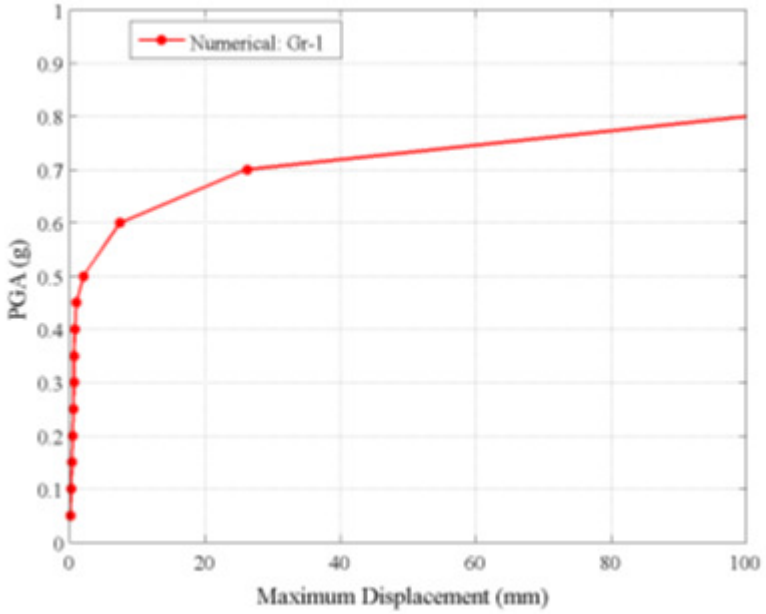

Figure 153: EUC-COMP-7: EUCENTRE blind prediction – Relative mid-height response vs. PGA for model under incremental dynamic testing procedure of ground motion Gr_1 (test phases #1)

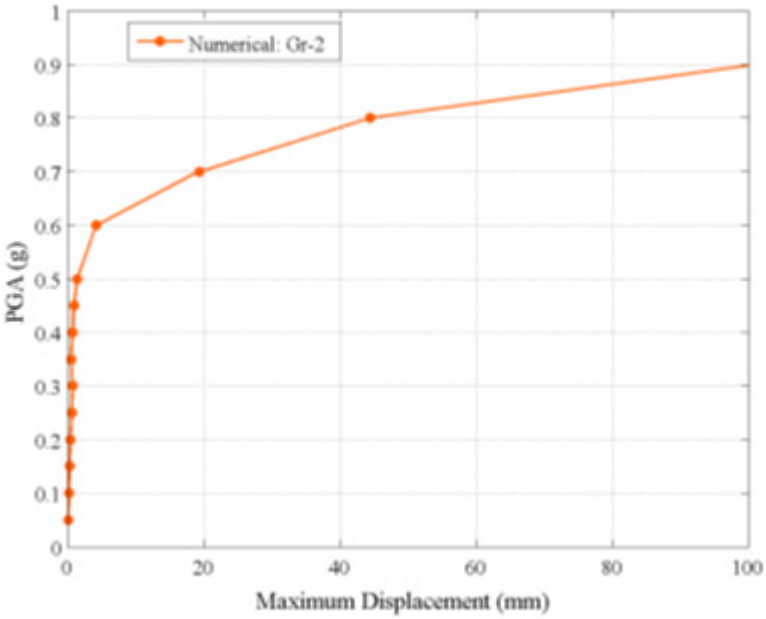

Figure 154: EUC-COMP-7: EUCENTRE blind prediction – Relative mid-height response vs. PGA for model under incremental dynamic testing procedure of ground motion Gr_2 (test phases #3 & 5)

3.1.9.4 TU-Delft Blind Prediction

A plane strain model has been constructed to account for the deformation over the thickness of the wall. Eight different setups are tested for acceleration signals with increasing PGAs. A discrete cracking model was used for the analyses, including interfaces at the top, bottom and middle of the panel.

The results of these analyses show that a mechanism occurs due to cracking in the interfaces. For an overburden of 0.1 MPa a maximum PGA of 0.5g before global instability was found.

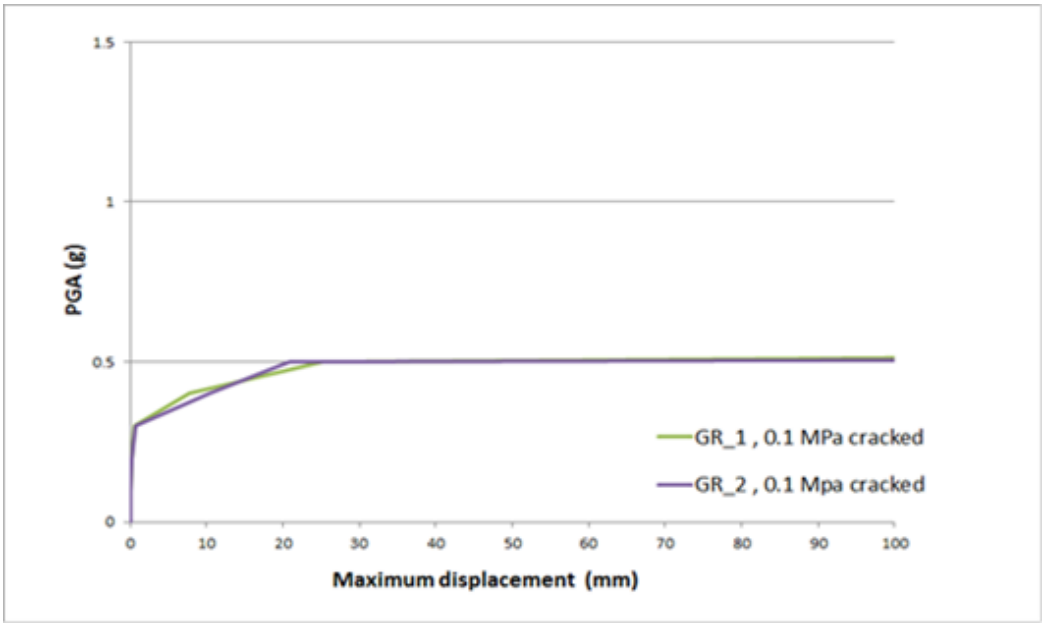

Figure 155: EUC-COMP-7: DIANA blind prediction – Relative mid-height response vs. PGA for 0.3 MPa overburden, under incremental dynamic testing procedure of ground motion Gr_1 (test phase #1) and Gr_2 (test phase #3 and 5)

3.1.10 Summary

The blind prediction results for the out-of-plane quasi-static tests are summarised in Table 43. Because of the differences between the protocols and overburden loading assumed in the simulations versus those actually applied in the tests, these comparisons are of limited value.

Table 43: LS-DYNA blind prediction results summary for out-of-plane quasi-static tests

Component	LS-DYNA		TREMURI		DIANA (*)		Test Result	
	Peak Strength [kN]	Max Achieved Drift (End of protocol) [mm]	Peak Strength [kN]	Max Achieved Drift (End of protocol) [mm]	Peak Strength [kN]	Max Achieved Drift [mm]	Peak Strength [kN]	Max Achieved Drift (End of protocol) [mm]
TUD-COMP-7	11	80	7.7	80	---	---	10	80
TUD-COMP-10	16 (no applied overburden, forces on top and bottom edges only)	90	---	---	53	8	46 (0.05 MPa overburden)	80
TUD-COMP-11	15 (no applied overburden, forces on top and bottom edges only)	73	---	---	---	---	31 (0.05 MPa overburden)	100
TUD-COMP-12	22 (forces on top and bottom edges only)	80	---	---	---	---	25	100

(*) Model failed to converge

Table 44: LS-DYNA blind prediction results summary for out-of-plane dynamic tests – part 1

Component	LS-DYNA		Tri-Linear model (EUCENTRE)		DIANA		Test Result	
	Max Achieved PGA for Gr_1 input motion	**Max Achieved PGA for Gr_2 input motion**	**Max Achieved PGA for Gr_1 input motion**	**Max Achieved PGA for Gr_2 input motion**	**Max Achieved PGA for Gr_1 input motion**	**Max Achieved PGA for Gr_2 input motion**	**Max Achieved PGA [g]**	**Increment cycle at failure**
EUC-COMP-4	0.9g for 0.1MPa overburden 1.0g for 0.3MPa overburden	1.1g for 0.1MPa overburden	0.7g for 0.1MPa overburden 1.0g for 0.3MPa overburden	0.6g for 0.1MPa overburden	0.8g for 0.1MPa overburden (no collapse) 2.0g for 0.3MPa overburden (no collapse)	1.0g for 0.1MPa overburden	0.96	5 (*)
EUC-COMP-5	0.7g	0.9g	---	---	0.6g	0.6g	0.66	6

Table 45: LS-DYNA blind prediction results summary for out-of-plane dynamic tests – part 2

Component	LS-DYNA		Tri-Linear model (EUCENTRE)		DIANA		Test Result	
	Peak Strength [kN]	Max Achieved Drift (End of protocol) [mm]	Max Achieved PGA for Gr_1 input motion	Max Achieved PGA for Gr_2 input motion	Max Achieved PGA for Gr_1 input motion	Max Achieved PGA for Gr_2 input motion	Max Achieved PGA [g]	Increment cycle at failure
EUC-COMP-6	0.74 (no collapse achieved)	4	---	---	1.1g	1.2g	1.17	5
EUC-COMP-7	0.74	4	0.8g	0.9g	0.5g	0.5g	0.75	5 (*)

(*) Increment cycles are defined as the first character of the 'Test #' in Table 39, Table 40, Table 41 and Table 42. This relates to the number of series of incremental ground motion which have been applied in order to reach failure. Note that for the simulations of components EUC-COMP-4 and EUC-COMP-7 the maximum PGA does not occur during the last series of incremental ground motion (Increment cycle at failure) but at an earlier stage in the analysis.

4 Conclusions

4.1 Arup Conclusion

General conclusions:

- The LS-DYNA models all ran robustly without abnormal termination, either completing the input protocol or predicting collapse of the specimen for physically plausible reasons.
- The peak strength of the in-plane specimens are in general fairly well predicted.
- For the out-of-plane specimens, bending about the horizontal axis is predicted reasonably accurately, but bending about the vertical axis (which contributes to the resistance in two-way spanning) is much weaker than indicated by the experiments. This could be due to the understanding that the net force that would be reported would be taken as the load transferred to the top and bottom timber reaction frames only. Therefore, the reported analysis net force is also only measured from the top and bottom edges of the blind prediction model, while the hysteresis from the test includes forces from all four edges.
- Predictions for the cavity wall dynamic test specimens are fair, although the assumptions made on the loading protocol that may or may not have matched the implemented loading protocol appear to affect results.
- In-plane and out-of-plane rocking modes absorb too little energy in the analyses compared to the tests.
- An important aspect of the analyses of existing buildings for the GESU project is to predict whether the building collapses or is in a near-collapse state. This is not fully exploited in the blind predictions but is a point of focus in the post-test refined predictions.

4.2 EUCENTRE Conclusion

The comparison of blind predictions and tests results for the component tests carried out at TU-Delft and EUCENTRE showed a general ability of the TREMURI models to predict the experimental back-bone curves and failure modes.

However, several exceptions to this general trend occurred. They were mainly associated with erroneous assumptions for material properties (few cases) and differences in the loading protocols. The actual load applied in many of the tests differed from the planned protocol significantly (for example, in respect of the applied overburden). The comparisons between the blind predictions and the actual test results are therefore of limited value for those tests.

In general, the macro-element model showed a limited capacity in simulating the hysteretic energy dissipation occurring during the tests of flexure-dominated calcium silicate specimens.

4.3 TU-Delft Conclusion

In many cases the comparison between experimental and numerical results cannot be considered completely valid given the differences found in the loading protocol and in the overburden. Nevertheless some general conclusions and observations on the performance of the numerical model can be drawn.

Concerning the in-plane tests, the DIANA models provided reasonable results in the prediction of shear capacity of the panels. A differentiation of material parameters at the boundaries and in the middle of the panel was needed for the correct separation of damage mechanisms related to rocking and shear respectively, highlighting the need for the development of a direction dependent material model. Several analyses prematurely failed due to convergence issues, not allowing to investigate the behaviour of the panel for high displacement levels. The level of energy dissipation predicted was significantly lower than the test result in all cases.

Regarding the static out-of-plane tests performed by the TUD laboratories, only TUD_COMP-10 was submitted before the execution of the test. The model was able to detect the main failure mechanism and provided a discrete estimation of the peak resistance but could not describe any post-peak behaviour. An orthotropic model might better represent the failure mechanism for two-way bending tests.

Concerning the dynamic out-of-plane tests performed by the EUCENTRE laboratories, a good estimation of the maximum PGA was achieved. In addition, the model was able to reproduce the main failure mechanism related to the out-of-plane behaviour of single and double leaf specimens that is characterised by rocking on top and bottom of the panel and a main crack at mid-height. However, the adopted model (a plane strain finite element model with the elements orientated in the thickness direction of the walls) cannot be employed in more complex structures (such as whole buildings). Also, the estimated displacements are far from those measured during the experiments.

References

[1] Arup, 229746_032.0_REP127, "Modelling and Analysis Cross-Validation – Arup, EUC, TU-Delft", July 2015, Rev A.01

[2] EUCENTRE, "Experimental campaign on cavity walls systems representative of the Groningen building stock", November 2015

[3] TU-Delft, "Preliminary test reports for in-plane tests on masonry walls at TU-Delft", October 2015

[4] TU-Delft, "Preliminary test reports for out-of-plane tests on masonry walls at TU-Delft", January 2016

[5] TU-Delft, "Tests for the characterisation of replicated masonry", October 2015

[6] TU-Delft, "Pull-out strength of wall ties", December 2015

[7] Tomassetti U., Graziotti F., Penna A., Magenes G. (2015). A single degree of freedom model for the simulation of the out-of-plane response of unreinforced masonry walls. Proc.Italian National Conference on Earthquake Engineering, L'Aquila, Italy.

[8] NAM, Basis for Design: Seismic Structural Upgrading of Existing Buildings in the Groningen Area, Rev 3, March 2015, Doc Ref: EP201403208456

[9] TU-Delft, "Tests for the characterisation of replicated masonry", August 2015, version 4

[10] Lagomarsino S., Penna A., Galasco A., Cattari S., (2013) "TREMURI Program: an equivalent frame model for the nonlinear seismic analysis of masonry buildings", ENGINEERING STRUCTURES, 56(11): 1787-1799.

[11] Penna A., Lagomarsino S., Galasco A., (2014) "A nonlinear macro-element model for the seismic analysis of masonry buildings", EARTHQUAKE ENGINEERING & STRUCTURAL DYNAMICS, 43(2): 159-179.